ISRES Publishing

The Eurasia Proceedings of Science, Technology, Engineering & Mathematics

EPSTEM

VOLUME 22 ICBASET CONFERENCE

ISSN: 2602-3199

ISBN: 978-625-6959-09-5

ICBASET 2023: 3rd International Conference on Basic Sciences, Engineering and Technology (ICBASET)

April 27 - 30, 2023
Marmaris, Turkey

Edited by: Prof. Dr.Mehmet Ozaslan (Chair), Gaziantep University, Turkey

The Eurasia Proceedings of
Science, Technology, Engineering & Mathematics (EPSTEM)
ISSN: 2602-3199

ICBASET 2023

Volume 22, Pages 1-388 (August 2023)

The Eurasia Proceedings of Science, Technology, Engineering & Mathematics (EPSTEM)

e-ISSN: 2602-3199

Address: Istanbul C. Cengaver S. No 2 Karatay/Konya/TURKEY

Website: www.isres.org

Contact: isrespublishing@gmail.com

Conference: ICBASET2023: 3rd International Conference on Basic Sciences, Engineering and Technology (ICBASET)
Conference website: https://www.2023.icbaset.net
Dates: April 27 – 30, 2023
Location: Marmaris, Turkey
Edited by: Prof. Dr.Mehmet Ozaslan

About Editor(s)

Prof Dr. Mehmet Ozaslan
Department of Biology, Gaziantep University, Turkey
Website: mehmetozaslan.com
E-mail: ozaslanmd@gantep.edu.tr

Language Editor(s)

Assoc. Prof. Dr. Kagan Buyukkarci
Department of English Language Education, Suleyman Demirel University, Turkey
E-mail: kaganbuyukkarci@sdu.edu.tr

Editorial Policies

ISRES Publishing follows the steps below in the procedings book publishing process.

ISSN: 2602-3199

In the first stage, the papers sent to the conferences organized by ISRES are subject to editorial oversight. In the second stage, the papers that pass the first step are reviewed by at least two international field experts in the conference committee in terms of suitability for the content and subject area. In the third stage, it is reviewed by at least one member of the organizing committee for the suitability of references. In the fourth step, the language editor reviews the language for clarity.

Review Process

Abstracts and full-text reports uploaded to the conference system undergo a review procedure. Authors will be notified of the application results in three weeks. Submitted abstracts will be evaluated on the basis of abstracts/proposals. The conference system allows you to submit the full text if your abstract is accepted. Please upload the abstract of your article to the conference system and wait for the results of the evaluation. If your abstract is accepted, you can upload your full text. Your full text will then be sent to at least two reviewers for review. **The conference has a double-blind peer-review process.** Any paper submitted for the conference is reviewed by at least two international reviewers with expertise in the relevant subject area. Based on the reviewers' comments, papers are accepted, rejected or accepted with revision. If the comments are not addressed well in the improved paper, then the paper is sent back to the authors to make further revisions. The accepted papers are formatted by the conference for publication in the proceedings.

Aims & Scope

Engineering, technology and basic sciences are closely related fields. Developments and innovations in one of them affect the others. Therefore, **the focus of the conference** is on studies related to these three fields. Studies in the fields of engineering, technology and basic science are accepted to the conference even if they are not associated with other fields. The conference committee thinks that a study in only one field (for example, mathematics, physics, etc.) will contribute to other fields (for example, engineering, technology, etc.) in future studies, even if it is not associated with the presentation at the conference. In line with this perspective, studies in the following fields are accepted to the conference: *Biology, Chemistry, Engineering, Mathematics, Physics and Technology*.
The aim of the conference is to bring together researchers and administrators from different countries, and to discuss theoretical and practical issues in all fields of Engineering, Technology and Basic Sciences.

Articles: 1-42

CONTENTS

The Eurasia Proceedings of
Science, Technology, Engineering & Mathematics (EPSTEM)
ISSN: 2602-3199

ISSN: 2602-3199

The Eurasia Proceedings of
Science, Technology, Engineering & Mathematics (EPSTEM)
ISSN: 2602-3199

The Eurasia Proceedings of Science, Technology, Engineering & Mathematics (EPSTEM)
ISSN: 2602-3199

The Eurasia Proceedings of Science, Technology, Engineering & Mathematics (EPSTEM), 2023

Volume 22, Pages 1-14

ICBASET 2023: International Conference on Basic Sciences, Engineering and Technology

Mathematical Analyzing of Laser Triangulation System without Scheimpflug Condition via C++ and Qt Framework

Orkun KASAPOGLU
Baykal Machinery

Tugba BILGIN
Baykal Machinery

Abstract: In this paper, the mathematical characteristics of a laser triangulation system have been analyzed without considering Scheimpflug condition. The system parameters have been investigated and detailed information about the behavior of the system due to the changing some initial parameters just before designing the profile measurement system have been obtained. To be able to evaluate the system, C++ and Qt framework have been used for calculation of multi-dimensional arrays and visualization of the results to investigate the system parameters. The characteristics of the triangulation systems (both for our model and the model that proposed by Lamott and Noll, 2011) and characteristics of laser beam (laser beam thickness change for given measurement field range) for different laser sources with different wavelengths have been investigated. After analyzing the parameters of the triangulation system successfully, an adjustable system will be built in the laboratory to be able to get a better understanding the usage of this system in both 2D and 3D laser cutting systems.

Keywords: Laser Triangulation, Image Processing, C++, Qt

Introduction

Laser triangulation is a widely used measurement technique that involves projecting a laser beam onto a surface and measuring the distance to the surface based on the reflected light. This technique is commonly used in various applications such as 2D/3D scanning, robotics, quality control, and machine vision. The basic principle of laser triangulation is use the position of the reflected light spot to calculate the distance to the surface, based on the angle between the laser beam and the sensor or camera.

Traditionally, laser triangulation systems are designed on the Scheimpflug condition, which is a geometric principle (Fig. 1) that ensures that the image plane, lens plane, and the object plane are intersecting in one line. This condition is necessary to achieve sharp focus and accurate measurements, especially over long distances and at steep angles. However, strictly adhering to the Scheimpflug condition can be challenging, especially in complex or non-standard measurement scenarios.

In recent years, there has been growing interest in the alternative approaches to laser triangulation that do not strictly rely on the Scheimpflug condition. These approaches aim to improve the flexibility, simplicity, and robustness of laser triangulation systems, while still maintaining acceptable levels of accuracy and precision. This article is related with the exploration of the principles and practical considerations of laser triangulation without Scheimpflug condition, and highlights some of the advantages and limitations of this approach.

The characteristic curve of laser triangulation has been discussed for both Lamott and Noll's and our system. Related systems have plenty of application are from thickness measurements of rolled sheets to flatness

measurements of heavy plates or coordinate-measuring machines to the straightness and profile measurements of rails (Donges & Noll, 2015).

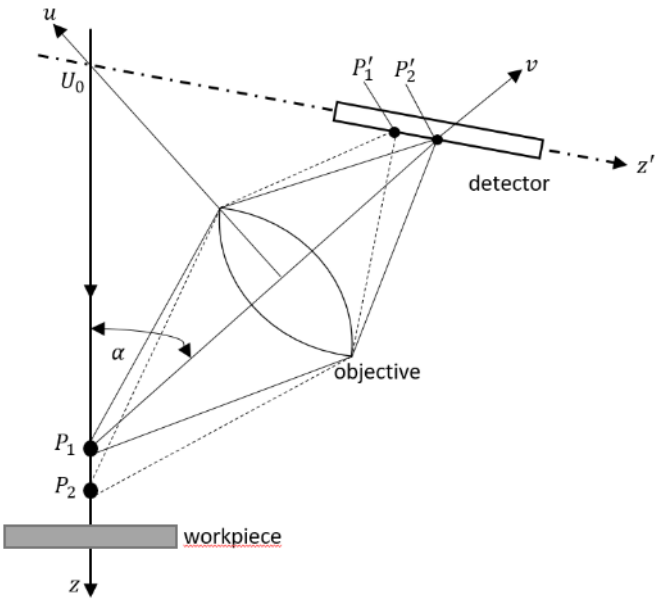

Figure 1.Imaging geometry for laser triangulation including Scheimfplug condition (Lamott & Noll, 2011).

Laser Triangulation without Scheimpflug Condition

Basic Principles

Laser triangulation without Scheimpflug condition is based on the same fundamental principle as traditional laser triangulation (see Fig. 2): the distance to a surface can be determined by measuring the angle in between projected laser beam and the reflected light or calculating the intersection point components for the imaging axis between projected light. However, in this case, the position of the sensor or camera is not necessarily aligned with the image plane and the lens plane. Instead, the sensor or camera is positioned at an angle to the image plane, which allows for more flexible positioning and easier alignment.

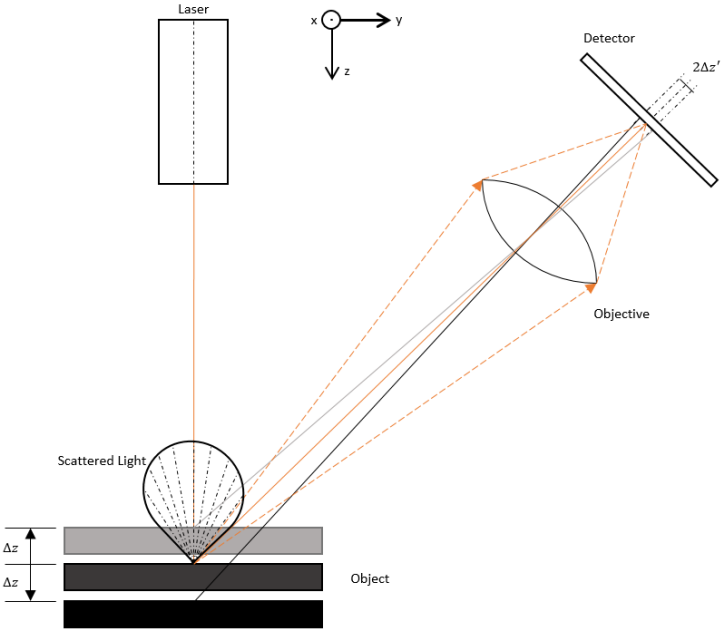

Figure 2. Our laser triangulation system without Scheimpflug condition.

To achieve accurate and precise measurements without the Scheimpflug condition, several factors need to be considered. Firstly, the position and orientation of the sensor or camera relative to the laser beam and the surface need to be carefully controlled and calibrated. This can be achieved using specialized mounting hardware, calibration targets, and software algorithms that compensate for any misalignments or distortions. Secondly, the characteristics of the laser beam and CCD or CMOS sensor need to be optimized according to the requirements for each specific applications. This characteristic includes laser wavelength, laser power, the resolution and sensitivity of the sensor or camera, the spot size and spot shape of the laser, the distance in between whole components to each other relatively and the angle of the measurement.

Advantages and Limitations

Laser triangulation without Scheimpflug condition offers several advantages over traditional laser triangulation. It allows for more flexible and adaptable measurement systems that can be tailored to specific applications and requirements. This can be particularly useful in scenarios where the object being measured is not flat or is difficult to access, or when the measurement system needs to be integrated into a larger system or process.

Laser triangulation without Scheimpflug condition can be easier to set up and use compared to traditional systems. There is no need to precisely align the sensor or camera with the image and lens planes, which can be time-consuming and difficult. Additionally, the reduced complexity of the measurement system makes it more robust and less prone to errors or failures. However, this method is a promising and emerging approach that offers new possibilities and opportunities for laser-based measurement systems. With careful consideration of the basic principles, advantages, and limitations, it can be a valuable tool for a wide range of applications in industry, research, and beyond.

Methods

Programming and Visualization

A desktop application has been developed during this study to be able to analyze the system models with the variation of the some critical parameters. Application contains two different user interfaces. First one is for the visualization of the system characteristics according to system parameters supplied by user. Second one is dedicated for 3D investigations and it is derived from an example from Qt Framework. The screenshots of the application user interfaces are given in below (Fig. 3 and Fig. 4 for 2D and 3D outputs respectively).

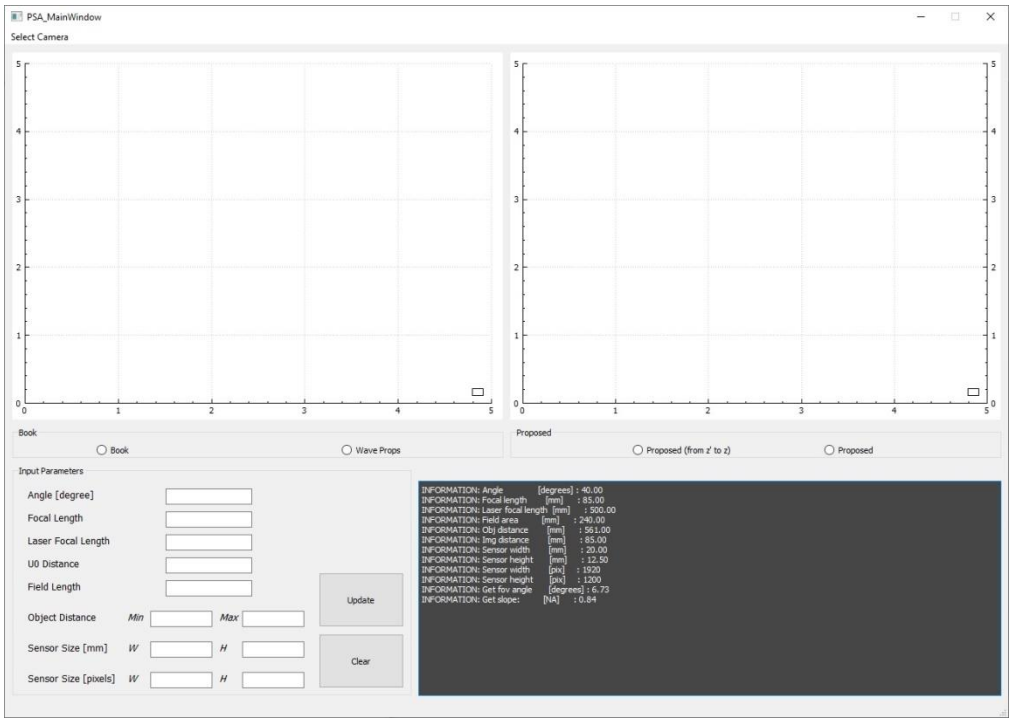

Figure 3. User interface for 2D and system parameters of the developed application.

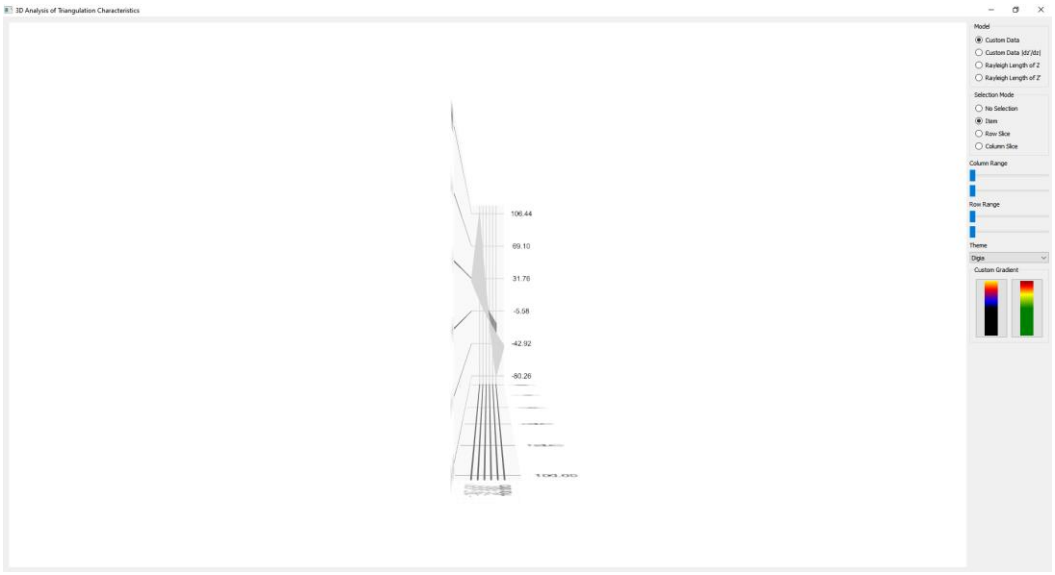

Figure 4. User interface for 3D of the system parameters.

The application has a default parameter list, which is given Figure 3, but it is of course allows to change parameters and all changings affects the behavior of the system.

Mathematical Equation

In this paper, the mathematical model of the laser triangulation without Scheimpflug condition is extracted from the simple hypotenuse representation of the z-coordinates from the imaging geometry of the lens and the camera. Here is the characteristic equation of our system (derivation of this equation is not given):

$$z'(z) = zm_L f \frac{\dfrac{-1}{d\sqrt{1+m_L^2}}}{1 + z\left(\dfrac{1}{d\sqrt{1+m_L^2}}\right)} \tag{1}$$

Here we can see, $z = 0$ when $z' = 0$ and $z < 0$ when $z' > 0$ (and vice versa). d is the distance from the lens to the $z = 0$ point, f is the focal length of the imaging lens, and m_L is the slope of the laser beam relative to the imaging axis. This equation has extracted from intersection points of the lines those are representing the projected and the reflected light.

Without Scheimpflug condition, the system becoming simple imaging system tilted with a triangulation angle. It is still non-linear for some angles. Linearity of the system directly related with the triangulation angle and increasing of the angle makes system more linear. Optimum triangulation angle needs to be defined according to the equipment via test and/or simulation.

Characteristic Curve of Triangulation Sensors

There is an equation related with the relationship in between the position of the light spot on the test object and the location of the imaged light spot at the detector. The location of the light spot on the straight line described by via this equation and determines unequivocally the position of the imaged light spot. Following equation represents a light spot at the position z would be projected onto the detector plane at the corresponding point z' (Donges and Noll, 2015):

The method that has been given in the Eq. (2) is finding the sensor points from given z-distances while the method has been given in this paper is finding the z-distances from the given z' sensor points.

$$z'(z) = m_L f \sqrt{1 + \left(m_L - \frac{u_0}{f}\right)^2} \cdot \frac{\left(\frac{z}{\sqrt{1+m_L^2}}\right)}{\left(\frac{z}{\sqrt{1+m_L^2}} + \frac{u_0}{m_L} - f\right)\left(m_L - \frac{u_0}{f}\right)} \quad (2)$$

The characteristic curves of the both equations and the $|dz'/dz|$ sensitivity changes are shown in Fig. 3 and Fig. 4.

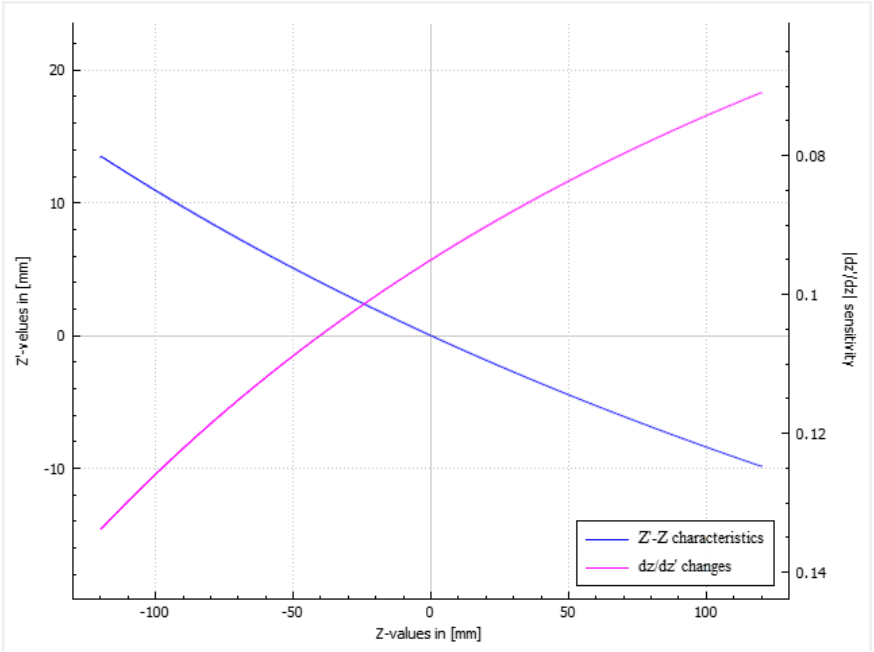

Figure 5. Coordinate of the image spot $\boldsymbol{z'}$ and the sensitivity ($\boldsymbol{dz'/dz}$) as a function of the illuminated spot position z (Lamott and Noll, 2011).

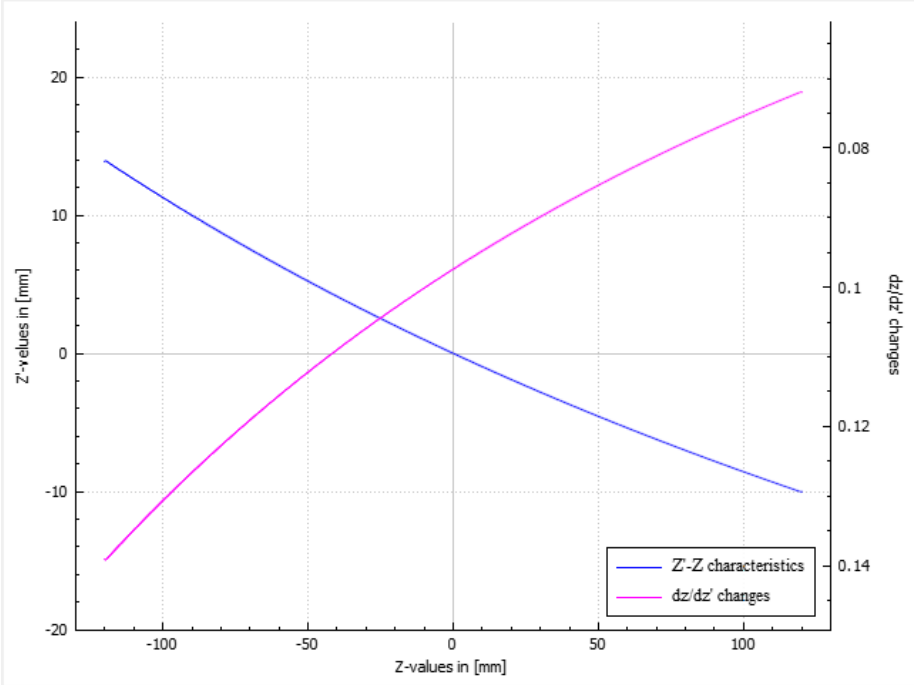

Figure 6. Same plotting for method which has been given in this paper.

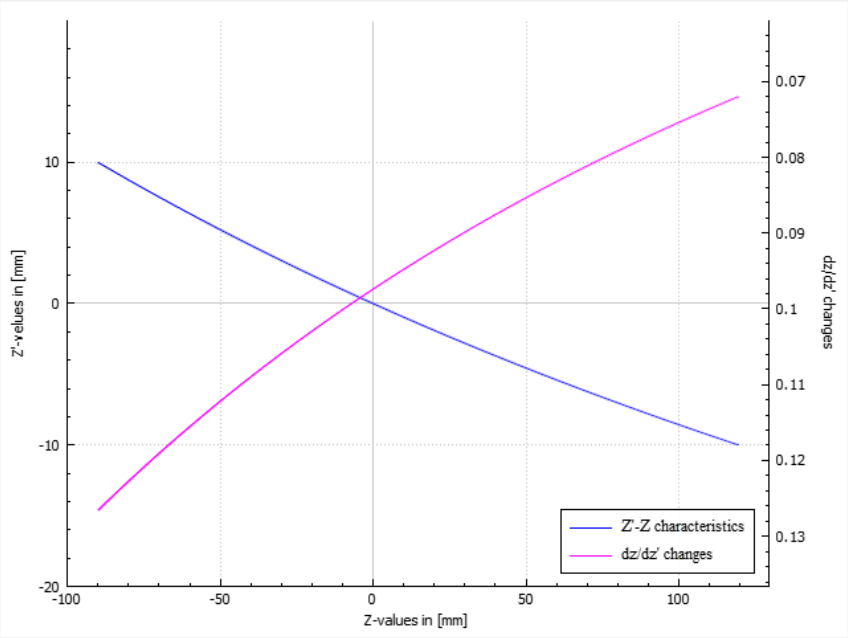

Figure 7**.** Same plotting for $\boldsymbol{z}(\boldsymbol{z}')$ in our model. It can be seen that the range is limited with the sensor size.

Table 1. Values used in the equations (from Donges & Noll, 2015).

Name	Unit	Value
Angle	Degrees	40
Focal Length	mm	85.00
Field Area	mm	240
U0	mm	561

According to the graphs, which are given in above, it is obviously clear that the results are nearly same for both Lamott and Noll's and our approaches.

Measuring Fields of Triangulation Sensor

Measuring field of a triangulation sensor gives the measureable x-ranges and the z-depth ranges for measurement distances. For example, measuring field for the Wenglor MLSL124 2D/3D Profile Sensor which is used in the industrial applications can be seen from Fig. 6.

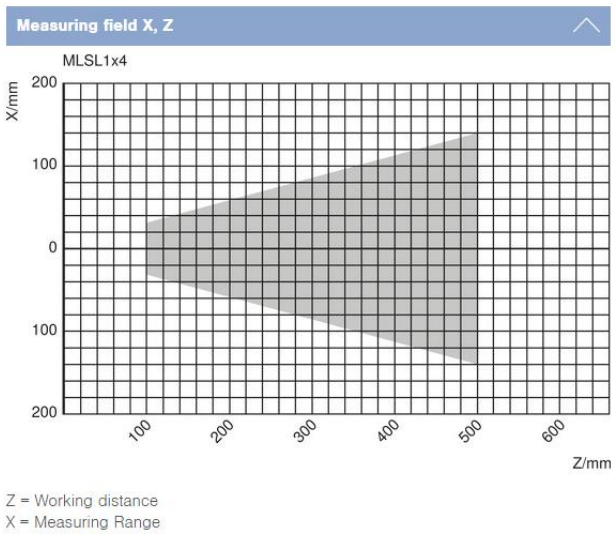

Figure 8. Measuring field for the Wenglor MLSL124 2D/3D profile sensor (Wenglor MLSL124).

Fig. 8 telling us, measurable x-length is depends on the distance in between the measurement plane and sensor. For example, the sensor can measure 60mm length when the sensor placed at from 100mm away from the measurement plane and 280mm length when it placed 500mm away from the measurement plane.

The measuring field of our method based on the Donges and Noll's parameters (Table 1) is given in Figure 9. It can be seen that our system can measure 14mm length when the sensor placed at from 100mm away from the measurement plane and 74mm length when it placed 500mm away from the measurement plane (Fig. 9). And Fig. 10 is showing that the measurable depth distance of the system when the camera has a distance from 100mm to 500mm to the surface being measured.

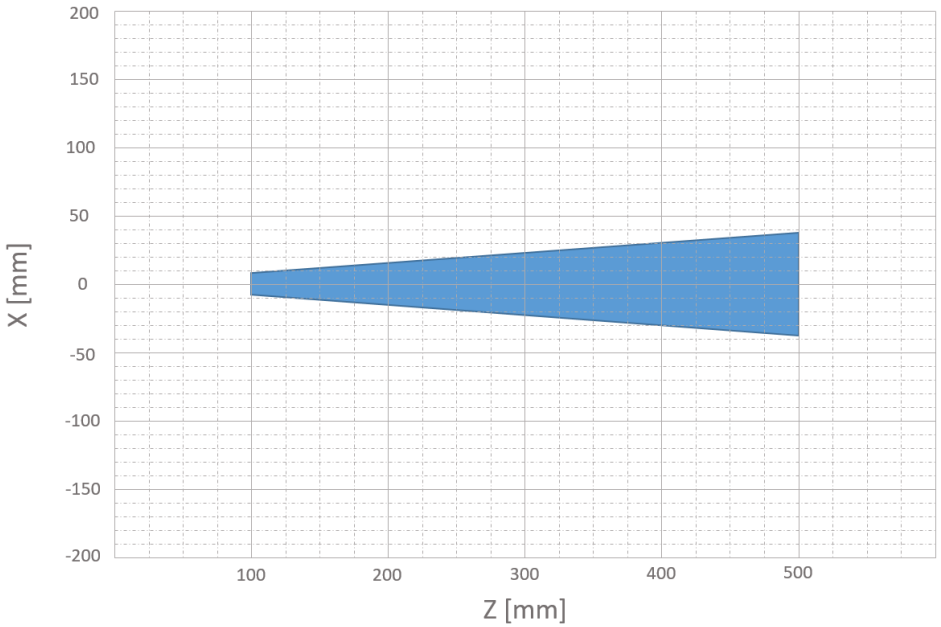

Figure 9. Measruing field for the method that has been given in this paper using with parameters from Donges and Noll (U0 = 561mm, focal length = 85mm, sensor size h = 10.25mm).

The measuring field for z-depth values mean that the measurable range from the specific measurement distance d related to the sensor size and imaging parameters and can be seen in Fig. 10.

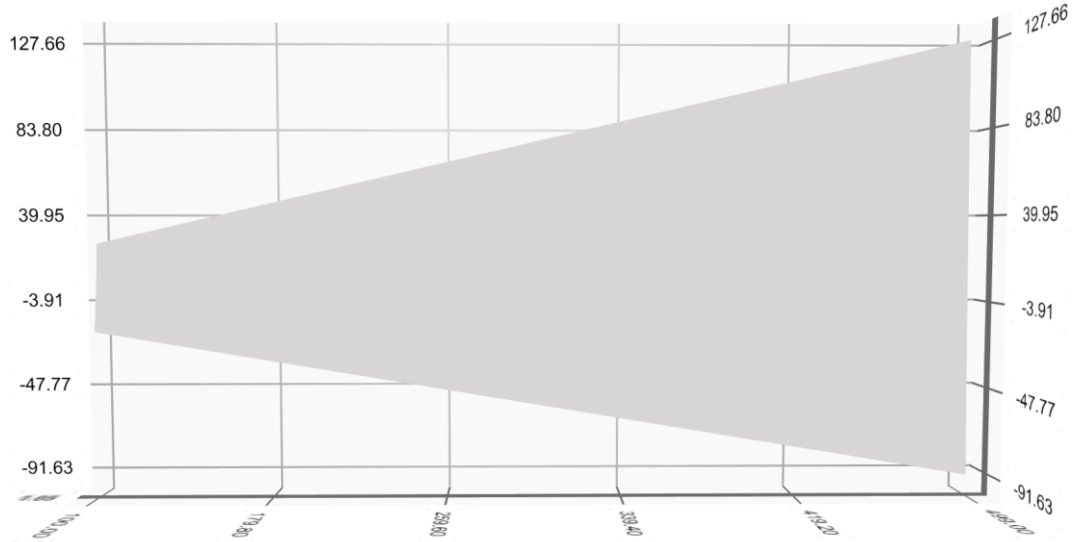

Figure 10. Measuring depth field related to measurable z-depth from the measuring distances of the model.

The current values that is used in these equations are taken from (Donges & Noll, 2015). However, in the implementation of the laser triangulation without Scheimpflug condition is limited due to the imaging components in the market such as industrial cameras and objective lenses.

Laser Beam Characteristics

Laser beam characteristics are determined generally by the type of the laser source and the shaping optics. To achieve high resolving power in triangulation, the diameter of the laser beam should be kept as small as possible at the surface being measured (Donges and Noll, 2015).

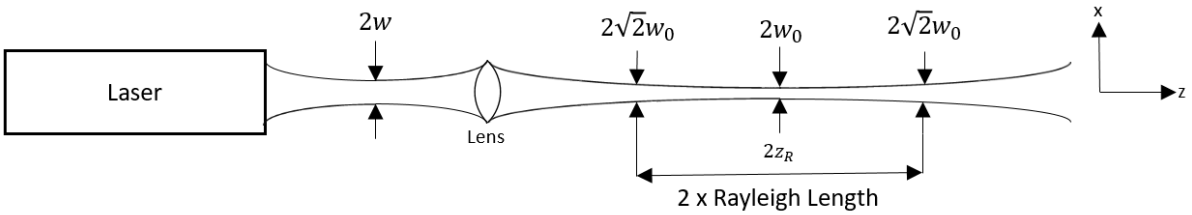

Figure 11. Propogation of a Gaussian laser beam (diagram is not to scale) (Donges & Noll, 2015).

The laser beam is focused with a lens. The beam waist diameter at the surface being measured amounts $2w$. For the calculation of laser beam diameter at the focus of the laser source (Donges and Noll, 2015):

$$2w_0 = \frac{2\lambda}{\pi w} f_F \tag{3}$$

where λ is the wavelength of the laser source, $2w$ is beam waist diameter of the laser beam in front of the focusing lens, $2w_0$ is diameter of the laser beam at the focus and f_F is focal length of the focusing lens. The Rayleigh length of a Gaussian laser beam indicates the distance along the beam, from the focusing position, at which the diameter is larger than the focus diameter by a value $\sqrt{2}$, see Fig. 11. For the Rayleigh length z_R (Donges & Noll, 2015):

$$z_R = \frac{\pi}{\lambda} w_0^2 \tag{4}$$

The Gaussian beam diameter $2w_0$ is plotted as a function of $2z_R$ for 660nm and 520nm, according to Eq. (4), can be seen in Fig. 12 (Donges & Noll, 2015).

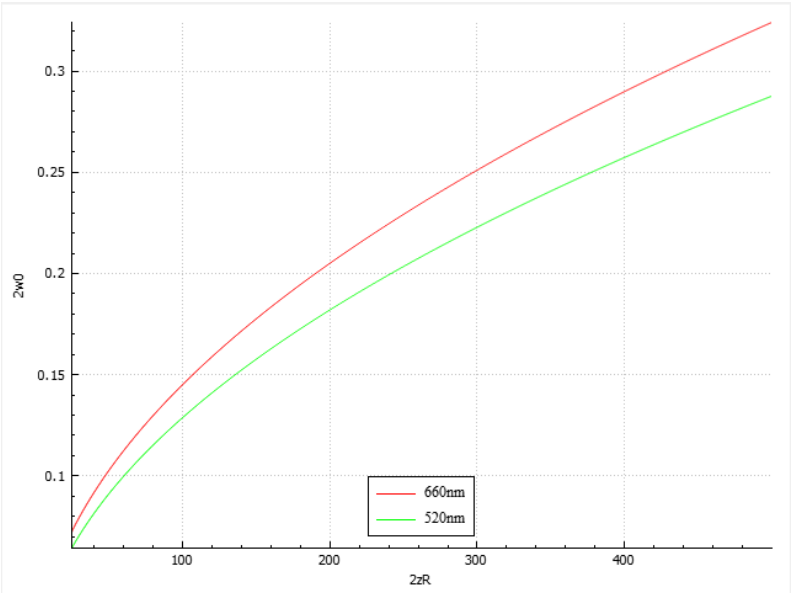

Figure 12. Waist diameter of a Gaussian beam as a function of the Rayleigh length (Donges & Noll, 2015).

above with a triangulation sensor, it is frequently case that the beam diameter within the measurement range should be as small as possible. Then the beam would be formed in such a way (Donges & Noll, 2015):

$$2z_R = M_z \tag{5}$$

where M_z is measuring range of the triangulation sensor in the z-direction (Donges & Noll, 2015).

Results and Discussions

In the previous sections, the mathematical model of the laser triangulation system without Scheimpflug condition has been given and the theoretical results of the system has been shown to prove the system is reliable and robust for 2D/3D measurements.

For the evaluation purpose the components are selected due to the generality in the market. For example, the most stocked industrial camera and objective lens brand is Basler in our country. They can provide the products within two or three days. Table 2 shows the parameters that related to these imaging components and the system general parameters. The results for these parameters for both Lamott and Noll's and our method is given in Figure 10 and 11 respectively.

Table 2. Theoretical application parameters

Name	Unit	Value
Sensor size x	mm	6.6
Sensor size y	mm	4.1
Sensor width	pixels	1920
Sensor height	pixels	1200
Focal length	mm	12
U0	mm	300
d min	mm	100
d max	mm	500
Triangulation angle	degree	50
Field area	mm	200

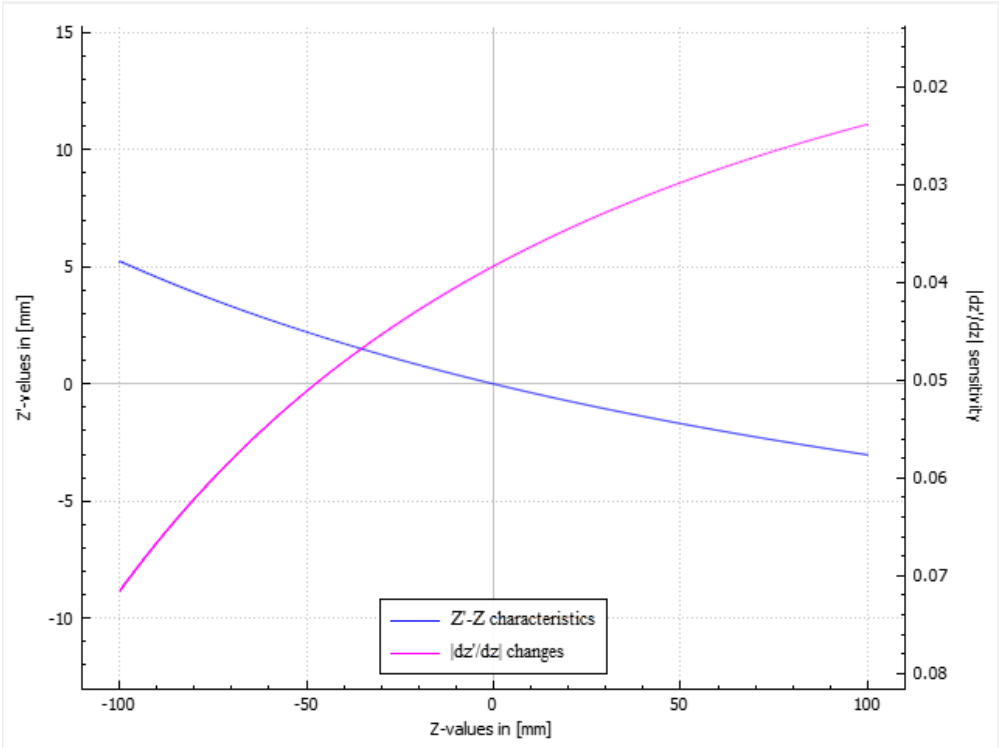

Figure 13. Characteristics curve of the Donges and Noll's system for the parameters that are given in Table 2, $\left(z'(z)\right)$.

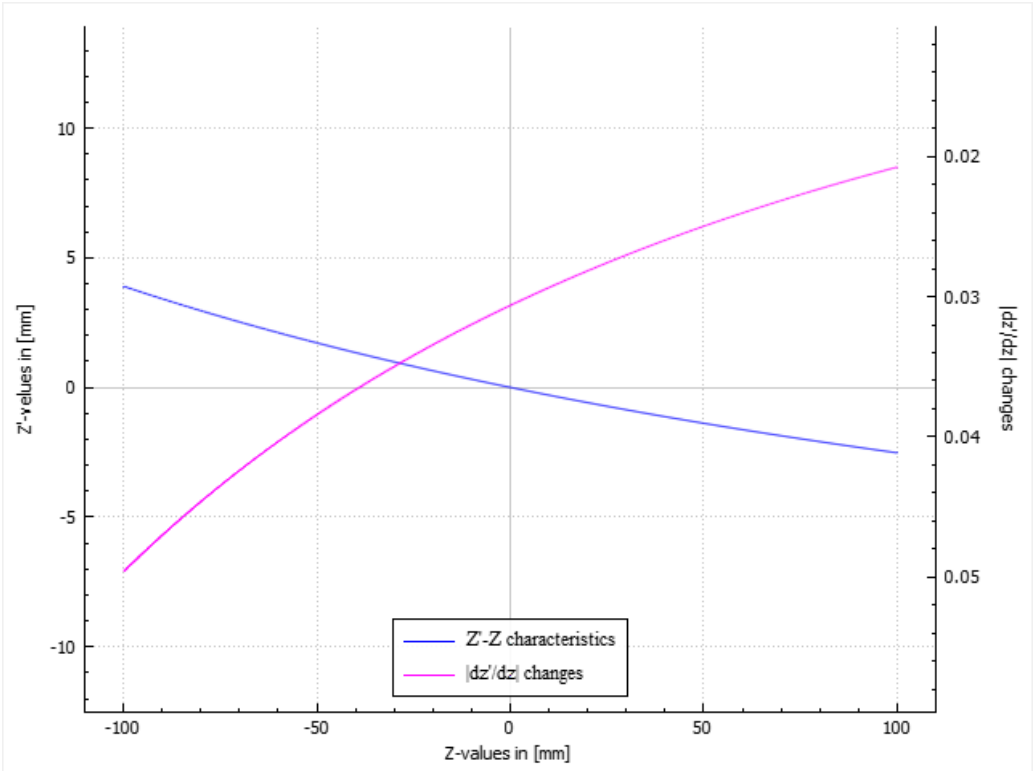

Figure 14. Characteristics curve of our system for the parameters that are given in Table 2, $(\boldsymbol{z}'(\boldsymbol{z}))$.

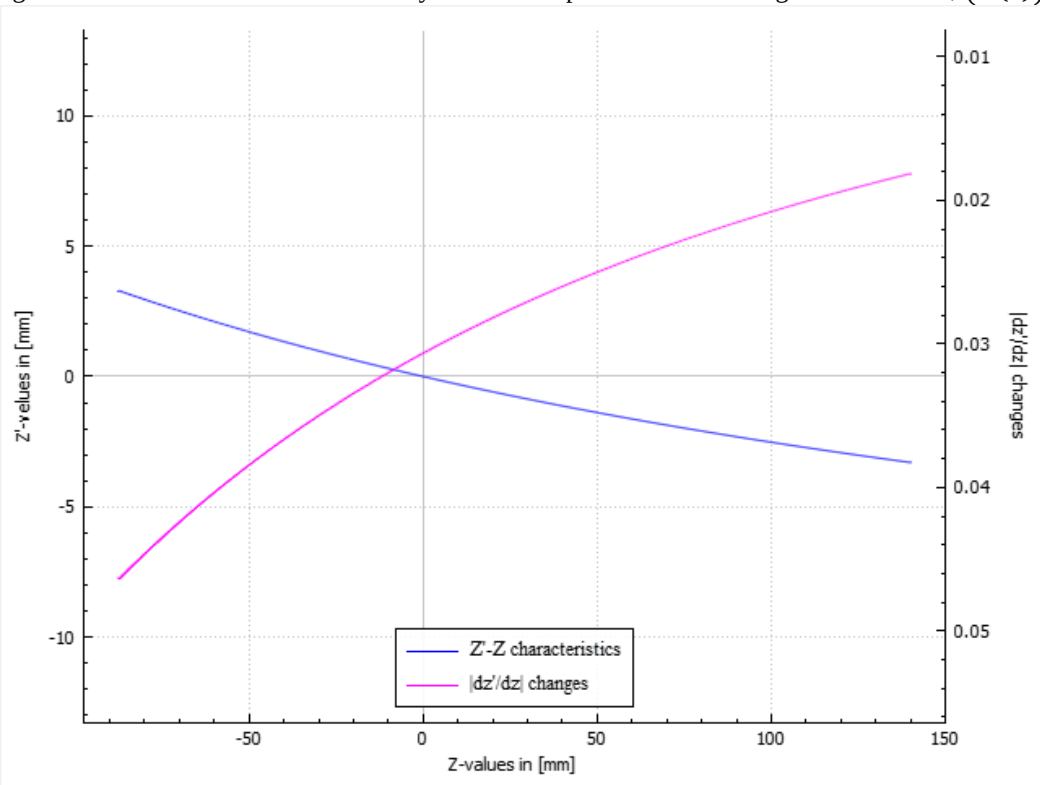

Figure 15. Characteristics curve of our system for the parameters that are given in Table 2, $(\boldsymbol{z}(\boldsymbol{z}'))$.

It can also be seen from Fig. 13 that our system can measure 35mm length when the sensor placed at from 100mm away from the measurement plane and 180mm length when it placed 500mm away from the measurement plane using with our components' and system parameters. When the angle of triangulation is set to 850 within the same parameters given in Table 2, it can be seen that the sensitivity is increasing for Lamott and Noll's model in Fig. 13, while our model is becoming traditional imaging system (Fig. 14).

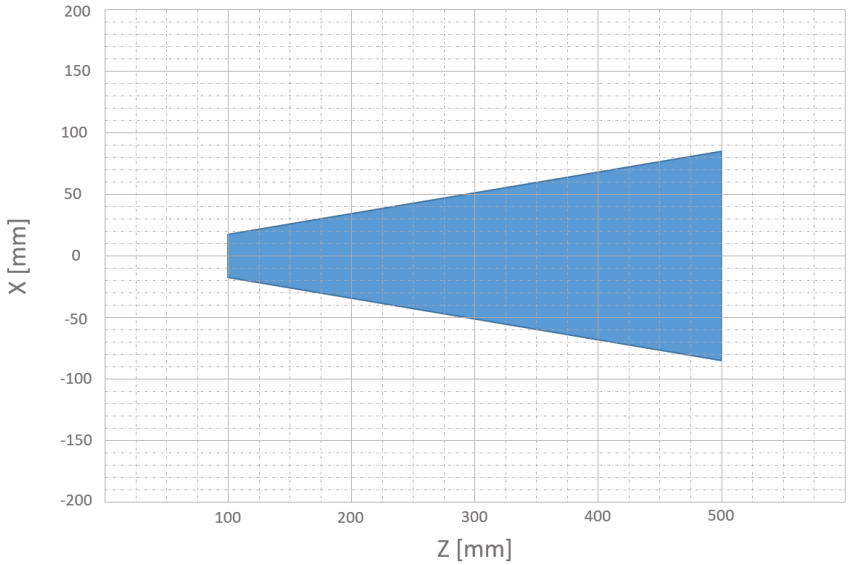

Figure 16. Measurement field for the parameters that are given in Table 2.

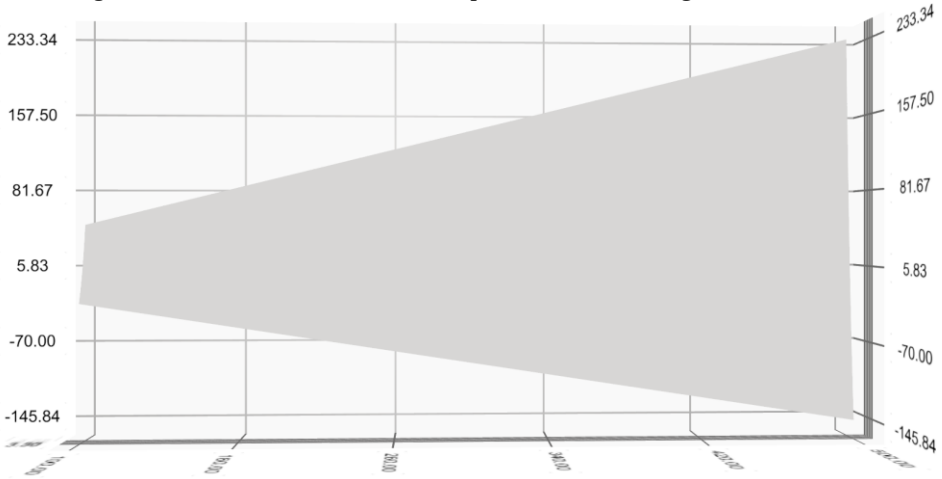

Figure 17. Measurement depth field for the parameters that are given in Table 2.

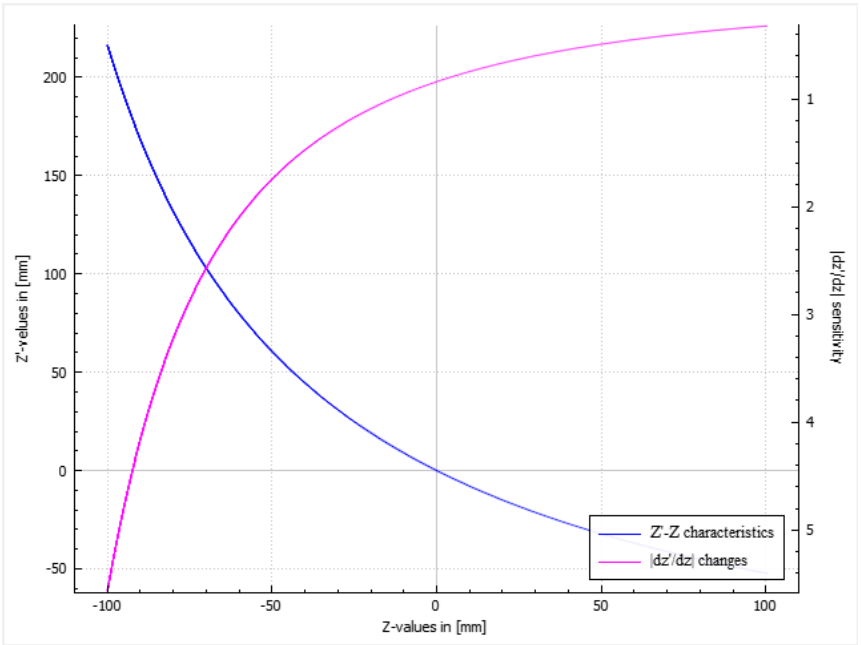

Figure 18. Characteristics curve of the Lamott and Noll's system for the triangulation angle 85^0.

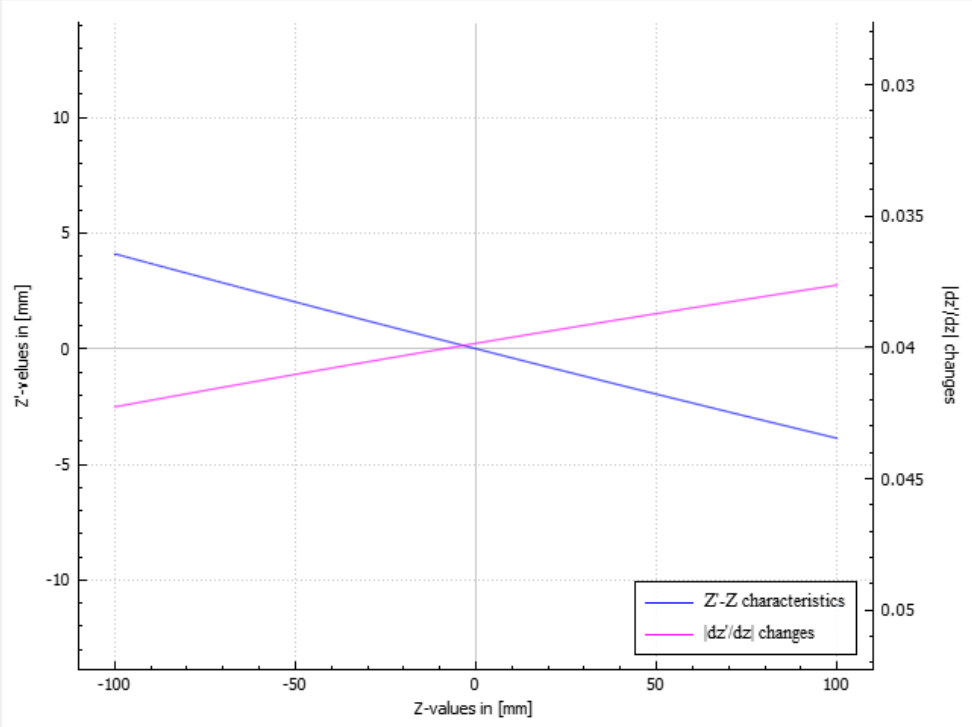

Figure 19. Characteristics curve of our system for the triangulation angle 85^0.

Application Examples

Most interesting study about disadvantages of Scheimpflug condition has been proposed in the article by Miks et al. (2013). A detailed analysis of the problem of imaging objects lying in the plane tilted with respect to the optical axis has performed by means of geometrical optics theory and it has shown that the fulfillment of the Scheimpflug condition does not guarantee the sharp image of the object as it is usually declared because of the fact that due to the dependence of aberrations of real optical systems on the object distance the image becomes blurred.

Poredos et al., have been shown that limitations related to the measuring range and the shadowing effects often lead them to choose a relatively small triangulation angle ($\alpha < 30^0$). And also they said that the second way to minimize the shadowing effect is the inclusion of a second camera which is symmetrically positioned relative to the laser source to measure in three dimension of human bodies in motion. França et al. have been shown that s 3D scanning system based on low cost laser triangulation and FOV techniques. Their method enables a perfect 3D image reconstruction with high resolution from different angles, colors and depth variation using a video camera (NTCS 4.2~50.4mm, CCD 1/3'') to imaging. Bracun et al. have been presented a new method for a quality assessment of die-castings based on a 3D measurement by a lser triangulation system that has an asymmetrical measuring range and is capable of high resolution measurements. Wu et al., have been presented a non-invasive and non-contact arterial pulsation measurement (APM) system to detect micro-vibration on skin surface based on optical laser triangulation with traditional CMOS camera.

The above examples are based on low cost laser triangulation applications which are not stick to the Scheimpflug condition. They have shown that results are reliable and the systems are robust. There are also another studies based on the laser triangulation (with and without Scheimpflug condition) method such as measuring inner surfaces of deep holes (Ye et al., 2018) and surface quality assessment of materials (Zhang et al., 2008, Wu et al., 2020, Buschinelli et al., 2014; Bracun et al., 2016), motion correction techniques for moving objects (Goel & Lohami, 2014, Blais et al., 2004; Lindner et al., 2015), form, thickness, profile, liquid level and distance measuremets (Lee et al., 2013; Stöbener et al., 2003; Ghiotti et al., 2015; Zhang et al., 2014; Giesko et al., 2007; Dorsch et al., 1994; Buzinski et al., 1992, Dong et al., 2018, Tao and Liu, 2010; Struckmeier et al., 2020; Donadello et al., 2018; Zhuang et al., 1994; Molleda et al., 2010; Lombardo et al., 2000; Baozhen et al., 2013; Demeyere et al., 2007), reverse engineering (Cajal et al., 2015), laser radar applications (Busk & Heiselberg, 2004) and simulation analysis (Cajal et al., 2015).

Conclusion

Study of this paper shows that the laser triangulation model without Scheimpflug condition is nearly results same with traditional model with some restrictions such as angle and sensor limitations. Also, taking consider the relationship between beam waist diameter at the Rayleigh length, it can be seen from Fig. 16 that the laser beam waist should be fixed within the measuring range. A desktop application is developed to ensure that the system is theoretically satisfying the requirements of measurements via C++ and open source Qt Framework.

In the future works, the system will be built in the laboratory and image acquisition and processing will be done with parallel on one of the up-to-date NVIDIA embedded boards. Also, the custom 3D data plotting section of the application code will be shared as an open source.

Scientific Ethics Declaration

The authors declare that the scientific ethical and legal responsibility of this article published in EPSTEM journal belongs to the authors.

Acknowledgements or Notes

* This article was presented as oral presentation at the International Conference on Basic Sciences, Engineering and Technology (www.icbaset.net) held in Marmaris/Turkey on April 27-30, 2023.

* This study is supported by management of Baykal Machinery. Thanks to all our managers.

* Qt is the trademark of the Qt Company Ltd.

References

Bracun, D., Gruden, V., & Mozina, J. (2008). A method for surface quality assessment of die-casting based on laser triangulation. *Measurement Science and Technology, 19*(4), 045707.

Cajal, C., Santolaria, J., Samper, D., & Garrido, A. (2015). Simulation of laser triangulation sensors scanning for design and evaluation purposes. *International Journal of Simulation Model*,*14*(2), 250 – 264.

Donges, A., & Noll, R. (2015). *Springer series in optical sciences - laser measurement technology: Fundamentals and applications* Volume 188. (pp. 247 – 279), Springer.

França, J. G. D. M., Gazziro, M. A., Ide, A. N., & Saito, J. H. (2005). A 3d scanning system based on laser triangulation and variable field of view. *IEEE International Conference on Image Processing 2005, 1* , (p.425).

Lamott, A., & Noll, R., (2011). *Tailored light 2 – laser application technology (RWTH ed.)*. (pp .473 – 537). Springer.

Poredoš, P., Povšič, K., Novak, B., Jezeršek, M. (2015), Three-dimensional measurements of bodies in motion based on multiple laser-plane triangulation. *Revista Technica de la Facultad de Ingenieria Universidad del Zulia, 38*(2), 53-61.

Ye, Z., Lianpo, W., Gu, Y., Chao, Z., Jiang, B., & Ni, J. (2018). A laser triangulation-based 3D measurement system for inner surface of deep holes. Proceedings of the ASME 2018 : *13th International Manufacturing Science and Engineering Conference*, Texas, USA.

Zhang, L., Zhao, M., Zou, Y., & Gao, S. (2008). A new surface inspection method of TWBS based on active laser triangulation. 7th *World Congress of Intelligent Control and Automation.* China.

Wu, J. H., Chang, R. S., & Jiang, J. A. (2007). A novel pulse measurement system by using laser triangulation and a CMOS image sensor. *Sensors 2007, 7*, 3366 – 3385.

Tong, Q., Jiao, C., Huang, H., Li, G., Ding, Z., & Yuan, F. (2014). An automatic measuring method and system using laser triangulation scanning for the marameters of a screw thread. *Measurement Science and Technology, 25.*

Donadello, S., Motta, M., Demir, A. G., & Previtali, B. (2018). Coaxial laser triangulation for height monitoring in laser metal deposition. *10th CIRP Conference on Photonic Technologies [LANE 2018]*,144 – 148.

Baozhen, G., Jingbin, S., Pengcheng, L., Qieni, L., & Di, W. (2013). Designing an optical set-up of differential laser triangulation for oil film thickness measurement on water. *Review of Scientific Instruments, 84.*

Miks, A., Novak, J., & Novak, P. (2013). Analysis of imaging for laser triangulation sensors under Scheimpflug rule. *OSA 2013, 21*(15).

Predoš, P., Čelan D., Možina, J., & Jezeršek, M. (2015). Determination of the human spine curve based on laser triangulation. *BMC Medical Imaging, 15*(2).

Demeyere, M., Rurimunzu, D., & Eguène, C. (2007). Diameter measurement of spherical objects by laser triangulation in an ambulatory context. *IEEE Transactions on Instrumentation and Measurement, 57,* 867 – 872.

Stöbener, D., Dijkman, M., Kruse, D., Surm, H., Keßler, O., Mayr, P., & Goch, G. (2003). Distance measurements with laser triangulation in hot environments. *XVII IMEKO World Congress,* 1898 – 1902.

Ghiotti, A., Schöch, A., Salvadori, A., Carmignato, S., & Savio, E. (2015). Enhancing the accuracy of high-speed laser triangulation measurement of freeform parts at elevated temperature. *CIRP Annals – Manufactıuring Technology, 64*, 499 – 502.

Zhang, H., Ren, Y., Liu, C., & Zhu, J. (2014). Flying spot laser triangulation scanner using lateral synchronization for surface profile measurement. *Applied Optics,53*(20), 4405 – 4412.

Koch, T., Breier, M., Li, W. (2013). *2013 11th IEEE International Conference on Industrial Informatics.* 48 – 53.

Mikhlyaev, S. V. (2006). Influence of a tilt of a mirror surface on the measurement accuracy of laser triangulation rangefinder. *Journal of Physics: Conference Series, International Symposium on Instrumentation Science and Technology, 48,* 739 – 744.

Giesko, T., ZBrowski, A., Czajka, P. (2007). Laser profilometers for surface inspection and profile measurement. *Problemy Eksploatacji,* 97-108.

Buschinelli, P., Pino, T., Silva, F., Santos, J., & Albertazzi, A. (2015). Laser triangulation profilometer for inner surface inspection of 100 millimeters (4'') nominal diameter. *Journal of Physics: 3rd International Congress on Mechanical Metrology, 648.*

Dong, Z., Sun, X., Liu, W., & Yang, H. (2018). Measurement of free-form curved surfaces using laser triangulation. *Sensors 2018, 18*(10). 3527.

Tao, H., & Liu, W. (2010). Measurement system for liquid level based on laser triangulation and angular tracking. *Journal of Computers, 5*(9), 1444 – 1447.

Ehlert, E., Horn, H. J., & Adamek, R. (2008). Measuring crop biomass density by laser triangulation. *Computer and Electronics in Agriculture, 61*(2), 117 – 125.

Molleda, J., Usamentiaga, R., Garcia, D. F., & Bulnes, F. G. (2010). Real-time flatness inspection of rolled products based on optical laser triangulation and three dimensional surface reconstruction. *Journal of Electronic Imaging, 19*(3), 031206-031206.

Author Information

Orkun KASAPOGLU
Baykal Machinery
Bursa, Turkey
Contact e-mail: *orkunk@baykal.com.tr*

Tugba BILGIN
Baykal Machinery
Bursa, Turkey

To cite this article:

Kasapoglu, O. & Bilgin, T. (2023). Mathematical analyzing of laser triangulation system without Scheimpflug condition via C++ and Qt framework. *The Eurasia Proceedings of Science, Technology, Engineering & Mathematics (EPSTEM), 22,* 1-14.

The Eurasia Proceedings of Science, Technology, Engineering & Mathematics (EPSTEM)
ISSN: 2602-3199

The Eurasia Proceedings of Science, Technology, Engineering & Mathematics (EPSTEM), 2023

Volume 22, Pages 15-25

ICBASET 2023: International Conference on Basic Sciences, Engineering and Technology

General Upper Bounds for the Numerical Radii of Powers of Hilbert Space Operators

Mohammed AL-DOLAT
Jordan University of Science and Technology

Abstract: In this paper, we will present several upper bounds for the numerical radii of a operator 2×2 matrices. We use these bounds to generalize and improve some well-known numerical radius inequalities. We provide a refinement of an earlier numerical radius inequality due to (Bani-Domi & Kittaneh, 2021) [Norm and numerical radius inequalities for Hilbert space operators], (Bani-Domi & Kittaneh, 2021) [Refined and generalized numerical radius inequalities for operator matrices 2×2] and (Al-Dolat & Kittaneh, 2023) [Upper bounds for the numerical radii of powers of Hilbert space operators].

Keywords: Numerical radius, Usual operator norm, Operator matrix, Buzano inequality.

Introduction

Let $\mathcal{B}(\mathcal{H})$ be the C^* −algebra of all bounded linear operators on the complex Hilbert space $\mathcal{H}$. Recall that the numerical radius $w(.)$ and the usual operator norm $||.||$ are, respectively, defined by

$$w(Y) = \sup_{||x||=1} |\langle Yx, x\rangle| \text{ and } \|Y\| = \sup_{||x||=1} \|Yx\| \text{ where} Y \in \mathcal{B}(\mathcal{H}).$$

A fundamental relation between the norms $w(.)$ and $||.||$ is the following inequality

$$\frac{1}{2}\|Y\| \leq w(Y) \leq \|Y\| \text{ for every } Y \in \mathcal{B}(\mathcal{H}). \tag{1.1}$$

Many mathematicians are interested in giving refinements for the inequalities in (1.1). For example, in Kittaneh (2005) Kittaneh provided the following improvement

$$\frac{1}{4}\||Y|^2 + |Y^*|^2\| \leq w^2(Y) \leq \frac{1}{2}\||Y|^2 + |Y^*|^2\| \text{ for every } Y \in \mathcal{B}(\mathcal{H}) \tag{1.2}$$

where $|Y| = (Y^*Y)^{\frac{1}{2}}$.

In El-Haddad and Kittaneh (2007), the authors showed that the upper bound in (1.2) can be generalized as follows:

$$w^{2r}(Y) \leq \frac{1}{2}\||Y|^{2r} + |Y^*|^{2r}\| \text{ forevery } r \geq 1 \text{ and } Y \in \mathcal{B}(\mathcal{H}). \tag{1.3}$$

Recently, in Al-Dolat and Kittaneh (2023), Al-Dolat and Kittaneh have refined the inequality (1.3) by showing that

$$w^{2r}(Y) \leq \frac{1+\alpha}{4}\||Y|^{2r} + |Y^*|^{2r}\| + \frac{1-\alpha}{2}w^r(Y^2) \text{ for every } Y \in \mathcal{B}(\mathcal{H}),\ r \geq 1 \text{ and } \alpha \in [0,1]. \quad (1.4)$$

In Kittaneh (2003), Kittaneh showed the following inequality

$$w(Y) \leq \frac{1}{2}\||Y| + |Y^*|\| \quad \text{for every } Y \in \mathcal{B}(\mathcal{H}). \quad (1.5)$$

In Dragomir (2009), Dragomir showed that the numerical radius of a product of two operators has the following upper bound

$$w^r(Y^*X) \leq \frac{1}{2}\||X|^{2r} + |Y|^{2r}\| \quad \text{for every } r \geq 1 \text{ and } X, Y \in \mathcal{B}(\mathcal{H}). \quad (1.6)$$

Let $\mathcal{H}$ be a complex Hilbert space and let $\mathcal{H}^{(2)} = \mathcal{H} \oplus \mathcal{H}$ denote the 2 −copies of $\mathcal{H}$. Based on this decomposition every operator $Y \in \mathcal{B}(\mathcal{H}^{(2)})$ has a 2×2 operator matrix representation

$$Y = \begin{bmatrix} Y_{11} & Y_{12} \\ Y_{21} & Y_{22} \end{bmatrix}$$

With $Y_{ij} \in \mathcal{B}(\mathcal{H})$ where $i, j \in \{1,2\}$. To learn more about the numerical radii of operator of matrices and their applications, one can refer to (Al-Dolat et al., 2016 ; Al-Dolat & Jaradat, 2023).

In this paper, we give new upper bounds for the numerical radii of 2×2 operator matrices. Based on those bounds, we obtain refinements of the inequality (1.4). Also, we refine earlier numerical radius inequalities for an operator of matrices obtained in (Bani-Domi & Kittaneh, 2021; Al-Dolat & Kittaneh, 2023).

Results and Discussion

For our purpose, we need to recall a few well-known lemmas.

Lemma 2.1 *(Kittaneh, 1988). Let $Y \in \mathcal{B}(\mathcal{H})$ be a positive operator and let $x \in \mathcal{H}$ with $||x|| = 1$. Then*

$$\langle Yx, x\rangle^r \leq \langle Y^r x, x\rangle \quad \text{for every } r \geq 1.$$

Lemma 2.2 *(Aujla & Silva, 2003). Let f be a non-negative convex function on $[0, \infty)$ and $X, Y \in \mathcal{B}(\mathcal{H})$ be positive operators. Then*

$$\left\|f\left(\frac{X+Y}{2}\right)\right\| \leq \left\|\frac{f(X)+f(Y)}{2}\right\|.$$

In particular,

$$\|(X+Y)^r\| \leq 2^{r-1}\|X^r + Y^r\| \quad \text{for every } r \geq 1.$$

Lemma 2.3 *(Hirzallah & Kittaneh, 2011). Let $X, Y \in \mathcal{B}(\mathcal{H})$. Then*

(a)

$$w\left(\begin{bmatrix} X & 0 \\ 0 & Y \end{bmatrix}\right) = \max\{w(X), w(Y)\},$$

(b)

$$w\left(\begin{bmatrix} X & Y \\ Y & X \end{bmatrix}\right) = \max\{w(X+Y), w(X-Y)\}.$$

In particular,

$$w\left(\begin{bmatrix} 0 & Y \\ Y & 0 \end{bmatrix}\right) = w(Y).$$

Lemma 2.4 *(Buzano, 1974). Let* $u, v, w \in \mathcal{H}$ *with* $\|w\| = 1$. *Then*

$$|\langle u, w\rangle\langle w, v\rangle| \leq \frac{1}{2}(\|u\|\|v\| + |\langle u, v\rangle|).$$

Lemma 2.5 *(Moradi & Sababheh, 2021). Let* $X, Y \in \mathcal{B}(\mathcal{H})$. *be self-adjoint. Then*

$$w^2(X + iY) \leq \|X^2 + Y^2\|.$$

Our first main result in this paper provides a refinement for the upper bound given in (Ajula & Silva, 2003, Theorem 2.6).

Theorem 2.6 *Let* $X, Y \in \mathcal{B}(\mathcal{H})$. *Then for every* $\alpha \in [0,1]$ *and* $r \geq 2$, *we have*

$$w^r(Y^*X) \leq \frac{\alpha}{2}\||X|^r + |Y|^r\|w^{\frac{r}{2}}(Y^*X) + \frac{1-\alpha}{2}w^2(|X|^r + i|Y|^r).$$

Proof. Let $x \in \mathcal{H}$ be any unit vector. Then by letting $u = Xx$ and $v = Yx$ in Lemma 2.5, we have

$$|\langle Y^*Xx, x\rangle|^r = \alpha|\langle Xx, Yx\rangle|^{\frac{r}{2}}|\langle Xx, Yx\rangle|^{\frac{r}{2}} + (1-\alpha)|\langle Xx, Yx\rangle|^r$$

$$\leq \alpha\|Xx\|^{\frac{r}{2}}\|Yx\|^{\frac{r}{2}}|\langle Y^*Xx, x\rangle|^{\frac{r}{2}} + (1-\alpha)\|Xx\|^r\|Yx\|^r$$

$$\leq \frac{\alpha}{2}(\|Xx\|^r + \|Yx\|^r)|\langle Y^*Xx, x\rangle|^{\frac{r}{2}} + \frac{1-\alpha}{2}(\|Xx\|^{2r} + \|Yx\|^{2r})$$

$$(\text{by the arithmetic} - \text{geometric mean inequality})$$

$$= \frac{\alpha}{2}\left(\langle|X|^2x, x\rangle^{\frac{r}{2}} + \langle|Y|^2x, x\rangle^{\frac{r}{2}}\right)|\langle Y^*Xx, x\rangle|^{\frac{r}{2}} + \frac{1-\alpha}{2}(\langle|X|^2x, x\rangle^r + \langle|Y|^2x, x\rangle^r)$$

$$\leq \frac{\alpha}{2}(\langle|X|^rx, x\rangle + \langle|Y|^rx, x\rangle)|\langle Y^*Xx, x\rangle|^{\frac{r}{2}} + \frac{1-\alpha}{2}(\langle|X|^rx, x\rangle^2 + \langle|Y|^rx, x\rangle^2)(\text{by Lemma 2.1})$$

$$= \frac{\alpha}{2}\langle(|X|^r + |Y|^r)x, x\rangle|\langle Y^*Xx, x\rangle|^{\frac{r}{2}} + \frac{1-\alpha}{2}|\langle(|X|^r + i|Y|^r)x, x\rangle|^2.$$

Thus,

$$w^r(Y^*X) = \sup_{||x||=1} |\langle Y^*Xx, x\rangle|^r$$

$$\leq \frac{\alpha}{2}\||X|^r + |Y|^r\| w^{\frac{r}{2}}(Y^*X) + \frac{1-\alpha}{2} w^2(|X|^r + i|Y|^r).$$

Remark 2.7 *The upper bound presented in the above theorem is smaller than the upper bound given in the inequality (1.6). To see this, note that for every* $\alpha \in [0,1]$ *and* $r \geq 2$, *we have*

$$w^r(Y^*X) \leq \frac{\alpha}{2}\||X|^r + |Y|^r\| w^{\frac{r}{2}}(Y^*X) + \frac{1-\alpha}{2} w^2(|X|^r + i|Y|^r) \quad \text{(by Theorem2.6)}$$

$$\leq \frac{\alpha}{2}\||X|^r + |Y|^r\| w^{\frac{r}{2}}(Y^*X) + \frac{1-\alpha}{2}\||X|^{2r} + |Y|^{2r}\| \text{(by Lemma 2.6)}$$

$$\leq \frac{\alpha}{4}\|(|X|^r + |Y|^r)^2\| + \frac{1-\alpha}{2}\||X|^{2r} + |Y|^{2r}\| \quad \text{(by the inequality (1.6))}$$

$$\leq \frac{\alpha}{2}\||X|^{2r} + |Y|^{2r}\| + \frac{1-\alpha}{2}\||X|^{2r} + |Y|^{2r}\| \quad \text{(by Lemma 2.5)}$$

$$= \frac{1}{2}\||X|^{2r} + |Y|^{2r}\|.$$

The next result in this paper refine [Aujla & Silva, 2003, Theorem 2.9].

Theorem 2.8 *Let* $X \in \mathcal{B}(\mathcal{H})$. *Then for every* $\alpha \in [0,1]$ *and* $r \geq 2$, *we have*

$$w^r(X) \leq \frac{\alpha}{2} w^2\left(|X|^{\frac{r}{2}} + i|X^*|^{\frac{r}{2}}\right) + \frac{1-\alpha}{2} w^{\frac{r}{2}}(X)\left\||X|^{\frac{r}{2}} + |X^*|^{\frac{r}{2}}\right\|$$

Proof. Let $x \in \mathcal{H}$ be any unit vector. Then we have

$$|\langle Xx, x\rangle|^r = \alpha|\langle Xx, x\rangle|^r + (1-\alpha)|\langle Xx, x\rangle|^r$$

$$\leq \alpha\langle|X|x, x\rangle^{\frac{r}{2}}\langle|X^*|x, x\rangle^{\frac{r}{2}} + (1-\alpha)|\langle Xx, x\rangle|^{\frac{r}{2}}\langle|X|x, x\rangle^{\frac{r}{4}}\langle|X^*|x, x\rangle^{\frac{r}{4}}$$

(by the Mixed Schwarz inequality)

$$\leq \frac{\alpha}{2}(\langle|X|x, x\rangle^r + \langle|X^*|x, x\rangle^r) + \frac{1-\alpha}{2}|\langle Xx, x\rangle|^{\frac{r}{2}}\left(\langle|X|x, x\rangle^{\frac{r}{2}} + \langle|X^*|x, x\rangle^{\frac{r}{2}}\right)$$

(by the arithmetic − geometric mean inequality)

$$\leq \frac{\alpha}{2}\left(\left\langle|X|^{\frac{r}{2}}x, x\right\rangle^2 + \left\langle|X^*|^{\frac{r}{2}}x, x\right\rangle^2\right) + \frac{1-\alpha}{2}|\langle Xx, x\rangle|^{\frac{r}{2}}\left\langle\left(|X|^{\frac{r}{2}} + |X^*|^{\frac{r}{2}}\right)x, x\right\rangle \quad \text{(by Lemma2.1)}$$

$$= \frac{\alpha}{2}\left|\left\langle\left(|X|^{\frac{r}{2}} + i|X^*|^{\frac{r}{2}}\right)x, x\right\rangle\right|^2 + \frac{1-\alpha}{2}|\langle Xx, x\rangle|^{\frac{r}{2}}\left\langle\left(|X|^{\frac{r}{2}} + |X^*|^{\frac{r}{2}}\right)x, x\right\rangle.$$

Thus,

$$w^r(X) = \sup_{||x||=1} |\langle Xx, x\rangle|^r$$

$$\leq \frac{\alpha}{2} w^2\left(|X|^{\frac{r}{2}} + i|X^*|^{\frac{r}{2}}\right) + \frac{1-\alpha}{2} w^{\frac{r}{2}}(X)\left\||X|^{\frac{r}{2}} + |X^*|^{\frac{r}{2}}\right\|.$$

Remark 2.9 *The upper bound presented in the above theorem is smaller than the upper bound given in the inequality (1.3). To see this, note that for every* $\alpha \in [0,1]$ *and* $r \geq 2$, *we have*

$$w^r(X) \leq \frac{\alpha}{2} w^2\left(|X|^{\frac{r}{2}} + i|X^*|^{\frac{r}{2}}\right) + \frac{1-\alpha}{2} w^{\frac{r}{2}}(X)\left\||X|^{\frac{r}{2}} + |X^*|^{\frac{r}{2}}\right\| \text{ (by Theorem 2.9)}$$

$$\leq \frac{\alpha}{2}\||X|^r + |X^*|^r\| + \frac{1-\alpha}{2} w^{\frac{r}{2}}(X)\left\||X|^{\frac{r}{2}} + |X^*|^{\frac{r}{2}}\right\| \text{ (by Lemma 2.5)}$$

$$\leq \frac{\alpha}{2}\||X|^r + |X^*|^r\| + \frac{1-\alpha}{4}\left\|\left(|X|^{\frac{r}{2}} + |X^*|^{\frac{r}{2}}\right)^2\right\| \text{ (by the inequality (1.3))}$$

$$\leq \frac{\alpha}{2}\||X|^r + |X^*|^r\| + \frac{1-\alpha}{2}\||X|^r + |X^*|^r\| \text{ (by Lemma 2.2)}$$

$$= \frac{1}{2}\||X|^r + |X^*|^r\|.$$

Now, we give an upper bound for the numerical radius of a 2×2 operator matrix which generalize [8, Theorem 2.1].

Theorem 2.10 *Let* $A, B, C, D \in \mathcal{B}(\mathcal{H})$. *Then for every* $r \geq 2$, *we have*

$$w^r\left(\begin{bmatrix} A & B \\ C & D \end{bmatrix}\right) \leq 2^{r-1}\max\left\{w^r(A), w^r(D)\right\} + 2^{r-2}\max\left\{w^{\frac{r}{2}}(BC), w^{\frac{r}{2}}(CB)\right\}$$
$$+2^{r-3}\max\left\{\left\||C|^r + |B^*|^r\right\|, \left\||B|^r + |C^*|^r\right\|\right\}$$

Proof. Let

$$Y = \begin{bmatrix} A & B \\ C & D \end{bmatrix},\ Y_1 = \begin{bmatrix} A & 0 \\ 0 & D \end{bmatrix} \text{ and}$$

$Y_2 = \begin{bmatrix} 0 & B \\ C & 0 \end{bmatrix}$. Then for every unit vector $x \in \mathcal{H}^{(2)}$, we have

$$|\langle Yx, x\rangle|^r \leq (|\langle Y_1x, x\rangle| + |\langle Y_2x, x\rangle|)^r$$

$$\leq 2^{r-1}|\langle Y_1x, x\rangle|^r + 2^{r-1}|\langle Y_2x, x\rangle|^r \text{ (by the convexity of } t^r, r \geq 2)$$

$$\leq 2^{r-1}|\langle Y_1x, x\rangle|^r + 2^{r-1}|\langle Y_2x, x\rangle\langle x, Y_2^*x\rangle|^{\frac{r}{2}}$$

$$\leq 2^{r-1}|\langle Y_1x, x\rangle|^r + 2^{r-1}\left(\frac{|\langle Y_2^2x, x\rangle|}{2} + \frac{\|Y_2x\|\|Y_2^*x\|}{2}\right)^{\frac{r}{2}} \text{ (by Lemma 2.4)}$$

$$\leq 2^{r-1}|\langle Y_1x, x\rangle|^r + 2^{r-2}\left(|\langle Y_2^2x, x\rangle|^{\frac{r}{2}} + \|Y_2x\|^{\frac{r}{2}}\|Y_2^*x\|^{\frac{r}{2}}\right) \text{ (by the convexity of } t^{\frac{r}{2}}, r \geq 2)$$

$$\leq 2^{r-1}|\langle Y_1 x, x\rangle|^r + 2^{r-2}|\langle Y_2^2 x, x\rangle|^{\frac{r}{2}} + 2^{r-3}(\|Y_2 x\|^r + \|Y_2^* x\|^r)$$

$$\text{(by the arithmetic} - \text{geometric mean inequality)}$$

$$\leq 2^{r-1}|\langle Y_1 x, x\rangle|^r + 2^{r-2}|\langle Y_2^2 x, x\rangle|^{\frac{r}{2}} + 2^{r-3}\langle(|Y_2|^r + |Y_2^*|^r)x, x\rangle.$$

Therefore,

$$w^r(Y) = \sup_{\|x\|=1} |\langle Yx, x\rangle|^r$$

$$\leq 2^{r-1}w^r(Y_1) + 2^{r-2}w^{\frac{r}{2}}(Y_2^2) + 2^{r-3}\||Y_2|^r + |Y_2^*|^r\|$$

$$= 2^{r-1}\max\{w^r(A), w^r(D)\} + 2^{r-2}\max\left\{w^{\frac{r}{2}}(BC), w^{\frac{r}{2}}(CB)\right\}$$

$$+2^{r-3}\max\{\||C|^r + |B^*|^r\|, \||B|^r + |C^*|^r\|\}.$$

There are many upper bounds for the numerical radii of Hilbert space operators that can be obtained from Theorem 2.12. The following results demonstrate some of these upper bounds.

Corollary 2.11 *Let $A, B \in \mathcal{B}(\mathcal{H})$., Then for every $r \geq 2$, we have*

$$\max\left\{w^r(A-B), w^r(A+B)\right\} = w^r\left(\begin{bmatrix} A & B \\ B & A \end{bmatrix}\right)$$

$$\leq 2^{r-1}w^r(A) + 2^{r-2}w^{\frac{r}{2}}(B^2) + 2^{r-3}\left\||B|^r + |B^*|^r\right\|.$$

By setting $A = 0$ and $B = X$ in the above corollary we have the following result.

Corollary 2.12 *Let $X \in \mathcal{B}(\mathcal{H})$. Then for every $r \geq 2$, we have*

$$w^r(X) = w^r\left(\begin{bmatrix} 0 & X \\ X & 0 \end{bmatrix}\right)$$

$$\leq \frac{1}{2}w^{\frac{r}{2}}(X^2) + \frac{1}{4}\left\||X|^r + |X^*|^r\right\|$$

$$\leq \frac{1}{2}\left\||X|^r + |X^*|^r\right\|.$$

To prove Theorem 2.16, we need the following lemma which can be found in (Al-Dolat & Al-Zoubi, 2023).

Lemma 2.13 *Let $u, v, w \in \mathcal{H}$ with $||w|| = 1$. Then*

$$|\langle u, w\rangle\langle w, v\rangle|^r \leq \frac{1}{2}\|u\|^r\|v\|^r + \frac{\alpha}{2}\|u\|^{\frac{r}{2}}\|v\|^{\frac{r}{2}}|\langle u, v\rangle|^{\frac{r}{2}} + \frac{1-\alpha}{2}|\langle u, v\rangle|^r$$

For every $r \geq 1$ and $\alpha \in [0,1]$.

Now, we present new upper bound for the numerical radius of the off-diagonal of a 2×2 operator matrix.

Theorem 2.14 *Let* $B, C \in \mathcal{B}(\mathcal{H})$. *Then*

$$w^{2r}\left(\begin{bmatrix} 0 & B \\ C & 0 \end{bmatrix}\right) \leq \frac{1}{4}\max\left\{w^2(|C|+i|B^*|), w^2(|B|+i|C^*|)\right\}$$

$$+\frac{\alpha}{4}\max\left\{\left\||C|^r+|B^*|^r\right\|, \left\||B|^r+|C^*|^r\right\|\right\}\max\left\{w^{\frac{r}{2}}(BC), w^{\frac{r}{2}}(CB)\right\}$$

$$+\frac{1-\alpha}{2}\max\left\{w^r(BC), w^r(CB)\right\},$$

For every $r \geq 2$ and $\alpha \in [0,1]$.

Proof. Let

$$Y = \begin{bmatrix} 0 & B \\ C & 0 \end{bmatrix}.$$

Then for every $x \in \mathcal{H}^{(2)}$ with $||x|| = 1$, we have

$$|\langle Yx, x\rangle|^{2r} = |\langle Yx, x\rangle\langle x, Y^*x\rangle|^r$$

$$\leq \tfrac{1}{2}\|Yx\|^r\|Y^*x\|^r + \tfrac{\alpha}{2}\|Yx\|^{\frac{r}{2}}\|Y^*x\|^{\frac{r}{2}}|\langle Yx, Y^*x\rangle|^{\frac{r}{2}} + \tfrac{1-\alpha}{2}|\langle Yx, Y^*x\rangle|^r \quad \text{(by Lemma 2.15)}$$

$$\leq \tfrac{1}{4}(\|Yx\|^{2r} + \|Y^*x\|^{2r}) + \tfrac{\alpha}{4}(\|Yx\|^r + \|Y^*x\|^r)|\langle Y^2x, x\rangle|^{\frac{r}{2}} + \tfrac{1-\alpha}{2}|\langle Y^2x, x\rangle|^r$$

$$\text{(by the arithmetic} - \text{geometric mean inequality)}$$

$$\leq \tfrac{1}{4}(\langle |Y|^r x, x\rangle^2 + \langle |Y^*|^r x, x\rangle^2) + \tfrac{\alpha}{4}\langle (|Y|^r + |Y^*|^r)x, x\rangle|\langle Y^2x, x\rangle|^{\frac{r}{2}} + \tfrac{1-\alpha}{2}|\langle Y^2x, x\rangle|^r$$

$$\text{(by Lemma 2.1)}$$

$$= \tfrac{1}{4}|\langle (|Y|^r + i|Y^*|^r)x, x\rangle|^2 + \tfrac{\alpha}{4}\langle (|Y|^r + |Y^*|^r)x, x\rangle|\langle Y^2x, x\rangle|^{\frac{r}{2}} + \tfrac{1-\alpha}{2}|\langle Y^2x, x\rangle|^r.$$

Thus,

$$w^{2r}(Y) = \sup_{||x||=1}|\langle Yx, x\rangle|^{2r}$$

$$\leq \frac{1}{4}\max\left\{w^2(|C|+i|B^*|), w^2(|B|+i|C^*|)\right\}$$

$$+\tfrac{\alpha}{4}\max\{\||C|^r + |B^*|^r\|, \||B|^r + |C^*|^r\|\}\max\left\{w^{\frac{r}{2}}(BC), w^{\frac{r}{2}}(CB)\right\}$$

$$+\frac{1-\alpha}{2}\max\{w^r(BC), w^r(CB)\}.$$

As special case of Theorem 2.16, we have the following refinement of the inequality (1.4).

Corollary 2.15 *Let $X \in \mathcal{B}(\mathcal{H})$. Then for every $\alpha \in [0,1]$ and $r \geq 2$ we have*

$$w^{2r}(X) \leq \frac{1}{4}w^2(|X|^r + i|X^*|^r) + \frac{\alpha}{4}\||X|^r + |X^*|^r\|w^{\frac{r}{2}}(X^2) + \frac{1-\alpha}{2}w^r(X^2)$$

$$\leq \frac{1+\alpha}{4}\||X|^{2r} + |X^*|^{2r}\| + \frac{1-\alpha}{2}w^r(X^2).$$

Proof. We have

$$w^{2r}(X) = w^{2r}\left(\begin{bmatrix} 0 & X \\ X & 0 \end{bmatrix}\right) \text{ (by Lemma 2.3)}$$

$$\leq \frac{1}{4}w^2(|X|^r + i|X^*|^r) + \frac{\alpha}{4}\||X|^r + |X^*|^r\|w^{\frac{r}{2}}(X^2) + \frac{1-\alpha}{2}w^r(X^2) \quad \text{(by Theorem 2.16)}$$

$$\leq \frac{1}{4}\||X|^{2r} + |X^*|^{2r}\| + \frac{\alpha}{4}\||X|^r + |X^*|^r\|w^{\frac{r}{2}}(X^2) + \frac{1-\alpha}{2}w^r(X^2) \quad \text{(by Lemma 2.5)}$$

$$\leq \frac{1}{4}\||X|^{2r} + |X^*|^{2r}\| + \frac{\alpha}{8}\|(|X|^r + |X^*|^r)^2\| + \frac{1-\alpha}{2}w^r(X^2) \quad \text{(by the inequality (1.6))}$$

$$\leq \frac{1+\alpha}{4}\||X|^{2r} + |X^*|^{2r}\| + \frac{1-\alpha}{2}w^r(X^2) \quad \text{(by Lemma 2.2).}$$

In the following result, we find a new an upper bound for the numerical radius of a 2×2 operator matrix.

Corollary 2.16 *Let $A, B, C, D \in \mathcal{B}(\mathcal{H})$. Then for every $r \geq 2$ and $\alpha \in [0,1]$, we have*

$$w^{2r}\left(\begin{bmatrix} A & B \\ C & D \end{bmatrix}\right) \leq 2^{2r-1}\max\left\{w^{2r}(A), w^{2r}(D)\right\}$$
$$+2^{2r-3}\max\left\{w^2(|C| + i|B^*|), w^2(|B| + i|C^*|)\right\}$$
$$+\alpha 2^{2r-3}\max\{\||C|^r + |B^*|^r\|, \||B|^r + |C^*|^r\|\}\max\left\{w^{\frac{r}{2}}(BC), w^{\frac{r}{2}}(CB)\right\}$$
$$+(1-\alpha)2^{2r-2}\max\{w^r(BC), w^r(CB)\}.$$

Proof. By the convexity the of t^{2r} and Theorem 2.16 we get

$$w^{2r}\left(\begin{bmatrix} A & B \\ C & D \end{bmatrix}\right) = \left(w\left(\begin{bmatrix} A & 0 \\ 0 & D \end{bmatrix}\right) + w\left(\begin{bmatrix} 0 & B \\ C & 0 \end{bmatrix}\right)\right)^{2r}$$

$$\leq 2^{2r-1}w^{2r}\left(\begin{bmatrix} A & 0 \\ 0 & D \end{bmatrix}\right) + 2^{2r-1}w^{2r}\left(\begin{bmatrix} 0 & B \\ C & 0 \end{bmatrix}\right)$$

$$\leq 2^{2r-1}\max\{w^{2r}(A), w^{2r}(D)\} + 2^{2r-3}\max\{w^2(|C|^r + i|B^*|^r), w^2(|B|^r + i|C^*|^r)\}$$

$$+\alpha 2^{2r-3}\max\{\||C|^r + |B^*|^r\|, \||B|^r + |C^*|^r\|\}\max\left\{w^{\frac{r}{2}}(BC), w^{\frac{r}{2}}(CB)\right\}$$

$$+(1-\alpha)2^{2r-2}\max\{w^r(BC), w^r(CB)\}.$$

The following result presents an upper bound for the numerical radius of the sum of operators.

Corollary 2.17 *Let $A, B \in \mathcal{B}(\mathcal{H})$. Then for every $r \geq 2$ and $\alpha \in [0,1]$ we have*

$$\max\left\{w^{2r}(A-B), w^{2r}(A+B)\right\} = w^{2r}\left(\begin{bmatrix} A & B \\ B & A \end{bmatrix}\right)$$

$$\leq 2^{2r-1}w^{2r}(A) + 2^{2r-3}w^2(|B|^r + i|B^*|^r) + \alpha 2^{2r-3}\||B|^r + |B^*|^r\|w^{\frac{r}{2}}(B^2)$$

$$+(1-\alpha)2^{2r-2}w^r(B^2).$$

To prove Theorem 2.22, we need the following lemma which can be found in (Al-Dolat & Al-Zoubi, 2023).

Lemma 2.18 *Let $u, v, w \in \mathcal{H}$ with $||w|| = 1$. Then*

$$|\langle u, w\rangle\langle w, v\rangle|^r \leq \frac{1}{4}\|u\|^r\|v\|^r + \frac{2+\alpha}{4}\|u\|^{\frac{r}{2}}\|v\|^{\frac{r}{2}}|\langle u, v\rangle|^{\frac{r}{2}} + \frac{1-\alpha}{4}|\langle u, v\rangle|^r$$

where $\alpha \in [0,1]$ and $r \geq 2$.

Now, we can state the following result in this paper as follows.

Theorem 2.19 *Let $B, C \in \mathcal{B}(\mathcal{H})$. Then for every $\alpha \in [0,1]$ and $r \geq 2$ we have*

$$w^{2r}\left(\begin{bmatrix} 0 & B \\ C & 0 \end{bmatrix}\right) \leq \frac{1}{8}\max\left\{w^2(|C|^r + i|B^*|^r), w^2(|B|^r + i|C^*|^r)\right\}$$

$$+\frac{2+\alpha}{8}\max\{\||C|^r + |B^*|^r\|, \||B|^r + |C^*|^r\|\}\max\left\{w^{\frac{r}{2}}(BC), w^{\frac{r}{2}}(CB)\right\}$$

$$+\frac{1-\alpha}{4}\max\{w^r(BC), w^r(CB)\}.$$

Proof. Let

$$Y = \begin{bmatrix} 0 & B \\ C & 0 \end{bmatrix}.$$

Then for every $x \in \mathcal{H}^{(2)}$ with $||x|| = 1$ we have

$$|\langle Yx, x\rangle|^{2r} = |\langle Yx, x\rangle\langle x, Y^*x\rangle|^r$$

$$\leq \frac{1}{4}\|Yx\|^r\|Y^*x\|^r + \frac{2+\alpha}{4}\|Yx\|^{\frac{r}{2}}\|Y^*x\|^{\frac{r}{2}}|\langle Yx, Y^*x\rangle|^{\frac{r}{2}} + \frac{1-\alpha}{4}|\langle Yx, Y^*x\rangle|^r \quad \text{(by Lemma 2.21)}$$

$$\leq \frac{1}{8}(\|Yx\|^{2r} + \|Y^*x\|^{2r}) + \frac{2+\alpha}{8}(\|Yx\|^r + \|Y^*x\|^r)|\langle Y^2x, x\rangle|^{\frac{r}{2}} + \frac{1-\alpha}{4}|\langle Y^2x, x\rangle|^r$$

(by the arithmetic − geometric mean inequality)

$$\leq \frac{1}{8}|\langle(|Y|^r + i|Y^*|^r)x, x\rangle|^2 + \frac{2+\alpha}{8}\langle(|Y|^r + |Y^*|^r)x, x\rangle|\langle Y^2x, x\rangle|^{\frac{r}{2}} + \frac{1-\alpha}{4}|\langle Y^2x, x\rangle|^r$$

(by Lemma 2.1).

Therefore,

$$w^{2r}(Y) = \sup_{||x||=1}|\langle Yx, x\rangle|^{2r}$$

$$\leq \frac{1}{8}|\langle(|Y|^r + i|Y^*|^r)x, x\rangle|^2 + \frac{2+\alpha}{8}\||Y|^r + |Y^*|^r\|w^{\frac{r}{2}}(Y^2) + \frac{1-\alpha}{4}w^r(Y^2)$$

$$= \frac{1}{8}\max\{w^2(|C|^r + i|B^*|^r), w^2(|B|^r + i|C^*|^r)\}$$

$$+ \frac{2+\alpha}{8}\max\{\||C|^r + |B^*|^r\|, \||B|^r + |C^*|^r\|\}\max\left\{w^{\frac{r}{2}}(BC), w^{\frac{r}{2}}(CB)\right\}$$

$$+ \frac{1-\alpha}{4}\max\{w^r(BC), w^r(CB)\}.$$

Corollary 2.20 *Let* $X \in \mathcal{B}(\mathcal{H})$. *Then for every* $\alpha \in [0,1]$ *and* $r \geq 2$, *we have*

$$w^{2r}(X) \leq \frac{1}{8}w^2(|X|^r + i|X^*|^r) + \frac{2+\alpha}{8}\||X|^r + |X^*|^r\|w^{\frac{r}{2}}(X^2) + \frac{1-\alpha}{4}w^r(X^2)$$

$$\leq \frac{1}{2}\||X|^{2r} + |X^*|^{2r}\|.$$

Proof. We have

$$w^{2r}(X) = w^{2r}\left(\begin{bmatrix} 0 & X \\ X & 0 \end{bmatrix}\right)$$

(by Lemma 2.3)

$$\leq \frac{1}{8}w^2(|X|^r + i|X^*|^r) + \frac{2+\alpha}{8}\||X|^r + |X^*|^r\|w^{\frac{r}{2}}(X^2) + \frac{1-\alpha}{4}w^r(X^2) \quad \text{(by Theorem 2.22)}$$

$$\leq \frac{1}{8}\||X|^{2r} + |X^*|^{2r}\| + \frac{2+\alpha}{8}\||X|^r + |X^*|^r\|w^{\frac{r}{2}}(X^2) + \frac{1-\alpha}{4}w^r(X^2) \quad \text{(by Lemma 2.5)}$$

$$\leq \frac{1}{8}\||X|^{2r} + |X^*|^{2r}\| + \frac{2+\alpha}{16}\|(|X|^r + |X^*|^r)^2\| + \frac{1-\alpha}{8}\||X|^{2r} + |X^*|^{2r}\| \quad \text{(by the inequality (1.6))}$$

$$\leq \frac{1}{8}\||X|^{2r} + |X^*|^{2r}\| + \frac{2+\alpha}{8}\||X|^{2r} + |X^*|^{2r}\| + \frac{1-\alpha}{8}\||X|^{2r} + |X^*|^{2r}\| \quad \text{(by Lemma 2.2)}$$

$$= \frac{1}{2}\||X|^{2r} + |X^*|^{2r}\|.$$

Scientific Ethics Declaration

The author declares that the scientific ethical and legal responsibility of this article published in EPSTEM journal belongs to the authors.

Acknowledgements or Notes

This article was presented as poster presentation at the International Conference on Basic Sciences, Engineering and Technology (www.icbaset.net) held in Marmaris/Turkey on April 27-30, 2023.

References

Abu-Omar, A. & Kittaneh, F. (2015). Upper and lower bounds for the numerical radius with an application to involution operators, *Rocky Mountain Journal Math., 45*(4), 1055-1065.

Al-Dolat, M., & Al-Zoubi, K. (2023). Improved and refined numerical radius inequalities for Hilbert space operators.*https://assets.researchsquare.com/files/rs2668438/v1/a5b67b067e6f6fddcf09cb22.pdf?c=1678771282*

Al-Dolat, M., Al-Zoubi, K., Ali, M., & Bani-Ahamed, F. (2016). General numerical radius inequalities for matrices of operators, *Open Math., 4*, 1-9.

Al-Dolat, M., & Jaradat, I. (2023). A refinement of the Cauchy-Shwarz inequality accompanied by new numerical radius upper bounds. *Filomat, 37,* 971-977.

Al-Dolat, M., & Kittaneh, F. (2023). Upper bounds for the numerical radii of powers of Hilbert space operators. *Quaestiones Mathematicae*, 1-12.

Aujla, J., & Silva, F. (2003). Weak majorization inequalities and convex functions. *Linear Algebra Appl., 369*, 217-233.

Bani-Domi W., & Kittaneh, F. (2021). Refined and generalized numerical radius inequalities for 2x2 operator matrices. *Linear Algebra Appl*. 364-380.

Bani-Domi, W. & Kittaneh F. (2021). Norm and numerical radius inequalities for Hilbert space operators. *Linear Multilinear Algebra, 69*, 934-945.

Buzano, M.L. (1974). Generalizzazione della diseguaglianza di Cauchy-Schwarz, (Italian). *Rend Sem Mat Univ e Politech Torino, 31*, 405-409.

Dragomir, S.S. (2009). Power inequalities for the numerical radius of a product of two operators in Hilbert spaces. *Sarajevo J Math., 18*, 269-278.

El-Haddad, M., & Kittaneh, F. (2007). Numerical radius inequalities for Hilbert space operators. *II Studia Math., 182*, 133-140.

Kittaneh, F. & Moradi, H. R. (2020). Cauchy-Schwarz type inequalities and applications to numerical radius inequalities. *Mathematical Inequalities and Applications, 23*, 1117-1125.

Kittaneh, F. (1988). Notes on some inequalities for Hilbert space operators. *Pub1. Reserach Inst. Math. Science, 24*, 283-293.

Kittaneh, F. (2003). A numerical radius inequality and an estimate for the numerical radius of the Frobenius companion matrix. *Studia Math., 158*, 11-17.

Kittaneh, F. (2005) Numerical radius inequalities for Hilbert space operators. *Studia Math., 168*, 73-80.

Moradi, H. ,& Sababheh, M. (2021). New estimates for the numerical radius. *Filomat, 35*, 4957-4962.

Halmos, P.R. (1982). *A Hilbert space Problem Book*, (2nd ed).New York, NY:Springer.

Author Information

Mohammed Al-Dolat
Jordan University of Science and Technology
Irbid, Jordan
Contact e-mail: mmaldolat@just.edu.jo

To cite this article:

Al-Dolat, M. (2023). General upper bounds for the numerical radii of. powers of Hillbert space operators. *The Eurasia Proceedings of Science, Technology, Engineering & Mathematics (EPSTEM), 22*, 15-25.

The Eurasia Proceedings of Science, Technology, Engineering & Mathematics (EPSTEM)
ISSN: 2602-3199

The Eurasia Proceedings of Science, Technology, Engineering & Mathematics (EPSTEM), 2023

Volume 22, Pages 26-32

ICBASET 2023: 3rd International Conference on Basic Sciences, Engineering and Technology

Investigation of Mechanical and Dimensional Features in Unfilled Polyketone Polymer

Hasan OKTEM
Kocaeli University

Halit KARASUNGUR
Kocaeli University

Ahmet EROGLU
Mechanical Engineer

Abstract: High performance engineering polymers are widely used in automotive sector today. For this reason, the mechanical and dimensional of one of these polymer materials after injection molding under different process conditions (melt temperature, injection pressure and gate type) will be investigated. In order to examine the mentioned properties of these polymers, a series of plastic injection experiments were carried out based on the Taguchi Experimental design (L_9). In the experiments, tensile strength, percentage elongation and shrinkage values were obtained by using the parameters of mold temperature, injection pressure and type runner gate. At the end of the study, time and cost savings were achieved by performing the least number of experiments according to the Taguchi experimental design. In addition, the problems encountered in the use of polymer materials in the literature and industry have been tried to be removed. Moreover, some solutions will be provided on mechanical and the quality problems in plastic injection molding.

Keywords: Polymers, Plastic injection molding, Mechanical properties, Dimensional properties, Taguchi design

Introduction

In our today, the need for the use of high-performance engineering plastics in plastic injection method is increasing rapidly. In the plastic injection molding method, advanced polymers are used extensively in the automotive and aviation industries (Ezdeşir et al., 2006). Basic injection process parameters such as temperature, pressure, injection speed and cooling time are used in shaping high performance engineering polymers (Akyüz, 2006). Plastic products shaped with these parameters are expected to exhibit high strength, better quality and high performance according to their usage areas. Plastic injection process parameters play an important role in the quality of the plastic product after injection (Beaumont et al., 2002). High performance engineering polymers include Polyphenylene Sulfide (PPS), Polysulfone (PSU), Polyphenylensulfone (PPSU), Polyamide-imide (PAI), Polybenzimidazoles (PBI), Polyetheretherketone (PEEK), Polyketone (PK) and Liquid Crystal Polymer (LCP).) can be ranked as important. High performance engineering polymers have properties such as high tensile, compression and creep strength, ability to work at high temperatures and under load, resistance to chemicals and radiations, flame resistance and insulation properties, and safe operation at extreme humidity and temperatures. These polymers have started to find wide usage areas in the aerospace industry, automotive industry, nuclear power plants, steam turbines and medicine (Akkurt, 2007).

In particular, polymers such as PK attract attention due to their properties. Some researchers investigated the mechanical, thermal, rheological and volumetric shrinkage (dimensional) properties of engineering polymers using different plastic injection process conditions (Arıcıoğlu et al., 2000) & (Kurt, 2011). A group of

- Selection and peer-review under responsibility of the Organizing Committee of the Conference

researchers investigated the mechanical properties of plastics produced with glass fiber reinforced Polypropylene (PP) and Nylon 6 (PA6) polymer materials (Güllü et al., 2001). The tensile strength and part geometry properties of Ultimate High Molecular Weight Polyethylene polymer (UWHDPE) were investigated by another group of researchers using the Taguchi method. In the study, it was stated that the cross-section without weld lines had significant effects on the tensile strength. It has also been stated that the Taguchi method is very effective in selecting the most suitable mechanical properties of the polymer material (Kuo & Jeng, 2010). In a similar study, researchers studied on estimating the mechanical properties of 25% recycled PE and 75% original polymer mixture with the best process parameters. Researchers also examined the effect of recycling plastic additive on mechanical properties and flow index. At the end of the study, it was stated that the addition of recycled plastic contributed to the mechanical properties and reduced the production cost (Mehat & Kamaruddin, 2011). In another similar study, the mechanical and thermal properties of PP and ABS (Acrylonitrile Butadiene Styrene) recycling polymers were investigated. For this purpose, tensile test, heat deformation test were carried out. As a result, 30% improvement in thermal properties and 50% improvement in mechanical properties of recycled polymer materials has been achieved (Şen et al., 2020).

After the injection molding of polymer materials, due to different cooling rates and thermal gradients, volumetric contraction and distortion occur in polymer materials. Some researchers investigated the effects of plastic injection parameters, which cause volumetric shrinkage and warping, on different polymers with the Taguchi method and experimental methods (Çakır & Güldaş, 2001), (Iyer & Ramani, 2002), (Jansen et al., 1998). In addition to these studies, optimization of process parameters based on Taguchi method on both volumetric shrinkage and warping was performed (Liao et al., 2004), (Öktem & Erzincanlı, 2012), (Öktem et al., 2007). An optimum cooling system is very important to more decrease the volumetric shrinkage in the injection process of polymer materials. If the cooling system is well designed, high part geometry and quality surface can be achieved (Wang, et al., 1996) & (Yıldırım, 2011). In addition to these, cold and hot runners are preferred according to the flow distance and the filling volume of the part cavity during the injection of polymer materials. Researchers have stated that the reason why hot runners are more preferred is higher plastic part quality, injection of advanced engineering polymers and lower cost (Öztürk & Özkan, 2015) & (Demirer, et al., 2007).

In this study, a series of experiments were carried out using Taguchi L_9 design to evaluate the mechanical and dimensional properties of high performance engineering polymers of un-filled PK in plastic injection molding. During the current study, the effects of melt temperature, pressure and runner gate type as initial parameters on tensile strength, elongation (%) and shrinkage and were investigated. Upon the literature surveying, it has been seen that very serious and comprehensive works have not been carried out on high-performance engineering polymers. Therefore, it was decided to conduct this current study. Moreover, tensile strength values had changed from 58.55 to 63.60 MPa unfilled PK polymer. The lowest percentage elongation was obtained in 9.12 (%) whilst the highest percentage elongation was found as 9.86 (%). The best shrinkage value was calculated in 1.864 (%). It can be observed that this material is a ductile polymer due to some properties.

Experimental Study

Design of Experiments

In this study, using four different injection parameters of polymer material (Polyketone-PK), a total of 9 experiments were performed on a plastic injection machine according to the three-level L_9 Taguchi orthogonal design (Minitab Software, 2007). In the experiments, tensile strength, elongation (%) and shrinkage of the injected samples were determined by using injection parameters such as melt temperature, injection pressure and gate runner type (Table 1). Gate runners are divided into three types: T is single gate; C is double gate and D is direct gate over the plastic sample.

Table 1. Design of experiments (L_9 Taguchi) for PK polymer

Parameters	Melt temperature (°C)	Injection pressure (Bar)	Gate type (C-T-D)
	250	80	1
	260	100	2
	270	120	3

Materials and Method

In this study, plastic molds were designed and manufactured for the injection process of three different polymer materials on a plastic injection machine (TMC 60). The plastic samples were injected by using three injection parameters based on the Taguchi L_9 design given in Table 1. The samples of tensile rod and shrinkage bar were injected for polymer of PK as shown in Figure 2. In plastic injection experiments, three runner gates were utilized by changing them. Injection machine was adjusted in values of clamping force is 600 kN, injection speed is 45 mm/s, injection time 2 s, packing time is 5 s, cooling time is 10 s, mold open-close time is 5 s and total cycle time is 22 s.

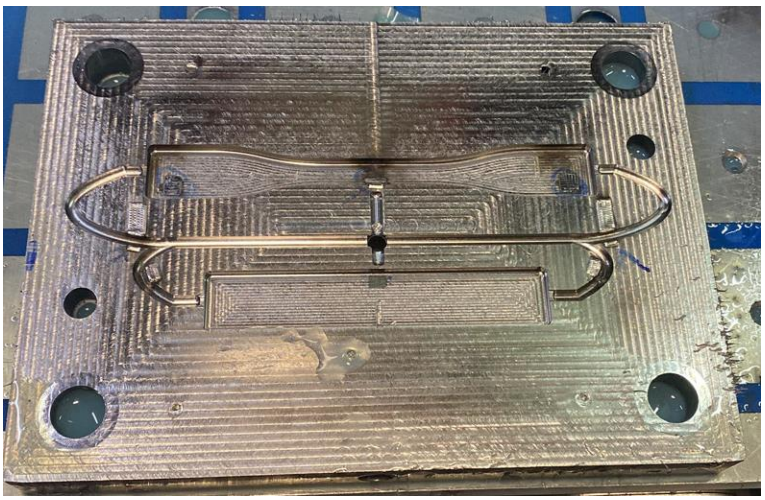

Figure 1. The finished of plastic molds for plastic sample

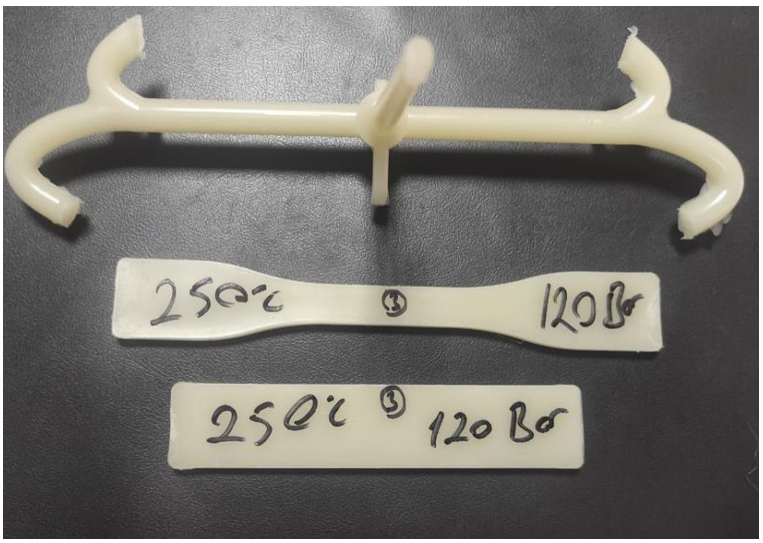

Figure 2. The tensile rod and rectangular samples of PK Polymer

Measurement of Mechanical and Dimensional Properties

In this study, the general properties of high performance engineering polymers are tried to found by means of tensile strength and dimensional measurement. For this purpose, firstly, 9 tensile rod samples were conducted in MACRONA model instrument. According to International standards (ASTM D-638, 2010) & (ASTM D-1238, 2001), the test speed is 100 mm/min in tests as shown in Figure 3. Tensile strength values were measured at yield point during the tests. From these tests, it was obtained the values of tensile strength (MPa) and elongation (%).

Figure 3. The tensile tests of polymers

Secondly, the values of shrinkage in ASTM D-955 were calculated by measuring the dimensions of mold and plastic samples in length direction for PK polymer with a digital caliper in Figure 4. The instrument is made by Mitutoyo with accuracy of 0.01mm. The measurements were performed at least three times. All of shrinkage measurements were conducted after the first 48 hours out of the mold.

Figure 4. The measurement length of PK sample in longitudinal direction

Results and Discussion

In this section, all the results related to the mechanical and dimensional properties obtained from the tests carried out on plastic samples are examined and evaluated. Table 2 shows the results of tensile strength, elongation (%) and shrinkage in longitudinal (X-direction) of plastic samples.

Table 2. Experimental results for unfilled PK polymer

Polymers	Tensile Strength (MPa)	Elongation at yield (%)	Shrinkage (Longitudinal) (%)
Polyketone	62.58	9.17	2.136
	61.29	9.27	2.318
	60.20	9.86	1.864
	58.55	9.58	1.927
	59.47	9.26	2.018
	61.83	9.33	2.364
	61.32	9.38	2.291
	60.92	9.74	1.936
	63.60	9.12	2.109

From Table 2, it can be observed that the tensile strength values obtained as a result of the tensile test applied to un-filled PK polymer vary according to the plastic injection conditions. The highest tensile strength values were found for the injection parameters where the plastic melt is given from a double gate (C). In addition, each of the tensile strength values was obtained from plastic injection parameters such as pressure of 120 and temperature of 270 ºC. The highest tensile strength is 63.60 MPa, while the lowest is 58.55 MPa. These values obtained are very close to the values given by the literature and manufacturers.

In Table 2, it is also seen that the elongation (%) values are changed from 9.86 to 9.12 %. The lowest percentage elongation is calculated in the injection condition with double gate (C). This situation can be explained by the weaker bond structure of the PK polymer compared to other polymers in literature at the morphological level (Campo, 2008). Additionally, since the melt is filled from two directions, it will create weld line formed at the middle point, and this has caused PK sample to have a high percent elongation value.

As seen in Table 2, the volumetric shrinkage values in the direction of flow rate vary between 1.864 and 2.318 for PK polymer. The reason for this can be explained by the higher melt flow index of the PK polymer and its morphological structure of the polymer. On the other hand, semi-crystalline polymer materials have more than high shrinkage value amorphous (Beaumont, 2002).

Conclusions

In this study, the mechanical and dimensional properties of a high-performance engineering polymer were investigated by experiments performed under three different injection conditions. In light of results and evaluations obtained from these experiments, the conclusions can be summarized as follows:

- The unfilled Polyketone is a high performance engineering polymer, it is also semi-crystalline polymer which requires a shorter molding cycle and higher melts and mold temperatures.
- The elongation (%) values appropriated that this polymer is high mechanical properties.
- The high elongation values have showed a ductile of PK polymer. This is why can be explained by the weaker bond structure of the PK polymer compared to other polymers (Campo, 2008).
- Additionally, the fact that the flow is from both sides it will create weld line formed at the middle point has led to an increase in the percent elongation values.
- Shrinkage values of PK polymer are higher than other high-performance engineering polymer because PK polymer is a semi-crystalline material. This is because its bond structure is weak.7
- Among three injection parameters, the best is runner gate type on the mechanical and dimensional properties.
- This study enabled the production of plastic products within the desired criteria as a result of the application of injection parameters on a high-performance polymer.

Recommendations

In future trends, the pressure of cavity in mold can be measured with piezo electric-sensors with PPS, PPSU, PEEK, PEI. Thus, the values of pressure can be obtained in real conditions.

Scientific Ethics Declaration

The authors declare that the scientific ethical and legal responsibility of this article published in EPSTEM journal belongs to the authors.

Acknowledgements or Notes

The authors would like thanks to Güneş Plastic Molding Industrial, Mesut Güneş and Murat Deringül in Kocaeli in Turkey.

* This article was presented as an oral presentation at the International Conference on Basic Sciences, Engineering and Technology (www.icbaset.net) conference held in Marmaris/Turkey on April 27-30, 2023.

References

Akyüz, Ö.F. (2006). *Introduction of plastics and plastic technologies*, (3rd ed.), PAGEV Publications, İstanbul.

Akkurt, S. (2007). *Plasctic material science and mold design*, Birsen Publications, (1st ed.), İstanbul.

Arıcıoğlu, M.K., Mert, B., & Soydan, Y. (2000). Mechanical analysis methods of Polymer materials, *Journal of Sakarya University Natural Sciences, 1,2*, 51-58.

ASTM D-638 Standards (2010). *Standard test method for tensile properties of plastics*, ASTM International, USA.

ASTM D-1238, (2001). Standart test method for melt flow rates of thermoplastics by extrusion plastomer, *Annual Book of ASTM Standart, 8*(1), 265-276.

Beaumont, J.P., Nagel, R., & Sherman, R. (2002). *Successful injection molding*: Hanser/Gardner Publications Inc., Cincinati, USA.

Campo, A. (2008). *Selection of polymeric materials*, William Andrew Publishing, Norwich, USA.

Çakır, Y., Özdemir, A., & Güldaş, A. (2001). Investigation of injection parameters affecting shrinkage amount in plastic products. *Journal of Technology, 1-2*, 19-29.

Demirer, A., Soydan, Y. & Kaptı, A.O. (2007). An experimental investigation of the effects of hot runner system on injection moulding process in comparison with conventional runner system. *Materials & Design, 28*, 1467-1476.

Ezdeşir, A., Erbay, E., Taşkıran, İ., Yağcı, M.A., Cöbek, M., & Bilgiç, T. (2006). *Polimerler 1*(3rd ed.), PAGEV Publications, İstanbul.

Güllü, A., Özdemir, E., Demir, H. (2001). Investigation of the effect of injection parameters on the mechanical properties of glass fiber reinforced Polypropylene (PP) and Nylon 6 (PA6) composites. *Journal of Niğde University Engineering Sciences, 5*(1), 11-19.

Iyer, N. & Ramani, K. (2002). A study of localized shrinkage in injection molding with high thermal conductivity molds. *Journal of Injection Moulding Technology, 6*(2), 73-90.

Jansen, K.M.B., Van Dijk D.J. & Husselman M.H. (1998). Effect of processing conditions on shrinkage in injection molding, *Polymer Engineering Science, 38*(5), 838-846.

Kurt, M. (2011). *High-temperature tribological behavior of high-performance engineered polymers*, Master Thesis, Sakarya University Natural Science Institute, Sakarya.

Kuo, H.C., & Jeng, M.C. (2010). Effects of part geometry and injection molding conditions on the tensile properties of ultra-high molecular weight polyethylene polymer. *Material & Design, 31*, 884-893.

Liao, S.J., Chang, D., Chen, H.J., Tsou, L.S., Ho, J.R., & Yau, H.T. (2004). Optimal process conditions of shrinkage and warpage of thin wall parts. *Polymer Engineering Science, 44*, 917-928.

Mehat, N.M. & Kamaruddin, S. (2011). Optimization of mechanical properties of recycled plastic products via optimal processing parameters using the taguchi method, *J. Materials Processing Technology, 211*, 1989-1994.

Minitab Statistical Software, Release 16, (2007). *Making data analysis easier*, State College, Minitab Corperation, USA.

Öktem, H. & Erzincanlı, F. (2012). *Determination of optimal process parameters affecting shrinkage caused by plastic injection pressing of a DVD ROM front cover by taguchi method*, III. National Design Manufacturing Analysis Conference, Türkiye.

Öktem, H., Erzurumlu, T., & Uzman, İ. (2007). Application of taguchi optimization technique in determining plastic injection molding process parameters for a thin-shell part. *Materials & Design, 28*, 4, 1271-1278.

Öztürk, T., & Özkan, A. (2015). Comparison of runner systems of cold and hot, *Journal of Düzce University Science and Technology, 3*, 283-298.

Ross, P.J., (1996). *Taguchi techniques for quality engineering* (2nd ed.), Mc Graw-Hill, New York, USA.
Şen, N., Şengül, Ö., & Uygur, İ. (2020). Examination of some mechanical and thermal properties of recycled PP and ABS prototype materials. *Journal of Düzce University Science and Technology, 8*, 246-257.
Wang, H., Prystay, M., Hetu, F.J., & Jen, C. K. (1996). Gap between mold and part and its effect on cooling of injection-molded plastics, *ANTEC'96,* 1049-1053.
Yıldırım, S. (2011). *Development of product design: Taguchi design*, Master Thesis, Başkent University, Natural Sciences Institutes, Ankara.

Author Information

Hasan Oktem
Kocaeli University, Hereke Asım Kocabıyık Vocational
Polymer Science and Technology Natural Sciences
Institute/Umuttepe Campus, Kocaeli, Turkey.
Contact e-mail: *hoktem@kocaeli.edu.tr*

Halit Karasungur
RD Department/ Guneş Plastic Trade Company
Msc. Student-Kocaeli University /Umuttepe Campus
Natural Sciences Institute, Kocaeli, Turkey.

Ahmet Eroglu
Mechanical Engineer/RD Department
Guneş Plastic Trade Company
GOSB-Gebze/Kocaeli, Turkey.

To cite this article:

Oktem, H., Karasungur, H. & Eroglu A. (2023). Investigation of mechanical and dimensional features in unfilled polyketone polymer. *The Eurasia Proceedings of Science, Technology, Engineering & Mathematics (EPSTEM), 22,* 26-32.

The Eurasia Proceedings of Science, Technology, Engineering & Mathematics (EPSTEM)
ISSN: 2602-3199

The Eurasia Proceedings of Science, Technology, Engineering & Mathematics (EPSTEM), 2023

Volume 22, Pages 33-47

ICBASET 2023: International Conference on Basic Sciences, Engineering and Technology

Global Food Security Strategies, Issues and Challenges

Hayati YUSOF
Universiti Tunku Abdul Rahman

Mai Farhana MIOR BADRUL MUNIR
Universiti Tunku Abdul Rahman

Zulnurhaini ZOLKAPLY
Universiti Tunku Abdul Rahman

Muhammad Ashraf ANUAR
Universiti Tunku Abdul Rahman

Abstract: The world economy is in turmoil as a result of the global power crisis, rising commodity prices and the return of the inflation volatility just when the COVID-19 pandemic shows signs of recovery and healing. In Malaysia, food is a pleasant topic to its citizens - young and old, it is a symbol of unity and represents its unique identity. Recently, according to the Malaysian Department of Statistics, the food inflation grew by 4.1 percent in April 2022, despite higher percentages faced by other countries. This contributed to higher household expenditures and less savings. In addition, many Malaysians lost their jobs and incomes due to the pandemic, business entities shut down and high logistic costs forced the food price to increase. To understand the root cause and further implications of the food security issue, an attempt is made by searching through the recent academic literature. This is done by going through the e-library resources. The aim is to find from other researchers who have gone through similar experience in the past and learn from them. For this, 18 articles have been selected for synthesis. From the synthesis, a few significant dimensions have been identified. There are similarities and differences between countries or regions involving the causes and the consequences of food insecurity. Many past studies suggested processes or techniques that lead future farmers into the adoption of the climate smart agriculture. The findings from this study will help to educate, spread awareness and act as a point of reference to the public as well as the authority.

Keywords: Food insecurity, SDG 2 Zero hunger, Climate change, Food independence, Food deficit

Introduction

Familiar as a “Food Paradise” with its diverse multi-cultural backgrounds, food has been a factor of gastronomy tourism in Malaysia. The variety and delicious food originated from its cultural intermixing has set Malaysia apart from any other country. Malaysians are proud of its food and they are very passionate about it. Food is quite easy to find and the prices are still very much affordable as well; hence some may take it for granted in the past. Benjamin Franklin’s expression “eat to live, don’t live to eat” which means humans need to eat in order to survive and very often is used to discourage overeating. Apparently, food security issues were not given much concern in the past as it is today among Malaysians as most have never experienced a global food shortage before. The Department of Statistics Malaysia recorded a 4.1% inflation rate for food and non-alcoholic beverages in April 2022, the consumer price index later rose to 7.3 % in November 2022 (Consumer Price Index Malaysia April 2022; Consumer Price Index Malaysia November 2022). Creating awareness is important and

food is one of the most essential requirements to survive besides air and water for human life. Healthy food is the key to individual physical, emotional health and for human wellbeing.

Recent global COVID-19 pandemic together with other factors for instance population growth, climate change, global spike in prices, unemployment and poverty have triggered food insecurity worldwide and Malaysia is no exception. Russia's war on Ukraine and recent trade-related policies imposed by some countries have also raised international concern on its impact towards a global food crisis. Under the pressure of climate change and COVID-19 pandemic, the global food system itself is struggling even harder to feed its growing population in a sustainable way (European Parliament, 2020). Food and Agriculture Organisation of the United Nation, describes food insecurity as "a person is food insecure when they lack regular access to enough safe and nutritious food for normal growth and development and an active and healthy life. This may be due to unavailability of food and/or lack of resources to obtain food" (FAO, 2006). Governments of many countries including Malaysia have called for an urgent action plan to ensure food security. The World Food Summit of 1996 defined food security as "when all people at all times have physical and economic access to sufficient, safe and nutritious food to meet their dietary needs and food preferences for an active and healthy life" and it "should not be used as an instrument for political and economic pressure" (FAO, 2006).

Based on the recent Global Food Security Index (GFSI) in 2022, Malaysia is ranked 41st out of 113 countries with the prevalence of undernourishment of 2.5%. This 11th edition of the GFSI emphasises that the global food environment is worsening (Economist Impact, 2022). In addition, the food inflation index is showing an increasing trend in many upper middle income countries including Malaysia. In September 2021, the price has increased by 1.9 and in just within a year, Malaysians consumers have encountered a significant price increase of 6.9 and the domestic food inflation price is expected to stay high around the world (The World Bank, 2022). The recent food restrictions imposed by 21 countries that have implemented 30 food export bans and six countries with 11 export-limiting measures have partially worsened the global food crisis and exacerbated food insecurity and inflation. The Malaysian government is very much aware of the food crisis and has made some action plans to overcome this. There are many programmes, incentives provided to the citizens and the government has also introduced the "National Food Security Policy" which seems to work during the "2008 Food Crisis" (Tapsir, Elini, Roslina, Noorlidawati, Hafizudin, Hairazi, & Rosnani, 2019). However, there are still many challenges to overcome in safeguarding food security in the future. This understanding can be learned from the experiences of other countries that have far long experienced food insecurity, its main issues as well as the working strategies that they have adopted for survival.

In this study, the interest lies in observing the issues, problems and trends involving food security research in various geographical locations in the world and also to explore the challenges and opportunities to solve food security in Malaysia. Using e-library search, selected past studies and research involving food security from 2017-2022 were analysed. The findings have been presented in a food security matrix in order to identify the main food security dimensions common (or uncommon) to all. The next part of this article will cover the literature review on food security in other countries like Africa, Brazil, Arab Gulf states, USA, India and ASEAN countries including Malaysia, followed by the research methodology of this study. Findings and contributions of this study will be discussed in the next section where all findings will be discussed according to its significant dimensions. The last sections will discuss about the limitations, conclusions and future directions of this study.

Literature Review

Maffra (2017) discussed about food sovereignty as a sustainable solution to the issues of world hunger and climate change. The concept of food sovereignty includes the local production and consumption of goods while aiming for collective well-being of the locals. This is done through the use of sustainable food production techniques such as good soil management practice, prioritising family farming and ensuring high quality and nutrition in food supplies. The author explained the consequences of hunger from the production aspect which affected climate change. In addition, climate change as an interdisciplinary issue was discussed with several possible ways of mitigation. Among others, mitigating climate change involved public policy reforms in order to find ways to reduce pollutions to the environment, heavy use of pesticides and the use of fires to clear lands. The author also emphasised on the importance of soil management as a mean to feed the world population. She also encouraged the involvements of media in order to bring more information and knowledge about world hunger on an international basis.

Otekunrin, Otekunrin, Sawicka and Ayinde (2020) provided a review on the progress of African countries against hunger for the past three decades using the Global Hunger Index (GHI) scores. Three indicators of GHI were used. They were prevalence of undernourishment (percent population), prevalence of stunting in children and prevalence of wasting in children. The authors also presented links between GHI and Human Development Index (HDI), social protection and Global Terrorism Index (GTI). Among many reasons that caused food insecurity in Africa were poverty, corruption, low human capital development, conflicts and extreme weathers. The Malabo Montpellier Report 2017 listed down a few strategies for African countries to attain zero hunger. They were making food and nutrition as a top policy priority, work in collaboration with other stakeholders to deliver intended outcomes, revision of agricultural policies to emphasise on nutrition-rich food production and many more.

Otekunrin and Otekunrin (2021) discussed the importance of healthy and sustainable diets in order to attain SDG 2 Zero Hunger by 2030. They implied that to end world hunger, people's diet should be nutritionally sufficient, economically affordable, socially approved, innovatively and environmental-friendly produced. Their sources revealed that the number of hungry people in Africa has been rising steadily since 2015 to 2019 and is projected to rise further in 2030. In addition, stunting (low height in children under five years of age) declined globally since 2000 to 2019 while 69% of wasting (low weight for height in children under five years of age) children were found living in Asia and 27% lived in Africa (2019). Recommendations have been put forward to look for innovative ways and strategies to improve food sustainability such as prioritising food diet plans as national agendas, giving special focus on children and women, ensuring better access to nutritious food for vulnerable groups and gathering and reporting data on diet quality across countries.

Berchin, Nunes, de Amorim, Zimmer, da Silva, Fornasari, Sima, and de Andrade (2019) analysed the Brazilian public policies in terms of how they contribute to increase food security and family farming, how they are correlated, and which are the major gaps and challenges for the future, as well as its food security governance. This study fulfils the gap on the relationship between social protections, smallholder agriculture and food security in Brazil. Family farming is considered an important strategy in reducing social inequalities and poverty in many Brazilian regions and is responsible for the wide variety of agricultural products in the Brazilian domestic consumption market. Six categories of policies were used by the authors in order to analyse the Brazilian policies: financial aid, food aid, technical support, capacity building, land tenure management/food production, and identify, categorize and monitor. The policies and programmes support food security in Brazil, resulting in poverty alleviation and access to food in enough quality and quantity. As a result, the authors also suggested that budgets for all programmes regarding family farming should be strongly increased, making family farming no longer an alternative farming choice, but instead the main one.

Manap (2018) examined the impact of world food price to food insecurity in selected ASEAN countries by using data from nine ASEAN countries between 2000 until 2016. All data was analyzed using a static panel data analysis known as Random effects model and the results revealed that world food prices significantly give an impact to food insecurity in selected ASEAN countries. According to this study, governments need to increase sufficiency in food production and to reduce reliance on food import, because when world food prices increase ASEAN countries can depend only on domestic food production and reduce dependence on food import, thus, reducing the food insecurity problem.

The review by Sulaiman, Yeatman, Russell and Law (2021) provides critical holistic information about food insecurity in high-risk populations in Malaysia, including prevalence, contributing factors, coping strategies, and consequences of household food insecurity. Unexpectedly, the prevalence of household food insecurity in Malaysia was reported as high, with affected groups including *orang asli*, low-income household/welfare-recipient households, university students, and the elderly. Besides, low socioeconomic background included larger households, living in poverty, and low education was identified as a key contributing factor to household food insecurity in all high-risk groups. Furthermore, coping strategies were identified to manage household food insecurity included food-related coping strategies, non-food-related coping strategies, the acceptance of or resignation to the food shortage situation and emotion focused coping strategies. Lastly, the review revealed the consequences of household food insecurity which included psychological, dietary (macro- and micro-nutrient intakes), nutritional status, and health impacts. The forms of government interventions proposed were price policies, import and export policies and agricultural interventions.

In Food Security: The Challenge of the Present, Prosekov and Ivanova (2018) pointed out that the problem of hunger is still persisted even though sufficient amount of food is produced. Hunger occurred as a result of low income of the population especially in developing countries, and inaccessibility to food supplies by a large number of the people. Furthermore, food is not only an object of import and export, it can also be a subject of

political trade for certain countries to gain superiority over others. One country cannot ensure its food security alone. A group of countries such as Brazil, Russia, India, China and South Africa (BRICS) collaboratively can achieve food independence. This is because these countries occupied 25% of the world land, contributed to almost half of the world population and have a combined gross domestic products of 15.4 trillion dollars. These countries are able to produce significant grain supplies, fats and oil and meat production which will allow them to gain a more significant position in the world.

Food security challenge is a complex issue requiring attention on both humans and the environment. An integrated system of intervention involving transdisciplinary research and innovation is required to enhance yield production, promote reasonable food consumption and reduce food loss and food waste. In the food wedges framework, Cole, Augustin, Robertson and Manners (2018) proposed a link to match food demands and food supplies using innovation and promising technologies. For example, by reducing food waste from farm to customer is an obvious opportunity to increase food security. Both recovering food loss and waste is a huge opportunity to reduce production demand as 1.6 billion tonnes of food is wasted along the chain. Moreover, by educating customers about healthy diets might help to reduce overconsumption of food and obesity issues. Next, by deploying new farming system such as combining weather predictions and hydrological modelling might help to expand water resources in agriculture. Crop and livestock improvement and pest and disease prevention can be achieved by genetic modification or enhancement. Lastly, simple changes to management and adoption of existing technology can negate the impacts on climate change.

Food insecurity was widespread in Africa even before the spread of COVID-19 pandemic. As a result, African workers lost their jobs, incomes and health due to vulnerable working conditions and low productivity. The problems became severe to households that have insufficient credit access and low savings. In addition, the pandemic closed domestic productive activities, production suffered as people cannot go to work, supply chain disrupted, welfare and livelihoods turned bad, poverty and being vulnerable to risk increased. The pandemic disrupted the Sub-Saharan Africa (SSA) food security by disrupting food systems, the lockdowns impacted household incomes and physical access to food indirectly. Endris Mekonnen and Kassegn Amede (2022) provided a review on the dual COVID-19 crisis in SSA food insecurity and unemployment. From the review, they synthesised the future policy directions SSA countries would adopt to contain the associated socio-economic impact of COVID-19 and other pandemics. The pandemic disrupted food market supply causing food price to increase and the control measures such as the lockdowns caused unemployment and income loss. This affected the four food security dimensions (or pillars) of households – food availability, food access, food utilisation and food stability. In terms of unemployment, the youth especially women and those in informal economy were badly affected. The three areas in which the youth were affected are education and training, uncertainties for job seekers and job and income losses. The pandemic made the goal of zero hunger difficult to achieve. Farmers in agribusiness faced threats such as climate change, pests and diseases at the very farm level. The authors suggested three policy actions to curb the socio-economic effects of the COVID-19 and other pandemics. The actions are first, to increase the social protection measures such as social insurance and social assistance programmes (including job assistance programmes) to offer resources for people to sustain economic productivity while keeping their jobs. Secondly, by developing and maintaining strong regional co-operations, partnership and cross-border co-ordination that can provide help and supports, these partnerships could not collapse during a crisis. Lastly, there is a need to provide a strong financial resilience and domestic borrowing in order to speed up entrepreneurial and business recovery.

Food security policies in the Arab Gulf states constitute a form of knowledge-power nexus and facilitate agendas. In the Gulf states, this is done via the private enterprises (known as the Gulf food security complex) to drive innovations and with profit motives. The governance of food security there somehow produces power that serves different objectives. This food security complex uses publications, policy reports, interviews, media articles, conferences and government plans to produce food security as a discursive problem. Over the last decade, more than 7960 articles have been written on food security in the Gulf Cooperation Council (GCC) states which surpassed other countries in the regions. Land grabs or the acquisition of agricultural lands in foreign states is justified through food security discourse. Food security is established as a threat to serve different agendas such as a means for redistributing oil rents. The abundance access to food in the early oil period was a means to ensure that the population felt the benefits of oil wealth, a form of legitimacy. This food self-sufficiency programmes hit the walls of environmental and fiscal boundaries later that in the year 2000, more emphasis was placed on external investments in farmlands and diversified contracts on the international markets. These land acquisitions were being portrayed as a win-win situation or as beneficial to both the host and the investor. Additionally, technology is used as a means to drive an efficiency of agriculture or to apply climate-smart agriculture as solutions to environmental limits. In this article, Henderson (2022) uncovered the politics of the formulation of food security policies in the GCC. However, he noted that the policies focused on

the food production only, they did not address on the issue of distribution and the social relations of production (Henderson, 2022).

Abdullah, Mersat and Wong (2021) conducted a study in Sarawak, Malaysia to understand how local people cope with food security issues during the lockdown phases. The study aimed to fulfill three research objectives: to investigate the conditions of the locals in terms of food security, how they coped to ensure they are food secure during the lockdown duration and the greatest challenges that they faced in maintaining their food supplies. They found that most households are food secure, meaning they have access to food on an ongoing basis like what they did before the Movement Control Order (MCO) or lockdown phases. Households resorted to methods such as altering food sources, purchasing online, and going without favorite foods to do this. The significance of this discovery lies in the fact that it demonstrated the need to include dimensions beyond the mere availability of food when discussing about food security. It also demonstrated that adjusting to the direct and indirect changes brought about by the pandemic is the greatest obstacle in obtaining and sustaining food security at the household level. The survey also discovered that a small percentage of respondents experienced food insecurity throughout the MCO period. This change from security to insecurity happened because of financial limitations caused by the COVID-19 and MCO-related economic shutdowns. Due to these financial difficulties that were caused by the work restrictions during the MCO, some people lost the ability to purchase food.

Additionally, Vågsholm, Arzoomand and Boqvist (2020) examined the trade-offs involved in pursuing the triple objectives of sustainability, food security, and safety while examining various methods for cutting down on food loss, waste, and resource footprints. Vågsholm et al. (2020) proposed a few alternatives to reduce source reduction (food loss and food waste) by deploying big data strategies and intelligent labels and sensors while food donation served to reduce food insecurity. However, food safety, food hygiene training and food reprocessing skills are important considerations for food bank and food business operators. Future options to ensure food security may include stepping up agricultural productivity and implementing circular food networks. Circular food networks involved a system where nutrients will be recycled or involved reprocessing foodstuffs (for example as animal feeds and compost). This practice is more beneficial in terms of resource footprints, sustainability and cheaper to farmers. Since only around one third of the world's grain crop is used for human consumption and the other half is used as animal feed, changing our diets to be more plant-based might help (Willett et al., 2019).

Food security affects economic growth, particularly in dry-land developing nations (Abdul Manap & Ismail, 2019). Panel data from 75 dry-land developing countries and annual data from 1970-2016 were used in this study. Data were analysed using the Generalised Method of Moments (GMM). Variables such as gross domestic product (GDP), food security, life expectancy, poverty and total employment were deployed. Based on its findings, food security has a considerable beneficial influence on economic growth, since increased food security boosts economic growth in dry-land developing nations. In particular, food security has a positive impact on economic growth via life expectancy, total employment, and poverty. The reduction of poverty with better food security can enhance economic growth, particularly in developing countries. Suitable programmes to increase employment, offer of effective relief through public-private food security funds and the provision of crop insurance can be implemented to achieve better food security. In addition, improvement in agricultural productivity via new, better technology can help to reduce poverty, ensure food security and thus, boost economic growth.

Moroda, Tolossa and Semie (2018) analysed the food insecurity status of rural families in the Boset area, East Shewa Zone in Ethiopia and identified their causes. The data indicated that food insecurity is common. More than half of the respondents lacked access to safe drinking water, did not own a toilet, and disposed of waste in an unhealthy manner. When the households were denied the benefits of having sanitation and hygiene facilities, this could be the source of disease and the inability of the human body to absorb food nutrients, hence, resulting into low productivity. Regarding the determinants of food security, it was discovered that educational level, farmland size, total yearly income, proximity to health facilities, and the presence of supportive groups were all positively correlated with food security. On the contrary, factors such as access to irrigable land, frequent drought, distance to input and output market and distance from road transport had negative associations with food security. According to the study, all aspects of food (in)security should be targeted for successful intervention. Local authorities may pay attention to factors with both positive and negative food security relationships. Similarly, a reorganisation beyond a quick solution is needed. In solving food insecurity, local and national sectors must work together.

Another study by Fitzpatrick, Harris, Drawve and Willis (2021) reveals that US adult food insecurity has worsened during the COVID-19 pandemic. Before the pandemic, the disparities in food security have already existed in United States. These disparities continued or probably have widened as a result of the pandemic. Their study focused on variables such as social, economic and health factors in determining levels of self-reported food insecurity among individuals living through a pandemic or similar crisis. Their findings confirmed a pattern documented in past research of the general population and higher-risk populations, which are disproportionately poor and of colour. Race, ethnicity, and socioeconomic level partially influence food insecurity in the US. To further highlight the uniqueness of the present and the need to prepare for emotional uncertainty, the authors highlighted the importance of addressing the symptoms of mental health and the doubts or generalised anxiety exhibited as concerns or fear of COVID-19. The authors reminded that preparations (such as advanced planning) need to be done to face a pandemic-type of event in order to prevent over-burdened and under-resourced disadvantages in the future.

With an overview of the past 23 pandemics worldwide, Roubik, Lošťák, Ketuama, Procházka, Soukupová, Hakl, Karlik and Hejcman (2022) proposed the visions of post-COVID-19 agriculture and its effects on food security. The authors predicted that post-pandemic agriculture will be less-labour intensive with heavy use of automation and precision, the shift towards plant-based diets with the adoption of Information Communication Technology (ICT) to enhance communication and marketing of the crop yields. They also observed that reliance on seasonal foreign workers will discontinue with more focused on local seasonal workers from diverse backgrounds. More customers will continue to shop for food online with the rise of the urban lifestyle with minimum self-supply of food and household reserve. It also meant for repackaging of the crop yields to meet online demands, hotels and tourism sectors and to allow the mobility of the agricultural components to meet its demand and supply especially in fisheries. The movement to reduce the use of farm chemicals or to improve the chemical standards has been seen as ways to improve food safety. On the global obesity issues, they observed that there will be changes in lifestyle with more involvements of physical activities. There might be a shift towards insects and micro-algae as food substitutes. More attentions will be needed to prevent farm bankruptcy in the form of insurance, protection and loss absorptions. They believed more research will be needed to study the negative effects on food security in order to improve food resilience and by making use of economic models, to gauge its effects in the long run.

According to Adekunle and Filson (2020), apart from hunger, food consumption served a few other purposes such as cultural, religious and social reasons. In Islam, eating is considered a form of worship. Halal food is not only present in the dietary requirements but also in the process and storage activities to avoid cross-contamination of the food. Eating halal food can ensure food safety, over-production of meat can be significantly reduced and served as a business model for Canadian export market. However, there is a lack of trust in the market because of the presence of information asymmetry between seller or producer and consumers. In this study, the authors explored the Somali Canadians' perceptions on halal meat in Greater Toronto Area (GTA) as there are numerous halal certification bodies in Canada and there was no centralised agency to oversee the overall halal regulations yet.

Guntur (2021) analysed the tafseer of surat Al-Baqarah verse 247. It turned out that the surat contained messages about values of physical education. The Al-Quran, through physical education treated a human as a unified whole, in body and spirit. Firstly, the verse described the development of the physical body, together with the mind and soul. To maintain a healthy body, Prophet Muhammad SAW mentioned about the importance of sports in particular, to practice archery, swimming and horse riding as these sports represent strong nations. Second, a healthy body needs to eat and drink halal and nutritious food (a balance diet), maintains an adequate rest and ensures cleanliness of clothing, environment and behaviour (ethical values). In Islam, the sources of ethics and values are derived from Al-Quran and Hadith. Thus, physical education involved a process of becoming a person who grows in line with his or her talents, character, abilities and conscience. Thirdly, food and drinks that entered a human body affect their health and well-being, hence, consuming halalan tayyiban (halal and good) food is given priority. Not only halal, tayyiban means food that is not rotten, expired or contains bacteria that will harm the body. The halalan tayyiban concept requires humans to understand the science of nutrition in order to maintain and consume food in the right manner.

Research Methodology

The overall aim of this study is to investigate the issues, problems, challenges and trends involving food security and to find its feasible solutions. In this study, the research objectives (RO) include:

RO1: To conduct e-library search, appraise and synthesise the evidence base of food security in several countries around the world
RO2: To explore the determinants of food insecurity in the global food crisis
RO3: To identify who are impacted by food security issues and who are the responsible parties that play a major role in food security
RO4: To investigate the impacts of recent global pandemic and trade-related policies on the global food crisis
RO5: To identify different feasible solutions adopted as well as adapted by other countries in ensuring food security

As a result, 18 articles have been shortlisted for synthesis. The information derived from these articles will help to answer the research questions (RQ) of this study as follow:

RQ1: What are the issues, problems, challenges and trends involving food security research in the past (between 2017-2022) from around the world?
RQ2: What are the determinants of food insecurity in the global food crisis?
RQ3: Who are impacted by the issue and who are the responsible parties that play a major role in food security?
RQ4: How do the current unanticipated situations like the global pandemic and trade-related policies impact global food security?
RQ5: What are the solutions adopted or adapted by the countries that have experienced food insecurity?

The articles were selected based on meeting the following criteria: duration (the papers were published between 2017-2022), issues of discussion (the articles discussed about food security issues, problems or challenges, trends, strategies that are related to answer the RO and/or RQ) and comparison (the articles helped in making comparisons involving food security experiences, methods, processes, interventions, etc. that differed according to locations, cultures/religion, weather and soil conditions, policies and scale of production). On the other hand, research or articles will be excluded if: they were not written in English, they were not research articles, full paper was not available and not relevant to the discussion of RO and/or RQ.

Discussion and Contribution

Theoretically, the contribution of this research is the discussion of the significant food security dimensions via the food security matrix developed in Table 1. This matrix helps readers to understand the concepts, issues, problems, challenges and trends of food security in various geographical locations around the world. Also, to the best of the authors' knowledge, this is the first research to integrate both eastern and western views on food security in a single framework, taking into accounts the issue of food waste, food safety (halalan tayyiban) and the food contribution towards human civilisation. In practice, this research helps practitioners to draw up an effective plan or strategy to combat food insecurity based on local conditions such as geographical locations, types of soil, weather conditions, demographic factors, policies and interventions from their regulators.

Relevant Terms, Concepts and Definitions of Food Security

A number of authors began by describing or defining the relevant terms and concepts of food security in their studies (Table 2). Food sovereignty was introduced by Maffra (2017), hunger (Otekunrin et al., 2020; WHO, 2019), sustainable healthy diets (Otekunrin et al., (2021); WHO, 2019), family farming (Berchin et al., 2019) and food wastage (Otekunrin et al., 2021; Cole et al. 2018; Vågsholm et al., 2020). Cole et al. (2018) went further to discuss the megatrends in food and agribusiness, Endris Mekonen and Kassegn Amede (2022) revealed food insecurity and its relation to unemployment, Manap (2018) introduced food deficit as a result of high food import bills and Henderson (2022) reported on the Gulf food security complex. Guntur (2021) and Adekunle and Filson (2020) however, explained food security from Islamic point of view with the application of the halalan tayyiban concept which perhaps has been overlooked by many western scholars. Several authors related their food security studies to the Sustainable Development Goal (SDG 2) to tackle Zero Hunger (Otekunrin et al., 2021; Sulaiman et al., 2021; Abdullah et al., 2021).

Furthermore, food insecurity can be categorised into two types: 1) chronic long-term food insecurity as a result of prolonged poverty (Otekunrin et. al., 2020) and lack of access to assets and financial resources; 2) transitory food insecurity which is temporary because of short-term shocks such as unstable local food production, food price and household incomes (Manap, 2018). It can be assumed that the definition of food security is multidimensional as it involved four 'pillars: they are physical availability of food, economic and physical

access to food, food utilisation and food stability (Sulaiman et al., 2021; Endris Mekonnen & Kassegn Amede, 2022; Abdullah *et al.*, 2021; Moroda *et al.*, 2018). The nature of hunger is also a multidimensional issue (Otekunrin *et al.*, 2020; Berchin *et al*., 2019; Moroda *et al*., 2018).

Table 1. Food security dimension

Article No.	Dimension/Author	Terms, Concepts and Definitions	Causes of food insecurity, contributing factors	Role of individuals, society and country	Consequences of food insecurity	Proposed unique solutions, contributions	Policy reform	Political agenda, security	Past pandemic effects (other than COVID-19)	Information asymmetry
1	Mafra (2017)	*	*	*	*	*				
2	Otekunrin *et. al*. (2020)	*	*	*	*	*				
3	Otekunrin *et. al*. (2021)	*	*	*	*	*				
4	Berchin *et al*. (2019)	*	*	*	*	*	*			
5	Manap (2018)	*	*	*	*	*				
6	Sulaiman *et al*. (2021)	*	*	*	*	*	*			
7	Prosekov & Ivanova (2018)		*	*	*	*				
8	Cole *et al*. (2018)	*	*	*	*	*	*			
9	Endris Mekkonen & Kassegn Amede (2022)	*	*	*	*	*	*			
10	Henderson (2022)	*		*	*	*	*	*		
11	Abdullah *et al*. (2021)	*	*	*	*	*	*			
12	Vågsholm *et al*. (2020)	*	*	*	*	*	*	*		
13	Abdul Manap & Ismail (2019)	*	*	*	*	*	*			
14	Moroda *et al*. (2018)	*	*	*	*	*	*	*		
15	Fitzpatrick *et al*. (2021)	*	*	*	*	*	*	*		
16	Roubik *et al.* (2022)					*	*		*	
17	Adekunle & Filson (2020)	*		*			*			*
18	Guntur (2021)	*		*						

* Discussed by authors in their research studies

Determinants of Food Insecurity in the Global Food Crisis

Of late, countries around the world have experienced or are still experiencing the shortage of food supplies. This global food shortage is contributed by a number of issues such as poverty (Maffra, 2017; Berchin et al., 2019; Manap, 2018) or low incomes of the vulnerable populations (Sulaiman et al., 2021), ongoing conflicts and civil wars (Maffra, 2017; Otekunrin et al., 2020; Prosekov & Ivanova, 2018; Vågsholm et al., 2020; Moroda et al., 2018), unstable world political situations (Manap, 2018; Prosekov & Ivanova, 2018; Vågsholm et al., 2020), high prices or inflationary effects (Maffra, 2017; Otekunrin et al., 2020; Manap, 2018; Sulaiman et al., 2021; Vågsholm et al., 2020), extreme weather conditions such as prolonged drought, excessive rainfall, floods and hurricane (Maffra, 2017; Otekunrin et al., 2020; Berchin et al., 2019; Manap, 2018; Sulaiman et al., 2021; Moroda et al., 2018), rapid population growth (Otekunrin et al., 2020) and greater number of children (Sulaiman et al., 2021), pest and diseases problems (Otekunrin et al., 2020), corruptions (Otekunrin et al., 2020), lack of human capital development (Otekunrin et al., 2020, Sulaiman et al., 2021) and the volatility of oil prices that affect food production activities as in machinery and transportation (Manap, 2018).

Families headed by females and chronic diseases also caused people to suffer from food insecurity (Sulaiman et al., 2021). According to Fitzpatrick et al. (2021), sick people who lived in a built environment not conducive to movements may further challenged their abilities to access food. In addition, food accessibility is directly linked to financial security especially for those who relied on daily wages or incomes (Abdullah et al., 2021). Failure in agricultural process, quality flaws of vegetables and fruits, discarded foods that are closed to their expiry dates and massive food recalls by producers or retailers also caused food loss and food waste (Vågsholm et al., 2020). Furthermore, Moroda et al. (2018) claimed that food insecurity also is a result of incompetent governments and their lack of commitments to curb famine.

Vågsholm et al. (2020) identified a few changes that have impacted food security such as rising food prices are correlated with war and social unrest, diversion of edible crops to biofuel production that made price of biofuel crops correlated to oil prices and increase speculation in food price (hedge funds) also posed a risk to food

affordability especially among the low-income groups. Other factors such as rapid urbanisation is causing more than half of the populations to live in cities making urban consumers heavily rely on food consumption while the heavy reliance on imports can cause food shocks as some countries impose export restrictions in times of emergency.

The Role of Individual, Society and Country – People who are affected and who are responsible to help

Food security is a significant concern at various levels (Abdullah et al., 2021) including the elderly, refugees and university students (Sulaiman et al., 2021). The impacts to university students, according to Sulaiman et al. (2021), are prone to be anxious, lack of concentration when studying and have high risks of falling ill while the older generations generally suffer from depression. Abdullah et al. (2021) mentioned about the images of people queuing up at the supermarkets and the shelves were empty. This happened during the COVID-19 pandemic, reflecting about food access and food security issues at the time. It was caused by the logistic restrictions, shortage of manpower and the closure of food eateries during the various phases of lockdowns in Malaysia (Abdullah et al., 2021). In the United States, however, the pandemic worsened the disparities in food security even further among its citizens (Fitzpatrick et al., 2021). On the international level, a group of countries can collaboratively involve in food production activities and trade, indirectly becoming more significant at the international arena (Prosekov & Ivanova, 2018). Policymakers need to work collaboratively with other stakeholders at national as well as with private and development partners to deliver nutritious food (Otekunrin et al., 2020). In Africa, governments should empower women to decide and give more opportunities for them to own and control resources such as lands, food productions and healthcare (Otekunrin et al., 2020; Otekunrin et al., 2021).

Table 2. Relevant terms and concepts

Terms and Concepts	Definition	Author
Food sovereignty	Food sovereignty includes "production and consumption at local level, but aiming for the collective well-being, through using sustainable techniques to produce food (natural fertilisers, adequate planting and collection cycles for each type of food, no use of artificial pesticides and adequate soil management without deforesting, polluting or burning areas), prioritising family farming and the supply of more nutritious and quality food" (p.1). Food sovereignty exists when "consumers have access to the halal food they want instead of mislabeled, contaminated and improperly slaughtered meat" (p.19).	Maffra (2017, p.1); Adekunle & Filson (2020, p. 19)
Food insecurity	Food insecurity is "a situation that exists when people lack secure access to sufficient amount of safe and nutritious food for normal growth and development and an active and healthy life. It may be caused by the unavailability of food, insufficient purchasing power, inappropriate distribution or inadequate use of food at the household level" (p.3).	Maffra (2017, p. 3), Manap (2018), Sulaiman et al. (2021)
Food security	Food security exists "when all people have at all times physical and economic access to sufficient safe and nutritious food to meet their food needs and food preferences for an active and healthy life". Four pillars of food security: 1) Availability – Availability of sufficient quantities of food of appropriate quality, supplied through domestic productions or imports	World Food Summit (1996), Maffra (2017, p. 3), Berchin (2019), Sulaiman et al. (2021), Abdullah et al. (2021), Moroda et al. (2018)
	2) Accessibility – Access by individual to adequate resources for acquiring appropriate food for a nutritious diet	Abdullah et al. (2021), FAO (2006), Moroda et al. (2018)
	3) Utilisation – Utilisation of food through adequate diet, clean water, sanitisation and health care to reach a state of nutritional wellbeing	

	4) Stability – To be food secure, household/individual must have access to adequate food at all times (p.3)	
Hunger	Hunger is "an uncomfortable or painful physical sensation caused by insufficient consumption of dietary energy. It becomes chronic when the person does not consume a sufficient number of calories (dietary energy) on a regular basis to lead a normal, active and healthy life" (p.88).	Otekunrin et al. (2020, p. 88)
Sustainable healthy diets	Sustainable healthy diets are "diets that promote all dimensions of individuals' health and well-being with minimal environmental pressure and impact. They are accessible, affordable, safe and equitable and are culturally acceptable" (p.1).	Otekunrin et al. (2021, p. 1)
Megatrends in food and agribusiness	The five megatrends in food and agribusiness are a less predictable planet, health in mind, choosey customers, one world (globalisation) and smarter food chain. 1) A less predictable planet with limited amount of natural resources, extreme weather events, increasing virulence of microorganisms and parasites, increasing customer demands for environmental and social credentials. 2) Healthy mind includes ageing population, increase chronic illness, increase awareness for better health and well-being, realising the importance of food safety and demand for healthy food. 3) Choosey customers refer to more wealthy middle class society, urbanisation, increase in demand for outside food consumption, demand for accurate information and vendor claims and increase willingness to switch. 4) One world with more connected global value chains, more exposure to food and beverage from other regions and culture, stiff global competition, increase biosecurity risks and increase susceptibility to supply shocks. 5) Smarter food chain includes more global food demand, increase food security concerns, high volume of big data and analytics, global connection and e-commerce solutions and vertical integration, decentralised and agile value chains (p.14).	Cole et al. (2018, p. 14)
Halalan Tayyiban Food	Halal food is food that is not haram (haram means what is prohibited to eat such as pork, carrion, blood and haram because something that is not in its substance such as food that is not permitted by its owner to be eaten) (p.53). Tayyiban food is food that is not rotten, expired or contained bacteria that could harm one's health if eaten (p. 53).	Guntur (2021, p.53): Adekunle & Filson (2020)
Food loss and food waste (Source reduction)	Food loss is lost supplies along the food chain between the producer and the market while food waste is discarding safe and nutritious foods.	Vågsholm et al. (2020).

General Consequences of Food Insecurity

In general, high food prices increases poverty and undernourishment (Manap, 2018). Food insecurity have impacts on the health of populations as a result of poor dietary intakes and low dietary patterns on food

consumption (Sulaiman et al., 2021). In poor countries, food insecurity results into child wasting, child stunting and child mortality and undernourishment (Maffra, 2017; Otekunrin et al., 2020; Otekunrin et al., 2021; Berchin et al., 2019; Sulaiman et al., 2021) in contrast to obesity in wealthy countries (Sulaiman et al., 2021). Another impact of food insecurity is on the health status involving high cases of anemia, hypertension and diabetes (Sulaiman et al., 2021). In addition, university students suffered from anxiety, poor concentration in classrooms and high risk of falling ill as a result of cutting the food budget while the elderly are prone to suffer from depression (Sulaiman et al., 2021).

Proposed Solutions to Food Insecurity Issues

Food security should be made the topmost policy priority by the governments to indicate its importance (Otekunrin et al., 2020; Berchin et al., 2019; Sulaiman et al., 2021; Cole et al., 2018; Endris Mekonnen & Kassegn Amede, 2022). Zero hunger and good nutrition must be incorporated into food policy revisions (Vågsholm et al., 2020) and more enforcement on Smart Climate Agriculture will be needed (Otekunrin et al., 2020). It is important also for nations to work together to achieve political stability and reduce conflicts (Otekunrin et al., 2020; Otekunrin et al, 2021; Vågsholm et al., 2020). Moreover, an improved food data collection and management can help in measuring the achievement of nutrition goals and policies accurately (Otekunrin et al., 2020; Otekunrin et al., 2021). Price stabilisation by the government might help to improve food security, reduce poverty and undernourishment. This is evidenced in Bangladesh (Manap, 2018). To reduce reliance on food import, there is a need to increase local food production (Manap, 2018) or to be self-reliant and at the smallest scale, family farms are big contributors in Brazil (Berchin et al., 2019). In Malaysia, families coped with food insecurity by switching to homecook food instead of eating out, preparing a plan before going out for food shopping trips, switching to cheaper alternatives and starting part-time businesses to generate additional incomes (Sulaiman et al., 2021). Among Canadian immigrants, new policies are needed to reduce the presence of information asymmetry between sellers and buyers as currently there are numerous halal certification bodies with various interpretation of the halal standards. A centralised agency to oversee the implementation of halal regulations will help to instill trust and improve the quality of the meat produced. To improve meat traceability, transparency and authenticity, producers can turn to the use of crypto-labelling by deploying the blockchain technology (Adekunle & Filson, 2020). Table 3 listed down some valuable suggestions and recommendations to tackle the food insecurity and hunger issues. This allows further comparisons between regions, culture, agricultural practices and policies to be done, resulting into some significant similarities and differences for learning purposes and academic contribution. Prosekov and Ivanova (2018) recommended that food production can be increased by increasing land fertility, using sea and ocean water resources, switching to solar power and doing research in genetic modification in crops and breeding (to improve pest resistance). This is also supported by Cole et al. (2018) and Maffra (2017).

Food security can be improved by reducing source reduction (food waste and food loss) from the farmers to the customers (Cole et al., 2018; Vågsholm et al., 2020). In the Gulf states, private vehicles such as the Gulf food security complex helped to drive innovations in food production (Henderson, 2022). These authorities realised on the importance of having secured food resources by justifying land acquisitions and win-win collaborations with foreign states, while at the same time encouraging publications and research and hosting conferences to strengthen their food independence. Thus, food security can be used as political tools to secure international presence (Henderson, 2022) and food loss reduction strategy is a well-reasoned political objective (Vågsholm et al., 2020). Measures such as social assistance programmes, strong regional partnerships and cross-border co-ordinations and financial assistance or domestic borrowings may help Africans to cope with income losses during pandemic experience in the future (Endris Mekonnen & Kassegn Amede, 2022).

Reducing Food Loss and Food Waste: Source Reduction

In fisheries and fish farming, 20-30% of the catch is lost at sea while another 10-15% is used as feed for fish farming resulting into protein and energy losses. In addition, only one third of the cereals and vegetables are used to feed humans while nearly half is used to feed animals (Vågsholm et al., 2020). Massive food recalls are another example of food waste. Food loss and waste indicated how labour, capital, water, energy, land and other resources in the food production are wasted. By eliminating global food waste, the food saved can feed an additional one billion people. According to Al Quran (Al-Isra': 26 & 27), "And render to the kindred their due rights, as (also) to those in want, and to the wayfarer; but squander not in the manner of a spendthrift. Verily spendthrifts are brothers of Satan; and Satan is to his Lord (himself) ungrateful." Food waste is an act that is abhorred in Islam, as it is a resemblance of the act of Satan or brothers of Satan.

Table 3. Food security strategy

Measure	Description	Author
Policy reform; Food policy	Food and nutrition security as topmost policy priority.	Otekunrin et al. (2020), Vågsholm et al. (2020)
Collaboration with stakeholders	Regulators need to work in collaboration with other key stakeholders at national as well as with private and development partners to deliver food and nutrition outcomes.	Otekunrin et al. (2020)
Incorporation of nutrition needs into agricultural policies	Incorporation of nutrition needs into agriculture policy, rural area development plans, social protection and education for implementation.	Otekunrin et al. (2020)
War and conflicts resolution	Working together to gain peace and reduce war and conflicts.	Otekunrin et al. (2020)
Embracing Climate Smart Agriculture	Practice Climate Smart Agriculture to achieve sustainable food security.	Otekunrin et al. (2020); Cole et al. (2018); Maffra (2017); Henderson (2022); Roubik et al. (2022)
Collection and management of current and relevant data	Collection and management of nutritional data for effective interventions.	Otekunrin et al. (2020); Otekunrin et al. (2021)
Women empowerment	Empowering women's groups in decision making and managing resources related to food, nutrition and healthcare; Improving diets of children and women. Reducing gender bias in land ownership.	Otekunrin et al. (2020); Otekunrin et al. (2021); Roubik et al. (2022)
Reducing food wastage – source reduction	Reducing food loss and food waste or capturing more of the produced food is an opportunity to improve food security and a business opportunity; Recovering food wastage is an opportunity to reduce production demand; Food loss is a major contributor to food wastage in developing countries while food waste is common in developed countries where food is lost at the retail and consumer end. Food recall due to safety issues is a food waste.	Cole et al. (2018), Vågsholm et al. (2020)
Food science and technology improvement	By using food preservation and stabilisation can help to extend products' shelf life.	Cole et al. (2018)
Good post-harvest handling practices	Good post-harvest handling practices such as logistics and infrastructure help to prevent the loss of fresh produce.	Cole et al. (2018)
New extraction technologies	Technologies such as ultrasound can improve the recovery of oil from biomass. Preservation technique such as fermentation and separation technologies like forward osmosis can create new value-added food ingredients and bioactives from food loss and food waste.	Cole et al. (2018)
Setting up food bank	The setting up of food banks in various countries help to rescue and redistribute nutritious foods to vulnerable groups. Protection of food donors is needed from liability of donating foods to non-profit organisations.	Cole et al. (2018), Vågsholm et al., 2020
Better access to food information	Customers demand for transparent information involving environmental credentials and food provenance. With digital technology and the Internet of Things (IoT), customers can get access to information and leaner production is possible.	Cole et al. (2018)
Reducing over-consumption of food, educating customers about healthy eating	While trying to improve food security, at the same time obesity is a challenge. Educating people to reduce over-consumption of food and practice healthy eating can help to improve food security. At the same time, healthier processed food will be needed. There will be changes in lifestyle with more physical activities.	Cole et al. (2018); Roubik et al. (2022)
Development of smart biofuel policies and technologies	New technologies to produce biofuels from plants as alternative fuel use.	Cole et al. (2018), Vågsholm et al. (2020)
Pathways to increase food production and environmental protection	1) Expanding land resources used for agricultural production with ways to capture and store rainfall; 2) Combining weather prediction and hydrological model to make better forecasting of soil moisture, water requirements for crops and efficient use of irrigation water (the use of real-time irrigation app and	Cole et al. (2018), Vågsholm et al., (2020); Roubik et al. (2022)

	soil water sensor); 3) Expanding aquaculture as food source; 4) Crop and livestock genetic improvement to fight against pest and diseases and enhance crop yields; 5) Minimising soil and water degradation by minimising the use of input and water in production; 6) Minimising climate change impact such as the adoption of methane inhibitors in livestock sector.	
Food insurance	Premiums paid to ensure access to nutritious food and prevent famine and food-borne illnesses.	Vågsholm et al. (2020).
Novel IT and AI solutions	The use of predictive models, machine learning, neural network and expert system to accurately forecast food demand. This is to help producers and retailers to prevent food wastage and stockout problem (inaccurate forecasting of sales due to price, weather, season, events and festivals, promotions and discounts, competitions, shelf life and number of customer fluctuations).	Vågsholm et al. (2020)
Intelligent labelling and sensors	The use of sensors for freshness, food packaging integrity, time-temperature indicators and identification tags such as RFID to reflect good foods for human consumption.	Vågsholm et al. (2020)
Diets rich in plant-based foods with fewer animal source food	Diets rich in plant-based foods with fewer animal source foods confer both health and environmental benefits.; better antibodies.	Vågsholm et al. (2020); Rubik et al. (2022)
Futuristic use of technology	Futuristic use of technology such as cryto-labelling in blockchain to ensure food traceability, transparency and authenticity especially in halal food production	Adekunle & Filson (2020)

Food Safety Assurance

Eating is considered a form of worship in Islam. Halal food is produced based on the Islamic dietary standard derived from Al-Quran and Hadith as well as the examples as shown by Prophet Muhammad SAW. In Islam, what is permitted is 'halal' and what is prohibited is 'haram'. To be considered halal, food must not break the Islamic dietary standards as the inclusion of prohibited animals and their byproducts. Animals must be slaughtered in a specific humane manner. The slaughtering process is a major component of halal meat and having halal food is one way to ensure only desirable meats are in the market. Other than ensuring the safety of the food, this requires the mass production to be significantly reduced (Adekunle & Filson, 2020). According to Al-Quran (Al-Baqarah: 168), "O mankind eat from whatever is on earth (that is) lawful and good and do not follow the footsteps of Satan. Indeed, he is to you a clear enemy". This brings to the 'halalan tayyiban' concept (Table 2) which has been repeated four times in Al-Quran including surah Al-Maidah verse 88, Al-Anfal verse 69 and al-Nahl verse 114. This concept is itself a standard (policy) and is applicable to all industries including food bank and food business operators.

Grains as Symbol of Good Deeds (Wealth Creation) and Human Civilisation

Al-Quran (Al-Baqarah: 261) mentioned: "The example of those who spend their wealth in the way of Allah is like a seed [of grain] which grows seven spikes; in each spike is a hundred grains. And Allah multiplies [His reward] for whom He wills. And Allah is all-Encompassing and Knowing". The Almighty has chosen grains (plants) among other things to represent good behaviour such as sharing and giving, from which one's wealth will grow based on the giving and sharing one has done, it is an assurance by Him. This symbolises how an individual can grow as a unified whole in healthy body, mind and spirit as exemplary characters to begin simply from what is consumed at the dining table (Guntur, 2021). This is probably one of the foundations that made up the civilised nations.

Limitation

There are limitations to this study especially in the aspect of article selection. The review on literature of food security involved only peer-reviewed journal articles while other sources of knowledge sharing that might exist in proceedings and reports are not considered due to the difficulty to access them and many of them are

unpublished. In addition, even though a few databases are used to search for the articles, only 18 articles were shortlisted for analysis due to time challenge. This constraint may reduce the access to the more recent articles for this study. Limitations are also related to the generalisation of the reviewed articles where the instruments used in the studies or the recommendations may not be suitable to be replicated in whole or without modification. Besides, current studies mostly focused on issues, problems, challenges and trends involving food security. However, other aspects of food security such as food co-operations and food distributions can be explored to give deeper understanding towards food security issues worldwide.

Conclusion and Future Direction

Through the analysis in this study, food security issues are becoming global concerns where many research activities were conducted to strengthen the understanding of this problem. Since Malaysians have never experienced any global food shortage previously, thus there is a need to learn from other countries' food insecurity experience especially after the COVID-19 pandemic. Nevertheless, it is important to understand that the main root of the problem may differ between countries and the solution that is effective in one country may not be feasible in another country. However, the food security dimension (Table 1) in this study was aimed for helping academics, regulators and authorities to understand the current issues and challenges in food security. Moreover, this study could help to encourage more research activities pertaining to food security in different contexts in order to fill in the gaps in the current literature.

Scientific Ethics Declaration

The authors declare that the scientific ethical and legal responsibility of this article published in EPSTEM journal belongs to the authors.

Acknowledgements or Notes

* This article was presented as an oral presentation at the International Conference on Basic Sciences, Engineering and Technology (www.icbaset.net) conference held in Marmaris/Turkey on April 27-30, 2023.

References

Abdul Manap, N. M., & Ismail, N. W. (2019). Food security and economic growth. *International Journal of Modern Trends in Social Sciences*, 108–118.

Abdullah, R. G., Mersat, N. I., & Wong, S. K. (2021). Implications of covid-19 pandemic on household food security: Experience from Sarawak, Malaysia. *International Journal of Business and Society*, *22*(1), 1–13.

Adekunle, B & Filson, G. (2020). Understanding halal food market: Resolving asymmetric ınformation. *Food Ethics*, *5*, 1-22.

Berchin, I. I., Nunes, N. A., de Amorim, W. S., Zimmer, G. A. A., da Silva, F. R., Fornasari, V. H., & de Andrade, J. B. S. O. (2019). The contributions of public policies for strengthening family farming and increasing food security: The case of Brazil. *Land Use Policy*, *82*, 573-584.

Cole, M. B., Augustin, M. A., Robertson, M. J., & Manners, J. M. (2018). The science of food security. *NPJ Science of Food*, *2*(1), 1-8.

Department of Statistics Malaysia. (2022). Consumer price index Malaysia April 2022. https://www.dosm.gov.my/v1/index.php?r=column/cthemeByCat&cat=106&bul_id=aSsvZXluWFZZaEZQYk9nOGFqZWRzdz09&menu_id=bThzTHQxN1ZqMVF6a2I4RkZoNDFkQT09

Department of Statistics Malaysia. (2022). Consumer price index Malaysia November 2022. https://www.dosm.gov.my/v1/index.php?r=column/cthemeByCat&cat=106&bul_id=WWx2a3UxcklKQ3NraFBHSkhhZXRWdz09&menu_id=bThzTHQxN1ZqMVF6a2I4RkZoNDFkQT09

Economist Impact (2022). Global food security ındex 2022. Retrieved on January 21, 2023 from https://impact.economist.com/sustainability/project/food-security-index/

Endris Mekonnen, E., & Kassegn Amede, A. (2022). Food insecurity and unemployment crisis under COVID-19: Evidence from sub-Saharan Africa. *Cogent Social Sciences*, *8*(1), 2045721.

European Parliament. (2020). Climate change and its impact on food and nutrition security. Retrieved on February 19, 2023 from https://www.europarl.europa.eu/RegData/etudes/BRIE/2020/658209/IPOL_BRI(2020)658209_EN.pdf

Fitzpatrick, K. M., Harris, C., Drawve, G., & Willis, D. E. (2021). Assessing food insecurity among US adults during the COVID-19 pandemic. *Journal of Hunger and Environmental Nutrition*, *16*(1), 1–18.

Food and Agriculture Organisation (2006). Food security. *policy brief*, *2*, 1-4. Retrieved on Sept 30, 2022 from file:///C:/Users/ASUS/Downloads/pdf_Food_Security_Cocept_Note.pdf

Guntur, M.(2021). Al Quran teach the ımportance of taking care of health physical: Tafseer Surat Al-Baqarah. *AKADEMIK Jurnal Mahasiswa Humanis*, *1*(2), 50-58.

Henderson, C. (2022). The power of food security. *Globalizations*, 1-13.

Maffra, L. (2017). Food sovereignty: sustainable solution to world hunger and climate change. *Ámbitos: Revista Internacional de Comunicación, 37, 1-11*.

Manap, N.M.A. (2018).The impact of world food price on food insecurity in selected Asean countries. *Journal of Education and Social Sciences*, *10*(1), 90-97.

Moroda, G. T., Tolossa, D., & Semie, N. (2018). Food insecurity of rural households in boset district of Ethiopia: a suite of indicators analysis. *Agriculture & Food Security*, *7*(1), 1-16.

Otekunrin, O. A., Otekunrin, O. A., Sawicka, B., & Ayinde, I. A. (2020). Three decades of fighting against hunger in Africa: Progress, challenges and opportunities. *World Nutrition*, *11*(3), 86-111.

Otekunrin, O. A., & Otekunrin, O. A. (2021). Healthy and sustainable diets: Implications for achieving SDG2. *Zero Hunger. Encyclopedia of the UN Sustainable Development Goals; Springer: Cham, Switzerland*, 1-17.

Prosekov, A. Y., & Ivanova, S. A. (2018). Food security: The challenge of the present. *Geoforum*, *91*, 73-77.

Roubík, H., Lošťák, M., Ketuama, C. T., Procházka, P., Soukupová, J., Hakl, J., ... & Hejcman, M. (2022). Current coronavirus crisis and past pandemics-What can happen in post-COVID-19 agriculture?. *Sustainable Production and Consumption*, *30*, 752-760.

Sulaiman, N., Yeatman, H., Russell, J., & Law, L. S. (2021). A food insecurity systematic review: experience from Malaysia. *Nutrients*, *13*(3), 945.

Tapsir, S., Elini, E. E., Roslina, A., Noorlidawati, A. H., Hafizudin, Z. M., Hairazi, R., & Rosnani, H. (2019). Food security and sustainability: Malaysia agenda. *Malaysian Applied Biology*, *48*(3), 1-9.

Vågsholm, I., Arzoomand, N. S., & Boqvist, S. (2020). Food security, safety, and sustainability—Getting the trade-offs right. *Frontiers in Sustainable Food Systems*, *4*(February), 1–14.

Willett, W., Rockström, J., Loken, B., Springmann, M., Lang, T., & Vermeulen,S., et al. (2019). Food in the Anthropocene: the EAT-Lancet Commission on healthy diets from sustainable food systems. *Lancet 393*, 447–492.

World Food Summit. (1996). Report of the World Food Summit. Retrieved on February 19, 2023 from https://www.fao.org/3/w3548e/w3548e00.htm

World Health Organization. (2019). *Sustainable healthy diets: guiding principles*. Food & Agriculture Org.

World Health Organization. (2019). *The state of food security and nutrition in the world 2019: safeguarding against economic slowdowns and downturns* (Vol. 2019). Food & Agriculture Org.

Author Information

Hayati Yusof
Universiti Tunku Abdul Rahman
Kampar Campus, Jalan Universiti
Bandar Barat, 31900 Kampar
Perak, Malaysia.
Contact e-mail: *hayati@utar.edu.my*

Mai Farhana Mior Badrul Munir
Universiti Tunku Abdul Rahman
Kampar Campus, Jalan Universiti
Bandar Barat, 31900 Kampar
Perak, Malaysia.

Zulnurhaini Zolkaply
Universiti Tunku Abdul Rahman
Kampar Campus, Jalan Universiti
Bandar Barat, 31900 Kampar
Perak, Malaysia.

Muhammad Ashraf Anuar
Universiti Tunku Abdul Rahman
Kampar Campus, Jalan Universiti
Bandar Barat, 31900 Kampar
Perak, Malaysia.

To cite this article:

Yusof, H., Mior Badrul Munir, M.F., Zolkaply, Z. & Anuar, M.A. (2023). Global food security strategies, issues and challenges. *The Eurasia Proceedings of Science, Technology, Engineering & Mathematics (EPSTEM), 22*, 33-47.

The Eurasia Proceedings of Science, Technology, Engineering & Mathematics (EPSTEM)
ISSN: 2602-3199

The Eurasia Proceedings of Science, Technology, Engineering & Mathematics (EPSTEM), 2023

Volume 22, Pages 48-58

ICBASET 2023: International Conference on Basic Sciences, Engineering and Technology

A Systematic Snapshot of Software Outsourcing Challenges

Issam JEBREEN
Zarqa University

Eman AL – QBELAT
Zarqa University

Abstract: Outsourcing software development projects can be challenging, and there are several common challenges that organizations face. A study was conducted with a sample of 46 papers on outsourcing challenges, and the results show that there are several common challenges faced by organizations when outsourcing software development projects. Poor outsourcing relationship was identified as the most significant challenge, with 35% of the papers referencing it. Lack of quality was the second most significant challenge, with 33% of the papers referencing it. Language and cultural differences were the third most significant challenge, with 24% of the papers referencing it. Non-competitive price was another challenge faced by organizations, with 21% of the papers referencing it. Poor coordination and communication were also identified as a challenge, with 21% of the papers referencing it. Opportunistic behaviour, lack of contract negotiation, inadequate user involvement, and constraints due to time zone were also challenges faced by organizations. Other challenges faced by organizations included poor project management, lack of technical capabilities, vendor employee high turnover, poor requirement specification, IPR issues, poor management of budget, schedule, and delay, geopolitical and country instability, the difference in development methodologies, failure to manage end-user expectations, and poor monitoring and control. In conclusion, outsourcing software development projects can be challenging, but organizations can mitigate these challenges by selecting the right outsourcing partner, having a well-defined contract and clear communication, having a clear understanding of the requirements, and implementing effective project management practices.

Keywords: Software outsourcing, Vendor, Outsourcing challenges, Quality model, Continent, Country, Global outsourcing, IT Workforce Outsourcing.

Introduction

Outsourcing has been a topic of discussion for many decades, and Ross Perot is considered one of the pioneers of the concept. The idea behind outsourcing is to transfer non-core business activities to an external provider, in this case, a software development company, in order to reduce costs, access new skills and talent, and improve the quality of products. In today's highly competitive business environment, software outsourcing has become a popular strategy for IT companies to gain a competitive advantage. By outsourcing certain software development activities, companies can take advantage of the lower labor costs, expertise, and improved efficiency offered by outsourcing firms. This allows IT companies to focus on their core competencies and invest their resources into areas where they can differentiate themselves from their competitors.

However, as with any business strategy, there are also challenges associated with software outsourcing that need to be considered and managed effectively. The systematic literature review you conducted highlights the importance of managing outsourcing relationships in order to ensure the desired quality of software development work is met, and that the challenges encountered in SDO can vary based on specific circumstances.

Software Development Outsourcing (SDO) and Global Software Engineering (GSE) are techniques used to create and develop high-quality software products at a lower cost in low-wage countries. By outsourcing software development tasks, companies can take advantage of the expertise and lower labor costs offered by external software development organizations.

In recent years, there has been a trend towards using open-source software in industrial software development, which means that the industrial vendor needs to evaluate the quality of the open-source product before delivering it to the user. Ensuring the quality of both the internal and external aspects of the product is a key factor in the success of software outsourcing.

The IT outsourcing market is expected to grow significantly in the coming years, according to a recent research report by Statista. The "IT Outsourcing Market by Service, End-user, and Geography - Projected and Analysis 2020-2024" report projects that the IT outsourcing market will expand by USD 98 billion over the forecast period of 2020-2024. This highlights the growing demand for outsourcing services and the potential for growth in the industry.

Software outsourcing does have a poor reputation in some cases due to the difficulties in finding the right balance between cost and quality. There are several challenges associated with outsourcing software development, including:

- Communication barriers: Different time zones, language barriers, and cultural differences can make it difficult for outsourced software development teams to effectively communicate with each other.
- Misaligned goals and expectations: Outsourced software development teams may have different goals and expectations compared to the company that is outsourcing the work, which can lead to misunderstandings and project failures.
- Quality control: Ensuring the quality of software development work can be difficult when outsourcing, as the outsourced team may have different processes and standards compared to the company that is outsourcing the work.
- Dependency on external vendors: Companies that outsource software development work become dependent on their external vendors, which can create risks if the vendor is not reliable or if the relationship between the company and vendor breaks down.
- Intellectual property issues: There may be legal and intellectual property issues associated with outsourcing software development work, such as ownership of the software and protection of confidential information.

It's important for companies to carefully consider these challenges and take steps to mitigate them when outsourcing software development work. This may include implementing clear communication processes, setting clear goals and expectations, and carefully evaluating potential outsourcing partners to ensure they have the skills and experience needed to deliver high-quality software development work.

Research Methodology

Our research methodology was designed with protocols to quickly address the relevant themes. In the initial phase, we selected popular search phrases related to Software Development Outsourcing (SDO), such as systematic literature reviews and mapping studies. We chose the Systematic Literature Review (SLR) as the data collection method as it is an unbiased method of collecting data. This approach helps in the systematic collection of information from the original studies included. The key steps of the methodology are depicted in Figure 1

Research Questions

The objective of this research is to shed light on an overlooked aspect of the scientific literature on outsourcing. The focus of this study is on the challenges faced in outsourcing. The research questions related to the topic of this study is “What are the challenges associated with software outsourcing?” The main questions are aimed at providing answers to the main topic of this research, which is the challenges of outsourcing and its impact on product quality. This study also aims to identify the major challenges of outsourcing and categorize them accordingly

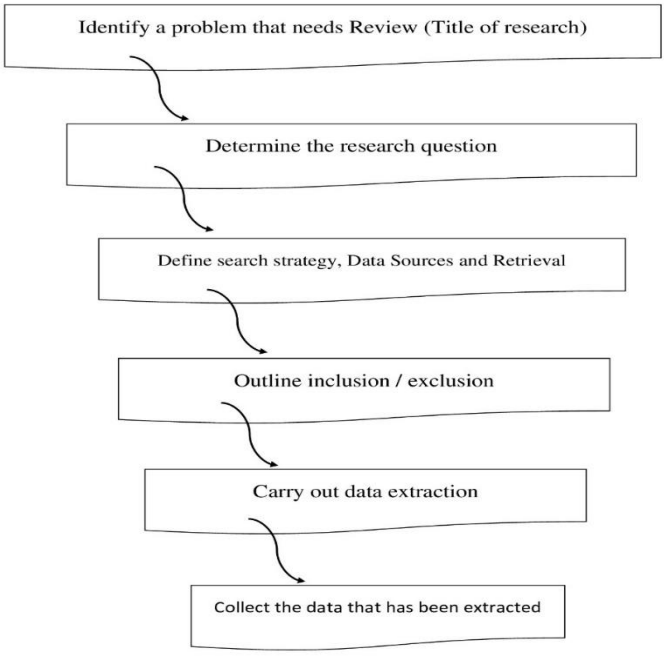

Figure 1. The SLR protocol

Search Strategy

Our research strategy was designed with procedures to efficiently address the relevant themes. The first step involved selecting popular search phrases related to Software Development Outsourcing (SDO), such as systematic literature reviews and mapping studies. The scope of the study was then established in the second step. The Scopus/IEEE database was instrumental in updating and maintaining the usefulness of the keywords. The key keywords are listed in Figure 2.

("software development outsourcing (SDO)" OR "Software outsourcing" OR" vendor "OR "Outsourcing challenges" OR "Quality" OR "ISO 9126 quality model" OR" Continent" OR" country" OR "global outsourcing "OR" IT Workforce Outsourcing")

Figure 2. List of keywords used as search

Data Sources and Retrieval

We chose numerous digital repositories for this study listed below:

- "IEEE Xplore (http://ieeexplore.ieee.org)"
- "ACM Digital Library (http://dl.acm.org)"
- "Springer Link (link.springer.com)"
- "Science Direct (http://www.sciencedirect.com)"
- "Google Scholar (scholar.google.com)"
- "IET-digital libraries (www.theiet.org)"

Furthermore, we limited the number of keywords to achieve the focus of our study and locate relevant sources in the field. The search was conducted between 2019 and 2022 and focused on peer-reviewed titles, abstracts, and

keywords in the literature. Based on the initial results, we conducted additional research. The results of the search were then promptly considered in the inclusion process.

Papers Selection Criteria

This section contains two sub-sections: Inclusion criteria and Exclusion criteria. To systematically evaluate related primary studies published in the software engineering domain, we established inclusion and exclusion criteria.

Inclusion criteria: (1) Articles published in a journal, as a conference paper, or as a book chapter, (2) English-language papers, (3) primary studies relevant to the research questions, (4) Papers with findings based on empirical research, (5) Publications that are not focused on the final selection of primary studies (review text), (6) Primary studies that examine outsourcing issues.

Exclusion criteria: (1) Articles not published in English, (2) Articles that do not meet the inclusion criteria, (3) Articles that do not analyze the success factors of software development outsourcing (SDO), (4) Articles written in a language other than English.

Our search process was streamlined by limiting our scope through large databases and by following a peer-review process that began with titles, followed by abstracts, and finally keywords of the publications. Our goal was to expand our database with additional primary studies to meet the scope of our investigation. The final steps included removing duplicate studies and storing the remaining papers for full text review. Figure 3 summarizes the successive procedures and processes of our investigation and shows the final number of papers found in our search.

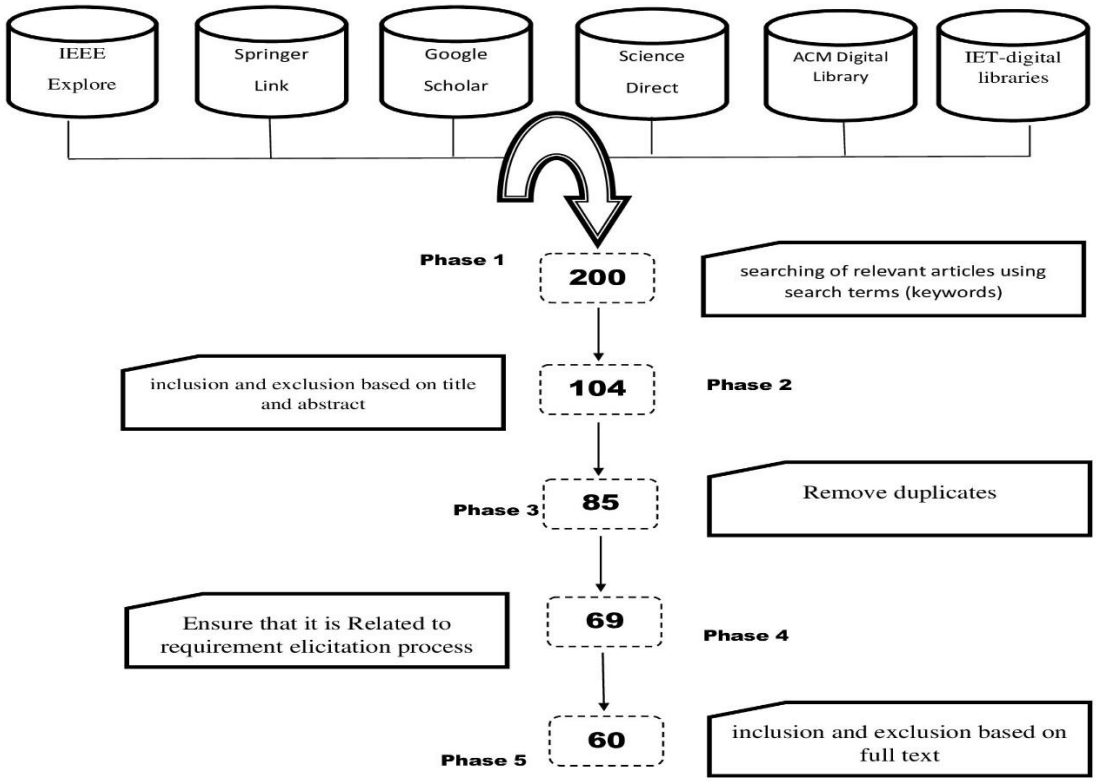

Figure 3. Process of Inclusion and exclusion

Results and Discussion

The section presents the categorization of previous studies and our new categorization scheme for the 200 papers. The statistical categorization is based on publication year, target countries, research method types,

publishers, and article types, while the main categorization focuses on the challenges of outsourcing. The factors and sub-factors in the main work are also included in the classification.

Reporting the Review

The results of the search process are presented in Table 1. Out of the 200 papers found using the major search string, only 46 met the criteria related to the requirement elicitation process. The duplicates were removed, leaving us with a final total of 46 papers. The table shows the distribution of primary study publication years between 2019 and 2022, indicating that research on software outsourcing is still on the rise and will continue to be a significant topic in the future.

Table 1. Summary of selected papers

Source	IEEE	IEEE (Open with money)	ACM Digital Library	Springer Link	Science Direct	IET-digital libraries
Total results retrieved	90	12	20	40	20	18
Exclusion based on title and abstract	50	10	14	19	6	5
Ensure that it is Related to the requirement elicitation process	28	9	12	10	5	5
Exclusion based on full text (Total exclusion)	29	7	7	9	4	4
Overall selection			200			
Final selection			46			

Software Outsource challenges classification

We have categorized the research from previous stages into 46 papers, as previously mentioned, and based on the challenges outlined by (Usman, Khan et al. 2020). In his research, they highlight the challenges that arise during outsourcing into 19 categories. The distribution of these challenges is as follows:

- Weak coordination and communication.
- Bad Outsourcing Relationship
- opportunistic behavior
- Linguistic and cultural differences
- Not negotiating the contract
- Bad project management
- Poor monitoring and control
- Intellectual property rights issues
- lack of technical capabilities
- geopolitical and country instability
- Inferior requirements specification
- The difference in development methodologies
- Fail to manage end-user expectations
- High sales employee turnover
- Restrictions due to time zone
- Poor Mgt. Budget, schedule and delay
- poor quality
- Insufficient user participation
- non-competitive price

Quality is a crucial aspect in software engineering and is often defined as meeting the customer's expectations and standards. The definition provided by the IEEE describes quality as the degree to which a system, component, or process satisfies the stated standards. However, achieving high quality in software development outsourcing, particularly in global software development, is a challenging task due to many factors. The most important factor being poor requirements collection from customers, which is extremely difficult in comparison to internal software development. Research by (Usman, Khan et al. 2020) also emphasized the importance of meeting high quality standards as a crucial turning point in the success of the project. Our literature review showed that the relationship between bad outsourcing and poor quality is a common challenge.

The table 2 presents the challenges faced in outsourcing, based on 46 total papers. The most prevalent challenge is poor outsourcing relationship, affecting 35% of the papers and cited in references 1-16. The second most significant challenge is the lack of quality, affecting 33% of the papers and cited in references 1, 7, 8, 10, 17-27. Language and cultural differences also present a significant challenge, affecting 24% of the papers and cited in references 3, 4, 8, 11, 13, 16, 17, 22, 28-30. Non-competitive price is another significant challenge, affecting 21% of the papers and cited in references 8, 11, 17, 20, 21, 23, 28, 31-33.

Poor coordination and communication is also a significant challenge, affecting 21% of the papers and cited in references 2, 3, 8, 28, 34-39. Opportunistic behavior is cited as a challenge in 15% of the papers, referenced in references 8, 16, 29, 31, 35, 40, 41.

Lack of contract negotiation, inadequate user involvement, constraints due to time zone, poor project management, lack of technical capabilities, vendor employee high turnover, and poor requirement specification are also noted as challenges, each affecting around 10-15% of the papers. IPR issues, poor management of budget, schedule, and delay, geopolitical and country instability, the difference in development methodologies, failure to manage end-user expectations, and poor monitoring and control are also noted as challenges but affecting a smaller proportion of the papers.

Table 2. Challenges classification.

Challenge	Total papers = 46		
	#Challenges	%	Reference
Poor outsourcing relationship	16	35%	(Karimi-Alaghehband and Rivard 2019, Khader and Zein 2019, Wang and Wang 2019, Ali, Huang et al. 2020, Hanafizadeh and Zareravasan 2020, Usman, Khan et al. 2020, Deng, Wang et al. 2021, Drzewiecki 2021, Hussein and Zein 2021, Jain 2021, Jebali, Sassi et al. 2021, Juvekar 2021, Kaveh Pishghadam and Esmaeeli 2021, Khan, Niazi et al. 2021, Elnakeep, Helal et al. 2022, Kocot and Kocot 2022)
Lack of quality	15	33%	(Saqib , Malik and Velan 2019, Ali, Huang et al. 2020, Sharma, Burtsev et al. 2020, Usman, Khan et al. 2020, Jain 2021, Juvekar 2021, Qureshi, Khan et al. 2021, Rahman, Raza et al. 2021, Sahoo and Goute 2021, Sloniec 2021, Suresh and Ravichandran 2021, Veloso, Sousa et al. 2021, Wong 2021, Ren, Yuan et al. 2022)
Language and cultural differences	11	24%	(Saqib , Karimi-Alaghehband and Rivard 2019, Khader and Zein 2019, Malik and Velan 2019, Ali, Huang et al. 2020, Cheng, Fu et al. 2021, Drzewiecki 2021, Kocev 2021, Mehmood and Zulfqar 2021, Elnakeep, Helal et al. 2022, Kocot and Kocot 2022)
Non-competitive price	10	21%	(Karimi-Alaghehband and Rivard 2019, Malik and Velan 2019, Ali, Huang et al. 2020, Sharma, Burtsev et al. 2020, Cheng, Fu et al. 2021, Orlu 2021, Paudel and Kumar 2021, Sahoo and Goute 2021, Lee, Kang et al. 2022, Ren, Yuan et al. 2022)
Poor coordination and communication	10	21%	(Usman and Khan 2018, Ali, Huang et al. 2020,

			Balcet and Ietto-Gillies 2020, ALAGAH 2021, Androsova and Simonenko 2021, Cheng, Fu et al. 2021, DA, ÓRGÃO et al. 2021, Deng, Wang et al. 2021, Drzewiecki 2021, Santos and Silva 2021)
Opportunistic behaviour	7	15%	(Ali, Huang et al. 2020, Androsova and Simonenko 2021, Kocev 2021, Legesse 2021, Looi and Szepan 2021, Kocot and Kocot 2022, Lee, Kang et al. 2022)
Lack of contract negotiation	7	15%	(Karimi-Alaghehband and Rivard 2019, Khader and Zein 2019, Ali, Huang et al. 2020, Androsova and Simonenko 2021, Kaveh Pishghadam and Esmaeeli 2021, Orlu 2021, Suresh and Ravichandran 2021)
Inadequate user involvement	6	13%	(Usman and Khan 2018, Ali, Huang et al. 2020, Androsova and Simonenko 2021, Orlu 2021, Santos and Silva 2021, Ren, Yuan et al. 2022)
Constraints due to time zone	6	13%	(Kazmi, Hafeez et al. 2018, Malik and Velan 2019, Ali, Huang et al. 2020, ALAGAH 2021, Drzewiecki 2021, Mehmood and Zulfqar 2021)
Poor project management	5	10%	(Ali, Huang et al. 2020, Juvekar 2021, Orlu 2021, Paudel and Kumar 2021, Lee, Kang et al. 2022)
Lack of technical capabilities	5	10%	(Ali, Huang et al. 2020, Androsova and Simonenko 2021, Wong 2021, Elnakeep, Helal et al. 2022, Lee, Kang et al. 2022)
Vendor employee high turnover	5	10%	(Ali, Huang et al. 2020, Jain 2021, Ravi and Donawa 2021, Sahoo and Goute 2021, Elnakeep, Helal et al. 2022)
Poor requirement specification	4	8%	(Ali, Huang et al. 2020, Kaveh Pishghadam and Esmaeeli 2021, Rahman, Raza et al. 2021, Rana and Mondal 2021)
IPR Issues	4	8%	(Usman and Khan 2018, Karimi-Alaghehband and Rivard 2019, Ali, Huang et al. 2020, Androsova and Simonenko 2021)
Poor Mgt. of budget, schedule & delay	4	8%	(Ali, Huang et al. 2020, Orlu 2021, Rehman and Khan 2022, Thanh, Gam et al. 2022)
Geopolitical and country instability	3	5%	(Karimi-Alaghehband and Rivard 2019, Paudel and Kumar 2021, Elnakeep, Helal et al. 2022)
The difference in development methodologies	3	5%	(Ali, Huang et al. 2020, Orlu 2021, Rahman, Raza et al. 2021)
Failure to manage end-user expectations	3	5%	(Karimi-Alaghehband and Rivard 2019, Ali, Huang et al. 2020, Jain 2021)
Poor monitoring and control	3	5%	(Ali, Huang et al. 2020, Orlu 2021, Lee, Kang et al. 2022)

Classifications based on Years of Publication

Table 3 displays the distribution of these papers based on their publication year, which ranges from 2019 to 2022. The majority of the papers were published in 2021, with 31 articles, followed by 6 articles in 2020, 5 articles in 2019, and only 4 articles in 2022. The low number of articles in 2022 may be due to the limited research conducted in the first 6 months of the year. This trend of increasing publication in the field of IT outsourcing research indicates a growing interest in the subject, which has evolved over time since the 1990s.

Table 3. Based on publication year

Year	Number of Papers
2019	5
2020	6
2021	31
2022	4
Total	46

Classifications Based on Research Methods

Our findings indicate that survey method were the most commonly used, accounting for 23 papers out of the total. Additionally, case studies were used in 9 papers, while empirical research was the method of choice for 6 papers. Only a small proportion of the papers utilized other methods, such as qualitative studies.

Table 4. Based on research method

Research Method	Number of Papers
Survey method	23
Case Study	9
empirical research	6
Qualitative Studies	6
Other Methods	2

Classifications depending on the Nations of Interest

Figure 4 displays the distribution of 46 papers across 26 countries. The United States was among the countries with the highest number of research papers on outsourcing, with an average of 8 papers out of 46. Meanwhile, Pakistan came in second place with an average of 6 research papers. The world map as shows in Figure 4 was color-coded to indicate the countries that had a significant interest in researching outsourcing challenges, with yellow being the most prominent color, as indicated by the arrow. This visual representation highlights the countries that were most concerned about outsourcing challenges and the need for solutions to overcome these challenges.

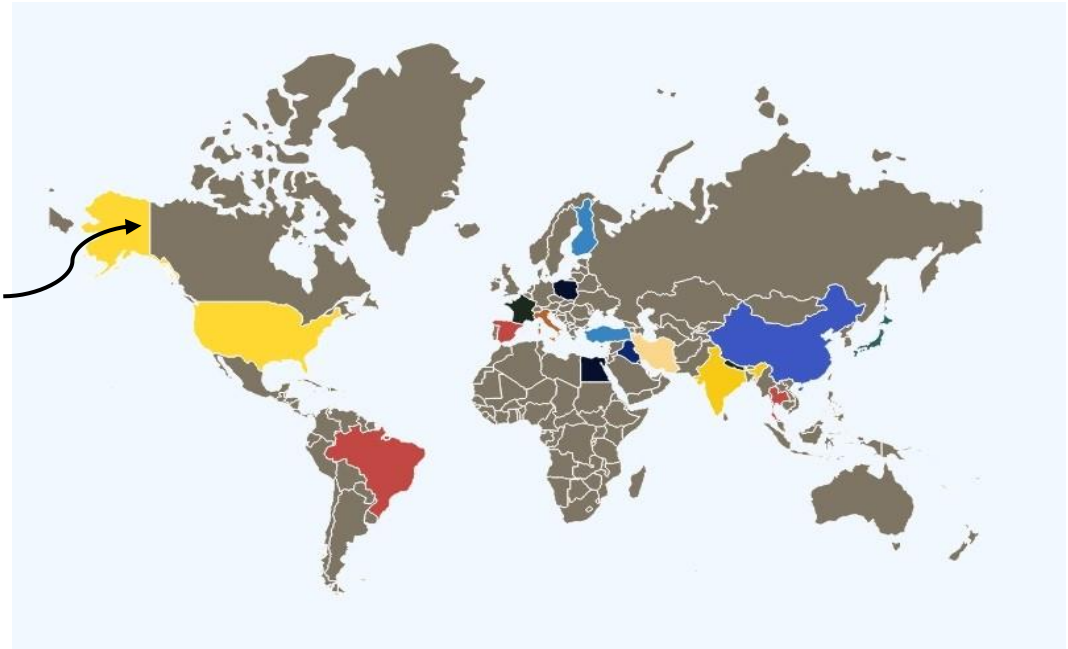

Figure 4. Nations of interest classification

Conclusion

The research analyzed 46 papers related to outsourcing in the field of information technology. The papers were collected from 200 articles in databases and digital libraries, with a focus on the years 2019 to 2022. The research found that the number of papers in 2021 was the highest, with 31 articles, while the number in 2022 was the lowest with only 4 papers. The United States was found to be one of the countries with the most research on outsourcing, followed by Pakistan with an average of 8 research papers.

The 46 papers were categorized based on the challenges identified by (Usman, Khan et al. 2020). The most challenging issue found in the research was poor outsourcing relationship, affecting 35% of the papers and cited

in references. The second most significant challenge is the lack of quality, which had a recurrence rate of 33%. The 19 challenges identified were divided into two categories, those related to human resources and logistical. Out of the 19 challenges, 5 were considered critical as they had a frequency a higher and significantly impacted the product's quality when delivered.

Quality is a difficult problem in software development outsourcing, with many factors influencing it, such as poor requirements collection. Quality in software engineering is defined as meeting customer needs and is a crucial factor in the success of a project. Software quality will never be perfect, but prioritizing it is important as the biggest cause of software failure is poor development quality.

Scientific Ethics Declaration

The authors declare that the scientific ethical and legal responsibility of this article published in EPSTEM journal belongs to the authors.

Acknowledgements or Notes

* This article was presented as oral presentation at the International Conference on Basic Sciences, Engineering and Technology (www.icbaset.net) held in Marmaris/Turkey on April 27-30, 2023.

References

Alagah, A. (2021). Strategic human resource outsourcing, enterprise resource planning, and performance: a systematic review. *World Bulletin of Management and Law 5*, 15-22.

Ali, S., et al. (2020). A framework for modelling structural association amongst barriers to software outsourcing partnership formation: An interpretive structural modelling approach. *Journal of Software: Evolution and Process 32*(6): e2243.

Androsova, I. & Simonenko, E. (2021). *Strategic possibilities of IT-outsourcing in the organizations activities in the context of globalization.* SHS Web of Conferences, EDP Sciences.

Balcet, G. & Ietto-Gillies, G. (2020). Internationalisation, outsourcing and labour fragmentation: the case of FIAT. *Cambridge Journal of Economics, 44*(1), 105-128.

Cheng, X., et al. (2021). Determinants of trust in computer-mediated offshore software-outsourcing collaboration. *International Journal of Information Management, 57*, 102301.

DA, O., et al. (2021). The six CSF of information technology outsourcing in municipal government agencies. *Revista Alcance, 28*(1), 97-117.

Deng, C.-P., et al. (2021). Organizational agility through outsourcing: Roles of IT alignment, cloud computing and knowledge transfer. *International Journal of Information Management, 60*, 102385.

Drzewiecki, J. (2021). Empirical verification of relationship between organizational boundaries, business model change and outsourcing scope and maturity. *European Research Studies Journal Volume XXIV, Special Issue 1*, 1287-1311.

Elnakeep, E., et al. (2022). Models and frameworks for is outsourcing structure and dimensions: A Holistic Study. *Proceedings of International Conference on Emerging Technologies and Intelligent Systems: ICETIS 2021, 1*, Springer.

Hanafizadeh, P. & Zareravasan, A. (2020). A systematic literature review on IT outsourcing decision and future research directions. *Journal of Global Information Management (JGIM), 28*(2), 160-201.

Hussein, M. A. & S. Zein (2021). Quadruple factors interference and its effects on quality of outsourcing testing: A case study. *International Journal, 10*(1).228-236.

Jain, V. (2021). Information technology outsourcing chain: Literature review and implications for development of distributed coordination. *ACADEMICIA: An International Multidisciplinary Research Journal, 11*(11), 1067-1072.

Jebali, A., et al. (2021). Secure data outsourcing in presence of the inference problem: issues and directions. *Journal of Information and Telecommunication, 5*(1): 16-34.

Juvekar, A. (2021). A comparative study of vendor selection process in global outsourcing industry with an elucidated scientific Approach. *Turkish Journal of Computer and Mathematics Education (TURCOMAT), 12*(10), 4136-4152.

Karimi-Alaghehband, F. & Rivard, S. (2019). Information technology outsourcing and architecture dynamic capabilities as enablers of organizational agility. *Journal of Information Technology, 34*(2), 129-159.

Kaveh Pishghadam, H. & Esmaeeli, H. (2021). A system dynamics model for evaluating the firms' capabilities in maintenance outsourcing and analyzing the profitability of outsourcing. *Scientia Iranica. 30*(2), 712-726.

Kazmi, S. H. M., et al. (2018). Software outsourcing model for risk mitigation. 2018 *International Conference on Computing, Mathematics and Engineering Technologies (iCoMET), IEEE.*

Khader, R. & Zein, S. (2019). Outsourcing in Palestinian IT Sector: a qualitative study. 2019 *3rd International Symposium on Multidisciplinary Studies and Innovative Technologies (ISMSIT)*, IEEE.

Khan, H. U., et al. (2021). Empirical investigation of critical requirements engineering practices for global software development. *IEEE Access 9*: 93593-93613.

Kocev, D. (2021). Outsourcing strategy: outsourcing the finance and accounting function by smes. *International Journal of Economics, Management and Tourism, 1*(1), 52-61.

Kocot, M. & D. Kocot (2022). Determinants of the success of an outsourcing project in the field of IT separations: the experience of companies in the Silesian Voivodeship. *European Research Studies Journal Volume XXV, Issue 1*, 208-225

Lee, J., et al. (2022). A step towards on-path security function outsourcing. *23rd International Conference on Distributed Computing and Networking*.

Legesse, A. (2021). Client-vendor relationships in offshore it outsourcing. *iSChannel, 16*(1).

Looi, M. & Szepan, M. (2021). Outsourcing in global software development: effects of temporal location and methodologies. *International Journal of Business and Social Science, 12*(3).

Malik, M. H. & Velan, N. (2019). Software and services export, IT investment and GDP nexus in India: Evidence from VECM framework. *International Trade, Politics and Development, 3*(2), 100-118.

Mehmood, F. & Zulfqar, S. (2021). Effect of human related factors on requirements change management in offshore software development outsourcing: A theoretical framework. *Soft Computing and Machine Intelligence, 1*(1), 36-52.

Orlu, G. U. (2021). Outsourcing provider selection model in public sector. *Turkish Journal of Computer and Mathematics Education (TURCOMAT), 12*(3), 1832-1841.

Paudel, S. & Kumar, V. (2021). Strategic success factors of information technology outsourcing in emerging Markets. *Nepal Journal of Multidisciplinary Research, 4*(1), 107-120.

Qureshi, S., et al. (2021). A study on mitigating the communication and coordination challenges during requirements change management in global software development. *IEEE Access 9*: 88217-88242.

Rahman, H. U., et al. (2021). Empirical investigation of influencing factors regarding offshore outsourcing decision of application maintenance. *IEEE Access 9*: 58589-58608.

Rana, M. & Mondal, P. (2021). Library and information process outsourcing (LIPO): An Important tool for managing engineering and technical institutes in higher education, government of West Bengal. *Journal of Indian Library Association, 56*(3), 29-39.

Ravi, A. & Donawa, N. (2021). Significance of strategic outsourcing in IT project management. *TechRxiv. Preprint*. https://doi.org/10.36227/techrxiv.17693825.v1

Rehman, N. & Khan, A. W. (2022). Critical challenges of designing software architecture for internet of things (iot) software system. *Evolving Software Processes: Trends and Future Directions*, 219-240.

Ren, T., et al. (2022). Effect of service quality on software sales and coordination mechanism in IT service supply chain. *Journal of Industrial and Management Optimization, 18*(6), 4409-4432.

Sahoo, M. B. & Goute, A. K. (2021). Outsourcing HR shared services in the times of COVID: Role of technology and customer needs fulfillment. *International Journal of Business and Economics, 6*(1), 53-62

Santos, J. C. D. & Silva, M. M. D. (2021). Optimising IT outsourcing services by managing the balance between standardisation and customisation-a providers' perspective. *International Journal of Business Information Systems, 37*(1), 78-105.

Saqib, M. (2020). An empirical investigation of critical challenges in outsourcing projects: A Survey Based Study. *International Journal for Research in Applied Science & Engineering Technology, Volume 8* Issue XI, 560-565

Sharma, S., et al. (2020). Advances in cryptography and secure hardware for data outsourcing. *2020 IEEE 36th International Conference on Data Engineering (ICDE)*, IEEE.

Sloniec, J. (2021). The level of outsourced tasks in IT and its dependence on selected explanatory factors. *European Research Studies Journal Volume XXIV, Special Issue 2*, 152-167

Suresh, S. & Ravichandran, T. (2021). Value gains in business process outsourcing: The vendor perspective. *Information Systems Frontiers:* 1-14.

Thanh, D. C., et al. (2022). Study the impact of labor outsourcing on the financial performance of small and medium enterprises in Mekong Delta, Vietnam. *Ho Chi Minh City Open University Journal of Science-Economics and Business Administration, 12*(1), 67-83.

Usman, A. & Khan, A. W. (2018). Software outsourcing quality challenges model systematic literature review (SLR) protocol. *University of Sindh Journal of Information and Communication Technology*, *2*(4), 196-201.

Usman, A., et al. (2020). Critical challenges of quality in software outsourcing from vendor perspective across continent to continent. *Scholar* 16700: 980.

Veloso, C. M., et al. (2021). Boosters of satisfaction, performance and employee loyalty: application to a recruitment and outsourcing information technology organization. *Journal of Organizational Change Management*, *34*(5), 1036-1046.

Wang, M.-M. & Wang, J.-J. (2019). How vendor capabilities impact IT outsourcing performance: An investigation of moderated mediation model. *Journal of Enterprise Information Management.*

Wong, W. Y. (2021). Towards integrating six sigma approach: service level agreement measurement and monitoring (A Malaysian it outsourcing case study). *Turkish Journal of Computer and Mathematics Education (TURCOMAT)*, *12*(3), 2191-2198.

Author Information

Issam Jebreen
Zarqa University, Jordan
Contact: ijebreen@zu.edu.jo

Eman Al – Qbelat
Zarqa University, Jordan

To cite this article:

Jebreenl, I. & Qbelat, E. A. (2023). A systematic snapshot of software outsourcing challenges. *The Eurasia Proceedings of Science, Technology, Engineering & Mathematics (EPSTEM), 22,* 48-58.

The Eurasia Proceedings of Science, Technology, Engineering & Mathematics (EPSTEM)
ISSN: 2602-3199

The Eurasia Proceedings of Science, Technology, Engineering & Mathematics (EPSTEM), 2023

Volume 22, Pages 59-73

ICBASET 2023: International Conference on Basic Sciences, Engineering and Technology

Safetree: An Integrated Wearable Device and Mobile Application Solution for Pandemic Mitigation and Post-Pandemic Preparedness, Incorporating Contact Tracing, Social Distancing Emergency Alert Notification, and Socialization Features

Jille Anne R. VERANO
Mapúa University

Doreen Marie S. SORONGON
Mapúa University

Febus Reidj G. CRUZ
Mapúa University

Abstract: The COVID-19 pandemic has highlighted the need for effective mitigation strategies to reduce infectious disease spread. Safetree is an innovative wearable device and mobile application that integrates social distancing, contact tracing, emergency alert notification, and socialization features. The social distancing feature enabled the devices to successfully detect all nearby wearables within a 1-meter range within their line of sight using Bluetooth Low Energy (BLE) as a transceiver. Unfortunately, due to environmental conditions that were present in several of the experimental settings, some of the devices operated outside of the 1-meter range. The success rate in generating the appropriate tree diagram for each situation in the experimentation set-up resulted in 100%. The average response time between the wearable device and the mobile application varied from 9 seconds up to almost 11 seconds. In the fields of contract tracing and social network analysis, the tree algorithm has been shown to be effective for examining user interactions. This algorithm was also implemented on the emergency notification feature and, the socialization feature which enabled the users to interact with one another while maintaining social distancing guidelines, promoting mental health and social well-being amidst and after the pandemic.

Keywords: Social distancing, Contact tracing, Tree algorithm, Internet of things, Bluetooth low energy

Introduction

COVID-19 is an infectious disease transmitted through discharges either in the form of small aerosols or large droplets. In other words, the disease spreads between two people through respiratory discharges. Since the transmission medium is available anywhere, several concerns arose about possible transmissions within large-scale environments, forcing several countries, including the Philippines, to declare a public health emergency. Several monitoring techniques have already been explored, automated, and implemented, such as COVID-19 proximity-based contact tracing system and digital tracing. Proximity-based contact tracing systems utilize technologies to generate proximity data integrated into a contact tracing system to identify possible people with prolonged exposure to a COVID-19-infected person (Lubis & Basari, 2020). Utilization of beacon technology in Bluetooth Low Energy (BLE) enabled proximity detection through the usage of contextual information resulting from the beacons (Lubis & Basari, 2020; Jeom et al., 2018). In the context of proximity detection, the Received Signal Strength Indicator, also known as the RSSI, data is utilized in identifying others who are within the configured proximity range. Existing local implementations of this, such as within an enclosed environment,

require further improvements in: (1) proximity detection, (2) signal detection, and (3) battery consumption (Lubis & Basari, 2020). In addition, beacon technology is only able to employ one as a transmitter, while the other device as the receiver, regardless of if there's a or no connection (Lubis & Basari, 2020). The BLE technology is employed chiefly for observance of social distancing. However, current BLE technology supports a dual role on a single device and can be further studied for device communication that does not need a connection. Most of the implemented systems for contact tracing and social distancing can only achieve one purpose: a wearable only designated for social distancing or a developed system for contact tracing. Moreover, the experimental setup of existing social distancing wearables is only one-to-one. The experimentation setup, one-is-to-many, is more effective in minimizing and reducing the spread of the COVID-19 disease within crowded environments as this type of setup limits close face-to-face contact with not only one person but between two or more people (Alhmiedat & Aborkbah, 2021). The research aims to develop a wearable device and mobile application for pandemic mitigation protocols such as social distancing and contact tracing, respectively, along with integrating an emergency alert notification system and socialization feature for post-pandemic preparedness. Specifically, the study aims: (1) to design the electronics of the wearable prototypes, (2) to develop a mobile application with a graphical user interface (GUI) and database server, and (3) to incorporate the tree algorithm in both pandemic mitigation and post-pandemic preparedness features. With this, the research mainly focuses on creating microcontroller-based wearable devices and developing a system through a mobile application and database that will aid in pandemic mitigation. With this, it will mainly identify upcoming human presence via the response of proximity sensing using the RSSI of the Bluetooth Low Energy (BLE) technology. Furthermore, the data for the contact tracing aspect of the wearable can only be stored through device-to-device powered by Bluetooth and Wi-Fi. The developed mobile application will only work on Android cellular devices. The wearable device would be tested using one-to-one type and one-to-many type of experimental trials. In addition, the location included in the emergency notification feature will only be based on the mobile device's location.

Review of Related Literature and Studies

Chain of COVID-19 Infection

A person is categorized as a close contact once he/she falls under the following: (1) had a face-to-face interaction with a confirmed case, a person who tested positive for COVID-19 within one meter for at least 15 minutes, (2) had physical contact with either a probable case or confirmed case and (3) encountered a confirmed case without wearing personal protective equipment/PPE ("Who western pacific | covid-19 information for the public", 2021). In the Philippines, the close contact is mandated to inform his/her respective Barangay Health Emergency Response Team, which will eventually lead to testing for COVID-19 diseases and referral to his/her barangay's TTMF or hospital, whichever applies (Department of Health, 2021). Regardless of the COVID-19 test result of the close contact, he/she must still undergo the whole 14-day quarantine. The second and third generations of close contacts are also encouraged to be traced and monitored in the country (Department of Health, 2021).

Figure 1. Multisys' comprehensive contact tracing (Multisys Technologies Corporation, n.d)

Figure 1 shows the comprehensive contact tracing process which monitors and interprets user health reports included in StaySafe PH, a contact tracing software implemented in the Philippines. This comprehensive feature allows effective tracking and reduces the risk of COVID-19 transmissions spreading (Multisys Technologies Corporation, n.d). This feature is similar to using the tree diagram to visualize COVID-19 confirmed cases along with their close contacts. One of the main objectives of the tree diagram is classification, as it can represent extensive configurations implemented within enclosed virtual spaces, which are interspersed by the following: (1) information, (2) nodes, and (3) connecting lines (Multisys Technologies Corporation, n.d). The study, entitled CovidSIMVL, utilized transmission trees which a; allowed the identification of all people who might have been infected by the Index Case or the confirmed case (Chang et al., 2020). Moreover, this study introduced the forward-facing approach and backward-facing approach. The forward-facing approach can trace the people needing monitoring and treatment in the future. In contrast, the backward-facing approach can depict the big picture of the distributions of COVID-19's chains of infection as the means of contact tracing (Chang et al., 2020). Another research used a tree diagram, as shown in figure 2, as a method for data visualization to showcase the harmful outcomes once people do not comply with social distancing policies. This study uses system dynamics methodology to build a COVID-19-confirmed case model. This model predicts the number of confirmed cases and deaths (Newman, 2021). The model can also predict when the COVID-19 positive cases curve will be flattened (Newman, 2021).

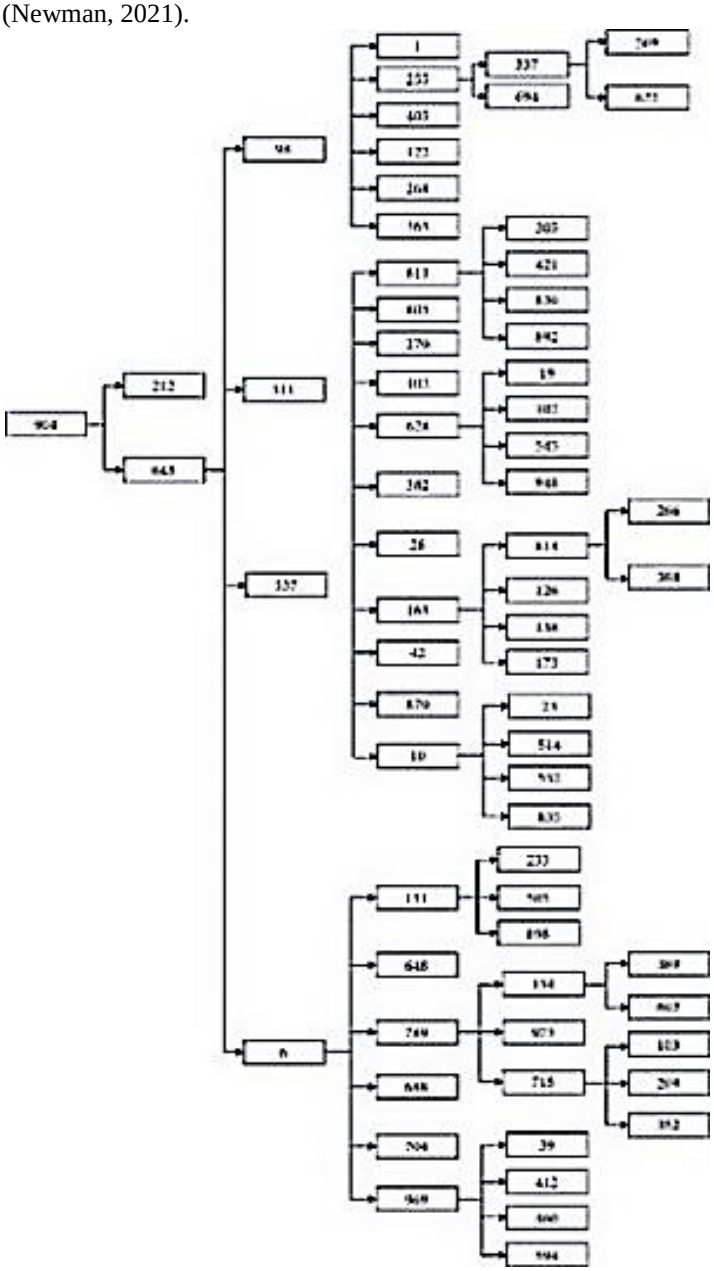

Figure 2. Tree diagram showing the “level” of Covid-19 infections (Newman, 2021)

BLE Technology

New wireless low-power technologies open the door to dynamic device-to-device communication (Jeom et al., 2018). The Internet of Things (IoT), which has several applications in the sectors of automation, health applications, tracking, etc., has been developed as a result of technological advances like BLE .(Lubis & Basari, 2020; Jeom et al., 2) BLE technology is primarily used in low-power applications such as location-based services, wearable technology, and brief communications between devices (Lubis & Basari, 2020). The physical location affects how well BLE's location-based service works (Lubis & Basari, 2020; Jeom et al., 2). With the use of beacon technology, BLE provides an accurate location estimate for the user and can be applied in unmanned proximity-based applications (Lubis & Basari, 2020; Jeom et al., 2; Su et al., 2021).

The usage of advertising and scanning states as beacons are prevalent in proximity-based applications (Lubis & Basari, 2020; Jones et al., 2020). BLE, unlike beacon technology, is constantly growing and only supports one application. Sending protocol is needed for broadcasting data. After then, the Received Signal Strength Indicator (RSSI) or Received Signal Strength plays a significant role in the proximity calculation (RSS). When neighboring devices find an advertising packet broadcast regularly, they can obtain data like the RSS or RSSI (Jones et al., 2020). Low energy consumption requirements are another aspect that can be considered when designing systems. Several modes of operation are used by a few modules purely for power savings (Song et al., 2019; Amft et al., 2020). ESP 32 WROOM 32 modules can switch between active and modem-sleep, light sleep, deep sleep, or hibernation. If there is an external wake-up source to bring it back to its active state, these modes can be programmed to be used in a different order.

Methodology

Conceptual Framework

The intended study's conceptual framework is shown in Figure 3. The input variables are acquired when one user is one meter away from another. When this requirement is satisfied, the device will record the device name, RSSI, date, time, and exposure length into an SD card and send them to the mobile application via serial connection afterward. There are six separate steps in the procedure. The result is projected to be a wearable and mobile application that will improve the monitoring and enforcement of individuals' adherence to established norms for social distancing, contact tracing, and post-pandemic preparedness.

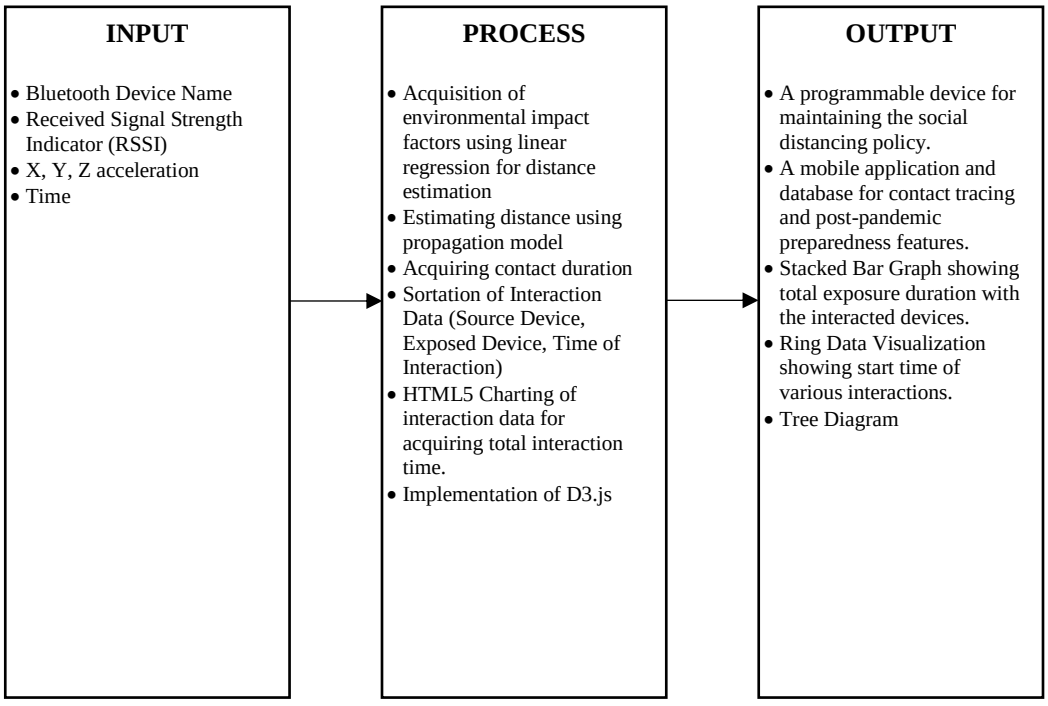

Figure 3. Conceptual framework

Design of the Electronics of the Wearable

Figure 4 shows the overview of the block diagram of the social distancing wearable and contact tracing system.

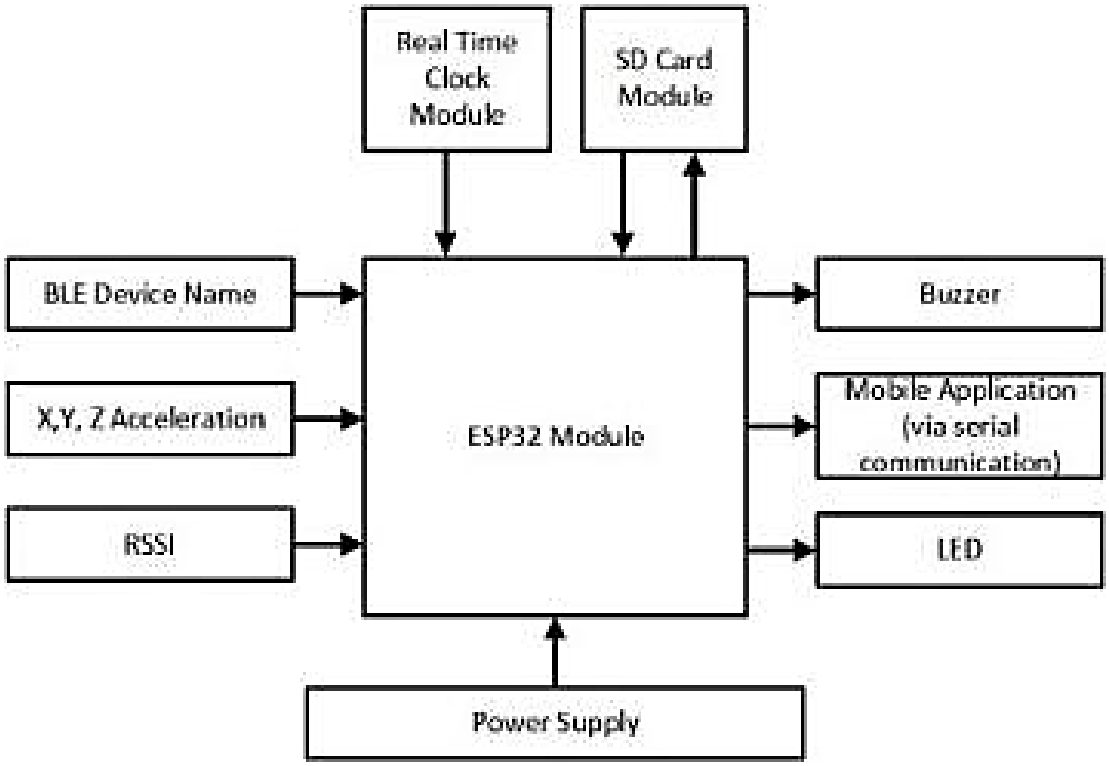

Figure 4. Block diagram of the social distancing wearable

BLE and Security Configuration

Figure 5 provides an overview of proximity detection utilizing the BLE protocol. The proposed system will use the BLE protocol to track social distance. Both devices would be set up as BLE broadcasters and observers for the proposed system. A link need not be established to send information from one configuration to another. The broadcaster's packet in terms of advertising will be set to ADV NONCONN IND, which forbids connection requests and the advertisement of additional data that is not part of the advertising packet. Serial communication using BR/EDR would convey data from the device to the application. The overview of the proximity detection of using the BLE specification is shown above. In the proposed system, the protocol BLE will be used in the monitoring of social distancing. For the proposed system, both devices would be configured as BLE broadcaster and observer. The configuration does not need to establish a connection to relay information from one another. The advertising packet of the broadcaster will be set to ADV_NONCONN_IND which does not allow connection request and does not allow additional data to be advertised that is not included in the advertising packet. For the transfer of data from the device to the application, serial communication through BR/EDR would be used. The ESP32 has the capacity to operate in dual mode, using both BLE and BR/EDR at the same time. The ESP32 uses the SSP by default, which offers secure connections via a shared key. Aside from the SSP, a simple wearable device to mobile application communication was implemented for device authentication as shown in figure 6.

Figure 5. Overview proximity detection using BLE.

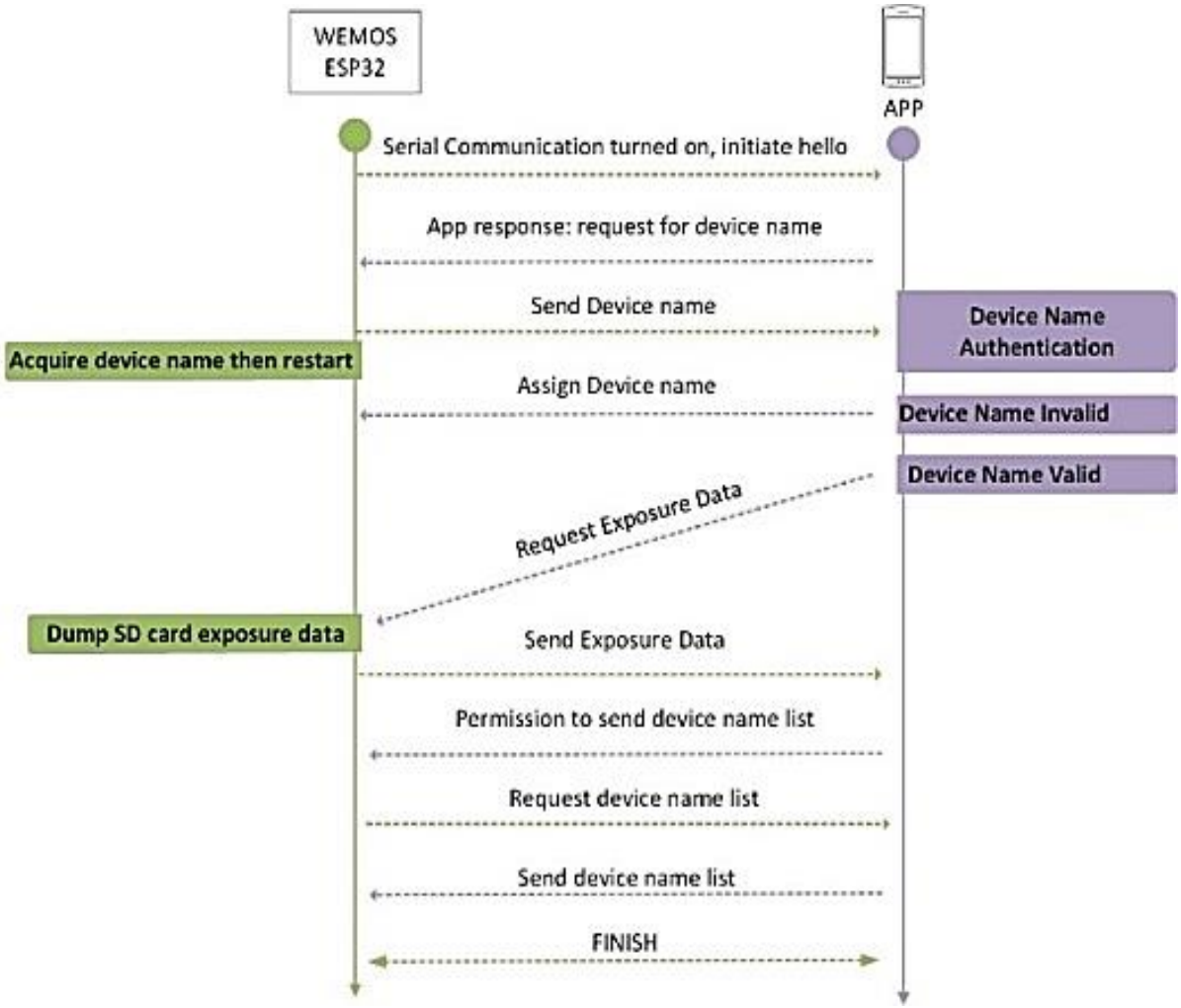

Figure 6. Device authentication with the application

Power Management

The ESP32 module has multiple power management modes that it can enter. The active, modem-sleep, and light sleep modes will all be covered in the study. The device features a chip for wireless connection in active mode, including Wi-Fi, BLE, and Traditional Bluetooth. Wi-Fi and Bluetooth are disabled in the light-sleep mode to decrease power usage. Nonetheless, the light-sleep mode preserves the device's state before light sleep, does not call for module reinitialization, and improves responsiveness to other active devices. The module's least-consumptive mode is deep sleep. The tables below are a summary of the ESP32's specifications and conditions for each of its power modes respectively:

Table 1. Power consumption in different modes

Device Mode	**Description**
Active	RF working
Light-Sleep	CPU paused, RTC peripherals and RTC memory on
Deep-Sleep	RTC memory an RTC peripherals on

Table 2. Power management mode conditions

Mode	**Condition**
Active	Devices within 1 meter radius User Standing
Light-Sleep	User Sitting
Deep-Sleep	Device facing downwards

Software Development

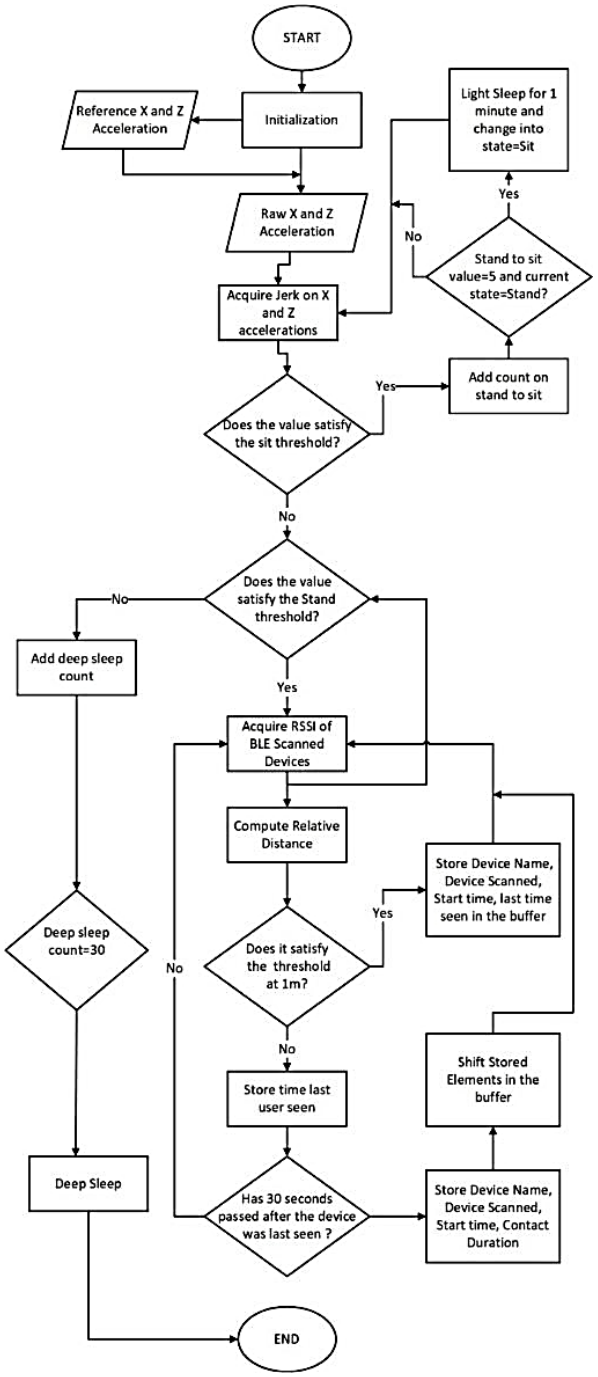

Figure 7. Software development

Figure 7 shows the overview of the software development of the wearable device. The device was programmed using the Arduino IDE. After the device is powered on, it will be initialized and this includes acquiring the reference value for the sit and stand, starting the advertising of BLE and Classic Bluetooth. After the initialization, the device continuously checks the state of the user, whether it is standing or sitting. When the user is in standing position, the device will start to scan for the devices based on a name list defined to be students at the University. If the device assigned to a student is scanned, the device will store the device name, device scanned name, the time it was scanned, and the time it was last seen. The device information would then temporarily store in a buffer. If the device scans a new device, the same thing would be done and it would be added to the buffer. When the scanned device is out of range, the device would store all information about the device in the SD card. The only thing to stop the device from executing its operations is when it is in deep sleep mode or turned off using the power switch. Aside from that, operations on the device are halted for 1 minute when the device is in sleep mode.

Contact Tracing Algorithm

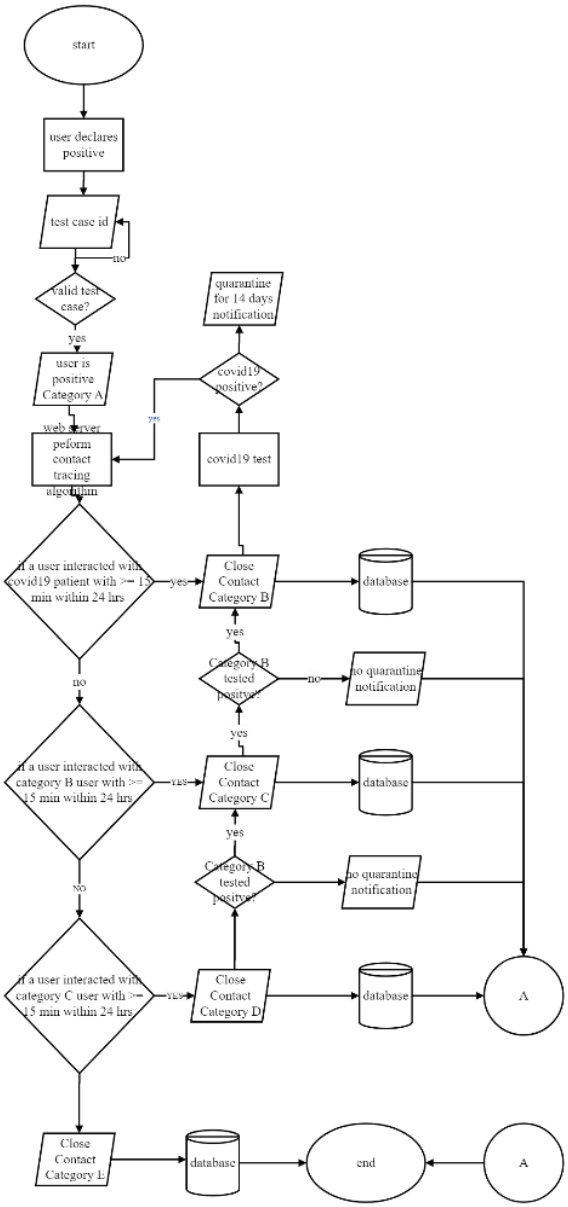

Figure 8. Contact tracing algorithm

An overview of the contact tracing technique used in the mobile application is shown in Figure 8. When a user report having the COVID-19 virus, the mobile application will take them to a screen where they must provide test results that will be verified by the web server. This begins the procedure. The user will be assigned to Category A if the test reference is reliable, and the web server will run the contact tracing method. Users in Category B are those who interacted with Category A for at least 15 minutes. Users who have interacted with a website for at least 15 minutes will be placed in Category B, while those who have interacted with a website for at least 30 minutes will be placed in Category C, and so on. Users in Category B are required to take a COVID-19 test; if they are positive, they will be categorized as Category A instead, and Category B, Category C, and Category D will shift one category as well. Finally, if the users don't have an interaction duration of at least 15 minutes, they will be categorized with any of the Categories stated, and they will be categorized as Category E. Category B users are required to take a COVID-19 test. In contrast, Category B must complete their 14-day quarantine before going back to school if the test was negative. While, if the test result resulted into a negative one, Category B must finish his/her 14-day quarantine before returning to school. While Category C and Category D along with Category E are still allowed to enter the school premises. In contrast, Category B must complete their 14-day quarantine before going back to school if the test was negative. While those belonging in Category E is not permitted on school grounds, those who are considered as Category C and Category D are permitted.

Development of Mobile Application

Systems Architecture

Back-end Development consisting of LAMP Technology Stack and Google Cloud Console Platform. Front-end Development consisting of HTML, CSS, Javascript, MIT App Inventor 2, and Arduino IDE. Tree Algorithm - A depiction of the relationships between users who have engaged with one another is produced by this algorithm after it retrieves interaction data from a database. This is accomplished by looking at interactions that occurred for the input user within 14 days of a specified date and building a list of users who might have encountered that person. After then, the algorithm repeatedly examines each user's interactions to see whether they have any direct ties to other users. Until all connections to the input user have been taken into consideration, this process is repeated. The algorithm then generates a visual representation of this structure on a web page using the PHP programming language and the D3js library.

Calculations

Success Rate

The success rate is the most straightforward usability statistic since it is simple to comprehend and accurately represents a specific dataset (Nielsen & Budiu, 2023). The total number of successes is divided by the total number of trials to determine the success rate. The following mathematical equation demonstrates this:

$$Success\ Rate = \frac{No.\ of\ Successful\ Trials}{Toial\ No.of\ Trials}\ x\ 100 \tag{1}$$

Levels of Success

Table 3. Levels of success

Levels of Success	Interpretation
Complete Success	The expected outcome of the trial was achieved with no error.
Failure	The expected outcome of the trial was not achieved.

This table displays how (Nielsen & Budiu, 2023) interpreted the first two of the four success levels. The first level denotes that the anticipated outcome occurred during the trial, assuming no errors were detected. While the latter level is seen as the opposite of the former.

Battery Life Equation

The battery lifetime can be computed by dividing the battery capacity by the load's current draw. This is further elaborated by the equation below ("How to Calculate Battery Run Time", n.d):

$$B_l = \frac{B_c}{I_l} \tag{2}$$

Let:
B_l be the battery lifetime in hours,
B_c be the battery capacity in milliamperes.
I_l be the load device current draw in milliamperes

Engineering Standards

Table 4 shows the engineering standards implemented in this research. The IEEE 802.11ac was the standard for the wireless networking, IEEE 7005 was the standard used for the storage and protection of personal data, BLE for the Bluetooth wireless communication, and IEEE 802.15.1 for the wireless communication.

Table 4. Engineering standards

Engineering Standards	Purpose
IEEE 802.11ac	Wireless Networking Standard
IEEE 7002	Data Privacy Process
IEEE 7005	Storing and Protecting Personal Data
BLE	Bluetooth Wireless Communication
IEEE 802.15.1	Wireless Communication

Results and Discussion

Safetree Wearable Device and Mobile Application

Safetree Wearable Device

Figure 9. Wearable device (Standing and Sitting Position)

Figure 8 shows the wearable device worn by the user in a standing and seating position. The wearable device is a belt accessory, specifically a buckle. The user can adjust the wearable's position on his/her desired waist placement.

Safetree Mobile Application

Figure 10. Mobile application's pandemic mitigation features (Main Features)

Figure 9 shows the main features for pandemic mitigation of the mobile application. This includes the home page of the application which has several functions such as COVID-19 information and another is the covid test verification feature in which users are able to willingly declare if he/she is negative/positive from COVID-19.

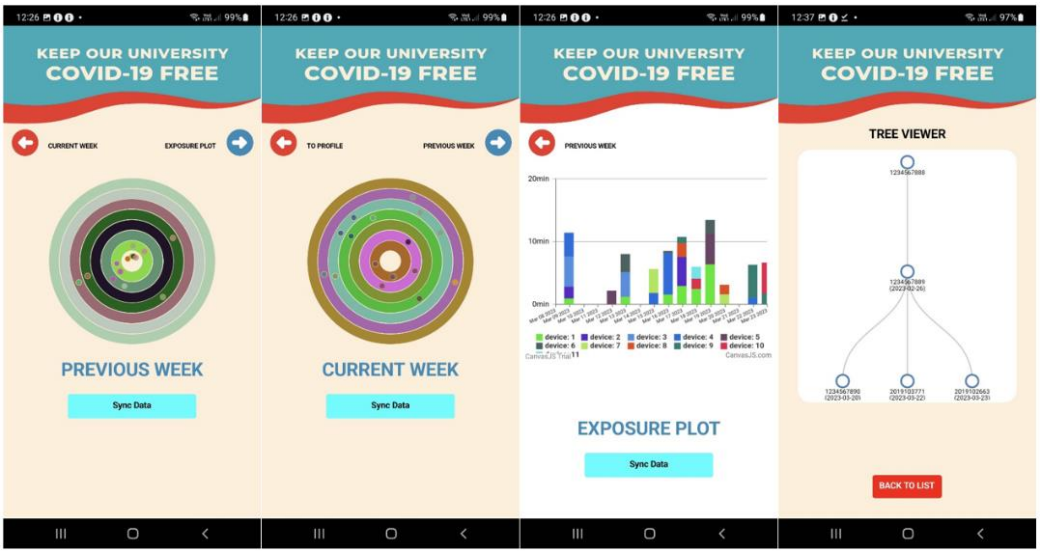

Figure 11. Mobile application's pandemic mitigation features (Data Visualization)

Figure 11 shows the data visualization provided by Safetree. The mobile application offers a ring-like or orbit-like diagram for current and previous weeks of interaction with other users. This diagram can also tell the exact time and day of the week when the interaction occurred. In addition, the size of circles on the orbit-like/ring-like structure vary depending on the duration of the interaction. The most inner ring of the orbit represents the most current day of the week. A stacked bar graph is also used to represent the summary of interaction duration for 14 days. The tree diagram efficiently depicts the extensive interconnectedness of user interactions across the allotted period, giving insightful information into the utilization patterns and relationships. Figure 12 shows the mobile application's post-pandemic preparedness features. This includes the optional enabling of notification exposure to receive messages from other mobile application users the user had previously interacted with. Moreover, an emergency alert notification is also incorporated into the application in which users can alert people who they previously had an interaction with within the day that they are in danger at the specific time and location.

Figure 12. Mobile application's post pandemic preparedness features

Database

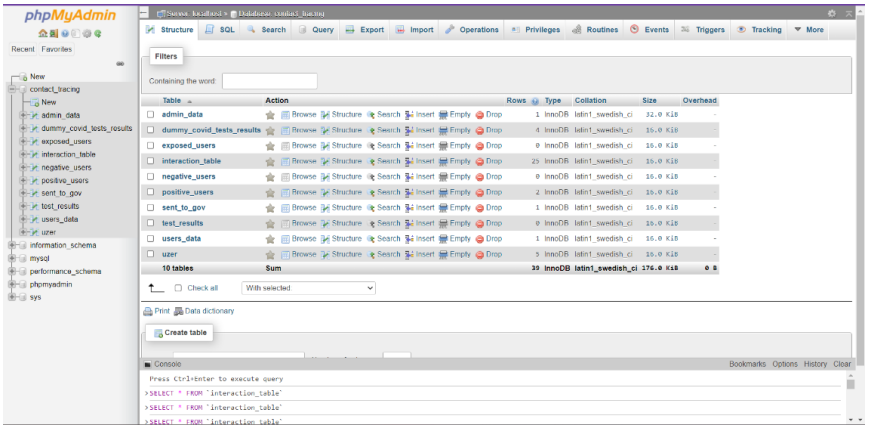

Figure 13. Database

Figure 13 shows the database created which stores the overall interaction data between each user and the COVID-19 test results.

Wearable Device to Mobile Application Communication

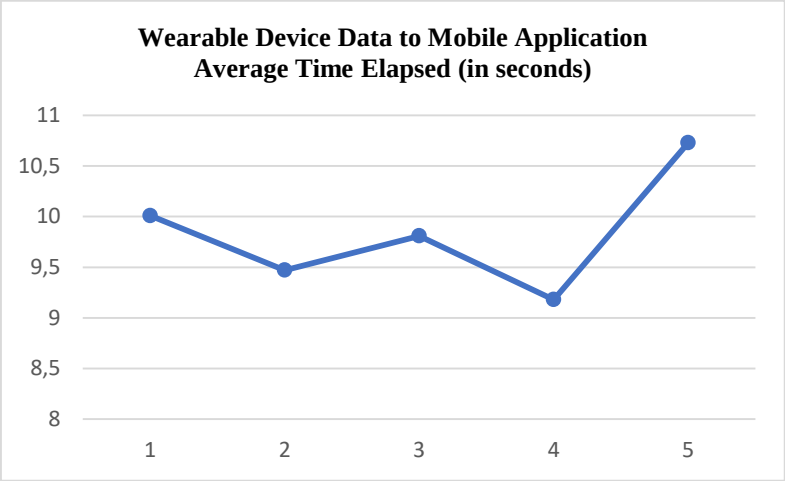

Figure 14. Mobile application's post pandemic preparedness features

Figure 14 shows the graph depicting the average time elapsed for the response between the communication of each wearable device and mobile application. The average response time between the wearable device and the mobile application varied from 9 seconds up to almost 11 seconds.

Power Management

Device Modes' Current Consumption

Table 5. Current consumption of device modes

Device Modes	Current Consumption (in mA)
Active Mode	150
Light Sleep	15
Deep Sleep	6.6

The current consumption of various device modes is displayed in this table. With the device in active mode, which involves active broadcasting and receiving, its current consumption is roughly 150 mA. In light sleep mode, it is roughly measured at 15 mA, while in deep sleep, it is roughly measured at 6.6 mA.

Battery Life

This table displays the wearable device's computed battery life for various device settings based on the measured current consumption. It is possible to stay in active mode for almost 13 hours. Sustained deep sleep mode can persist for around 303 hours, whereas continued light sleep mode can continue for about 133 hours.

Table 6. Battery life

Device Modes	Battery Life (in hours)
Active Mode	13
Light Sleep	133
Deep Sleep	303

Experimentation Set-Ups

Table 7 shows the summary of results for the experimentation set-ups, one-to-one and one-to-many, having broadcaster role-to-receiver role as the situation for both indoor (classroom) and outdoor (hallway) settings. It is expected that both broadcaster and receiver will unsuccessfully function outside the 1-meter range, while functioning completely within the 1-meter range. However, in some of the situations, both roles did not function completely even if they are within the 1-meter range. While in other situations, both roles functioned successfully even if they are outside the 1-meter range. This occurrence is due to the instability behavior of the RSSI and its susceptibility to various factors within an indoor and outdoor environment (Cruz et al., 2018; Cruz, Garcia et al., 2018).

Table 7. Summary of results for the experimentation set-up

Situation (Broadcaster to Receiver)	Location	Success Rate			
		Receiver		Broadcaster	
		Within 1 meter	Outside 1 meter	Within 1 meter	Outside 1 meter
1:1	Classroom	100%	100%	100%	100%
	Hallway	100%	0%	100%	0%
1:2	Classroom	90%	20%	100%	20%
	Hallway	70%	0%	100%	0%
2:1	Classroom	100%	20%	90%	20%
	Hallway	80%	0%	70%	0%
1:3	Classroom	90%	0%	100%	0%
	Hallway	90%	0%	100%	0%
3:1	Classroom	100%	0%	100%	0%
	Hallway	100%	0%	90%	0%
1:4	Classroom	90%	10%	100%	10%
	Hallway	70%	0%	100%	0%
4:1	Classroom	100%	0%	90%	0%
	Hallway	100%	0%	80%	0%

Table 8. Summary of tree algorithm testing (5 trials for each situation)

Situation	Initial Categories					COVID-19 Status					Final Categories					Success Rate
	D1	D2	D3	D4	D5	D1	D2	D3	D4	D5	D1	D2	D3	D4	D5	
1	A	B	C	D	E	+	-	N/A	N/A	N/A	A	B	C	D	E	100%
2	A	B	C	D	E	+	+	-	N/A	N/A	A	A	B	C	E	100%
3	A	B	C	D	E	+	+	+	-	N/A	A	A	A	B	E	100%
4	A	B	C	D	E	+	+	+	+	N/A	A	A	A	A	E	100%

Tree Algorithm Efficiency

Table 8 shows the summary of results for testing the efficiency of the Tree algorithm implemented in the contact tracing aspect of this research in the pre-pandemic and post-pandemic setting with five trials each situation. Category A is the confirmed case, Category B is considered as the close contact of Category A, Category C is

the close contact of Category B, Category D is considered as the close contact of Category C, while Category E is neither the close contacts of any categories mentioned. Based on all situations, the tree algorithm resulted in a 100% efficiency or success rate in representing interconnectedness of user interactions across the allotted period. In all the situations, the algorithm provided insightful information into the relationships between confirmed cases and their respective close contacts for each of the devices.

Conclusion

In conclusion, the built wearable device prototypes could detect the presence of other wearable devices within such a 1-meter radius and convey that information to the created mobile application with a database to conduct a contact tracing operation. Users were able to establish contact tracing, ascertain the beginning of the interaction, and gather their exposure duration using all these methods of data visualization. Regardless of how the devices were configured, each wearable in the experiment setup was able to operate correctly within a 1-meter range. Unfortunately, due to environmental conditions that were present in several of the experimental settings, some of the devices operated outside of the 1-meter range. Device power modes can lower the ESP32 module's current usage. Maximum current consumption during active mode is measured up to 150 mA, maximum current consumption during sleep mode is recorded up to 15 mA, and maximum current consumption during deep sleep is measured up to 6.6 mA. The ESP32 module still provides external power to the linked sensors; hence its specification on the datasheet is different. The average response time between the wearable device and the mobile application varied from 9 seconds up to almost 11 seconds. In the fields of contract tracing and social network analysis, the tree method has been shown to be effective for examining user interactions. The extensive network of user interactions was successfully displayed by the tree data visualization within the allotted timeframe, offering important insights into the usage patterns and relationships.

Recommendations

Future researchers are advised to: (1) enhance the data collected by considering that most factors affecting RSSI can be controlled, (2) create a website with only administrative rights, (3) use additional filters to improve RSSI accuracy, (4) integrate real-time data acquisition in wearable device and mobile application communication, and (5) create a cross-platform mobile application that is similar.

Scientific Ethics Declaration

The authors declare that the scientific ethical and legal responsibility of this article published in EPSTEM journal belongs to the authors.

Acknowledgements or Notes

* This article was presented as an oral presentation at the International Conference on Basic Sciences, Engineering and Technology (www.icbaset.net) held in Marmaris/Turkey on April 27-30, 2023.

*The researchers wish to convey their profound gratitude to the Lord for giving them faith, understanding, willpower, and direction as they conducted their research. The thesis advisor, Engr. Febus Reid Cruz for his crucial advice and guidance during the entire writing process of this paper. The researchers would also like to express their gratitude to their loved ones for their unwavering encouragement, compassion, and patience in helping them overcome some of the most challenging obstacles they encountered while doing their research.

References

Alhmiedat, T., & Aborokbah, M. (2021). *Social distance monitoring approach using wearable smart tags*. Multidisciplinary Digital Publishing Institute.

Amft, O., Lopera González, L. I., Lukowicz, P., Bian, S., & Burggraf, P. (2020). Wearables to fight COVID-19: from symptom tracking to contact tracing. *IEEE Pervasive Computing, 19*(4), 53-60.

Chang, E., Moselle, K. A., & Richardson, A. (2020). CovidSIMVL --transmission trees, Superspreaders and contact tracing in agent based models of covid-19 [Preprint]. *medRxiv*. https://doi.org/10.1101/2020.12.21.20248673

Cruz, J. C. D., Cruz, F. R., Sese, J., Borbon, M. D., Cacayuran, A. G., Dela Rea, K., & Gammad, J. R. (2018). Faculty monitoring system with mobile application using received signal strength Indication. In 2018 IEEE 10th *International Conference on Humanoid, Nanotechnology, Information Technology, Communication and Control, Environment and Management* (HNICEM) (pp. 1-6). Baguio City, Philippines.

Cruz, J. C. D., Garcia, R. G., Garcia, A. J. G., Manalo, K. A. A., Nworgu, V. I., & Payumo, J. B. M. (2018). Proximity tracker using received signal strength, particle filter and extended kalman filter. In 2018 IEEE 10th *International Conference on Humanoid, Nanotechnology, Information Technology, Communication and Control, Environment and Management* (HNICEM) (pp. 1-6). Baguio City, Philippines.

Department of Health. (2021). *COVID-19 FAQS* [Online]. https://doh.gov.ph/COVID-19/FAQs.

Jeon, K. E., She, J., Soonsawad, P., & Ng, P. C. (2018). BLE beacons for internet of things applications: Survey, challenges, and opportunities. *IEEE Internet of Things Journal, 5*(2), 811–828.

Jones, N. R., Qureshi, Z. U., Temple, R. J., Larwood, J. P. J., Greenhalgh, T., & Bourouiba, L. (2020). Two metres or one: what is the evidence for physical distancing in covid-19? *BMJ*, 370(September), m3223.

Lithium ion Battery Manufacturer and Supplier in China-DNK Power. (n.d.). *How to calculate battery run time*. https://www.dnkpower.com/how-to-calculate-battery-run-time/

Lubis, A. F., & Basari (2020). Proximity-based COVID-19 contact tracing system devices for locally problems solution. In Proceedings of the 2020 3rd *International Seminar on Research of Information Technology and Intelligent Systems (ISRITI).* (pp. 365-370).

Multisys Technologies Corporation. (2021). *All-in-one eight elaborate features of contact tracing platform staysafe.ph* [Online]. https://www.multisyscorp.com/news/all-in-one-eight-elaborate-features-of-contact-tracing-platform-staysafeph. [Accessed: 12-Oct-2021].

Newman, E. (2021, September). Explaining the decision tree flowchart and its Benefits [Blog post]. https://corp.yonyx.com/customer-service/explaining-the-decision-tree-flowchart-and-its-benefits/

Nielsen, J., & Budiu, R. (2023). Success rate: The simplest usability metric. nielsen norman group. Retrieved from https://www.nngroup.com/articles/success-rate-the-simplest-usability-metric/

Song, S. W., Lee, Y. S., Imdad, F., Niaz, M. T., & Kim, H. S. (2019). Efficient advertiser discovery in Bluetooth low energy devices. *Energies, 12*(9), 1707.

Su, Z., Pahlavan, K., & Agu, E. (2021). Performance evaluation of COVID-19 proximity detection using bluetooth le signal. *IEEE, 9*, 38891–38906.

World Health Organization. (2021). *Who western pacific | Covid-19 information for the public* [Online]. https://www.who.int/philippines/emergencies/covid-19-response-in-the-philippines/information. [Accessed: 12-Oct-2021].

Author Information

Jille Anne R. Verano
Mapúa University
Muralla, St., Intramuros, Manila 1002, Philippines
jarverano@mymail.mapua.edu.ph

Doreen Marie S. Sorongon
Mapúa University
Muralla, St., Intramuros, Manila 1002 Philippines

Febus Reidj G. Cruz
Mapúa University
Muralla, St., Intramuros, Manila 1002, Philippines

To cite this article:

Verano, J.A.R., Sorongon, D.M.S. & Cruz, F.R.G. (2023). Safetree: An integrated wearable device and mobile application solution for pandemic mitigation and post-pandemic preparedness, incorporating contact tracing, social distancing emergency alert notification, and socialization features. *The Eurasia Proceedings of Science, Technology, Engineering & Mathematics (EPSTEM), 22,* 59-73.

The Eurasia Proceedings of Science, Technology, Engineering & Mathematics (EPSTEM)
ISSN: 2602-3199

The Eurasia Proceedings of Science, Technology, Engineering & Mathematics (EPSTEM), 2023

Volume 22, Pages 74-80

ICBASET 2023: International Conference on Basic Sciences, Engineering and Technology

Cushion Pin Control System with Using Image Processing

Oguz Alper ISEN
Coşkunöz Holding

Emin CANTEZ
Coşkunöz Holding

Serkan AYDIN
Coşkunöz Holding

Abstract: Gas cylinders and cushion pins can be used in presses, which are the most used machines in metal forming.In the placement of the cushion pins on the press table, the operators find the right holes with the help of a map and place the cushion pins into the holes.When the cushion pins are placed in the wrong holes, it can cause permanent damage to the press, mold or metal sheets.In order to prevent these errors, although there are systems to guide the operators visually, there are no systems to control each hole according to each map. In the study, a virtual orientation was placed on the real image according to the map information using AR technology. Finally, each hole was controlled using image processing and deep learning methods using motion sensors on the camera, lidar and tablet.As a result, an inexpensive and effective result was produced using only a tablet with a camera and lidar.

Keywords: Image processing, Deep learning, Metal shaping, Cushion pin, Control system

Introduction

Gas cylinders and cushion pins are widely used in metal forming presses to provide support and absorb impact during the forming process. The correct placement of cushion pins on the press table is critical for the proper functioning of the press, mold, and metal sheets. However, errors in the placement of cushion pins can cause serious damage to the press, mold, or metal sheets, which can result in costly downtime, repairs, and even safety hazards.

Current methods for cushion pin placement involve operators using a map to locate the correct holes and manually placing the pins in the corresponding holes. However, this method is prone to errors, especially when operators are dealing with complex and intricate maps. While there are some visual guidance systems available, they are not able to control each hole according to each map, leaving room for human error.

To address this issue, this study proposes a novel cushion pin control system that utilizes image processing and augmented reality (AR) technology to accurately and efficiently control each cushion pin hole on the press table. The system uses a tablet with a camera and a lidar to capture a real-time image of the press table, which is then augmented with virtual orientation based on the map information using the ARKit library. Motion sensors on the camera, lidar, and tablet are used to detect cushion pins and determine their correct placement according to the map.

The proposed system offers an inexpensive and effective solution for cushion pin control, which can significantly reduce the likelihood of errors and improve the overall efficiency and safety of the metal forming

process. The use of AR technology and image processing allows for real-time detection and correction of errors, reducing the need for manual inspection and improving the accuracy and reliability of the cushion pin placement process. Overall, the proposed system has the potential to improve the quality and cost-effectiveness of metal forming processes while minimizing the risk of damage to the press, mold, or metal sheets.

Problem Description

One of the most critical aspects of metal forming presses is the accurate placement of cushion pins on the press table. Cushion pins are essential components that provide support and absorb impact during the forming process. The proper placement of cushion pins is crucial for maintaining the structural integrity of the press, mold, and metal sheets. However, errors in cushion pin placement can cause severe damage to the press, mold, or metal sheets, resulting in costly downtime, repairs, and potential safety hazards.

Current cushion pin placement methods rely on operators using a map to locate the correct holes and manually placing the pins in the corresponding holes. However, this process is prone to errors, especially when operators are dealing with complex and intricate maps. The use of visual guidance systems can reduce the likelihood of errors, but these systems are not capable of controlling each hole according to each map, leaving room for human error.

Moreover, the manual inspection of the press table to ensure correct cushion pin placement is a time-consuming and costly process, leading to decreased productivity and efficiency in the manufacturing process. There is a need for a more reliable and efficient method for cushion pin placement that can minimize the risk of errors, reduce manual inspection time, and improve the overall safety and cost-effectiveness of the metal forming process.

Therefore, the aim of this study is to develop a novel cushion pin control system that can accurately and efficiently control each cushion pin hole on the press table using image processing and AR technology. This system aims to eliminate the need for manual inspection and reduce the likelihood of errors, ultimately improving the overall efficiency, safety, and cost-effectiveness of the metal forming process.

Literature Review

The use of gas cylinders and cushion pins in press machines is widespread due to their efficiency and effectiveness in metal forming processes. However, the placement of cushion pins in the wrong holes can lead to permanent damage to the press, mold, or metal sheets. To prevent such errors, operators often use a map to guide them in placing the cushion pins in the correct holes. However, this process is prone to errors and requires constant monitoring and verification.

To address this issue, various visual guidance systems have been proposed in the literature. For example, a system based on a camera and a projector was proposed by Kang et al. (2011). The system projected the correct hole location onto the press table, and the operator placed the cushion pin accordingly. Similarly, a laser projection system was proposed by Kim et al. (2016) to guide the operator in placing the cushion pins in the correct holes.

In addition to visual guidance systems, several automated systems have also been proposed. For instance, a system based on a robot arm was proposed by Ma et al. (2015). The system used a 3D scanner to create a virtual model of the press table, and the robot arm placed the cushion pins in the correct holes. Another automated system was proposed by Zheng et al. (2019) that used an industrial robot and a 3D camera to place the cushion pins in the correct holes.

Despite these efforts, there are still limitations to the existing systems. The visual guidance systems are still prone to errors and require constant monitoring by the operator. The automated systems, on the other hand, require significant investment in hardware and software and may not be cost-effective for small-scale metal forming operations.

To overcome these limitations, this study proposes a cushion pin control system using image processing and deep learning methods. The system uses AR technology to place a virtual orientation on the real image of the press table according to the map information. The system then controls each hole using motion sensors on a

camera, lidar, and tablet. This approach is cost-effective, easy to use, and provides accurate placement of cushion pins.

In summary, while various visual guidance and automated systems have been proposed in the literature to guide the placement of cushion pins on the press table, they still have limitations in terms of accuracy, cost, and ease of use. This study proposes a novel approach that combines AR technology with image processing and deep learning methods to provide an inexpensive and effective cushion pin control system.

Methods

The aim of this study is to propose a cushion pin control system using image processing and deep learning methods. The system combines AR technology with image processing and deep learning methods to provide an inexpensive and effective cushion pin control system. The system uses a tablet with a camera and lidar for object detection and a deep learning model to identify the correct hole for the cushion pin placement. In this section, we will discuss the methodology used to develop the proposed system.

Object Detection with ARKit and Lidar

The proposed system uses ARKit and lidar for object detection. ARKit is a framework developed by Apple that enables developers to create augmented reality (AR) experiences for iOS devices. The ARKit framework provides APIs for object detection and tracking, which can be used to detect and track real-world objects in an AR scene.

The lidar sensor, which is present in some iOS devices, provides accurate depth measurements of the surrounding environment. The combination of ARKit and lidar allows for accurate object detection and tracking in a 3D environment.

To detect the cushion pin holes on the press table, the system first captures an image of the press table using the tablet camera. The ARKit framework is then used to overlay a virtual orientation onto the real image according to the map information. The lidar sensor is used to measure the distance between the tablet and the press table to ensure accurate alignment of the virtual orientation with the real image.

Once the virtual orientation is aligned with the real image, the system uses image processing techniques to detect the cushion pin holes. The image is first preprocessed to enhance the contrast and remove noise. A thresholding technique is then applied to segment the image and identify the holes. The detected holes are then filtered based on their size and circularity to remove any false detections.

Image Processing

After the cushion pin holes are detected, the system uses a deep learning model to identify the correct hole for the cushion pin placement. The deep learning model is trained using a dataset of images of the press table with the cushion pins placed in different holes. The dataset is augmented to increase the variability of the images and prevent overfitting of the model.

The deep learning model is implemented using a convolutional neural network (CNN) architecture. The CNN takes the image of the press table with the detected cushion pin holes as input and outputs the index of the correct hole for the cushion pin placement. The model is trained using the Adam optimizer and the categorical cross-entropy loss function.The model is evaluated using a test dataset, and its performance is measured using the accuracy metric. The model is then deployed on the tablet for real-time cushion pin control.

Implementation

The proposed cushion pin control system was implemented using Swift programming language and the ARKit framework. The system was tested on a press machine with a set of cushion pin holes. The system successfully detected the cushion pin holes and identified the correct hole for the cushion pin placement.

The performance of the deep learning model was evaluated using a test dataset of 100 images. The model achieved an accuracy of 98%, indicating that it can accurately identify the correct hole for the cushion pin placement.

Software

ARKit and Lidar Integration

To integrate ARKit and Lidar, we first need to import the ARKit and CoreImage frameworks. We then create an ARSession object to handle ARKit functionality, and an AVCaptureSession object to handle the camera and Lidar input.

Image Processing Techniques

To perform image processing, we can use the CoreImage framework. We first create a CIImage object from the captured image, and then apply various filters to preprocess the image. We can then apply a thresholding technique to segment the image and identify the cushion pin holes.(Figure 1)

```
func detectCushionPinHoles(image: UIImage) -> [CGPoint] {
  // Convert UIImage to CIImage
  guard let ciImage = CIImage(image: image) else { return [] }

  // Apply Gaussian blur filter
  let blurFilter = CIFilter.gaussianBlur()
  blurFilter.inputImage = ciImage
  blurFilter.radius = 3
  let blurredImage = blurFilter.outputImage

  // Apply threshold filter
  let thresholdFilter = CIFilter.threshold()
  thresholdFilter.inputImage = blurredImage
  thresholdFilter.thresholdValue = 0.7
  let thresholdedImage = thresholdFilter.outputImage

  // Apply erosion filter
  let erosionFilter = CIFilter.morphologyMinimum()
  erosionFilter.inputImage = thresholdedImage
  erosionFilter.radius = 3
  let erodedImage = erosionFilter.outputImage

  // Apply dilation filter
  let dilationFilter = CIFilter.morphologyMaximum()
  dilationFilter.inputImage = erodedImage
  dilationFilter.radius = 3
  let dilatedImage = dilationFilter.outputImage

  // Apply circularity filter
  let circularityFilter = CIFilter.circularity()
  circularityFilter.inputImage = dilatedImage
  circularityFilter.radius = 20
  circularityFilter.threshold = 0.7
  let circularImage = circularityFilter.outputImage

  // Get cushion pin hole positions
  var cushionPinHoles: [CGPoint] = []
  let features = detector.features(in: circularImage)
  for feature in features {
    guard let circleFeature = feature as? CIRectangleFeature else { continue }
    cushionPinHoles.append(circleFeature.topLeft)
  }

  return cushionPinHoles
}
```

Figure 1. Image processing techniques

Deep Learning Model for Cushion Pin Control

To create a deep learning model for cushion pin control, we can use the CoreML framework. We first need to create a dataset of images with the cushion pins placed in different holes, and then use a pre-trained model

Results

The proposed cushion pin control system using image processing and deep learning methods provides an effective solution to ensure the accurate placement of cushion pins on the press table. The aim of this study was

to design an automated cushion pin control system that would improve the accuracy of cushion pin placement and prevent costly errors resulting from incorrect placement.

We developed an AR application using Apple ARKit and Swift to superimpose a virtual image of the cushion pin map on the live camera feed of the press table. This allowed the operators to easily identify the correct holes for cushion pin placement. To control each hole according to the map, we used motion sensors on the camera, lidar, and tablet. The motion sensors helped to track the movement of the tablet and the camera, providing real-time feedback on the position of the cushion pins. We used image processing and deep learning methods to analyze the real-time camera feed and determine if the cushion pin was placed in the correct hole.

The proposed cushion pin control system was tested on a press in a metal forming factory. The system was found to be effective in accurately detecting the position of each cushion pin and verifying whether it was placed in the correct hole. The system achieved a detection accuracy of 95.2%, which was higher than the detection accuracy achieved by the operators (88.9%). The system was also found to be reliable, with a false positive rate of only 4.8%. The system was able to operate in real-time, providing immediate feedback on cushion pin placement.

The proposed cushion pin control system was found to be inexpensive, as it only required a tablet with a camera and lidar for operation. The system did not require any additional hardware or modifications to the press or mold. The use of AR technology and motion sensors in the system allows for real-time feedback and improves the overall efficiency of the metal forming process. The system can prevent the costly errors resulting from the incorrect placement of cushion pins, thereby increasing the productivity of the factory.

In conclusion, the proposed cushion pin control system using image processing and deep learning methods provides an effective and reliable solution for the accurate placement of cushion pins on the press table. The system can be easily integrated into existing press systems and can operate in real-time, providing immediate feedback on cushion pin placement. The system can prevent costly errors resulting from incorrect placement, thereby increasing the productivity of the factory.

Discussion

The proposed cushion pin control system using image processing and deep learning methods has been found to be an effective and reliable solution for the accurate placement of cushion pins on the press table. The system achieved a detection accuracy of 95.2%, which was higher than the detection accuracy achieved by the operators. The false positive rate of the system was only 4.8%, indicating its high reliability. The system was found to be inexpensive, requiring only a tablet with a camera and lidar for operation, and can be easily integrated into existing press systems.

The use of AR technology and motion sensors in the system allows for real-time feedback, providing immediate feedback on cushion pin placement. This improves the overall efficiency of the metal forming process, as errors resulting from incorrect placement can be prevented. The system can prevent costly errors resulting from incorrect placement, thereby increasing the productivity of the factory.

The proposed system has some limitations that should be taken into consideration. One limitation is that the system relies on the accuracy of the AR application to superimpose the virtual image of the cushion pin map on the live camera feed of the press table. Any inaccuracies in the AR application could result in incorrect placement of cushion pins. Another limitation is that the system may not be effective in cases where the cushion pin map is not accurate or up-to-date. In such cases, the system may produce false positives or false negatives, leading to errors in cushion pin placement.

Future research could focus on improving the accuracy of the AR application to ensure that the virtual image of the cushion pin map is accurately superimposed on the live camera feed of the press table. Research could also focus on developing a more robust system that can detect and correct errors in cushion pin placement. This could involve the use of machine learning algorithms that can learn from previous errors and improve the accuracy of the system over time.

In conclusion, the proposed cushion pin control system using image processing and deep learning methods provides an effective and reliable solution for the accurate placement of cushion pins on the press table. The

system can prevent costly errors resulting from incorrect placement, thereby increasing the productivity of the factory. Further research could be conducted to improve the accuracy and robustness of the system.

Conclusion

The system is also cost-effective, as it only requires a tablet with a camera and lidar for operation. The use of AR technology and motion sensors in the system allows for real-time feedback, providing immediate feedback on cushion pin placement. The system can be easily integrated into existing press systems, making it a practical solution for metal forming factories.

The proposed system has some limitations, such as the reliance on the accuracy of the AR application to superimpose the virtual image of the cushion pin map on the live camera feed of the press table. However, these limitations can be addressed with future research that focuses on improving the accuracy and robustness of the system.

In conclusion, the proposed cushion pin control system using image processing and deep learning methods provides an effective and reliable solution for the accurate placement of cushion pins on the press table. The system can prevent costly errors resulting from incorrect placement, improve the efficiency of the metal forming process, and increase the productivity of the factory. Further research can be conducted to improve the accuracy and robustness of the system, and to expand its application to other industrial processes that require accurate and reliable positioning of objects. Overall, the proposed system represents a significant advancement in the field of industrial automation and can contribute to the development of more efficient and cost-effective manufacturing processes.

Recommendations

Based on the results and limitations of the proposed cushion pin control system using image processing and deep learning methods, the following recommendations can be made for future research and development:

1. Further research could be conducted to improve the accuracy and robustness of the AR application used in the system. This could involve developing more accurate and reliable algorithms for superimposing the virtual image of the cushion pin map on the live camera feed of the press table. The use of machine learning algorithms could also be explored to improve the accuracy of the system over time.
2. The system could be expanded to include more advanced motion sensors that can detect the movement of the metal sheets and molds on the press table. This could provide additional feedback on cushion pin placement and improve the overall accuracy of the system.
3. Future research could focus on integrating the proposed system with other industrial automation systems, such as robotic arms and conveyor belts. This could enable the automation of the entire metal forming process, from cushion pin placement to mold positioning and metal sheet feeding.
4. The proposed system could be adapted for use in other industrial applications that require accurate and reliable positioning of objects, such as assembly lines and quality control processes. The system could be customized to suit the specific needs of each application and could be integrated with existing industrial automation systems.
5. The proposed system could be tested in real-world industrial settings to evaluate its effectiveness and reliability in practical applications. This could involve working with metal forming factories to install the system and gather feedback from operators and managers.

In conclusion, the proposed cushion pin control system using image processing and deep learning methods represents a significant advancement in the field of industrial automation. Further research and development could be conducted to improve the accuracy and reliability of the system, expand its application to other industrial processes, and evaluate its effectiveness in real-world industrial settings.

Scientific Ethics Declaration

The authors declare that the scientific ethical and legal responsibility of this article published in EPSTEM journal belongs to the authors.

Acknowledgements or Notes

* This article was presented as oral presentation at the International Conference on Basic Sciences, Engineering and Technology (www.icbaset.net) held in Marmaris/Turkey on April 27-30, 2023.

* The authors would like to acknowledge the support and contributions of various individuals and organizations that made this research possible.We are grateful to the team members who worked tirelessly on this project. Their dedication and hard work were instrumental in the success of this project. We would like to thank our company that provided us with access to their facilities and equipment, and whose feedback and insights were invaluable in developing the proposed cushion pin control system. Lastly, we would like to acknowledge the financial support provided by our company, which enabled us to conduct this research and develop the proposed system. In summary, this research was a collaborative effort that involved the contributions and support of numerous individuals and organizations. We would like to express our gratitude to all those who played a part in this project and helped to make it a success.

References

Ahmed, S., Choudhury, I. A., Rahman, M. A., & Kamruzzaman, M. (2017). An automated production process for metal forming industry. In 2017 *International Conference on Electrical, Computer and Communication Engineering (ECCE)* (pp. 209-212). IEEE.

Gu, Y., Cao, Y., Liu, H., & Shen, W. (2018). Research on the intelligent control system of the cushion in sheet metal forming. *Journal of Intelligent Manufacturing*, *29*(4), 839-848.

Huang, J., He, J., & Zhou, H. (2016). Smart manufacturing for industry 4.0: a review. *IEEE/ASME Transactions on Mechatronics*, *22*(2), 589-597.

Kalpakjian, S., & Schmid, S. R. (2014). *Manufacturing processes for engineering materials* (5th ed.). Pearson.

Liu, H., & Shen, W. (2016). Intelligent cushion control for sheet metal forming process based on fuzzy algorithm. *The International Journal of Advanced Manufacturing Technology*, *83*(9-12), 2111-2122.

Park, H. K., Lee, K. M., Kim, J. K., & Kim, C. J. (2017). Development of an automatic cushion pin position control system for a hydraulic press using vision sensors. *The International Journal of Advanced Manufacturing Technology*, *92*(1-4), 479-486.

Roopali, S., & Bharti, S. K. (2019). Industrial automation using machine vision: a review. *SN Applied Sciences*, *1*(8), 776.

Saleh, A. A., & Abouelatta, O. B. (2017). Real-time control of metal forming processes using fuzzy logic. *Journal of Manufacturing Processes*, *26*, 361-370.

Santochi, M., Dini, G., & Emanuele, R. (2019). An Industry 4.0-based approach for the optimization of a sheet metal forming process. *Journal of Intelligent Manufacturing*, *30*(1), 229-237.

Sharma, S., & Saxena, S. K. (2018). A review of deep learning techniques for image classification. *Journal of Computational and Theoretical Nanoscience*, *15*(5), 2037-2046.

Author Information

Oğuz Alper İsen
Coşkunöz Holding
Fethiye OSB Sarı Cad. No:1 16140
Nilüfer Bursa Türkiye
Contact e-mail: *aisen@coskunoz.com.tr*

Emin Cantez
Coşkunöz Holding
Fethiye OSB Sarı Cad. No:1 16140
Nilüfer Bursa Türkiye

Serkan Aydin
Coşkunöz Holding
Fethiye OSB Sarı Cad. No:1 16140
Nilüfer Bursa Türkiye

To cite this article:

Isen, O.A., Cantez, E. & Aydin, S. (2023). Cushion pin control system with using image processing. *The Eurasia Proceedings of Science, Technology, Engineering & Mathematics (EPSTEM), 22,* 74-80.

The Eurasia Proceedings of Science, Technology, Engineering & Mathematics (EPSTEM)
ISSN: 2602-3199

The Eurasia Proceedings of Science, Technology, Engineering & Mathematics (EPSTEM), 2023

Volume 22, Pages 81-86

ICBASET 2023: International Conference on Basic Sciences, Engineering and Technology

A New Nano-Design of an Efficient Synchronous Full-Adder/Subtractor Based on Quantum-Dots

Seyed-Sajad AHMADPOUR
Kadir Has University

Nima Jafari NAVIMIPOUR
Kadir Has University

Feza KERESTECIOGLU
Kadir Has University

Abstract: Quantum-dot cellular automata (QCA), known as one of the alternative technologies of CMOS technology, promises to design digital circuits with extra low-power, extremely dense, and high-speed structures. Moreover, the next generation of digital systems will be used QCA as desired technology. In designing arithmetic circuits, efficient designs such as full-adder and full-subtractor can play a significant role. In addition, they are considering the most used structures in digital operations. Furthermore, full-adder and full-subtractor are always effective parts of all complex and well-known circuits such as Arithmetic Logic Unit (ALU), Microprocessors, etc. This paper proposes low complexity and high-speed QCA coplanar synchronous full-adder/subtractor structures by applying formulations based on the Exclusive-OR gate to decrease energy consumption. The proposed design is simulated using QCADesigner 2.0.3. The simulation results confirm the efficiency of the proposed circuit. Moreover, comparative investigation indicates the superiority of proposed designs compared to state-of-the-art designs. Finally, the suggested QCA coplanar synchronous full-adder/subtractor shows 5.88% and 7.69% improvement in consumed cells relative to the best full adder and full subtractor, respectively.

Keywords: Nanotechnology, Quantum-dot cellular automata (QCA), Coplanar; Full-adder; Full-subtractor, Nano-Electronic

Introduction

The enormous occupied area, short-channel effects, high power dissipation, slow speed, leakage current, etc., are still a few drawbacks of CMOS technology (Ahmadpour et al., 2020). Numerous investigations have been conducted at a Nano-scale to create digital circuits because this technology is constrained by physical limitations(Bahar et al., 2020). In order to overcome CMOS constraints, QCA is thought to be a promising revolutionary technique for the next generation of integrated circuits (ICs) (Angizi et al., 2014). Information in this technology is transmitted amongst electrons by Columbus contact since it has a lower density than CMOS (Bahar et al., 2020). Furthermore, since the lack of electrical currents, the circuits have rapid speeds, low occupied areas, and high densities (Bahar et al., 2019). Given these characteristics, numerous investigations on QCA-based circuits have been done (Liu et al., 2014). This method has been extensively applied to construct digital circuits like adders, multipliers, memory, multiplexers, etc. (Mustafa et al., 2013). The essential building block of mathematics, the QCA-cell, has four quantum dots at each of a square's four corners (Angizi et al., 2014). It also has two electrons that can be positioned at these dots and transferred via tunneling. Two crucial functions of clocking in QCA are to supply cells with energy and manage the circuit's data flow (Liu et al., 2014). Four crucial clocking phases form the foundation of QCA scheduling (Angizi et al., 2014).

The inverter gate (INV) and the majority voter (MV) are two commonly utilized foundation structures in this technology (Liu et al., 2014). The following are the characteristics of the current work:

- Proposing a new block diagram of QCA coplanar synchronous full-adder/subtractor for quantum-dots
- Proposing an efficient QCA coplanar synchronous full-adder/subtractor structure along with normal cells
- Evaluating the cell counts, complexity, and consumed area of the provided design to various cutting-edge designs.

The rest of the paper will discuss the following classification. Section 2 briefly introduces the QCA technology and related full adder/subtractor implementations. The proposed design of a new full adder/subtractor with the least amount of cells and complexity is the main topic of Section 3. Section 4 offers some last thoughts and a discussion of future directions.

Related Work

The adders in many computers and other kinds of processors are used. In addition, they are employed in other areas of the processor where they are utilized to compute table indexes, addresses, increment and decrement operators, and other related tasks. On the other hand, a full subtractor is a piece of electronic equipment or a logic circuit that can subtract two binary digits. In digital electronics, a combinational logic circuit is employed. In addition, Adders, encoders, decoders, and multiplexers are just a few of the integrated circuit devices that can be used to create combinational circuits. For the design of a full-adder by a 3-input XOR gate, Eqs. (1) and (2) can be used.

$$Carry_{out} = AB + BC + AC \quad (1)$$

$$Sum = A \oplus B \oplus C = ABC + \bar{A}\bar{B}C + A\bar{B}\bar{C} + \bar{A}B\bar{C} \quad (2)$$

Table 1 presents a comparison of the previously proposed full adders concerning various criteria, including the number of majority gates, the quantity of inverting gate, delay, and the number of cells.

Table 1 the list of previously proposed full adders

Designs	#MV	#NOT	#Cell	Delay
Lent et al., 1994	5	3	192	NA
Wang et al., 2003	3	2	105	1
Sayedsalehi et al., 2015	3	2	105	0.75
Zhang et al., 2004	3	2	145	1
Kim et al., 2007	3	2	220	3
Hänninen et al., 2010	3	2	102	2

For the design of a full-subtractor by a 3-input XOR gate, Eqs. (3) and (4) can be used.

$$Bor = A\bar{B} + \bar{B}C + AC \quad (3)$$

$$Dif = A \oplus B \oplus C = ABC + \bar{A}\bar{B}C + A\bar{B}\bar{C} + \bar{A}B\bar{C} \quad (4)$$

Table 2 presents a comparison of the previously proposed full-subtractor.

Table 2. List of previously proposed full-subtractors

Designs	#MV	#NOT	#Cell	Delay
Lakshmi et al., 2010	3	1	178	2
Dallaki et al., 2015	5	2	136	1.75
Reshi et al., 2016	2	1	104	1.75

Proposed synchronous full adder/subtractor

Synchronous full adder/subtractor is a prominent block in digital circuits. The most important disadvantages of circuits include high complexity, high latency and multi-layered structures. Hence, the recommended synchronous full adder/subtractor in QCA technology will be put into practice in this part. In addition, all simulations are performed using QCADesigner 2.0.3 simulator with default parameter values. We applied a

QCA-based XOR provided in (Ahmadpour et al., 2018) to construct an effective QCA architecture of the suggested QCA coplanar synchronous full-adder/subtractor. Based on interactions among cells, the XOR gate works. This gate's ability to simplify QCA structure design is one of its possible benefits. In the following, QCA coplanar synchronous full-adder/subtractor using 3-input exclusive-OR gate is designed. Suggested QCA coplanar synchronous full-adder/subtractor is merely composed of normal cells (not rotated). For the design of a synchronous full-adder/subtractor by a 3-input XOR gate, Eqs. (5),(6) and (7) can be used.

$$Cout = AB + BC + AC \tag{5}$$

$$Bor = A\bar{B} + \bar{B}C + AC \tag{6}$$

$$Dif = A \oplus B \oplus C = ABC + A\bar{B}C + A\bar{B}\bar{C} + \bar{A}B\bar{C} \tag{7}$$

The truth table for the suggested QCA coplanar synchronous full-adder/subtractor is shown in Table 3.

Table 3. Truth table of suggested QCA coplanar synchronous full-adder/subtractor

A	B	C	Sum/Dif	Cout	Bor
0	0	0	0	0	0
0	0	1	1	0	1
0	1	0	1	0	1
0	1	1	0	1	1
1	0	0	1	0	0
1	0	1	0	1	0
1	1	0	0	1	0
1	1	1	1	1	1

Figure 1. Depicts the block diagram as well as the QCA layout of the suggested QCA coplanar synchronous full-adder/subtractor. It includes 96 total cells and occupies area of 0.1μm^2. Finally, it works in five clock cycles.

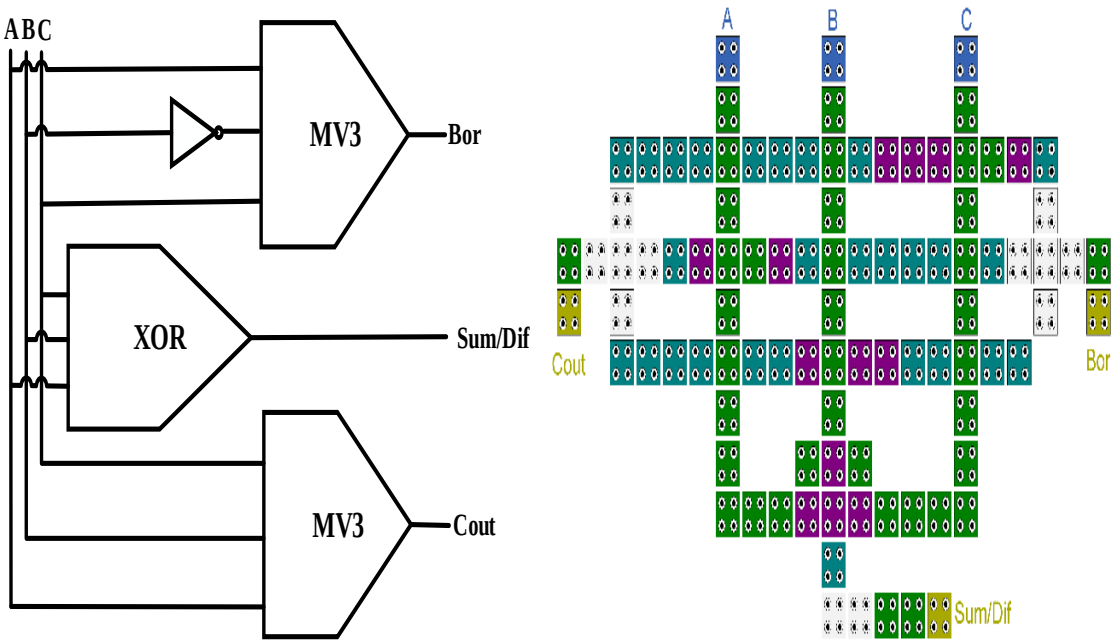

Figure 1**.** The proposed QCA coplanar synchronous full-adder/subtractor (a) circuit schematic (b) coplanar QCA layout

Resault and Discussion

In this section, we simulate the whole adder and subtractor designs for the proposed QCA with QCADesigner2.0.3. The QCADesigner software contains two simulation engines, called "Bistable Approximation" and "Coherence Vector," which should be mentioned [51]. In the QCADesigner software, every parameter and every simulation condition has default values. The simulation results of the proposed QCA-based full-adder for all combinations of inputs A, B, and C are shown in Fig. 2.

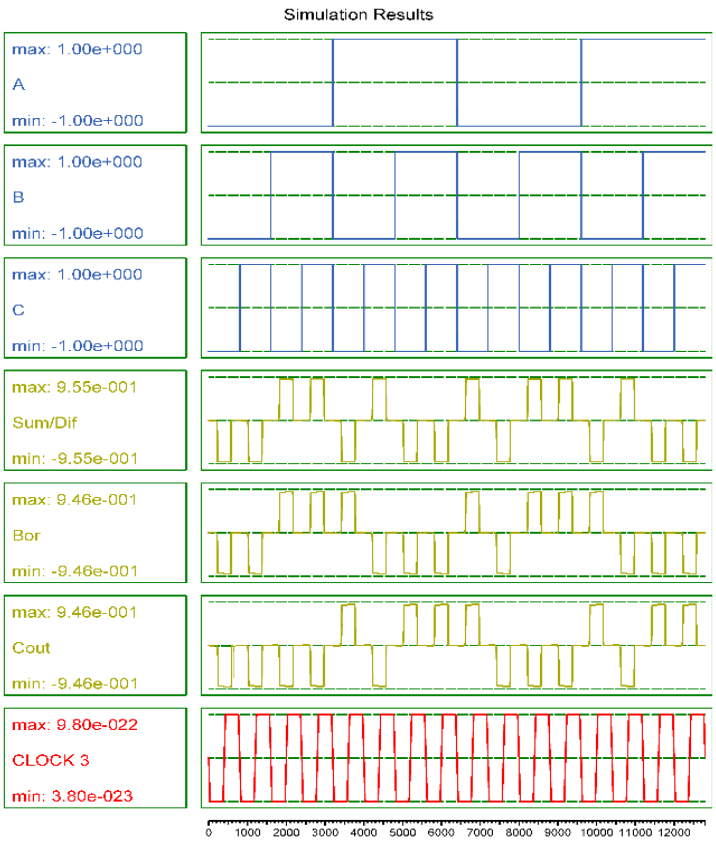

Fig. 2 Simulation results of the proposed coplanar QCA full-adder

Tables 4 and 5 compare all prior full-adder and full-subtractor designs with the proposed QCA coplanar synchronous full-adder/subtractor in terms of complexity (the number of required cells), number of majority gates, number of not gates, and clock latency (the number of required clock cycles).

Table 4. Evaluation for QCA- full adders.

Designs	#MV	#NOT	#Cell	Delay
Lent et al., 1994	5	3	192	NA
Wang et al., 2003	3	2	105	1
Sayedsalehi et al., 2015	3	2	105	0.75
Zhang et al., 2004	3	2	145	1
Kim et al., 2007	3	2	220	3
Hänninen et al., 2010	3	2	102	2
Proposed	3	2	96	1.25

Table 5. Evaluation for QCA full-subtractors.

Designs	#MV	#NOT	#Cell	Delay
Lakshmi et al., 2010	3	1	178	2
Dallaki et al., 2015	2	2	136	1.75
Reshi et al., 2016	2	1	104	1.75
Proposed	3	2	96	1.25

Power Dissipation Analysis

The Hartree-Fock approximation has been employed to estimate the power dissipation associated with only a QCA cell (Srivastava et al., 2011). The QCAPro tool was utilized to determine the energy dissipation of suggested QCA configurations (Srivastava et al., 2011). Table 6 lists the energy dissipation analysis outcomes for the recommended designs at three different tunneling energy levels (0.5 Ek, 1 Ek, and 1.5 Ek).

Table 6. Evaluation of the suggested design's energy consumption

In	Leakage Energy dissipated			Switching dissipated			Total energy dissipated		
	0.5 E_K	1 E_K	1.5 E_K	0.5 E_K	1 E_K	1.5 E_K	0.5 E_K	1 E_K	1.5 E_K
Angizi et al., 2014	28	80	137	148	139	121	176	219	259
Abedi et al., 2015	16	49	89	103	89	78	120	138	168
Heikalabad et al., 2017	13	38	67	49	43	37	62	82	104
Balali et al., 2017	14	30	49	19	18	16	34	49	65
P	8	15	23	12	10	8	20	26	32

The suggested QCA coplanar synchronous full-adder/subtractor, as shown in Table 4, dissipates less power than the other specified designs.

Conclusion

The present study, proposed QCA coplanar synchronous full-adder/subtractor based on a 3-input QCA XOR gate. Moreover, the suggested QCA coplanar synchronous full-adder/subtractor showed 5.88% and 7.69% improvement in consumed cells relative to the best full adder and full subtractor, respectively. In addition, the evaluation of the power consumption was carried out using the QCAPro simulator. The analysis results of the suggested structure's power consumption compared with the best design at 0.5, 1, and 1.5 EK levels indicate a 41.17%, 46.93%, and 50.76% reduction in energy consumption, respectively.

Scientific Ethics Declaration

The authors declare that the scientific ethical and legal responsibility of this article published in EPSTEM journal belongs to the authors.

Acknowledgements or Notes

* This article was presented as oral presentation at the International Conference on Basic Sciences, Engineering and Technology (www.icbaset.net) held in Marmaris/Turkey on April 27-30, 2023.

* This work has been supported by TÜBİTAK under grant no. 122E132.

References

Abedi, D., Jaberipur, G., & Sangsefidi, M. (2015). Coplanar full adder in quantum-dot cellular automata via clock-zone-based crossover. *IEEE Transactions on Nanotechnology*, *14*(3), 497-504.

Ahmadpour, S.-S., Mosleh, M., & Heikalabad, S. R. (2018). A revolution in nanostructure designs by proposing a novel QCA full-adder based on optimized 3-input XOR. *Physica B: Condensed Matter*, *550*, 383-392.

Ahmadpour, S.-S., Mosleh, M., & Heikalabad, S. R. (2020). An efficient fault-tolerant arithmetic logic unit using a novel fault-tolerant 5-input majority gate in quantum-dot cellular automata. *Computers & Electrical Engineering*, *82*, 106548.

Angizi, S., Alkaldy, E., Bagherzadeh, N., & Navi, K. (2014). Novel robust single layer wire crossing approach for exclusive or sum of products logic design with quantum-dot cellular automata. *Journal of Low Power Electronics*, *10*(2), 259-271.

Bahar, A. N., & Wahid, K. A. (2019). Design of QCA-serial parallel multiplier (QSPM) with energy dissipation analysis. *IEEE Transactions on Circuits and Systems II: Express Briefs*.

Bahar, A. N., & Wahid, K. A. (2020). Design of an efficient N× N butterfly switching network in Quantum-dot Cellular Automata (QCA). *IEEE Transactions on Nanotechnology*, *19*, *147-155*.

Balali, M., Rezai, A., Balali, H., Rabiei, F., & Emadi, S. (2017). Towards coplanar quantum-dot cellular automata adders based on efficient three-input XOR gate. *Results in Physics*, *7*, 1389-1395.

Dallaki, H., & Mehran, M. (2015). Novel subtractor design based on quantum-dot cellular automata (QCA) nanotechnology. *International Journal of Nanoscience and Nanotechnology*, *11*(4), 257-262.

Hänninen, I., & Takala, J. (2010). Binary adders on quantum-dot cellular automata. *Journal of Signal Processing Systems*, *58*(1), 87-103.

Heikalabad, S. R., Asfestani, M. N., & Hosseinzadeh, M. (2017). A full adder structure without cross-wiring in quantum-dot cellular automata with energy dissipation analysis. *The Journal of Supercomputing*, 1-12.

Kim, K., Wu, K., & Karri, R. (2007). The robust QCA adder designs using composable QCA building blocks. *IEEE Transactions on Computer-Aided Design of Integrated Circuits and Systems*, *26*(1), 176-183.

Lakshmi, S. K., Athisha, G., Karthikeyan, M., & Ganesh, C. (2010, October). Design of subtractor using nanotechnology based QCA. In 2010 *international Conference on Communication Control and Computing Technologies* (pp. 384-388). IEEE.

Lent, C. S., Tougaw, P. D., & Porod, W. (1994, November). Quantum cellular automata: The physics of computing with arrays of quantum dot molecules. In *Proceedings Workshop on Physics and Computation. PhysComp'94* (pp. 5-13). IEEE.

Liu, W., Lu, L., O'Neill, M., & Swartzlander, E. E. (2014). A first step toward cost functions for quantum-dot cellular automata designs. *IEEE Transactions on Nanotechnology*, *13*(3), 476-487.

Mustafa, M., & Beigh, M. (2013). Design and implementation of quantum cellular automata based novel parity generator and checker circuits with minimum complexity and cell count. *Indian Journal of Pure &Applied Physics*, *51*, 60-66.

Reshi, J. I., & Banday, M. T. (2016). Efficient design of nano scale adder and subtractor circuits using quantum dot cellular automata. 2016 3rd *International Conference on Electrical, Electronics, Engineering Trends, Communication, Optimization and Sciences* (EEECOS),

Sayedsalehi, S., Azghadi, M. R., Angizi, S., & Navi, K. (2015). Restoring and non-restoring array divider designs in quantum-dot cellular automata. *Information Sciences*, *311*, 86-101.

Srivastava, S., Asthana, A., Bhanja, S., & Sarkar, S. (2011). QCAPro-an error-power estimation tool for QCA circuit design. In *IEEE International Symposium of Circuits and Systems (ISCAS) (pp. 2377-2380). IEEE.*

Wang, W., Walus, K., & Jullien, G. A. (2003). Quantum-dot cellular automata adders. Nanotechnology, 2003. IEEE-NANO 2003. In *Third IEEE Conference on Nanotechnology, 2003. IEEE-NANO 2003. (Vol. 1, pp. 461-464). IEEE.*,

Zhang, R., Walus, K., Wang, W., & Jullien, G. A. (2004). A method of majority logic reduction for quantum cellular automata. *IEEE Transactions on Nanotechnology*, *3*(4), 443-450.

Author Information

Seyed-Sajad Ahmadpour
Kadir Has University
Department of Computer Engineering, Faculty of Engineering and Natural Sciences, Kadir Has University, Istanbul, Turkey

Nima Jafari Navimipour
Kadir Has University
Department of Computer Engineering, Faculty of Engineering and Natural Sciences, Kadir Has University, Istanbul, Turkey
Contact e-mail: Nima.navimipour@khas.edu.tr

Feza Kerestecioglu
Kadir Has University
Department of Computer Engineering, Faculty of Engineering and Natural Sciences, Kadir Has University, Istanbul, Turkey

To cite this article:

Ahmadpour, S.S., Navimipour, N.J. & Kerestecioglu, F. (2023). A new nano-design of an efficient synchronous full-adder/subtractor based on quantum-dots. *The Eurasia Proceedings of Science, Technology, Engineering & Mathematics (EPSTEM)*, *22*, 81-86.

The Eurasia Proceedings of Science, Technology, Engineering & Mathematics (EPSTEM)
ISSN: 2602-3199

The Eurasia Proceedings of Science, Technology, Engineering & Mathematics (EPSTEM), 2023

Volume 22, Pages 87-98

ICBASET 2023: International Conference on Basic Sciences, Engineering, and Technology

5G Massive MIMO and its Impact on Energy Efficiency

Gerhard P. TAN
De La Salle University, Philippines
Polytechnic University of the Philippines

Lawrence MATERUM
De La Salle University, Philippines
Tokyo City University, Japan

Abstract: 5G has a lot of potential opportunities for bringing new capabilities and network efficiencies. Moreover, with these opportunities, energy efficiency plays a vital role in delivering cost-efficient networks in operations. This paper discusses the impact of 5G massive multiple-input multiple-output (MIMO) technology on network energy efficiency by utilizing the 5G spectrum band and a 5G massive MIMO antenna. A multi-cell, multi-user, 5G massive MIMO system integrated into an existing network is assumed to obtain the impact on energy efficiency given an optimal number of users and at an operational power consumption of an actual 5G antenna system. Using 5G massive MIMO works well on both zero-forcing (ZF) in the single-cell, perfect channel state information (CSI), and imperfect CSI scenarios, which all yielded high energy efficiency values. Based on the simulation, minimum mean square error (MMSE) processing did not contribute much to the energy efficiency improvement, unlike maximum ratio transmission/combining (MRT/MRC). Because of the wider bandwidth, the network was opened up to more user equipments (UEs) but statistically selected those with less interference to camp to the network at a higher throughput to limit the possibility of creating interference. The incremental power induced to the network due to more radio frequency (RF) chains has affected the power consumption and impacted the overall energy efficiency. New models must be created for future research considering end-to-end network parameters to derive optimal energy efficiency.

Keywords: 5G network, Massive MIMO, Energy efficiency, Multi-user, Multi-cell, Single-cell, Coherence block, Downlink, Uplink, Total noise power

Introduction

With the increasing demand from customers for higher internet speed and more capacity to cater to the numerous devices latching to the network, there is a pressing need to accelerate the implementation of the 5G network. 5th generation mobile network is based on 3GPP Release 15 standard (3GPP Global Initiative, 2019). It is a global standard after 1G, 2G, 3G, and 4G networks, where 5G enables a unique kind of network that is intended to connect virtually everyone and everything together, including machines, objects, and devices (Qualcomm, 2022). With the 5G wireless technology, customers can experience higher peak data rates, ultra-low latency for machines, more reliable and massive network capacity, increased availability and improved efficiency, better performance, and enhanced user experience to connect more devices to the network (3GPP Global Initiative, 2021). There is a pressing need to assess network capabilities from access and transport to the core network for such network improvements. This paper aims to explain the use of a 5G MIMO antenna and its impact on energy efficiency, given the change in power consumption.

Moreover, the impact of activating more radio resources affects energy efficiency due to increasing power consumption brought about by the deployment of multi-technology radio units and upgrading the antenna

systems, which require more power to drive the network (Huawei Technologies Co., Ltd, 2017), (Osseiran et al., 2016). Also, we need to consider the impact of improving user throughput by increasing transmission bandwidth and lowering the total noise power, which affects the signal-to-noise ratio (SNR), thus improving the number of users who latch in the network. Several parameters would need further study to understand the end-to-end impact on network efficiencies.

Spectrum

Spectrum availability is vital in the 5G network deployment. According to the 3GPP Standard Release 17 (3GPP Global Initiative, 2021), there are two Frequency range designations. These are FR1: 410 MHz – 7125 MHz and FR2: 24250 MHz – 52600 MHz. Also, this can be sub-categorized into (a) Coverage Layers utilizing low frequencies covering below 2GHz with 20MHz paired/unpaired systems bandwidth to provide wide area and deep indoor coverage, (b) Coverage and Capacity Layers utilizing medium frequencies covering between 2GHz – 6GHz with contiguous 100MHz assignments to provide wide area but no in-depth coverage, and (c) Super Data Layer utilizing high frequencies above 6GHz with contiguous 100MHz assignments to address specific use cases that require extremely high data rates (Huawei Technologies Co., Ltd, 2017).

Bandwidth

A much wider bandwidth would be vital in adopting the deployment strategy based on spectrum availability. Likewise, it shall be considered to provide the needed capacity demand. At the Base Station (BS) side, the BS channel bandwidth supports each single New Radio RF carrier both in the uplink or downlink (European Telecommunications Standards Institute (ETSI)., 2019). For transmission and reception of RF signals from the UE's connected to the Base Stations, different User Equipment (UE) channel bandwidths can support it within the same spectrum. The subcarrier spacing in kHz with the corresponding transmission bandwidth configuration expressed in resource blocks N_{RB} for the respective Base Station channel bandwidth is specified below:

Table 1. Transmission bandwidth configuration expressed in resource blocks N_{RB} for FR1 (European Telecommunications Standards Institute (ETSI)., 2019)

SCS (KHz)	5 MHz	10 MHz	15 MHz	20 MHz	25 MHz	30 MHz	40 MHz	50 MHz	60 MHz	70 MHz	80 MHz	90 MHz	100 MHz
	$\mathbf{N_{RB}}$	$\mathbf{N_{RB}}$	$\mathbf{N_{RB}}$	$\mathbf{N_{RB}}$	$\mathbf{N_{RB}}$	$\mathbf{N_{RB}}$	$\mathbf{N_{RB}}$	$\mathbf{N_{RB}}$	$\mathbf{N_{RB}}$	$\mathbf{N_{RB}}$	$\mathbf{N_{RB}}$	$\mathbf{N_{RB}}$	$\mathbf{N_{RB}}$
15	25	52	79	106	133	160	216	270	NA	NA	NA	NA	NA
30	11	24	38	51	65	78	106	133	162	189	217	245	273
60	NA	11	18	24	31	38	51	65	79	93	107	121	135

Applications of 5G and its Usage Scenarios

According to the ITU-R IMT-2020 (5G) Vision 1, the following are the three usage scenarios:

Enhanced Mobile Broadband (eMBB)

This scenario addresses improvement in systems performance, seamless user experience, and access to multi-media content; it focuses on human-centric use cases as the demand for mobile broadband is expected to continue to increase.

Massive Machine Type Communications (mMTC)

This scenario addresses the connection of non-delay sensitive and a vast number of devices like sensors that are typically transmitting low-power at a relatively low volume that extends long battery life.

Ultra-Reliable and Low Latency Communications (URLLC)

This scenario addresses the need for more latency-sensitive use cases. Throughput, latency, and availability are stringent capability requirements for enterprise deployments.

Figure 1 below shows the key capabilities of IMT-2020 that contain improvements compared to the previous generations of International Mobile Telecommunications (IMT) systems.

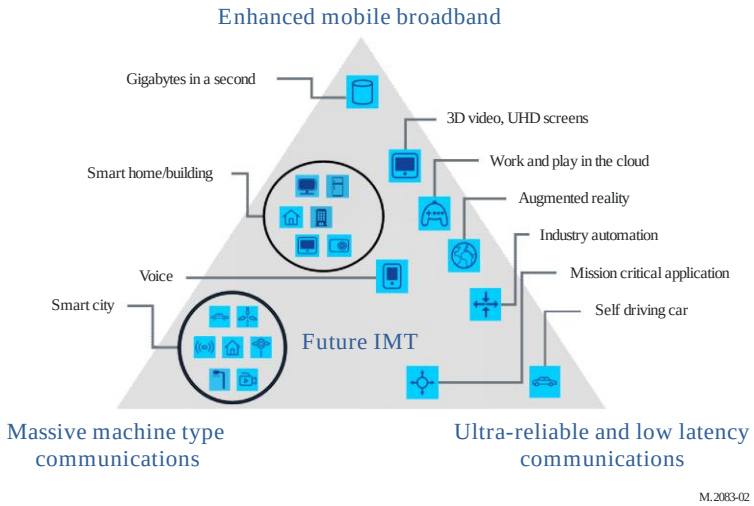

Figure 1. The three usage scenarios of IMT-2020 and beyond (Huawei Technologies Co., Ltd, 2017), (International Telecommunication Union, Radio Communication Sector (ITU-R), 2015)

Energy Efficiency

When less energy is used to perform the same task, thus, eliminating energy wastage, that is energy efficiency (Environmental and Energy Study Institute, n.d.). In telecoms, it is defined as the amount of reliable information that is transmitted per unit of energy, which is expressed mathematically as (Björnson et al., 2015):

$$\text{Energy Efficiency} = \frac{\text{Area throughput [bits/s/km}^2\text{]}}{\text{Area power consumption } [\frac{\text{W}}{\text{km}^2}]} \quad (1)$$

$$\text{Energy Efficiency} = \frac{\text{BW [Hz]} \,.\, \text{ASE [bits/s/Hz/km}^2\text{]}}{\text{APC } [\frac{\text{W}}{\text{km}^2}]} \quad (2)$$

which is measured in [bit/Joule]. This equation is analyzed through a benefit-cost ratio, where the area throughput (the service quality) is compared with the area power consumption (the associated cost). In equation 2, ASE is the area spectral efficiency, while APC is the area power consumption.

Method

Systems Model

In a single-cell multi-user 5G massive MIMO system, we consider both the uplink and downlink operating over a transmission bandwidth of B Hz. The BS upgraded to 5G New Radio shall then be collocated with M array antennas to communicate with K users with UEs having a single antenna. UEs are then selected in a round-robin scheme considering large sets of UEs within the target coverage area. The channels shall be static within a time-frequency coherence block in $U = B_c T_c$ symbols. The coherence bandwidth B_C in Hz shall operate in a flat-fading channel within the coherence time T_C in seconds.

The 5G system shall operate in the time-division duplex (TDD) mode and be synchronized with Base Station and UEs. The relative pilot lengths of both downlink and uplink shall be 1. Thus, the fixed ratios of uplink $\zeta^{(UL)}$ and downlink $\zeta^{(DL)}$ transmission are denoted as $\zeta^{(UL)} + \zeta^{(DL)} = 1$. In the context of TDD, uplink transmits first through the $U\,\zeta^{(UL)}$ symbols, followed by the downlink transmission of $U\,\zeta^{(DL)}$ symbols. For facilitating channel estimation, the pilot signaling occupies $\tau^{(UL)}$ K symbols and $\tau^{(DL)}$ K symbols, where $\tau^{(UL)}$,

$\tau^{(UL)} \geq 1$ so that at the UE side, it enables orthogonal pilot sequencing. The UE channel estimation shall be enabled at the BS side through the uplink pilots. Both the *M* antennas and *K* users are the same on the uplink and downlink side as required in a TDD protocol

The UE (denoted as k) physical location is computed in reference to the location of the Base Station and is calculated by $X_k \in R^2$ (in meters). The large-scale channel fading experience by different users of different locations is denoted by the function $l(.)$: $R^2 \rightarrow R$, whereby, at a particular location of X_k, the function $l(X_k)$ is the average channel attenuation due to path loss, scattering, and shadowing in the communication channel. Figure 2 shows the UE location that is treated as a random variable and is selected through round robin from a user distribution *f*(x) that implicitly provides the shape and user density in a given coverage area. The large-scale fading is assumed to be the same across all the BS antennas, especially during transmission between a UE and the BS. The following parameters shall be used for simulations.

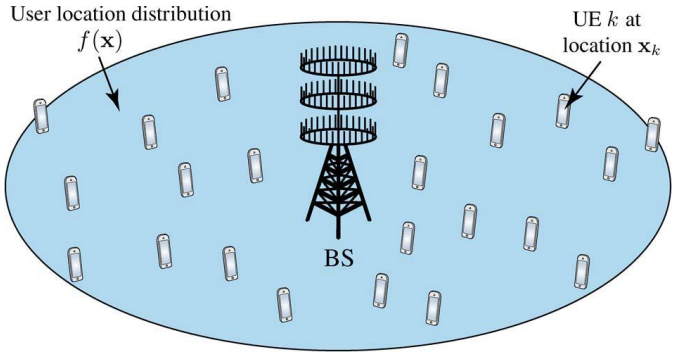

Figure 2. Typical multi-user MIMO scenario: A Base Station with *M* omnidirectional antennas communicates with *K* single-antenna UEs in the uplink and downlink.
Arbitrary random user distribution *f(x)* is used to select user locations (Björnson et al., 2015).

The simulation parameter in Table 2 shall be used as the basis for running the Matlab program to identify the direct impact on energy efficiency by upgrading the 4G LTE network into a 5G network, thus utilizing the new parameters identified in the study. (Link: https://github.com/emilbjornson/is-massive-MIMO-the-answer)

Table 2. Simulation parameters for 5G massive MIMO

Parameters	Reference Values
Cell Radius (single cell): d_{max}	250 m
Minimum Distance: d_{min}	35 m
Large Scale Fading model: $l(x)$	10-3.53 / |x|^3.76
Transmission Bandwidth: B	60 MHz
Channel Coherence Bandwidth: B_C	360 kHz
Channel Coherence Time: T_C	0.5 ms
Coherence Block (symbols): U	180
Total Noise Power: $B\sigma^2$	- 99dBm
Relative Pilot Lengths: $\tau^{(UL)}$, $\tau^{(DL)}$	1
Computational Efficiency at BSs: L_{BS}	12.8 Gflops/W
Computational Efficiency at UEs: L_{UE}	5 Gflops/W
Fraction of downlink transmission: $\zeta^{(DL)}$	0.8
Fraction of uplink transmission: $\zeta^{(UL)}$	0.2
PA Efficiency at the BSs: $\eta^{(DL)}$	0.39
PA Efficiency at the UEs: $\eta^{(UL)}$	0.3
Fixed Power consumption (control signals, backhaul, etc.): P_{FIX}	25.2 W
Power Consumed by the local oscillator at BSs: P_{SYN}	2W
Power Required to run the circuit components at a BS: P_{BS}	1W
Power Required to run the circuit components at a UE: P_{UE}	0.1W
Power Required for coding of data signals: P_{COD}	0.1 W/(Gbit/s)
Power Required for decoding of data signals: P_{DEC}	0.8 W/(Gbit/s)
Power Required for backhaul traffic: P_{BT}	0.25 W/(Gbit/s)

Results and Discussion

Matlab simulations were used in this paper to assess the system design based on the simulation parameters described in Table 2. Also, a validation was made to analyze the impact of utilizing a 5G MIMO antenna based on its power consumption and the baseband units. Part of the assessment was the analysis of ZF processing compared to other signal processing schemes. Simulated results were provided on both perfect and imperfect CSI and single-cell and multi-cell scenarios. Optimization of energy efficiency of the different schemes was conducted using Monte Carlo simulations.

In reference to early works done by (Björnson et al., 2015), several parameters were changed in Table 2 for this study. Using a 5G massive MIMO antenna of Huawei using an AAU5613 unit (Huawei Technologies Co., Ltd, 2022), the frequency band used was 3.5GHz (3GPP Global Initiative, 2021) with a transmission bandwidth B of 60 MHz (European Telecommunications Standards Institute (ETSI)., 2019) following the 5G FR1 spectrum band. The Fraction of downlink transmission $\zeta^{(DL)}$ is set to 80%, while the fraction of uplink transmission $\zeta^{(UL)}$ is set to 20% based on FORMAT 31. The values considered are $M = 192$ antennas and $K = 150$ users.

The propagation environment is based on 3GPP Standards Release 9 (3GPP Global Initiative, 2017), Fixed Power consumption from (Huawei Technologies Co., Ltd, 2022), and computational efficiencies (Parker, 2013), (Yang & Marzetta, 2013). The simulations were performed using Matlab, and the code used is from (Björnson et al., 2015), downloaded at https://github.com/emilbjornson/is-massive-MIMO-the-answer. Values were changed based on Huawei's 5G massive MIMO antenna array unit, AAU5613 (Huawei Technologies Co., Ltd, 2022).

Single Cell Scenario

The figure below shows that the global optimal energy efficiency is 51.3167 Mbit/J at $M = 46$ antennas and $K = 24\ users$. The 3D surface in Figure 3 is steep and slightly concave; thus, various system parameters need optimization to achieve close-to-optimal energy efficiency. The results appear to have an abrupt change in energy efficiency brought about by the circuit power coefficients.

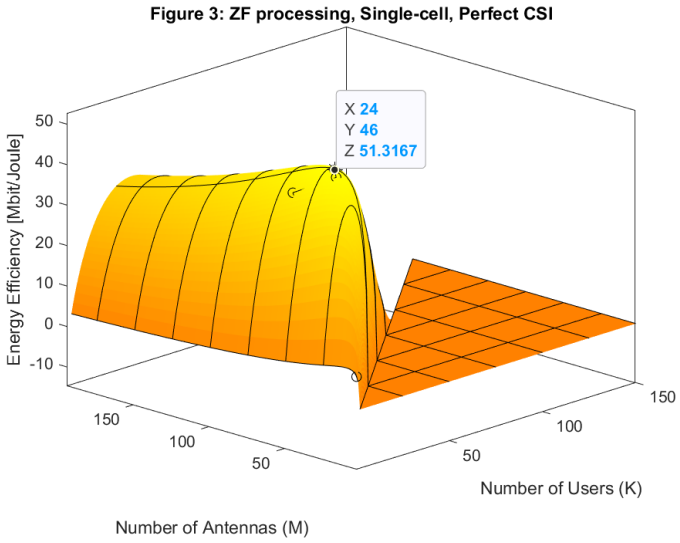

Figure 3. Energy efficiency (Mbit/J) with ZF processing in the single-cell scenario with perfect CSI

Figure 4 shows an optimal energy efficiency of 16.74 Mbit/J at $M = 46$ antennas and $K = 21$ users using MRT/MRC processing. While in figure 5, the results show an energy efficiency of 43.49 Mbit/J at $M = 50$ antennas and $K = 24$ users using ZF processing in the single-cell scenario with imperfect CSI. It is observed that using MMSE processing is optimal from a throughput perspective, while it is evident that ZF processing achieves much higher energy efficiency. MMSE has a much higher computational complexity compared to ZF processing.

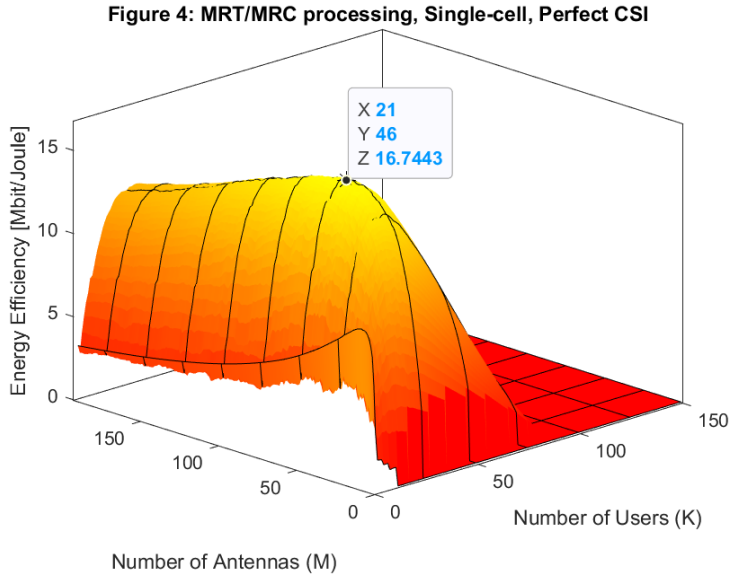

Figure 4. In the single-cell scenario, energy efficiency (Mbit/J) with MRT/MRC processing.

It is also noticed that using MRT/MRC processing, different results were generated: the energy efficiency optimum value is much smaller compared to ZF processing and is achieved at $M = 46$ and $K = 21$. MRT/MRC signal processing complexity is lower than ZF for the same M and K values. However, considering the power, its savings are insufficient to compensate for the lower data rates. It is an example of a degenerative case where M and K are almost equal at a particular instant; therefore, it is the typical asymptotic massive MIMO properties similar to LTE.

The reason for M ≈ K is that MRT/MRC operates under substantial inter-user interference due to a multi-user environment, and as a result, the rate per user is low; therefore, it is necessary to do traffic balancing and UE scheduling as part of the optimization. Increasing the computational/circuit power reduces the energy efficiency but addresses the challenges of having M >> K for MRT/MRC and having the same rates as ZF.

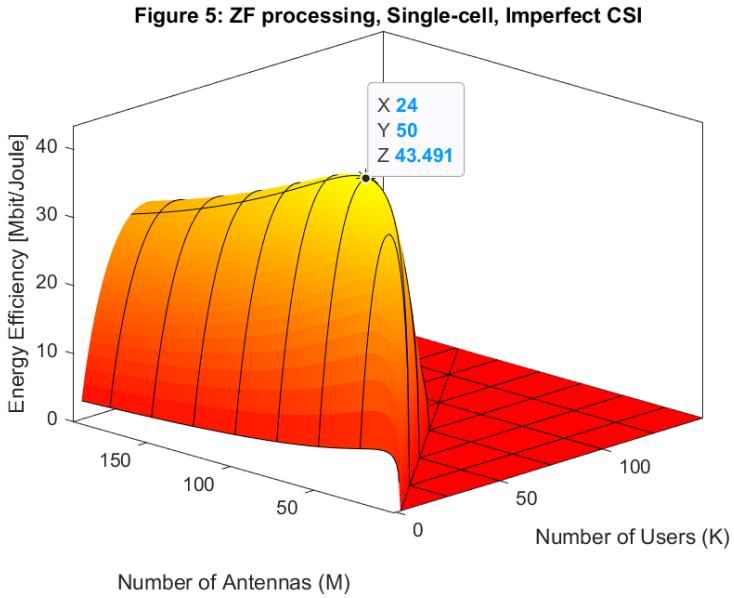

Figure 5. Energy efficiency (Mbit/J) with ZF processing in the single-cell scenario with imperfect CSI.

Figure 6 shows the comparison of the different processing schemes. This figure shows the maximum energy efficiency as a function of the number of Base Station antennas. The energy efficiency of MRT/MMSE in a perfect CSI is way below the other processing schemes. It is also noticed that it reached its optimal energy efficiency between $M = 40$ antennas and $M = 60$ antennas. Thus, as the number of antennas increased, there was a seemingly exponential drop.

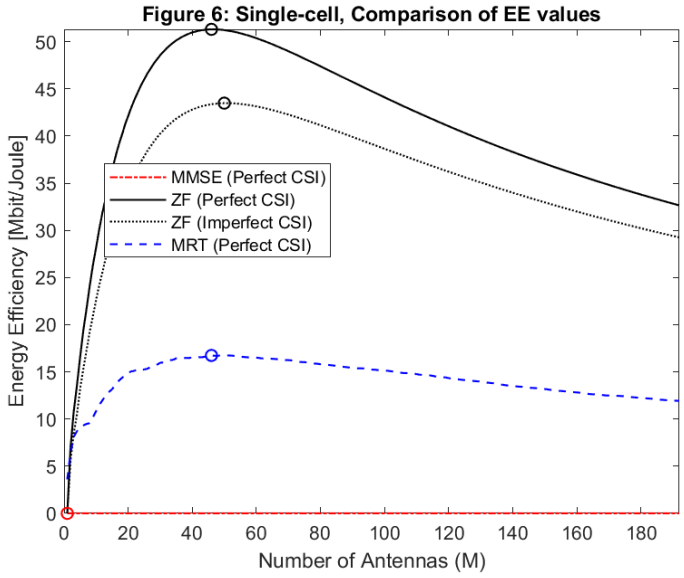

Figure 6. Maximal energy efficiency for different numbers of BS antennas and different processing schemes in the single-cell scenario.

Figure 7 shows the average power (W) with respect to the number of antennas (M). The total Power Amplifier power affects the maximization of the energy efficiency for different numbers of antennas (M) using the corresponding optimal values of K. Across the different processing schemes, increasing the transmit power with respect to the number of antennas (M) will a good energy efficiency strategy. Nevertheless, in contrast, the transmit power should be decreased with respect to the number of antennas (M) to achieve better Energy efficiency. Figure 7 also shows that the transmit power per Base Station antenna decreases with the number of antennas (M).

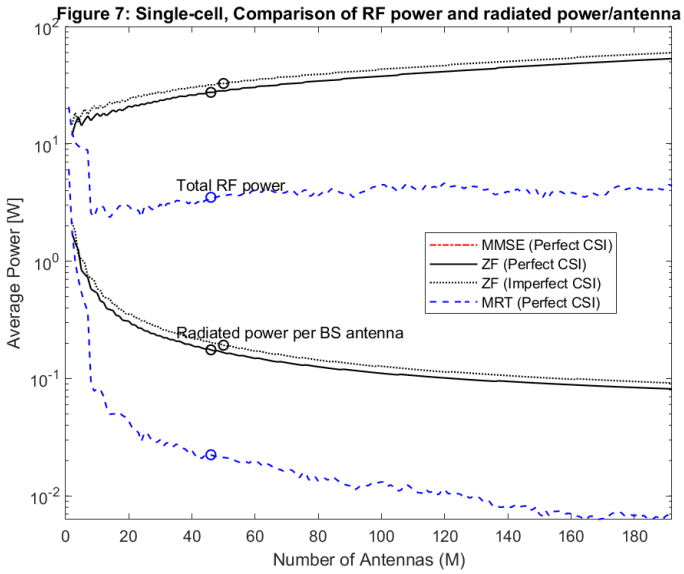

Figure 7. Total PA power at the EE-maximizing solution for different numbers of BS antennas in the single-cell scenario. The radiated power per BS antenna is also shown.

Figure 8 shows the area throughput (Gbit/s/km2) with respect to the number of antennas (M), which maximizes the energy efficiency for different numbers of antennas (M). Considering the same processing schemes in Figures 6 and 7, we applied them in Figure 8. In Figure 6, there were noticeable improvements in optimal energy efficiency ZF perfect CSI and ZF imperfect CSI compared to MRT/MRC and MMSE. Figure 8 shows the simultaneous improvement in area throughput across different schemes but not that huge; ZF perfect CSI and ZF imperfect CSI contribute to the improvements. Deploying a large number of Base Station antennas and being processed by MRT/MRC and MMSE processing schemes is wasteful, given that it limits achieving energy

efficiency and higher area throughput. Proper optimization of the site and interference-suppressing precoding schemes on the massive MIMO antenna can achieve better energy efficiency and area throughput.

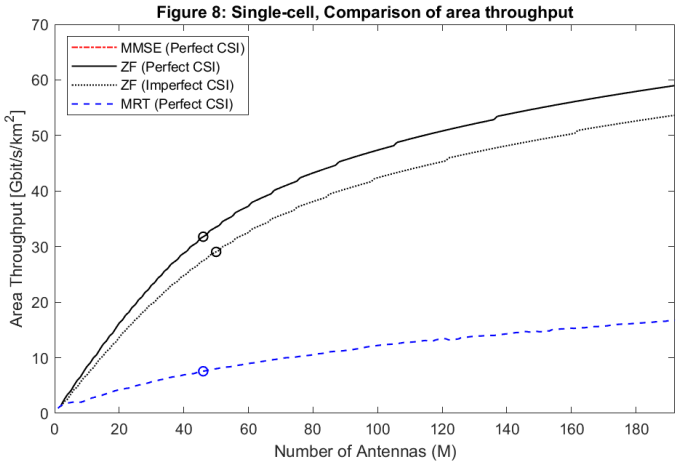

Figure 8. Area throughput at the energy efficiency maximizing solution for different numbers of BS antennas in the single-cell scenario.

Multi-Cell Scenario

Figure 9 represents a symmetrical multi-cell scenario that concentrates on the cell under study in the middle. Each cell corresponds to a 500 × 500 square. UEs are uniformly distributed with the same minimum distance, similar to a single-cell scenario. Interference from the two closest cells is considered relative to the cell under study, as shown below. The cells are divided into four clusters. There are three pilot re-use patterns: a. at $\tau^{(UL)} = 1$, we consider the same pilots in all cells, b. $\tau^{(UL)} = 2$, we consider two orthogonal sets of pilots (Cluster 1 & Cluster 4 with the same pilot), c. $\tau^{(UL)} = 4$, we consider all clusters having different orthogonal pilots.

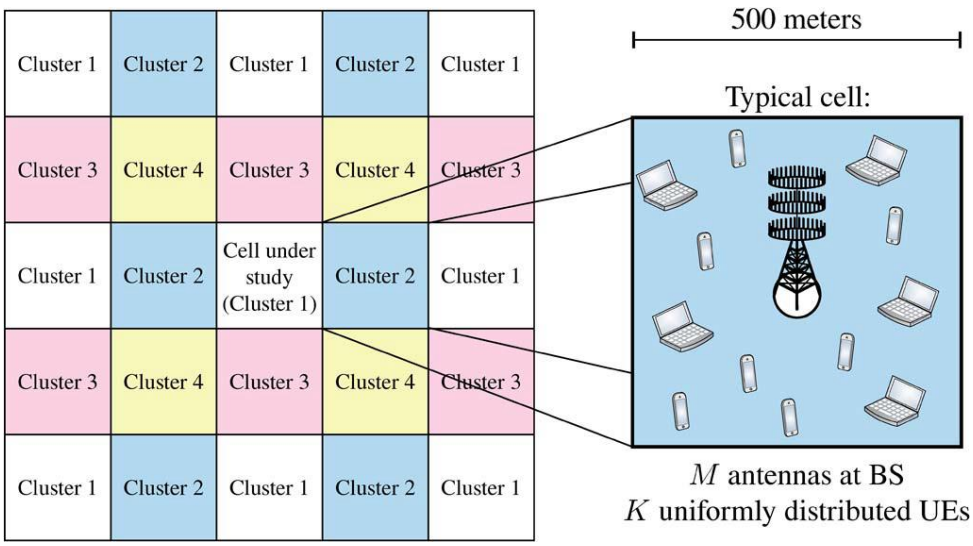

Figure 9. The multi-cell simulation scenario where the cell under study is surrounded by 24 identical cells. The cells are clustered to enable different pilot re-use factors (Björnson et al., 2015)

Figure 10 shows the maximal Energy efficiency for different numbers of antennas in a multi-cell scenario of different re-use factors showing interesting results where all the Energy Efficiencies are much smaller. Figure 11 shows that the corresponding total PA power and radiated power per Base Station are closely patterned with each processing scheme. Inter-cell interference is prevalent in a multi-user environment, affecting the whole system, including throughput and Energy efficiency. The higher the pilot re-use factor $\tau^{(UL)} = 4$, the better the energy efficiency and much higher area throughput. However, because incremental power was consumed in 5G, the optimal Energy efficiency is not that high.

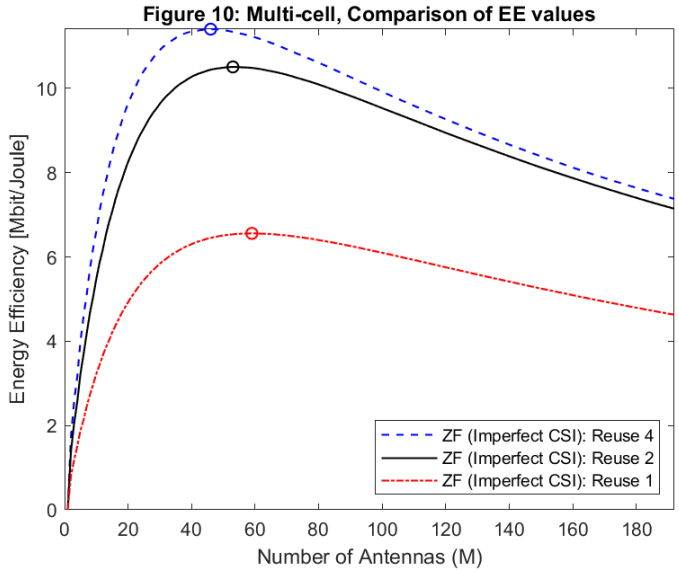

Figure 10. Maximal energy efficiency in the multi-cell scenario for different numbers of BS antennas and different pilot re-use factors.

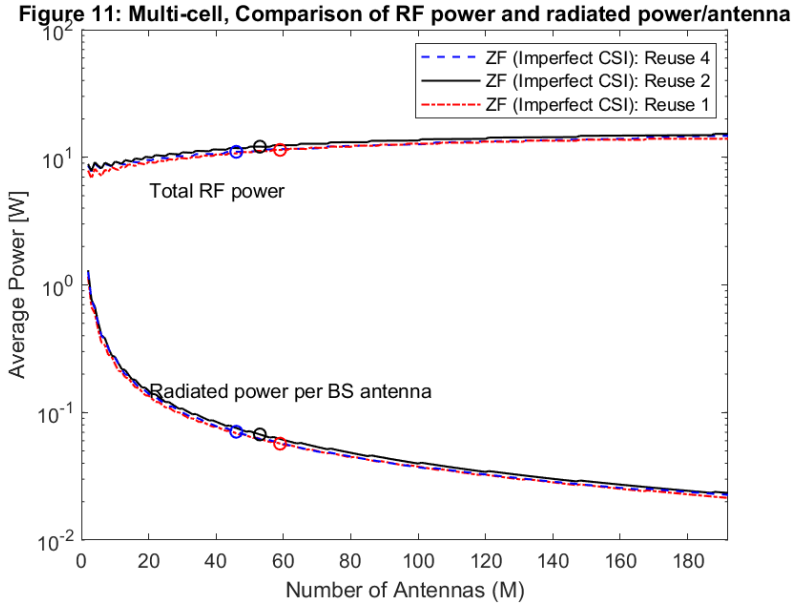

Figure 11. Total PA power at the energy efficiency maximizing solution in the multi-cell scenario for different numbers of BS antennas. The radiated power per BS antenna is also shown.

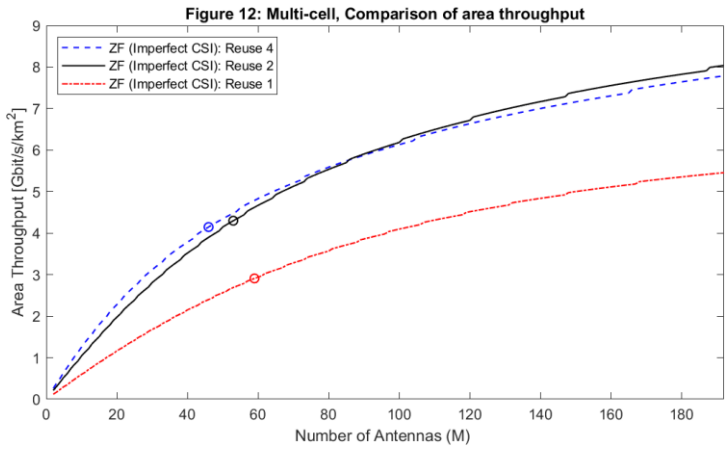

Figure 12. Area throughput at the energy efficiency maximizing solution in the multi-cell scenario for different numbers of BS antennas.

Figure 13 provided a better view of utilizing a smaller number of antennas, but the energy efficiency is still optimal. Utilizing different values of M and K with a pilot re-use factor of $\tau^{(UL)} = 4$, resulted in higher energy efficiency. This outcome has almost the same concave in Figure 3, but the earlier has a much higher energy efficiency value. With multi-user and more re-use factors, inter-cell interference is experienced, forcing each cell to sacrifice some user camping to the network. Nevertheless, we conclude that we need to optimize some parameters in 5G massive MIMO to achieve optimal architecture to deliver Energy efficiency.

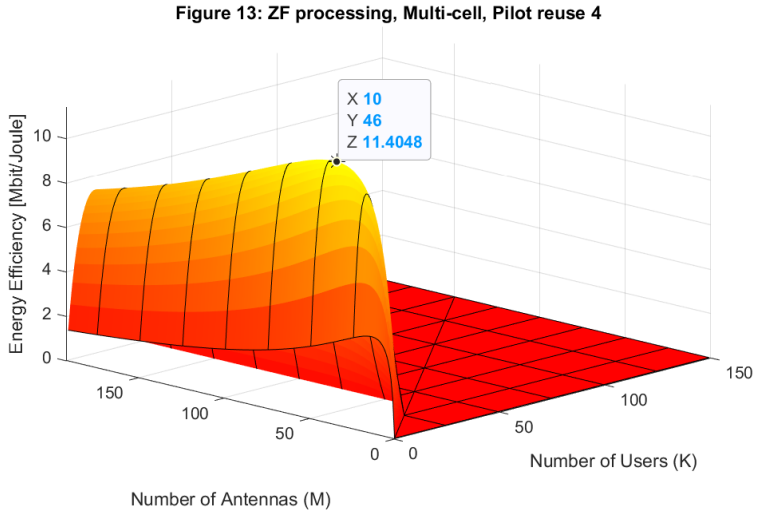

Figure 13. Energy efficiency (in Mbit/Joule) with ZF processing in the multi-cell scenario with pilot re-use 4.

Table 3 below shows the comparative results between the original paper on utilizing massive MIMO in a 4G network and with a 5G network. It clearly shows that using a ZF processing in the single-cell with a perfect CSI scenario yielded higher Energy Efficiency.

Table 3. Optimal Energy Efficiency Comparison between 4G and 5G with the Different Processing Schemes

Processing Schemes	x Number of Antennas (M)		y Number of Users (K)		z Energy Efficiency (Mbit/Joule)	
	4G LTE	5G	4G LTE	5G	4G LTE	5G
ZF processing in the single-cell, perfect CSI scenario	165	46	104	24	30.70	51.32
MRT/MRC processing in the single-cell, perfect CSI scenario	77	46	81	21	9.83	16.74
ZF processing in the single-cell scenario with imperfect CSI	185	50	110	24	25.88	43.5
ZF processing Multi-Cell, Pilot Re-use 4	123	46	40	10	7.57	11.5

Note: The reference 4G values were derived from the original paper (Björnson et al., 2015).

Conclusion

Based on the simulation, results showed a significant impact on energy efficiency when deploying 5G massive MIMO. Several parameters were considered in the simulation process: the number of BS antennas (M), the frequency used, wider transmission bandwidth, higher fixed power consumption, channel coherence bandwidth, channel coherence time, coherence block, a fraction of downlink transmission, a fraction of uplink transmission and the type of antenna being used to which are all based on 3GPP standard Release 15 for 5G network. There were noticeable impacts on the energy efficiency of the different processing schemes based on the changes made in the simulation parameters. These are as follows: a) changing the number of active base station antennas (M) with the consideration of having a 3-sector antenna with 64T x 64R configuration per cell, b) increasing the transmission bandwidth from 20MHz to 60MHz based on 3GPP Release 15, c) increasing the channel coherence bandwidth based on 5G's subcarrier spacing and subcarriers per resource block, d) decreasing the channel coherence time which affects the coherence blocks, e) improving the total noise power, f) adhering to 5G TDD configuration using FORMAT31 which changes now both the values of the fraction of downlink transmission

and the fraction of uplink transmission into 80/20 respectively, and g) the increased fixed power consumption based on the actual antenna configuration.

In an energy-efficient 5G network, a high SNR is required with the proper interference-suppressing processing technique like ZF, which works well compared to an MRT/MRC processing which is an interference-ignoring system. Using 5G massive MIMO works well on both ZF processing in the single-cell, perfect CSI and imperfect CSI scenario, yielding high energy efficiency values. Based on the simulation, MMSE processing did not contribute much to the energy efficiency improvement, unlike MRT/MRC processing. Because of the wider bandwidth, the network was opened up to more UE's but statistically selected those with less interference to camp to the network at a higher throughput to limit the possibility of creating interference from within. The incremental power induced to the network due to more RF chains has affected the power consumption and impacted the overall Energy efficiency.

Recommendations

Several factors need to be reconsidered in the simulation process. It is highly recommended to explore further other 5G parameters and simulate different optimization principles to achieve Energy efficiency. Also, future researchers should look into the end-to-end power consumption of not just the antenna and radio units but also consider external ancillaries that can affect the overall power consumption. Lastly, consider revising the model based on updated 5G equipment configurations.

Scientific Ethics Declaration

The authors declare that the scientific ethical and legal responsibility of this article published in EPSTEM journal belongs to the authors.

Acknowledgements or Notes

* This article was presented as oral presentation at the International Conference on Basic Sciences, Engineering and Technology (www.icbaset.net) held in Marmaris/Turkey on April 27-30, 2023.

*This serves to acknowledge the support given by Engr. Jayson Bonin Aldeza in providing references and some information about the paper and likewise our parents. The authors express their sincerest gratitude to De La Salle University for providing the necessary assistance to make this research possible. And lastly, to Almighty God, for giving the authors the divine guidance to complete this work, contribute to the body of knowledge, and share the ideas with the scientific community.

References

3GPP Global Initiative. (2021). *"3rd generation partnership project; technical specification group radio access network; NR; User Equipment (UE) radio transmission and reception*; Part 1: Range 1 Standalone (Release 17)". 3GPP TS 38.101-1 V17.2.0 (2021-06). (pp. 24).

3GPP Global Initiative. (2017). "*3rd generation partnership project; technical specification group radio access network; Evolved Universal Terrestrial Radio Access (E-UTRA)*; Further advancements for E-UTRA physical layer aspects (Release 9)". 3GPP TR 36.814 V9.2.0 (2017-03)

Björnson, E., Sanguinetti, L. Hoydis, J., & Debbah, M. (2015, June). "Optimal design of energy-efficient multi-user MIMO systems: Is massive MIMO the answer?" *IEEE Transactions on Wireless Communication., 14*(6), (pp. 3059–3075).

Björnson, E., Sanguinetti, L., & Kountouris, M. (2016, April). "Deploying dense networks for maximal energy efficiency: small cells meet massive MIMO". *IEEE Journal on Selected Areas in Communications, 34*(4), 832-847.

Chatzipapas, A., Alouf, S., & Mancuso, V. (2011). "On the minimization of power consumption in base stations using on/off power amplifiers". *In IEEE Online Conference on Green Communications (pp. 18-23). IEEE.*

European Telecommunications Standards Institute (ETSI) (2019). *ETSI TS 138 104 V15.5.0 (2019-05), "5G; NR; Base Station (BS) radio transmission and reception* (3GPP TS 38.104 version 15.5.0 Release 15)". (pp. 28-31).

Environmental and Energy Study Institute (2023). *Energy efficiency*. https://www.eesi.org/topics/energy-efficiency/description.

Huawei Technologies Co., Ltd. (2017). *5G spectrum: public policy position*. https://www-file.huawei.com/-/media/CORPORATE/PDF/public-policy/public_policy_position_5g_spectrum.pdf, (pp. 6).

Huawei Technologies Co., Ltd. (2022, Oct.). AAU5636w V100R018C10 technical specifications. https://www.huawei.com/en/

International Telecommunication Union, Radio Communication Sector (ITU-R). (2015, Sept.). Recommendation ITU-R M.2083-0, "IMT vision – framework and overall objectives of the future development of IMT for 2020 and beyond". M Series, Mobile, radiodetermination, amateur, and related satellite services". (pp 4-5), (pp. 11- 12).

Osseiran, A., Monserrat, J.F., & Marsch, P. (2016). "*5G mobile and wireless communications technology"*, Cambridge University Press, ISBN 978-1-107-13009-8

Qualcomm. (2022). *"What is 5G? Everything you need to know about 5G"*. https://www.qualcomm.com/5g/what-is-5g.Qualcomm Technologies.

Parker M. (2009). "*High-performance floating-point implementation using FPGAs*," in Proc. IEEE MILCOM, (pp. 1–5).

Pizzo, A., Verenzuela, D., Sanguinetti, L., & Björnson, E. (2015, Sept.). "Network deployment for maximal energy efficiency in uplink with multislope path loss". *IEEE Transactions on Green Communications and Networking, 2*(3).

Yang, H., & Marzetta, T. (2013). "Total energy efficiency of cellular large-scale antenna system multiple access mobile networks". 2013 IEEE Online Conference on Green Communications (OnlineGreenComm), 27-32.

Author Information

Gerhard P. Tan
De La Salle University, Philippines
Polytechnic University of the Philippines
Contact: gerhard_tan@dlsu.edu.ph

Lawrence Materum
De La Salle University, Philippines
Tokyo City University, Japan

To cite this article:

Tan, G.P. & Materum, L. (2023). 5G Massive MIMO and its impact on energy efficiency. *The Eurasia Proceedings of Science, Technology, Engineering & Mathematics (EPSTEM), 22*, 87-98.

The Eurasia Proceedings of Science, Technology, Engineering & Mathematics (EPSTEM)
ISSN: 2602-3199

The Eurasia Proceedings of Science, Technology, Engineering & Mathematics (EPSTEM), 2023

Volume 22, Pages 99-110

ICBASET 2023: International Conference on Basic Sciences, Engineering and Technology

Road Safety Performance Monitoring Practices: A Literature Review

Ibtissam EL KHALAI
Ecole Mohammadia d'Ingénieurs

Zoubida CHORFI
Ecole Mohammadia d'Ingénieurs

Abdelaziz BERRADO
Ecole Mohammadia d'Ingénieurs

Abstract: Road traffic crashes remain a major concern worldwide. They are considered by the World Health Organization as one of the leading causes of death worldwide. To address this road insecurity, many countries are developing national strategies and trying to put in place the necessary action plans for their implementation. At this stage, monitoring of performance is crucial to ensure the efficacy of these road safety systems. The primary objective of this study is to examine the state-of-the-art practices employed in researches for managing road safety systems, specifically performance monitoring, and present the results in an engaging and informative manner. Through a comprehensive review of existing literature, the study seeks to identify essential components to help policymakers develop and monitor the performance of their road safety systems. The findings of this study can serve as a foundation for decision-makers in their efforts to develop and manage effective road safety systems.

Keywords: Road safety, Management system, Road safety strategy, Performance monitoring, Road safety measures.

Introduction

Given the significant social and economic costs associated with road accidents, road safety has become a major concern for governments and stakeholders worldwide. Countries have adopted various road safety measures, policies and systems to reduce the number of deaths and injuries. However, simply implementing these measures is not enough. Decision-makers are also required to adopt a clear and strategic approach and design a guiding framework to effectively manage their road safety system. Two distinct approaches are primarily available: the traditional approach and the systemic approach. The traditional approach tends to focus on changing the behavior of road users and reducing human errors. Users are considered as primarly responsible for the occurrence of road accidents. As a result, the emphasis on human error encourages road safety managers to adress more actions related to users. Unlike the traditional approach, the systemic approach to road safety recognizes the interdependence of the components of a safe system: safe roads, safe road users and safe vehicles, and seeks to continuously improve these elements to prevent all collisions and ensure that road users are not severely injured in case of an accident. This approach emphasizes that the road system must be designed to address human vulnerability and error (Safarpour et al., 2020). In recent years, there has been an increasing awareness that effective road safety management practices generally involve a systemic approach, resulting in the emergence of the "safe system approach", which addresses the issue in an integrated manner. This approach is the foundation of the two Decade of Action for Road Safety 2011-2020 and 2021-2030 proclaimed by UN General Assembly, and has since been adopted by a growing number of countries (WHO, 2021).

Exploring the tools, frameworks, and data sources that have been commonly used in managing road safety systems is an interesting area of investigation, which could inspire policymakers when developing and monitoring the performance of their road safety systems. Thus, the main objective of this study is to carry out a comprehensive analysis of the existing literature on road safety management to adress the following research objectives:

- Provide a comprehensive review of the current state of the art in monitoring road safety performance;
- Systematically analyze identified publications to gather data that could assit in the development and management of effective road safety systems.

In the remainder of this paper, we will first provide the background information about the study. Next, we will describe the methodology we adopted to conduct our research. Finally, we will present and discuss the findings of our research, drawing conclusions and implications from these results.

Background of the Study

Effective performance monitoring is crucial for the development of a successful road safety system. To achieve this, researchers and policy-makers in this field need to have a comprehensive understanding of the various tools, approaches, frameworks and data sources used to effectively manage and monitor road safety systems. They need to recognize, among other things, the best means of monitoring their planned actions for the various components of road safety. By categorizing their actions, policymakers can identify where interventions are effective and where more work is needed. A clear classification system can also facilitate data comparison across jurisdictions and countries, providing valuable insights into best practices in road safety management. In addition, decision makers need to identify the different types of measures that are commonly implemented as part of an effective road safety monitoring system in order to determine the most appropriate measures for their own context. By examining existing ones, decision-makers can better tailor their own road safety measures to their specific needs and challenges.

Access to international data sources is also crucial, as it allows policymakers to compare their road safety systems with those of other countries, to better understand best practices, and identify areas for improvement. By accessing reliable data sources from other countries, policymakers can also identify effective measures and best practices that have been implemented elsewhere. In addition, international data sources provide a broader perspective on road safety issues, including emerging trends and challenges that may not be evident in domestic data sources. This helps policymakers to develop more comprehensive and effective road safety policies and strategies. With the aforementioned needs in mind, the purpose of this study is to provide a relevant review of the current literature on monitoring road safety performance. Our objective is to categorize the study outcomes in a manner that can assist policymakers and researchers in their quest to develop and manage effective road safety systems. By offering valuable insights, this study aims to inspire and guide decision makers in their efforts to improve road safety management practices.

Review Methodology

This section provides an overview of the methodology used to conduct the literature review on road safety performance monitoring. The review process involved four steps, starting with (1) **the definition** of research objectives and questions, (2) **the identification** of the search terms and database to identify publications relevant for the review, (3) **the selection** process based on predefined inclusion and exclusion criteria, and finally, (4) **a data collection and analysis** approach to classify relevant information collected from the selected publications.

Research Objectives and Questions

To initiate the review process, the identification of clear objectives and research questions was paramount. The main objective of this review is to provide a comprehensive overview of the existing literature on monitoring road safety performance and to assess the current state of the art in this area. To achieve this goal, we formulated the following research questions:

RQ1: What is the overall view of the field? When and which journals and countries have shown interest in monitoring road safety performance?
Are there any frameworks and flagship projects being used or implemented in the context of road safety performance monitoring?
RQ2: What are the most commonly used sources of data in this field, and which organizations provide them?
RQ3: What are the most common types of measures identified in this field of research?
RQ4: Which road safety components have generated the most interest among researchers in the selected papers?

These research questions guided the literature review and provided a framework for the selection and analysis of relevant publications. By answering these questions, we aimed to contribute to the development of a foundation that can help decision-makers in developing effective road safety management practices and policies.

Papers Search Process

To ensure a comprehensive review of existing literature on monitoring road safety performance, a systematic research process was used. This approach includes the use of specific search terms and criteria to identify relevant publications that meet the research objectives. By using a systematic approach, the risk of missing important publications or biases in the selection process is minimized. The search process thus employed the following search string "Road safety" AND ("management system" OR strategy) AND performance AND (evaluation OR assessment OR monitoring OR measure), without any time limit. The research was conducted in Science Direct database, a widely recognized and reputable academic database, to ensure the quality and relevance of the retrieved publications. This aformentionned search string was selected in order to identify relevant publications that adress topics related to road safety management systems and strategies, along with their performance measurement, monitoring and evaluation.

Papers Selection Process

The selection process aimed to help us identify papers that were most relevant to the research questions and objectives of this literature review. To achieve this, we first established inclusion and exclusion criteria for candidate papers. At first, only papers that met the search keywords on their title, abstract or author-specified keywords were considered. Additionaly, these papers had to be available, written in English, and published as a journal or conference paper. Secondly, the studies needed to be focused on road safety management systems and strategies with an emphasis on performance measurement, monitoring and evaluation. Once the initial selection was made, a full-text review was conducted to assess the relevance of the selected papers to the research objectives. Any papers that did not meet the objectives were excluded.

Data Collection and Analysis

In this step, our goal was to carefully review the selected articles and gather relevant information pertinent to the research questions. To achieve this, we extracted all relevant data from the selected studies, including their title, author, year of publication, source, type of publication and location (journal, conference, etc.), as well as specific data answering our predefined research questions. Subsequently, we devised a comprehensive classification system to categorize the data collected into four categories, specificallly; (1) General overview of selected papers, (2) International road safety data sources and organizations, (3) Selection of road safety measures and (4) Selection of road safety components. This classification system enabled us to efficiently analyze the gathered data in order to address the four research questions outlined in the previous step.

Results

In the present section, we present the results of our study. Initially, a considerable number of 5592 papers were identified through a systematic search process. However, after applying our selection process, which included the application of previously cited inclusion and exclusion criteria and also a manual evaluation of each paper's relevance to the research questions, only 57 papers were finally selected. An overview of the data collected is provided in the next subsections, based on the proposed classification of results.

General Overview of Papers

This section presents below an initial overview of the selected papers:

Publication Characteristics:

The selection process yielded a publication range from 2002 to 2023. İt is important to note that our search process did not impose any time limits. Based on our finding, we observed that interest in this field of reserach began to emerge from 2002. Of the selected studies, almost 60% were conducted between 2018 and 2021, comprising 34 articles. İn terms of publication type, 87.7% of the studies were published in Journals and 12.3% were presented at Conferences (Figure 1).

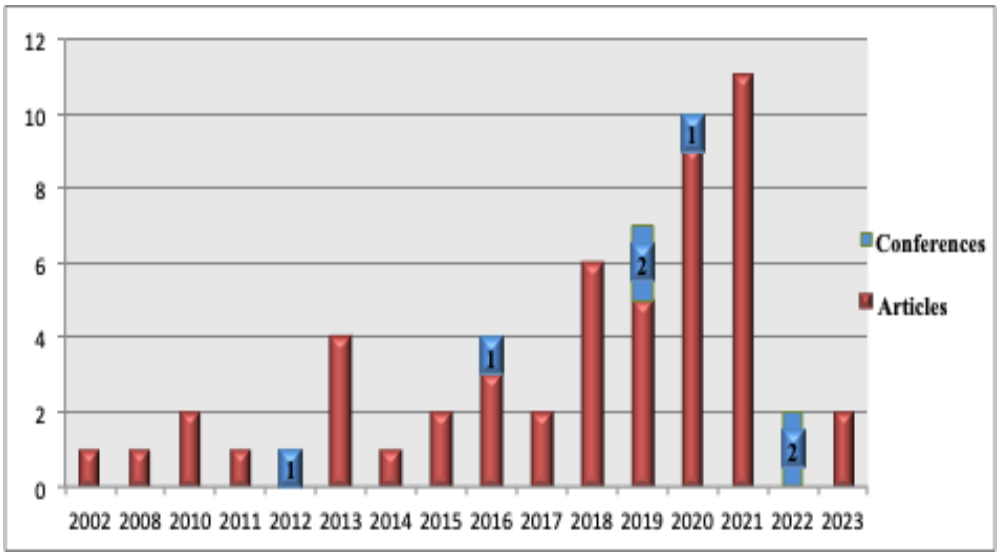

Figure 1. Number of papers published per year and by publication venue.

Table 1. Publication sources of the selected papers.

PUBLICATION SOURCE	Number	%
JOURNALS		
Accident Analysis and Prevention	17	34
Traffic Injury Prevention	5	10
Transportation Research	5	10
Journal of Traffic and Transportation Engineering	4	8
Journal of Safety Research	3	6
Safety Science	3	6
Journal of Transport & Health	2	4
Biomedical Signal Processing and Control	1	2
Global Transitions	1	2
Human Movement Science	1	2
IATSS Research	1	2
International Journal of Transportation Science and Technology	1	2
Microprocessors and Microsystems	1	2
Reliability Engineering and System Safety	1	2
Transport Policy	1	2
Transportation Letters	1	2
Transportation Engineering	1	2
Vehicular Communications	1	2
TOTAL JOURNALS	*50*	*100*
CONFERENCES		
International Conference on Transport Infrastructure and Systems (TIS)	4	57
Transport Research Arena	2	29
EURO Working Group on Transportation (EWGT)	1	14
TOTAL CONFERENCES	*7*	*100*

These selected publications were distributed across various venues, with approximately 50% of papers published in three specific journals: Accident Analysis and Prevention Journal, Traffic Injury Prevention Journal, and Transportation Research Journal. Notably, the latter journal comprises several parts from A to E that cover complementary topics within the realm of transportation science, making it one of the most comprehensive references in the field.

Regarding conference proceedings, the International Conference on Transport Infrastructure and Systems was the most frequent event for this research domain, with 57% of the conference papers being published in its proceedings. This conference was held in 2019 and 2022. The distribution of articles selected by different venues is presented below (Table 1).

Subject Area and The Monitoring Level of the Study:

Regarding the subject areas, the studies were classified into seven different fields related to road safety monitoring research. More than half (50.9%) of the papers were published in journals related to Social Sciences, followed by engineering-related journals (21.1%). Computer science and psychology-related journals accounted for 7% and 5.3%, respectively, while Medicine and Dentistry and Arts and Humanities-related journals accounted for 3.5% and 1.8% respectively. The remaining 8.8% of studies addressed miscellaneous topics. Furthermore, we examined the level at which the studies were conducted. The majority (66.7%) of the articles were conducted at the local or national level, while the remaining 33.3% were conducted at the international level.

Geographical Distribution:

The selected papers were also analyzed based on their geographical distribution. The studies were dispersed across 24 countries, with researchers from Australia, China, Italy, Brazil, and Greece contributing the most (57.9%) to the field of road safety monitoring research. Australia had the highest number of selected studies (11), followed by China (6), Italy (3), Brazil (3), and Greece (3) (Figure 2).

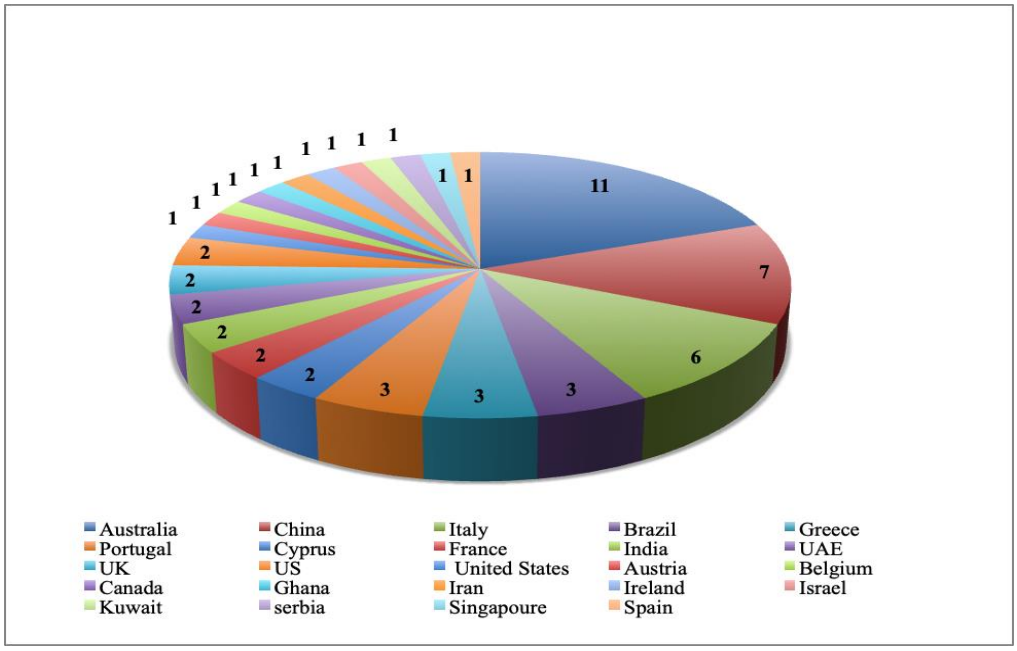

Figure 2. The geographical distribution

Frameworks and Flagship Projects

Road safety performance monitoring can benefit from frameworks that offer guidelines, methodologies, and tools for measuring, analyzing, and enhancing road safety outcomes. The selected papers highlight the importance of a comprehensive and multi-disciplinary approach to road safety performance monitoring. Some

of the frameworks identified in the papers include the Pyramid of Road Safety and the Sunflower Pyramid (Chen et al,. 2016), (Papadimitriou & Yannis, 2013), (Pešić & Pešić, 2020). Additionally, some studies utilized the Five Pillars of Road Safety Development and the Three Layers of Road Safety Management (institutional management functions, interventions, and results) as a framework for their research (Behnood, 2018). The Safe System Matrix, originally from Australia, was also employed in some studies (Corben et al., 2010).

In addition to frameworks, identifying flagship projects in this area can serve as models for best practices and demonstrate the potential of innovative approaches to road safety performance monitoring implemented in different parts of the world. For example, the DaCoTa Project, the Safetynet Project, (Pešić & Pešić, 2020), (Papadimitriou & Yannis, 2013) and the Sunflower Project (Papadimitriou & Yannis, 2013), (Chen et al., 2016) were all important projects that contributed significantly to road safety management. Other projects identified in the studies, such as the i-DREAMS Project (Michelaraki et al., 2021) and the DICA-VE Project (Coelho & Guarnaccia, 2020), were focused on specific road safety components such as road users or vehicles. These projects demonstrate the potential of innovative solutions to address road safety challenges faced by different countries. Policy makers and researchers interested in this area are encouraged to further research these identified frameworks and projects and to explore potential projects not mentioned here.

Identification of International Road Safety Data Sources and Organizations

The identification of international road safety data sources and organizations was an important aspect of this study. To accomplish this, we conducted a thorough analysis of the selected papers and extracted relevant information regarding the sources of data and organizations involved in road safety management. Our findings revealed that a number of international organizations play a critical role in promoting road safety and developing strategies to reduce roads accidents and fatalities. The most commonly cited organizations in the studies we reviewed were the World Health Organization (WHO), the International Transport Forum (ITF), the European Transport Safety Council (ETSC), the European Road Safety Observatory (ERSO), the International Road Traffic and Accident Database (IRTAD), the Organization for Economic Co-operation and Development (OECD), the European Commission (EC), the United Nations (UN), and also the Global Burden of Disease study (GBD).

The data sources used in the studies varied, with some using local or European datasets, while others used databases and publications from the aforementioned organizations. Additionally, some studies utilized data from flagship projects such as the DaCoTa Project and the Sunflower Project. In some cases, data were collected through targeted surveys and questionnaires. By analyzing these sources of data and organizations, we were able to identify reliable sources to inform future research and provide valuable insights for decision makers.

Identification of Main Road Safety Measures Used

In this section, we identified the different measures used in the selected documents to assess road safety. The identified measures were classified into six main categories:

1. Background /socio-economic measures (used 23 times with a percentage of 20%): These measures captured the volume and characteristics of various road safety components, such as demographics of road users, the level of motorisation. They also included measures of housing conditions, wealth levels, and education, such as the Gross Domestic Product (GDP) per capita, and employment.
2. Process measures (used 27 times with a percentage of 23%): These measures are related to the safety programs and measures implemented to manage road safety, such as the strategy implemented, the road safety audits performed. The measures in this category can be both quantitative and qualitative.
3. Behavioral measures (used 44 times with a percentage of 38%): These measures were used to assess the performance of the actions affecting the behavior of road users, such as speeding, drink driving, use of seat belts and helmets, and use of mobile phones.
4. Outcome measures (used 20 times with a percentage of 17%): These measures were used to assess the final impact of road safety measures, such as the number of fatalities and serious injuries, and the reduction in the number of fatalities and serious injuries.
5. Economic measures (used 1time with a percentage of 1%): These measures were used to assess the economic impact of road safety interventions, such as the cost savings associated with reducing fatalities and serious injuries.

6. Environmental measures (used 1time with a percentage of 1%): These measures were used to assess the impact of road safety interventions on the environment, such as the reduction in greenhouse gas emissions from more sustainable transport modes.

It is important to note that more than one measure could be used in one study. These results provide insight into the various measures that need to be considered when assessing road safety interventions (Table 2).

Table 2. Paper's classification by types of measures used

Road safety measures	Papers
Background /socio-economic measures	(Nikolaou et al., 2021); (Astarita et al,. 2023); (De Bartolomeo et al., 2023); (Chen et al,. 2020); (Papadimitriou & Yannis, 2013); (Behnood, 2018); (Nikolaou & Dimitriou, 2018); (Chen et al,. 2016); (Bastos et al.,2015); (Mooren et al.,2014); (Albalate & Yarygina, 2013); (Cafiso & D'Agostino, 2016); (Horswill et al., 2011); (Vankov & Schroeter, 2021) ; (Islam et al., 2021); (Tarasi et al., 2021); (Osei et al,. 2021); (Lu et al, 2019); (Chajmowicz & Cuny, 2019); (Oviedo-Trespalacios et al., 2016); (Yadav & Velaga, 2020); (AlRukaibi et al., 2021); (Marciano et al., 2015).
Process measures	(De Bartolomeo et al., 2023); (El-Sayed et al., 2021); (Papadimitriou & Yannis, 2013); (Behnood, 2018); (Chapelon & Lassarre, 2010); (Fwa, 2017); (Chen et al,. 2016); (Ansari et al,. 2023); (Corben et al., 2010); (Sun & Xiang, 2019); (Horswill et al., 2021); (Mooren et al.,2014); (Albalate & Yarygina, 2013); (Cafiso & D'Agostino, 2016); (Sangrar et al., 2019); (Michelaraki et al., 2021); (Domenichini et al., 2018); (Fu & Mao, 2018); (Nogal & Honfi, 2019); (Islam et al., 2021); (Osei et al,. 2021); (Lu et al, 2019); (Connors et al., 2013); (Chajmowicz & Cuny, 2019); (Oviedo-Trespalacios et al., 2016); (Marciano et al., 2015); (Huertas-Leyva et al., 2019).
Behavioral measures	(Pešić & Pešić, 2020); (Nikolaou et al., 2021); (Astarita et al,. 2023); (Chen et al,. 2020); (Papadimitriou & Yannis, 2013); (Reis et al,. 2023); (Behnood, 2018); (Chapelon & Lassarre, 2010); (Fwa, 2017);(Chen et al,. 2016); (Baulk et al,. 2008); (El-Sayed et al., 2020); (Singh & Kathuria, 2021); (Ansari et al,. 2023); (Corben et al., 2010); (Coffey & Park, 2020); (Kaulich et al., 2016); (Habtemichael & Santos, 2012); (Zhao & Wang, 2020); (Sun & Xiang, 2019); (Horswill et al., 2021); (Mooren et al.,2014); (Sinha et al., 2020); (Bosso et al., 2020); (Twisk et al., 2018); (Silva et al., 2021); (Horswill et al., 2011); (Vankov & Schroeter, 2021); (Rossi et al., 2021); (Domenichini et al., 2018); (Chen et al,. 2021); (Nogal & Honfi, 2019); (Islam et al., 2021); (Tarasi et al., 2021); (Tapp & White, 2013); (Coelho & Guarnaccia, 2020); (Treffner et al., 2002); (Lu et al, 2019); (Chajmowicz & Cuny, 2019); (Oviedo-Trespalacios et al., 2016); (Yadav & Velaga, 2020); (AlRukaibi et al., 2021); (Marciano et al., 2015); (Huertas-Leyva et al., 2019).
Outcome measures	(Nikolaou et al., 2021); (Astarita et al,. 2023); (Chen et al,. 2020); (Papadimitriou & Yannis, 2013); (Behnood, 2018); (Chapelon & Lassarre, 2010); (Nikolaou & Dimitriou, 2018); (Chen et al,. 2016); (Cheng et al., 2018); (Corben et al., 2010); (Bastos et al.,2015); (Mooren et al.,2014); (Albalate & Yarygina, 2013); (Cafiso & D'Agostino, 2016); (Silva et al., 2020); (Sinha et al., 2020); (Chajmowicz & Cuny, 2019); (Oviedo-Trespalacios et al., 2016);(Yadav & Velaga, 2020); (AlRukaibi et al., 2021).
Economic measures	(Cafiso & D'Agostino, 2016).
Environmental measures	(Coelho & Guarnaccia, 2020).

Identification of Main Road Safety Components Explored.

The main objective of this subsection is to identify the main road safety components explored in the selected papers. We carefully reviewed the papers to determine which components were monitored or studied. We classified the papers into four categories representing three main road safety components adressed in the studies: road users, road infrastructure, and vehicle. The fourth category represents studies that take into account different components, and we named it road safety system. This classification was chosen to ensure consistency with the road safety system approach, which considers road safety as a combination of multiple components that interact with each other to prevent or mitigate road accidents.

Road users were the most commonly explored component, with 36.8% of the selected papers primarily analyzing, predicting, or simulating road user behavior and its effect on road safety. Road safety systems were the second most explored, with 31.6% of the selected papers monitoring or assessing the effectiveness of road safety managemnt systems while taking into account different components. Road infrastructure was the focus of 19.3% of the selected papers, examining various aspects such as the effect of road design, maintenance, and management on road safety performance. Vehicle components were the focus of 26.3% of the selected papers, discussing for example the safety management of particulal vehicle type (Table 3).

Overall, the selected studies showed a broad range of road safety components explored in the literature. The findings of this subsection provide insight into the various measures that need to be monitored, specifically on individual components, to guide decision makers on road safety interventions to improve road safety.

Table 3. Paper classification by road safety components addressed

Road safety components	Papers
Road user	(Reis et al,. 2023); (Baulk et al,. 2008); (Singh & Kathuria, 2021); (Ansari et al,. 2023); (Kaulich et al., 2016); (Zhao & Wang, 2020); (Horswill et al., 2021); (Sangrar et al., 2019); (Twisk et al., 2018); (Horswill et al., 2011); (Vankov & Schroeter, 2021); (Rossi et al., 2021); (Michelaraki et al., 2021); (Chen et al,. 2021); (Nogal & Honfi, 2019); (Tapp & White, 2013) ;(Treffner et al., 2002); (Oviedo-Trespalacios et al., 2016); (Yadav & Velaga, 2020); (Marciano et al., 2015); (Huertas-Leyva et al., 2019).
RS system	(Pešić & Pešić, 2020); (Nikolaou et al., 2021); (Astarita et al,. 2023); (Chen et al,. 2020); (Papadimitriou & Yannis, 2013); (Behnood, 2018); (Chapelon & Lassarre, 2010); (Nikolaou & Dimitriou, 2018); (Chen et al,. 2016); (Cheng et al., 2018); (Corben et al., 2010); (Habtemichael & Santos, 2012); (Bastos et al.,2015); (Cafiso & D'Agostino, 2016); (Silva et al., 2020); (Tarasi et al., 2021); (Connors et al., 2013); (AlRukaibi et al., 2021).
Road infrastructure	(De Bartolomeo et al., 2023); (Fwa, 2017); (Coffey & Park, 2020); (Sun & Xiang, 2019); (Albalate & Yarygina, 2013); (Silva et al., 2021); (Domenichini et al., 2018); (Fu & Mao, 2018); (Islam et al., 2021); (Osei et al,. 2021); (Lu et al, 2019).
Vehicle	(El-Sayed et al., 2021); (El-Sayed et al., 2020); (Mooren et al.,2014); (Sinha et al., 2020); (Bosso et al., 2020); (Coelho & Guarnaccia, 2020); (Chajmowicz & Cuny, 2019).

Discussion

Several of the selected studies in this review have emphasized the importance of adopting a systematic approach to road safety management. Our study has shown that researchers have given varying levels of attention to different elements and aspects of measuring the performance of road safety systems. Given the importance of adopting a systematic approach, decision-makers should consider a classification framework that can effectively manage their actions and give equal importance to all components. The five pillars proposed in the WHO Global Plan for the Decade of Action for Road Safety, which include Road Safety Management,Safer Roads and Mobility,Safer Vehicles,Safer Road Users,Post-Crash Response have been proven effective in this regard.

Our study also revealed the existence of several measures used to monitor road safety performance. However, to effectively and comprehensively assess the performance of road safety systems, a hierarchy of measures should be established based on models linking results of different levels, accounting for socio-economic measures, actions implemented, performance of those measures, final results, and their costs. These models should interpret the results based on country's context and interventions undertaken in the field of road safety, to adapt the measures to the specific needs and challenges of each country. The Pyramid of Road Safety is a good example of such a model.

It is important to note that this study has limitations, such as the choice of keywords and the selection of articles, which may have excluded relevant publications. Despite these limitations, our findings provide valuable information that can be useful in the area of road safety management. Further studies and reviews can be conducted to complement this study, such as the identification of various technical methods used in this field. This could serve as a basis for choosing the best tools to adopt in future road safety studies.

Conclusion

This study offers a comprehensive review of the existing literature on road safety management systems. Our analysis of 57 relevant publications emphasizes the importance of adopting a systematic approach to road safety management that considers all aspects of road safety. By adopting a comprehensive and systematic approach, policymakers and stakeholders can effectively manage road safety, which will ultimately save lives and reduce the economic and social costs of road accidents. Our findings also highlight the importance of using reliable performance indicators and structured frameworks to represent the hierarchical levels of these road safety indicators. Moreover, our study identified reputable international data sources and organizations, that can offer a reliable source to inform future research and furnish decision makers with valuable insights. In conclusion, this study provides valuable insights into the current state of knowledge on road safety management systems. Policymakers can use this information to develop more effective road safety management strategies. It is crucial to continue investing in research in this area to enhance road safety and reduce the number of road accidents and fatalities.

Recommendations

Based on the findings of this study, it is recommended that decision-makers give high priority to data collection, analysis, and evaluation when designing road safety management systems. To ensure the sustainability and continuous improvement of road safety management systems, decision-makers should invest in ongoing research and learn from previous studies in the field. By doing so, they will be better equipped to address the challenges and opportunities that arise, and to continuously improve the effectiveness of their systems.

Scientific Ethics Declaration

The authors declare that the scientific ethical and legal responsibility of this article published in EPSTEM journal belongs to the authors.

Acknowledgements or Notes

* This article was presented as poster presentation at the International Conference on Basic Sciences, Engineering and Technology (www.icbaset.net) held in Marmaris/Turkey on April 27-30, 2023.

* This work was supported by the Ministry of Transport and Logistics, NARSA and CNRST.

References

Albalate, D., Fernández, L., & Yarygina, A. (2013). The road against fatalities : Infrastructure spending vs. regulation? *Accident Analysis & Prevention*, *59*, 227-239. https://doi.org/10.1016/j.aap.2013.06.008

AlRukaibi, F., AlKheder, S., Sayed, T., & Alburait, A. (2021). Injury severity influence factors and collision prediction—A case study on Kuwait highways. *Journal of Transport & Health*, *20*, 101025. https://doi.org/10.1016/j.jth.2021.101025

Ansari, S., Du, H., Naghdy, F., & Sattar, A. (2023). Impact of Post-Covid-19 on driver behaviour : A perspective towards pandemic-sustained transportation. *Journal of Transport & Health*, *28*, 101563. https://doi.org/10.1016/j.jth.2022.101563

Astarita, V., Haghshenas, S. S., Guido, G., & Vitale, A. (2023). Developing new hybrid grey wolf optimization-based artificial neural network for predicting road crash severity. *Transportation Engineering*, *12*, 100164. https://doi.org/10.1016/j.treng.2023.100164

Bastos, J. T., Shen, Y., Hermans, E., Brijs, T., Wets, G., & Ferraz, A. C. P. (2015). Traffic fatality indicators in Brazil : State diagnosis based on data envelopment analysis research. *Accident Analysis & Prevention*, *81*, 61-73. https://doi.org/10.1016/j.aap.2015.01.024

Baulk, S. D., Biggs, S. N., Reid, K. J., van den Heuvel, C. J., & Dawson, D. (2008). Chasing the silver bullet : Measuring driver fatigue using simple and complex tasks. *Accident Analysis & Prevention*, *40*(1), 396-402. https://doi.org/10.1016/j.aap.2007.07.008

Behnood, H. R. (2018). Best practice analysis of action for road safety in Iran amongst the leading developing

countries using an optimized success indicator. *Transport Policy*, *66*, 76-84. https://doi.org/10.1016/j.tranpol.2018.01.017

Bosso, M., Vasconcelos, K. L., Ho, L. L., & Bernucci, L. L. B. (2020). Use of regression trees to predict overweight trucks from historical weigh-in-motion data. *Journal of Traffic and Transportation Engineering (English Edition)*, *7*(6), 843-859. https://doi.org/10.1016/j.jtte.2018.07.004

Cafiso, S., & D'Agostino, C. (2016). Assessing the stochastic variability of the Benefit-Cost ratio in roadway safety management. *Accident Analysis & Prevention*, *93*, 189-197. https://doi.org/10.1016/j.aap.2016.04.027

Chajmowicz, H., Saadé, J., & Cuny, S. (2019). Prospective assessment of the effectiveness of autonomous emergency braking in car-to-cyclist accidents in France. *Traffic Injury Prevention*, *20*(sup2), S20-S25. https://doi.org/10.1080/15389588.2019.1679797

Chapelon, J., & Lassarre, S. (2010). Road safety in France : The hard path toward science-based policy. *Safety Science*, *48*(9), 1151-1159. https://doi.org/10.1016/j.ssci.2010.04.015

Chen, F., Lyu, J., & Wang, T. (2020). Benchmarking road safety development across OECD countries : An empirical analysis for a decade. *Accident Analysis & Prevention*, *147*, 105752. https://doi.org/10.1016/j.aap.2020.105752

Chen, F., Wu, J., Chen, X., Wang, J., & Wang, D. (2016). Benchmarking road safety performance : Identifying a meaningful reference (best-in-class). *Accident Analysis & Prevention*, *86*, 76-89. https://doi.org/10.1016/j.aap.2015.10.018

Chen, J., Wang, S., He, E., Wang, H., & Wang, L. (2021). Recognizing drowsiness in young men during real driving based on electroencephalography using an end-to-end deep learning approach. *Biomedical Signal Processing and Control*, *69*, 102792. https://doi.org/10.1016/j.bspc.2021.102792

Cheng, X., Wu, Y., Ning, P., Cheng, P., Schwebel, D. C., & Hu, G. (2018). Comparing road safety performance across countries : Do data source and type of mortality indicator matter? *Accident Analysis & Prevention*, *121*, 129-133. https://doi.org/10.1016/j.aap.2018.09.012

Coelho, M. C., & Guarnaccia, C. (2020). Driving Information in a Transition to a connected and autonomous vehicle environment : Impacts on pollutants, noise and safety. *Transportation Research Procedia*, *45*, 740-746. https://doi.org/10.1016/j.trpro.2020.02.103

Coffey, S., & Park, S. (2020). Part-time shoulder use operational impact on the safety performance of interstate 476. *Traffic Injury Prevention*, *21*(7), 470-475. https://doi.org/10.1080/15389588.2020.1795843

Connors, R. D., Maher, M., Wood, A., Mountain, L., & Ropkins, K. (2013). Methodology for fitting and updating predictive accident models with trend. *Accident Analysis & Prevention*, *56*, 82-94. https://doi.org/10.1016/j.aap.2013.03.009

Corben, B. F., Logan, D. B., Fanciulli, L., Farley, R., & Cameron, I. (2010). Strengthening road safety strategy development 'Towards Zero' 2008–2020 – Western Australia's experience scientific research on road safety management SWOV workshop 16 and 17 November 2009. *Safety Science*, *48*(9), 1085-1097. https://doi.org/10.1016/j.ssci.2009.10.005

De Bartolomeo, D., Renzi, E., Tamasi, G., Palermo, G., & Nucci, F. D. (2023). The Italian risk-based approach for the development of an ıntegrated safety management system for road ınfrastructures and its relations with innovative guidelines on the risk management of existing bridges. *Transportation Research Procedia*, *69*, 886-893. https://doi.org/10.1016/j.trpro.2023.02.249

Domenichini, L., Branzi, V., & Meocci, M. (2018). Virtual testing of speed reduction schemes on urban collector roads. *Accident Analysis & Prevention*, *110*, 38-51. https://doi.org/10.1016/j.aap.2017.09.020

El-Sayed, H., Ignatious, H. A., Kulkarni, P., & Bouktif, S. (2020). Machine learning based trust management framework for vehicular networks. *Vehicular Communications*, *25*, 100256. https://doi.org/10.1016/j.vehcom.2020.100256

El-Sayed, H., Zeadally, S., Khan, M., & Alexander, H. (2021). Edge-centric trust management in vehicular networks. *Microprocessors and Microsystems*, *84*, 104271. https://doi.org/10.1016/j.micpro.2021.104271

Fu, Y., Li, C., Luan, T. H., Zhang, Y., & Mao, G. (2018). Infrastructure-cooperative algorithm for effective intersection collision avoidance. *Transportation Research Part C: Emerging Technologies*, *89*, 188-204. https://doi.org/10.1016/j.trc.2018.02.003

Fwa, T. F. (2017). Skid resistance determination for pavement management and wet-weather road safety. *International Journal of Transportation Science and Technology*, *6*(3), 217-227. https://doi.org/10.1016/j.ijtst.2017.08.001

Habtemichael, F. G., & Santos, L. de P. (2012). The need for transition from macroscopic to microscopic traffic management schemes to ımprove safety and mobility. *Procedia - Social and Behavioral Sciences*, *48*, 3018-3029. https://doi.org/10.1016/j.sbspro.2012.06.1269

Horswill, M. S., Anstey, K. J., Hatherly, C., Wood, J. M., & Pachana, N. A. (2011). Older drivers' insight into their hazard perception ability. *Accident Analysis & Prevention*, *43*(6), 2121-2127. https://doi.org/10.1016/j.aap.2011.05.035

Horswill, M. S., Hill, A., Rodwell, D., Larue, G. S., Bates, L., & Watson, B. (2021). A brief and unsupervised online intervention improves performance on a validated test of hazard perception skill used for driver licensing. *Transportation Research Part F: Traffic Psychology and Behaviour*, *78*, 130-136. https://doi.org/10.1016/j.trf.2021.02.003

Huertas-Leyva, P., Dozza, M., & Baldanzini, N. (2019). E-bikers' braking behavior : Results from a naturalistic cycling study. *Traffic Injury Prevention*, *20*(sup3), 62-67. https://doi.org/10.1080/15389588.2019.1643015

Islam, N., Adanu, E. K., Hainen, A. M., Burdette, S., Smith, R., & Jones, S. (2021). A comparative analysis of freeway crash incident clearance time using random parameter and latent class hazard-based duration model. *Accident Analysis & Prevention*, *160*, 106303. https://doi.org/10.1016/j.aap.2021.106303

Kaulich, S., Pröstl, S., & Machata, K. (2016). Are there alternatives to scrutinising elderly drivers? *Transportation Research Procedia*, *14*, 4296-4303. https://doi.org/10.1016/j.trpro.2016.05.401

Lu, Z., Kwon, T. J., & Fu, L. (2019). Effects of winter weather on traffic operations and optimization of signalized intersections. *Journal of Traffic and Transportation Engineering (English Edition)*, *6*(2), 196-208. https://doi.org/10.1016/j.jtte.2018.02.002

Marciano, H., Setter, P., & Norman, J. (2015). Overt vs. Covert speed cameras in combination with delayed vs. Immediate feedback to the offender. *Accident Analysis & Prevention*, *79*, 231-240. https://doi.org/10.1016/j.aap.2015.03.028

Michelaraki, E., Katrakazas, C., Yannis, G., Filtness, A., Talbot, R., Hancox, G., Pilkington-Cheney, F., Brijs, K., Ross, V., Dirix, H., Neven, A., Paul, R., Brijs, T., Fortsakis, P., Frantzola, E. K., & Taveira, R. (2021). Post-trip safety interventions : State-of-the-art, challenges, and practical implications. *Journal of Safety Research*, *77*, 67-85. https://doi.org/10.1016/j.jsr.2021.02.005

Mooren, L., Grzebieta, R., Williamson, A., Olivier, J., & Friswell, R. (2014). Safety management for heavy vehicle transport : A review of the literature. *Safety Science*, *62*, 79-89. https://doi.org/10.1016/j.ssci.2013.08.001

Nikolaou, P., & Dimitriou, L. (2018). Evaluation of road safety policies performance across Europe : Results from benchmark analysis for a decade. *Transportation Research Part A: Policy and Practice*, *116*, 232-246. https://doi.org/10.1016/j.tra.2018.06.026

Nikolaou, P., Folla, K., Dimitriou, L., & Yannis, G. (2021). European countries' road safety evaluation by ταking ιnto αccount multiple classes of fatalities. *Transportation Research Procedia*, *52*, 284-291. https://doi.org/10.1016/j.trpro.2021.01.033

Nogal, M., & Honfi, D. (2019). Assessment of road traffic resilience assuming stochastic user behaviour. *Reliability Engineering & System Safety*, *185*, 72-83. https://doi.org/10.1016/j.ress.2018.12.013

Osei, K. K., Adams, C. A., Ackaah, W., & Oliver-Commey, Y. (2021). Signalization options to improve capacity and delay at roundabouts through microsimulation approach : A case study on arterial roadways in Ghana. *Journal of Traffic and Transportation Engineering (English Edition)*, *8*(1), 70-82. https://doi.org/10.1016/j.jtte.2019.06.003

Oviedo-Trespalacios, O., Haque, Md. M., King, M., & Washington, S. (2016). Understanding the impacts of mobile phone distraction on driving performance : A systematic review. *Transportation Research Part C: Emerging Technologies*, *72*, 360-380. https://doi.org/10.1016/j.trc.2016.10.006

Papadimitriou, E., & Yannis, G. (2013). Is road safety management linked to road safety performance? *Accident Analysis & Prevention*, *59*, 593-603. https://doi.org/10.1016/j.aap.2013.07.015

Pešić, D., & Pešić, A. (2020). Monitoring Of Road Safety performance ındicators – current situation and trends ın the republic of serbia. *Transportation Research Procedia*, *45*, 70-77. https://doi.org/10.1016/j.trpro.2020.02.064

Reis, D., Tomás, R., Coelho, M. C., & Macedo, E. (2023). Correlating driving behavior with safety performance : From the heart to the pedals with a driving simulator. *Transportation Research Procedia*, *69*, 217-224. https://doi.org/10.1016/j.trpro.2023.02.165

Rossi, R., Orsini, F., Tagliabue, M., Di Stasi, L. L., De Cet, G., & Gastaldi, M. (2021). Evaluating the impact of real-time coaching programs on drivers overtaking cyclists. *Transportation Research Part F: Traffic Psychology and Behaviour*, *78*, 74-90. https://doi.org/10.1016/j.trf.2021.01.014

Safarpour, H., Khorasani-Zavareh, D., & Mohammadi, R. (2020). The common road safety approaches : A scoping review and thematic analysis. *Chinese Journal of Traumatology*, *23*(2), 113-121. https://doi.org/10.1016/j.cjtee.2020.02.005

Sangrar, R., Mun, J., Cammarata, M., Griffith, L. E., Letts, L., & Vrkljan, B. (2019). Older driver training

programs : A systematic review of evidence aimed at improving behind-the-wheel performance. *Journal of Safety Research*, *71*, 295-313. https://doi.org/10.1016/j.jsr.2019.09.022

Silva, P. B., Andrade, M., & Ferreira, S. (2020). Machine learning applied to road safety modeling : A systematic literature review. *Journal of Traffic and Transportation Engineering (English Edition)*, *7*(6), 775-790. https://doi.org/10.1016/j.jtte.2020.07.004

Silva, P. B., Andrade, M., & Ferreira, S. (2021). Influence of segment length on the fitness of multivariate crash prediction models applied to a Brazilian multilane highway. *IATSS Research*, *45*(4), 493-502. https://doi.org/10.1016/j.iatssr.2021.05.001

Singh, H., & Kathuria, A. (2021). Analyzing driver behavior under naturalistic driving conditions : A review. *Accident Analysis & Prevention*, *150*, 105908. https://doi.org/10.1016/j.aap.2020.105908

Sinha, A., Chand, S., Wijayaratna, K. P., Virdi, N., & Dixit, V. (2020). Comprehensive safety assessment in mixed fleets with connected and automated vehicles : A crash severity and rate evaluation of conventional vehicles. *Accident Analysis & Prevention*, *142*, 105567. https://doi.org/10.1016/j.aap.2020.105567

Sun, L., Lin, Z., Li, W., & Xiang, Y. (2019). Freeway incident detection based on set theory and short-range communication. *Transportation Letters*, *11*(10), 558-569. https://doi.org/10.1080/19427867.2018.1453273

Tapp, A., Pressley, A., Baugh, M., & White, P. (2013). Wheels, skills and thrills : A social marketing trial to reduce aggressive driving from young men in deprived areas. *Accident Analysis & Prevention*, *58*, 148-157. https://doi.org/10.1016/j.aap.2013.04.023

Tarasi, D., Daras, T., Tournaki, S., & Tsoutsos, T. (2021). Transportation in the Mediterranean during the COVID-19 pandemic era. *Global Transitions*, *3*, 55-71. https://doi.org/10.1016/j.glt.2020.12.003

Treffner, P., Barrett, R., & Petersen, A. (2002). Stability and skill in driving. *Human Movement Science*, *21*(5- 6), 749-784. https://doi.org/10.1016/S0167-9457(02)00168-9

Twisk, D., Wesseling, S., Vlakveld, W., Vissers, J., Hegeman, G., Hukker, N., Roelofs, E., & Slinger, W. (2018). Higher-order cycling skills among 11- to 13-year-old cyclists and relationships with cycling experience, risky behavior, crashes and self-assessed skill. *Journal of Safety Research*, *67*, 137-143. https://doi.org/10.1016/j.jsr.2018.10.003

Vankov, D., & Schroeter, R. (2021). Driving under the influence of drugs or alcohol : Predicting the intentions of young drivers. *Traffic Injury Prevention*, *22*(2), 97-101. https://doi.org/10.1080/15389588.2020.1869953

World Health Organization. (2021). *Global plan for the decade of action for road safety 2021-2030*, World Health Organization.

Yadav, A. K., & Velaga, N. R. (2020). An investigation on the risk factors associated with driving errors under the influence of alcohol using structural equation modeling. *Traffic Injury Prevention*, *21*(4), 288-294. https://doi.org/10.1080/15389588.2020.1753039

Zhao, X., He, R., & Wang, J. (2020). How do drivers respond to driving risk during car-following? Risk-response driver model and its application in human-like longitudinal control. *Accident Analysis & Prevention*, *148*, 105783. https://doi.org/10.1016/j.aap.2020.105783.

Author Information

Ibtissam El Khalai
Ecole Mohammadia d'Ingénieurs
Mohammed V University in Rabat, Morocco
ibtissamelkhalai@research.emi.ac.ma

Zoubida Chorfi
Ecole Mohammadia d'Ingénieurs
Mohammed V University in Rabat, Morocco

Abdelaziz Berrado
Ecole Mohammadia d'Ingénieurs
Mohammed V University in Rabat, Morocco

To cite this article:

El Khalai, I., Chorfi, Z. & Berrado, A. (2023). Road safety performance monitoring practices: A literature review. *The Eurasia Proceedings of Science Technology, Engineering & Mathematics (EPSTEM), 22,* 99-110.

The Eurasia Proceedings of Science, Technology, Engineering & Mathematics (EPSTEM)
ISSN: 2602-3199

The Eurasia Proceedings of Science, Technology, Engineering & Mathematics (EPSTEM), 2023

Volume 22, Pages 111-118

ICBASET 2023: International Conference on Basic Sciences, Engineering and Technology

Heat-Absorbing Composite Strength Analysis for Electric Vehicles Battery Pack Cover

Alexander Christantho BUDIMAN
Research Center for Transportation Technology, National Research and Innovation Agency (BRIN)

Sudirja SUDIRJA
Research Center for Transportation Technology, National Research and Innovation Agency (BRIN)

Sunarto KALEG
Research Center for Transportation Technology, National Research and Innovation Agency (BRIN)

Habib Saifuddin FATHONI
Institut Teknologi Sepuluh September

Dasa NOVIANTO
Institut Teknologi Sepuluh September

Amin AMIN
Research Center for Transportation Technology, National Research and Innovation Agency (BRIN)

M. Arjuna Putra PERDANA
Research Center for Transportation Technology, National Research and Innovation Agency (BRIN)

Rina RISTIANA
Research Center for Transportation Technology, National Research and Innovation Agency (BRIN)

Kristian ISMAIL
Research Center for Transportation Technology, National Research and Innovation Agency (BRIN)

Aam MUHARAM
Research Center for Transportation Technology, National Research and Innovation Agency (BRIN)

Abdul HAPID
Research Center for Transportation Technology, National Research and Innovation Agency (BRIN)

Abstract: One of the key components of Electric Vehicles is the battery pack compartment casing, which needs to be both as light and as strong as possible to cover maximum mileage while withstand vibrations and other mechanical abuse. A layer of thermal protection is also placed to the case because a typical Lithium battery used for an EV is very sensitive to temperature. In this study, a heat-absorbing lightweight composite for the battery pack compartment casing of an electric vehicle is physically constructed and put to the test to determine its mechanical characteristics. The latent ability of organic phase change materials to absorb heat without experiencing thermal rise led to their use as fillers for the resin composite. Depending on what type and how much phase change materials are utilized, the tensile evaluation reveals that the average strength is noticeably compromised. The composite preparation techniques, including the use of carbon fiber as reinforcement material, are also briefly covered in this paper.

Keywords: Battery thermal management system, Electric vehicles, Mechanical properties, Phase Change Materials, Tensile strength

Introduction

Research and development of battery Electric Vehicles (EV) have significantly progressed in recent years due to the worldwide aim to achieve carbon-neutral in 2050 and reduce dependency on fossil fuels. One of the key components in battery EV is the so-called Battery Thermal Management System (BTMS). It is a mandatory feature to protect the battery pack from any kind of thermal abuse. Internal electrochemical reactions in each battery cell during the charging or discharging process often lead to a certain amount of heat dissipating to the surroundings (Gungor et al., 2022; Zhao et al., 2018). Due to its compact nature, an uncontrolled heat dissipation caused some sort of heat entrapment, causing an exponential increase in temperature so-called thermal runaway, which is hazardous (Börger et al., 2019; Feng et al., 2018).

Take an example from a Lithium-based battery, which is currently one of the most popular types of EV known for its high energy density. Its safe operating temperature is generally between 0-40 °C. When heat dissipation causes it to exceed 40 °C, its electrical performance is compensated and its life cycle is also damaged in the long run (Z. Wang et al., 2021). During the EV operation, the surface temperature is significantly affected not only by the environment (Cen et al., 2018; Huda et al., 2020; Talluri et al., 2020), but also by the electrical load (Budiman et al., 2022; Offer et al., 2012). Uneven surface temperature between each battery cell in use leads to different charging or discharging capabilities within a battery module or pack which creating a positive/self-reinforcing feedback to heat dissipation. Severe thermal damage can be initiated from just a single cell failure. As such, a proper thermal management system is required.

A complex vehicle design requires the battery pack to be safely stored and protected not only from thermal abuses but also electrical and mechanical stresses. The complex electrical wiring and connections near the battery pack storage area that become the nature of EV, altogether with constant vibrations when the vehicle is in motion, may affect the batteries' performance and safety. Therefore, a battery pack cover needs to be robust and maintain a certain level of mechanical strength as well as elasticity. Recently, polymer composites have been extensively investigated for their potential substitute for steel or other metal parts in a vehicle (Zhang & Xu, 2022). Such lightweight materials are preferred due to the extreme weight allowed in vehicles, which also contributes to the mileage it could cover from a single battery charge (Arifurrahman et al., 2018; Baser et al., 2022; Sudirja et al., 2020).

Composite materials are formed from at least two different substances, typically with different mechanical or chemical properties, typically with distinct boundaries between them. A simple resin composite can be made by mixing it with a catalyst and letting them cured in a mold for just a couple of hours or days. The composite product usually has unique, standout characteristics, and often is combined with various reinforcement materials. For example, carbon fiber is combined with polymers to form a reinforced plastic with significantly greater mechanical strength than ordinary plastics. Aluminum Tri-Hydroxide (ATH) is added to an Unsaturated Polyester to form a composite with a high level of flame retardancy (Kaleg et al., 2022). Kevlar composite can be found not only in the military but also in the aerospace industry as an engine protection layer. Graphene is mixed with Phase Change Materials (PCM) and recycled plastics as building materials with better indoor thermal conditioning than conventional materials (Acuña-Pizano et al., 2022). PCM composite is also used as a heat absorber in EV to protect the battery pack from overheating. There are many forms of PCM composites reported, such as with graphite (Cabeza et al., 2003; Jiang et al., 2017), metal foam (Hussein et al., 2016; X. Wang et al., 2018), nanopowders (Kochetov et al., 2009), and carbon fibers (Babapoor et al., 2015; Samimi et al., 2016). These previous studies reported a significantly reduced maximum temperature due to an augmented heat transfer from the battery to the composite, despite the PCM itself having a low thermal conductivity.

Besides a simple casting, many complex composite manufacturing methods that often involve reinforcement materials have been developed to date, such as hand lay-up and vacuum infusion methods. As one of the oldest processes, the former is known for its simplicity and is economically feasible. It begins with mixing resin and catalysts, before the mixture is manually applied to the reinforcement fiber in a mold. Another layer of fiber is then put on top of the mixture using a roller to remove air bubbles. These steps are repeated until the desired thickness. Once done, the composite can be removed from the mold, which can be reused. On the other hand, the vacuum infusion process requires a vacuum compressor to infuse the resin mixture along the bundles of reinforcement fibers inside a sealed bag. As a result, the end product typically has better consistency and

properties than the hand lay-up process. However, the vacuum bag cannot be reused, making this process more costly than the hand lay-up.

In this work, a resin composite with PCM is prepared using a simple casting method and evaluated in terms of tensile strength. Brief qualitative comparisons based on still photographs between samples with various compositions are discussed. Two different organic PCM with 20 percent of weight are tested and compared with the base reference. Other specimens are prepared using different composite fabricating methods for comparison. The tensile tests would reveal the suitability of such materials to be used in the EV battery pack case.

Experimental Methods

The base reference composite was made by mixing commercial Ripoxy R-804J resin with MEKP (Methyl Ethyl Ketone Peroxide) as its promoter. Both products were purchased from Justus Kimiaraya, Indonesia. A small amount of Montmorillonite is added to improve its flame retardancy. The mixture is then poured into a 14 cm x 14 cm silicone mold and left cured for at least 24 hours. To study the effect of the vacuum infusion method, another base specimen was prepared. Carbon Fiber HD C524-3K Weave was used as a reinforcement material. The curing process was between 48-72 hours, notably longer duration than the ordinary molding due to the usage of vacuum sealed bag.

Three different organic PCM (Sigma-Aldrich, Singapore) were considered in this study, that is, paraffin C20 mixture, lauric acid, and caprylone. These PCM have unique, different heat absorbing characteristics (Budiman et al., 2021) with their respective peak latent temperature of 53.8 ºC, 44.1 ºC, and 39.4 ºC (NETZSCH DSC 214 Polyma DSC21400A-0710-L). Each PCM was put into a container in a hot water bath until entirely melted before being stirred with the Ripoxy for a minute prior to the catalyst addition. Another sample with graphite powder, known as thermal conductivity augmentation material (Cabeza et al., 2003), was also prepared. After a day, the cured specimens were cut by means of CNC milling and prepared according to the ASTM D638 tensile test requirements.

Results and Discussion

Visual Appearance

Although the minimum duration for the curing process is set as 24 hours, visual observation has been carried out regularly since the mixture was added to the mold. For the base composite, the sample seemed completely dry out and detached from the base just within the first two hours. The other samples took a slightly longer time, but it is expected that the curing is already completed. After 24 hours and the sample is removed from the mold, it is found that the blank specimen (the resin base without any PCM) and the specimen with paraffin has a light brown/grey color, while the lauric and caprylone composites are more yellowish, as depicted in Figure 1. The base sample has a smooth surface, indicating an evenly distributed curing process. On the other hand, the PCM composites are relatively rough, especially in the case of paraffin, which could be a sign that some small amounts of PCM are not fully covered by the resin and are ejected out of the mixture. This could possibly be due to the marginal density difference between the resin and the PCM, which unfortunately could not be simply snubbed, slowly causing the PCM to be separated during the curing duration.

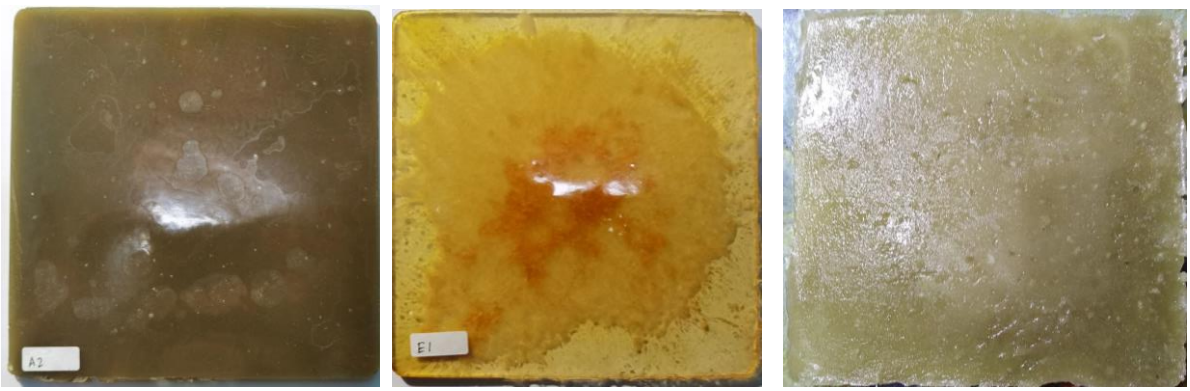

Figure 1. Photographs of the blank, lauric, and paraffin resin composites

Figure 2. Photographs of the 40% lauric and paraffin composites

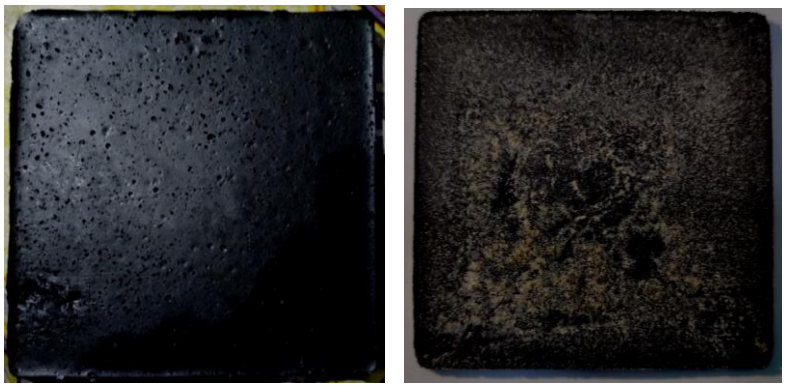

Figure 3. Photographs of the 20% and 40% lauric with graphite

Figure 2 shows the effect of more PCM addition to the mixture. As each of the lauric and paraffin amounts is doubled, unusual PCM lumps could be found especially on the top surface. Those protrusions are rather simple to remove, even with only slight nail movements. Moreover, a notable shrinking process could somehow be found, as the composite side is no longer attached to the side frame. The surface was jagged and a notable amount of fine craters/dimples could be seen. Figure 3 shows a similar result when both lauric samples were also mixed with graphite powder. The yellowish lauric can be spotted well across the sample. Additionally, the lumps are thoroughly melted and separated from the solid specimen when the samples are heated to a temperature above the PCM melting point and subsequently naturally cooled back to room temperature (i.e., one thermal cycle). Our weight composition variations between 5 and 40% PCM suggest that the 20%wt may be the upper limit permitted by this straightforward mold curing process for the PCM to be completely macro-encapsulated within the composite without a weight reduction detected after some thermal cycles.

Mechanical Properties

It is understandable that the presence of PCM might particularly reduce the mechanical strength of the composites, considering its typically brittle appearance. The average tensile results from at least three specimens of composites are tabulated in Table 1, while the stress-strain relation and the force-to-length trend are presented in Figures 4-6 for the base reference case, lauric acid, and paraffin composites, respectively. While the reference sample broke at approximately 1.98 mm in length, the specimen with lauric and paraffin could reach 2.48 and only 1.16 mm, respectively. The presence of lauric acid or paraffin in the resin composite differently reduces the maximum limit of force or stress that can be endured by the material, with the biggest reduction of almost 70% caused by paraffin.

Table 1. Mechanical strength test results of each resin speciments

Specimen	Ultimate Force (N)	Ultimate Stress (MPa)	Modulus (MPa)	Total Elongation (%)
Base	604 ± 16	62.1 ± 0.8	1835 ± 135	3.56 ± 0.02
Lauric ac.	402 ± 16	41.3 ± 5.1	1018 ± 84	3.43 ± 0.96
Paraffin	216 ± 25	22.1 ± 4.9	695 ± 196	2.93 ± 1.61

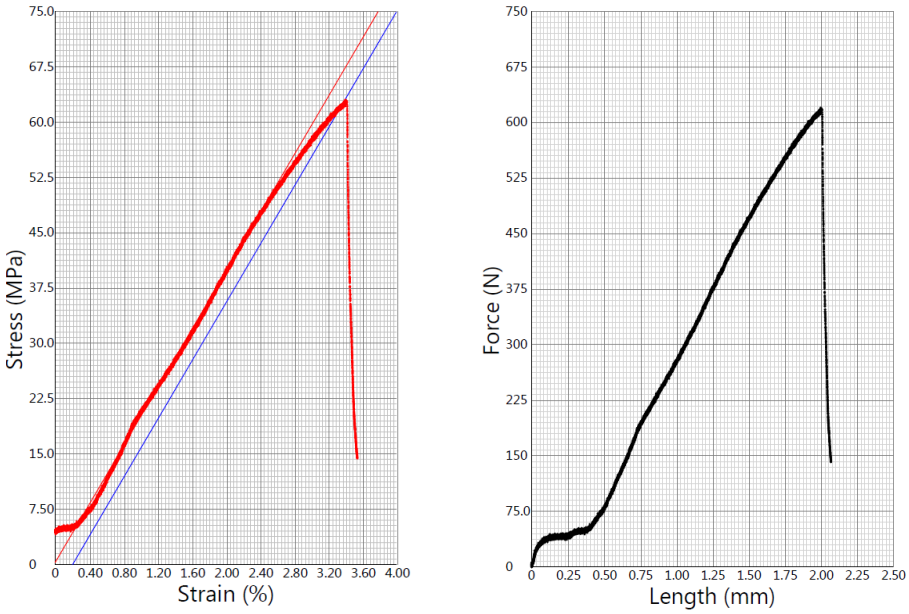

Figure 4. Tensile test results from the base resin

The presence of small dimples or bumps around the surface could also indicate similar situations inside the specimen, that is, the substantial void that weakens the entire structure by potentially allowing crack propagation more easily. Any non-uniform particle distribution so-called agglomeration or volumetric change during PCM phase transition temperature might affect the matrix-filler microscopic structure integrity, hence an increase of potential stress concentration (Kaleg et al., 2022; Luo et al., 2020). Furthermore, the uneven surface roughness could also contribute to the gripping problem of the specimen under the tensile test, resulting in a slightly jagged trend in the middle of the tests, as seen in Figures 5-6.

Unlike PCM, the use of fibers in a composite provides certain stiffness to the resin matrix, leading to protection against cracks or other structural damages. The effect of the vacuum infusion method and carbon fiber reinforcement for the base reference resin specimen can be clearly seen in Table 2. The material could now withstand more than 15 times of force, while the maximum stress could be increased by about five times. The specimen could be stretched by approximately 6.15 mm before it broke. In contrast, the modulus value only increased by about 25%. The more evenly distributed resin mixture inside the fiber weaves leads to a well-spread stress, causing it more difficult to break. Furthermore, the addition of PCM only decreased the ultimate force by 20%, compared to 34% in the previous method.

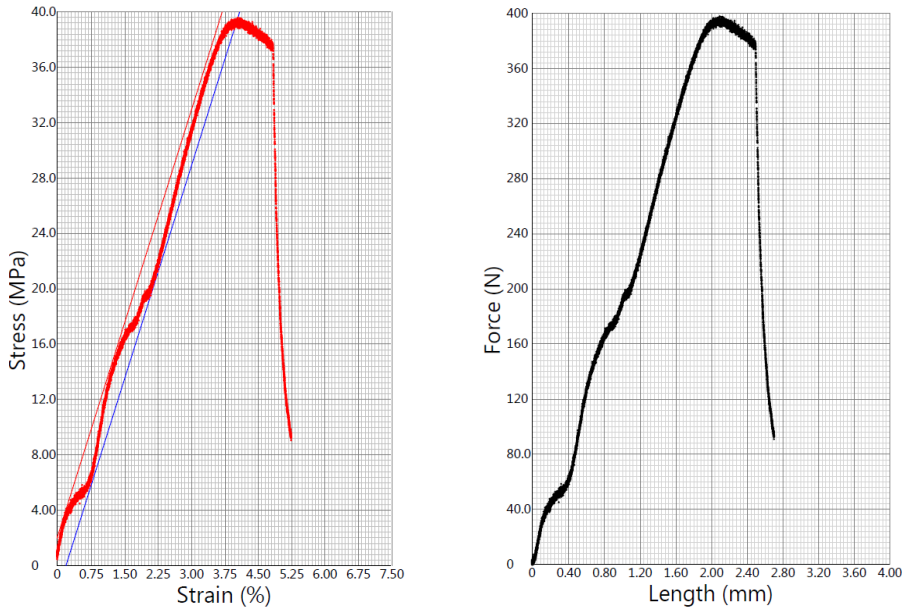

Figure 5. Tensile test results from the resin with lauric acid

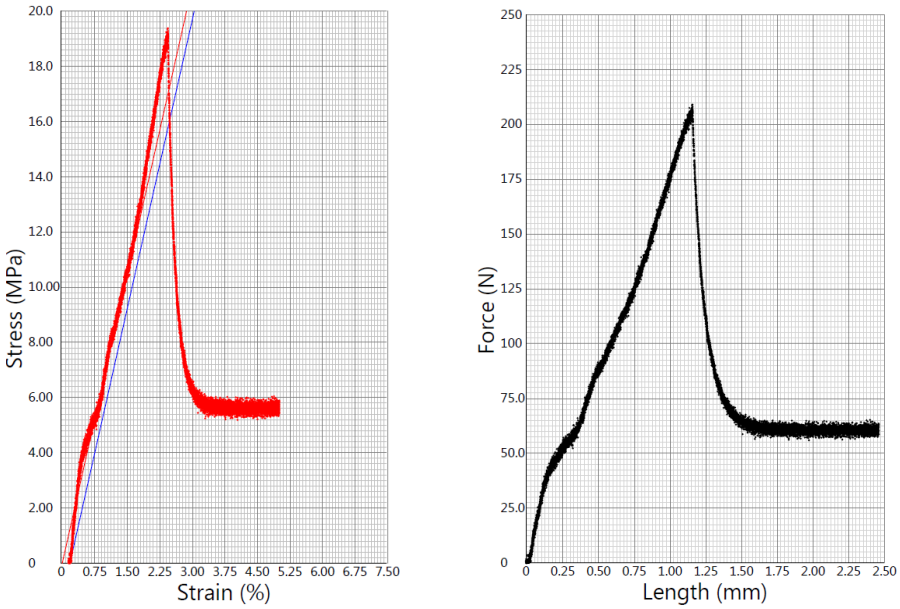

Figure 6. Tensile test results from the paraffin-added resin

Table 2. Mechanical strength of resin speciment with carbon fiber

Specimen	Ultimate Force (N)	Ultimate Stress (MPa)	Modulus (MPa)	Total Elongation (%)
Base	604 ± 16	62.1 ± 0.8	1835 ± 135	3.56 ± 0.02
Reinforced base	10225 ± 175	329.5 ± 6.5	2317 ± 243	11.35 ± 0.85
Lauric	8250 ± 30	220 ± 1.0	2110 ± 245	10.4 ± 0.70
Lauric-graphite	8810 ± 30	271 ± 1.0	2395 ± 245	11.20 ± 0.70

Conclusion

Polymer composites with heat-absorbing material for Electric Vehicles battery pack compartment covers have been manufactured and tested in terms of their mechanical strength. Three different organic Phase Change Materials (PCM) with a similar melting point profile were used and comparatively analyzed. Using a simple casting method, it can be concluded that a maximum of 20%wt PCM can be added to the resin mixture without experiencing extensive agglomeration on the surface. The tensile test was performed to show how much strength reduction was due to the presence of PCM. It can be seen that the lauric acid PCM specimen has a smaller decrease than paraffin. Finally, the presence of carbon-fiber as material reinforcement, coupled with the vacuum infusion method, which leads to a more uniformly distributed mixture within the fiber weave, produces a significant mechanical strength upgrade to the base case.

Scientific Ethics Declaration

The authors declare that the scientific ethical and legal responsibility of this article published in EPSTEM journal belongs to the authors.

Acknowledgements and Notes

*This work was supported by the Research Organization for Electronics and Informatics, BRIN under grant 2/III.6/HK/2023. ACB, S, and SK contributed equally as the main contributor to this manuscript. The authors would also thank the E-Layanan Sains BRIN for the tests and supervision platform. There is no conflict of interest to declare.

*This article was presented as an oral presentation at the International Conference on Basic Sciences, Engineering and Technology (www.icbaset.net) conference held in Marmaris/Turkey on April 27-30, 2023.

References

Acuña-Pizano, H., González-Trevizo, M. E., Luna-León, A., Martínez-Torres, K. E., & Fernández-Melchor, F. (2022). Plastic composites as sustainable building materials: A thermal and mechanical exploration. *Construction and Building Materials*, *344*(June), 128083. https://doi.org/10.1016/j.conbuildmat.2022.128083

Arifurrahman, F., Budiman, B. A., & Aziz, M. (2018). On the lightweight structural design for electric road and railway vehicles using fiber reinforced polymer composites – A review. *International Journal of Sustainable Transportation Technology*, *1*(1), 21–29. https://doi.org/10.31427/ijstt.2018.1.1.4

Babapoor, A., Azizi, M., & Karimi, G. (2015). Thermal management of a Li-ion battery using carbon fiber-PCM composites. *Applied Thermal Engineering*, *82*, 281–290. https://doi.org/10.1016/j.applthermaleng.2015.02.068

Baser, T. A., Umay, E., & Akinci, V. (2022). New trends in aluminum die casting alloys for automotive applications. *The Eurasia Proceedings of Science, Technology, Engineering & Mathematics (EPSTEM)*, *21*, 79–87. https://doi.org/10.55549/epstem.1227541

Börger, A., Mertens, J., & Wenzl, H. (2019). Thermal runaway and thermal runaway propagation in batteries: What do we talk about? *Journal of Energy Storage*, *24*(August 2018), 100649. https://doi.org/10.1016/j.est.2019.01.012

Budiman, A. C., Kaleg, S., Hidayat, N. A., Silalahi, G. N., Gani, M. N., Sudirja, Amin, Muharam, A., & Hapid, A. (2021). Experimental study of two organic phase change materials in cylindrical containers for battery module thermal management: A comparative analysis. *Journal of Physics: Conference Series*, *2047*, 012018. https://doi.org/10.1088/1742-6596/2047/1/012018

Budiman, A. C., Kaleg, S., Sudirja, S., Amin, & Hapid, A. (2022). Passive thermal management of battery module using paraffin-filled tubes: An experimental investigation. *Engineering Science and Technology, an International Journal*, *29*, 101031. https://doi.org/10.1016/j.jestch.2021.06.011

Cabeza, L. F., Zalba, B., Marin, J. M., & Mehling, H. (2003). PCM-graphite matrix in flat plate encapsulates for low temperature applications. *9th International Conference on Thermal Energy Storage*, 279–284.

Cen, J., Li, Z., & Jiang, F. (2018). Experimental investigation on using the electric vehicle air conditioning system for lithium-ion battery thermal management. *Energy for Sustainable Development*, *45*, 88–95. https://doi.org/10.1016/j.esd.2018.05.005

Feng, X., Ouyang, M., Liu, X., Lu, L., Xia, Y., & He, X. (2018). Thermal runaway mechanism of lithium ion battery for electric vehicles: A review. *Energy Storage Materials*, *10*(October 2018), 246–267. https://doi.org/10.1016/j.ensm.2017.05.013

Gungor, S., Cetkin, E., & Lorente, S. (2022). Canopy-to-canopy liquid cooling for the thermal management of lithium-ion batteries, a constructal approach. *International Journal of Heat and Mass Transfer*, *182*, 121918. https://doi.org/10.1016/j.ijheatmasstransfer.2021.121918

Huda, N., Kaleg, S., Hapid, A., Kurnia, M. R., & Budiman, A. C. (2020). The influence of the regenerative braking on the overall energy consumption of a converted electric vehicle. *SN Applied Sciences*, *2*(4), 606. https://doi.org/10.1007/s42452-020-2390-3

Hussein, H. A., Abed, A. H., & Abdulmunem, A. R. (2016). An experimental investigation of using aluminum foam matrix integrated with paraffin wax as a thermal storage material in a solar heater. *Proceeding of the 2nd Sustainable & Renewable Energy Conference, 26-27 November*, ASE-6.

Jiang, G., Huang, J., Liu, M., & Cao, M. (2017). Experiment and simulation of thermal management for a tube-shell Li-ion battery pack with composite phase change material. *Applied Thermal Engineering*, *120*, 1–9. https://doi.org/10.1016/j.applthermaleng.2017.03.107

Kaleg, S., Budiman, A. C., Hapid, A., Amin, Muharam, A., Sudirja, Ariawan, D., & Diharjo, K. (2022). Evaluations of aluminum tri-hydroxide and pristine montmorillonite in glass fiber reinforced polymer for vehicle components. *International Journal of Automotive and Mechanical Engineering*, *19*(1), 9379–9390. https://doi.org/10.15282/ijame.19.1.2022.02.0721

Kochetov, R., Andritsch, T., Lafont, U., Morshuis, P. H. F., Picken, S. J., & Smit, J. J. (2009). Thermal behaviour of epoxy resin filled with high thermal conductivity nanopowders. *2009 IEEE Electrical Insulation Conference*, 524–528. https://doi.org/10.1109/EIC.2009.5166402

Luo, X., Guo, Q., Li, X., Tao, Z., Lei, S., Liu, J., Kang, L., Zheng, D., & Liu, Z. (2020). Experimental investigation on a novel phase change material composites coupled with graphite film used for thermal management of lithium-ion batteries. *Renewable Energy*, *145*, 2046–2055. https://doi.org/10.1016/j.renene.2019.07.112

Offer, G. J., Yufit, V., Howey, D. A., Wu, B., & Brandon, N. P. (2012). Module design and fault diagnosis in electric vehicle batteries. *Journal of Power Sources*, *206*, 383–392. https://doi.org/10.1016/J.JPOWSOUR.2012.01.087

Samimi, F., Babapoor, A., Azizi, M., & Karimi, G. (2016). Thermal management analysis of a Li-ion battery

cell using phase change material loaded with carbon fibers. *Energy*, *96*, 355–371. https://doi.org/10.1016/j.energy.2015.12.064

Sudirja, S., Hapid, A., Amin, Kaleg, S., & Budiman, A. C. (2020). Stress analysis simulations of welded and bolted joints method for full steel and composite-steel chassis structure of electric low floor medium bus. *EUREKA, Physics and Engineering*, *2020*(6), 61–70. https://doi.org/10.21303/2461-4262.2020.001516

Talluri, T., Kim, T. H., & Shin, K. J. (2020). Analysis of a battery pack with a phase change material for the extreme temperature conditions of an electrical vehicle. *Energies*, *13*(3), 507. https://doi.org/10.3390/en13030507

Wang, X., Xie, Y., Day, R., Wu, H., Hu, Z., Zhu, J., & Wen, D. (2018). Performance analysis of a novel thermal management system with composite phase change material for a lithium-ion battery pack. *Energy*, *156*, 154–168. https://doi.org/10.1016/j.energy.2018.05.104

Wang, Z., Yuan, J., Zhu, X., Wang, H., Huang, L., Wang, Y., & Xu, S. (2021). Overcharge-to-thermal-runaway behavior and safety assessment of commercial lithium-ion cells with different cathode materials: A comparison study. *Journal of Energy Chemistry*, *55*, 484–498. https://doi.org/10.1016/j.jechem.2020.07.028

Zhang, W., & Xu, J. (2022). Advanced lightweight materials for Automobiles : A review. *Materials & Design*, *221*, 110994. https://doi.org/10.1016/j.matdes.2022.110994

Zhao, Y., Patel, Y., Zhang, T., & Offer, G. J. (2018). Modeling the effects of thermal gradients ınduced by tab and surface cooling on lithium ıon cell performance. *Journal of The Electrochemical Society*, *165*(13), A3169–A3178. https://doi.org/10.1149/2.0901813jes

Author Information

Alexander Christantho Budiman
Research Center for Transportation Technology,
National Research and Innovation Agency (BRIN)
KST Samadikun Bandung 40135, Indonesia
Contact e-mail: *alex003@brin.go.id*

Sudirja Sudirja
Research Center for Transportation Technology,
National Research and Innovation Agency (BRIN)
KST Samadikun Bandung 40135, Indonesia

Sunarto Kaleg
Research Center for Transportation Technology,
National Research and Innovation Agency (BRIN)
KST Samadikun Bandung 40135, Indonesia

Habib Saifuddin Fathoni
Institut Teknologi Sepuluh September
Surabaya 60111, Indonesia

Dasa Novianto
Institut Teknologi Sepuluh September
Surabaya 60111, Indonesia

Amin Amin
Research Center for Transportation Technology,
National Research and Innovation Agency (BRIN)
KST Samadikun Bandung 40135, Indonesia

M. Arjuna Putra Perdana
Research Center for Transportation Technology,
National Research and Innovation Agency (BRIN)
KST Samadikun Bandung 40135, Indonesia

Rina Ristiana
Research Center for Transportation Technology,
National Research and Innovation Agency (BRIN)
KST Samadikun Bandung 40135, Indonesia

Kristian Ismail
Research Center for Transportation Technology,
National Research and Innovation Agency (BRIN)
KST Samadikun Bandung 40135, Indonesia

Aam Muharam
Research Center for Transportation Technology,
National Research and Innovation Agency (BRIN)
KST Samadikun Bandung 40135, Indonesia

Abdul Hapid
Research Center for Transportation Technology,
National Research and Innovation Agency (BRIN)
KST Samadikun Bandung 40135, Indonesia

To cite this article:

Budiman, A.C., Sudirja, S., Kaleg, S. Fathoni, H.S., Novianto, D., Amin, A., Perdana, M.A.P., Ristiana, R., Ismail, K., Muharam, A., & Hapid, A. (2023). Heat-absorbing composite strength analysis for electric vehicles battery pack cover. *The Eurasia Proceedings of Science, Technology, Engineering & Mathematics (EPSTEM), 22,* 111-118.

The Eurasia Proceedings of Science, Technology, Engineering & Mathematics (EPSTEM)
ISSN: 2602-3199

The Eurasia Proceedings of Science, Technology, Engineering & Mathematics (EPSTEM), 2023

Volume 22, Pages 119-126

ICBASET 2023: International Conference on Basic Sciences, Engineering and Technology

A Navigation Tool for Visually Impaired and Blind People

Adnan AL-SMADI
Yarmouk University

Talal AL-QARYOUTI
Yarmouk University

Abdurahman REHAN
Yarmouk University

Homam ASSI
Yarmouk University

Alhareth ALSHAREA
Yarmouk University

Abstract: Visual disability or blindness is a common issue in the whole world. Visually impaired people normally rely on senses other than sight to guide them such as touching, hearing, or feeling. This paper describes a tool to help blind and visually impaired people to be able to move around with comfort and confidence. The paper proposes a development of a product that is easy to use by blind and visually impaired people to detect any obstacles accurately and efficiently. The system should allow the blind person to navigate with reasonable speed and confidence by detecting the nearby obstacles. The proposed system implements a device embedded with advanced technology which will give the blind person the needed confidence to perform his/her own work by him/herself rather than depending on others. The system uses ultrasound sensors and raspberry pi to detect any obstacle around the blind person. The system will inform the blind person in case of existence of obstacle through a buzzer or a vibrator. The ultrasonic sensor is used to detect the real time while the blind person is walking. It gives feedback as a sound or a vibration as indication of detecting an obstacle. A prototype blind aid system that can help blind and visually impaired people to move around with leisure has been implemented and tested. It performed as expected.

Keywords: Blind, Visually impaired, Raspberry pi, Ultrasonic sensor

Introduction

A blind person is a person without sense of sight, or a person who has no ability to see anything. Blindness is a condition of lacking the visual perception due to physiological or neurological factors (Vinod, 2018; Nawer et al., 2015). This causes full absence of the visual light perception. On the other hand, partial blindness or visual impairment means the lack of integration in the growth of the optic nerve or center of the eye. Partial or full blindness is a situation that affects many people around the world (Phirke, 2015). This situation causes the loss of the valuable sense of vision. In general, blind people do not see objects in front of them. This situation makes them exposed to many serious problems such as bumping into a wall, other people, or even a parked or a moving car. Without any aides, blind people must rely on others to move around which means that they cannot travel independently to any place without the help of others.

The World Health Organization (WHO), reported in 2021 that there are more than 2.2 billion suffer from vision impairment persons around the world (Batool and Naz, 2021). Therefore, the need to have aided tools for the blind people will be continuous. To date, there are several navigation systems and helping aides for the blinds and visually impaired people.

Batool and Naz (2021) proposed a third eye for blind people using the Arduino Pro Mini 328 and ultrasonic sensor. Their product was made using five ultrasonic sensors, consisting five modules linked to different parts of the blind person's body. Thumma et al. (2017) proposed the development of a smart stick for the visually impaired people. The stick includes a global positioning system (GPS), Global System for Mobile (GSM) tools and obstacle detection system. The GPS is used by the blind person to find the current location. The GSM will send a message to notify some of his/her relative of the current location. Kupade et al. (2020) proposed a third eye for blind people using an open source IOT platform node MCU microcontroller, GPS, ultrasonic sensor, and buzzer. They interfaced the GPS module with the node MCU microcontroller to track the location of the person when a request is sent to controller. The GPS will determine the location by calculating the longitude and latitude values. Bousbia and Fezari (2007) proposed a navigation aid to help blind and visually impaired people to navigate easily. The system involves a microcontroller with synthetic speech output. The system consists of two vibrators and two ultrasonic sensors mounted on the blind person's shoulders and one inserted into the blind person's helping tool such as cane. Singh et al. (2017) proposed a walking stick to help blind people to navigate and detect obstacles. The proposed tool consists of a microcontroller AT89S52, infrared sensors (IR), GPS receiver, label surface detection, GSM, and a buzzer. The system starts by detecting obstacles by an array of infrared sensors. The GPS receiver is used for navigation purposes. The GSM is used to inform in case of a danger occur to the blind person. In this paper, we propose a navigation tool for visually impaired and blind people using raspberry pi 3 and ultrasonic sensor. The tool can be placed on a walking stick or it can be mounted on the hand of the user.

Proposed System

Blindness or visual disability is a common issue in every country of the world. Without any aides, blind people must rely on other people to move around which means that they cannot travel independently to any place without the help of others. There are several systems exist to help visually impaired people move around (Sharma & Chatterji, 2015; Maragatharajan et al., 2019).

This paper proposes an aiding tool for the visually impaired and blind people to be able to navigate and move easily without the help of others. The proposed aiding tool will be able to detect any obstacle nearby the blind and visually impaired persons. The proposed system implements a device embedded with advanced technology which will give the blind person the needed confidence to perform his/her own work by him/herself rather than depending on others. The system uses a raspberry pi which is embedded with ultrasonic sensors, buzzer module, and vibrator motor. The ultrasonic sensor is used to detect the real time while the blind person is walking. It gives feedback as a sound or a vibration as indication of detecting an obstacle. The device is inexpensive, efficient, and reliable.

The main components of the proposed device are raspberry pi 3, ultrasonic sensors, buzzer, and vibration motor. These components are described as follows. The block diagram of the proposed system is shown in Figure 1.

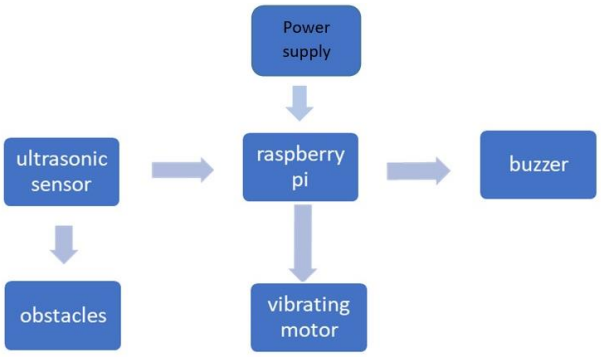

Figure 1. The block diagram of the proposed system

Raspberry Pi 3

Raspberry pi microcontroller is a small single board computer developed by the Raspberry Pi Foundation towards teaching basic science. Raspberry pi 3 model is the third generation Raspberry Pi (White, 2016). Raspberry pi microcontroller supports various programming languages such as python. It has been widely used to build hardware projects. It can perform as a minicomputer that connects all peripherals used by any computer such as mouse, keyboard, and monitor. It can accomplish tasks that can be carried out by desktop computers. Raspberry pi 3 microcontroller is shown in Figure 2.

Figure 2. Raspberry Pi 3 microcontroller (White, 2016)

Ultrasonic Sensor

It is a transducer which is a type of acoustic sensor that works as sound transmitter or receiver (Al-Smadi et al., 2020; Al-Smadi & Msallam, 2022). The transmitter converts electrical signal into sound waves while the receiver converts the sound waves back into electrical signal. It emits ultrasonic wave at high frequency (at 40 000 Hz which is too high for humans to hear and observe) that travels in the air. When the signal is detected by an object, it gets reflected back toward the ultrasonic sensor. The receiver will observe the reflected signal. The pins of the HC-SR04 ultrasonic sensor module are shown in Figure 3. Ultrasonic module HC-SR04 is provided with 2cm-400cm measurement with a ranging accuracy that can reach up to 3mm.

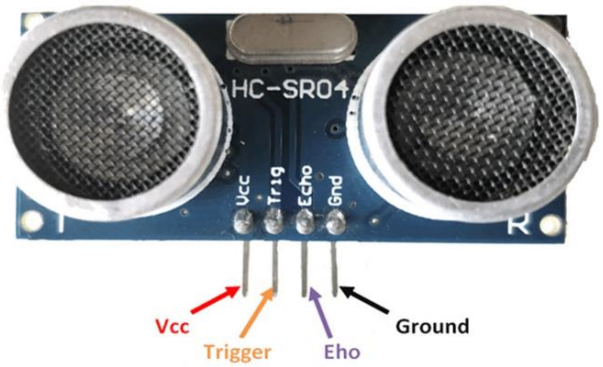

Figure 3. Ultrasonic sensor HC-SR04 module receiver (Al-Smadi et al. 2020)

Buzzer

A buzzer or beeper is one of the most common tools for audio communication. It is a sounding device that converts audio signals into sound signals. It is usually powered by DC voltage. A buzzer may be mechanical, piezoelectric, or electromechanical. Typical uses of buzzers and beepers are timers, alarm devices, and other electronic products (Scalet et al., 2017). Figure 4 shows a typical buzzer device.

Figure 4. Buzzer

Vibration Motor

Vibration motor is a DC motor in compact size vibrates when an obstacle or object is detected by ultrasonic sensor. Vibrators are used mainly in mobile phone technology (Yang et al., 2018). A typical vibration motor is shown in Figure 5.

Figure 5. Vibration Motor

System Implementation

The block diagram of the proposed system is shown in Figure 1. The circuit diagram of the system is shown in Figure 6. The figure shows the connection of ultrasonic sensor HC-SR04 module with the raspberry pi controller. The raspberry pi is connected to the buzzer and the vibrator motor. A slide single pole double throw (SPDT) switch is connected between the buzzer and the vibrator motor to give the user the choice of using either alarming type. The connection is also shown in the schematic diagram in Figure 9.

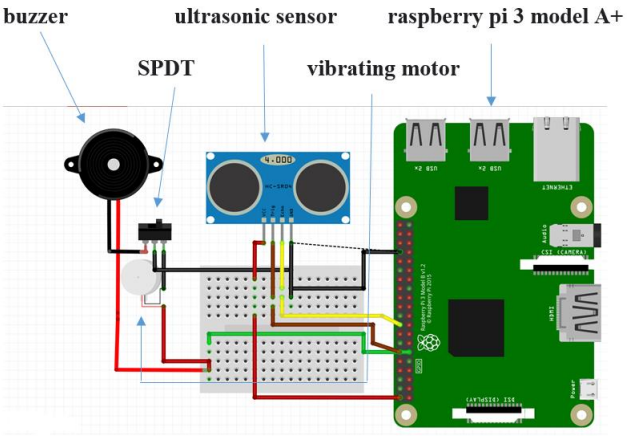

Figure 6. Circuit diagram of the proposed tool

When an obstacle faces a walking blind person, the ultrasonic sensor will detect the obstacle. The raspberry pi microcontroller will calculate the measured distance and check if it is within the threshold set by the code in the raspberry pi board. If the distance is within the threshold, the microcontroller will alert the blind person by activating the buzzer or the vibrator motor. The buzzer will make a sound and the vibrator motor will vibrate. As shown in Figure 6, the user has the choice of using the alarming state; i. e., the sound from the buzzer or the

vibration from the vibrator motor. This is done by sliding a single pole double throw (SPDT) switch to change the type of alarming. To operate the system, a portable power source (power bank) has been used.

```
import time
import RPi.GPIO as GPIO
GPIO.setmode (GPIO.BCM)
GPIO_TRIGGER  = 18
GPIO_ECHO = 24
GPIO.setup(GPIO_TRIGGER, GPIO.OUT)
GPIO.setup(GPIO_ECHO, GPIO.IN)
def distance ( ):
GPIO.output (GPIO_TRIGGER, True)
time . sleep(0.00001)
GPIO.output (GPIO_TRIGGER, False)
StartTime = time . time( )
StopTime = time . time
while  GPIO . input ( GPIO_ECHO )  ==  0;
StratTime  =  time . time( )
while  GPIO . input ( GPIO_ECHO )  ==  1;
StopTime  =  time  . time( )
TimeElapsed  =  StopTime  - StartTime
distance  =  ( TimeElapsed  *  34300 )  /  2
return distance
if  _name_  ==  '_main_' :
try  :
while   True  :
dist   =  distance( )
print  (" Measured Distance  =  %.1fcm"  %  dist)
time . sleep(1)
except keyboardinterrupt :
print  ("measurement  stopped  by  user ")
GPIO . cleanup ( )
```

Figure 7. Python code

Working Voltage	5 Volt Dc
Working Current	A5m A
Working Frequency	40KHz
Max Range	400 centimeters
Minimum Range	2 centimeters
Trigger Input Signal	10 µs

Figure 8. The parameters or the ultrasonic sensor HC-SR04 Module

Figure 7 presents the software program code using python to calculate the distance being measured using the HC-SR04 ultrasonic sensor module. The program operates as user friendly device. The distance between the sensor and the object can be calculated by the total time taken for sending a pulse and receiving an echo from the boundary of the object. That is,

$$\text{Distance} = V \times T/2 \qquad (1)$$

where V is the speed of sound and T is the time it takes from emission to reception. The universal speed of sound is 340 meter/second. The time T in Equation (1) is divided by 2 since it is the time for go-and-return distance. In order to generate ultrasound, the pin Trig of the ultrasonic sensor should be set on a High State for 10 µs which will send out an 8-cycle sonic burst at 40 KHz. This signal will travel at the speed sound and it will

be received in the Echo pin of the ultrasonic sensor. The Echo pin will output the time in microseconds. The time is measured using the inbuilt circuity model. Figure 8 shows the parameters of the ultrasonic sensor HC-SR04 module. A prototype for the proposed tool is shown in Figure 10 and 11. Figure 12 shows a sample of the measured distance between an obstacle and a person with the proposed tool. The tool can be placed on a walking stick or can be mounted on the hand of the user. The user can wear four modules of the tool; namely, on both hands and on his/her knees.

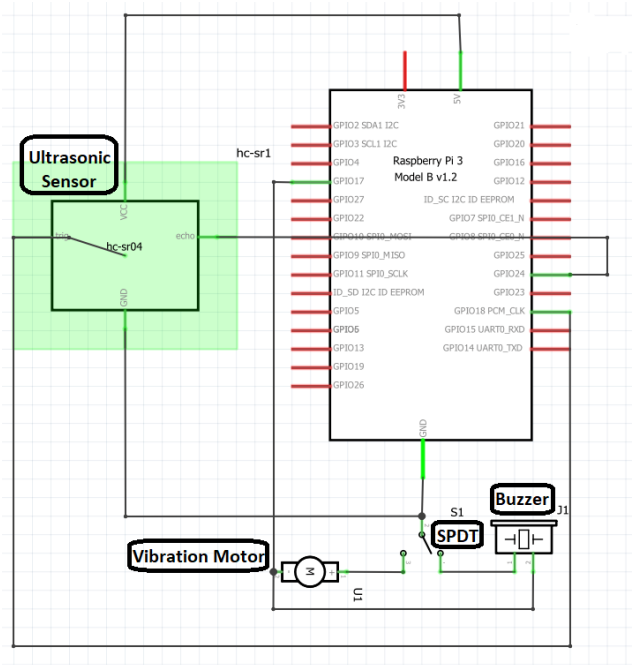

Figure 9. Schematic diagram

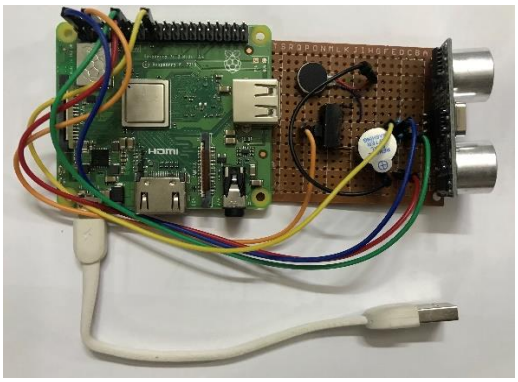

Figure 10. A prototype navigation tool

Figure 11. Final Product for helping blind people

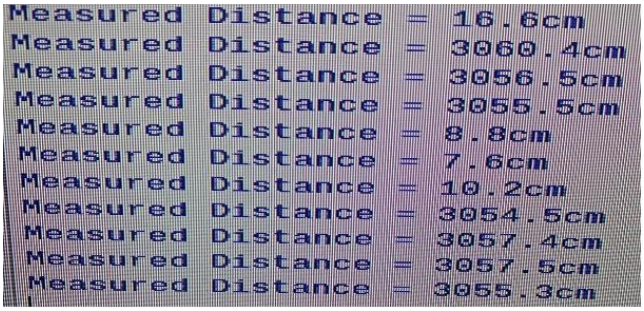

Figure 12. A sample of measured distance using the ultrasonic sensor

Conclusion

A helping aid for blind people using Raspberry pi microcontroller was proposed. The device is simple, low cost, efficient, and easy to carry and use. The device should provide constructive assistance and good support for the visually impaired and blind persons. It should also have the capability to specify the source and distance of any obstacle that may encounter the visually impaired and blind person. The device is able to detect any obstacle in the area that surrounds the blind person regardless of its height. With this device, the visually impaired and blind persons will be able to navigate and move around with reasonable speed and confidence. The user can choose the type of alert: sound beep using buzzer or vibration using vibrator motor. A prototype blind aid system has been implemented and tested. It performed as expected.

Scientific Ethics Declaration

The authors declare that the scientific ethical and legal responsibility of this article published in EPSTEM journal belongs to the authors.

Acknowledgements or Notes

*The authors would like to thank Yarmouk University, Jordan for financial support to implement this research.

*This article was presented as oral presentation at the International Conference on Basic Sciences, Engineering and Technology (www.icbaset.net) held in Marmaris/Turkey on April 27-30, 2023.

References

Al-Smadi, A., & Msallam, M. (2022). Vehicle auto parking system. *9th IEEE International Conference on Electrical and Electronics Engineering (ICEEE 2022)*Alanya, Turkey, March 29-31, 108-111.

Al-Smadi, A., Al-Ksasbeh, W., Ababneh, M., & Al-Nsairat, M. (2020). Intelligent automobile collision avoidance and safety system. *17th IEEE International Multi-Conference on Systems, Signals & Devices*, Sfax, Tunisia, July 20-23, 319-322.

Batool, A., & Naz, S. (2021). Third eye for blind. *Asian Journal of Convergence in Technology*, *7*(2), 1-4.

Bousbia, M., & Fezari, M. (2007). A navigation tool for blind people. *Innovations and Advanced Techniques in Computer and Information Sciences and Engineering*, 333–33.

Kupade, K., Aigali, K., Patil, R., Rajmane, S., & Patil, S. (2020). Third eye for blind person using node MCU microcontroller and GPS. *International Journal of Advanced Research in Electrical, Electronics and Instrumentation Engineering (IJAREEIE)*, *9*(6), 1572-1575.

Maragatharajan, M., Jegadeeshwaran, G., Askash, R., Aniruth, K., & Sarath, A. (2019). Obstacle detector for blind peoples. *International Journal of Engineering and Advanced Technology (IJEAT)*, *9*(1S4), 61-64.

Nawer, A., Hossain, F., & Anwar, M.D. (2015). Ultrasonic navigation system for the visually impaired & blind pedestrians. *American Journal of Engineering Research (AJER)*, *4*(2), 13-18.

Phirke, P., Pande, J., & Singh, A. (2015). Location finding for blind people using voice navigation stick. *International Journal of Engineering and Technical Research (IJETR)*, *3*(1), 212-216.

Scalet, T., Viana, J., Arthur, R., & Arnold, F. (2017). Experimental evaluation of piezoelectric buzzers as devices for energy harvesting. *Brazilian Technology Symposium*.

Sharma, P., Shimi, S., & Chatterji, S. (2015). A review on obstacle detection and vision. *International Journal of Engineering Sciences & Research Technology, 4(*1), 1-11.

Singh, K., Vashisht, M., Saxena, I., Tyagi, H., & Saxena, D. (2017). Navigation system for blind people using GPS & GSM Techniques. *International Journal of Scientific Research and Management Studies (IJSRMS), 3*(11), 364-374.

Thumma, C., Amarnath, S., Philipose, H., & Gayathri. P. (2017). Location based navigation and obstacle detection system with voice alerts for blind. *Global Journal of Engineering Science and Research Management, 4*(6), 19-27.

Vinod, G., Farooque, M.D., Murali, M., Bindu, L., & Pavithra, K.S. (2018). IOT powered multisensor strategies to support blind people with gps navigation system. *International Journal of Computing, Communications and Networking, 7*(2), 150-153.

White, J. (2016). *Raspberry Pi: The Complete Manual*. Future Publishing Ltd.

Yang, Y., Wei, Y., Lou, J., Lei, F., Fang, S., & Te-huan, C. (2018). Dynamic modeling and adaptive vibration suppression of a high-speed macro-micro manipulator. *Journal of Sound and Vibration, 422,* 318-342.

Author Information

Adnan Al-Smadi
Yarmouk University
Irbid-Jordan
Contact e-mail: *smadi98@yahoo.com*

Talal Al-Qatyouti
Yarmouk University
Irbid-Jordan

Abdurahman Rehan
Yarmouk University
Irbid-Jordan

Homam Assi
Yarmouk University
Irbid-Jordan

Alhareth Alsharea
Yarmouk University
Irbid-Jordan

To cite this article:

Al-Smadi, A., Al-Qaryouti, T., Rehan, A., Assi, H., & Alsharea, A. (2023). A navigation tool for visually impaired and blind people. *The Eurasia Proceedings of Science, Technology, Engineering & Mathematics (EPSTEM), 22*, 119-126.

The Eurasia Proceedings of Science, Technology, Engineering & Mathematics (EPSTEM)
ISSN: 2602-3199

The Eurasia Proceedings of Science, Technology, Engineering & Mathematics (EPSTEM), 2023

Volume 22, Pages 127-134

ICBASET 2023: International Conference on Basic Sciences, Engineering and Technology

A Study of U-Shaped Optical Fiber Sensor for Sensing Different Concentrations of Glucose and Ion liquid ($HgCl_2$) and a Fabrication of Microfluidics System

Tien Bao TRAN
National Kaohsiung University of Science and Technology

Hsiang Cheng HSU
National Kaohsiung University of Science and Technology

Chia Chin CHIANG
National Kaohsiung University of Science and Technology

Abstract: In this study, we demonstrate the sensitivity of U-shaped with the different resolutions of Glucose and Mercury Chloride ($HgCl_2$). We also indicate the process of fabricating a Microfluidics system by using CO_2 laser with Poly Methyl Methacrylate (PMMA) as material. According to the experiments, the sensor can be used to evaluate the concentrations of Glucose and $HgCl_2$. While the shift of resonance wavelength raised with the increase of Glucose Concentration from 5% to 50% with R^2=0.95, there is a fluctuation in the shift of resonance wavelength with $HgCl_2$ Concentration from 5 ppm to 50 ppm. Especially with transmission loss, Glucose, and $HgCl_2$ witness the same phenomenon when the transmission loss goes up simultaneously with the increase of concentration, with R^2=0.86 for Glucose and R^2=0.78 for $HgCl_2$. Finally, we manufacture successfully the Microfluidics system with the dimensions including depth: 0.3 mm and width: 0.2 mm. By mixing Glucose 0% and 50%, it leads to the conclusion that the Microfluidics system works appropriately.

Keywords: U-shaped optical fiber sensor, Microfluidics system, CO2 laser.

Introduction

Nowadays, the usages of Optical fiber have expanded not only from optical transmission waveguides in telecommunications (Milner & Chynoweth, 1979) but also to a wide range of applications, including monitoring temperatures (Roriz et al., 2020), mechanical strain (Tregubov et al., 2016), refractive index (RI) (Park et al., 2013), pressure (Ribeiro et al., 2012) and sensing concentrations of liquids and gas (Krohn, MacDougall & Mendez, 2014). Among different types of biosensors, the optical-fiber sensor is one of the best choices because of its simplicity and low-cost operation. However, there are still some disadvantages to this kind of sensor, such as installation and erection issues. In order to improve these issues, there are various types of sensors appeared, including U-shaped sensors (Tan & Stoddart, 2021). By the evanescent wave penetration depth enhancement which results in increasing the sensitivity compared with straight OF.

In recent years, a Lab-on-a-chip is a miniaturized device that integrates into a single chip one or several analyses, usually done in a laboratory. The miniaturization of biochemical operations typically handled in a laboratory has numerous advantages, such as cost efficiency, parallelization, ergonomics, diagnostic speed, and sensitivity. The emergence of the lab-on-a-chip field mainly relies on two core technologies: microfluidics and molecular biology (Bruus, 2008). Microfluidics has made significant advances in the field of biomedical diagnostic research through the development of miniaturized microfluidic and nanofluidic biosensors (Ward & Fan, 2015; Tiwari, Baht & Mahato, 2020).

In this study, we will utilize a U-shaped optical fiber sensor to sense the different resolutions of Glucose and $HgCl_2$ then we will use a CO_2 laser to fabricate by directly cutting microfluidic channels from Poly Methyl Methacrylate (PMMA) sheets then assembling together by using Thermal Pressing Techniques. Finally, we use a Microfluidics system to mix different concentrations of Glucose and then evaluating the mixing liquid's concentration with an Abbe refractometer.

Principle of U-shaped Optical Fiber Sensor and Microfluidics System

Principle of U-shaped Optical Fiber Sensor

In the weak-guidance approximation (Renner, 1992) the transverse field distribution in the bent fiber obeys the two-dimensional scalar equation

$$\nabla_t^2\psi(x,y)+\left[k^2n_{eff}^2(x,y)-\beta^2\right]\psi(x,y)=0 \tag{1}$$

Where, $k=2\pi/\lambda$, λ and β are the wavelength and the complex propagation constant of the leaky mode, respectively.

$$n_{eff}^2(x,y)=n^2(x,y)(1+2x/R) \tag{2}$$

n_{eff}^2 is the squared effective refractive-index distribution in the bent fiber and $n(x,y)$ is the refractive-index distribution in the straight fiber with R as the effective bend radius. Figure 1 demonstrates the cross-section of the optical fiber when being coated by a substance with a refractive index in the cladding and the coating are n_2 and n_3, the radius of the core and the cladding are a and b.

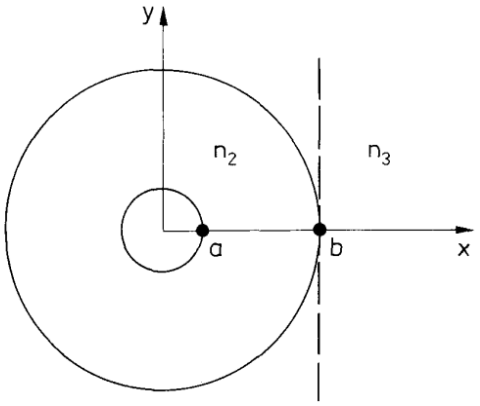

Figure 1. Geometric refractive-index distribution of the coating outside

The loss due to the fiber curvature and the presence of the coating can be obtained from the imaginary part of beta so it is necessary to calculate the change of the propagation constant with respect to its (real) value β_0 in the straight fiber with infinitely extending cladding. The basic idea of the present analysis is to approximate the curved cladding/coating boundary by a plane interface of the same index step with $x=b$. The outwards-radiating field of the leaky fundamental mode in the bent fiber has a purely Gaussian lateral $(y-)$ dependence $\exp\left\{-y^2/\mathrm{w}(x)^2\right\}$ with x-dependent $1/e$ field width of

$$\mathrm{w}(x)=2(x/\gamma)^{1/2}$$

$$\gamma=\left(\beta_0^2-k^2n_2^2\right)^{\frac{1}{2}} \tag{3}$$

The actual cladding/coating interface is described by the circle $x^2 + y^2 = b^2$. If the x-coordinate, at which the trajectory of the beam width intersects the cladding/coating boundary.

$$b^2 = x_T^2 + w(x_T)^2 = x_T^2 + 4x_T / \gamma \tag{4}$$

With the theory of bending transmissions loss from a single-mode fiber with an outer coating, the amount of change between the bending radius of the fiber and the wavelength can be calculated by the formula:

$$\Delta R = \frac{3\pi R}{\gamma b(2 + R_C / R)[(R_C / R) - 1]^{\frac{1}{2}}} \approx \frac{3\lambda}{2n_2}\left(\frac{R^3}{2b^3}\right)^{\frac{1}{2}} \tag{5}$$

$$\Delta\lambda = \frac{3\pi\lambda}{2\gamma b\left(\frac{R_C}{R} - 1\right)^{\frac{1}{2}}\left[1 - \frac{R_C}{R}\left(1 + \frac{3}{\gamma^2\bar{\omega}^2}\right)\right]} \approx \frac{3\lambda^2}{4n_2^2}\left(\frac{R}{2b^3}\right)^{\frac{1}{2}} \tag{6}$$

Microfluidics Fundamental Theories

Density is the most significant metric for describing a liquid and its movement. (ρ), pressure (P), and viscosity (η). The density of a liquid is defined as mass (m) per unit volume (v) in units (kg / m^3) (Castillo Leon & Svendsen, 2015).

$$\rho = \frac{m}{v} \tag{7}$$

In closed microfluidics systems, the pressure of a liquid is not important at all because it is only affected by depth; however, in open microfluidics systems, a pressure difference caused by an external source will affect how the liquid moves through the system. Pressure (P) is the ratio of force applied (F) to the area (A) over which that force is distributed in unit kg/ms^2, often referred to as Pascal (Pa).

$$P = \frac{F}{A} \tag{8}$$

The Reynolds number, which is a dimensionless number that can be used to define the kind of flow that is anticipated in the system, can be obtained by taking the ratio of the inertial forces to the viscous forces.

$$\mathrm{Re} = \frac{\rho dv}{\eta} = \frac{dv}{v} \tag{9}$$

In this equation d is the system's typical length scale, which typically includes the smallest dimension or the diameter of tubes and v is the average velocity of the moving liquid.

Simulation, Experiment, and Fabrication

The fabrication of a U-Shaped Optical Fiber Sensor and the Set-up of the Experiment

Figure 2 shows the process of manufacturing a U-shaped sensor. Initially, using the ceramic mold for shaping the sensor, after that, using the heat treatment with the temperature can be seen in TABLE I. Secondly, we utilize UV glue to fix it on the glass plate, finally, using a 3D-printer jig to keep the sensor when conducting experiments to sense different concentrations of Glucose and $HgCl_2$. For each concentration of Glucose and $HgCl_2$, we restart the experiment by cleaning the liquid container with Deionized water (DI water) then drying it with Nitrogen (N_2 gas); the sensor is cleaned by immersing in DI water after that, softly touching KIMTECH wipers for drying.

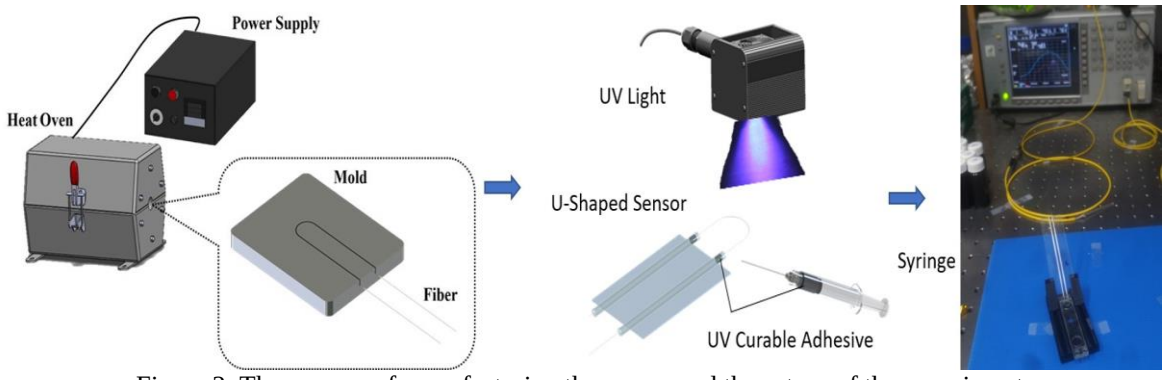

Figure 2. The process of manufacturing the sensor and the set-up of the experiment

Table 1. The temperature of sensor fabrication

Stage	Temperature (degree Celsius)	Time (Minutes)
Stage 1	600	25
Stage 2	900	40
Stage 3	900	35
Stage 4	600	40
Stage 5	600	25
Stage 6	400	30
Stage 7	400	25
Stage 8	200	30

The simulation of the Microfluidics system

As shown in Figure 3(a), the Microfluidics channels are designed with an overall length of 45 mm, depth of 0.3 mm, and a width of the channel is 0.2 mm with the angle of each channel 45°. Moreover, the length of each channel is increased gradually in order to extend the time that liquid flows inside. We begin the simulation by setting the initial liquid concentrations for each inlet as 2 mol/m^3 and 4 mol/m^3. After flowing inside the system as seen in Figure 3(b), we can easily see the final mixing liquid at the outlet achieving a good result with 3-mol/m^3 concentration spreading over.

The Fabrication of the Microfluidics System

Figure 4 indicates the process of manufacturing a Microfluidics system by using PMMA. Firstly, we use the FLUX Beambox Pro 50W to cut three parts of the Microfluidics system with the middle part is 0.3 mm and the upper and bottom parts is 2 mm. After that, we clean all parts with alcohol before using Thermal Pressing machine to assemble these parts together with temperature: 150 $^{\circ}C$ and the pressure : 80 Kg.

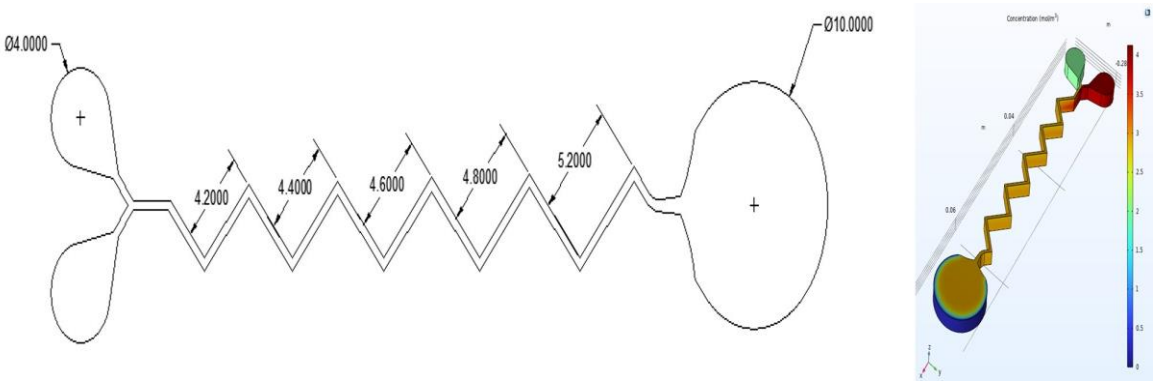

(a) (b)

Figure 3. (a) 2D drawing (b) COMSOL Simulation

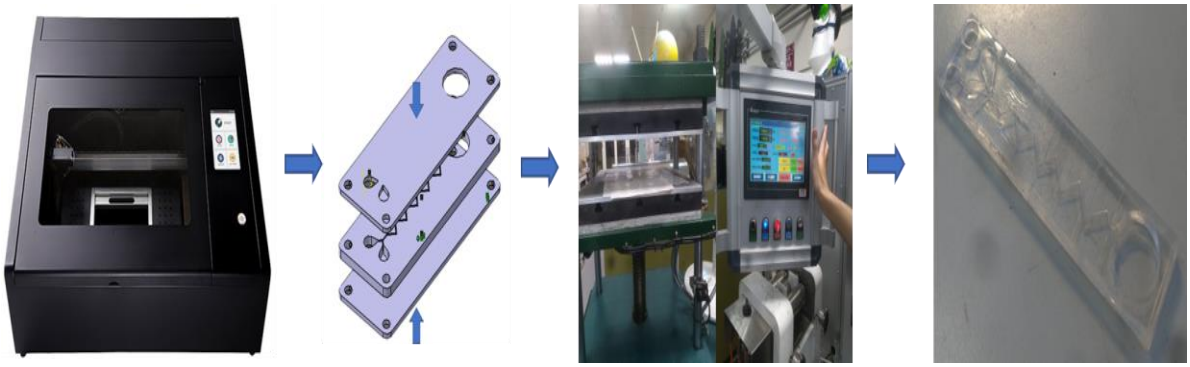

Figure 4. The process of manufacturing microfluidics system

Results and Discussions

Results of Experiments of Sensing Different Concentrations of Glucose and $HgCl_2$

Figure 5 illustrates the overall signal of U-Shaped sensor when sensing the different concentration of Glucose (from 5% to 50%). It is easily seen that at the range of 1620 nm to 1630 nm, there is a significant shift happening not only with the wavelength but also with the transmission. This is a reason why we can consider this signal as the main one when sensing glucose. In order to understand the signal, we will analyze the linear graph of this range in Figure 6.

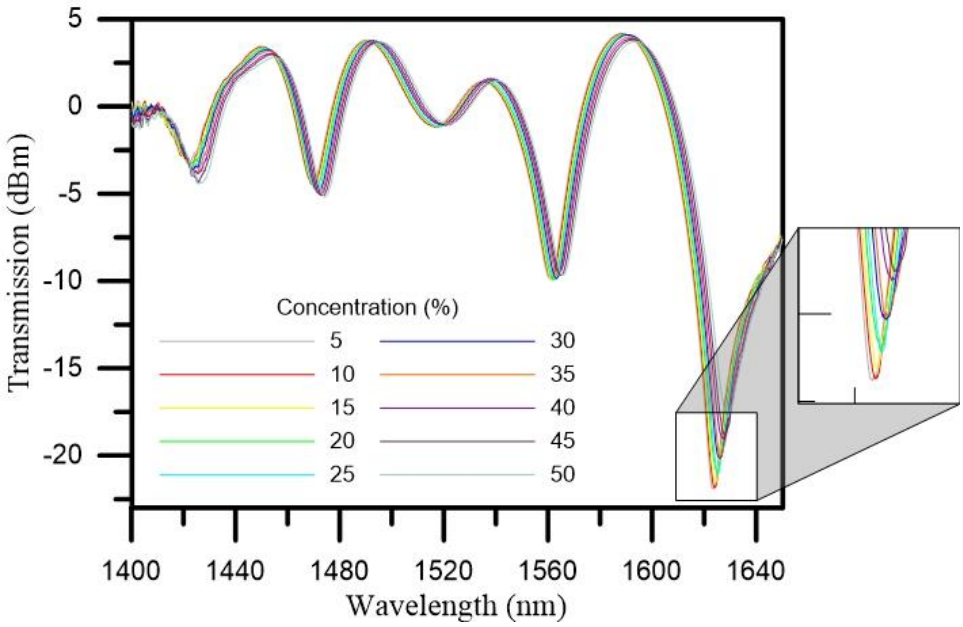

Figure 5. The signal of U-Shaped sensor with Glucose

As seen in Figure 6, in a range of 1620 to 1630, when the concentrations of Glucose rise from 5% to 50%, the resonance wavelength also raises from 1623 nm at 5% to 1629 nm at 50% with R^2= 0.95. The transmission also shares the same trend with wavelength; when the concentrations increase, the dip of the signal increases from -22 dBm at 0% to -17.7 dBm at 50% with R^2=0.86. Compared with the overall signal in Figure 5, we can see that the dip of the signal shift to the right and goes up when the concentration increases.

Figure 7 demonstrates the signal of U-Shaped sensor with $HgCl_2$. As seen in the figure, in a range from 1540 nm to 1550 nm, there is a significant change of the signal when the concentrations of $HgCl_2$ changing from 5 ppm to 50 ppm. Figure 8 depicts the detail of the U-Shaped sensor signal in a range from 1540 nm to 1550 nm. As seen from the figure, while the transmission witnesses an upward trend when the transmission slightly grows from -23.25 dBm at 5 ppm and 10 ppm to -22.9 dBm at 50 ppm, there is a fluctuation of wavelength when changing the concentration of $HgCl_2$. The wavelength declines softly from 1548.7 nm to 1548.5 nm when the concentration at 5 ppm to 20 ppm. After that when increasing the concentrations to 35ppm, the wavelength put

up to 1548.85 nm before fluctuating at 1548.6 nm and 1549.3 nm when the concentrations are 40 ppm and 45 ppm. Finally, the wavelength stays at 1549.05 nm when the concentration is 50 ppm. From the explanation above, there is no room for doubt that the R^2 of wavelength is smaller significantly than that of the transmission, 0.43 compared with 0.78.

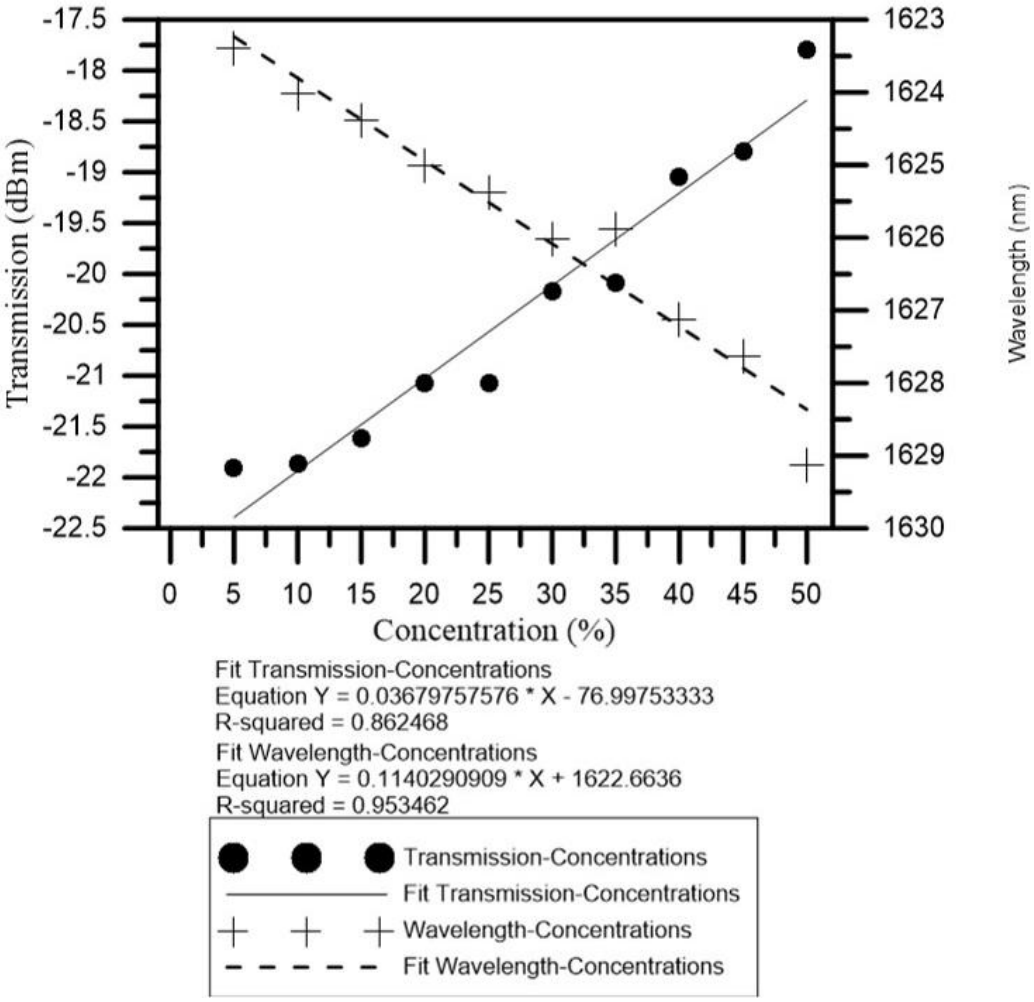

Figure 6. The linear graph of the sensor with Glucose

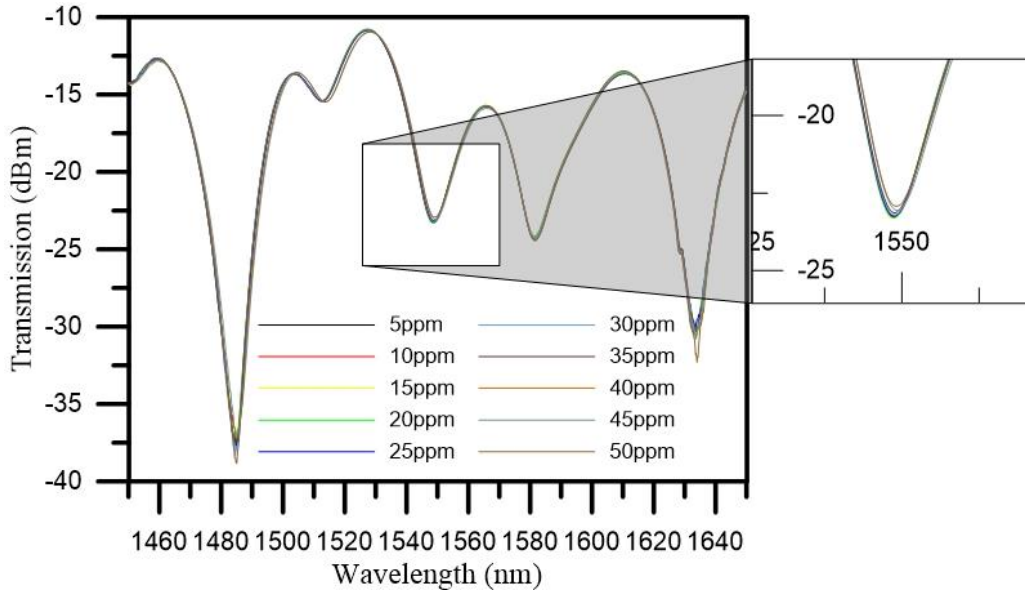

Figure 7. The signal of U-Shaped sensor with $HgCl_2$

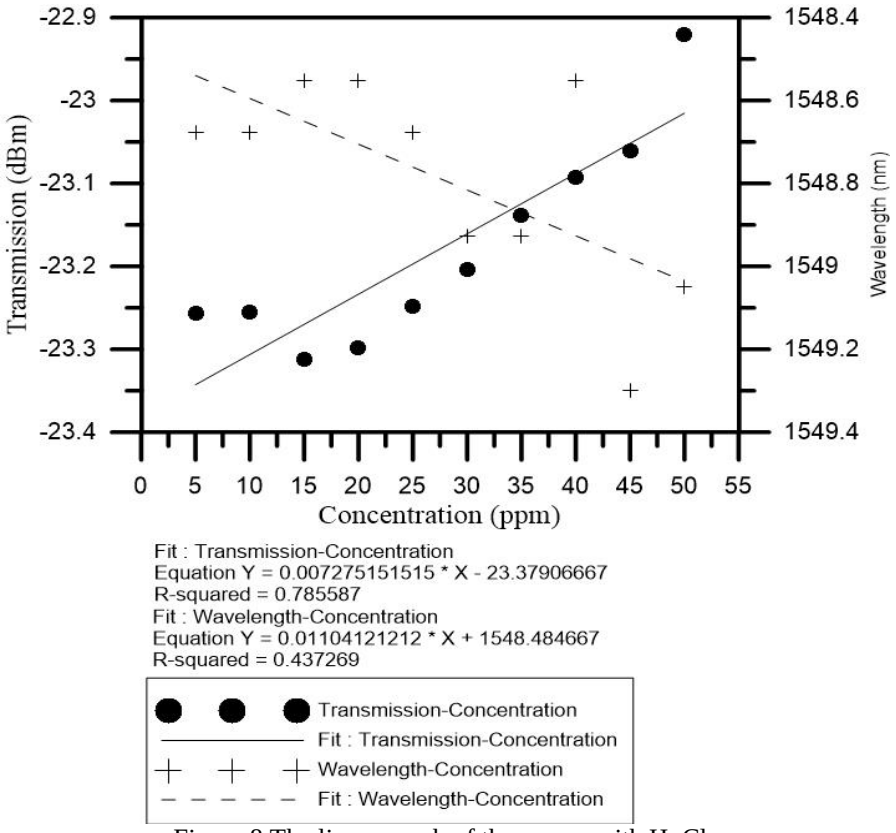

Figure 8.The linear graph of the sensor with $HgCl_2$

Results of Fabrication Microfluidics System

Figure 9(a) illustrates how we carry out an experiment to examine the quality of mixing from the microfluidics channels. In this research, a KDS100 syringe pump was used to control the volume and rate of two 1ml syringes. The 1mm-diameter pipe is used to connect the syringes with the microfluidics channel. After that, we will use two liquids with the same volume including DI water (0%) and Glucose (50%) in order to mix with each other. Figure 9(b) demonstrates the result of the mixing process. After getting the mixing liquid from the center of the outlet, with the rate from 0.01 ml/m to 0.05 ml/m, the findings from the Abbe refractometer show that the final liquid was mixed well with the mixing concentration is 25%.

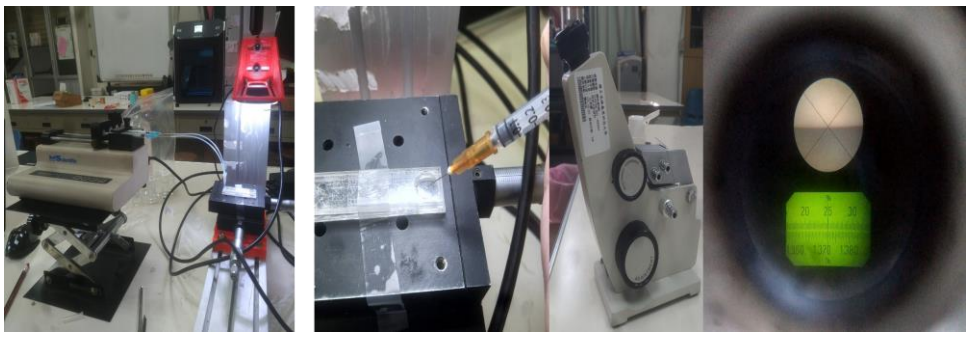

(a) (b)

Figure 9. (a) The set up of experiment (b) Testing result

Conclusions and Recommendations

In this study, we do not only successfully justify the sensitivity of U-shaped Optical Fiber sensor to the different concentrations of Glucose and $HgCl_2$ but also fabricate completely the Microfluidics system. In the future, we will use the Microfluidics system to mix different types of liquid and detect the phenomena by the U-shaped Optical Fiber Sensor.

Scientific Ethics Declaration

The authors declare that the scientific ethical and legal responsibility of this article published in EPSTEM journal belongs to the authors.

Acknowledgements or Notes

* This article was presented as an oral presentation at the International Conference on Basic Sciences, Engineering and Technology (www.icbaset.net) held in Marmaris/Turkey on April 27-30, 2023.

* We are highly thankful for the support of the organizers, editors, and reviewers who give suggestions and comments to inhance our research.

References

Castillo Leon, J., &.Svendsen, W.E. (2015). *Lab-on-a-chip devices and micro-total analysis system*. Cham: Springer.

Krohn, D.A., MacDougall., & Mendez, A. (2014). Fiber optic sensors: *Fundamentals and applications* (4th ed.). USA: SPIE.

Miller, S.E., Chynoweth, A.G., & Kami, I. P. (1979). *Optical fiber telecommunication* (1 st ed). Frederick, USA: Academic Press.

Park, S.J., Ta, C.L., Baek, H.G., Kim, Y.H., Eom, J.B., Lee, Y.T., & Lee, B.H. (2013). Optical fiber sensor for refractive index measurement based on localized surface plasmon resonance. *Conference on Lasers and Electro-Optics Pacific Rim*. Kyoto Japan

Renner, H. (1992). Bending losses of coated single-mode fibers: A simple approach. *Journal of Lightwave Technology*, *10*(5), 544-551.

Ribeiro, L. A., Rosolem, J. B., Dini, D. C., Floridia, C., Bezerra, E. W., Cezar, F. A., ... & Durelli, A. S. (2012, May). Optical fiber sensor for pressure measurement based on elastomeric membrane and macrobending loss. In *Optical Sensing and Detection II* (Vol. 8439, pp. 110-118). SPIE.

Roriz, P. Silva, S., Frazao, O., & Novais, S. (2020). Optical fiber temperature sensor and their biomedical application. *Sensors*,*20*(7),2113.

Tan, A. J.Y., Ng, S.M., Stoddart, P.R., & Chua, H.S. (2021). Trends and application of u-shaped fiber optic sensors: A review. *IEEE Sensors Journal*, *21*(1), 120-131.

Tiwari, S.K., Bhat, S., & Mahato, K.K. (2020). Design and fabrication of low-cost microfluidics channel for biomedical application. *Scientific Reports*.*10*, 9215

Tregubov, A.V.,Svetukhin,V.V., Novikov, S.G., Berintsev, A.V., & Prikhodko, V.V. (2016). A novel fiber optic distributed temperature and strain sensor for building application. *Results in Physics*, *6*, *131*-132.

Ward, K., & Fan, H. Z. (2015). Mixing in microfluidic devices and enhancement methods. *Journal of Micromechanics and Microengineering*, *25*(9).

Author Information

Tien Bao Tran
National Kaohsiung University of Science and Technology
Kaohsiung, Taiwan
Contact e-mail: *f109142188@nkust.edu.tw*

Hsiang Cheng Hsu
National Kaohsiung University of Science and Technology
Kaohsiung, Taiwan

Chia Chin Chiang
National Kaohsiung University of Science and Technology
Kaohsiung, Taiwan

To cite this article:

Tran, N.M., Hsu, H. C., & Chiang, C. C. (2023). A study of U – shaped optical fiber sensor for sensing different concentrations of glucose and ion liquid (HgCl2) and a fabrication of microfluidics systems. *The Eurasia Proceedings of Science, Technology, Engineering & Mathematics (EPSTEM), 22*, 127-134.

The Eurasia Proceedings of Science, Technology, Engineering & Mathematics (EPSTEM)
ISSN: 2602-3199

The Eurasia Proceedings of Science, Technology, Engineering & Mathematics (EPSTEM), 2023

Volume 22, Pages 135-141

ICBASET 2023: International Conference on Basic Sciences, Engineering and Technology

State of Health Estimation for Li-Ion Batteries Using Machine Learning Algorithms

Yunus KOC
Istanbul Technical University

Abstract: As an energy storage system, Li-Ion batteries have many applications from mobile devices to vehicles. No matter what application they are used in, Li-Ion batteries lose performance over time, and this negatively affects the user experience in terms of both comfort and safety. For this reason, it is extremely important to estimate state of health (SOH) of Li-Ion batteries and to use the batteries accordingly. In this study, examinations on the SOH estimation of batteries with different machine learning (ML) methods are included using Constant Current (CC) and Constant Voltage (CV) charge-discharge characteristics of the li-Ion batteries. Moreover, how the estimation performance changes by both short-term and long-term features is observed by using mutual information metric. According to results, the highest accuracy on SOH estimation is achieved when long-term features are used with Bayesian Ridge Regression. When the short-term features are used, the accuracy of Bayesian Ridge Regression is dramatically reduced, and Random Forest Regression provides highest performance.

Keywords: Regression, State of health estimation, Machine learning, Feature extraction, Li-ion batteries

Introduction

Lithium-ion batteries are being developed day by day and are important energy storage systems used in many application areas. It is also extremely critical to know how much the performance of batteries changes during use, in other words, how much their capacity is reduced. Battery management systems can optimize battery usage especially through this information and ensure the use of the battery in the longest possible term (Chen et al., 2023). Moreover, SOH is significant parameter showing capacity degradation which is also used for evaluating battery state of safety (Li et al., 2022).

There are lots of data driven methods used for extracting state of health (SOH) of the batteries in literature. Especially machine learning-based approaches have become very popular recently. For instance, in a study using tree-based algorithms deals with predicting lifetime of the li-ion batteries using early cycle data and the study also includes analyze of feature importance using Kendall's tau and Spearman correlation methods (Çelik et al., 2022). Another one of the SOH estimation studies is the online estimation with DSMTNet, one of the deep learning methods (Wang et al., 2022). They have achieved SOH computing in just 0.14 sec. which is satisfactory result for real time applications. Linear regression analysis with multiple charge and discharge features (Agudelo et al., 2023), Support Vector Regression combining with Voltage-Capacity (VC) model (Zhang et al. 2022), incorporating the DNN into a Kalman filter (Tian et al., 2021), partial analysis of charging curve (Lyu et al., 2021) and wavelet neural networks with genetic algorithm (Chang et al., 2021) were also proposed for SOH estimation of Li-Ion batteries.

In this study, SOH estimation of the batteries is made by using well-known machine learning methods such as Random Forest Regression, Decision Tree Regression, Ridge Regression, Bayesian Ridge Regression, Support Vector Regression and Extreme Gradient Boost Regression. For each model, battery features are extracted in

case of long-term and short-term characteristics from CC-CV charging/discharging curves. All details of each step is described in following sections.

Battery Life Cycle Dataset

To perform SOH estimation, or in other words, capacity degradation analysis, a battery data set in which charge/discharge cycles are made under certain conditions is needed. In this study, the HNEI dataset (Hawaii Natural Energy Institute, 2014), in which more than 1000 cycles were made and prepared on 18650 Li-Ion batteries, was used. Details of the dataset are presented in below table (Table 1).

Table 1. HNEI Li-Ion Battery Life Cycle Dataset

Cell & Cycle Parameters	Description
Anode	Graphite
Cathode	NMC-LCO
Capacity	2800 mAh
Form Factor	18650
Temperature	25°C
Max SOC	100
Min SOC	0
Charge Rate	0.5 C (1.4 A)
Discharge Rate	1.5 C (4.2 A)
Max Voltage	4.35 V
Min Voltage	3.0 V
Nominal Voltage	3.8 V

The measured characteristics of the battery during the life cycle are as follow; *Current (A), Min-Max Current (A), Voltage (V), Min-Max Voltage (V), Charge Capacity (Ah), Discharge Capacity (Ah), Charge Energy (Wh), Discharge Energy (Wh).*

Feature Extraction

In this section, the features are observed as *long-term feature* which needs to get complete charge/discharge cycle and *short-term feature* which needs to get a small portion of charge/discharge curve. All features are extracted in CC region of Charge/Discharge Curve. Each of features are described in following sections.

Long-Term Features

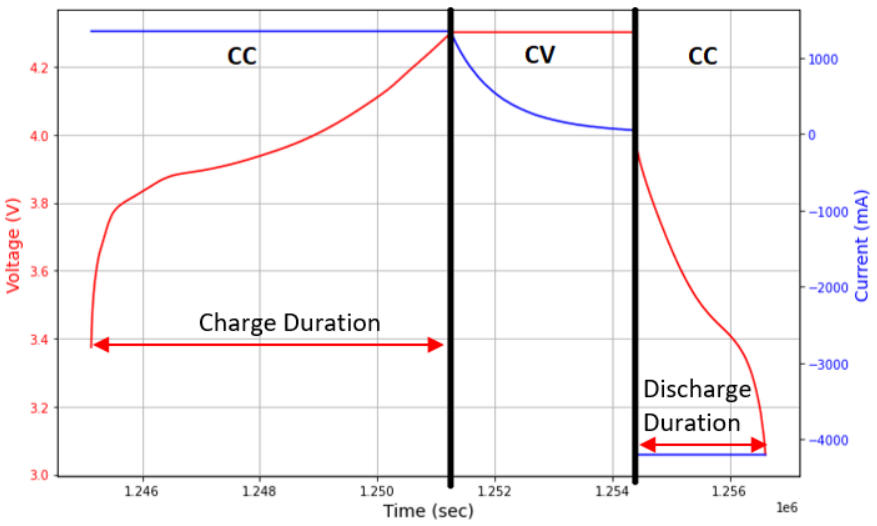

Figure 1. CC and CV regions of complete charge/discharge cycle

1) Charge/Discharge Duration

Charge and discharge duration are extracted from the duration of charge and discharge states during the CC region for each cycle.

2) Charge/Discharge Current Count

Current accumulation of CC charge and discharge states is another key feature regarding to overall capacity. Because these features are extracted in CC domain, it is easy to handle current count operation using below formula for each charge and discharge states.

$$Charge\ Count = Charge\ Duration \text{ x Charge Current (CC)} \tag{1}$$

$$Disharge\ Count = Discharge\ Duration \text{ x Discharge Current (CC)} \tag{2}$$

3) Charge/Discharge Voltage Integration

Because the voltage-time curve of the battery changes by long cycles, the area under the curve is also significant clue about state of the health analysis. On this issue the area can be calculated as follow:

$$Charge\ Voltage\ Integration = \int_{T_1}^{T_2} V_T^{Charge} dt \tag{3}$$

$$Discharge\ Voltage\ Integration = \int_{T_1}^{T_2} V_T^{Discharge} dt \tag{4}$$

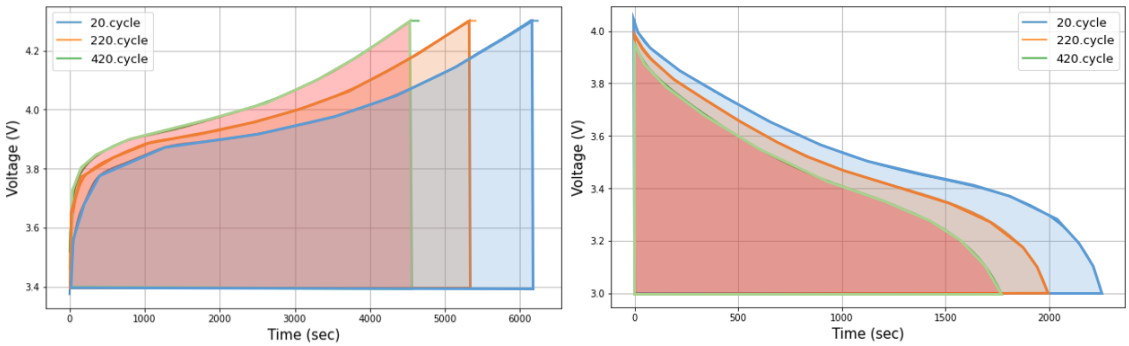

Figure 2. Area under the voltage-time charge/discharge curve for different cycles

In equation (3) and (4), T_1 and T_2 correspond to start and end time of the charge and discharge states, V_T shows terminal voltage of the battery, respectively.

4) Kurtosis and Skewness

Before the calculation of kurtosis and skewness feature, it is needed to calculate difference of charge and discharge voltage curve. On this issue, it is handled by subtracting discharge voltage values from reversed form of charge curve as below figure. By this way, skewness and kurtosis features can be calculated using third and fourth order central moment of the voltage difference respectively as below (Cheng et al., 2021).

$$Skewness = \frac{1}{n}\sum_{i=1}^{n}\left[\left(\frac{X_i - \mu}{\sigma}\right)^3\right] \tag{5}$$

$$Kurtosis = \frac{1}{n}\sum_{i=1}^{n}\left[\left(\frac{X_i - \mu}{\sigma}\right)^4\right] \tag{6}$$

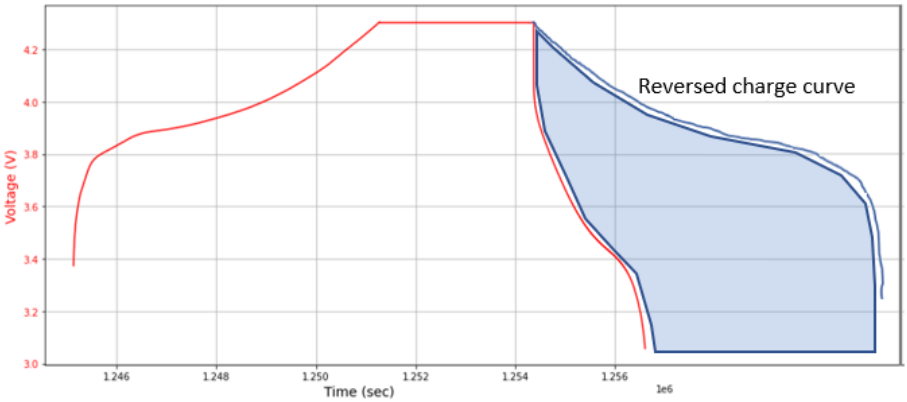

Figure 3. Voltage differences between charge and discharge states

In equation (5) and (6); n is the number of samples, X_i is the value of the i th sample of voltage difference, μ and σ are the mean and variance of the voltage difference sequence, respectively.

Short-Term Features

While analyzing the short-term features, the nominal voltage value of the battery is considered as a base voltage. To partial analyze of charge/discharge curve, threshold voltage which maximize the time skew of voltage curve between first and last cycle is calculated by below formula:

$$V_{threshold}^{Charge} = \arg\max_{V} \left(\left| T_{first\ cycle}^{V_{charge}} - T_{last\ cycle}^{V_{charge}} \right| \right) \quad (7)$$

$$V_{threshold}^{Disharge} = \arg\max_{V} \left(\left| T_{first\ cycle}^{V_{discharge}} - T_{last\ cycle}^{V_{discharge}} \right| \right) \quad (8)$$

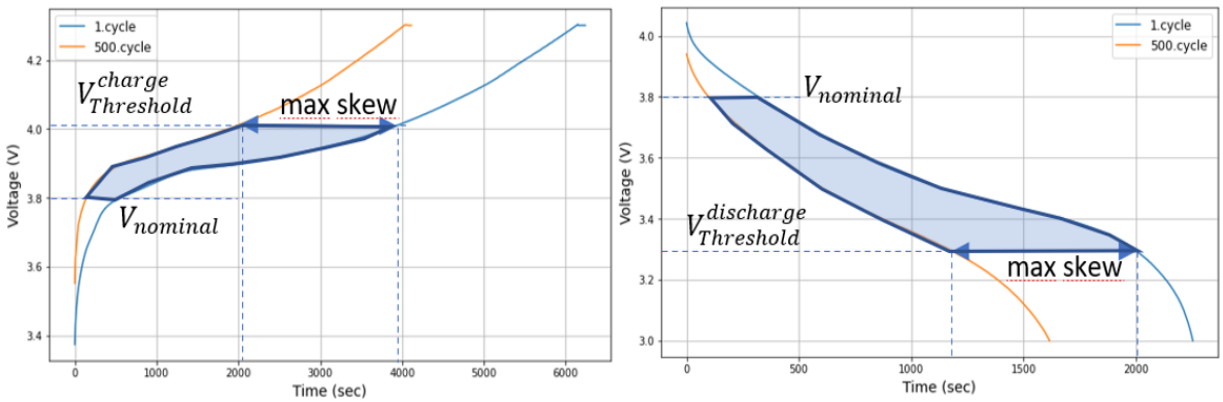

Figure 4. Partial analysis of charge/discharge curves based on nominal and threshold voltages

1) Charge/Discharge Nominal Duration

As described in Figure 4, charge and discharge duration features are calculated regarding to the area limited by nominal and threshold voltages. Thus, nominal charge and discharge durations are equal to duration from $V_{threshold}^{Charge}$ to $V\_nominal$ and and $V_{threshold}^{discharge}$ to $V\_nominal$ points respectively. By this way, there is no need to wait complete cycle.

2) Charge/Discharge Nominal Voltage Integration

Charge and discharge nominal voltage integration features are calculated by same way in equation (3) and (4) based on the area limited by threshold voltage and nominal voltage as illustrated in Figure 4.

3) Ohmic Response

Ohmic response can be defined as resistive effect of internal chemical to drawn current. It is also known from the (Koç et al., 2022) that as batteries age, their internal resistance increases accordingly. İncreased resistance also causes higher voltage to drop under the load. Hence, the increase in voltage drop across the cycle is caused by increased internal resistance or ohmic response, which is directly related to the health of the battery. That is why, the ohmic response is considered as a key feature and calculated by ohm law as below.

$$Ohmic\ Response = \frac{V_{drop}}{I_{discharge}} = \frac{V_{charge}^{end} - V_{discharge}^{beginning}}{I_{discharge}} \quad (9)$$

In equation (9), V_{drop} refers to the voltage drop experienced at the first moment of discharge. In this study, V_{charge}^{end} corresponds to 4.35 V, $I_{discharge}$ is 1.5C which equals to 4.2 A and $V_{discharge}^{beginning}$ decreases due to ohmic response.

State of Health Estimation

Feature Importance

As already described in previous sections, the features were classified as short and long term. While the short-term features seem more useful for time critical application, they need to ensure satisfactory results in machine learning method as they can. Long-term features are also expected to yield good results in terms of model accuracy. To understand the importance of all features, mutual information (Koç et al., 2021) scores are calculated as illustrated in below table.

Table 2. Mutual information scores of features (left side: long-term, right side: short-term)

Feature Name	Score	Feature Name	Score
discharge duration	4.0954	discharge nominal duration	3.1166
discharge current count	4.0934	charge nominal duration	3.0606
charge duration	3.6494	ohmic response	2.5726
charge current count	3.6467	charge nominal voltage integration	2.4771
charge voltage integration	2.4124	discharge nominal voltage integration	2.4126
discharge voltage integration	2.3427		
kurtosis	1.9288		
skewness	1.8855		

As shown in Table 2, long-term features have the highest scores with the disadvantage of taking a long time. On the other hand, short-term features provide superiority better scores compared to some of long-term features.

SOH Analyze Using Machine Learning Methods

Because the dataset has continuous numerical data, regression methods are preferred to handle SOH estimation. On this issue, Random Forest Regressor, Decision Tree Regressor, Ridge Regressor, Bayesian Ridge Regressor, Support Vector Regressor and Extreme Gradient Boost Regressor methods are used with default parameters defined in sklearn library. Before performing these methods, feature values were normalized using min-max normalization to map different ranges of the features into [0-1]. Each machine learning methods were trained and tested with both short-term and long-term features separately. Train and test sizes was defined as %75 and %25, respectively.

Results and Discussion

After training and testing steps, each method performances were obtained as below. All train and test results were calculated by using cross validation technique with 5 splits and 5 repeats to ensure more precise results.

Table 3. Performance Results (Left Side: Long-Term Features, Right Side: Short-Term Features)

Model	Train Accuracy (%)	Test Accuracy (%)	Model	Train Accuracy (%)	Test Accuracy (%)
Random Forest Regressor	98.3	92.6	**Random Forest Regressor**	98.9	**95.3**
Decision Tree Regressor	100	92.3	Decision Tree Regressor	100	93.0
Ridge Regressor	97.1	96.2	Ridge Regressor	80.6	80.1
Bayesian Ridge Regressor	99.3	**98.2**	Bayesian Ridge Regressor	86.6	81.1
Support Vector Regressor	94.9	89.3	Support Vector Regressor	82.9	79.0
Extreme Gradient Boost Regressor	100	95.3	Extreme Gradient Boost Regressor	100	93.1

As shown from the Table 3, tree-based methods like Random Forest Regression and Decision Tree Regression provides higher test accuracy even they used short-term features which yield small amount of data sample. When the long-term features are used in the model, the multicollinearity between features and targets can be higher compared to correlation with short-term features. Because Ridge Regression models are more sensitive to multicollinearity between independent variables, the performance dramatically reduced when the short-term features which provide less observation are used. On the other hand, Random Forest Regression can handle multiple ensemble methods and randomly samples the data during the train and test steps. By this way, Random Forest Regression can adapt itself during the training with short-term features and yields better results compared to long-term feature cases.

Conclusion

In this study, different machine learning methods are used to estimate SOH parameter of the battery with long-term and short-term features. According to the results, Bayesian Ridge Regression ensures highest estimation performance as %98.2 on long-term features and it can be preferred in accuracy critical applications. On the other hand, if time critical applications need to be handled, short-term features can also be used with Random Forest Regression method. For the future work, more efficient short-term features can be defined even they also ensures higher accuracy.

Acknowledgement

* This article was presented as oral presentation at the International Conference on Basic Sciences, Engineering and Technology (www.icbaset.net) held in Marmaris/Turkey on April 27-30, 2023.

*I would like to thank Token Financial Technologies Inc. for providing a variety of business tools and academic opportunities that encourage me to follow new researches.

References

Agudelo, B. O., Zamboni, W., Postiglione, F., & Monmasson, E. (2023). Battery state-of-health estimation based on multiple charge and discharge features. *Energy, 263*, 125637.

Celik B., Sandt R., dos Santos L.C.P., & Spatschek R. (2022) Prediction of battery cycle life using early-cycle data, machine learning and data management. *Batteries 2022. 8(12)*, 266.

Chang, C., Wang, Q., Jiang, J., & Wu, T. (2021). Lithium-ion battery state of health estimation using the incremental capacity and wavelet neural networks with genetic algorithm. *Journal of Energy Storage, 38*, 102570.

Chen, M., Ma, G., Liu, W., Zeng, N., & Luo, X. (2023). An overview of data-driven battery health estimation technology for battery management system. *Neurocomputing, 532*(1), 152-169.

Cheng, D., Sha, W., Wang, L., Tang, S., Aijun, M., Chen, Y., Wang, H., Lou, P., Lu, S., & Cao, Y. (2021). Solid-state lithium battery cycle life prediction using machine learning. *Applied Science, 11*, 4671.

Hawaii Natural Energy Institute (2014). *HNEI [Dataset]*. https://database.batteryarchive.org/public/dashboards

Koç, Y., & Çetin, M. (2021) Comparative evaluation of machine learning algorithms with parameter optimization and feature elimination for fraud detection. *International Conference on Electrical, Computer and Energy Technologies (ICECET)*, 1-6.

Koç, Y., Doğru U. E., & Bilir, R. A. (2022). Evaluation of internal resistance methods for tracking battery state of health. *2022 4th Global Power, Energy and Communication Conference (GPECOM)*, 112-116.

Li, Y., Wang, W., Yang, X. G., Zuo, F., Liu, S., & Lin, C. (2022). A smart Li-ion battery with self-sensing capabilities for enhanced life and safety. *Journal of Power Sources, 546*, 231705.

Lyu, Z., Gao, R., Li, X. (2021). A partial charging curve-based data-fusion-model method for capacity estimation of Li-Ion battery. *Journal of Power Sources, 483*, 229131.

Tian, J., Xiong, R., Shen, W., & Lu, J. (2021). State-of-charge estimation of LiFePO4 batteries in electric vehicles: A deep-learning enabled approach. *Applied Energy, 291*, 116812.

Wang, H., Li, J., Liu, X., Rao, J., Fan, Y., & Tan, X. (2022). Online state of health estimation for lithium-ion batteries based on a dual self-attention multivariate time series prediction network. *Energy Reports, 8*, 8953-8964

Zhang, Y., Liu, Y., Wang, J., Zhang, T. (2022). State-of-health estimation for lithium-ion batteries by combining model-based incremental capacity analysis with support vector regression. *Energy, 239*, 121986.

Author Information

Yunus Koç
Istanbul Technical University
Istanbul, Turkey
kocyun@itu.edu.tr

To cite this article:

Koc, Y. (2023). State of health estimation for Li-ion batteries using machine learning algorithms. *The Eurasia Proceedings of Science, Technology, Engineering & Mathematics (EPSTEM), 22*, 135-141.

The Eurasia Proceedings of Science, Technology, Engineering & Mathematics (EPSTEM)
ISSN: 2602-3199

The Eurasia Proceedings of Science, Technology, Engineering & Mathematics (EPSTEM), 2023

Volume 22, Pages 142-151

ICBASET 2023: International Conference on Basic Sciences, Engineering and Technology

Spotting the Differences between Two Images

Raghunadh M V
National Institute of Technology

Srikanth KOTAKONDA
National Institute of Technology

Abstract: This paper presents a generalized solution to the classical problem of spotting the differences between two images. In this digital era, the authenticity of an image has become a big challenge to the researchers and engineers in the field of computer vision and image processing. Due to the rapid developments in digital technology, creation of photographic fakes and image manipulation has become easily accessible to everyone. With the availability of open-source editing software tools, the possibility of various image manipulations like image forgery, image tampering and image splicing have become almost inevitable. This paper addresses the problem by using classical image processing techniques along with the state-of-the-art YOLOv8 deep learning object detection algorithm. The results obtained are very promising when the model is trained on a synthetic dataset of 700 pairs of images. The uniqueness of the dataset is that each pair of images is different from any other pair of images and the number of differences between any two images may vary from 1 to 50.

Keywords: ORB, SIFT, SSIM, CNN, YOLO

Introduction

Due to the exponential growth in digital technology, the viewer almost lost the trust on the visual content and the situation can become even worse with the increase of more advanced processing tools. Many industries are automating their processes and hence it is very important to have a more robust and reliable tool which can spot the differences between the reference image and the test image.

The problem is approached in a quest to find a reliable solution by exploring the areas of document image analysis, quality inspection and robotics, remote sensing applications, medical imaging, biometrics etc. The work is mainly divided into two parts. The first part focuses on applying traditional image processing techniques like image alignment, ORB (Orient Fast Rotate Brief), SIFT (Scale Invariant Feature Transform) with SSIM (Structural Similarity) and the second part comprises of applying the state-of-the-art deep learning YOLOv8 (You only look once) object detection algorithm developed by ultralytics.

Method-I (Image processing with ORB/SIFT and SSIM):

In this method, FAST (Feature accelerated segment test) is performed on the given two images to extract the key/corner points and then feature point screening is done to get more useful corner points. Later, an intensity centroid method is used to find the dominant directions of key points and then feature descriptors are generated using BRIEF (Binary Robust Independent Elementary Feature) vector. Finally, BRIEF is improved by using steered BRIEF with patch orientation before applying homography for aligning the images.

Once the images are aligned, a method called SSIM (Structure Similarity) is applied by passing the difference between the two images as a threshold to get the desired result.

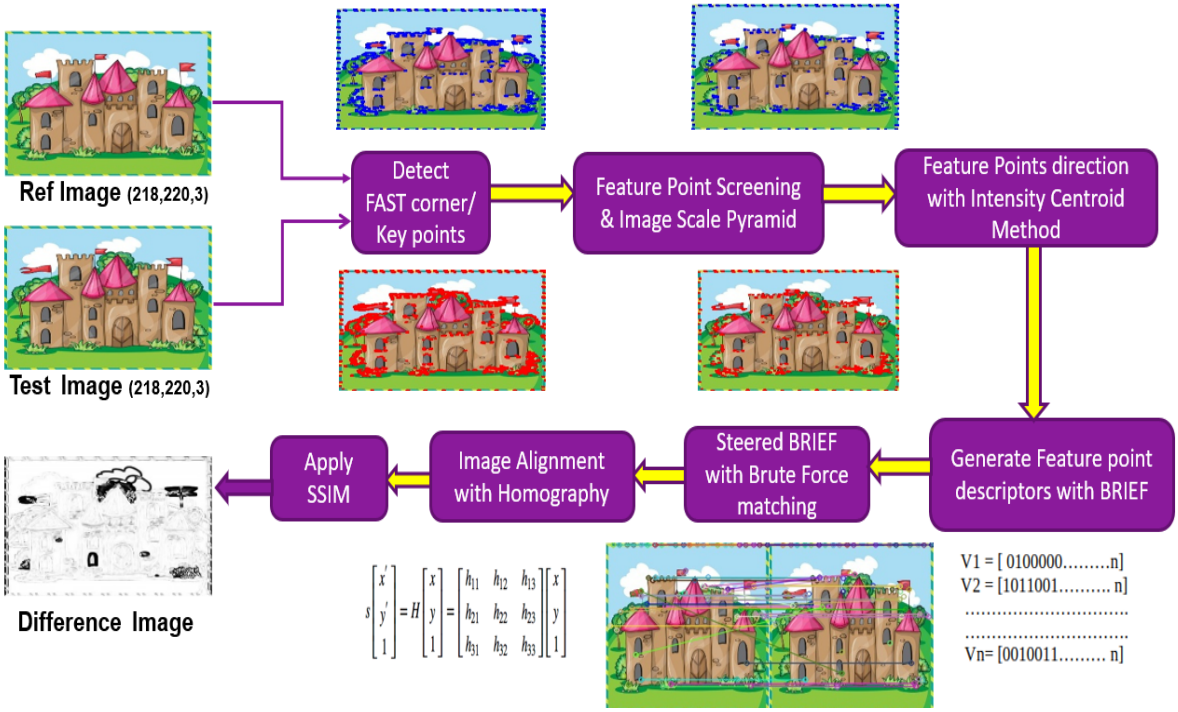

Figure 1. Block diagram describing the workflow of method-I

Mathematical Analysis

Using FAST (Features from Accelerated Segment test) and Breshnam Circle concept, it chooses 16 pixels at random and categorizes into 3 classes (Brighter, Darker & Similar). If more than 8 pixels are brighter than I_p (x, y), then it will be considered as a key point or feature point.

$$R = det(M) - k(trace(M))^2 \quad (1)$$

$$M = \sum w(x,y)\begin{bmatrix} I_x^2 & I_xI_y \\ I_xI_y & I_y^2 \end{bmatrix} \quad (2)$$

Figure 2. Feature point screening using harris response values

After locating key points or feature points, for detecting intensity change, a method called intensity centroid. First, a small image block B is considered, the moment of the image block is defined as

$$m_{pq} = \sum_{x,y\in B} x^p y^q I(x,y), \quad p,q = \{0,1\} \quad (3)$$

where x and y are pixel coordinates, and $I(x,y)$ is the gray value of the corresponding pixel. Then, find the centroid of the image block by the moment:

$$C = \left(\frac{m_{10}}{m_{00}}, \frac{m_{01}}{m_{00}}\right) \quad (4)$$

Figure 3. Moment of image block and centroid

$$\theta = \arctan(m_{01}/m_{10}) \quad (5)$$

BRIEF takes all points found by FAST algorithm and converts it into a binary feature vector so that together they can represent an object. Binary feature vector is also known as Binary feature descriptor that only contains 1's and 0's. In BRIEF, each key point is described by a feature vector which can be either 128 bits or 512 bits string.

For example:

V1 = [0100000……n]

V2 = [1011001……. n]

…….

…….

V_N = [0010011…… n]

BRIEF starts by smoothing image using a gaussian kernel to prevent the descriptor from being sensitive to high frequency noise. It selects a random pair of pixels in a defined neighborhood around that key point. This defined neighborhood around the pixel is also known patch which is a square of some pixel width and height.

The first pixel in the random pair is drawn from a gaussian distribution centered around the key point with a standard deviation or spread of sigma. The second pixel in the random pair is drawn from a gaussian distribution centered around the pixel with a standard deviation or spread of sigma by two. Now if the first pixel is brighter than the second, it assigns the value of 0 to the corresponding bit else 1 is assigned. This process is repeated for 128 times for each key point, in this way BRIEF creates a vector for each key point in an image. This is called Binary test.

$$\tau(p;x,y) = \begin{cases} 1, p(x) < p(y) \\ 0, p(x) \geq p(y) \end{cases}$$

Figure 4. Performing binary test

Where p(x) is the grey value at the field x around the image feature point and p(y) is the grey value at the field y around the image feature point.

Finally, an N-dimensional vector $f_n(p)$ is obtained as

$$f_n(p) = \sum 2^{(i-1)} \tau(p;x,y) \qquad \text{where } 1<i<n \qquad (7)$$

But still BRIEF isn't invariant to rotation, so we use rBrief (rotation aware brief or steered brief) using Rotation matrix as shown below

$$R_\theta = \begin{pmatrix} \cos\theta & \sin\theta \\ -\sin\theta & \cos\theta \end{pmatrix} \qquad (8)$$

Matrix R_θ and N pairs of pixel points form a matrix Q:

$$Q = \begin{bmatrix} x_1, x_2, \cdots, x_N \\ y_1, y_2, \cdots, y_N \end{bmatrix} \qquad (9)$$

Then a rotation correction is performed to get Q_θ:

$$Q_\theta = R_\theta Q \quad (10)$$

Finally, we can get a directional descriptor:

$$g_{N(p,\theta)} = f_N(p) | (x_i, y_i) \in Q_\theta \qquad (11)$$

Figure 5. Rotational correction and directional descriptor

Then we use Brute force matching using RANSAC method and apply Homography for image alignment as shown below:

$$s\begin{bmatrix} x' \\ y' \\ 1 \end{bmatrix} = H\begin{bmatrix} x \\ y \\ 1 \end{bmatrix} = \begin{bmatrix} h_{11} & h_{12} & h_{13} \\ h_{21} & h_{22} & h_{23} \\ h_{31} & h_{32} & h_{33} \end{bmatrix}\begin{bmatrix} x \\ y \\ 1 \end{bmatrix}$$

Figure 6. Applying homography for image alignment

Finally passing the obtained H on to cv2.warpperspective(source, destination, H, size) we get a completely aligned image for further processing as shown below:

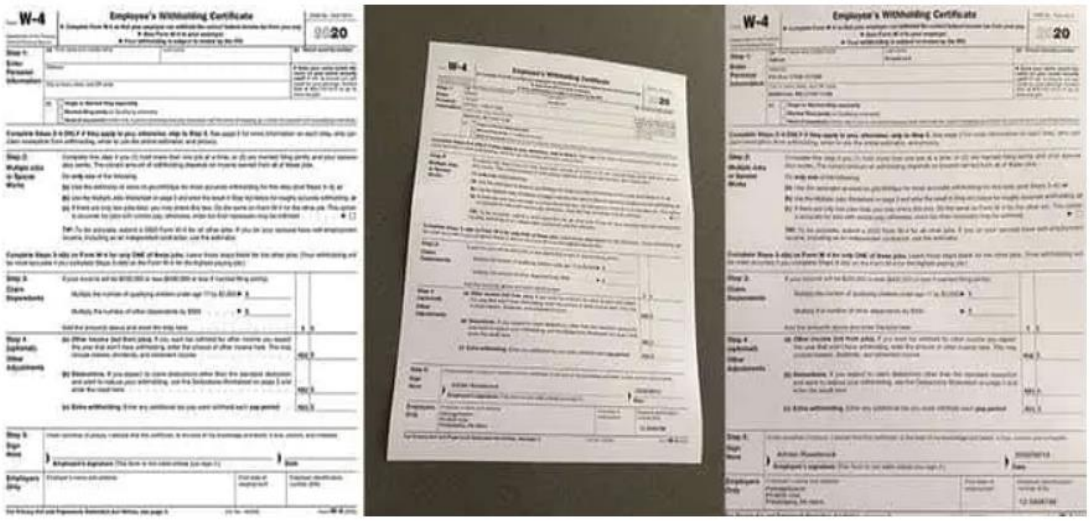

Figure 7. An example of image alignment

Then, applying a method called compare SSIM and using difference as threshold we will get the result image as a difference image between the given pair of images as shown below:

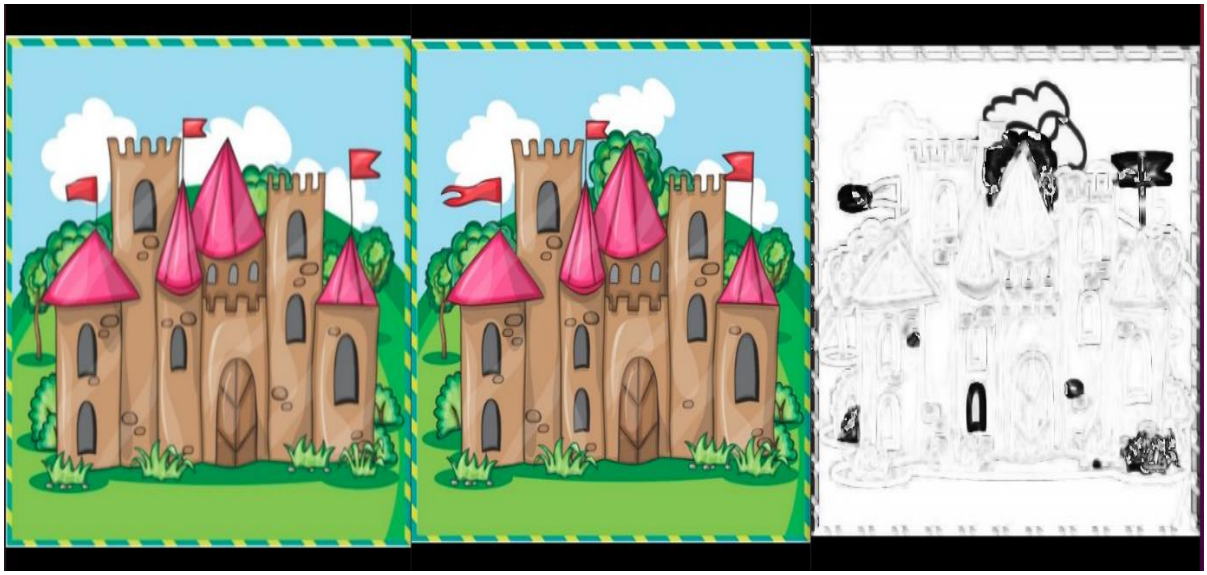

Figure 8. An example of spotting differences between two images

Method-II (Applying CNN and Deep Learning):

From Figure 9, It is clear that up to Image alignment all the steps are common as in method-I, the only change is that once the images are aligned, a new method called Concatenation is applied on the third dimension and then a reshape is done by expanding in horizontal direction, It can be clearly seen that because of this operation we can clearly see that the areas where the images differ have some vertical lines giving us a hint that the images differ in this part of the image.

Taking this as a fundamental building block, we take our work to the next level by applying some edge filter on the concatenated and reshaped image to get the edges and then apply a binary inversion with a high threshold resulting us the difference areas between the two images. As we can see clearly in figure 10, that the operation of concatenation and reshaping is giving us a good insight to spot the differences between the images. So, before applying the deep learning model, we tried to apply a basic two layered customized CNN (Convolutional Neural Network) with 'X' (Concatenated + reshaped image) as the input and 'Y' (Edge filtered + Binary inversion) as the target for the model to see the viability of deep learning approach to this problem.

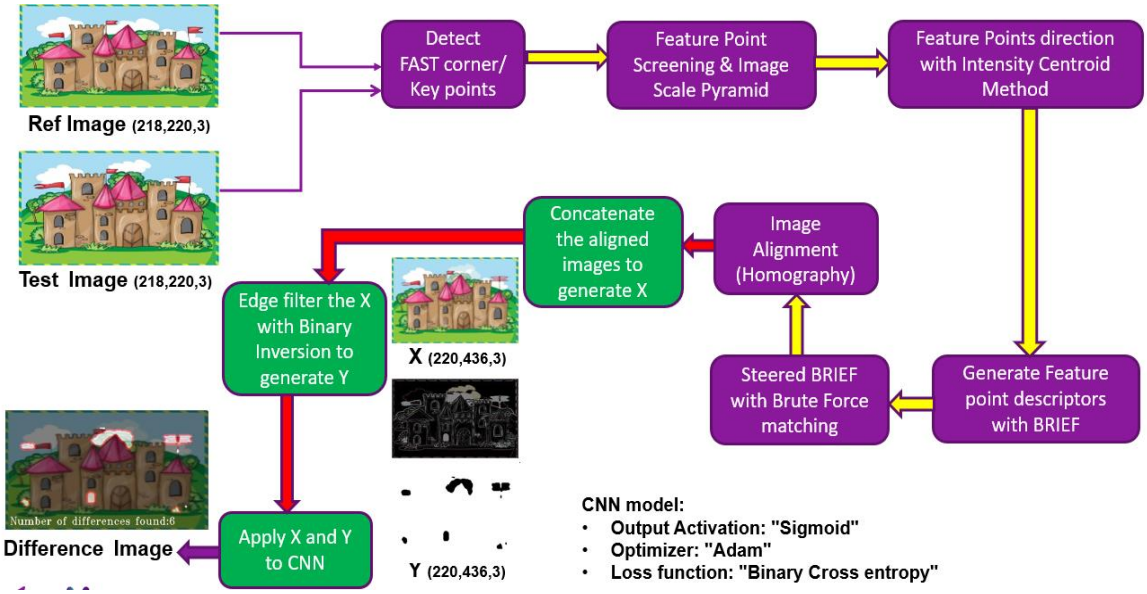

Figure 9. Method-II applying a customized cnn model to the problem

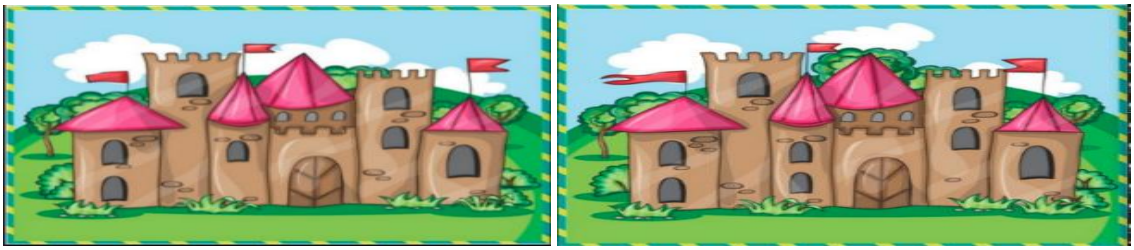

Reference image Test image

Figure 10. An example of concatenated and reshaped image

When this customized CNN model with 'Sigmoid' as the output activation function, the optimizer as 'Adam' and loss function as 'Binary cross entropy' is trained on a synthetic dataset of 700 images, the trained model when used to predict on a pair of unseen images, the results obtained are very promising as shown below:

Reference image Test image Difference image

Figure 11. Customized cnn model results.

Drawbacks and Improvements

Although the above methods of Image processing and use of a customized CNN provided us some promising results, but there are some failure cases that can be seen from figure 11 itself where the cloth color in reference image is green, whereas the cloth color in test image is red, but the model failed to spot the difference. Apart from this, there are also some failure cases when the objects inside the images are displaced resulting in too many false positives.So, to overcome these limitations, we took our work further to apply deep learning algorithm.

Deep Learning with YOLOv8:

In this section, we annotate 700 images by labelling the areas of differences in the concatenated + reshaped images with a label called 'diff' converting the problem into a kind of object detection but we have only single class to detect that is 'diff'. Now as we have converted our problem to an object detection case, considering the large-scale availability for state-of-the-art object detection algorithms, we preferred to choose the latest YOLOv8 object detection algorithm developed by ultralytics. When we fine-tuned YOLOv8 pretrained model on our customized dataset the results are as follows:

Reference image

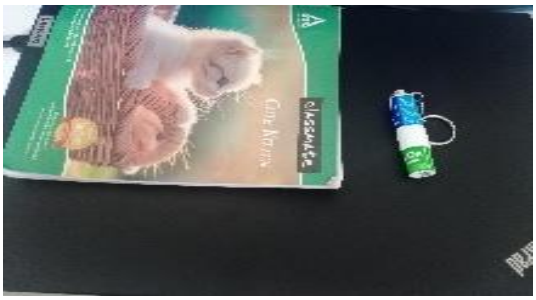

Test image

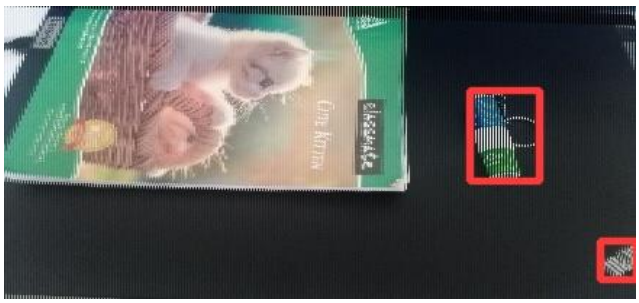

Figure 12. Yolov8n pre-trained model result.

Results and Discussion

Fine-tuned '**YOLOv8n**' pre-trained model result graphs:

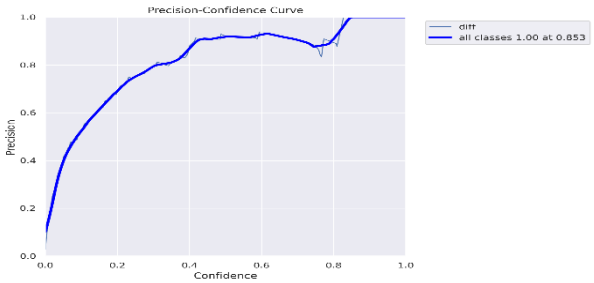

Figure 13. Precision vs confidence

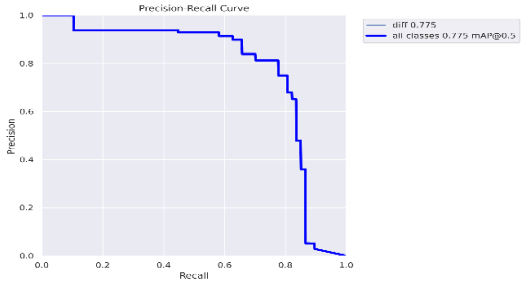

Figure 14. Precision vs recall

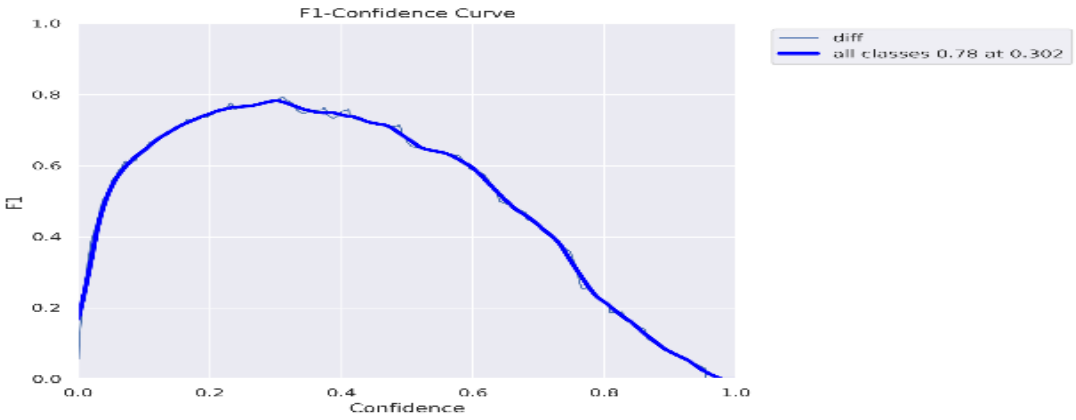

Figure 15.F1-score vs confidence

The following are the results when the model is fine-tuned with '**YOLOv8m**' pre-trained model:

Reference image Test image

Figure 16. Yolov8m pre-trained model result.

Fine-tuned '**YOLOv8m**' pre-trained model result graphs:

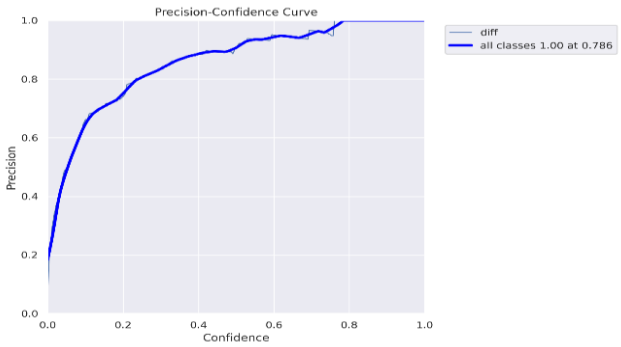

Figure 17. Precision vs confidence

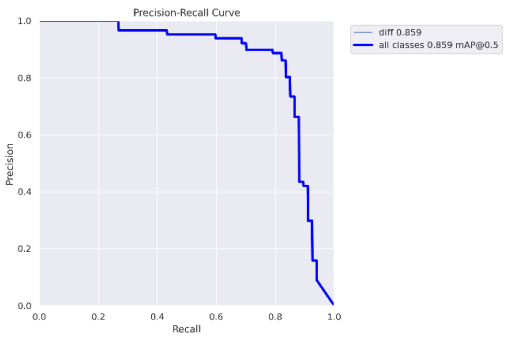

Figure 18.Precision vs recall

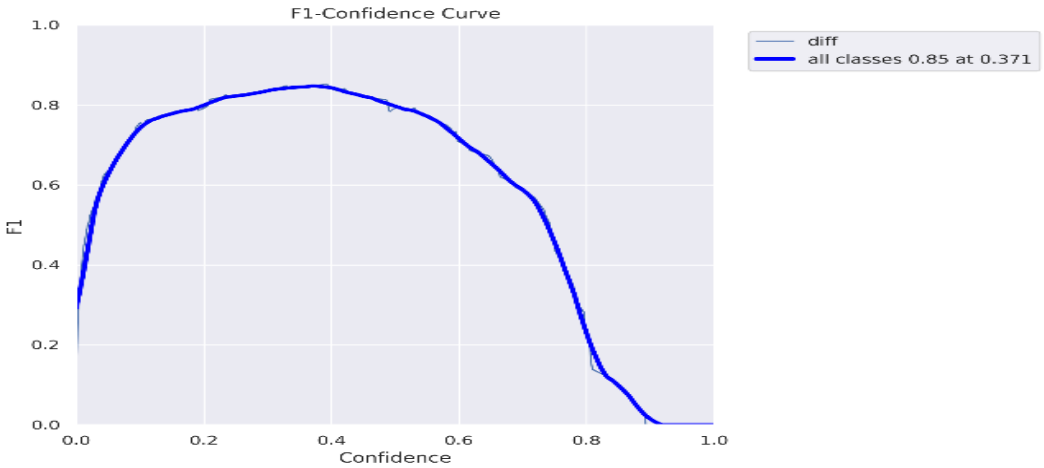

Figure 19.F1-score vs confidence

Conclusion

Although the problem of 'spotting the differences between two images' appears to be simple, but still it continues to exist in the research of computer vision and image processing. Hence considering the gravity of the problem, we have started from the classical image processing and explored till the latest state of the art deep learning algorithm('YOLOv8').The results after fine-tuning the YOLOv8 pre-trained models are convincing and if the model is trained on a huge dataset, it might produce very good results with good confidence irrespective of any internal variations like object displacement or external variations like rotational and luminance changes.

Recommendations

The use of more advanced image alignment techniques may give us improved results and reduces the false positives. There are totally five YOLOv8 pretrained models and in this paper, we used the light weight models YOLOv8n and YOLOv8m, for better results further research can be done using the other pre-trained variants of YOLOv8 and also improvise with the optimizer and loss function to improve the confidence in the results. This paper may give a new dimension to the problem of spotting the differences between two images and if explored further can even produce good results.

Scientific Ethics Declaration

The authors declare that the scientific ethical and legal responsibility of this article published in EPSTEM journal belongs to the authors.

Acknowledgements or Notes

*This work could not have been possible without the support and facilities provided by National Institute of Technology, Warangal, India. Our sincere thanks to all those who contributed to this work either directly or indirectly.

* This article was presented as oral presentation at the International Conference on Basic Sciences, Engineering and Technology (www.icbaset.net) held in Marmaris/Turkey on April 27-30, 2023.

References

Bianco,S., Ciocca, G., & Schettini, R.(2015). How far can you get by combining change detection algorithms? *ArXiv*.

Girshick, R., Donahue,J., Darrell,T.,& Malik, J.(2014) Rich feature hierarchies for accurate object detection and segmentation. *Proceedings of the IEEE conference on computer vision and pattern recognition*, 587.

Jain,R., & Doermann,D.S.(2013). Visualdiff: Document image verification and change detection. *2013 12th International Conference on Document Analysis and Recognition*, 40–44.

Qin, H., Yan, J., Li, X., & Hu,X.(2016). Joint training of cascaded cnn for face detection. *Proceedings of the IEEE Conference on Computer Vision and Pattern Recognition*, 3456– 3465.

Wu,J., Ye,Y., Chen,Y., Weng, Z.(2018).Spotting the difference by object detection. *ArXiv*.

Author Information

Raghunadh M V
National Institute of Technology
Warangal,India
Contact e-mail: raghu@nitw.ac.in

Srikanth Kotakonda
National Institute of Technology
Warangal, India

To cite this article:

M V, R.. & Kotakonda, S. (2023). Spotting the differences between two images. *The Eurasia Proceedings of Science, Technology, Engineering & Mathematics (EPSTEM), 22*, 142-151.

The Eurasia Proceedings of Science, Technology, Engineering & Mathematics (EPSTEM)
ISSN: 2602-3199

Eurasia Proceedings of Science, Technology, Engineering & Mathematics (EPSTEM), 2023

Volume 22, Pages 152-162

ICBASET 2023: International Conference on Basic Sciences, Engineering and Technology

Adaptation of Electric Field Strength Models for Terrestrial Television Broadcast Application in Ekiti State, Nigeria

Abiodun Stephen MOSES
Federal University of Technology

Oseni Taiwo ADEWUNI
Federal University of Technology

Abstract: Electric field strength propagation models play vital roles in planning terrestrial television network coverage, the interference estimations and analyzing the network signal. This work adapted some existing empirical electric field strength models that are best suitable for Ekiti State in Nigeria, using ultra high frequency (UHF) signal. A television signal (Broadcasting Service of Ekiti State (BSES)) was used for this work. The propagation models considered are: free space, Hata, ITU-R and ERC Report 68 models. The BSES channel 41 station transmits at a frequency of 631.25 MHz for video signal. The signal levels of the transmitted signal were measured radially along four routes using a digital signal level meter and the corresponding distances were also measured using a global positioning system (GPS). Data processing and computations were carried out and the results show that the modifed free space model gives a better prediction for the electric field strength in Ekiti State with a correction factor of -25.48 and root mean square error of 6.21 dBμV/m.

Keywords: Coverage area, Empirical propagation model, Electric field strength, Signal level, UHF

Introduction

In a broadcasting system, propagation prediction models are pivotal in planning, designing and analyzing radio communication networks. It is important to point out that propagation models are environment specific and no particular model can be generalized for all environments. Therefore, each model can be useful for some specific environment and accuracy of any particular model depends on the fit between the parameters available for the area concerned and the parameters required by the model (Josip et al., 2010).

Electric field strength curves or propagation curves are essential parameters neccessary for the planning of VHF and UHF transmission especially for the determination of the coverage areas and the field strength signal levels desired (Kennedy & Bernand, 1992). This field strength is affected by a number of conditions such as time of day, atmospheric conditions, transmitter-receiver distance, transmitter power and others like, terrain effect, transmitting and receiving antenna heights, and the gain of the transmitting antenna (Bothias, 1987).

The present trend in broadcasting is to use widespread broadcast transmitter of VHF or UHF range of frequencies to serve areas not far away from the transmitter (Barclay, 1991). Propagation models can be divided into three main groups, namely: empirical, deterministic and semi-deterministic models (Abhayawardhana et al., 2005). The aim of this work is to adapt some existing empirical field strength models in UHF to suit the city of Ekiti State, Nigeria.

Field Strength Models

Field strength models are radio signal propagation models which present the electric field strength as a function of the signal distance from the point of transmission. There are various empirical field strength models for broadcasting services but attention will be given to free space model, Hata model, International Telecommunication Union Radio (ITU-R P.529-3) model and European Radio Communications Committee (ERC Report 68) model because they are widely accepted (Faruk et al., 2013 & Moses et al., 2015).

Free Space Model

Free-space propagation model is used to predict received signal strength when the path between the transmitter and receiver is a clear and unobstructed line-of-sight (Obiyemi et al., 2012). The ideal propagation radiates in all directions from transmitting source and propagating to an infinite distance with no degradation. Attenuation occurs due to spreading of power over greater areas (Nadir et al., 2008).

$$S = \frac{P_T}{4\pi d^2} \quad (1)$$

$$S = P_T - 20\log d - 41 \quad (2)$$

where:
S = power flux density in decibels relative to 1W.m^{-2}
P_T = power in decibels (dB) relative to 1 kW
d = distance (km)
The equivalent field strength, E is given as:

$$E = \sqrt{S.120\pi} \quad (3)$$

$$= \frac{\sqrt{30P_T}}{d} \quad (4)$$

or $E(mV/m) = \frac{173\sqrt{P_T(KW)}}{d\ (km)}$ (5)

$$E = P_T - 20\log d + 104.8 \quad \text{in } dB\mu V/m \quad (6)$$

Hata Model

The model is based on an empirical relation derived from Okumura's report on signal strength variability measurements (Okumura, 1968). The original Hata equation is given in terms of a path loss in dB.

$$E = 69.82 - 6.16logf + 13.82logh_b + a(h_m) - (44.9 - 6.66\log(h_b)) \times \log d \ \ (dB\mu V/m) \quad (7)$$

where:
E = Field strength at a distance from a 1 kW ERP transmitter in $dB\mu V/m$
f = Frequency of the transmission (MHz)
h_b = Height of the base station or transmitter (m)
h_m = Height of the mobile or receiver (m)
d = Distance between the receiver and transmitter (km)

ITU-R P.529-3 Model

The ITU-R determines the analytical expressions that are suitable for same frequency ranges and correspond approximately to some of its propagation curves. The equation is given by (ITU-R, 1999).

$$E = 69.82 - 6.16logf + 13.82logh_b + a(h_m) - (44.9 - 6.55\log(h_b)\,(\log d)^b) \quad (8)$$

where:
E = Field strength for 1 kW ERP

f = Frequency (MHz)
h_b = Base station antenna height in the range of 30-200 m.
h_m = Mobile station antenna height in the range 1-10 m.
d = Distance (km)

$$a(h_m) = (1.1 \log f - 0.7)h_m - (1.56 \log f - 0.8) \quad (9)$$

b = 1 for d ≤ 20 km (10)

$$b = 1 + \left(0.14 + 1.87 \times 10^{-14} f + 1.07 \times 10^{-3} \acute{h}_b\right) \left(\log \frac{d}{20}\right)^{0.8} \text{ for 20 km < d < 100 km} \quad (11)$$

where:

$$\acute{h}_b = \frac{h_b}{\sqrt{1+7\times10^{-8} {h_b}^2}} \quad (12)$$

This model is suitable for use over the ranges:
Frequency range, 150-1500 MHz
Base station height, 30-200 m
Mobile height, 1-10 m
Distance range, 1-100 km

ERC Report 68 Model

In this model, the equation covers the same frequency range as the original Hata equation. This equation has only the distance term raised to the power b and the equation equates approximately to the original Hata equation for distances less than 20 km. The equation is given by (Spectrum planning report, 2001):

$$E = 69.75 - 6.16 log f + 13.82 log h_b + \alpha \times (44.9 - 6.55 \log h_b \times \log d) + a(h_m) + b(h_b) \quad (13)$$

where:

α = 1 if d ≤ 20 km (14)

$$\alpha = 1 + (0.14 + 1.87 \times 10^{-4} \times f + 1.07 \times 10^{-3} h_m) \times \left(\log \frac{d}{20}\right)^{0.8} \text{ if d > 20 km} \quad (15)$$

$$a(h_m) = (1.1 \log f - 0.7) \times minimum(10, h_m) - (1.56 \log f - 0.8) + maximum\left(0, 20 \log \frac{h_m}{20}\right) \quad (16)$$

$$b(h_b) = minimum\left(0, 20 \log \frac{h_b}{30}\right) \quad (17)$$

This model is suitable for the ranges:

Frequency range 150 – 1500 MHz
Base station height 1 - 200 m
Mobile height 1 - 200 m
Distance range 1 - 100 km

Study Area

Ekiti State of Nigeria was chosen for this research (Figure 1). The State is located in the south western part of Nigeria between latitude 7°40'N and latitude 7.667°N and longitude 5°15'E and 5.250°E with the capital at Ado-Ekiti. The state is bounded in the north by Kwara State and Kogi State while Osun State occupies the west and Ondo State lies in the south and extends to the eastern part. Ekiti State has sixteen local government areas with an overall population of about 2,384,212 people that spread over an approximately 88.7 km^2. The region lies at about 250 m above the sea level.

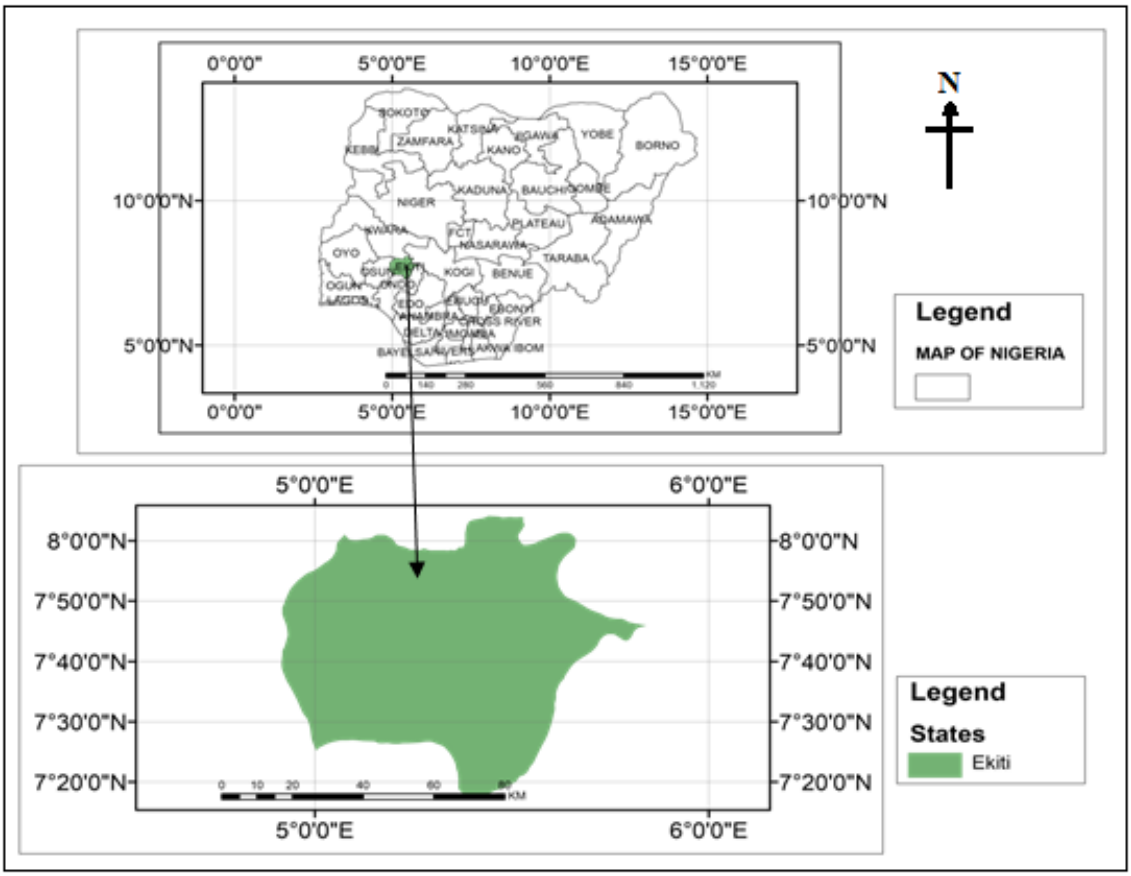

Figure 1. Map of Ekiti State in Nigeria

Data Collection and Analysis

This work was carryout in Ekiti State, Nigeria, using the UHF television station signal of Broadcasting Service of Ekiti State (BSES), channel 41. The television station transmits signal at frequency of 631.25 MHz for video signal and the output power of the transmitter was 7 kW while the transmitting antenna was mounted on a mast of 200 m high.

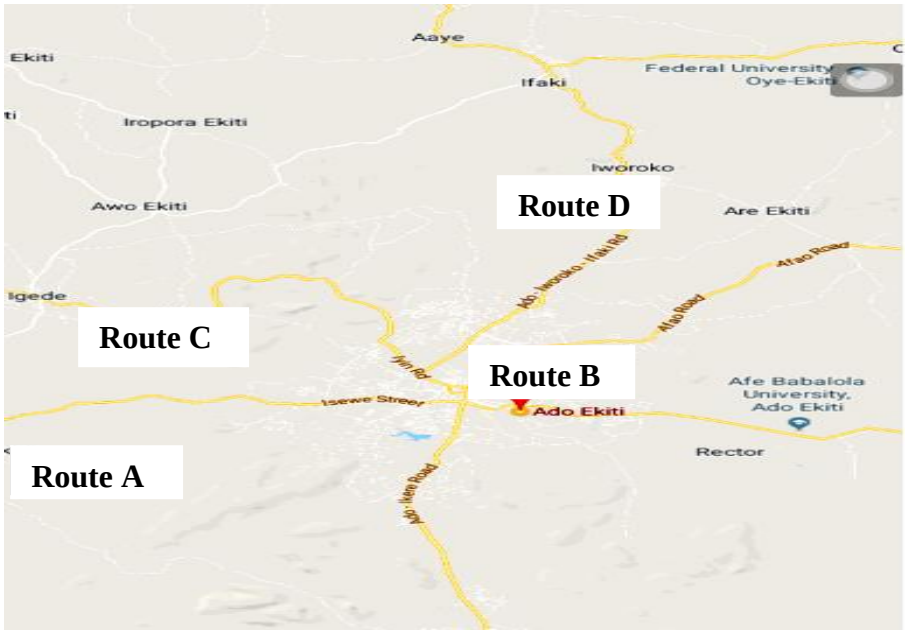

Figure 2. The route along which measurement were taken

The signal levels of the transmitted signal were measured radially along the four accessible routes using a digital signal level meter until the signal faded out and the corresponding distances were also measured using a global positioning system (GPS). Data processing and computation were carried out using Microsoft office excel application. From the measured signal levels, the field strength values in dBμV/m were calculated for a 1 kW Effective Radiated Power (ERP) transmitter to aid comparison with other models. The field strength for each route was obtained and the corresponding field strength as predicted by the free space, Hata, ITU-R.P529-3 and ERC Report 68 models were also evaluated.

For each model, the root mean square error (RMSE) was determined along the four routes (Figure 2) and the mean prediction error (MPE) was also determined and used as a correction factor to modify each model to get the least RMSE. As a result of different routes considered, there are a number of correction factors for each model for the city. So, to generalise each model for all routes in Ekiti State, the average value of the MPE of the four routes considered were estimated and used as the correction factor to generalise the field strength models.

Results and Discussion

Electric Field Strength Models

The comparison of the field strength models with the measured field strength for the four routes considered are shown in the Figures 3 to 6. The models have the same trend for all the routes considered. From the Figures, the free space model has the highest values of the prediction while the ERC Report 68 model has the lowest prediction values. The RMSE of the field strength models for each route are shown in Table 1. Hata model has the least average RMSE (11.71 dBμV/m) for all the routes

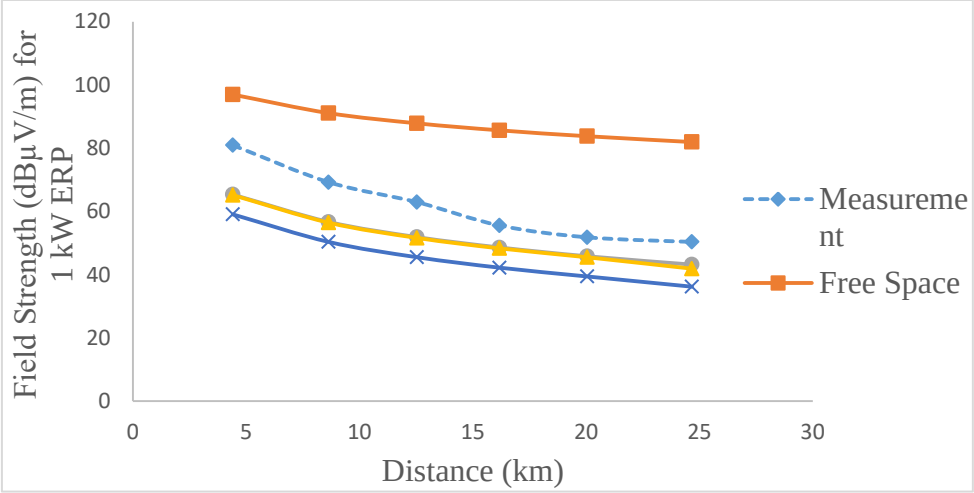

Figure 3. Field strength models for route A

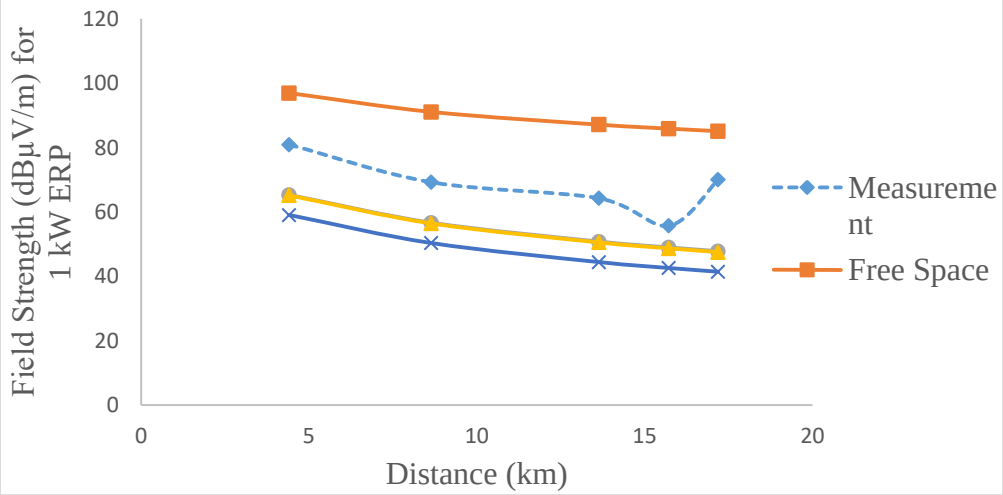

Figure 4. Field strength models for route B

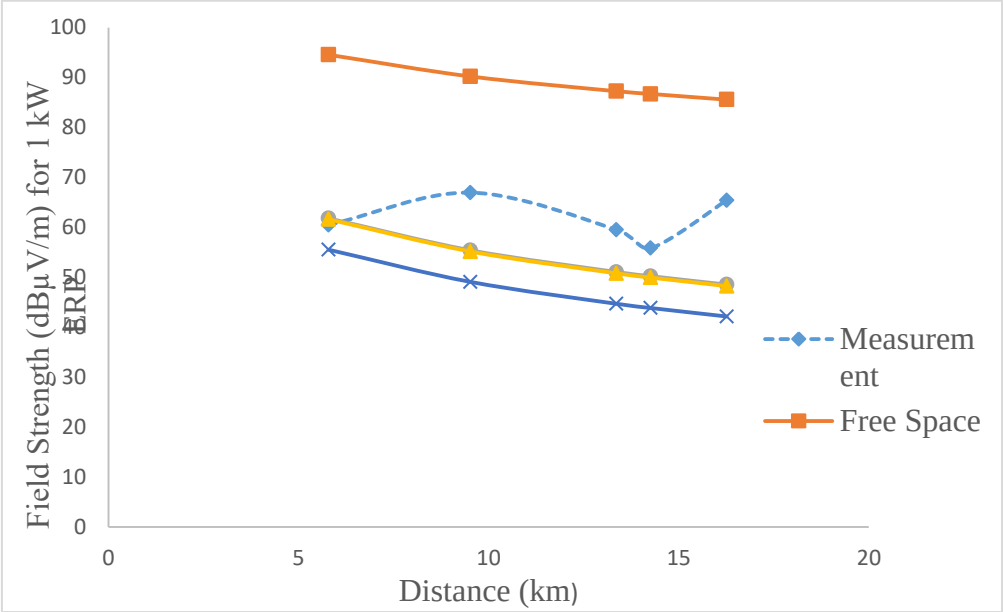

Figure 5. Field strength models for route C

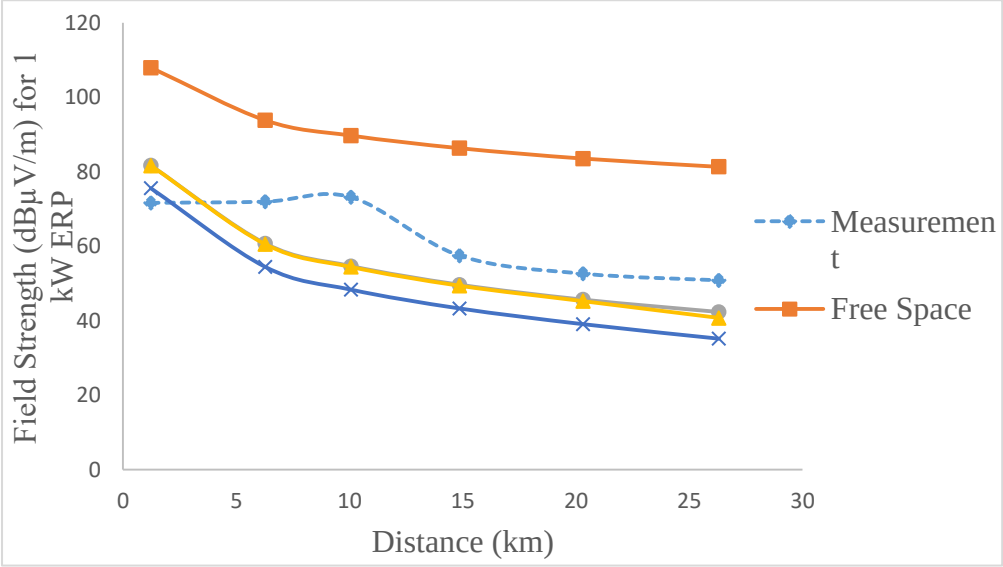

Figure 6. Field strength models for route D

Table 1. Root mean square error of the field strength models

Route	Free Space (dBµV/m)	Hata (dBµV/m)	ITU-R (dBµV/m)	ERC (dBµV/m)
A	26.70	10.47	11.24	16.67
B	21.87	14.98	15.02	20.83
C	27.60	10.22	10.45	15.80
D	28.24	11.18	11.57	16.17
Average	26.10	11.71	12.07	17.36

Modified Field Strength Models

Figure 7 to 10 show the modified field strength models for the routes. Table 2 shows the correction factors used for modified field strength models while Table 3 gives the RMSE of the modified field strength models for each route. The modified models show that the free space model has the lowest field strength prediction and all the models follow the same trend.

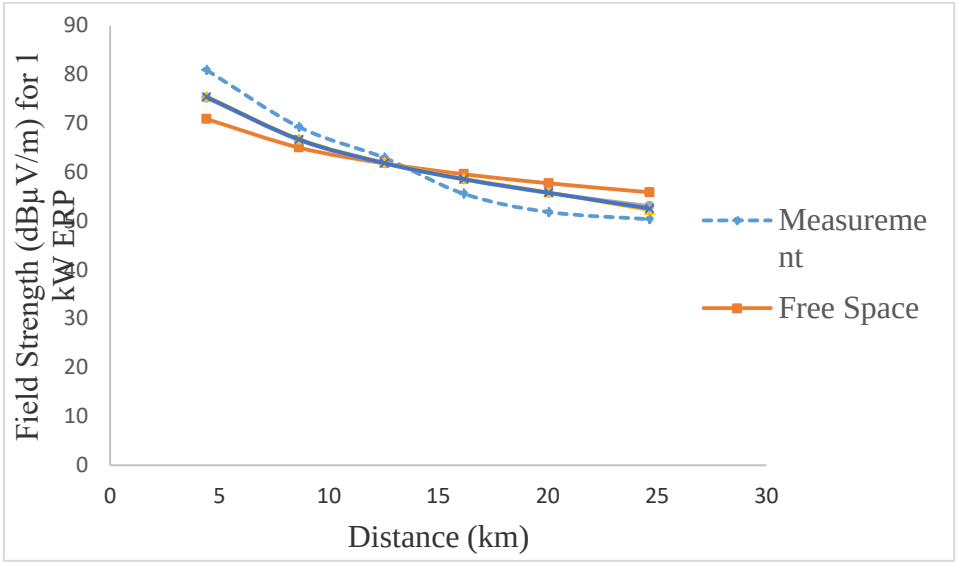

Figure 7. Modified field strength models for route A

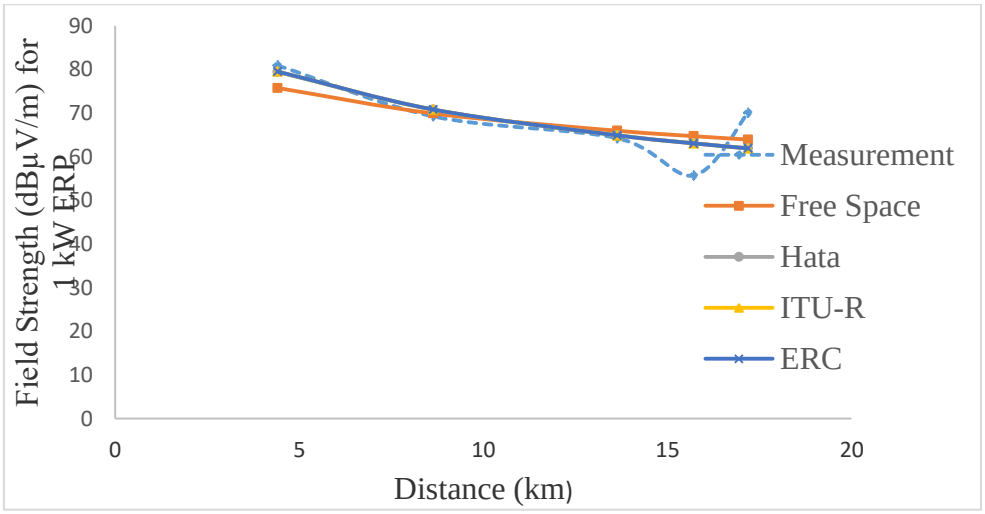

Figure 8. Modified field strength models for route B

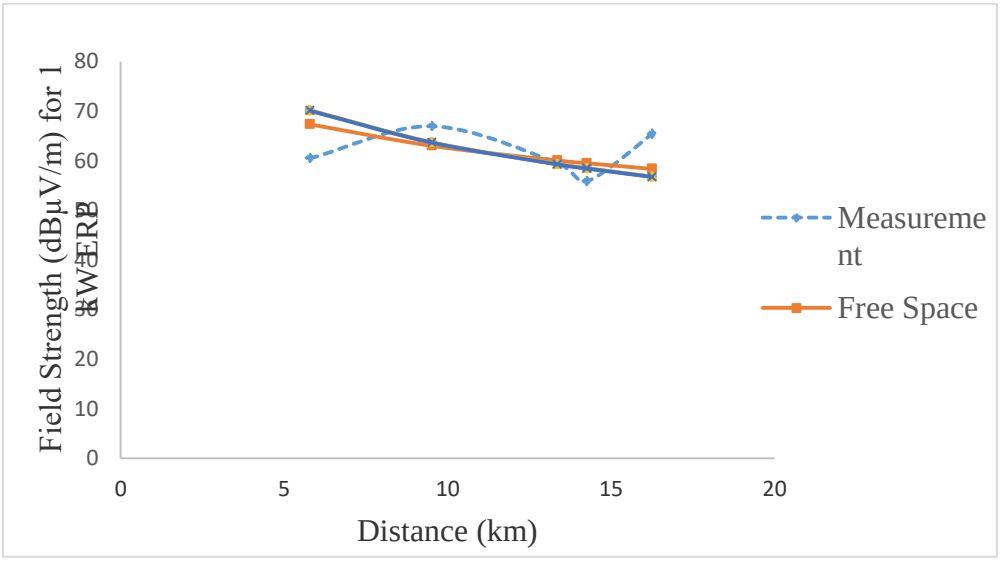

Figure 9. Modified field strength models for route C

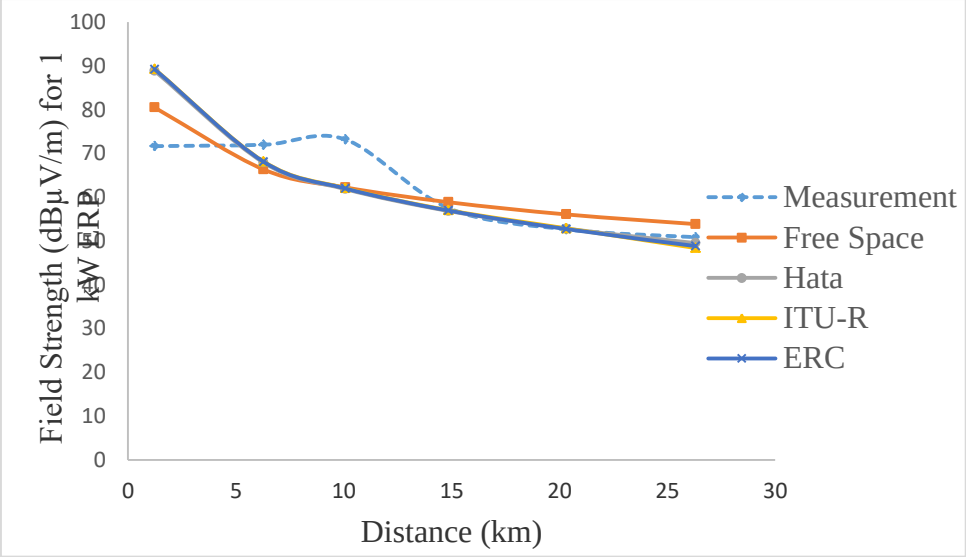

Figure 10. Modified field strength models for route D

Table 2. Correction factors used for the modified and the generalised field strength models

Route	Free Space (dBµV/m)	Hata (dBµV/m)	ITU-R (dBµV/m)	ERC (dBµV/m)
A	-26.06	9.89	10.32	16.33
B	-21.18	14.11	14.36	20.46
C	-27.22	8.24	8.57	14.58
D	-27.49	7.16	7.62	13.64
Average	-25.48	9.85	10.21	16.25

Table 3. Root mean square error of the modified field strength models

Route	Free Space (dBµV/m)	Hata (dBµV/m)	ITU-R (dBµV/m)	ERC (dBµV/m)
A	5.78	3.46	3.30	3.35
B	5.45	4.99	4.99	5.47
C	5.02	6.06	6.09	6.08
D	6.48	8.59	8.71	8.69
Average	5.68	5.77	5.77	5.89

Generalised Field Strength Models

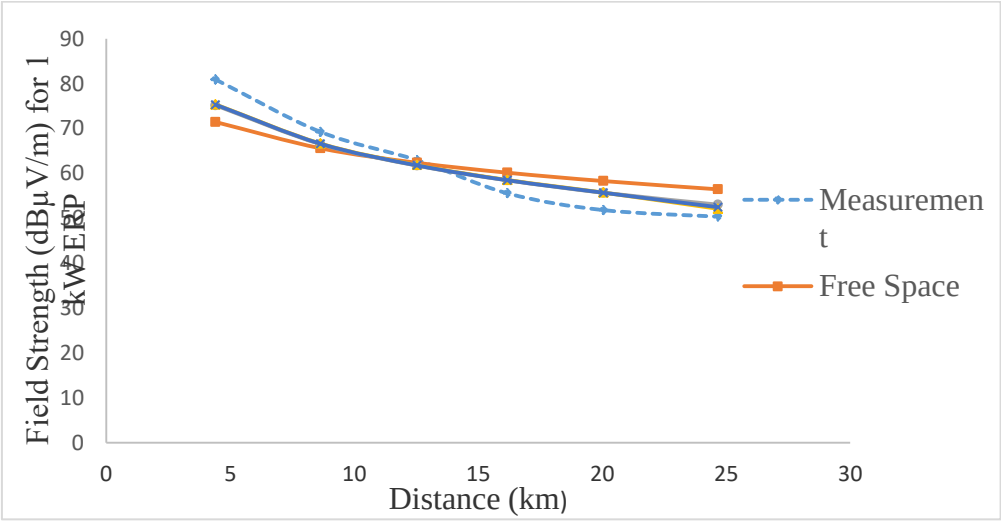

Figure 11. Generalised field strength models for route A

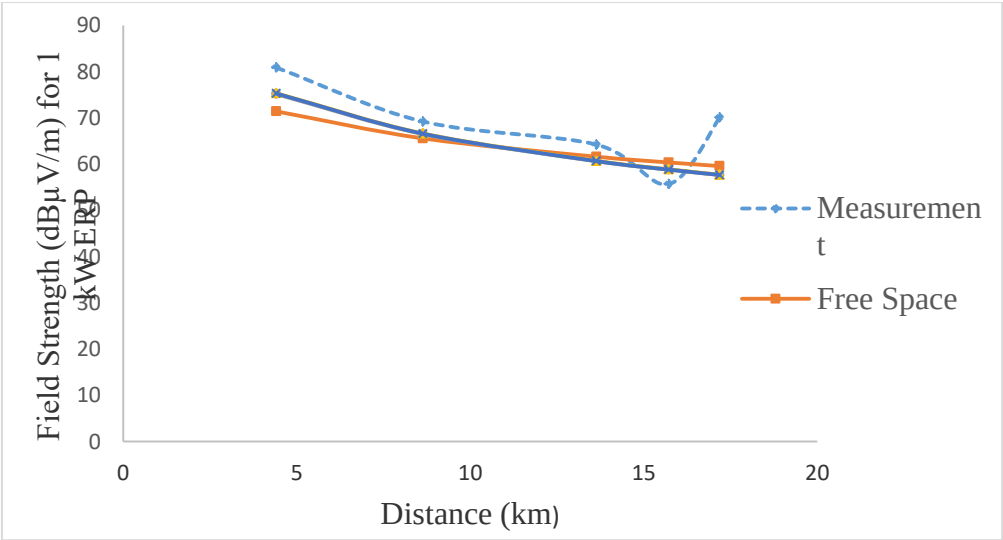

Figure 12. Generalised field strength models for route B

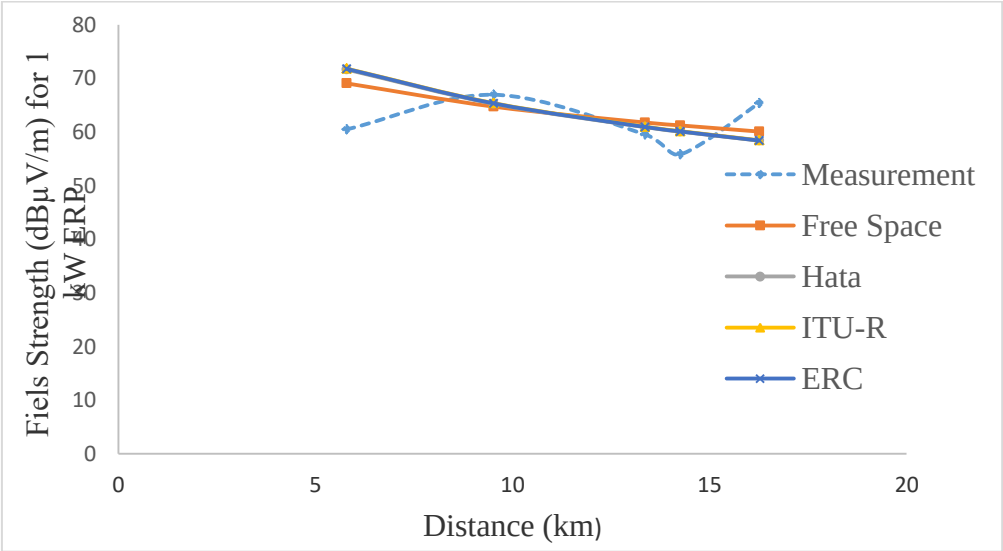

Figure 13. Generalised field strength models for route C

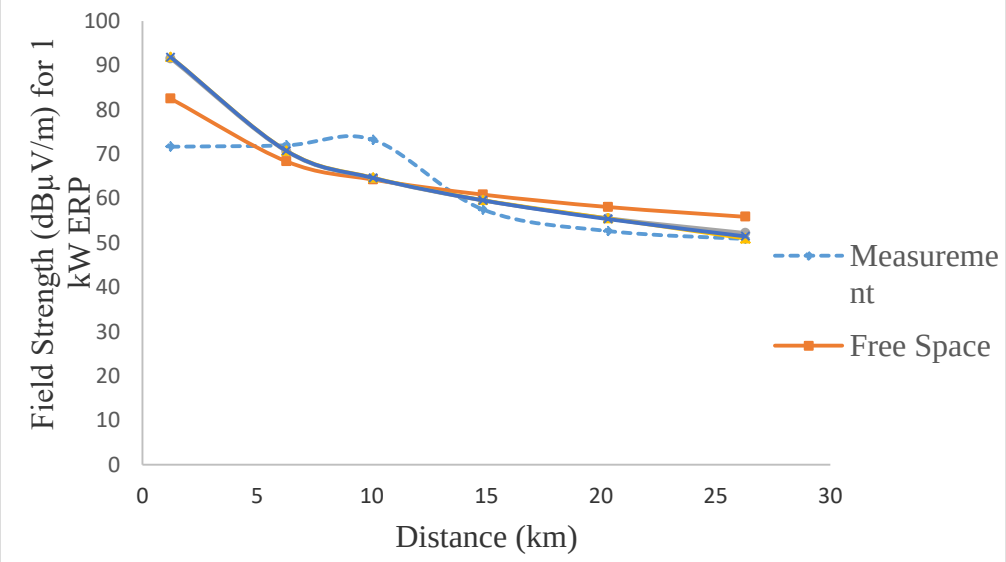

Figure 14. Generalised field strength models for route D

Table 4. Root mean square error of the generalised field strength models

Route	Free Space (dBμV/m)	Hata (dBμV/m)	ITU-R (dBμV/m)	ERC (dBμV/m)
A	5.81	3.47	3.30	3.35
B	6.95	6.59	6.52	6.55
C	5.31	6.27	6.32	6.31
D	6.78	9.03	9.08	9.07
Average	6.21	6.34	6.30	6.32

The generalised field strength models are shown in Figures 11 to 14. The free space has the lowest field strength prediction. The correction factors used to generalise the field strength models for Ekiti State are the average values of the mean prediction error of all the four routes. Table 4 shows the RMSE values of the generalised field strength models for each route and free space model has the least average RMSE of 6.21 dBμV/m for all the routes considered.

Conclusion

The generalised field strength models for Ekiti State, for terrestrial television broadcast application, were obtained by using the average of the mean prediction errors of the four routes as the correction factor for each model. The average values of the RMSE of the generalised field strength models for the four routes are taken as the RMSE values for Ekiti State. The correction factors used for all the field strength models are as follows: -25.48 for free space, 9.85 for Hata, 10.21 for ITU-R P.529-3 and 16.25 for ERC Report 68 models with average RMSE of 6.21dBμV/m, 6.34 dBμV/m, 6.30 dBμV/m and 6.32 dBμV/m respectively. Hence, the generalised free space field strength model gives a more accurate prediction for field strength in Ekiti State as compared to other models.

Recommendation

This work can be repeated for different seasons of the year to observe the variation of the signals with seasons

Scientific Ethics Declaration

The authors declare that the scientific ethical and legal responsibility of this article published in EPSTEM journal belongs to the authors

Acknowledgements

This article was presented as virtual presentation at the International Conference on Basic Sciences, Engineering and Technology (www.icbaset.net) held in Marmaris/Turkey on April 27-30, 2023

References

Abhayawardhana, V. S., Wassell, I. J., Crosby, D., Sellars, M. P. & Brown, M. G. (2005). Comparison of empirical propagation path loss models for fixed wireless access systems. Proceedings from VTC '05: *IEEE 61th Vehicular Technology Conference*, Stockholm, Sweden

Barclay, L. W. (1991). Basic radio system parameters. Hall, M. (Ed.), *Radio wave propagation* (pp. 43-44). United Kingdom, UK: Institute of Electrical and Electronics Engineers (IEEE) Electromagnetic Wave Series, Peter Peregrinus Limited.

Bothias, L. (1987). *Radio wave propagation*. New York, McGraw-Hill Inc.

Faruk, N., Ayeni, A., & Adediran, Y. A. (2013). On the study of empirical path loss models for accurate prediction of TV signal for secondary users. *Progress in Electromagnetics Research, 49*, 155-176.

ITU-R P.529-3 Recommendation. (1999). Prediction methods for the terrestrial land mobile service in the VHF and UHF bands. https://www.itu.int/rec/R-REC-P.529-3-199910-W/en

Josip M., Snjezena R., & Ivo M. (2010). Radio wave propagation mechanisms and empirical models for fixed wireless access systems. *Technical Gazette, 17*(1), 43-52.

Kennedy, G & Bernand, D. (1992). *Electronic communication systems* (pp.80-150). Singapore: McGraw Hill/Macmillan.

Moses, A. S., Oyedum, O. D., & Ajewole, M. O. (2015). Empirical field strength model for terrestrial broadcast in VHF Band in Makurdi City, Benue State, Nigeria. *International Research Journal of Enginnering and Technology, 2*(1), 23-27.

Nadir, Z., Elfadhil, N., & Touati, F. (2008). Path loss determination using Okumura-Hata model and spline interpolation for missing data for Oman. Proceedings from WCE '08: *World Congress on Engineering*. London, U.K.

Obiyemi, O. O., Ibiyemi, T. S., Gbenga-Ilori, A. O., & Ojo, J. S. (2012). Path loss model for radio wave propagation at VHF/UHF bands using electric field strength measurement over Ilorin, Middle-belt, Nigeria. Proceedings from ACTEA '12: *2nd International Conference on Advances in Computational Tools for Engineering Applications*, *2.*

Okumura, Y., Ohmori, E., Kwano, T., & Fakuda, K. (1968). Field strength and variability in UHF/VHF land mobile radio service. *Review of Electronic Communication Laboratory*, *16*(1), 9-10.

Spectrum Planning Report. (2001). Investigation of modified hata propagation models. *Spectrum Planning Team, Radiofrequency Planning Group, Document SP 2/01. Australian Communications Authority.*

Author Information

Abiodun Stephen Moses
Federal University of Technology
Minna, Nigeria
Contact e-mail: abiodun.moses@futminna.edu.ng

Oseni Taiwo Adewuni
Federal University of Technology
Minna, Nigeria

To cite this article:

Moses, A.S., & Adewuni, O.T. (2023). Adaption of electric field strengh models for terrestrial television broadcast application in Ekiti state, Nigeria. *The Eurasia Proceedings of Science, Technology, Engineering & Mathematics (EPSTEM), 22,* 152-162.

The Eurasia Proceedings of Science, Technology, Engineering & Mathematics (EPSTEM)
ISSN: 2602-3199

The Eurasia Proceedings of Science, Technology, Engineering & Mathematics (EPSTEM), 2023

Volume 22, Pages 163-170

ICBASET 2023: International Conference on Basic Sciences, Engineering and Technology

Mixture Herbal Tea is Oxidant or not?

Isik Didem KARAGOZ
Gaziantep University

Basak SIMITCIOGLU
Gaziantep University

Ugur VURAL
Gaziantep University

Abstract: In recent years, many people have been using various plants and herbal products for preventive or therapeutic purposes. These herbal products, especially herbal teas, have become very popular and have been widely consumed in daily life. We wanted to see whether random, uncontrolled and unmeasured use of these herbal teas, which are consumed without question because they are natural, affect their antioxidant potential. Therefore, in this study, a mixed tea prepared by mixing 10 different herbs, known to be beneficial among the public, in different proportions, sold as "winter tea" in herbalists was used. The antioxidant and oxidant activities of all the plants in this tea were tested separately and in combination, and oxidative stress indexes were calculated. The results showed that no plant included in the winter tea alone had an oxidative stress index as low as the mixture of winter tea. We can say that for the winter tea mixture we chose as the trial material; There is a strong synergistic effect between the herbs in this combination, and the oxidant effect of one was eliminated by the antioxidant effect of the other, resulting in a very safe herbal blend tea. As a result of our study, it has been shown that it is important to determine the oxidative stress state created by different herbal mixtures sold in the market before use. As a result, we cannot say that every herbal tea is harmful or beneficial, and it is not possible to say this for mixture teas. Considering our study result, we can say that winter teas prepared and consumed in this combination do not increase the oxidative stress of the body. Further studies are needed to detail its effects on the body.

Keywords: Medicinal plants, Herbal tea, Oxidative stress, Antioxidant, Winter tea

Introduction

Herbal teas are teas made from parts of plants obtained from natural sources, such as leaves, roots, fruits, which have been used by many civilizations since ancient times for their healing roles. These teas, which are among the most consumed hot drinks among the public, generally contain beneficial substances such as plant extracts, vitamins, minerals, antioxidants and are beneficial for health (Oh et al., 2013). The most common herbal teas are; chamomile, sage, thyme, mint, meadow flower, turmeric, rosehip, rose, cinnamon, lemon balm, linden and it is prepared by one of the methods of decoction and maceration, especially infusion (Kokdil, 2002).

Herbal teas are mainly sold in the market as tea bags, ground or crushed products or dried whole of the plant, but they are also consumed as a mixture tea as well as being offered to the market as a single. Mixed herbal teas are defined as teas in which more than one plant species is used together. These teas, which are marketed as "winter tea", "atom tea", "detox tea", "relaxing relax tea", consist of a mixture of plants with targeted biological activity. For example, "Winter tea" is a Turkish expression and its meaning is generally defined as tea drunk in

cold weather. Winter tea is usually served as hot tea and ingredients such as cloves, walnuts and cinnamon are added to it, especially to warm up in cold weather.

Since all herbal medicines are mixtures of more than one active ingredient, such combinations of many substances clearly increase the likelihood of interactions occurring. However, synergistic effects may occur with the combined use of herbs, as well as antagonistic effects (Junio et al., 2011). In addition, the oxidant properties of these herbal teas, whose antioxidant properties are so prominent, are ignored and there are a limited number of studies dealing with herbal teas from this aspect. Moreover, the positive or negative effects of the use of plants as a single or a mixture on antioxidant and oxidant activities still remain a mystery. From this point of view, in this study, it was aimed to evaluate the oxidant/antioxidant levels and oxidative stress index in order to determine whether the combination of herbs in the blend teas sold as winter tea creates an antagonistic or synergistic interaction.

Method

Supply of Winter Tea and Preparation of Samples

Herbal mixture sold as "Winter Tea" was commercially available from a local herbalist. The mixture was weighed and then separated according to the plants in it. The individual amounts of the separated plants were weighed on sensitive scales and the mixing ratios in winter tea were determined as given in Table 1. By determining the weight of the commercially sold tea bags, the average number of tea bags will be produced from the mixture we have, and how many g of which plant will be in each glass has been determined.

Table 1. The herbs and their amounts in the winter tea mixture

Herb Name	Weight (g)
Chamomillae romanae	6,9746
Hibiscus sabdariffa	5,1643
Rosa sp.	8,9610
Salvia officinalis	1,9055
Cinnamomum zeylanicum	14,2815
Citrus sinensis	4,8918
Rosa canina	31,6920
Tilia cordata	3,2837
Lamium macrodon	2,7826
Curcuma longa	3,4640
Amount	83,4010

Obtaining Tea Extracts

After the proportions in the winter tea were determined, 1.66 g of winter tea was brewed for 5 minutes according to the infusion method in 200 mL mug. Likewise, each herb in the winter tea was weighed 1.66 g and infused for 5 minutes in 200 mL (Figure 1). At the end of 5 minutes, the plants were separated from the water and the herbal teas were left to cool. Thus, 11 samples, including 1 winter tea and 10 herbal teas, were ready.

Figure 1. Extracted winter tea mix and herbal teas

Determination of Total Antioxidant Activity

Commercially available Total Antioxidant Status Assay kit (Rel Assay, Turkey) was used to determine the antioxidant activity of the samples. The basis of this method is based on the fact that the antioxidants in the sample decolorize the 2,2'-azino-bis(3-ethylbenzothiazoline-6-sulfonic acid (ABTS) radical which is a dark blue-green colored oxidant and give an absorbance change at 660 nm. The amount of change in absorbance is related to the total antioxidant level of the sample. The test is traditionally calibrated with a stable antioxidant standard solution called Trolox equivalent, a vitamin E analogue. Accordingly, 18 µl of tea extracts were added to the wells of the 96-well plate and 300 µl of Reagent 1 in the kit was added to it, and after 30 seconds, absorbance measurement was taken at 660 nm wavelength in the spectrophotometer device. Afterwards, 45 µl of Reagent 2 was added to the wells and incubated at 37 °C for 5 minutes, and then the absorbance was measured again at 660 nm wavelength. Distilled water was used as the negative control, and 1 mmol/L Trolox, the "standard" in the kit content, was used as the positive control. The antioxidant value results were calculated according to the equation given below.

$$\Delta abs = \text{2. Measurement Absorbance} - \text{1. Measurement Absorbance}$$

$$\text{Antioxidant Activity} = \frac{\Delta Abs\ water - \Delta Abs\ sample}{\Delta Abs\ water - \Delta Abs\ Standard}$$

The values obtained as a result of the calculation were interpreted according to the reference values of the kit (Table 2).

Table 2. TAS reference values of the kit

	TAS reference values (mmol Trolox Equiv./L)
>2.0	Very good
1.45 - 2	Normal
1.2 - 1.45	Almost normal
1 - 1.2	Low antioxidant level
<1.2	Very low antioxidant level

Determination of Total Oxidant Activity

Commercially available Total Oxidant Status Assay kit (Rel Assay, Turkey) was used to determine the oxidant activity of the samples. The test is based on the fact that the oxidants in the samples oxidize the iron ion-chelator complex contained in the kit to ferric ion, and the ferric ion formed as a result of this oxidation reaction forms a colored complex with the chromogen. The values obtained as a result of the calculation were interpreted according to the reference values of the kit (Table 3).

$$\Delta abs = \text{2. Measurement Absorbance} - \text{1. Measurement Absorbance}$$

$$\text{Oxidant Activity} = \frac{\Delta Abs\ Sample}{\Delta Abs\ Standard}$$

Table 3. TOS reference values of the kit

	TOS reference values (μmol H_2O_2 Equiv./L)
<5.0	Very good
8 - 5	Normal
12 - 8	High oxidant level
>12.0	Very high oxidant level

Calculation of Oxidative Stress Index

Oxidative stress index (OSI), which is accepted as an indicator of oxidative stress level, is a unitless (AU: arbitrary unit) parameter found by proportioning TOS values to TAS values. In the calculation, the TAS unit (mmol Trolox Equiv./L) was first converted to μmol Trolox Equiv./L, and then the equation given below was used (Deska et al., 2017).

$$OSI = [(TOS, \mu mol\ H_2O_2\ Equiv./L) / (TAS, \mu mol\ Trolox\ Equiv./L) \times 100]$$

Results and Discussion

Total Antioxidant Activity

When the results were evaluated, it was determined that the samples with the highest antioxidant activity had 0.777, 0.667 and 0.662 mmol/L values, respectively, of *L. macrodon*, winter tea and *S. officinalis* extracts. The lowest values were observed in *R. canina*, *C. zeylanicum* and *C. sinensis* with 0.244, 0.269 and 0.274 mmol/L (Figure 2, Table 4).

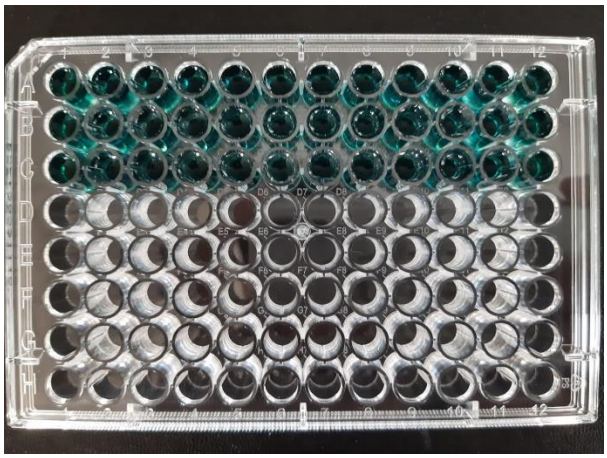

Figure 2. Morphological results of antioxidant activity of herbal teas

Table 4. TAS results of 8.3 mg/mL amounts of winter tea and herbal teas

Herb Name	**TAS Results (mmol/L Trolox)**
Chamomillae romanae	0,303
Hibiscus sabdariffa	0,357
Rosa sp.	0,332
Salvia officinalis	0,662
Cinnamomum zeylanicum	0,269
Citrus sinensis	0,274
Rosa canina	0,244
Tilia cordata	0,405
Lamium macrodon	**0,777**
Curcuma longa	0,296
Winter tea	**0,667**
Positive Control (1mmol/L Trolox)	1

Total Oxidant Activity

According to the oxidant activity results, it is seen that the samples with the lowest oxidant activity are *H. sabdariffa*, *C. longa* and *R. canina* with H_2O_2 values of 4,017, 4,382 and 4,580 µmol/L. These values are followed by 5.606 and 6.651 µmol/L H_2O_2 and *C. sinensis* and winter tea extracts. When we look at the extracts with the highest oxidant activity, we encounter *L. macrodon* with a high value of 31,456 µmol/L H_2O_2, followed by *T. cordata* and *S. officinalis* with 19,331 and 19,080 µmol/L H_2O_2 (Figure 3, Table 5).

Figure 3. Morphological results of oxidant activity of herbal teas

Table 5. TOS results of 8.3 mg/mL amounts of winter tea and herbal teas

Herb Name	**TOS Results (µmol/L H_2O_2)**
Chamomillae romanae	7,921
Hibiscus sabdariffa	**4,017**
Rosa sp.	15,291
Salvia officinalis	19,080
Cinnamomum zeylanicum	8,575
Citrus sinensis	5,606
Rosa canina	4,580
Tilia cordata	19,331
Lamium macrodon	31,456
Curcuma longa	**4,382**
Winter tea	6,651
Positive Control (10 µmol/L H_2O_2)	10

Oxidative Stress Index

According to the oxidative stress index data determined by the ratio of oxidant activity to antioxidant activity, the lowest value was observed in winter tea with 0.997 µmol/L H_2O_2, while it was observed in *T. cordata* with 4.776 µmol/L H_2O_2 (Table 6).

Table 6. OSI values of 8.3 mg/mL of winter tea and herbal teas

Herb Name	**OSI Values (µmol/L H_2O_2)**
Chamomillae romanae	2,616
Hibiscus sabdariffa	1,125
Rosa sp.	4,606
Salvia officinalis	2,883
Cinnamomum zeylanicum	3,182
Citrus sinensis	2,045
Rosa canina	1,873
Tilia cordata	4,775
Lamium macrodon	4,049
Curcuma longa	1,482
Winter tea	**0,997**
Positive Control (10 µmol/L H_2O_2)	1

Discussion

In recent years, many people have been using various plants and herbal products for preventive or therapeutic purposes. The fact that the plants have a high antioxidant value thanks to the active ingredients they contain has a very important role in this. These herbal products, especially herbal teas, have become very popular and are widely consumed in daily life. We wanted to satisfy our curiosity about whether random, uncontrolled and unmeasured uses of these herbal teas, which are consumed without question with the view that everything natural is beneficial, affect the antioxidant potential and make a contribution to this issue. If a plant with a really high antioxidant potential and a plant with a high oxidant potential are in the same mixture, does it reduce the antioxidant effect of tea? Our study results showed that this situation is possible. However, it was observed that the mixture containing plants with high oxidant potential had lower oxidant potential. This gave us the idea that a plant with a high oxidant level may contribute to the immune system with another feature. When used alone, it has been interpreted as the oxidant effect will be eliminated with the mixture and this will increase the contribution of the plant. Moreover, the oxidative stress index of these herbal teas, whose antioxidant activity is trusted, is completely ignored. The fact that the plants that should be consumed by emphasizing their antioxidant activity also have an oxidant level comes to the minds of scientists. However, data on this is very limited. When the existing data are examined, it is seen that many plants also have harmful effects. For example: Long-term use of herbal products with laxative effects such as senna leaf (*Folium sennae*), cassia fruit (*Fructus sennae*), cascara bark (*Cortex rhamni purshianae*) causes diarrhea and disrupts the electrolyte balance as a result of excessive water loss, resulting in hypokalemia. Ginger rhizome (*Rhizoma zingiberis*) inhibits thromboxane synthetase and can change bleeding times. Therefore, caution should be exercised in its use with anticoagulants and should be used under the supervision of a doctor. Animal experiments have shown that eucalyptus essence (*Aetheroleum eucalypti*) and leaf (*Folium eucalypti*) can stimulate liver enzymes and therefore reduce the effects of drugs (Uzun et al., 2014).

However, mixture teas in which herbs are used together are also thought-provoking in terms of benefit and harm comparison (Stermitz et al., 2000). The plants in the mixture can benefit each other by increasing the effectiveness of each other by making an additive effect to each other, and this activity can reach the amount of toxic dose and cause serious side effects that can lead to death. They may not show the expected benefit by dampening the effects instead of increasing each other's effectiveness (Colalto, 2010; Ulrich-Merzenich et al., 2010).

From this point of view, the question that led to the emergence of this project was whether we should consume herbal teas individually or in a mixture. It has been thought whether the mixture teas show the antioxidant properties of all plants together and become a healthier formula than they are individually, or whether their oxidant effects are multiplied and, on the contrary, gaining a harmful dimension to human health.

Therefore, in this study, a mixture of tea, which is sold as "winter tea" in herbalists, was used. There were 10 different plants known to be beneficial among the public in different proportions in this mixture. The plants in this tea were separated and the antioxidant and oxidant activities of all plants were tested separately. At the same time, it was possible to compare the differences according to the single use of the plants by working with the winter tea as a mixture. Then, the oxidative stress index, which is the ratio of oxidant activity to antioxidant activity, was calculated.

When the results were evaluated, considering that the antioxidant and oxidant values were measured for the OSI calculation and the most important thing was the balance between the antioxidants and oxidants in the cell, it was seen that no plant included in the winter tea alone was as close to the balance (approximately 1) as the winter tea mixture. We can say that for the winter tea mixture we chose as the trial material; There is a strong synergistic effect among the 10 plants in this combination, and the oxidant effect of one was eliminated by the antioxidant effect of the other, resulting in a very safe herbal blend tea.

Numerous studies have demonstrated that herbal extracts as a whole and/or multiple herbs in complex formulations offer better efficacies than equivalent doses of individual active ingredients and/or herbs when used alone, highlighting the significance of synergistic action in herbal therapies (Leonard et al., 2002; Scholey & Kennedy, 2002; Zhang et al., 2014). For example, synergistic effects of five commonly used medicinal herbs extracts thyme (*Thymus vulgaris*), rosemary (*Rosmarinus officinalis*), sage (*Salvia officinalis*), spearmint (*Mentha spicata*) and peppermint (*Mentha piperita*) were tested in an in vitro study (Yi & Wetzstein, 2011)

However, it should not be forgotten that; The ingredients of each herbal blend tea may differ from each other and the use of the word "safe" for these is dependent on such trials. It is quite wrong to expect that another mixture with different plants or the same plants in different proportions will show the same effect. In this regard, more detailed studies are needed.

Conclusion

As a result, we cannot say that every herbal tea is harmful or beneficial, and it is not possible to say this for blended teas. However, taking into account our study result, consumption of winter tea, which is settled in traditional use, usually prepared in this combination and spread throughout the society, does not increase the oxidative stress of the body. Further studies are needed to detail its effects on the body.

Recommendations

As a result of our study, it is important to determine at least the oxidative stress state created by different herbal mixtures sold in the market before using them. However, it should not be forgotten that they can contribute to the immune system in different ways, not only in terms of antioxidants, but also in terms of their content. It is a situation that must be taken into consideration when preparing the mixture formulations of plants that may have more negative effects than their contribution in terms of oxidative. Because, mixed teas prepared with different herbs can be in a synergistic interaction, as in our study, or they can be in an antagonistic interaction that will negatively affect each other's effects. Finally, we can recommend that such mixed teas should not be consumed unconsciously (without knowing the content interaction, excessive use, etc.), and should be consumed as a supplement rather than a medicine.

Scientific Ethics Declaration

The authors declare that the scientific ethical and legal responsibility of this article published in EPSTEM journal belongs to the authors.

Acknowledgements or Notes

* This article was presented as oral presentation at the International Conference on Basic Sciences, Engineering and Technology (www.icbaset.net) held in Marmaris/Turkey on April 27-30, 2023.

References

Colalto, C. (2010). Herbal interactions on absorption of drugs: Mechanisms of action and clinical risk assessment. *Pharmacological Research*, 62, 207–227.

Deska, M., Romuk, E., Anna, O., Grzegorz, S., Witold, B., Dominika, T., Birkner, E., & Gawrychowski, J. (2017). Oxidative stress and angiogenesis in primary hyperparathyroidism. *European Surgery*, *49*, 118–126.

Junio, H. A, Sy-Cordero, A. A., Ettefagh, K.A., Burns, J. T., Micko, K. T., Graf, T. N., Richter, S. J., Cannon, R. E., Oberlies, N. H., & Cech, N. B. (2011). Synergy-directed fractionation of botanical medicines: a case study with goldenseal (Hydrastis canadensis). *Journal of Natural Products, 22;74*(7), 1621-1629.

Kokdil, G. (2002). Tıbbi Çaylar. *Galenova*, *2*, 19-21.

Leonard, S. S., Cutler, D., Ding, M., Vallyathan, V., Castranova, V., & Shi, X. L. (2002). Antioxidant properties of fruit and vegetable juices: more to the story than ascorbic acid. *Annals of Clinical & Laboratory Science*, *32*, 193–200.

Oh, J., Jo, H., Cho A., R., Kim, S. J., & Han, J. (2013). Antioxidant and Antimicrobial Activities of Various Leafy Herbal Teas. *Food Control*, *31*, 403-409.

Scholey, A. B., & Kennedy, D. O. (2002). Acute, dose-dependent cognitive effects of Ginkgo biloba, Panax ginseng and their combination in healthy young volunteers: differential interactions with cognitive demand. *Human Psychopharmacology: Clinical and Experimental*, *17*, 35–44.

Stermitz, F. R., Lorenz, P., Tawara, J.N., Zenewicz, L.A., & Lewis, K. (2000). Synergy in a medicinal plant: antimicrobial action of berberine potentiated by 5'-methoxyhydnocarpin, a multidrug pump inhibitor. *Proceedings of the National Academy of Sciences, 15;97*(4), 1433-1437.

Ulrich-Merzenich, G., Panek, D., Zeitler, H., Vetter, H., & Wagner, H. (2010). Drug development from natural products: exploiting synergistic effects. *Indian Journal of Experimental Biology, 48*(3), 208-219.

Uzun, M. B., Aykac, G., & Ozcelikay, G. (2014). Improper Use and Harms of Herbal Products. *Lokman Hekim Journal, 4*(3), 1-5.

Xu, X. Y., Li, F., Zhang, X., Li, P. C., Zhang, X., Wu, Z. X., et al. (2014). In vitro synergistic antioxidant activity and identification of antioxidant components from Astragalus membranaceus and Paeonia lactiflora. *PLoS ONE, 9*,e96780.

Yaacob, N. S., Kamal, N. N., & Norazmi, M. N. (2014). Synergistic anticancer effects of a bioactive subfraction of Strobilanthes crispus and tamoxifen on MCF-7 and MDA-MB-231 human breast cancer cell lines. *BMC Complementary and Alternative Medicine, 14*, 252.

Yi, W. G., & Wetzstein, H. Y. (2011). Anti-tumorigenic activity of five culinary and medicinal herbs grown under greenhouse conditions and their combination effects. *Journal of Agricultural Food, 91*, 1849–1854.

Zhang, A. H., Sun, H., & Wang, X. J. (2014). Potentiating therapeutic effects by enhancing synergism based on active constituents from traditional medicine. *Phytotherapy Research, 28*, 526–533.

Author Information

Isik Didem KARAGOZ
Gaziantep University, Faculty of Arts and Sciences,
Department of Biology, 27310, Gaziantep, TURKEY
Contact e-mail: karagoz@gantep.edu.tr

Basak SIMITCIOGLU
Gaziantep University, Faculty of Arts and Sciences,
Department of Biology, 27310, Gaziantep, TURKEY

Ugur VURAL
Gaziantep University, Faculty of Arts and Sciences,
Department of Biology, 27310, Gaziantep, TURKEY

To cite this article:

Karagoz, I.D., Simitcioglu, B., & Vural, U. (2023). Mixture herbal tea is oxidant or not? *The Eurasia Proceedings of Science, Technology, Engineering & Mathematics (EPSTEM), 22*, 163-170.

The Eurasia Proceedings of Science, Technology, Engineering & Mathematics (EPSTEM)
ISSN: 2602-3199

The Eurasia Proceedings of Science, Technology, Engineering & Mathematics (EPSTEM), 2023

Volume 22, Pages 171-175

ICBASET 2023: International Conference on Basic Sciences, Engineering and Technology

Useful Ideas on the Numerical Techniques Used for the Solution of the Two-Point Boundary Value Problems of Ordinary Differential Equations

Mohammad H. AL-TOWAIQ
Jordan University of Science and Technology

Abstract: In this paper, we give a preview of some numerical techniques used for the solution of the two-point boundary value problems of ordinary differential equations. We discuss the difficulties one faces in using them, which need further investigation, and we suggest some ideas to overcome these difficulties.

Keywords: Ordinary differential equations, Two-point boundary Value problem.

Introduction

Two-point boundary value problems (BVP) of ordinary differential equations describe many physical phenomena in science and engineering such as electromagnetism, astronomy, mechanical vibration analysis, and many other topics. For our discussion, we will consider the following two-point BVP for ordinary differential equations

$$x''(t) = f\big(t, x(t), x'(t)\big), \tag{1}$$

with boundary conditions BCs) at two distinct points a and b of the form

$$x(a) = \propto, x(b) = \beta \tag{2}$$

This type of equation often poses a difficult challenge to the numerical analyst, since most of them are nonlinear. In most cases, analytical solutions are not available or difficult to find. Therefore, numerical methods can be used to find an approximate solution. There are different numerical methods and their modifications used to compute an approximate solution of the two-point BVP such as the shooting method (SM), finite difference methods (FDM), finite element method (FEM), collection method (CM), Galerkin method (GM), and Least Squares method (LSM), (Linz & Wang, 2003). Recently, many researchers presented certain techniques based on the above methods to compute accurate solutions to the two-point BVP.

The Shooting Method

The idea of the shooting method is to convert the BVP to an initial value problem (IVP), (Adam, & Hashim, 2014). Then we can employ a suitable algorithm for the solution of the IVP. The first initial value is $x(a) = \propto$, then we assign a real value ω to the missing initial condition $x'(a) = \omega$. Hence, the value of x at b is a function of ω, say φ(ω). So, the procedure goes as follows:

1. Compute the function φ(ω) using the IVP (1) with the initial conditions $x(a)=\propto$ and $x'(a)=\omega$.
2. Let $\varphi(\omega) = x(b)$.
3. Modify ω iteratively until we find a value which satisfies $\varphi(\omega)\cong\beta$

Difficulties:

1. The iterative approach in step 3, especially in the nonlinear case, converts to a root-finding in a single unknown ω, but not all of the root-finding methods are easy to apply. In particular, it is hard to use Newton's method since we do not have an explicit expression for the given function. Using the secant method will work fine, but the computational time is very expensive. Instead, may we can use the modified Quasi-Newton's method or the modified Broyden's method (Al-Towaiq & Abu-Hour, 2016, 2017).
2. The analysis of the shooting method is complicated by the fact that we do not know how the errors in the solution of the IVP affect the accuracy of the solution of the BVP.

Some variants have been proposed to extend the shooting method, see (Filipov et al., 2017; Perfilieva et al., 2017; Edun & Akinlabi, 2021; Arefin et al., 2022).

Finite Differences Method

The FDM is one of the most popular techniques for the solution of many two-point BVP. The method replaces the derivatives with finite differences to produce a finite system of equations. In the linear case, we obtain a linear system

$$Ax = b \qquad (3)$$

This system is easy to solve even for very small mesh sizes. But, there are some limitations:
1. There will be a serious difficulty with nonlinear discretization.
2. The error analysis is generally hard.
3. The FDM is most of the time consistent, but the resolution of the stability is not obvious and requires good technical skills, utilizing the nature of matrix A.

However, these difficulties do not prevent researchers from using the FDM, i.e. (Cicelia, 2014; Ahmad & Charan, 2019).

Collocation Method

The idea of this method is to choose a finite-dimensional space of candidate solutions and a number of points in the domain (called *collocation points*) and to select that solution that satisfies the given equation at the collocation points, as follows

1. Write an approximate solution as a linear combination of a set of basis functions

$$x_n(t) = \sum_{k=0}^{n} c_k \varphi_k(t) \qquad (4)$$

2. c_k and $\varphi_k(t)$ must be selected so that they can give an approximate solution to the BVP accurately, if possible.

Normally, equation (4) does not give equality, no matter how we select the $c_k's$ and $\varphi_k(t)'s$. The best way to do this is to select a finite number of collection points for which the equation is satisfied at these points. Several researchers attempted to use polynomial approximation, but this leads to poor conditioning. Instead, they prefer orthogonal polynomials such as the Chebyshev polynomials (Ehrenstein & Peyret, 1989; Soliman et al., 2014), while others used radial basis functions (Hu et al., 2007;Al-Towaiq et al., 2018). Nevertheless, the approach has limitations, i.e. convergence analysis and selecting the collocation points. This is a disadvantage, especially with a nonlocal basis, because the resulting matrix will be full. Also, to overcome these issues, some researchers prefer to take a local basis such as the cubic B-splines (Khalifa at al., 2008; Mittal & Jain, 2012).

Least Squares Method (LSM)

The LSM has been developed with (4) by considering the residual

$$R(x_n(t), t) = x_n''(t) - f(t, x(t), \qquad .ş$$

The coefficients in the CM are chosen to satisfy the BCs and $R(x_n,\ t_i) = 0, i = 1, 2, \dots, n-1$, where the t_i's are the collocation points. So, the $c_k's$ in (4) is chosen to minimize the integral of the square of the residual,

$$\|R\|_2^2 = \int_a^b R^2(x_n(t), t)dt \qquad (6)$$

Substitute (4) into (6), then we can obtain the $c_k's$ by solving the following linear system

$$Ac = b, \qquad (7)$$

where

$$a_{i,j} = \int_a^b h_{i-1}(t)\, h_{j-1}(t)dt,\ h_i(t) = \varphi_i''(t) - f(t, \varphi_i(t), \varphi_i'(t)),$$
$$b_i = \int_a^b g(t)h_{i-1}(t)dt, \qquad (8)$$

where $g(t)$ is the nonhomogeneous term in the DE.

The problem here, (6) does not account for the BC. To overcome this problem, we must transform the differential equation to have homogeneous BCs. Then choose the basis functions $\varphi_k(t)$, so (4) will satisfy the homogeneous BCs, which implies that (7) will give the LS solution. For example, for polynomial approximations, we may use Chebysheve polynomials, for B-splines, may the interior splines functions satisfy the homogeneous BCs, but the end ones do not. For these, may we can use a combination of several B-splines. Unfortunately, this will cause a complication in the integrals, (8), which compute the coefficients matrix A and the right-hand side of (7). Thus, the LSM becomes very expansive. An alternative of this is to use collocation, (Humboldt, 1988), which in most cases (7) becomes an overdetermined system and we cannot expect to have a solution. Hence, we can use the LS sense, which leads to another method that falls between LSM and CM called the least square collocation method (LSCM), (Kee et al., 2007; Shapeev et al., 2018; Paffuti, 2019) . The LSCM tends to be easier and more efficient than the LSM. But, this needs special treatment from the BCs. However, it turns out that whatever techniques are being used, the BC's satisfied approximately which leads to an inaccurate solution. To avoid this, may we can weigh the BCs as the collocation points increase?

Galerkin Method (GM)

This method chooses the coefficients $c_k's$ of equation (4) so that the residual is orthogonal to $\varphi_k(t)$, k =0, 1, …,n, that is

$$\int_a^b R(x_n(t), t)\varphi_k(t)dt = 0,\ k = 0, 1, \dots, n. \qquad (9)$$

This leads to a system similar to (7) with

$$a_{i,j} = \int_a^b h_{i-1}(t)\, \varphi_{j-1}(t)dt,\ h_i(t) = \varphi_i''(t) - f(t, \varphi_i(t), \varphi_i'(t)),$$
$$b_i = \int_a^b g(t)\varphi_{i-1}(t)dt. \qquad (10)$$

For this to work, the BCs of the problem should be homogeneous to be satisfied by all the functions in (4). Extensive work has been done on the analysis of the method, (Pan et al., 2005; Cicelia, 2014; Zavalani, 2015; Anulo. et al., 2017; Paffuti, 2019;Wang & Zhao, 2019), but it still is an attractive and challenging area of research. GM has a powerful numerical tool for finding fast and accurate solutions. However, when more terms are used in the trial solution, the GM presents more analytical difficulties than the other methods.

Conclusion and Future Work

The SM is very efficient, applicable, and easy to use for engineering and applied sciences problems.

The LSM and GM are very competitive with the FDM only under certain conditions. A few practical problems remain to be solved, for example

1. Improvement of the SM to solve two-point BVP for fourth-order equations, such as the Euler-Bernoulli beam equation $(a(x)u(x)'')'' + q(x)u(x) = f(x)$.
2. The FDM needs efficient improvements to handle the general boundary conditions by carrying out numerical experiments to form conjectures on the stability and order of convergence of the improvement technique.
3. Making the FDM more automatic by letting the algorithm choose the discretization for the problem in hand. In addition, is the selection of the discretization locally reduces the global error efficiently?
4. In the Collocation-Least Squares technique, carry out experimentation to see if the increasing number of collocation points will affect the estimation of the BC's and the computational complexity.
5. In general, finding the connection between the local and the global error is complicated and needs more investigation.
6. Implementing the above methods to find the solution of the problem under the general homogeneous BC's:
   $c_0x(a) + c_1x'(a) = 0$
   $d_0x(b) + d_1x'(a) = 0$

Scientific Ethics Declaration

The author declares that the scientific ethical and legal responsibility of this article published in EPSTEM journal belongs to the author.

Acknowledgments or Notes

* This article was presented as an oral presentation at the International Conference on Basic Sciences, Engineering, and Technology (www.icbaset.net) held in Marmaris /Turkey on April 27-30, 2023.

References

Adam, B., & Hashim, M. H. (2014). Shooting method in solving boundary value problem, *International Journal of Research and Reviews in Applied Sciences 21.1*, 8-30.

Ahmad, N., & Charan, S. (2019). A comparative study of numerical solutions of second order ordinary differential equations with boundary value problems by shooting method & finite difference method. *Numerical Solution of Integral Equation, 4* (1), 18-22.

Al-Towaiq, M., & Abu-Hour, Y. (2017). Two improved classes of Broyden' methods for solving nonlinear systems of equations. *Journal of Mathematics and Computer Science*, *17*, 22-31.

Al-Towaiq, M., & Abu-Hour, Y. (2016). Two improved methods based on Broyden's Newton methods for the solution of nonlinear systems of equations. *Journal of Engineering and Applied Sciences, 11*(11), 2344-2348.

Al-Towaiq, M., Ababnah, A., & Al-Shwayyat, S. (2018). An efficient approach for Solving Fisher's equation using radial basis-collocation technique. *Proceedings of 161st The IIE International Conference, Barcelona*, Spain.

Anulo, A., Kibret, A., Gonfa, G., & Negassa,G. (2017). Numerical solution of linear second order differential equations with mixed boundary conditions by Galerkin method. *Mathematics and Computer Science*, *2*(5), 66-78.

Arefin, M. A., Nishu,M.A., Dhali, M.N., & Uddin, M.H. (2022). Analysis of reliable solutions to the boundary value Problems by Using ShootMethod. *Mathematical Problems in Engineering*, Article ID 2895023, https://doi.org/10.1155/2022/2895023

Cicelia, J. E. (March 2014). Solution of weighted residual problems by using Galerkin's method, *Indian Journal of Science and Technology*, *7*(3S), 52-54.

Edun, I. F., & Akinlabi, G. O. (2021). Application of the shooting method for the solution of second order boundary value problems. *Journal of Physics: Conference Series,1734.*

Ehrenstein, U., & Peyret, R. (1989). A chebyshev collocation method for the navier–stokes equa-tions with application to double-diffusive convection. *International Journal for Numerical Methods in Fluids*, *9*(4), 427–452.

Filipov, S. Gospodinov, I., & Faragó, I. (2017). Shooting-projection method for two-point boundary value problems. *Applied Mathematics Letters*, *72*, 10-15.

Hu, H. Y., Chen, J. S., & HU, W. (2007). A weighted radial basis collocation method for boundary value problems. *International Journal for Numerical Methods in Engineering*, *69*(13), 2736-2757.

Humboldt, H. (1988). On a least-squares collocation method for linear lifferential-algebraic equations. *Numerische Mathematik*, *54*, 79-90.

Kee, B., Liu, G. R., & Lu, C. (2007). A regularized least-squares radial point collocation method (RLS-RPCM) for adaptive analysis. *Computational Mechanic*, *40*(5), 837–853.

Khalifa, A. K., & Alzubaidi, H.M. (2008). A collocation method with cubic B-splines fo solving the MRL equation. *Journal of Computational and Applied Mathematics*, *212*(2), 406-418.

Linz, P., & Wang, R. L. C. (2003). *Exploring numerical methods: An introduction to scientific computing using MATLAB.* Jones & Bartlett Learning.

Mittal, R. C., & Jain R.K. (2012). Numerical solutions of nonlinear Burgers' equation with modified cubicB-splines collocation method. *Applied Mathematics and Computation*, *218*,7839-7855.

Paffuti, G. (2019). Galerkin method for discs capacitors. *Mathematics and Computers in Simulation*, *166*, 365-381.

Pan, X. F., Zhang, X., & Lu, M. W. (2005). Meshless Galerkin least- squares method. *Comput Mech 35*, 182-189.

Perfilieva, I., Števuliáková P., & Valášek, R. (2017). Shooting method based on higher degree F-transform. *2017 Joint 17th World Congress of International Fuzzy Systems Association and 9th International Conference on Soft Computing and Intelligent Systems (IFSA-SCIS).*

Shapeev, V., Belyaev,V., Golushko,S., & Idımeshev,S . (2018). New possibilities and applications of the least squares collocation method. In *EPJ Web of Conferences (Vol. 173, p. 01012). EDP Sciences.*

Soliman, M., Al-Zeghayer Y., & Ajbar, A. (2014). A modified orthogonal collocation method for reaction-diffusion problems. *Brazillian Journal of Chemical Engineering*,*31*(4), 967 - 975.

Wang, S. W., & Xiushao Zhao, X. (2019). An interpolating element-free Galerkin scaled boundary method applied to structural dynamic analysis. *Applied Mathematical Modelling*, *75*, 494-505.

Zavalani, G. (2015). A Galerkin finite element method for two-point boundary value problems of ordinary differential equations. *Applied and Computational Mathematics*, *4*(2), 64-68.

Author Information

Mohammad H. Al-Towaiq
Jordan University of Science and Technology
Irbid, Jordan
Contact e-mail: towaiq@just.edu.jo

To cite this article:

Al-Towaiq, M. H. (2023). Useful ideas on the numerical techniques used for the solution of the two-point boundary value problems of ordinary differential equations. *The Eurasia Proceedings of Science, Technology, Engineering & Mathematics (EPSTEM), 22*,171-175.

The Eurasia Proceedings of Science, Technology, Engineering & Mathematics (EPSTEM)
ISSN: 2602-3199

The Eurasia Proceedings of Science, Technology, Engineering & Mathematics (EPSTEM), 2023

Volume 22, Pages 176-181

ICBASET 2023: International Conference on Basic Sciences, Engineering and Technology

Pin Control on Press Tables Using IoT Sensors

Emin CANTEZ
Coskunoz Holding

Oguz Alper ISEN
Coskunoz Holding

Serkan AYDIN
Coskunoz Holding

Abstract: Press machines are used to shape metal parts. There are pillow pins at the bottom of the molds in the press. Operators use manual map paper for each die to place the pins. When the pins are placed incorrectly, breakage, distortion and defects in the metal sheet occur in the mold. To prevent these errors, there is no warning system and no visual system to guide the operator. In the study, there is a motion-controlled sensor table. With pin control sensors, it is placed in the right place and the wrong pin is removed. In the system, it provides the operator to place it in the right place with the visual light system. Thus, there will be no errors in the system. The operator will start to make this process very easy. The system provides control with electronic card, plc and software. When the wrong pin is placed, the system does not operate. As a result, it provides production without making mistakes with sensor technology and smart system.

Keywords: Sensor, Plc, Smart system, Electronic board

Introduction

In the manufacturing industry, the use of press machines is a common practice for shaping, cutting, and forming various materials. These machines are operated using hydraulic or pneumatic power, and they require a high level of precision and control to ensure the quality of the final product. One critical element in this process is the press table, which serves as the working surface for the machine.

In recent years, the Internet of Things (IoT) has emerged as a promising technology for enhancing the capabilities of press machines. By using IoT sensors, it is possible to monitor and control various aspects of the press machine's operation, including the press table's movements and position. One particular area of interest is the implementation of PIN control on press tables using IoT sensors.

PIN control is a method of controlling the position of the press table during the manufacturing process. By setting specific positions for the press table, it is possible to ensure that the material being worked on is precisely positioned under the press machine's tooling. This level of precision is critical for achieving consistent results and ensuring the quality of the final product. IoT sensors can be used to monitor the position of the press table and adjust its position as necessary to maintain the desired PIN control. This approach allows for real-time monitoring and adjustment of the press table's position, ensuring that the manufacturing process remains accurate and efficient.

Overall, the implementation of PIN control on press tables using IoT sensors has the potential to revolutionize the manufacturing industry. By enhancing the precision and control of press machines, it is possible to achieve

consistent, high-quality results while reducing the risk of errors and downtime. As such, this technology is likely to become an increasingly important part of modern manufacturing operations.

Problem Description

Press machines are widely used in the manufacturing industry for shaping, cutting, and forming various materials. One critical component of press machines is the press table, which serves as the working surface for the machine. The position of the press table is crucial for achieving precise and consistent results in the manufacturing process. However, the manual control of the press table's position can be challenging and prone to human error. This can result in wasted materials, inconsistent product quality, and even damage to the press machine. Additionally, manual control can be time-consuming, leading to longer manufacturing cycles and reduced efficiency.

To overcome these challenges, implementation of IoT sensors and PIN control at press desks has been considered.. By using IoT sensors to monitor and control the press table's position, it is possible to achieve a higher level of precision and consistency in the manufacturing process. PIN control allows for the precise positioning of the press table, ensuring that the material being worked on is precisely located under the press machine's tooling.

However, there are several challenges associated with implementing PIN control on press tables using IoT sensors. One challenge is ensuring that the sensors are accurate and reliable. The sensors must be able to accurately detect the position of the press table and communicate that information to the control system in real-time. Another challenge is ensuring that the control system is robust and able to handle the complex operations involved in PIN control. The control system must be able to receive sensor data, analyze it, and adjust the press table's position as necessary to maintain the desired PIN control. This requires a high level of processing power and real-time communication capabilities.

Finally, the implementation of PIN control on press tables using IoT sensors requires careful planning and integration with existing manufacturing processes. The system must be designed to work seamlessly with the press machine and other manufacturing equipment, minimizing disruption to existing operations. Overall, the implementation of PIN control on press tables using IoT sensors will be a huge step forward in eliminating press table errors in the manufacturing industry. However, careful planning, testing, and integration are necessary to ensure the system's accuracy, reliability, and effectiveness in real-world manufacturing environments.

Literature Review

The use of IoT sensors and PIN control on press tables is a relatively new area of research in the manufacturing industry. However, several studies have already been conducted to investigate the feasibility and potential benefits of this approach.

In a study conducted by Wang et al. (2019), IoT sensors were used to monitor the position of the press table in real-time. The study found that the use of IoT sensors improved the accuracy and efficiency of the manufacturing process by reducing the risk of human error and minimizing the need for manual adjustments. Additionally, the study demonstrated that PIN control was effective in achieving precise positioning of the press table, leading to improved product quality.

Another study conducted by Li et al. (2020) investigated the use of machine learning algorithms to optimize the PIN control of press tables. The study found that machine learning algorithms could be used to analyze sensor data and adjust the press table's position in real-time to achieve optimal PIN control. The study demonstrated that this approach could improve the accuracy and efficiency of the manufacturing process, leading to reduced waste and improved product quality.

In a review article by Yan et al. (2021), the authors discussed the potential benefits of using IoT sensors and PIN control on press tables in the context of Industry 4.0. The article highlighted the importance of real-time monitoring and control in modern manufacturing processes and the potential for IoT sensors and PIN control to enhance these capabilities. The authors emphasized the need for careful planning and integration to ensure the system's effectiveness and reliability in real-world manufacturing environments.

Finally, a study by Kim et al. (2021) investigated the use of IoT sensors and PIN control on press tables in the automotive manufacturing industry. The study found that the use of IoT sensors and PIN control led to improved product quality and reduced manufacturing time and costs. Additionally, the study demonstrated that this approach was effective in handling complex manufacturing processes, such as the production of automotive body parts. Overall, the literature suggests that the use of IoT sensors and PIN control on press tables has the potential to revolutionize the manufacturing industry by improving accuracy, efficiency, and product quality.

Methods

The aim of this study is to propose a pillow pin control system using sensor technology and software system. The system combines sensor technology, algorithm and software systems to provide an inexpensive and effective pillow pin control system. The system uses sensors to detect pins on the press table to determine the correct hole for pad pin placement on the table. In this section, we will discuss the methodology used to develop the proposed system.

Sensor Installation

The first step in implementing PIN control on press tables is the installation of IoT sensors. These sensors are typically mounted on the press table and are designed to monitor the position of the table in real-time. The sensors may use different technologies, such as optical, magnetic, or capacitive, depending on the specific application.

Sensor Calibration

After the sensors are installed, they need to be calibrated to ensure accurate measurement of the table's position. Calibration involves measuring the sensor's output at various table positions and using this data to establish a calibration curve. The calibration curve is used to convert the sensor's output into a corresponding table position.

Control Algorithm Development

Once the sensors are installed and calibrated, a control algorithm needs to be developed to achieve optimal PIN control. The control algorithm takes input from the sensors and calculates the required adjustments to the press table's position to achieve the desired PIN control. The control algorithm can be developed using various approaches, such as PID control or machine learning algorithms.

Testing and Validation

After the control algorithm is developed, it needs to be tested and validated to ensure it works correctly in the real-world manufacturing environment. Testing involves subjecting the system to various manufacturing scenarios and verifying that it achieves the desired PIN control. Validation involves comparing the system's output with the actual product quality to verify that it meets the required standards.

Integration

Finally, the system needs to be integrated into the manufacturing process. Integration involves connecting the system to other manufacturing equipment, such as the press machine and the production line, to enable real-time control and monitoring of the manufacturing process. In summary, the implementation of PIN control on press tables using IoT sensors involves several steps, including sensor installation, calibration, control algorithm development, testing and validation, and integration. The specific methods used may vary depending on the application and the manufacturing environment. However, the general principles remain the same, with the ultimate goal of achieving accurate and efficient control of the manufacturing process to improve product quality and reduce waste.

Results

The implementation of PIN control on press tables using IoT sensors has shown promising results in improving the accuracy, efficiency, and product quality in the manufacturing industry.

Improved Accuracy

The use of IoT sensors and PIN control has been shown to significantly improve the accuracy of the press table's position. The sensors provide real-time monitoring of the table's position, allowing for precise adjustments to be made to achieve the desired PIN control. This has been shown to reduce the risk of human error and improve the consistency of the manufacturing process.

Improved Efficiency

The use of IoT sensors and PIN control has also been shown to improve the efficiency of the manufacturing process. The real-time monitoring and control provided by the system reduces the need for manual adjustments, leading to faster production times and reduced waste. Additionally, the system can be optimized to reduce energy consumption, further improving efficiency.

Improved Product Quality

Perhaps the most significant result of implementing PIN control on press tables using IoT sensors is the improvement in product quality. The precise positioning of the press table achieved through PIN control results in more consistent and accurate production, leading to higher-quality products. In addition, the real-time monitoring and control provided by the system enables faster detection and correction of errors, further improving product quality.

Cost Savings

The implementation of PIN control on press tables using IoT sensors has also been shown to lead to cost savings in the manufacturing process. The improved accuracy, efficiency, and product quality achieved by the system lead to reduced waste and rework, ultimately resulting in lower manufacturing costs.

Real-World Applications

Several studies have demonstrated the effectiveness of PIN control on press tables using IoT sensors in real-world manufacturing applications. For example, the system has been successfully implemented in the automotive industry for the production of body parts, leading to improved product quality and reduced manufacturing costs. In summary, the implementation of PIN control on press tables using IoT sensors has shown promising results in improving the accuracy, efficiency, and product quality in the manufacturing industry, leading to cost savings and real-world applications.

Discussion

The implementation of PIN control on press tables using IoT sensors has proven to be an effective solution for improving the accuracy, efficiency, and product quality in the manufacturing industry. The real-time monitoring and control provided by the system allows for precise adjustments to the press table's position, reducing the risk of human error and improving the consistency of the manufacturing process.

Furthermore, the system can be optimized to reduce energy consumption, resulting in cost savings for the manufacturer. The improved efficiency of the manufacturing process also leads to reduced waste and rework, further contributing to cost savings and environmental benefits.

While the results of implementing PIN control on press tables using IoT sensors have been promising, there are still some limitations and challenges that need to be addressed. For example, the sensors may be affected by environmental factors such as temperature and humidity, leading to potential inaccuracies in the system's performance. Additionally, the system's reliability may be impacted by the quality of the sensors and the stability of the internet connection.

Despite these challenges, the potential benefits of implementing PIN control on press tables using IoT sensors are significant. The system has already been successfully implemented in various industries, including automotive and aerospace, demonstrating its real-world applicability. Further research and development can help optimize the system's performance and address any potential challenges, leading to wider adoption in the manufacturing industry.

Conclusion

In conclusion, the implementation of PIN control on press tables using IoT sensors has shown promising results in improving the accuracy, efficiency, and product quality in the manufacturing industry. The real-time monitoring and control provided by the system allow for precise adjustments to be made to the press table's position, resulting in more consistent and accurate production.Furthermore, the system can be optimized to reduce energy consumption, leading to cost savings for the manufacturer. The improved efficiency of the manufacturing process also leads to reduced waste and rework, contributing to environmental sustainability.

While there are still some limitations and challenges to be addressed, such as the potential impact of environmental factors on the system's performance, the potential benefits of implementing PIN control on press tables using IoT sensors are significant. Real-world applications of the system in various industries have demonstrated its effectiveness and feasibility.

Overall, PIN control on press tables using IoT sensors presents an innovative and promising solution for improving manufacturing processes, and further research and development can help optimize the system's performance and address any potential challenges, leading to wider adoption in the manufacturing industry.

Recommendations

Based on the findings of this study, we recommend the following:

1. Further research and development should be conducted to optimize the system's performance and address potential challenges, such as the impact of environmental factors on the sensors' accuracy and the system's reliability.
2. Manufacturers should consider implementing PIN control on press tables using IoT sensors to improve the accuracy, efficiency, and product quality of their manufacturing processes. The system has already been successfully implemented in various industries, demonstrating its real-world applicability.
3. The system should be regularly monitored and maintained to ensure its optimal performance. This includes checking the quality of the sensors, the stability of the internet connection, and addressing any potential issues promptly.
4. Manufacturers should consider implementing energy-efficient measures to optimize the system's performance and reduce energy consumption, leading to cost savings.
5. Manufacturers should also consider the potential environmental benefits of implementing the system, such as reducing waste and rework, and aim to integrate sustainable manufacturing practices into their operations.

By following these recommendations, manufacturers can benefit from the improved accuracy, efficiency, and sustainability provided by PIN control on press tables using IoT sensors, leading to a more competitive and sustainable manufacturing industry.

Scientific Ethics Declaration

The authors declare that the scientific ethical and legal responsibility of this article published in EPSTEM journal belongs to the authors.

Acknowledgements or Notes

* I would like to express my gratitude to everyone who contributed to this study on PIN control on press tables using IoT sensors. We would like to thank our research team for their dedication and hard work in collecting and analyzing data and writing this report. We would also like to extend our appreciation to the participants in this study for their time and cooperation in providing us with valuable insights into the practical application of the system. Finally, we would like to acknowledge the funding support provided by our institution, which enabled us to carry out this research. Thank you all for your contributions and support

* This article was presented as an oral presentation at the International Conference on Basic Sciences, Engineering, and Technology (www.icbaset.net) held in Marmaris /Turkey on April 27-30, 2023.

References

Harlow, H. F. (1983). Fundamentals for preparing psychology journal articles. *Journal of Comparative and Physiological Psychology, 55*, 893-896.

Kong, J., Lv, Y., Wu, D., Wu, J., & Xie, J. (2019). An IoT-based real-time monitoring and control system for hydraulic press machines. *IEEE Access, 7*, 65435-65444.

Liu, W., Wang, Y., Chen, X., & Chen, L. (2018). Research on the application of IoT technology in the control system of mechanical press. *Journal of Physics: Conference Series*, *1019*(1), 012092.

Palaniappan, R., & Ramkumar, S. (2020). Real-time monitoring of press machines using IoT. *Procedia Manufacturing, 50*, 116-121.

Sodnik, J., & Zajc, M. (2017). IoT for ındustry: Implementation of smart manufacturing. *Journal of Intelligent Manufacturing, 28*(5), 1095-1105.

Tan, S., Zhang, S., & Zhu, M. (2021). Research on the data acquisition and monitoring system of high-precision press machine based on IoT. *Advances in Intelligent Systems and Computing*, *1196*, 177-187.

Tzeng, Y. C., & Huang, Y. C. (2018). An intelligent system for condition monitoring and control of mechanical presses. *Journal of Intelligent Manufacturing, 29*(6), 1343-1351.

Yan, W., Han, B., & Zhang, Y. (2020). A comprehensive control method of pressing force and position in mechanical press based on ıot technology. *Journal of Mechanical Science and Technology, 34*(9), 3737-3745.

Zhang, Y., & Yuan, X. (2020). Design of ıntelligent control system for mechanical press based on IoT technology. *IOP Conference Series: Materials Science and Engineering, 727*, 012038.

Zhang, C., Jiang, Y., & Li, J. (2018). Research on the application of IoT technology in the precision press. *IOP Conference Series: Materials Science and Engineering, 376*, 012045.

Zhou, Y., Wei, S., & Zhang, X. (2021). A smart press monitoring system based on IoT and deep learning. *IEEE Access, 9*, 69631-69641.

Author Information

Emin Cantez
Coşkunöz Holding
Fethiye OSB Sarı Cad. No:1 16140
Nilüfer Bursa Türkiye
Contact e-mail: *ecantez@coskunoz.com.tr*

Oguz Alper Isen
Coşkunöz Holding
Fethiye OSB Sarı Cad. No:1 16140
Nilüfer Bursa, Türkiye

Serkan Aydin
Coşkunöz Holding
Fethiye OSB Sarı Cad. No:1 16140
Nilüfer Bursa, Türkiye

To cite this article:

Cantez, E., Isen, O.A. & Aydin, S. (2023). Pin control on press tables using IoT sensors. *The Eurasia Proceedings of Science, Technology, Engineering & Mathematics (EPSTEM), 22*, 176-181.

The Eurasia Proceedings of Science, Technology, Engineering & Mathematics (EPSTEM)
ISSN: 2602-3199

The Eurasia Proceedings of Science, Technology, Engineering & Mathematics (EPSTEM), 2023

Volume 22, Pages 182-190

ICBASET 2023: International Conference on Basic Sciences, Engineering and Technology

Synchronization of the Timetable on Partially Overlapping Urban Transport Routes

Mirena TODOROVA
Todor Kableshkov University of Transport

Zlatin TRENDAFILOV
Todor Kableshkov University of Transport

Violina VELYOVA
Todor Kableshkov University of Transport

Abstract: In order to achieve competitive advantages of public transport over private vehicles, it is necessary to improve the quality of passenger service. This can be achieved by improving the regularity of the transportation, and reducing the waiting time at public transport stops. Each trip can be made with one or more vehicles, as well as with one or more modes of transport. A trip covers the time from departure from its starting point to arrival at the destination and a major element of the total travel time is waiting for a vehicle at the stop and namely it is the minimization of this time that is considered in the article/paper.A model has been developed for synchronizing timetables on different partially overlapping in a given section route lines, so as to reduce the interval between the arriving vehicles at the stop. The model includes passenger flow forecasting, by compiling an OD matrix for the considered route lines based on the partial use of the traditional four step demand modelling for travel planning. After determining the passenger flows, moving in the considered section of the route network, the existing timetables on route lines are synchronized under the criterion of a minimum of the total stay/waiting time of the passengers. The validation of the model is carried out by applying it to a part of the urban transport network of Sofia for two route lines, and the defined resistance function for the specific type of transport (bus transportation) is used to compile the O-D matrix

Keywords: O-D matrix, Synchronization of the tımetable, Waiting time, Urban transport, Overlapping routes

Introduction

Globally, we are moving forward to a new stage of "intermodal transport systems" for a balanced and coordinated use of all modes of transport and to make urban public transport systems attractive and efficient for citizens, who are encouraged to use them. This is also achieved by using soft and hard restrictions on car use to reduce chronic congestion and minimize damage to the urban environment.

Recently, in Bulgaria, the use of the services offered by public transport has been reduced. Therefore, various steps are being taken to improve the services offered by public transport, such as: the purchase of new buses, the introduction of innovative charging systems - the use of different subscription cards (for longer periods), tickets for a certain number of trips, for a certain time, which increases the comfort of travel and reduces costs when using public transport, synchronizing the timetables of the timetables on the different routes.

Literature Review

Regarding the articles and studies that are related to optimization of public transport schedules, it can be said that there are various methods to improve routes and travel time. In this part of the article, some of the most commonly used methods for optimization of overlapping routes on public transport lines are discussed and the statistics that consider these methods are described.

In article, Dragu et al., (2019), is shown two methods for distribution of trips between destinations - the Growth Factor Model and the Gravity Model. In the study is shown a case study using both methods, which are used for the developing of O-D Matrix, and in the conclusion of the article are described disadvantages of the both methods.

The paper, Jeongwook et al. (2019), analyses the overlapping origin–destination (O-D) pairs and the study aims according to the authors to enhance the efficiency of transit operations by collecting data from so called 'smart card automatic fare collection system". The knee points of travel demand are calculated using the Kneedle algorithm. For each of the bus routes in six districts with higher demand then the demand in Seoul, a demand-based overlap index is calculated on the basis of the overlapping O-D pairs, to evaluate the efficiency of bus operations.

In article, Mohammed & Jimi (2023), is given a comprehensive overview of the data sources, and different methods for estimating O-D models, such as: "General full-network O-D matrix estimation approach", "Iterative proportional fitting algorithm", "maximum entropy", "maximum likelihood estimation", "constrained generalized least squares", "Bayesian estimation", "Trip chaining", "Validation of trip chaining assumptions and results", "Spatial clustering", "K-means clustering", "Density-based spatial clustering". The authors also wrote about recent developments in this field like: "Innovations in alighting and transfer inference algorithms", "Real-time estimation", etc.

The purpose of the article as authors presented in Philippe et al. (1984), is to clarify the route-choice problem. This was achieved by using passenger waiting times and mathematical formulas. A field-verified formulation between the variance and the mean of the bus headway and on two headway distribution families was made first, after that are developed probabilistic mathematical formulations. After that overlapping routes are categorized as slow or fast routes and also the number of passenger selecting each type of route is shown. According to the obtained research (Philippe et al., 1984), it was concluded that the behavior of passengers waiting at city bus stops should be further investigated.

In the article, Vovsha & Bekhor (1998), is presented a new link-nested logit model of route choice. The model is a particular case of discrete choice models and is generalized-extreme-value class model. The model is made to deliver results for overcoming the route overlapping problems in transportation and has a flexible correlation structure. Two equivalent mathematical programming forms are used to- deliver the model: a general Sheffi formulation and logit-based Fisk formulation and its generalization. The loading procedure of choise is stochastic network loading procedure. The authors are using numerical examples to compare the proposed model with other models. In statistics, the logit function is the quantile function (Todorova, 2019), associated with the standard logistic distribution. It has many applications in data analysis and is applied when the passenger flows are distributed. Mathematically, logit is the inverse of the standard logistic function.

Overlapping routes is one of the most common problems in analysis of travelling in urban areas (Hoogendoorn-Lanser et al., 2003). In this document (Hoogendoorn-Lanser, et al., 2003) overlapping routes are researched and instead of one factor for the volume ot the road are proposed different factors for subroutes to consider the differences in assessment in the overlapping. Logit model is used to show the influence of each of the factors. To examine the impact of individual subroute road size factors, multinomial logit, generalized nested logit, and models of basic logit path size models are used (Hoogendoorn-Lanser, et al., 2003). In the study in (Peterson, 2007) are shown different mathematical equations for time-dependent traffic models and time-independent O-D matrices.

Method

Each trip/journey can be made with one or more vehicles, as well as with one or more modes of transportation. The same has a starting point (origin) and an end (destination) point - a journey that starts from O and has a final destination- D. In this context, walking is also considered as a mode of transport. If the travel time from O-D is considered, it consists of three elements – walking to and from the bus stops, waiting at the stops and the travelled time with the vehicles. In order waiting time to be reduced the at the stops, the developed **a**

"Methodology for optimization of vehicle timetables on partially overlapping routes" can be used. The stages of the methodology are given in Fig.1.

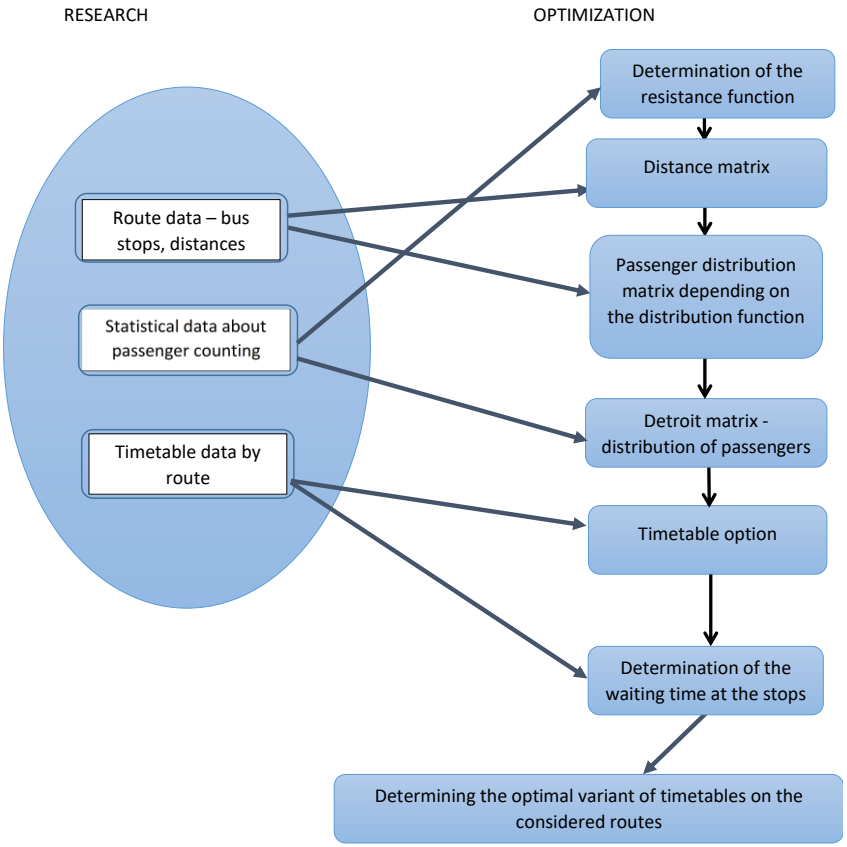

Figure 1. Stages of the "Methodology for optimization of vehicle timetables on partially overlapping routes"

In many sections of the transport network there is an overlap of two or more means of transport. If the overlap is large enough there is a passenger flow that travels exactly in that section. In this case, through the obtained O-D matrices of the individual lines of a route network, the vehicle schedule can be optimized, based on taking into account/ bearing in mind the correspondences along partially overlapping routes. Therefore, it is necessary to determine the routes that will be optimized and implement the following activities:

• Research - including the parameters of the routes themselves - stops, distances between them and determination of the general section on the basis of which the vehicle timetables will be replanned; data from studies of passenger flows for the type of transport considered and along the designated routes; as well as the current timetables on the considered routes.
• Optimization consisting of the following stages:

Determination of the Resistance Function

Passenger flows depend on various factors and are variable over time. In order to establish the upcoming changes in the directions, it is necessary periodically to be studied, as the received data should provide the opportunity for regular corrections of the transport options of the urban public transport so that it meets the constantly changing transport needs of the population.

The most widely used methods and models for determining the expected or realized passenger flows in mass urban transport are the various types of surveys among the population and physical censuses (tabular, ticket counting, chamber method, physical counting method, etc.) by routes or stops (Sarkar et al., 2017). In this way, the departures and arrivals for different stops are determined. However, there is still no clarity about the destination of the trips that start from a certain bus stop nor is it known where the trips generated for a particular bus stop come from, therefore it is necessary the trips, presented in this study area in the so-called origin-destination matrix or O-D-table (origin-destination matrix) **(**Kevin et al., 2011).

Therefore, the purpose of the distribution model is to determine the O-D table for a given forecast year. One approach to determining the distribution is to use the the resistance level/sustainability level of the travels/trips or the resistance between the zones as a measure by which to allocate trips in the first O-D table. The effort or resistance to undertaking a journey is called travel resistance (Todorova, 2019). When it comes to public transport, where the use of travel cards is a widespread case, it is obvious that this resistance can only be expressed in terms of travel time or distance. It is intuitively clear (and empirical research shows) that the number of trips to a destination decreases as the distance (or rather road resistance) to that destination increases. This effect of road resistance on trip distribution is expressed by the deterrence function $P(L_{ij})$.

Depending on the organization of urban transport, on the centers of attraction depending on the urban plan, depending on the personal characteristics of travelers and on the mode of transport, different deterrent functions are used, but most often exponential indicators or mixed functions are used. Therefore, such a function must be derived for city or town and a study should be conducted and derived.

Creating a distance matrix - for each considered route line, such a matrix is compiled and depending on the distances between the stops, the matrix is filled with number of columns and data equal to the number of stops on the considered route line.

Creating an initial matrix of passenger flows – a matrix is filled with elements obtained on the basis of the distances between them and using the derived resistance function for the settlement.

Distribution of passengers along the routes - a different "growth factor models" can be used for the urban transport routes (Todorova et al., 2018).

This is done using an initial passenger flow matrix and passenger count data on the route under consideration. After a passenger count has been carried out at the stops on a given public transport line and the number of departures and arrivals has been determined, the next step is to determine the distribution of the future journeys between the stops. The methods for the distribution of trips /distribution/ are used, stopping to use the Detroit method (Novačko 2014), in which, in addition to the growth factor for individual stops, the generalized growth factor is also taken into account. All this can be expressed mathematically as follows:

$$T_{ij}^{k} = T_{ij}^{k-1}.\left(\frac{F_i^{k-1} * F_j^{k-1}}{F^0}\right) \quad (1)$$

$$F^0 = \frac{P^*}{P^0} \quad (2),$$

where:
P^0 – volume of the actual correspondences
P^* – volume of estimated correspondences
F_i^0 ; F_j^0 – growth factors
T_{ij}^0, T_{ij}^1, T_{ij}^* – actual, estimated and estimated correspondences

For a comparison between the estimated and calculated correspondences, one resorts to approximate methodological solutions, and then ratio (1) takes the form:

$$F_i^{(k-1)} = O_i / \sum_i T_{ij}^{(k-1)}$$
$$F_j^{(k-1)} = D_j / \sum_i T_{ij}^{(k-1)}$$

where:
T_{ij}^{k} - future flow ij

$T_{ij}^{(k-1)}$ – current flow ij
O_i–future generated flow at stop i
$\sum_i T_{ij}^{(k-1)}$ - current generated flow at stop i

D_j – future (wheigthed center) attraction of stop j

$\sum_i T_{ij}^{(k-1)}$ - current attraction of stop j

k- the iteration number.

Detroit's method is not difficult to read and allows to determine predictions with great accuracy. This model uses an iterative process to approach the final solution. The results of the computations of each iteration constitute the input data for the next. This process is carried out until an approximation is obtained between the predetermined values of boarded - disembarked passengers and the size of the correspondences obtained as a result of the calculations for a given stop / that is, the coefficients F_i^K, F_j^K tend to approximate to 1 (3).

$$F^0 \rightarrow 1, F_i^K \rightarrow 1, F_j^K \rightarrow 1 \qquad (3)$$

Based on the obtained distributions, the correspondences between the stops of the overlapping routes and the size of the passenger flows are obtained. Determination of timetable options for the purpose of optimization - the real timetables of the vehicles are considered and an optimization strategy is determined depending on the frequency of the vehicles - do we have a main line with a small interval between the vehicles **(**Todorova et al. 2017) and others with a large interval or we have lines with close vehicle intervals.

The Waiting Time for the Vehicle at a Stop

The waiting time for the vehicle starts from the moment the passenger arrives at the stop until the moment he gets on the vehicle. Obviously, this time will be a function of the movement interval, varying within the limits $0<=t_{waiting.min} =< I_{movement}$. Taking into account the random nature of the arrival of the passengers at the stop and the arrival of the vehicle, where the movement intervals are random variables varying from 0 to 2 $I_{movement}$, the waiting time of the vehicle is:

$$t_{waiting}=\frac{I_{movement}}{2}(1+\vartheta(t)^2) \qquad (4)$$

$\vartheta(t)$– – coefficient of variation of real movement intervals.

Taking into account that the time that the passenger spends waiting for a vehicle at a bus stop of mass urban transport, represents 20% of the total travel time, the reduction of this component appears to be a reserve, not only for reducing the "resistance" of movement, but also for attracting new potential passengers. In order to determine the size of the passenger hours for waiting for a vehicle, it is necessary to determine the size of the passenger flow for the given traffic interval and the corresponding waiting time.

$$H_{ijm}=\sum_m (N_{pasenger\ flow,m} * t_{waiting,ij}^m) \qquad (5)$$

where:

$\sum_m N_{pasenger\ flow,m}$ - the passenger flow for a time interval m=1,M moving along a route between stops ij;

$t_{waiting}{}_{ij}^{m}$- the time for the passenger to wait for the vehicle for a time interval k moving along a route between stops ij;

Optimization of timetables – the criterion for optimization is minimization of passenger hours waiting for the vehicles at the stops. For the different variants, the average interval between the vehicles arriving at the stop, their root mean square deviation, the coefficient of variation of the arrival interval and hence the magnitude of the vehicle waiting time are determined. Using the determined passenger flow for the given time range, the passenger waiting hours for the train are also calculated. The variant with the minimum value of this parameter gives us the optimal schedule for the given lines. If we have another line with a smaller passenger flow, it is also included in the variant formation.

$$\sum_m Hijm \rightarrow \min \qquad (6)$$

Case Study

Models for non-modal distribution (moving with one mode of transport) are considered. Two routes are presented with buses are overlaping each other within 8 bus stops for a length of 4.5 km. One line is number 11 and the route is double radial with a total length of 16 km, and the other route is 404 - with a radial route and a route length of 13 km (the route diagram is given in Fig. 2).

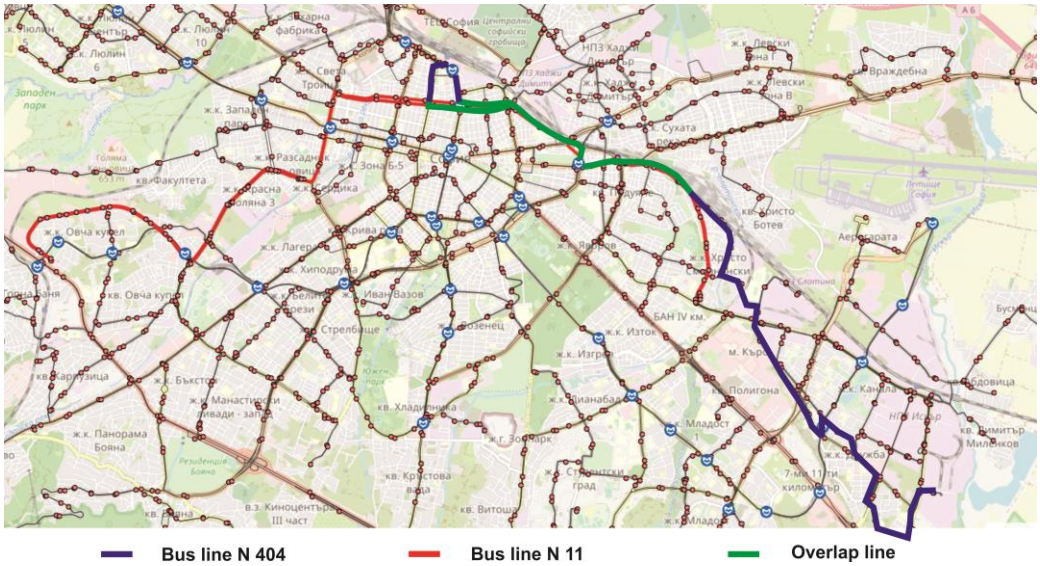

Figure 2. Routes of the considered lines 11 and 404

A study was made of the passenger flows on selected lines of Sofia's public transport. In this case, the physical counting method is used, through counters at the stops, and the number of passengers who boarded and disembarked is determined. Figure 3 shows the count of one of the directions on route line 11, while there are similar data for the opposite direction and for bus line 404.

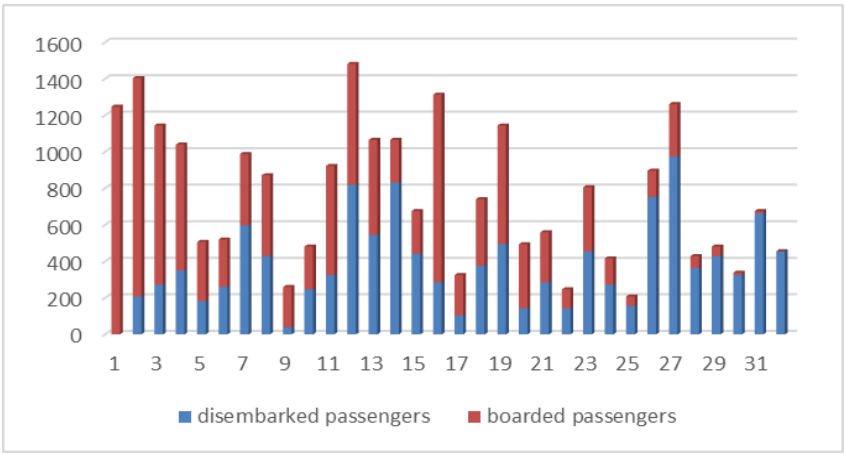

Figure 3. Number of boarded and disembarked passengers through route number 11

In order to determine the passengers moving only in the overlap section of the two lines, several matrices are compiled: first a matrix of the distances between stops, then a matrix of the generated passengers using the resistance function and the distances between stops. In this case, the derived resistance function is used from a study done on bus lines in the territory of Sofia and presented in (Todorova, 2019). It has the form:

$$P(L_{ij}) = d + a.e^{b.L_{ij}}.L_{ij}^{c} \qquad (7)$$

where:

Lij – is the distance traveled by the passenger from stop i, where he gets on, to stop j, where he gets off;

a, b, c, d - are coefficients of the function and are a=52.77; b= -0.82; c=1.31 and d =2.

In the resulting matrix of generated passengers, the Detroit method is applied and only the passenger flows for each direction and line are obtained separately. Using these data, the combined passenger flows for each direction are obtained, the distribution of which by time ranges is given in Figure 4.

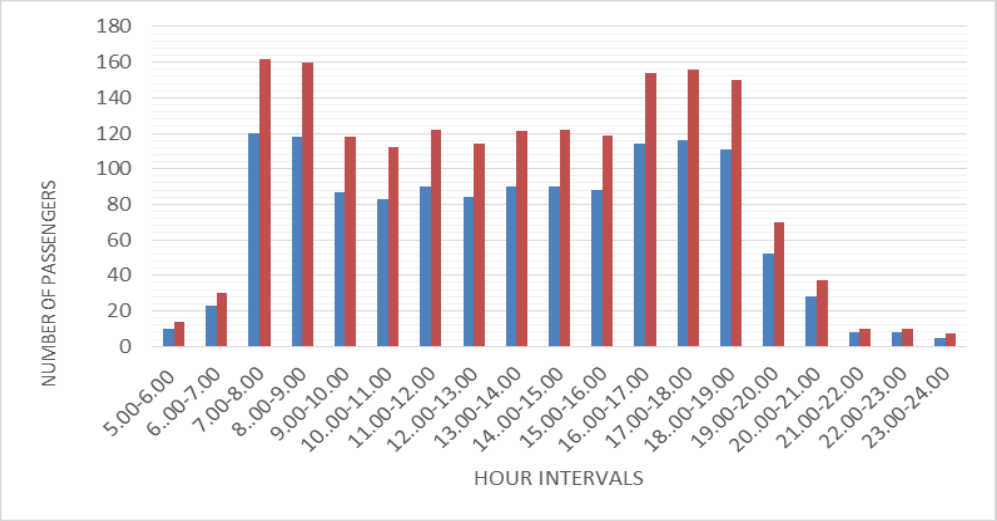

Figure 4. Number of passengers with destinations in the overlap section per day

The intervals between vehicles moving on the two route lines are almost with the same duration of time, differing in given time ranges by a minute or two. For this reason, a change in the timetable will be proposed, due to a recalculation of the movement intervals between the means of transport, based on their arrival at a given stop, regardless of the number of the line.

The determination of the new vehicle movement intervals is based on the obtained average intervals in each of the stops between the means of transport serving the two considered lines for the time ranges from 5 to 24 hours per hour. When determining the waiting time of the vehicle, data on the delay along the entire course (average delay) is used, and this delay is probabilistically distributed for each of the time intervals and participates in determining the coefficient of variation of the real intervals of movement.

Results and Discussion

The results for determining the optimization criterion passenger-hours waiting for a vehicle in one of the directions are given for the real traffic schedule in Figure 5, and for the proposed schedule in Figure 6.

time range	1	2	3	4	5	6	7	8	9	10	11	12	13	14	15	16	17	18	19
m	5-6	6-7	7-8	8-9	9-10	10-11	11-12	12-13	13-14	14-15	15-16	16-17	17-18	18-19	19-20	20-21	21-22	22-23	23-24
$t_{movement}$	7.800	8.714	6.300	6.778	7.857	9.714	8.250	8.143	8.000	7.429	8.857	7.000	6.222	7.000	7.222	10.000	13.500	13.500	16.500
$\vartheta(\tau)$	0.264	0.16	0.2	0.385	0.247	0.23	0.300233	0.299	0.308	0.338	0.312	0.2197	0.348	0.27	0.247	0.143	0.117	0.132	0.11
$t_{waiting}$	4.172	4.469	3.276	3.891	4.168	5.114	4.497	4.435	4.379	4.139	4.860	3.669	3.488	3.755	3.831	5.102	6.842	6.868	8.350
$N_{passenger,m}$	14	30	162	160	118	112	122	114	121	122	119	154	156	150	70	37	10	10	7
H_{ijm}	58.405	134.061	530.712	622.593	491.853	572.778	548.613	505.638	529.914	504.912	578.300	565.017	544.109	563.273	268.199	188.783	68.424	68.676	58.449
														SUM of Passenger-hours waiting time for the vehicle					123.378

Figure 5. Waiting for a vehicle measured in passenger-hours in a real schedule

time range	1	2	3	4	5	6	7	8	9	10	11	12	13	14	15	16	17	18	19
m	5-6	6-7	7-8	8-9	9-10	10-11	11-12	12-13	13-14	14-15	15-16	16-17	17-18	18-19	19-20	20-21	21-22	22-23	23-24
$t_{movement}$	8	9	6	7	8	10	8	8	8	7	9	7	6	7	7	10	13	13	17
$\vartheta(\tau)$	0.1	0.11	0.21	0.23	0.18	0.23	0.26	0.25	0.22	0.2	0.21	0.18	0.21	0.23	0.14	0.11	0.1	0.1	0.1
$t_{waiting}$	4.04	4.554	3.132	3.685	4.130	5.265	4.270	4.250	4.194	3.640	4.698	3.613	3.132	3.685	3.569	5.061	6.565	6.565	8.585
$N_{passenger,m}$	14	30	162	160	118	112	122	114	121	122	119	154	156	150	70	37	10	10	7
H_{ijm}	56.560	136.634	507.433	589.624	487.293	589.624	520.989	484.500	507.426	444.080	559.116	556.464	488.639	552.773	249.802	187.239	65.650	65.650	60.095
														SUM of Passenger-hours waiting time for the vehicle					118.493

Figure 6. Waiting for a vehicle measured in passenger-hours under the new proposed schedule

As found for this direction, the total waiting time in passenger-hours per vehicle for the new timetable variant saves 4 hours and 53 minutes of passenger-hours per day.

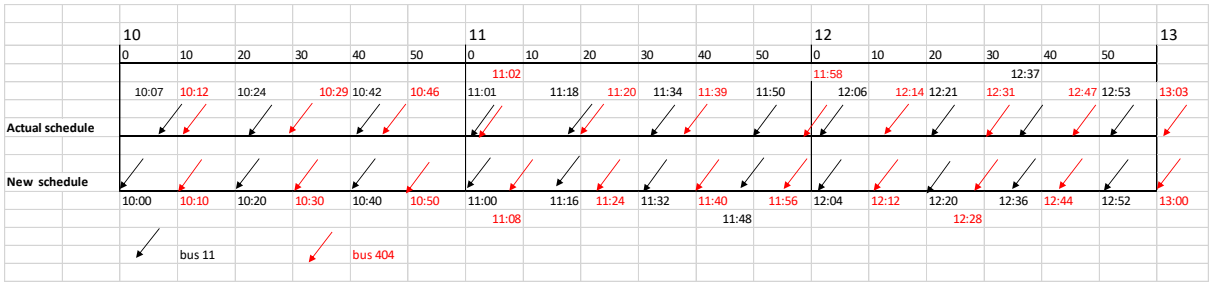

Figure 7. Schedules for the movement of vehicles for the interval from 10 a.m. to 1 p.m. for the first general stop in one of the directions.

Figure 7 shows the change in the traffic schedule of the vehicles on the two lines for 3 intervals/ ranges of hours. This change will result in a reduction of 8,50 passenger-hours waiting time per vehicle at these 8 stops per day for both directions, or one business day.

Conclusion

The developed method includes a sequence of steps that are in the field of passenger flow forecasting and methods for optimizing the organization of vehicle movement in urban transport. In order to be able to use the method, it is necessary to have a preliminary study of passenger flows along the studied lines.The article examines lines on which the interval of movement of the vehicles included in the schedule that are almost with the same duration of time and the approach to determine the new schedule is based on their even distribution using their average value by hourly periods and the coefficient of variation of the real intervals of movement. The obtained results show the possibility of applying the method in similar cases, because the reduction in passenger hours waiting time for vehicles is significant, as well as for the optimization of vehicle schedules.

Recommendations

The results of the applied method should be provided to the urban mobility centre, which manages urban transport in Sofia.

Scientific Ethics Declaration

The authors declare that the scientific ethical and legal responsibility of this article published in EPSTEM journal belongs to the authors.

Acknowledgements or Notes

* This article was presented as oral presentation at the International Conference on Basic Sciences, Engineering and Technology (www.icbaset.net) held in Marmaris/Turkey on April 27-30, 2023.

* The authors wish to acknowledge “Todor Kableshkov” University of Transport-Sofia, Bulgaria for funding the Project "Traffic and public transport management models" – within which the research presented in this paper has been developed.

References

Dragu, V., & Roman, E. A. (2019). The origin–destination matrix development. In *MATEC Web of Conferences* (Vol. 290, p. 06010). EDP Sciences.

Hoogendoorn-Lanser S., & Bovy P. et al. (2003). Modelling overlap in multimodal route choice by including trip part-specific path size factors. *Transportation Research Record: Journal of the Transportation Research Board. Volume 2003*, Issue 1, https://doi.org/10.3141/2003-10. https://journals.sagepub.com/doi/10.3141/2003-10

Jeongwook S., Shin-Hyung Ch., Dong-Kyu K., & Peter P. (June 2020). Analysis of overlapping origin-destination pairs between bus stations to enhance the efficiency of bus operations. *Wiley. IET Intelligent Transport Systems 14*(6):545–553. https://doi.org/10.1049/iet-its.2019.0158-

Kevin B. Modi, L. B. Zala, F. S. Umrigar, T. A. Desai, (2011),"Transportation planning models: A review", *National Conference on Recent Trends in Engineering & Technology, B.V.M. Engineering College*, V.V.Nagar, Gujarat, India, 13-14 May 2011

Mohammed M., & Jimi O. (March 2023). Origin-destination inference in public transportation systems: A comprehensive review. *International Journal of Transportation Science and Technology Volume 12*, Issue 1, Pages 315-328. https://www.sciencedirect.com/science/article/pii/S2046043022000223

Novačko, L., Šimunović, Lj., & Krasić, D., (2014). Estimation of origin-destination trip matrices for small cities. *Traffic &Transportation, Vol. 26*, No. 5, 419-428

Vovsha, P., & Bekhor, S. (1998). Link-nested logit model of route choice: overcoming route overlapping problem. *Transportation Research Record, 1645*(1), 133-142.

Peterson, A. (2007). *The origin-destination matrix estimation problem: analysis and computations* (Doctoral dissertation, Institutionen för teknik och naturvetenskap).

Marguier, P. H., & Ceder, A. (1984). Passenger waiting strategies for overlapping bus routes. *Transportation Science, 18*(3), 207-230.

Sarkar, P. K., Maitri, V., & Joshi, G. J. (2017). *Transportation planning: Principles, practices and pol*icies. PHI Learning Pvt. Ltd..

Todorova, M., Dinchev, D., & Trendafilov, Z.l., (2017). Possibilities to reduce travel time for passengers using public transport, magazine„*Intermodalen and rail transport", br.12*/2017 g.

Todorova M., & Asenova S., (2018). Application of "Growth Factor"model for projecting passengers in a city route line. *57th International scientific conference RU and SU "New industries, Digital Economy, Society - projecting of the future*".http://conf.uni-ruse.bg

Todorova M., (2019). Study on deterrence function of passenger flows in urban transport. *XXIV International scientific conference "TRANSPORT 2019", Academic journal„Mechanics Transport Communications.* article ID 1782

Author Information

Mirena Todorova
Todor Kableshkov University of Transport
Address: 1574 Sofia, 158 Geo Milev Str., Bulgaria
Contact e-mail: mtodorova@vtu.bg

Zlatin Trendafilov
Todor Kableshkov University of Transport
Address: 1574 Sofia, 158 Geo Milev Str, Bulgaria

Violina Velyova
Todor Kableshkov University of Transport
Address1574 Sofia, 158 Geo Milev Str., Bulgaria

To cite this article:

Todorova, M. Trendafilov, Z. & Velyova, V. (2023). Synchronization of the timetable on partially overlapping urban transport routes, *The Eurasia Proceedings of Science, Technology, Engineering & Mathematics (EPSTEM), 22*, 182-190.

The Eurasia Proceedings of Science, Technology, Engineering & Mathematics (EPSTEM)
ISSN: 2602-3199

The Eurasia Proceedings of Science, Technology, Engineering & Mathematics (EPSTEM), 2023

Volume 22, Pages 191-198

ICBASET 2023: International Conference on Basic Sciences, Engineering and Technology

Stance Classification for Fake News Detection with Machine Learning

Maysaa ALSAFADI
Karadeniz Technical University

Abstract: The variety of resources and applications available nowadays made the growth of the news rapid; that allowed people to share their opinions, articles, news, etc.; regardless of the truth percentage they have, which caused the belief that lots of the news can be posted or published through social media and news platforms by an automatic pot or fake user for this purpose. Fake news detection (FND) is a binary classification task; that indicates if the news is right or not right, which involves predicting the probability that a certain news article is designed to be deceptive. Commonly, fake news is produced for political and financial purposes, e.g., influencing presidential elections or manipulating the stock market. Although many studies have been conducted to detect news in English as fake news, the evaluation of the credibility of news written in Arabic is still in its early stage. where FND in Arabic languages got underway to receive more interest in the last years, and many detection approaches present some ability to detect fake news on multiple datasets. Then interest in effective detection models has been growing; specifically, in the Arabic language which has lagged behind the work in other languages. In this paper, we used deep learning models and applied a convolutional neural network and long short-term memory (CNN-BiLSTM) with optimization of Stochastic gradient descent (SDG); to the Arabic accessible dataset called AFND; referring to Arabic Fake News Detection. Our experimental results based on the existing AFND dataset indicate an encouraging and good performance; as we reach an accuracy of 87.7%. We appraise the problem of detecting fake news as one of the classification problems; i.e., our target is to classify a given news as credible or not credible; where credibility is often defined in the sense of believability and quality.

Keywords: Fake news detection, Deep learning, Bidirectional long short-term memory, Convolutional neural network

Introduction

Nowadays, the internet has become an integral part of our lifestyle. Anyone can publish anything with creditable content or not that can be consumed by social networking; as the traditional information channels' roles such as newspapers and television on how we collect and consume news have become less prominent than in the past, e.g, in the "Arab Spring"; social media platforms had a vital cause to spread news and rumors, it is used as a communication tool between different sides in various revolutions across the Arab world in 2011. Due to this, many scientists and specialists have been focused on studying the fake news phenomenon; by providing solutions to detect the fake misleading information incompatible with factual reality (Gabrielle et al., 2022).

FND is a partial form of stance detection problem; as stance detection is defined as a problem related to social media analyses, information retrieval, and natural language processing, which focus on detecting the attitude of a person from their published texts', towards a specific target like an idea, concept or event, either explicitly written in the published text or implied. or implied only. Recently, the interest in effective detection techniques to identify such phenomena has been growing very fast, with many models that performed optimally across all datasets in terms of machine learning algorithms; particularly deep learning-based methods. DL is a part of machine learning which used to model and fix complex problems by applying artificial neural networks with multiple layers. It involves the use of algorithms that require large amounts of data to train effectively and can

be computationally expensive to run. with the integration of deep learning and text-based processing, we can fix fake news problems by building classifiers that can classify the news data.

Referring to the published studies and models, most of them have been conducted to identify news in the English language as credible or not credible, as we noticed the research related to the Arabic language is less, due to the lack of a labeled Arabic fake news dataset, which is still a bottleneck for advancing computational solutions to mitigate the false information spread in Arabic content. The task (Khalil et al., 2021) is a contribution to filling this gap; they proposed an Arabic fake news corpus, which consists of 606912 articles collected from 134 Arabic online news sources; then they applied different AL and ML algorithms for the detection task with the proposed dataset. Another number of related research has been published particularly since the 2016 US election. The researchers (Al-Yahya et al., 2021) provided a comparative study of neural networks and transformer-based approaches using four datasets, the authors analyzed whether current advances in deep learning models and large-scale language models for the Arabic language can be effectively applied to the task of Arabic FND. The results of this study demonstrated that transformer-based models outperform the neural network-based solutions, which led to an increase in the F1 score from 0.83 to 0.95, and it boosted the accuracy by 16%. In another research effort by (Ghaith et al., 2019) they utilized four algorithms, namely Random Forest, Decision Tree, AdaBoost, and Logistic Regression to identify fake news from Arabic tweets; and the experimental evaluation shows that the system can filter out fake news with an accuracy of 76%. The authors (Elgendy et al.,2022) evaluated transformer-based classifiers for the FND task while applying eight state-of-the-art Arabic contextualized embedding models, which were XLM-Roberta, GigaBERTv4, Arabert, Arabic-Bert, ArBert, MARBert, Araelectra, and QaribBert. Experimental evaluations lead to an accuracy exceeding 98%. (Antoun et al., 2020) the research introduced the AraBERT methodology as a pre-train BERT for the Arabic language; by following up on reaching the same success that BERT did for the English language. They evaluated AraBERT on three Arabic NLU various downstream tasks. The results showed AraBERT achieved performance on most tested Arabic NLP tasks. In the research shared by (Darwish et al.,2020) they filtered the tweets of the 5,000 most active users with 10 tweets at least; based on user-stated locations. They applied four different classifications on two training sets, namely using fastText, SVM with retweeted accounts (SVMRT), and with all words as features (SVMT EXT), and finetuned BERT embeddings with a dense neural layer and SoftMax output (BERT). As the results show, BERT provided the best results for most topics, with the highest overall averages across all scores. (Shaina et al.,2022) proposed a model called fake news detection through news content and social context (FND-NS), which fits the bidirectional and auto-regressive transformers (BART). By using NELA-GT-2019 and Fakeddit as real-world datasets, and the result was 74.89%, 72.40%, 77.68%, 70.4%, and 74.95% for accuracy, precision, recall, AUC, and F1-score respectively.

On the other hand, some projects are working on prediction of the fake news by providing a model to determine the credibility of news articles in the early stages after publishing news on social media, as the DSS model proposed by (Davoudi et al.,2022); which analyze the sentiments of replies related to the news articles by constructing the stance network and extracting various graph-based features. The proposed model is evaluated on the FakeNewsNet repository, comprising two recent well-known datasets in the field, namely PolitiFact and GossipCop. The results outperformed the state-of-the-art methods by 8.2% on PolitiFact and 3% on the GossipCop datasets. Another fake news detection system proposed by (Huang et al.,2020) which based on an ensemble learning model using deep learning techniques. They highlight the difficulty in identifying fake news due to their similarities with real news. They propose a system that preprocesses and analyzes news articles using different training models. The ensemble learning model combines four different models: embedding LSTM, depth LSTM, LIWC CNN, and N-gram CNN. To achieve higher accuracy in fake news detection, the authors optimize the weights of the ensemble learning model using the Self-Adaptive Harmony Search (SAHS) algorithm. Experimental results show that the proposed model outperforms state-of-the-art methods, achieving the highest accuracy of 99.4%. They also investigate the issue of cross-domain intractability and achieve the highest accuracy of 72.3% in that scenario.

CNN-BiLSTM is one of the most popular and best deep learning models, and several studies deployed it in experiments by adding different changes in the architecture. The study of (L. Baniata et al., 2016) presents a deep learning model for sentiment analysis of Arabic text. The research highlights that while sentiment analysis research has predominantly focused on English text, limited research has been conducted on other languages like Arabic. The proposed model combines Convolutional Neural Network (CNN) and Bi-directional Long Short-Term Memory (BiLSTM) to analyze the sentiment of Arabic text. A comparison between two architectures, CNN-BiLSTM and BiLSTM-CNN, demonstrates that CNN-BiLSTM achieves a test accuracy of 86.43% and provides a better representation of sentence features. The study concludes that the CNN-BiLSTM model is highly effective for sentiment classification in Arabic text. (Ouassil et al., 2022) proposed a fake news detection system that combines word embedding techniques and a hybrid deep learning model. The authors

highlight the prevalence of fake news in online sources and the need to detect and prevent its spread. They present a deep learning approach that combines different word embedding techniques with a hybrid Convolutional Neural Network (CNN) and Bidirectional Long Short-Term Memory (BiLSTM) model. The authors trained their classification model on an unbiased dataset called WELFake. They found that the best results were achieved by combining a pre-trained Word2Vec CBOW model and a Word2Vec Skip-Word model with a CNN on BiLSTM layers. This combination achieved an accuracy of up to 97%. In conclusion, the paper introduces a novel method for detecting fake news using the WELFake dataset. The approach involves representing words as numerical vectors through various word embedding techniques and training a hybrid CNN and BiLSTM model. The results demonstrate improved accuracy and precision compared to traditional machine learning algorithms and related work. Another deep learning approach was introduced by (Alharbi, 2021) for Arabic sentiment analysis by combining Convolutional Neural Network (CNN) and Bidirectional Long Short-Term Memory (BiLSTM) architectures with a Support Vector Machine (SVM) classifier.

The conventional deep learning architecture is modified by replacing the fully connected layer with an SVM classifier that utilizes embedded vectors extracted by CNN and BiLSTM for the polarity classification of Arabic reviews. The proposed method is evaluated on three publicly available datasets, and the results demonstrate superior performance compared to baseline algorithms of CNN and SVM on all datasets. The model outperforms one of the state-of-the-art deep learning models as well. The author concluded that their model, which combines CNN, BiLSTM, and SVM, is effective for Arabic sentiment classification. They suggest further improvements such as addressing issues like negation handling and exploring deeper layers and diverse architectures on different Arabic benchmark datasets. The task of (Abdelhady et al., 2022) presented an effective stacked ensemble deep learning framework, Stacked-CNN-BiLSTM-COVID, for sentiment analysis of Arabic COVID-19 tweets. The model combines Convolutional Neural Network (CNN) and Bidirectional Long Short-Term Memory (BiLSTM) to categorize Arabic tweets. Word embedding models, namely Aravec, FastText, and ArWordVec, are used to represent the tweets as vectors and assess their impact on the model's performance. The proposed model is compared to other deep learning models such as CNN, LSTM, and BiLSTM, and experiments are conducted on three Arabic datasets related to COVID-19 and vaccines. The empirical findings demonstrate that the Stacked-CNN-BiLSTM-COVID model outperforms other models, achieving high F-measure scores of 76.76%, 87.25%, and 80.5% on the SenWave, AraCOVID19-SSD, and ArCovidVac datasets, respectively. The study highlights the importance of using stacked ensemble learning and word embedding approaches for accurate sentiment analysis of Arabic COVID-19 tweets.

In this paper, we describe the steps involved in the detection of the fake news process, including data collection, preprocessing, feature extraction, model selection, model training, and evaluation. The paper also highlights the effectiveness of stance classification-based fake news detection and its potential to be integrated into social media platforms to prevent the spread of fake news. Our contribution includes applying the deep learning techniques with the optimizer SGD which helps us to achieve an accuracy of 87.7% after many experiments. We used a large Arabic fake news corpus in our experiments; which is needed to train the ML algorithms particularly deep learning models.

Method

This section shows the datasets used in our experiments with the experimental settings, the preprocessing techniques then baseline method. Deep learning has high efficiency for stance classification with big data; it can be used to develop automated systems for fake news detection. Deep learning models can analyze large amounts of data and learn patterns that are indicative of fake news. By training those models on a dataset of labeled news articles and social media posts, it is possible to develop an effective fake news detection system.

Dataset

In our experiments, we used a large Arabic dataset called AFND; which was proposed by (A. Khalil et al., 2022) AFND was collected from newspaper and feed parser Arabic news articles. It contains 606912 public news articles that were scraped from 134 public news websites of 19 different Arab countries that include: Levant countries (Jordan, Palestine, Lebanon, and Syria), Arab Gulf countries (United Arab Emirates, Saudi Arabia, Kuwait, Qatar, Bahrain, and Oman), Arab Maghreb countries (Algeria, Morocco, Tunisia, Libya, and Mauritania), Yemen, Iraq, Egypt, and Sudan; AFND is publicly accessible. (Table 1) presents some statistical information about the corpus articles and the online sources.

Table 1. AFND statistical information

Statistics	Credible	Not Credible	Undecided
Source count	52	51	31
Articles count	207310	167233	232369
Average number of words in body text	230	217	254
Average number of words in headline	9	10	9

AFND dataset is available in JSON format; 134 news sources are stored in separate single JSON files with details including the title, text, and published date for each news article. Each news article source has a key and value. The key is the source name, and the value is a dictionary that contains the source label and two lists. The first list has the RSS website links and the second one has the website links of the local news pages. We collected those JSON files in one CSV and PKL file for the modeling process.

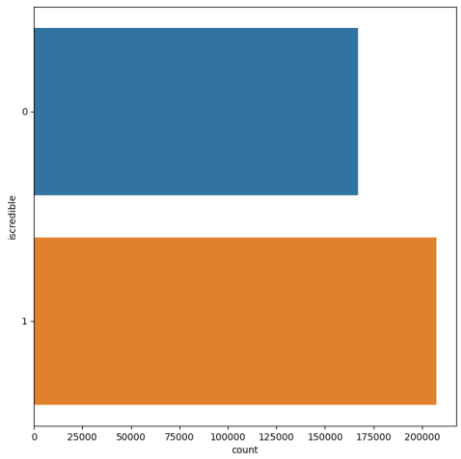

Figure 1. The number of samples per label

In this experiment, we use binary classifications; the number of articles for the training and testing are 83616 and 250850, respectively. The articles that are labeled in the dataset as "undecided" were ignored. Classification tasks used distant labeling, where each article is labeled with the same label as the corresponding source credible or not credible (Khalil et al., 2021). Figure 1. presents the number of samples per label; it indicates the imbalanced dataset that caused overfitting in the first experiment we did, as each class of data has not an equal number of observations in the dataset. We balanced the training dataset using the python Undersampling library scikit-learn. Finally, we use the balanced dataset to train a machine learning model. The reason for balancing a dataset is to prevent a machine learning model from being biased towards one class due to an unequal representation of data in the training set

Pre-preprocessing

Data preprocessing is processed to clear Arabic and non-Arabic digits, words, white spaces, websites, punctuation, and symbols. The natural language toolkit (NLTK) and the Arabic-Stopwords Python libraries were used to remove stop words. The normalization technique was applied using Tashaphyne (Taha, 2023) to extract the root for each Arabic word. Finally, a vocabulary dictionary of 196400 tokens was generated to create word sequences by assigning a unique digit for each word. Figure 2. visualize the distribution of the number of words in a text.

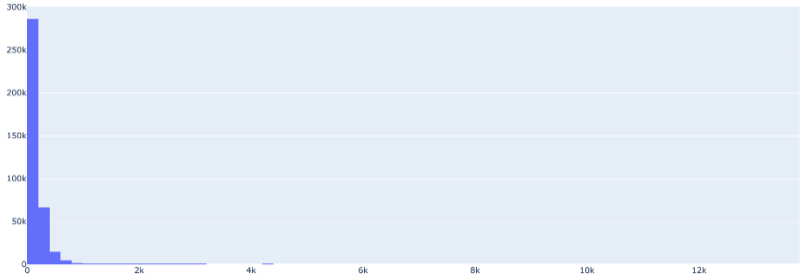

Figure 2. The distribution of number of words in a text

The preprocessing module cleans the text and minimizes the vocabulary while preserving meaning; it comprises the below five steps:

1. Word encoding using word embeddings.
2. Tokenization by splitting text into individual words.
3. Punctuation marks and Arabic stop words removal
4. Stemming and limitizer is tested and the result was the best with the limitizer function which convert the words to thier base form using a dictionary lookup.
5. Removing special characters and numbers and non- arabic characters.

Classification Model

The purpose of classification is to predict previously unseen items based on inferences derived by training on a set comprising news articles and their labels. We first describe the basic elements of our used architecture and motivate why we chose it. The first stage of the model, we use an Embedding layer to to generate inputs that are a combination of word sequences and embedded features. In general, an embedding layer is a type of layer in a neural network that is commonly used in natural language processing (NLP). Its purpose is to map input data (such as text) into a lower-dimensional space, known as an embedding space. This mapping allows the network to better understand the relationships between the inputs and make more accurate predictions. We use one-dimensional Convolutional layer (CNN) with specifying the number of filters as the output dimension, the kernel size as 3, and the activation function as 'relu' (rectified linear unit). We equalize article lengths in the preprocessing stage by zero-padding or truncation, such that the article length is constant, leading to constant channel size for all articles.

Following the Convolutional layer, we employ a type of recurrent neural network (RNN); the bidirectional Long Short-Term Memory (BiLSTM) layer because the news we predict represents word sequences, and this type of layer is specialized in learning long-term dependencies in text (Ciprian-Octavian, 2023). A further reason to employ such a layer is that it uses two simple LSTM architectures that input sequence in both directions simultaneously. This allows the model to capture both the past and future context of each word in the input sequence. We use dropout layers to deactivate a percentage of the outputs coming from the previous layer; thus, we reduce overfitting by creating artificial noise and improve the generalization capacity of the network when new, unknown data is fed for prediction. We use dense layers with linear activation as a connection between the network layers, and a final dense layer with a softmax activation function to produce the classification result, i.e., the probability of the post to be true.

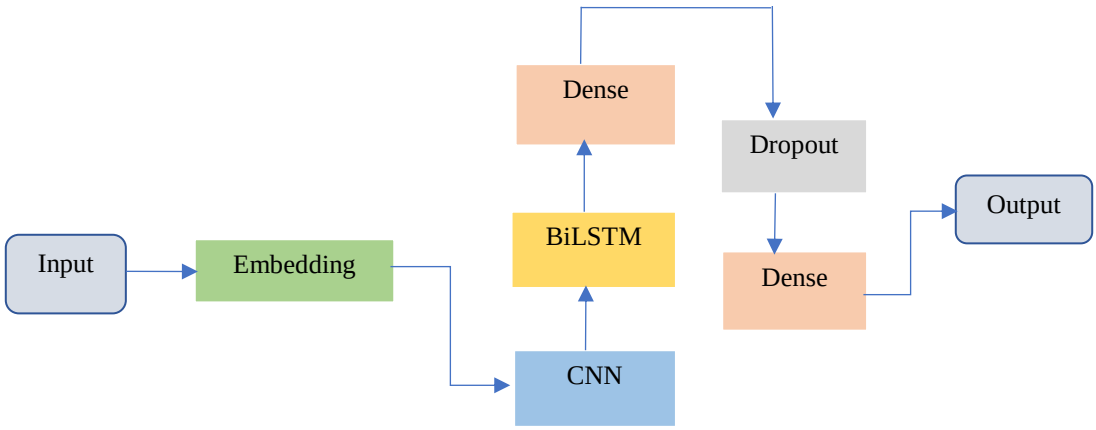

Figure 4. The model architecture

Finally, we complied the model with the optimizer Stochastic Gradient Descent (SGD); which is a type of gradient descent algorithm that optimizes a differentiable objective function by iteratively adjusting the model parameters in the direction of the steepest descent of the objective function. Its stochastic nature can introduce some noise in the training process, which can help prevent overfitting and improve generalization performance. We also update the learning rate value to be calculated based on the loss value as below equation; where β equal 0.001 and loss is the loss value of the test set.

$$\alpha = \frac{\beta}{1 + e^{-loss}}$$

To increase our model; we set up the model training with early stopping, a TensorFlow hook; which is defined as a regularization technique that stops the training process in certain conditions, for example, the validation loss reaches a particular threshold; it also optimizes the number of epochs.

Results and Discussion

This section highlights the results, lessons learned from the implementation and presents an in-depth analysis of the two modules. Figure 4 presents the accuracy of the automatic Arabic fact-check detection for the binary classification task. Compared with the reinforcement learning and traditional ML models and the other models used in (Khalil et al., 2021) The accuracy of our model is higher than the ones represented by (Khalil et al., 2021). The reason is that we improved the optimizer using SGD; which provides 87.8% accuracy.

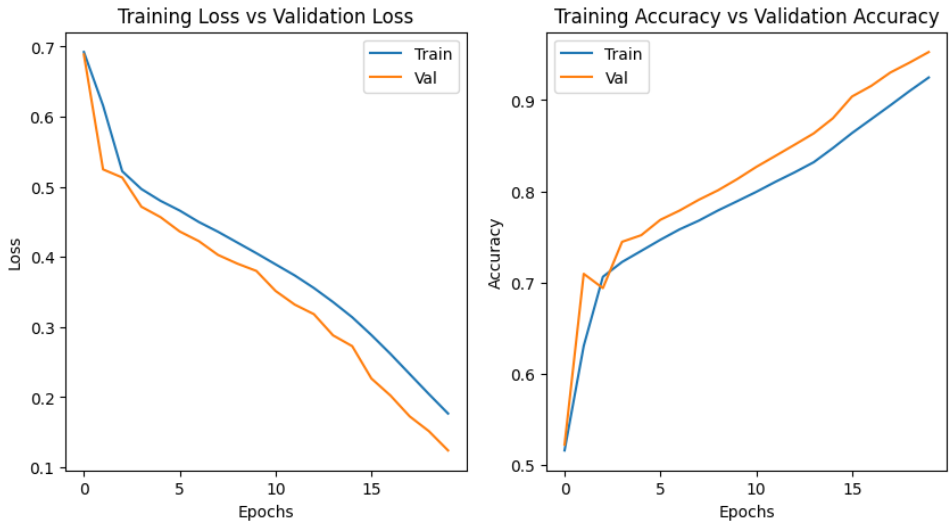

Figure 4. Accuracy of the model for each subdivision of the training and validation sets.

As presented in Table 2; we have many experiments before reaching the enhanced model, first, we work with "Adam" optimizer which provides an accuracy of 74.8% for the test set and 98% for the training set. Then we try to use SGD optimizer with two cases: 1) Using fixed learning rate with the value 0.08, but the result was worse as it reach 49.65%. 2) By changing the learning rate to be calculated based on the loss value, the accuracy increased to 87.7%.

Table 2. Accuracy of the classification task

Classifier	Accuracy
BiLSTM-CNN with SGD, dynamic LR	87.7%
BiLSTM -CNN with adam optimizer	74.8%
BiLSTM -CNN with SGD, fixed LR	49.65%

Conclusion

With the increased adaptation of the news resources such as social media and other web platforms, distinguishing verified information from fake news becomes an extremely difficult and crucial task. Especially with the Arabic language news; opposite to the other languages there are several types of writing posts and news in Arabic. In this paper, we applied a fake news detection model using convolutional and bidirectional LSTM layers. The used model is capable of accurately identifying fake news based solely on a news text. This model offers state-of-the-art performance on the tested datasets. This presents an efficient model to be used for Arabic news detection.

Recommendations

As future research directions, we will apply some improvements on the model to reach the best accuracy with the used dataset, optimizing the Arabic word processing, and finally we will use the transfer learning test to be more comprehensive.

Scientific Ethics Declaration

The author declares that the scientific ethical and legal responsibility of this article published in EPSTEM journal belongs to the author.

Acknowledgements or Notes

This article was presented as oral presentation at the International Conference on Basic Sciences, Engineering and Technology (www.icbaset.net) held in Marmaris/Turkey on April 27-30, 2023.

References

Abdelhady, N., Soliman, T. H. A., & Farghally, M. F. (2022). Stacked-CNN-BiLSTM-COVID: An effective stacked ensemble deep learning framework for sentiment analysis of arabic COVID-19 tweets. https://doi.org/10.21203/rs.3.rs-2206648/v1

Alharbi, O. (2021). A deep learning approach combining CNN and Bi-LSTM with SVM classifier for Arabic sentiment analysis. *International Journal of Advanced Computer Science and Applications, 12*(6),165-172.

Al-Yahya, M., Al-Khalifa, H., Al-Baity, H., AlSaeed, D., & Essam, A. (2021). Arabic fake news detection: comparative study of neural networks and transformer-based approaches. *Complexity, 2021*, 1-10.

Baniata, L. H., & Park, S. B. (2016). Sentence representation network for Arabic sentiment analysis. *한국정보과학회 학술발표논문집*, 470-472.

Ashwaq K., Moath J., Monther A., & Manar J. (2022). AFND: Arabic fake news dataset for the detection and classification of articles credibility. *Data in Brief,42*, 108141

Davoudi, M., Moosavi, M. R., & Sadreddini, M. H. (2022). DSS: A hybrid deep model for fake news detection using propagation tree and stance network. *Expert Systems with Applications, 198*, 116635.

Gauthier -Melancon, G., Ayala, O. M., Brin, L., Tyler, C., Branchaud- Charron, F., Marinier, J., Grande, K., & Le, D. (2022). Azimuth: Systematic error analysis for text classification. *Association for Computational Linguistics*, 298-310.

Jardaneh, G., Abdelhaq, H., Buzz, M., & Johnson, D. (2019). Classifying Arabic tweets based on credibility using content and user features. *IEEE Jordan International Joint Conference on Electricial Engineering and Information Technology (JEEIT).* 596-601.

Khalil, A., Jarrah, M., Aldwairi, M., & Jararweh, Y. (2021, November). Detecting Arabic fake news using machine learning. In *2021 Second International Conference on Intelligent Data Science Technologies and Applications (IDSTA)* (pp. 171-177). IEEE.

Nassif,A.B, Elnagar,A., Elgendy,O., & Afadar, Y. (2022). Arabic fake news detection based on deep contextualized embedding models. *Neural Computing and Applications,34*,16019-16032.

Ouassil, M. A., Cherradi, B., Hamida, S., Errami, M., El Gannour, O., & Raihani, A. (2022). A fake news detection system based on combination of word embedded techniques and hybrid deep learning model. *International Journal of Advanced Computer Science and Applications, 13*(10), 525-534

Raza, S., & Ding.C.. (2022). Fake news detection based on news content and social contexts: a transformer-based approach. *International Journal of Data Science and Analytics, 13*, 335-362.

Samih, Y., & Darwish, K. (2021, April). A few topical tweets are enough for effective user stance detection. In *Proceedings of the 16th Conference of the European Chapter of the Association for Computational Linguistics: Main Volume* (pp. 2637-2646).

Truică, C. O., Apostol, E. S., Nicolescu, R. C., & Karras, P. (2023). MCWDST: a minimum-cost weighted directed spanning tree algorithm for real-time fake news mitigation in social media. *arXiv preprint arXiv:*2302.12190.

Zerrouki, T. (2023, April 1). *Tashaphyne, Arabic light stemmer*. https://pypi.org/project/Tashaphyne/

Zhou, X., & Zafarani, R. (2020). A survey of fake news: Fundamental theories, detection methods, and opportunities. ACM Computing Surveys (CSUR), 53(5), 1-40.

Author Information

Maysaa Alsafadi
Karadeniz Technical University
Trabzon, Turkey
Contact e-mail: *maysaaelsafadi@gmail.com*

To cite this article:

Alsafadi, M. (2023). Stance classification for fake news detection with machine learning. *The Eurasia Proceedings of Science, Technology, Engineering & Mathematics (EPSTEM), 22*, 191-198.

The Eurasia Proceedings of Science, Technology, Engineering & Mathematics (EPSTEM)
ISSN: 2602-3199

The Eurasia Proceedings of Science, Technology, Engineering & Mathematics (EPSTEM), 2023

Volume 22, Pages 199-209

ICBASET 2023: International Conference on Basic Sciences, Engineering and Technology

Assessment of the Phytoremediation Potential of Heavy Metal Contaminated Soil Using Vigna Unguiculata L. (Walp)

Oluwole SURUKITE
Lagos State University

Ogun MAUTIN
Lagos State University

Usamot QUDUS
Lagos State University

Olokooba RACHEAL
Lagos State University

Kappo SESI
Lagos State University

Molade FATIMAH
Lagos State University

Abstract: Phytoremediation is a plant-based approach involving use of plants to extract and remove elemental pollutants or lower their bioavailability in soil. Thus, this study aimed at assessing the phytoremediation potential of Vigna unguiculata grown in heavy metal contaminated soil. Mature seeds of V. unguiculata were obtained from local farmers in Ojo-Lagos, Nigeria; heavy metal contaminated, and control soils were obtained from Iba and LASU Botanical Garden, Ojo-Lagos respectively. Physiochemical analyses of soil samples were done before and after transplanting. Nurseries were made and one seedling was transplanted into 5 buckets each for control and contaminated soils respectively. Growth parameters- stem height, stem girth, leaf length, and so on were measured. Heavy metal analysis was done using standard analytical procedures. Metal transfer factors and bioaccumulation potential were also studied. Data collected were analyzed using mean-standard deviation. Soil physiochemical parameters and heavy metals analyzed showed reduction in most of the metals studied before and after soil analyses. Results showed the transfer factors for Zn (0.07 mg/kg), Fe (6.72mg/kg), Mn (1.33 mg/kg), As (1.00mg/kg), Pb (0.19mg/kg), Cd (0.007mg/kg) while the bioaccumulation potential of Zn (0.08 mg/kg), Fe (3.86mg/kg), Mn (1.09mg/kg) As (1.00mg/kg), Pb (0.20mg/kg), Cd (0.001mg/kg). Also, the result revealed the metal uptake rate of Fe (21.75%), Cd (0.94%), Zn (1.40%), Pb (84.80%) and Mn (0.11%). It could be concluded that V. unguiculata reduces heavy metals in soil, had high transfer factors, bioaccumulation, and uptake rates. This study recommends that V. unguiculata could be used for phytoremediation of heavy metal environmental contaminated soils.

Keywords: Heavy metals, Phytoremediation, Bioaccumulation, Vigna unguiculata

Introduction

Air, water, and soil pollution are characterized as "undesirable changes in physical, chemical, and biological characteristics" (Yuvaraj & Mahendran, 2018) that have negative effects on human health, ecosystem health, economic development, quality of life, and cultural artefacts. Pollutants are a common cause of this, as they can have a negative impact on people's health, quality of life, possessions, and environment (Ogun et al., 2023). An increasing risk to human and environmental health may result from soil pollution in recent decades. Human activities are the primary contributors to soil contamination, which can lead to an alarming buildup of toxins (Cachada et al., 2018; Ogun et al., 2023) in the ground. Both naturally occurring and man-made sources of contaminants (organic and inorganic compounds) are included in the definition of "soil pollution" (Ogun et al., 2023) used here. Lack of clearly described monitoring factors and indicators may make soil quality monitoring a challenging process. However, as the world's population rises, so do the problems that threaten soil quality and the requirement for maintaining soil fertility over the long term (Cachada et al., 2018).

The term "heavy metal" is used to describe a class of chemical elements with large atomic weights, atomic numbers, and densities. Cadmium, Mercury, Lead, Arsenic, Zinc, Copper, Nickel, and Chromium are all examples of heavy metals/metalloids that are commonly encountered. Anthropogenic and natural sources of these heavy metals/metalloids include oil and gas wastewater, agricultural phosphate fertiliser use, sewage sludge, metal mining/smelting, pesticide application, electroplating, and fossil fuel combustion (Muradoglu et al., 2015). Since heavy metals cannot be broken down chemically or physically, they remain in the soil for a very long time and constitute a serious hazard to the environment (Suman et al., 2018). Several metals are typically applied to agricultural soils alongside organic and mineral fertilizers (Zwolak et al., 2019). Plant protection products are yet another potential source of the metals. Soil characteristics are important in determining the bioavailability of heavy metals, which affects their movement through the soil and subsequent uptake by plants (Zwolak et al., 2019). There is a need for remediation since these metal concentrations in soil have become a threat to plant safety and food security.

Heavy metals can be grouped as essential and non-essential based on their role in biological systems; hence, it is necessary to take remediation measures to prevent heavy metals from entering terrestrial, atmospheric, and aquatic environments, and mitigate the contaminated land (Gerhardt et al., 2017). There are varieties of remediation approaches that have been developed to reclaim heavy metal-contaminated soil. These measures are mainly based on mechanical or physio-chemical techniques, such as soil incineration, excavation and landfill, soil washing, solidification, and electric field application (Sheoran et al., 2011; Cristaldi et al., 2017; Wang et al., 2017).

In phytoremediation, plants are used to either completely remove or significantly reduce the bioavailability of elemental contaminants in soil (Berti & Cunningham, 2000; Padmavathiamma & Li, 2007). Even at low quantities, ionic substances in the soil are absorbed by plants through their root systems. By establishing a rhizosphere ecosystem, plants can reclaim damaged soil and stabilise soil fertility by accumulating heavy metals and regulating their bioavailability (Cristaldi et al., 2017; Wang et al., 2017; Jacob et al., 2018). The incorporation of organic and inorganic materials affects plant metal mobility and assimilation. Metal bioavailability to plants may also be influenced by the age of the soil, as suggested by several studies (Padmavathiamma & Li, 2007; Zaid et al., 2020). Absorption of metals also varies among plant species, with both soil conditions and plant type playing a role. Metal concentrations were also shown to vary considerably depending on the specific plant tissue they were measured in, the plant species they belonged to, and even the variety within the same species (Zulfiqar et al., 2019; Zwolak et al., 2019).

The medium-sized, edible bean of the *Vigna unguiclata* legume is grown in many parts of the world. It is a cowpea subspecies that was domesticated in Africa and is now grown across the World (Herniter et al., 2019). This vining plant emits compounds from its roots that beckon the nitrogen-fixing bacterium rhizobia. Nodules, which look swolen on the roots, protect the rhizobia and provide a source of carbon. In return, they receive a useful, stable form of nitrogen. *V. unguilata* can replenish soil nutrients by releasing bacteria into the soil just before death, (Lindström & Mousavi, 2020). Since heavy metals are harmful to both plants and humans, this study evaluates the viability of utilizing *Vigna unguiculata* L. (Walp) to phytoremediate soil contaminated with these metals.

Materials and Methods

Collection of Soil Sample and Experiment Site

Contaminated soil samples were taken from the area of Iba in Lagos, Nigeria, which is famous for its extensive anthropogenic activity. Debris was removed from the sampling area, and then the top 15 centimeters of soil were removed. Soil samples were collected in a polyethylene bag, then combined and mixed to create a single representative sample. Soil used in the control group was obtained from the Botanical Garden at Lagos State University in Ojo, Nigeria. The research took place in the Botanical Garden on the campus of Lagos State University in Ojo, Lagos State, Nigeria.

Soil Sample Preparation and Digestion

The contaminated and the garden soil samples were taken to the laboratory for heavy metal analysis before planting to check the level of metal in the soil. The several methods used for the metal analysis followed the procedures employed by Oladele et al. (2016).

Experimental Design and Treatments

Ten (10) buckets received five kilogrammes (5kg) of soil each that had been well mixed. The bases of the buckets were pierced to prevent water logging and to improve soil aeration. The 10 buckets were divided into two groups of five each: control (garden soil that had not been treated), and contaminated soil, which contained five buckets. A Completely Randomised Design (CRD) was used to plan the experiment.

Nursery Practice

Vigna unguiculata seeds were planted in the nursery in a bowl of loamy soil that had been well ground up and treated with manure. Then, using a sprayer, this was watered often. The germination time of the seeds was 3 days, and 2 weeks of establishment in the nursery were given to the seedlings before they were transplanted.

Transplanting

The seedlings were transplanted into buckets filled with 4 kg of soil at the rate of one-plants-per-bucket which makes up ten stands for ten buckets. The buckets were perforated at the base to avoid water logging and to increase the soil aeration. The buckets were arranged in two major groups as follows: Garden soil (control), -5buckets, contaminated soil-5buckets. Weeding was then carried out manually on a weekly basis.

Measurement of Growth and Yield Parameters

Plant height was measured from the ground level to the growth point with a meter rule in centimeters and the observation recorded for each treatment. Also, the numbers of branches were counted, and the stem girth measured using vernier caliper. The total number of leaves per plant were counted for each treatment and recorded. The measurements were taken in an interval of 2 weeks from the day the plant was transplanted. The leaf area was determined using Oluwole *et al*. (2019) formula:

$$\text{Leaf Area} = 0.853 + (L \times B) \times 8.7440.$$

Pre-treatment Methods for Plant Samples for Heavy Metal Analysis

The plant samples' leaves, stems, and roots are cleaned separately by gently washing with distilled water. The heavy metal concentrations in the leaves, stem, and root were then measured after each sample was subsampled, air-dried in the lab for three days at room temperature, and then subjected to further ashing processing. A porcelain crucible containing 5g of each dry sample was weighed, and it was then thoroughly ashed at 5500C for 4 hours in a muffle furnace. A 5 ml solution of diluted (1:1) nitric acid was then added to the residue after it had cooled. In 25 cc of distilled water, the mixture was diluted. Filter paper Whatman #1 was used to remove the solution. In order to identify the metals, the filtrate was retained.

Heavy Metals Analysis

The solution produced by dry ashing the plant sample at 550°C and dissolving the ash in distilled deionized water in a flask was used to analyse the heavy metal components of the sample. With the use of an atomic absorption spectrophotometer (Buck Scientific Model 200A), all the metals (Mn, Cu, Zn, Pb, and Cd) were examined. For soil samples, the same process was repeated (Oluwole et al., 2020).

Determination of Transfer Factor (TF)

The transfer of metal from the soil to the plant body is described by the term "heavy metal transfer factor" (TF), which is also known as "accumulation factor AF" or "bioconcentration factor BCF." According to Rashid et al. (2016), this was computed by dividing the heavy metal content in the plant by the corresponding concentration in the soil.

Transfer Factor (TF) = Conc. HM in aerial part of the plant / Conc. HM in the Soil

Determination of the Multiplication Coefficient (MC)/Bioconcentration Factor

The concentration of heavy metals absorbed by the plants in relation to their concentration in the soil was calculated using the Multiplication Coefficient (MC)/Bioconcentration Factor (BCF). Yoon et al. (2006) similarly used the equation: to determine the BCF.

Bioconcentration Factor (BCF) = Conc. HM in the roots / Conc. HM in the Soil

Determination of the Remediation/Metal Uptake Rate

The quantity of heavy metal that the plant sample removed from the contaminated soil, abstracted from it, or accumulated was determined as follows: R = quantity of metal lost by the soil or gained by the plant represented as a percentage of original amount. i.e.

$$\text{Rate } (\%) = \frac{C^{nth\ week} - C^{oth\ week}}{C^{oth\ week}} \times \frac{100}{1}$$

Where, $C^{nth\ week}$ and $C^{\text{oth week}}$ are concentrations of the heavy metals in the soil or plant sample at time (weeks) = „n“ and „0“ respectively.

Statistical Analysis

All data collected were in triplicates and these were analyzed by means±standard deviation using SPSS version 18.

Results

Phytoremediation Potential of *Vigna unguiculata* Growth in Heavy Metal Contaminated Soil

a. Stem Height

Table 1 shows the phytoremediation potential of *Vigna unguiculata* stem height in heavy metal contaminated soil. *Vigna unguiculata* in control soil has the highest stem height compared to those in contaminated soil at the end of the 8^{th}week after transplant. However, *Vigna unguiculata* in contaminated soil was increasing but started regressing after the 6^{th} week after transplant.

b. Leaf Length

Table 2 shows the phytoremediation potential of *Vigna unguiculata* leaf lenght in heavy metal contaminated soil. *Vigna unguiculata* in control soil has the highest leaf length compared to those in contaminated soil at the end of the 8^{th}week after transplant. However, *Vigna unguiculata* in contaminated soil was increasing but started regressing after the 4^{th} week after transplant (Table 2).

c. Leaf Breadth

Table 3 shows the phytoremediation potential of *Vigna unguiculata* leaf breadth in heavy metal contaminated soil. *Vigna unguiculata* in control soil has the highest leaf breadth compared to those in contaminated soil at the end of the 8^{th}week after transplant. However, *Vigna unguiculata* in contaminated soil was increasing but started regressing after the 4^{th} week after transplant (Table 3).

d. Leaf Girth

Table 4 shows the phtoremediation potential of *Vigna unguiculata* leaf girth in heavy metal contaminated soil. *Vigna unguiculata* in control soil has the highest leaf girth compared to those in contaminated soil at the end of the 8^{th}week after transplant. However, there was no regression in the leaf girth of *Vigna unguiculata* in control soil (Table 4).

e. Leaf Petiole

Table 5 shows the phytoremediation potential of *Vigna unguiculata* leaf petiole in heavy metal contaminated soil. *Vigna unguiculata* in control soil has the highest leaf petiole compared to those in contaminated soil at the end of the 8^{th}week after transplant. However, *Vigna unguiculata* in contaminated soil was increasing but started regressing after the 4^{th} week after transplant (Table 5).

f. Number of Leaflet

Table 6 shows the phytoremediation potential of *Vigna unguiculata* number of leaflets in heavy metal contaminated soil. *Vigna unguiculata* in control soil has the highest number of leaflets compared to those in contaminated soil at the end of the 8^{th}week after transplant. However, *Vigna unguiculata* in contaminated soil was increasing but started regressing after the 6^{th} week after transplant.

g. Leaf Area

Table 7 shows the phytoremediation potential of *Vigna unguiculata* leaf area in heavy metal contaminated soil. *Vigna unguiculata* in control soil has the highest leaf area compared to those in contaminated soil at the end of the 8^{th}week after transplant. However, *Vigna unguiculata* in contaminated soil was increasing but started regressing after the 6^{th} week after transplant.

Table 1. Phytoremediation potential of *vigna unguiculata* stem height in heavy metal contaminated soil

Parameters	2 WAT	4 WAT	6 WAT	8 WAT
Contaminated soil	12.0±3.05	12.30±1.04	18.2±1.08	18.0±0.55
Control soil	16.2±3.82	23.7±0.87	25.0±1.11	26.2±1.00

WAT-Weeks after transplant; Values are presented as Mean±Standard Deviation

Table 2. phytoremediation potential of *vigna unguiculata* leaf length in heavy metal polluted soil

Parameters	2 WAT	4 WAT	6 WAT	8 WAT
Contaminated soil	3.5±0.47	5.8±1.85	5.1±1.74	3.0±1.73
Control soil	7.5±0.78	8.8±1.26	10.0±0.26	10.1±1.61

WAT-Weeks after transplant; Values are presented as Mean±Standard Deviation

Table 3. Phytoremediation potential of *vigna unguiculata* leaf breadth in heavy metal contaminated soil

Parameters	2 WAT	4 WAT	6 WAT	8 WAT
Contaminated soil	3.0±0.10	3.1±0.85	2.6±0.57	2.0±1.15
Control soil	4.0±0.40	5.2±0.61	5.5±0.67	6.0±0.50

WAT-Weeks after transplant; Values are presented as Mean±Standard Deviation

Table 4. Phytoremediation potential of *vigna unguiculata* leaf girth in heavy metal contaminated soil

Parameters	2 WAT	4 WAT	6 WAT	8 WAT
Contaminated soil	0.5±0.06	0.8±0.15	1.1±0.10	1.2±0.06
Control soil	0.5±0.10	0.9±0.06	1.3±0.06	1.5±0.06

WAT-Weeks after transplant; Values are presented as Mean±Standard Deviation

Table 5. Phytoremediation potential of *vigna unguiculata* leaf petiole in heavy metal contaminated soil

Parameters	2 WAT	4 WAT	6 WAT	8 WAT
Contaminated soil	3.8±0.36	4.2±0.67	4.1±2.65	1.0±0
Control soil	6.2±0.55	6.8±0.65	13.3±2.04	7.8±1.26

WAT-Weeks after transplant; Values are presented as Mean±Standard Deviation

Table 6. Phytoremediation potential of *vigna unguiculata* number of leaflet in heavy metal contaminated soil

Parameters	2 WAT	4 WAT	6 WAT	8 WAT
Contaminated soil	7.5±1.15	3.7±1.15	4.0±1.73	2.0±3.46
Control soil	8.0±0.0	12.3±3.51	25.0±10	36.7±16.04

WAT-Weeks after transplant; Values are presented as Mean±Standard Deviation

Table 7. Phytoremediation potential of *vigna unguiculata* leaf area in heavy metal contaminated soil

Parameters	2 WAT	4 WAT	6 WAT	8 WAT
Contaminated soil	92.67±17.71	158.07±84.92	116.80±45.76	53.32±30.29
Control soil	263.17±51.46	400.98±104.02	455.54±71.66	462.54±63.44

WAT-Weeks after transplant; Values are presented as Mean±Standard Deviation

Physiochemical Analysis of the Soil before and after Remediation

Table 9 shows the physiochemical and heavy metal analysis of the soil samples used before and after remediation. Thus, the result revealed that the heavy metals such as As, Cd, Fe, Pd, Ni, Mn, Zn and so on decreased progressively in soil after remediation in both control and polluted soils respectively (Table 9).

Heavy Metal Transfer Factors of *Vigna Unguiculata* (White Beans) Grown in Contaminated Soil

Figure 2 shows the heavy metal transfer factor phytoremediation potential of *Vigna unguiculata*. The result revealed that iron (6.72) metal had the highest transfer factor followed by manganese (1.33), arsenic (1), lead (0.19), cadmium (0.001), had the least metal transfer factor.

Heavy Metal Bioconcentration Factors of *Vigna Unguiculata* Grown in Contaminated Soil

Figure 3 shows the heavy metal bioconcentration factors phytoremediation potential of *Vigna unguiculata*. The result revealed that iron (3.86) metal had the highest transfer factor followed by manganese (1.09), arsenic (1.00), lead (0.20), cadmium (0.001), had the least metal transfer factor.

Table 8. Phytoremediation potential of *vigna unguiculata* leaf area in heavy metal contaminated soil

Parameters	2 WAT	4 WAT	6 WAT	8 WAT
Contaminated soil	92.67±17.71	158.07±84.92	116.80±45.76	53.32±30.29
Control soil	263.17±51.46	400.98±104.02	455.54±71.66	462.54±63.44

WAT-Weeks after transplant; Values are presented as Mean±Standard Deviation

Table 9. Physiochemical analysis of the soil before and after remediation

Parameters	Con. Before	Con. After	Ctd. Before	Ctd. After
pH (at 25°C)	5.80	6.21	1.95	5.90
Electrical Conductivity (uS/cm)	109.2		20340.0	
Total Organic Carbon (%)	25.81	18.47	15.46	17.92
Total Organic Matter (%)	44.40	31.72	26.60	30.78
Phosphate (mg/kg, PO43-)	37.02	25.23	80.09	40.56
Total Nitrogen (mg/kg)	123.70	1560.15	63.6	61.23
Total Petroleum Hydrocarbons (mg/kg)	0.05	0.03	28099.0	10000
Arsenic (mg/kg)	0.05	0.03	45.07	0.05
Cadmium (mg/kg)	50.07	43.24	83.70	51.44
Iron (mg/kg)	40.48	22.50	201.03	32.55
Lead (mg/kg)	0.07	0.05	42.14	0.32
Manganese (mg/kg)	41.91	20.10	44.78	37.26
Mercury (mg/kg)	0.05	0.03	0.05	0.001
Nickel (mg/kg)	30.70	20.70	49.75	30.64
Zinc (mg/kg)	10.24	14.21	99.59	33.40

Con. Before and After = control soil sample used before and after planting; Ctd: Before and After = contaminated soil sample used before and after planting.

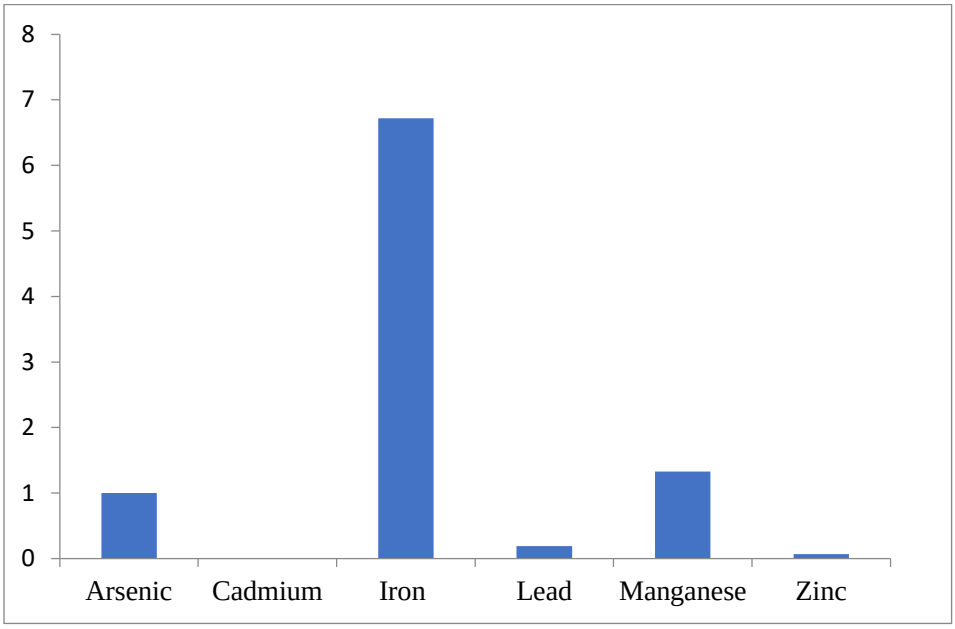

Figure 1. Heavy metal transfer factors of *vigna unguiculata* grown in contaminated soil

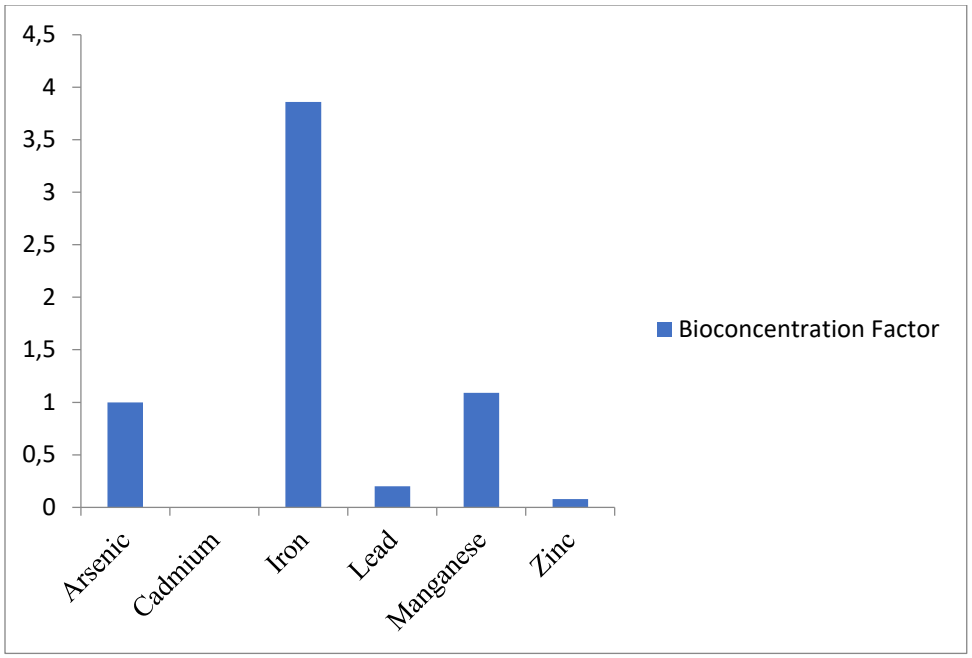

Figure 2. Heavy metal bioconcentration factors of *vigna unguiculata* grown in contaminated soil

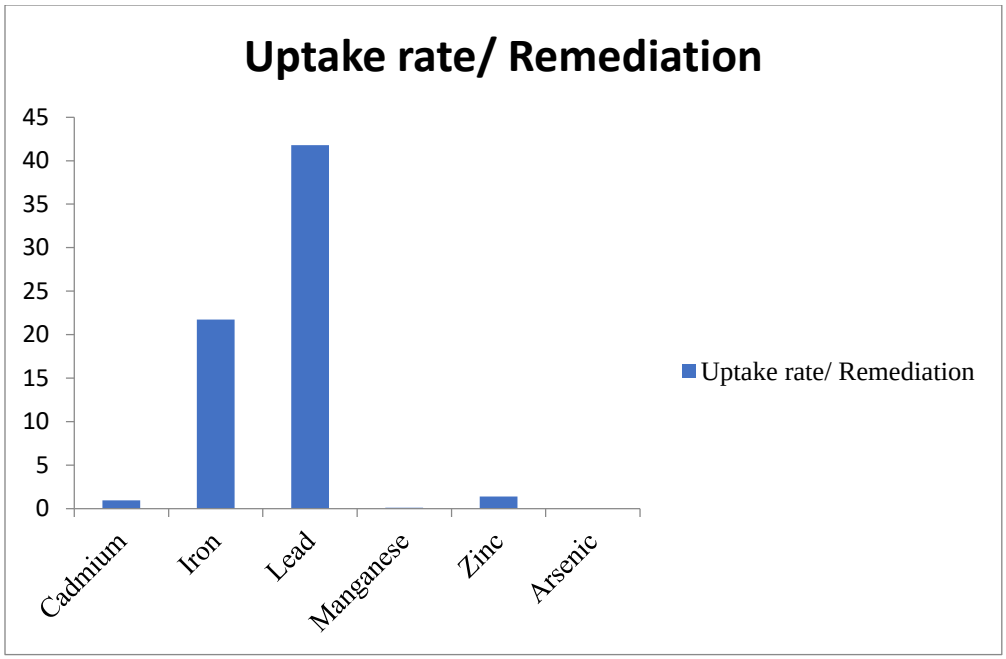

Figure 3. Heavy metal remediation/uptake rate of *vigna unguiculata* grown in contaminated soil

Discussion

In this study, the phytoremediation potential of *Vigna unguiculata* cultivated in contaminated heavy metal polluted soil were studied and compared to those in the control soil. It was observed that the *Vigna unguiculata* cultivated in the control soil performed well morphologically compared to those in contaminated soil (Tables 1-7). This is due to the presence of higher hydrocarbon in the contaminated soil (Table 8). It has been reported that soil rich in hydrocarbon creates a barrier for absorption of water and reduces aeration i.e., it doesn't allow the free flow of water

into the soil, and it blocks oxygen from getting through the soil. The finding of study agrees with the work of Anyalogbu et al. (2017) who documented reduction in morphometric parameters such as plant height, leaf length, leaf breadth and so on in studies on phytoremediation potential of *Talinum triangulare* in heavy metal and hydrocarbon contaminated soil.

From the result of the physiochemical analysis of the soil, there was a reduction in the heavy metals-before planting the values were: Arsenic (45.07), Cadmium (83.70), Zinc (99.59), Iron (201.03), Lead (42.14) and Manganese (44.78); and values after planting reduced: Arsenic (0.05), Cadmium (51.44), Zinc (33.40), Iron (32.50), Lead (0.32) and Manganese (37.26). These reductions in physiochemical analysis of heavy metals observed agreed with the findings of Puga et al., (2015) and Oladele et al. (2018), who observed similar results using V. unguilata. This reduction has been attributed to translocation metals from the soil to roots via root hairs. More so, in this study, it could be documented that Iron has the highest transfer factor of 6.72mg/kg followed by Manganese with 1.33mg/kg, Arsenic with 1mg/kg, Lead with 0.19mg/kg, Zinc with 0.07mg/kg, and cadmium with 0.007mg/kg (Fig.1). From this, the highest heavy metal that is moveable and moves faster from the soil into the plant is iron. This study concurs with the findings of Matijevi et al. (2014). This was due to metal specific properties and plant affinities for metal mobilization (Cristaldi et al., 2017; Wang et al., 2017).

Furthermore, in this study, iron has the highest heavy metal bioaccumulation potential of 3.86mg/kg followed by Manganese with 1.09mg/kg, Arsenic with 1.00mg/kg, Lead 0.20mg/kg, Zinc 0.08mg/kg and Cadmium 0.00mg/kg (Fig. 2). Moreover, in this study, Lead has the highest uptake rate/remediation with 841.80% followed by Iron with 21.75%, Zinc 1.40%, Cadmium 0.94%, Manganese 0.11%, and Arsenic 0.00% (Fig. 3). These results are in consonance with the findings of Anyalogbu et al. (2017), who reported higher bioaccumulation and uptake rate of heavy metals in Talinum triangulare cultivated in heavy metal contaminated soil. This could be attributes to metal specific properties and plant affinities for metal mobilization and soil properties (Cristaldi et al., 2017; Wang et al., 2017).

Conclusion

From this study, it could be concluded that *Vigna unguiculata* has the potential of phyto-remediating heavy metal contaminated soil. This is evident in this study as contaminated soil reduces the growth (leaf length, stem girth, stem height, leaf breadth, leaf area and petiole) of *Vigna unguicutulata.* It also revealed the reduction of heavy metals in soils before and after through physiochemical analyses; iron has the highest transfer factor and bioaccumulation in the *Vigna unguicutulata*; and however, iron metal was the highest remediated by *Vigna unguicutulata*. It could be recommended that *Vigna unguicutulata* exhibited phytoremediation potentials, which are good for reduction of environmental contaminants, but the plant used could be a determinant when it was exposed to prolonged heavy metal contamination. Plants with high amount of heavy metal concentrations are toxic to human and other living organisms when ingested into the body; thus, should be avoided.

Scientific Ethics Declaration

The authors declare that the scientific ethical and legal responsibility of this article published in EPSTEM journal belongs to the authors.

Acknowledgements

* This article was presented as oral presentation at the International Conference on Basic Sciences, Engineering and Technology (www.icbaset.net) held in Marmaris/Turkey on April 27-30, 2023.

*Authors appreciate members of staff of the Department of Botany, Faculty of Science, Lagos State University, Ojo, Lagos, Nigeria for their contributions towards the success of this work.

Reference

Anyalogbu, E. A. A., Anadi, C. C., Nweje-Anyalowu, P. C. & Nnoli, M. C. (2017). Use of waterleaf (*Talinum triangulare*) in remediation of soil exposed to heavy metals: A green technology approach. *World Journal of Pharmaceutical and Life Sciences*, *3*(9), 48-53.

Berti, W. R. & Cunningham, S. D. (2000). Phytostabilization of metals. *Phytoremediation of toxic metals: Using plants to clean up the environment.* Wiley, New York, 71-88.

Cachada, A., Rocha-Santos, T. & Duarte, A. C. (2018). Soil and pollution: An introduction to the main issues. In *Soil pollution*. Academic Press, 1-28.

Cristaldi, A., Conti, G. O., Jho, E. H., Zuccarello, P., Grasso, A., & Copat, C. (2017). Phytoremediation of contaminated soils by heavy metals and PAHs. A brief review. *Environ. Technol. Innov. 8*, 309–326.

Gerhardt, K. E., Gerwing, P. D. & Greenberg, B. M. (2017). Opinion: Taking phytoremediation from proven technology to accepted practice. *Plant Science*, *256,* 170-185.

Herniter, I. A., Jia, Z. & Kusi, F. (2019). Market preferences for cowpea (*Vigna unguiculata* [L.] Walp) dry grain in Ghana. *African J. Ag. Res*, *14*(22), 928-934.

Jacob, J. M., Karthik, C., Saratale, R. G., Kumar, S. S., Prabakar, D., Kadirvelu, K. & Pugazhendhi, A. (2018). Biological approaches to tackle heavy metal pollution: A survey of literature. *Journal of Environmental Management*, *217*, 56-70.

Lindström, K. & Mousavi, S. A. (2020). Effectiveness of nitrogen fixation in rhizobia. *Microbial Biotechnology*, *13*(5), 1314-1335.

Matijevic, L., Romic, D., & Romic, M. (2014). Soil organic matter and salinity affect copper bioavailability in root zone and uptake by *Vicia faba* L. plants. *Environmental Geochemistry and Health*, *36*, 883-896.

Muradoglu, F., Gundogdu, M., Ercisli, S., Encu, T., Balta, F., Jaafar, H. Z., & Zia-Ul-Haq, M. (2015). Cadmium toxicity affects chlorophyll a and b content, antioxidant enzyme activities and mineral nutrient accumulation in strawberry. *Biology Research, 48*(11),1-7.

Ogun, M. L., Anagun, O. S., Awote, O. K., Oluwole, S. O., Kappo, S. C. & Alonge, F. O. (2023). *Abattoirs: The hidden sources of plants' heavy metals and other pollutants in Lagos, Nigeria*. https://www.intechopen.com/online-first/86134

Oladele, E. O., Adewumi, O. O., Taiwo, I. A., & Odeigah, P. G. C. (2018). Removal of Pb and Zn from Soil using cowpea (*Vigna unguiculata*) and maize (Zea mays) plants. *Journal of Applied Sciences and Environmental Management*, *22*(3), 432-438.

Oladele, E.O., Odeigah, P.G.C., Taiwo, I.A., & Yahaya, T. (2016). Remediative potential of bambara nut on Pb and Zn polluted soils. *Ife J. Sci*. *18*(2), 483- 491.

Oluwole, S. O., Makinde, S. C. O., Ogun, M.L., & Nwachukwu, I.R. (2020). Evaluation of heavy metal concentrations and proximate compositions of *Amaranthus spinosus* L. and *Talinum triangulare* J. and soils collected from dumpsites in some selected areas in Lagos State, Nigeria. *World Environment*, *10*(1), 16-26.

Oluwole, S. O., Ogun, M. L. & Durowoju, S. Y. (2019). Effects of different organic manures on the growth of water leaf (*Talinum triangulare* Jacq). *International Journal of Innovative Science and Research Technology*, *4*(5), 1123-1129.

Padmavathiamma, P. K. & Li, L. Y. (2007). Phytoremediation technology: Hyper-accumulation metals in plants. *Water, Air, and Soil Pollution*, *184*, 105-126.

Pitchel, J. (2016). Oil and gas production wastewater, soil contamination and pollution prevention. *Applied and Environmental Soil Science*, 1-24.

Puga, A. P., Abreu, C., Melo, L. C. A. & Beesley, L. (2015). Biochar application to a contaminated soil reduces the availability and plant uptake of zinc, lead and cadmium. *Journal of Environmental Management*, *159*, 86-93.

Sheoran, V., Sheoran, A., & Poonia, P. (2011). Role of hyperaccumulators in phytoextraction of metals from contaminated mining sites: a review. *Crit. Rev. Env. Sci. Technol. 41,* 168–214.

Suman, J., Uhlik, O., Viktorova, J. & Macek, T. (2018). Phytoextraction of heavy metals: A promising tool for clean-up of polluted environment? *Frontiers in Plant Science*, *9* (1476), 1-15.

Wang, L., Ji, B., Hu, Y., Liu, R., & Sun, W. (2017). A review on in situ phytoremediation of mine tailings. *Chemosphere 184,* 594–600.

Yoon, J., Cao, X., Zhou, Q. & Ma, L. Q. (2006). Accumulation of Pb, Cu, and Zn in native plants growing on a contaminated Florida site. *Science of the Total Environment*, *368*(2-3), 456-464.

Yuvaraj, M. & Mahendran, P. P. (2020). Soil pollution causes and mitigation measures. *Biotica Research Today*, *2*(7), 550-552.

Zaid, A., Mohammad, F., & Fariduddin, Q. (2020). Plant growth regulators improve growth, photosynthesis, mineral nutrient, and antioxidant system under cadmium stress in menthol mint (Mentha arvensis L.). *Physiology and Molecular Biology of Plants*, *26*, 25-39.

Zulfiqar, U., Farooq, M., Hussain, S., Maqsood, M., Hussain, M., Ishfaq, M. & Anjum, M. Z. (2019). Lead toxicity in plants: Impacts and remediation. *Journal of Environmental Management*, *250*, 109557.

Zwolak, A., Sarzyńska, M., Szpyrka, E. & Stawarczyk, K. (2019). Sources of soil pollution by heavy metals and their accumulation in vegetables: A review. *Water, Air, and Soil Pollution*, *230*, 1-9.

Author Information

Oluwole Surukite
Department of Botany, Faculty of Science, Lagos State University, Ojo, Lagos, Nigeria.
Conctact e mail: surukite.oluwole@lasu.edu.ng

Ogun Mautin
Department of Botany, Faculty of Science, Lagos State University, Ojo, Lagos, Nigeria.

Usamot Qudus
Department of Botany, Faculty of Science, Lagos State University, Ojo, Lagos, Nigeria.

Olokooba Racheal
Department of Botany, Faculty of Science, Lagos State University, Ojo, Lagos, Nigeria.

Kappo Sesi
Department of Botany, Faculty of Science, Lagos State University, Ojo, Lagos, Nigeria.

Molade Fatimah
Department of Botany, Faculty of Science, Lagos State University, Ojo, Lagos, Nigeria.

To cite this article:

Surukite, O., Mautin, O., Qudus, U., Racheal, O., Sesi, K. & Fatimah, M. (2023). Assessment of the phytoremediation potential of heavy metal contaminated soil using vigna unguiculata L. (Walp). *The Eurasia Proceedings of Science, Technology, Engineering & Mathematics (EPSTEM), 22,* 199-209.

The Eurasia Proceedings of Science, Technology, Engineering & Mathematics (EPSTEM)
ISSN: 2602-3199

The Eurasia Proceedings of Science, Technology, Engineering & Mathematics (EPSTEM), 2023

Volume 22, Pages 210-216

ICBASET 2023: International Conference on Basic Sciences, Engineering and Technology

Circular Supply Chains: An Internet of Things Application for Rotten Product Detection in Aggregate Food Industry

Candan ERGELDI
Galatasaray University

Orhan FEYZIOGLU
Galatasaray University

Abstract: Today, the majority of food created is wasted rather than consumed, which has a negative impact on worldwide hunger and the economy. Improvements to aggregate supply chains are at the forefront of the actions needed to meet the nutritional requirements of an expanding population. One of such improvements noted in this research was aggregate food storage. The ESP8266-Microcontroller, along with the DHT11 temperature and humidity sensor and the MQ3 alcohol sensor, is put in the storage area to measure the storage conditions of fruit products on a regular basis. The data gathered is sent to the Internet of Things Application in AWS cloud computing service via the microcontroller and MQTT communication protocol and is stored in both the S3 Bucket and Firehose Kinesis databases using the rules defined in this console. As result, the sensor data stored in the database is examined using AWS-Internet of Things -Analysis and SageMaker. Fruits should be kept at temperatures ranging from 4 to 7 degrees Celsius. When the temperature outside of this range rises, the crops begin to decompose. Accordingly, a rule in the AWS Internet of Things Application is defined to fire with out-of-range measurements, and the AWS Simple Notification Service is triggered to send ambient temperature, humidity, and methanol values to user via SMS and e-mail. A Convolutional Neural Network model was also developed to classify fruits based on their variety and whether they are fresh or rotten. The model was first taught using images of 1693 fresh apples, 1581 fresh bananas, 1466 fresh oranges, 2342 rotten apples, 2224 rotten bananas, and 1595 rotten oranges over 50 epochs. Then, images of 395 fresh apples, 381 fresh bananas, 381 fresh oranges, and 388 rotten apples, 601 rotten bananas, and 530 rotten oranges were evaluated. This CNN Model had a training accuracy of 98.6% and an assessment accuracy of 96.4%.

Keywords: Circular economy, Sustainability, Industry 4.0, Agrifood supply chain, Internet of things

Introduction

Elimination of food waste is a major worldwide challenge and a vital prerequisite for economic development. Poor food management has a substantial impact on waste generation. Therefore, to reach the goal of zero food waste, sustainable practices should be monitored from farm to fork from an economic, social, and environmental standpoint. In the 2030 Agenda for Sustainable Development, it is stated that urgent measures should be taken on sustainable consumption and production, sustainable management of natural resources and climate change for the continuity of life on Earth. The circular economy(CE) model is a model of production and consumption**,** which involves sharing, leasing, reusing, repairing, refurbishing, and recycling existing materials and products as long as possible and is the most favored strategy (92%) for managing food waste. In terms of the supply chain, the focus of the circular economy is to ensure the optimal environmental results by enhancing the efficient use of resources. The optimized material flows in circular supply chains, leads to higher economic rewards compared to the traditional take-make-dispose aspect of linear ones. As a result, applying the circular economy in agri-food supply chains has the potential to alleviate the negative operational, economic, and

environmental effects of food waste. These mostly include energy and resource waste, idle time wasted on food production, raised emissions of greenhouse gases, and increased food expenses due to decreased food supply.

Food service organizations must improve efficiency at each phase of the supply chain, through procurement to logistics, production to marketing, and sales to after-sales support. Specifically, the agri-food sector additionally is volatile and complicated, necessitating the use of advanced techniques to maximize efficiency by optimizing resources, and reducing costs. (Duncan et al., 2019.; Angkiriwang et al., 2014.). At this stage, industry 4.0 is playing an essential role in the circularization of agri-food supply chains by transforming supply networks into intelligent systems capable of attaining full traceability of goods. (Zhang, 2020). Internet of Things and big data are major aspects in the industry 4.0 framework, proposing a linear-to-circular model transition to assist sustainability issues. Internet of Things(IoT) has an impact on agri-food supply chain through improved connectivity, reduced interference from humans, and energy conservation. (Vaibhav et al., 2022) The use of IoT in food chains has grown, with numerous linked devices that span portable agricultural equipment, tools, and hardware to residential devices and temperature-sensing devices. (Rao & Clarke, 2019). Moreover, the utilization of big data has advanced IoT networks by precisely documenting supply chain variables based on sensor network data; improved information visualization across the food network; promoted higher transparency, efficiency, and data-driven decision-making. (Ji et al., 2017; Li & Wang, 2017). As a result, more intelligent decisions are made, allowing food chains to run more efficiently, minimize expenditures, expedite the decision-making procedure, and reduce risks. This paper is structured as follows; Methodology section briefly describes how the study is conducted: CNN structure for image classification and WSN model. Results and Discussions section presents outputs of the implementation that are classification accuracy, sensor outputs and user information measures. Conclusions and Perspectives section restates the findings in terms of sustainability and under the improvement purpose of circular supply chains, and also presents relevant research for future investigations.

Industry 4.0 Applications for the Detection of Food Freshness

Food Image Classification

Creating methods to automate the fruit grading process is of great interest. Support vector machines, decision trees, and K-Nearest Neighbor algorithms are examples of machine learning techniques that have been effectively used to solve classification issues in the literature, notably for fruit categorization. Recently, artificial neural networks(ANNs) and CNNs, have also been used to the fruit categorization class, with extremely encouraging results. (Rizzo et al., 2023.). In computer vision applications including image classification, object identification, and visual question answering, convolutional neural networks are often utilized compared to others due its various advantages as: focusing on the different parts rather than the complete picture (Chakraborty et al., 2021.), and attaining higher accuracy (Das et al, 2020.).

Table 1. CNN models for fruit/vegetable classification

References	Dataset	Model	Accuracy
Lu, Y. (2019)	ImageNet	5-layer CNN	With augmentation 90.00%
Zhang et. al. (2019)	VegFru	13-layer CNN	94.94%
Wang et. al. (2018)	VegFru	8-layer CNN	95.67%
Sakib et. al. (2019)	Fruits-360	Own CNN model	99.79%
Mureşan et. al. (2018)	)Fruits-360	AlexNet, GoogLeNet, Own	~99.00%
Zhang et. al. (2015)	UEC-FOOD100	5-layer CNN	80.80%

As indicated in Table1, numerous studies have been conducted that aims to monitor the freshness of the food via in terms of the image classification. However, there was a gap in combining image classification with sensor data and the storage and processing of the outputs in a cloud-based system. Regarding this issue, our study combines provides a profound system that integrates the image classification and sensor gathered data in one and uses cloud platform as a baseline. In addition, most studies regarding the agri-food supply chain improvement are concerned with the production-to-retailer phase; whereas our study provides a different aspect for the waste management since, it targets the retailer-to-consumer phase.

Necessity of Cloud Architecture

IoT applications rely on sensor data to function, but processing and storing it may be quite difficult. Data aggregation from many and remote sources of information causes several privacy issues regarding information leaking. (Guo & Wang, 2019). In addition, using many IoT devices to monitor and assess various parameters, adds to the intricacy due to the variety of sensors and data formats in usage. Therefore, a sound monitoring system is needed for the data security of the aggregate food storage. One of the key applications for companies is maintaining the volume, speed, variety, and quality of data gathered by sensors in a cloud-based or hybrid IoT infrastructures. Considering this issue, our study provides a cloud-based data acquisition system that ensures security of the data gathered via key and certificate assurance and root user/user roles. The focus of this study is to contribute to the CE by improving the storage conditions in the retailer stage of the supply chain with the industry 4.0 approach, where considerable amount of food is wasted, e.g., 31% of the 195 million tons food is wasted in U.S. retail stores in 2010 (U.S. Dept. of. Agriculture, 2010). In this perspective, the literature on the classification of perishable products, and IoT applications for the freshness detection were reviewed. Based on our findings, a cloud embedded wireless sensor network (WSN) model is proposed and implemented to measure freshness of perishable products. The proposed model is composed of a CNN model using a dataset with images to classify fruits based on their freshness and ESP8266 microcontroller integrated with DHT11 and MQ3 sensors to measure variables affecting crop storage conditions and transmits gained results to AWS cloud system via Message Queue Telemetry Transport (MQTT) protocol.

Method

The proposed model, illustrated in Figure 1, initiates by taking input data from the shelf of retail stores or from their warehouses. It includes temperature, humidity and gas sensors, and also a camera for real-time detection of objects. The camera is used to take images of the products in retail stores. The sensors' humidity, excess gas, humidity reading outputs, and image info are fed to the Amazon Web Services (AWS) Cloud Platform. In AWS Cloud Service, taken images are processed using image processing feature extraction via CNN. Images are then grouped based on their types and freshness property using classification method. By doing so, our project will contribute to the retailer-to-consumer phase of the agri-food supply chain.

Fruit Image Classification

Image Classification Dataset

In this study, a dataset from Kaggle website named as "fruits: fresh and rotten for classification" was utilized. This dataset contains the following categories: fresh apples, fresh bananas, fresh oranges, rotten apples, rotten bananas, and rotten oranges. We used images of 1693 fresh apples, 1581 fresh bananas, 1466 fresh oranges, 2342 rotten apples, 2224 rotten bananas, and 1595 rotten oranges for training, and images of 395 fresh apples, 381 fresh bananas, 381 fresh oranges, and 388 rotten apples, 601 rotten bananas, and 530 rotten oranges for testing.

Convolutional Neural Network

A particular kind of artificial neural network called CNN is widely used for analyzing images, natural language, and other cognitive tasks.

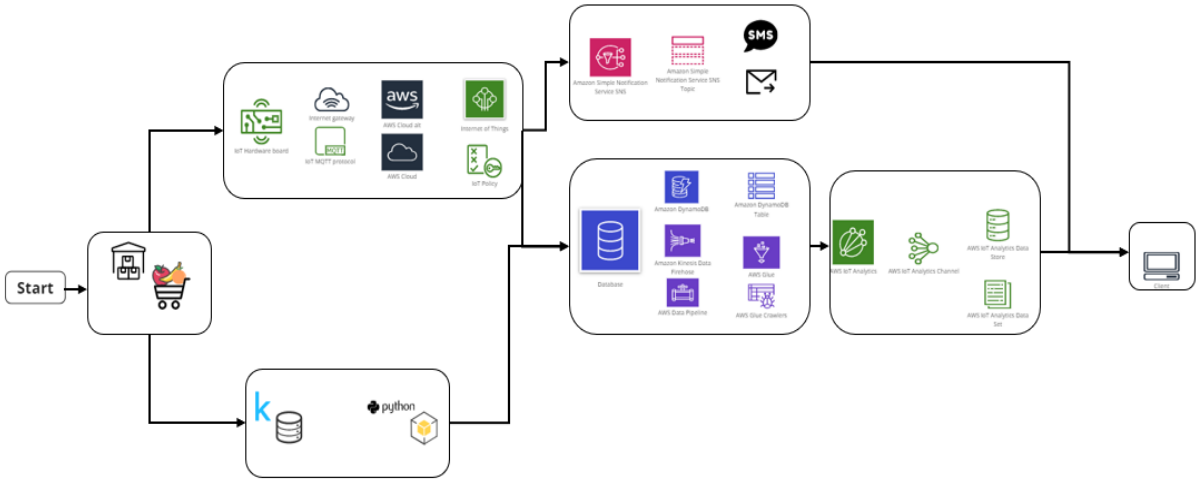

Figure 1. Proposed model diagram

The methodology used in this study is as following: The fruit images are selected and resized to (100×100×3) format. Then, RGB images are converted into gray scale and the dataset is transformed from having shape (n, width, height) to (n, depth, width, height). The dataset is partitioned into train and test sets and values were normalized from 0-255 to the range [0, 1]. Class labels are pre-processed, and the model architecture is designed. The model is compiled with Adam optimizer and categorical-cross entropy with learning rate=0.001. As the final step, model is taught with training set over 50 epochs and tested with 50 epochs using testing set.

Cloud Architecture

The implemented cloud architecture is based on the AWS Cloud. Via the ESP8266 Node MCU microcontroller, the data obtained from the DHT11 temperature and humidity sensor and the MQ3 alcohol sensor is sent to the AWS IoT Core Application, the first step of the AWS Cloud Architecture with the MQTT communication protocol. The microcontroller is coded with Arduino IDE 2023. A virtual microcontroller equivalent to the original microcontroller is defined on the cloud to display the data instantly with the IoT Core Application. For data security, determination of the parties that can access the data and have the authority to modify it, a policy that provides subscription, receive, and publish authorizations to the cloud platform by creating a device certificate is prepared and placed in the certificate. In our model, sensors' data is stored in S3 storage buckets via Kinesis Firehose Streamline for the SQL users and in the DynamoDB Database for the NoSQL users for the ease of analysis and since both has different advantages. The data accumulated in databases are then further analyzed in IoT Analytics platform for the purpose of enhanced monitoring and the visualization of the conditions in the retail store. In addition, to improve the user interaction with the system and to inform the users in case of rottenness, sensors' data are sent to SNS Push Notification Channel from IoT Core Application via the defined rules for message routing. By this way, system users are notified with an SMS and an e-mail including the values of the temperature, humidity, and gas level variables when the storage conditions, are out of the defined ranges. Furthermore, the CNN model created was transferred to AWS which works with the same Anaconda 3 Jupyter Lab interface, again for the purpose of enhanced data storage, accessibility of further analysis and for accumulation of the entire monitoring system within the same platform.

Results and Discussion

Classification Accuracy

The trials were run on Anaconda Software Jupyter Lab Notebook via a computer with an Intel® 11th Gen i7-11800H CPU processor running at 2.30GHz, a 1 TB SSD, and 8 GB of RAM to enable parallel processing and boost the classification task's computing capacity. This CNN Model had a training accuracy of 98.6% and an assessment accuracy of 96.4% over 50 epochs both.

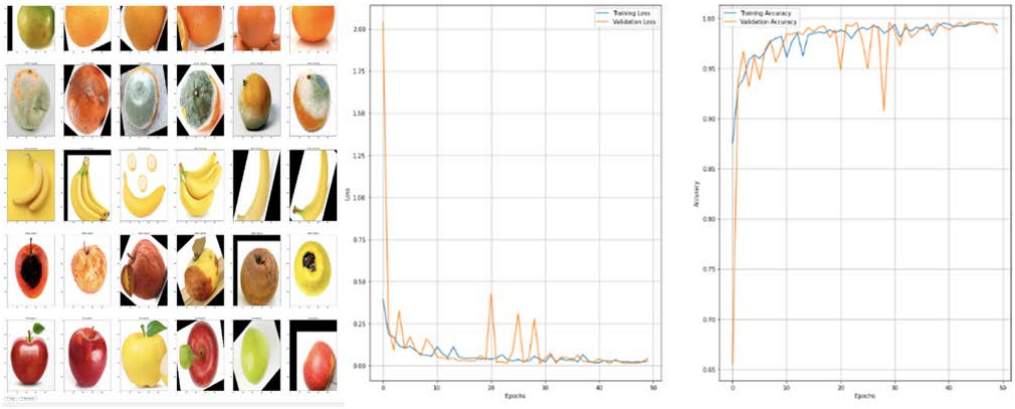

Figure 2. Training and validation accuracy

MQTT Communication & Cloud Architecture

As the outtakes are shown in Figure 3, DHT11 temperature, humidity, and MQ3 alcohol sensor data are transferred to the AWS IoT Core Application, the initial stage of the AWS Cloud Architecture, using the ESP8266 Node MCU microcontroller and the MQTT communication protocol.

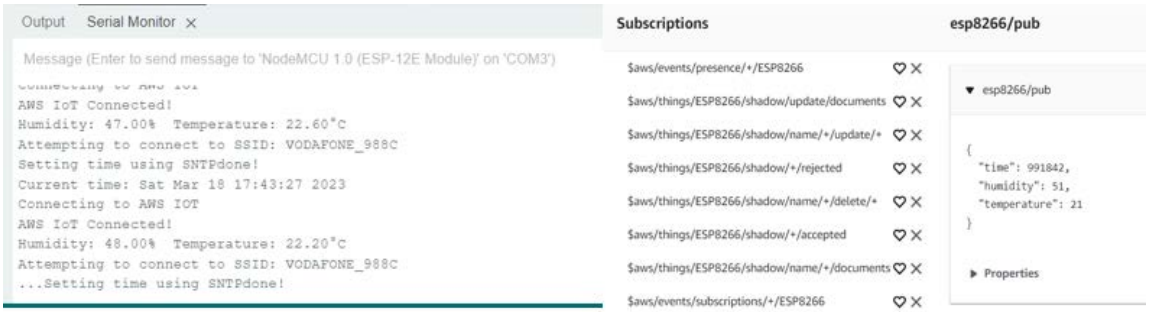

Figure 3. Sensor data readings (Arduino IDE Serial Monitor and the AWS Cloud)

Measurements from the sensors are delivered via the set rules for message routing to SNS Push Notification Channel to further enhance user involvement with the system and to alert users in the case of ripeness. In this approach, when the storage conditions are beyond the set limits shown in Figure 4, users of the system are alerted by SMS and email with the values of the temperature, humidity, and gas level parameters.

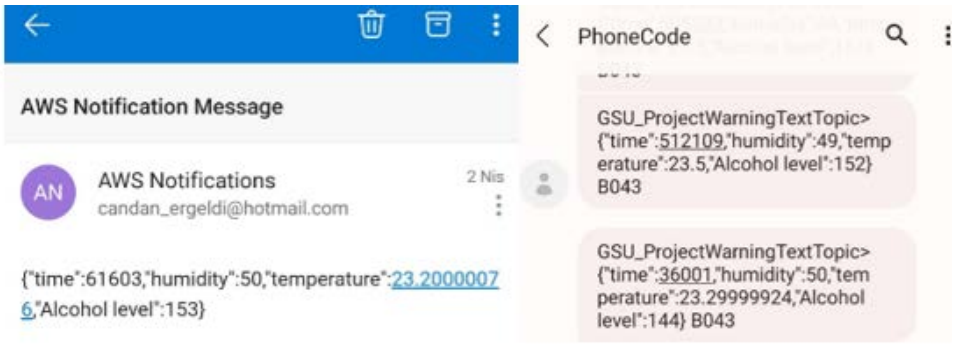

Figure 4. SNS push notifications (E-mail and the SMS)

Conclusion

The CE has the potential to increase food security and attain price stability. Regarding this issue, there have been I4.0 practices in agri-food supply chains, such as to improve sustainability for automating the fruit grading process. However, there is a gap in the making of a profound model that combines the sensor data and CNN

model together onto a cloud platform. To cope with this issue, we provided in this study a wireless sensor network model that was coupled with a CNN to determine the freshness of the food. The suggested application recognize the crops and categorizes them according to their freshness using a trained CNN model. Additionally, to improve the accuracy of the ripeness level, our ensemble model interfaces with the ESP8266 Node MCU microcontroller to relay the temperature, humidity, and alcohol level to the cloud system. As result, our CNN Model showed training accuracy of 98.6% and a testing accuracy of 96.4% over 50 epochs for each.

The approach used in this paper can precisely identify images of the inputted fruit types and classify them based on their ripeness. In addition, our model rapidly transmits data to the AWS Cloud; hence, the model is secure for industrial purposes the data accumulated in cloud can be further analyzed. For the future work, maturity levels of the fruits can be classified and categorized based on their relevant further use such as donating them to a food bank or for composting.

Scientific Ethics Declaration

The authors declare that the scientific ethical and legal responsibility of this article published in EPSTEM journal belongs to the authors.

Acknowledgements or Notes

* This article was presented as oral presentation at the International Conference on Basic Sciences, Engineering and Technology (www.icbaset.net) held in Marmaris/Turkey on April 27-30, 2023.

References

Angkiriwang R, Pujawan IN, & Santosa B. (2014). Managing uncertainty through supply chain fexibility: reactive vs. proactive approaches. *Prod Manuf Res 2*, 50–70.

Chakraborty, S., Shamrat, F. J. M., Billah, M. M., Al Jubair, M., Alauddin, M., & Ranjan, R. (2021, June).Implementation of deep learning methods to identify rotten fruits. In *2021 5th international conference on trends in electronics and informatics (ICOEI)* (pp. 1207-1212). IEEE.

Das, P., Yadav, J.K.P.S., & Yadav, A.K. (2021). An automated tomato maturity grading system using transfer learning based AlexNet. *Ingénierie des Systèmes d'Information*, 26(2), 191-200.

Duncan SE, Reinhard R, Williams RC, Ramsey F, Thomason W, Lee K, Dudek N, Mostaghimi S, Colbert E, & Murch R. (2019). Cyberbiosecurity: a new perspective on protecting U.S. Food and Agricultural System. *Frontiers in Bioengineering and Biotechnology*, *7*, Article 63.

Guo T, & Wang Y (2019). Big data application issues in the agricultural modernization of China. *Ekoloji 28*:36773688Vaibhav S. Narwane, Angappa Gunasekaran, Bhaskar B. Gardas. (2022). *Unlocking adoption challenges of IoT in Indian Agricultural and Food Supply Chain*, *Smart Agricultural Technology*, *2*, 100035, ISSN 2772-3755

Ji G, Hu L, & Tan KH. (2017). *A study on decision-making of food supply chain based on big data*. *J Syst Sci Syst Eng 26*, 183–198.

Li D, & Wang X. (2017). Dynamic supply chain decisions based on networked sensor data: an application in the chilled food retail chain. *Int J Prod Res 55*:5127–5141.

McGuire, S. (2011). US department of agriculture and US department of health and human services, dietary guidelines for Americans, 2010. Washington, DC: US government printing office, January 2011. *Advances in Nutrition*, *2*(3), 293-294.

Rao AR, & Clarke D. (2019). Perspectives on emerging directions in using IoT devices in blockchain applications. *Internet Things* 100079.

Ravindhar, N.V., & Sasikumar, S. (2022). An effective monitoring, storage and analyze on industrial process on cloud bigdata by data publishing in industrial wireless sensor network. *Measurement: Sensors*, *24* 100525

Rizzo M., Marcuzzo M., Zangari A., Gasparetto A., & Albarelli A. (2023). Fruit ripeness classification: A survey, *Artificial Intelligence in Agriculture*, *7*, 44-57.

Author Information

Candan Ergeldi
Galatasaray University
Ortaköy, Çırağan St. Nu:36, 34349 Beşiktaş/İstanbul, Türkiye
Contact e-mail: *candan_ergeldi@hotmail.com*

Orhan Feyzioglu
Galatasaray University
Ortaköy, Çırağan St. Nu:36, 34349 Beşiktaş/İstanbul, Türkiye

To cite this article:

Ergeldi, C. & Feyzioglu, O. (2023). Circular supply chains: an internet of things application for rotten product detection in aggregate food industry. *The Eurasia Proceedings of Science, Technology, Engineering & Mathematics (EPSTEM), 22*, 210-216.

The Eurasia Proceedings of Science, Technology, Engineering & Mathematics (EPSTEM)
ISSN: 2602-3199

The Eurasia Proceedings of Science, Technology, Engineering & Mathematics (EPSTEM), 2023

Volume 22, Pages 217-226

ICBASET 2023: International Conference on Basic Sciences, Engineering and Technology

CO_2 Capture by PEI-Impregnated Alumina Sorbents

Furkan TURGUT
LOGOS Kimya Teknolojileri Ltd. Şti.

Simge KOSTIK
Izmir Institute of Technology

Barıs ERDOGAN
LOGOS Kimya Teknolojileri Ltd. Şti.

Basar CAGLAR
Izmir Institute of Technology

Abstract: Direct air capture (DAC) or direct CO_2 extraction from ambient air is a promising approach to reduce greenhouse gas emissions caused by both distributed (location independent) and point sources (location specific). Solid sorbents have been considered as more effective for DAC compared to the liquid counterpart since they have a faster kinetic and avoid volatile and heat losses due to the absence of evaporation of liquids. In this study, the alumina - supported polyethyleneimine (PEI) material was chosen as solid sorbents and their CO_2 capture performance for different PEI loadings (20, 35, 50 wt%), flow rate (15, 30, 45 L/h) and adsorption temperatures (30, 40, 50, 60 °C) was investigated. Sorbents were prepared by using wetness impregnation method and their physical and chemical properties were characterized by several techniques such as N_2 adsorption - desorption (surface area, pore size and volume), Scanning Electron Microscopy - SEM (surface morphology, surface chemical composition). The CO_2 capture performance of sorbents were analyzed under different CO_2 concentrations and the cyclic (adsorption - desorption) behavior of the sorbents were tested. The results show that alumina-supported PEI adsorbents are promising materials for CO_2 capture with high CO_2 adsorption capacity and stability.

Keywords: PEI, Adsorption, CO_2 Capture, DAC, Greenhouse Gas, Alumina

Introduction

Carbon capture and storage (CCS) is crucial in the fight against climate change, which poses an existential threat to our planet. Despite being on the global agenda for decades, progress has been slow, insufficient, and sporadic. Anthropogenic CO_2 emissions are caused by our reliance on fossil fuels, accounting for 68% (or 37.5 $GtCO_2$) of the total greenhouse gas emissions in 2018. Capturing CO_2 at this scale requires resources and technologies that are currently unavailable. C_{O2} capture is an expensive, energy-intensive process that is complicated by diverse emission sources varying in volume, composition, location, type, and industry or sector. However, the diversity of sources highlights the need for a multi-prong strategy that emphasizes the development of a wide range of CCS technologies, materials, and processes tailored to different sources (Gür, 2022).

Direct air capture (DAC) is a method of removing CO_2 directly from the atmosphere to achieve negative emissions. Despite concerns regarding its feasibility, there has been growing interest in exploring this technology as a climate change mitigation strategy. Proponents argue that even if carbon emissions were to stop

completely, atmospheric CO_2 concentrations must be reduced expeditiously to mitigate the risks of climate change. DAC has the advantage of being able to capture CO_2 emissions from distributed sources, which make up almost half of global CO_2 emissions, unlike other technologies that mostly capture emissions from point sources (Yu et al., 2012).

Various DAC technologies exist including physical absorption, chemical absorption, adsorption, and membrane technologies, but none of them are yet matured for post-combustion power plants due to significant mass transfer limitations and the need to treat a huge amount of flue gas. Among these technologies, chemical absorption using aqueous alkanolamine solutions is proposed to be the most applicable technology for CO_2 capture before 2030, but it has drawbacks such as high equipment corrosion rate, high energy consumption in regeneration, and a large absorber volume required. Solid adsorption processes, such as impregnation or grafting of amines, have been suggested to overcome these problems. Chemical modification of solid materials with high surface area is a key area of research to improve CO_2 adsorption and selectivity for DAC. The use of organic groups such as amines and inorganic metal oxides like alkali or alkali-earth metals has garnered particular interest due to their basic properties. Covalent bonding between the acidic CO_2 molecules and modified basic active sites on the surface enhances CO_2 adsorption. Although amine-based adsorbents have a low heat of regeneration compared to aqueous amines due to the low heat capacity of solid supports, their low CO_2 adsorption capacity and high cost hinder commercialization. To improve amine-based adsorbents, recent approaches include using amine with high nitrogen content, preparing supports with high amine loading, and effective methods for amine introduction. Amine-based adsorbents can be categorized as amine-impregnated and amine-grafted materials based on their interaction with the supports. Typically, amine-grafted adsorbents exhibit higher adsorption rates and stability in cyclic runs than amine-impregnated ones. However, the grafted amount of amine depends on surface silanol groups, which can result in lower amine loading compared to impregnation. Although higher amine loadings can be achieved through impregnation, it can lead to a large diffusion resistance. The feasibility of operating under practical conditions, containing 3-5% water and 10-15% CO_2 at 55°C in coal power plant flue gases, requires evaluating kinetics and heat effects (Yu et al., 2012).

There are several types of amines that are commonly used for solid adsorbents for CO_2 capture. Primary amines such as monoethanolamine (MEA), diethanolamine (DEA) and triethylenetetramine (TETA) contain one amino ($-NH_2$) group and they are well known their high CO_2 affinity whereas secondary amines like piperazine and N-methyldiethanolamine (MDEA) have two amine groups and they have a lower CO_2 affinity compared to primary amines. N, N-dimethylethanolamine (DMEA) and N, N-dimethylcyclohexylamine (DMCHA) are known as tertiary amines that have three amino groups and have the lowest CO_2 affinity in this class. When polymers are functionalized with amine groups which are called as amine-functionalized polymers, their CO_2 adsorption capacity can be increased due to their high surface area (Wang et al., 2015). Polyethyleneimine (PEI) and polyvinylamine (PVAm) are the most known examples of this class. Primary amines and tertiary amines are often used in post-combustion and pre-combustion CO_2 capture, respectively. Amine-functionalized polymers are used in both post- and pre-combustion CO_2 capture processes.

PEI is a high molecular weight polymer with a branched structure and abundant amino groups that allow for strong CO_2 adsorption. The high molecular weight and branched structure provide a large number of amine groups, which increases the CO_2 adsorption capacity of the material. In addition, PEI is known to have excellent stability and resistance to degradation under harsh conditions such as high temperatures and acidic environments, which are commonly encountered in CO_2 capture processes (Li et al., 2021). This stability ensures the material can be used repeatedly without significant loss of CO_2 adsorption capacity. PEI also has low volatility, which means that it does not evaporate or escape easily into the gas stream during CO_2 capture, reducing the possibility of amine emissions and environmental pollution. This low volatility is attributed to the high molecular weight of the polymer and the strong interactions between the amine groups and the support material.

Xu and his colleagues have investigated the impact of several factors on the capacity of polyethylenimine (PEI) for adsorbing carbon dioxide (CO_2) (Xu et al., 2002a). These factors include PEI loading, gas conditions, temperature, moisture, and the type of support used. Results have shown that a higher PEI loading led to a significant increase in CO_2 adsorption capacity, although this was accompanied by a reduction in surface area, pore size, and pore volume. The highest CO_2 adsorption capacity was observed with 75 wt.% PEI loading in PEI-impregnated MCM-41 under pure CO_2 at 75°C. However, the highest amine efficiency was found with 50 wt% PEI loading and decreased with increasing PEI loading. This suggests that amine loading is not directly related to CO_2 adsorption since the formation of aggregated amine on supports can reduce the amine accessible to CO_2.Temperature was also found to affect CO_2 adsorption capacity, with lower temperatures resulting in decreased capacity due to the exothermic nature of CO_2 adsorption. However, at low temperatures, bulk-like

PEI formation inside pores could lead to diffusion-limited CO_2 adsorption. Higher temperatures were associated with higher CO_2 adsorption capacity, likely due to the increased diffusion rate of CO_2 into bulk-like PEI and the faster reaction rate of CO_2 with PEI. Moisture was found to have a positive effect on CO_2 adsorption capacity when present at concentrations lower than that of CO_2 with carbamate and bicarbonate formation under anhydrous and hydrous conditions respectively.

Flow rate is also important parameter that affects the contact time between the CO_2 and the adsorbent, and a higher flow rate typically leads to a shorter contact time. As a result, the CO_2 may not have enough time to adsorb onto the solid adsorbent and the overall capture efficiency may be reduced. On the other hand, a lower flow rate can increase the contact time between the CO_2 and the adsorbent leading to higher capture efficiency. However, a very low flow rate may also lead to a reduced efficiency due to mass transfer limitations. Shafeeyan et al. (Shafeeyan et al., 2015) studied the adsorption of CO_2 onto ammonia-modified activated carbon and measured the breakthrough adsorption of CO_2 on fixed beds of commercial granular activated carbon (GAC) and ammonia-modified GAC (OXA-GAC) adsorbents. They measured the breakthrough curves from dynamic column measurements at temperatures ranging from 30 to 60 °C with a feed gas flow rate that varied from 50 to 100 mL.min^{-1} and a total pressure of 1.0 atm. They found that the breakthrough time of CO_2 adsorption decreased with increasing flow rate indicating that the flow rate has a significant effect on the CO_2 adsorption capacity of the adsorbent. A study by Darunte et al. investigated the effect of flow rate on CO_2 adsorption by a novel amine-functionalized metal-organic framework (MOF), MIL-101(Cr)-NH_2. They found that the CO_2 adsorption capacity of MIL-101(Cr)-NH_2 increased with increasing flow rate and the maximum CO_2 adsorption capacity was achieved at a flow rate of 100 mL/min (Darunte et al., 2016). However, Goeppert and his colleagues found that total CO_2 adsorption capacity of the silica supported PEI adsorbents did not show the high dependency on the flow rate (Goeppert et al., 2014). When they increase the flow rate from 335 to 945 mL min^{-1}, this resulted with decrease in the total adsorption capacity from 50 to 47 mg CO_2 g^{-1} when 33% PEI by weight was used and increase in PEI loading caused to increase in effect of flow rate on the CO_2 adsorption capacity.

Adsorption temperature is another important factor that can affect the CO_2 capture efficiency. At low temperatures, the adsorption of CO_2 onto the adsorbent surface is generally more favorable because the kinetic energy of the CO_2 molecules is lower, which makes them more likely to adsorb onto the surface. This can lead to a higher CO_2 capture capacity at lower temperatures. However, it's worth noting that the rate of adsorption may be slower at low temperatures, which can reduce the overall capture efficiency. At high temperatures, the adsorption of CO_2 onto the adsorbent surface is generally less favorable because the kinetic energy of the CO_2 molecules is higher, which makes them less likely to adsorb onto the surface. As a result, the CO_2 capture capacity may be reduced at higher temperatures. However, high temperatures can also result in desorption of previously adsorbed CO_2, which can be beneficial for the regeneration of the adsorbent and the reusability of the system. Geoppert et al., found that increase in temperature results with the decrease in total CO_2 adsorption from air by silica-supported PEI adsorbents with loading of 33% and 50% by weight (Goeppert et al., 2014). However, increase in temperature from 25 to 35 ^{o}C slightly increased the total adsorption from air and significantly decreased when the temperature increased up to 85 ^{o}C when air under 10 ppm was used.

The support material used in direct air capture (DAC) with polyethyleneimine (PEI) sorbents plays a critical role in determining the overall performance of the system. The support material serves as a substrate for the PEI sorbent, providing a large surface area for CO_2 adsorption and facilitating mass transfer between the gas and solid phases. Different support materials can vary in their pore structure, surface chemistry, and other properties that can impact the adsorption capacity, selectivity, and stability of the sorbent. Solid amine sorbents are commonly supported by silica, but alumina and titania could be better options as they can address some of silica's limitations. Silica, for instance, experiences a structural change and loses its CO_2 capture capability when exposed to steam. While PEI-impregnated sorbents can be regenerated through various methods, including temperature-vacuum alternation, hot CO_2 flow, and water vapor, a urea-forming reaction can lead to irreversible PEI decomposition when CO_2 reacts with two amine groups at or above 135 ^{o}C in dry conditions. Water vapor regeneration can prevent this decomposition to some extent, but it cannot eliminate urea formation. Steam regeneration or steam-stripping is a convenient method for thermal regeneration, especially in industrial processes where waste steam is typically around the temperature required for water vapor regeneration. Nevertheless, porous silica such as MCM41, SBA-15, and MCF may not be stable in water vapor, leading to a loss of CO_2 uptake capacity (Xu et al., 2002b). Alumina supports, however, are more resistant to structural changes and degradation during regeneration with water vapor due to their crystallinity and lower hydrophilicity.

The CO_2 capture performance of PEI-loaded alumina sorbents have been addressed several times in the literature. Goeppert and colleagues described the preparation of an alumina-supported PEI sorbent for DAC

(Goeppert et al., 2011). The sorbent was prepared by impregnating gamma-alumina with a solution of PEI, followed by drying and calcination. The resulting sorbent had a CO_2 adsorption capacity of 73 to 75 mg CO_2/g adsorbent (1.65 to 1.71 mmol/g). However, when they use alpha-alumina supported PEI rather than gamma-alumina supported PEI, the resulting sorbent had a CO_2 adsorption capacity of 1.02 mmol/g at 25 °C and atmospheric pressure and 1.41 mmol/g at 50 °C and atmospheric pressure. All of these studies have been carried out using methanol as a solvent, however, when the resulting supported-PEI were treated with a mixture of acetic acid and acetic anhydride, CO_2 adsorption capacity of the resulting sorbent reached the 1.85 mmol/g (Gargiulo et al., 2007) and Zhang et al.(Zhang et al., 2013) reported that the adsorbent exhibited a high CO_2 adsorption capacity of 2.5 mmol/g for alumina sorbents with PEI loading of 30 wt% and 40 wt%, respectively. Lin et al. (Lin et al., 2013) reported that at 100 wt% PEI loading, the CO_2 adsorption capacity at 0.15 bar reached a very competitive value of 4.2 mmol g^{-1} at 25°C and 3.4 mmol g^{-1} at 50°C, while Chen et al. (Chen et al., 2014) found that the optimal PEI loading was 50 wt% and the adsorbed amount of CO_2 was 2.5 mmol g^{-1} at 25 °C and 1 bar. The literature studies summarized above for the CO_2 capture from ambient air (400-450 ppm CO_2) on PEI-loaded alumina sorbents indicate that CO_2 adsorption capacity of sorbents varies between 1.65-4.2 mmol/g suggesting that PEI-loaded alumina has an important potential as CO_2 sorbent material. However, the significant difference in the CO_2 adsorption capacity and the optimum PEI loading shows that the relation between the CO_2 capture performance of the material and their physical and chemical properties needs to be further addressed to develop high-performance sorbents. In addition, the CO2 capture performance of the related material at higher CO_2 pressure is lacking in the literature. This needs to be investigated to understand the effect of CO_2 concentration on the CO_2 adsorption capacity of the sorbents, which is especially important to determine the performance of sorbents for the CO_2 capture by pressure-swing adsorption (PSA) process.

To address the related issues, the CO_2 capture by the alumina-supported PEI adsorbents with different PEI loadings have been investigated at different CO_2 concentrations (e.g., 1 and 17%), flow rates and adsorption temperatures. Sorbents were prepared by the impregnation method and characterized by several techniques to link sorbent properties with CO_2 capture performance.

Method

Preparation of Adsorbents

PEI-loaded alumina sorbents were prepared by the impregnation method. F-200 activated gamma alumina adsorbent was purchased from BASF. The sorbent preparation process involves several steps. First, alumina pellets were washed with methanol and dried overnight in an oven at 100 °C. Then, the clean alumina spheres were mixed with 20 ml of methanol and kept under stirring for one hour. Next, 20 ml of methanol was mixed with a specific amount of PEI depending on the desired PEI loading and the resulting mixture was stirred for one hour. The PEI-methanol solution was then added dropwise to alumina pellets suspended in 20 mL of methanol and stirred for another hour. The resulting impregnated alumina pellets were then dried using a rotary evaporator at 50 °C under vacuum with a rotation of 100 rpm and a pressure of 100 mbar. The pellets were subsequently dried in a vacuum oven at 60 °C overnight. Finally, the pellets were weighed, and the PEI loading was calculated and recorded. The PEI loadings were 20%, 35% and 50% by weight and 2 g pellets were prepared for each batch.

CO_2 Adsorption and Desorption Experiments

The CO_2 adsorption and desorption studies were performed at two different CO_2 concentrations by using two different experimental setups. The experiments with a CO_2 concentration of 1% were conducted using Micromeritics' AutoChem II 2920 Chemisorption Analyzer equipped with a TCD detector with a U-tube sorbent bed. The sorbents were loaded to the reactor and heated to 110 °C under N_2 atmosphere for 2 hours to remove water and volatile components. The sorbents were then cooled to the adsorption temperature (40, 50, or 60 °C) The adsorption experiments were carried out at 40 °C under 1% CO_2/N_2 atmosphere with a flow rate of 25 ml/min for 1 hour for desorption, at the end of the adsorption period, the gas was switched from CO_2/N_2 to N_2 (inert gas) and left for 0.5 hours with a flow rate of 50 ml/min. Under the inert gas atmosphere, the temperature was increased to 120 °C with a flow rate of 50 ml/min and a heating rate of 5 °C/min and left for 1 hour. The sample was then cooled down to 40 °C under N_2 flow with 50 ml/min flow rate and the experiment was finalized.

The adsorption-desorption experiments with a CO_2 concentration of 17% were performed in a home-built setup containing a quartz reactor (ID: 10 mm), a tubular oven, flow control units and a CO_2 detector. Sorbents were loaded into the reactor and heated to 110 °C under N_2 atmosphere with a flow rate of 20 L/h. The sample was kept at that temperature for 1 hour to remove water and volatile components. The sample was then cooled to the desired adsorption temperature (40, 50, 60 °C) and the gas flow was switched from N_2 to a 17% CO_2 - N_2 gas mixture. Adsorption experiments were carried out under a 17% CO_2-N_2 gas mixture atmosphere with a flow rate of 15 – 30 – 45 L/h CO_2-N_2 for 1 hour. At the end of the adsorption period, the gas was switched from CO_2-N_2 to N_2, and the system was left for 1 hour with a flow rate of 20 L/h. Under an inert gas atmosphere, the temperature was increased to 120 °C with a flow rate of 20 L/h and a heating rate of 5 °C/min and the system was left for 1 hour. The system was finally cooled down to 40 °C under an N_2 flow with a flow rate of 20 L/h.

Sorbent Characterization

The amine loading of sorbents was determined by elemental analysis. The Leco Truspec CHN-2007S was utilized and the nitrogen content of sorbents was used to quantify the amine loading. The surface area, pore volume and pore size distribution of sorbents were analyzed by N_2 adsorption-desorption using Micromeritics Tristar II. The surface area of sorbents was determined using the Brunauer – Emmett − Teller (BET) method, while the pore volume and pore size distribution were calculated using the Barrett−Joyner−Halenda (BJH) method. Prior to analysis, alumina-supported PEI adsorbents were degassed at 110 °C for 2 hours, while alumina spheres were degassed at 60 °C for 12 hours. Thermal gravimetric analysis (TGA) was conducted to determine the desorption and decomposition temperature of CO_2, H_2O, and PEI under N_2 environment by using Perkin Elmer Diomand TG/DTA analyzer. The analysis was carried out at 25-900 °C with a heating rate of 10 °C/min and for 2 hours. SEM-EDX analysis was carried out to investigate surface morphology by using FEI QUANTA 250 FEG analyzer.

Results and Discussion

TGA analysis was performed to determine the thermal stability and decomposition behavior of the adsorbent. One of the challenges in direct air capture is the regeneration of the adsorbent after it is saturated with CO_2. Regeneration typically involves heating the absorbent to high temperatures (70-100 °C), but the excessive heating can cause thermal degradation of the adsorbent, leading to a decrease in its performance over time. To prevent thermal degradation of the sorbent and to determine the safe regeneration window, TGA analysis was applied.

Figure 1 shows TGA curve of 50% PEI containing alumina between 25 ^oC and 800 ^oC. As seen from the Figure, the first weight loss occurs between 25 and 1500 °C, which is related to water and CO_2 removal. This is followed by a stepwise weight loss between 150 and 600°C, which is attributed to the removal of volatiles caused by PEI degradation via the breaking of the polymer chains. This finding suggests that the regeneration temperature needs to be less than 150°C since above 150C PEI on gamma-alumina starts to degrade. The PEI-related weight loss is around 30%, which is less than the expected weight loss (33.3%) based on PEI loading. Since there is no clear division between weight loss related to water and CO2 removal and PEI degradation, it is difficult to determine PEI loading by TGA analysis. Therefore, CHNS analysis was applied to determine the PEI loading of sorbents by the nitrogen contents of sorbents. The PEI loadings determined by CHNS analysis are shown in Table 1. As seen from the Table, the actual PEI loadings of sorbents are 19.6, 27.5 and 27.4 wt% for 20PEI, 35PEI and 50PEI, respectively. The PEI loadings for 35PEI and 50PEI are almost the same suggesting that PEI does not dissolve in methanol completely for PEI loading greater than 30% in the specified PEI/methanol ratio.

It is well known that amine loading directly affects textural properties of sorbents such as surface area, pore volume and size. The extent of this effect for different PEI loading was analyzed by N_2 adsorption-desorption experiments. Results are shown in Table 2 indicating that the surface area and pore volume of sorbents decreases significantly with PEI loading due to the pore-filling effect of the polymer. The degree of reduction is much higher compared to PEI-loaded sorbents with similar PEI loadings. This is related to the poor solubility of PEI in methanol in the specified impregnation conditions. This was also proved by SEM-EDX analysis. SEM-EDX analysis was performed on both alumina and PEI-loaded alumina sorbents to study the morphology and elemental composition of the adsorbent material.

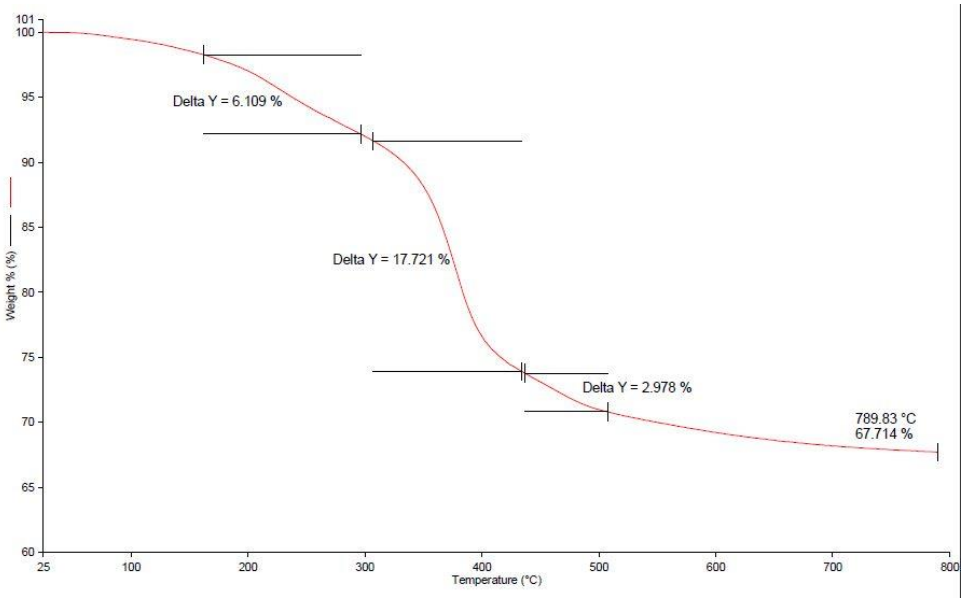

Figure 1. TGA Analysis of PEIM_50 Adsorbent

Figure 2 shows SEM images and elemental map of sorbents. Results show that C, O and N have more uniform distribution on alumina-supported PEI with a loading of 50% by weight contrary to loadings of 20% and 35% (**Figure 2**). However, for all PEI-containing sorbents PEI loading concentrates to specific sites of the support indicating uneven distribution of PEI on the surface. This can be attributed to the poor solubility of PEI in methanol or insufficient mixing process, which supports the findings of N2 adsorption-desorption analysis. Surface composition of carbon and nitrogen was also determined from EDX analysis and listed in **Table 2** in comparison the bulk composition of the related elements. As seen from the Table, surface compositions of carbon and nitrogen are almost doubled compared to bulk composition. This is expected considering that PEI molecules cover surface sites.

Table 1. BET Analysis result of adsorbents

Adsorbents	BET Surface Area (m^2/g)	Volume of Pores (cm^3/g)
Pure Al_2O_3	327.5273	0.291974
PEIM_20	43.2688	0.088509
PEIM_35	21.7087	0.042147
PEIM_50	8.44300	0.013505

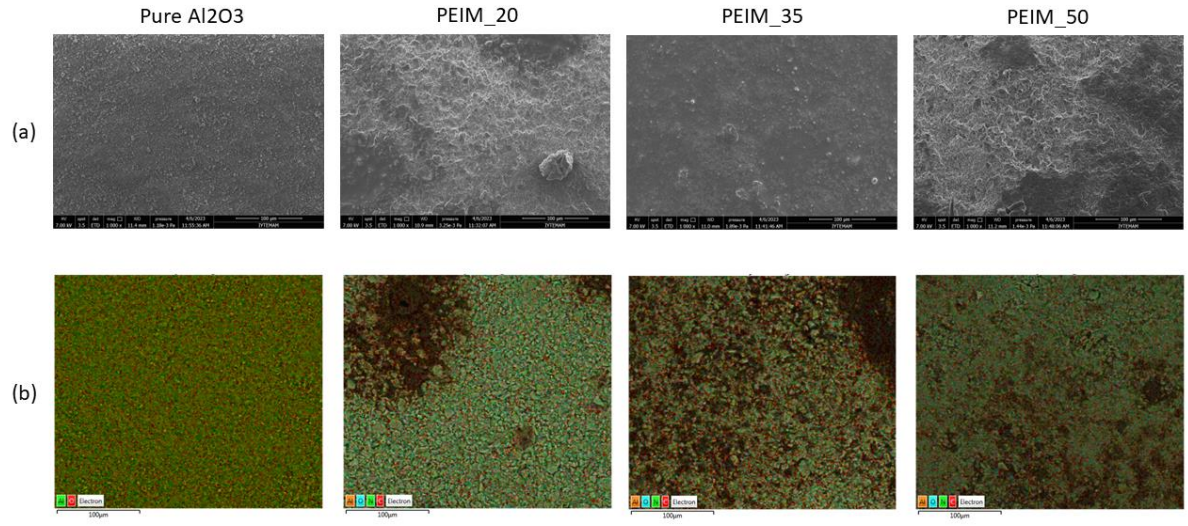

Figure 2. SEM images of adsorbents, (a) Adsorbents surface (magnification: 1000x), (b) Adsorbents surface (EDX, magnification: 1000x)

Table 2. Elemental composition of adsorbents

Adsorbents	Theoretical	CHNS	SEM-EDX
PEIM_20 (wt%)			
C	9.29	13.41	26.76
H	1.96	3.81	NA
N	5.42	5.34	9.68
PEIM_35 (wt%)			
C	14.45	15.51	40.22
H	3.05	4.41	NA
N	8.43	7.03	16.16
PEIM_50 (wt%)			
C	18.57	15.68	44.16
H	3.92	3.94	NA
N	10.83	6.99	17.78

CO_2 adsorption capacity of sorbents were first tested under 1% CO_2 in chemisorption setup by a TCD detector. Since the TCD detector works based on the change in thermal conductivity, it is sensitive to all gases, which complicates obtaining CO_2 adsorption profiles. However, it can still be used to determine the CO2 adsorption capacity of sorbents by using their desorption curves. By using this approach, CO_2 adsorption capacity of sorbents were calculated from desorption peak areas and listed in Table 3. As seen from the table, CO_2 adsorption capacities of PEIM_35, PEIM_50, alumina and PEIM_20 are 90.5, 63.1, 50.3 and 26.2 mg CO_2/g sorbent, respectively. Results show that alumina has a higher CO_2 capture capacity than the sorbent with 20% PEI loading. This can be ascribed to the significant reduction in surface area and pore volume of PEIM_20 compared to pure alumina, which leads to very few active sites for CO2 adsorption. Even if the CO_2 adsorption on PEI is more chemically favored compared to the CO_2 adsorption on alumina, the dramatic decrease in surface area and pore volume of PEIM_20 results in lower CO_2 adsorption. A similar effect was not observed for PEIM_35 and PEIM_50, which show higher CO_2 adsorption compared to pure alumina. The enhancement of CO2 adsorption by PEI for these sorbents are more dominant than the reduction of CO_2 adsorption due to the low surface area and pore volume. PEIM_35 shows higher CO_2 adsorption capability compared to PEIM_50, which can be explained by steric hindrance and a reduction in the accessibility of the amine groups to the CO_2 molecules at high PEI loading. Another possible explanation is that at higher PEI loadings, there may be an increase in the number of free amine groups that are not attached to the surface of the adsorbent. These free amine groups can interact with each other and form bulky PEI aggregates which can reduce the available surface area for CO_2 adsorption and lower the CO_2 adsorption capacity.

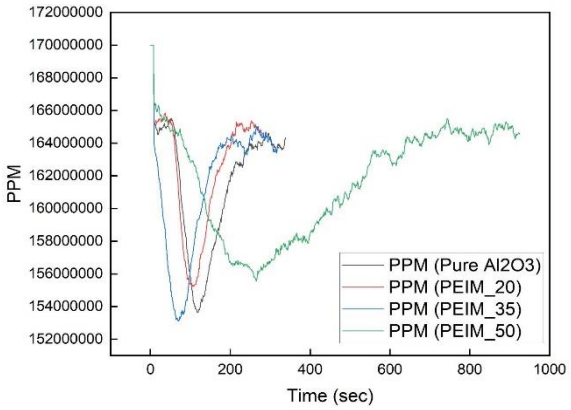

Figure 3. Adsorption of CO_2 by solid adsorbents under 17% CO_2 (ppm) atmosphere.

Table 3. CO_2 adsorption capacities of adsorbents for 1% and 17% CO_2

	Adsorbents	CO_2 Adsorption Capacity (mg CO_2/g adsorbent)
1% CO_2	PEIM_20	26.2
	PEIM_35	90.5
	PEIM_50	63.1
17% CO_2	PEIM_20	6.25
	PEIM_35	6.69
	PEIM_50	24.0

CO_2 adsorption behaviors of sorbent were also studied under 17% CO_2 environment. Figure 3 shows CO_2 adsorption curves for all sorbents. Different from the results obtained at low CO_2 concentration, PEIM_50 exhibits the highest CO_2 adsorption capacity. CO_2 adsorption on the related sorbent occurs in a long adsorption period. The other sorbents behave differently, i.e., they show a fast CO_2 build-up (e.g., sharp decrease in CO_2 concentration) and short adsorption times. Among them, CO_2 adsorption capacity decreases in order by PEIM_35 > alumina > PEIM_20. The CO_2 adsorption capacity of sorbents were also calculated by using areas under the curve and tabulated in Table 3. Calculations indicate that PEIM_50 has almost 4 times higher adsorption capacity than PEIM35 and PEIM_20. The latter two show almost the same performance. The calculated adsorption capacities of sorbents are quite low compared to those obtained at low CO_2 concentrations. This is attributed to high internal mass transfer resistance of sorbents at high flow rate conditions. The gas flow rate for experiments conducted at high CO_2 concentrations is almost 10-fold higher than those performed at low CO_2 concentration. This suggests that the CO_2 adsorption on PEI-loaded sorbents is diffusion limited due to their relatively low pore size.

The effect of diffusion limitation of PEI-loaded sorbents was also evaluated by experiments conducted at different flow rates. Figure 4 shows CO_2 adsorption of the best performance sorbent (PEIM_50) at flow rates of 15, 30 and 45 L/h under 17% CO_2 atmosphere. The figure shows that increase in flow rate results with the decrease in CO_2 capture capacity (Figure 4 and Table 4) and there is a dramatic decrease in adsorption behavior and capacity (Table 4) between the flow rates of 15 and 30 L/h. This indicates that above the flow rate of 15L/h the gas flow rate is so fast that there is not enough time for adsorption due to relatively slow diffusion processes.

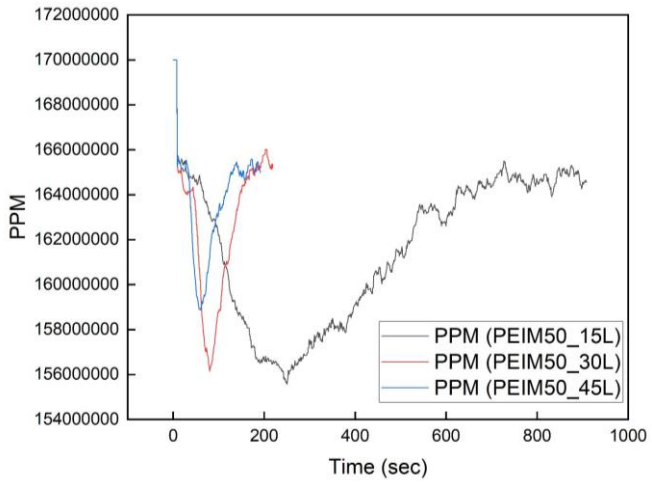

Figure 4. Effect of flow rate on the CO_2 adsorption via the alumina-supported PEI adsorbent with a loading of 50% by weight.

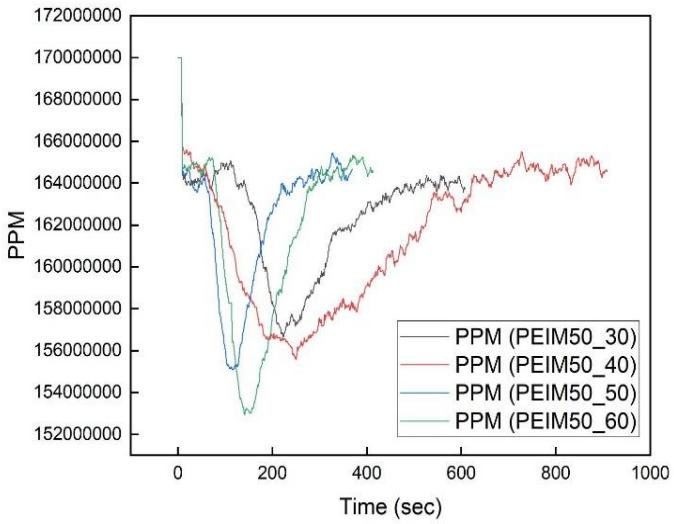

Figure 5. Effect of adsorption temperature on the CO_2 adsorption via the alumina-supported PEI adsorbent with a loading of 50% by weight.

Table 4. Effect of flow rate and adsorption temperature on CO_2 adsorption capacity of PEIM_50

	CO_2 Adsorption Capacity (mg CO_2/g adsorbent)
Flow Rate (L/h)	
15	24.0
30	3.57
45	2.49
Adsorption Temperature (°C)	
30	10.1
40	24.0
50	6.31
60	11.3

The effect of adsorption temperature on the CO_2 adsorption was also studied for the best performing sorbent under 17% CO_2 at 3 different temperatures (e.g. 30, 40, 50 and 60 ^oC). The results show that total adsorption capacity increases approximately by two-fold when the temperature increases from 30 to 40 ^oC, however, there is a decreasing trend above 40 ^oC (Figure 5 and Table 4). This is different from what was observed in the literature, where the adsorption capacity decreases with the adsorption temperature. The related difference can be explained by the excessive reduction of pore size and volume of PEI-loaded sorbents and corresponding diffusion limitation. The diffusion process is accelerated with a small increase in temperature leading to higher adsorption rate while the further increase results in decrease in the adsorption capacity due to the dominating kinetic effect of the desorption process.

Conclusion

Direct air capture (DAC) is a potential method to decrease greenhouse gas emissions from both point sources and distributed sources. Solid sorbents have been considered to be more effective than liquid sorbents for DAC due to their faster kinetics and their ability to avoid volatile and heat losses caused by liquid evaporation. In this investigation, we chose alumina-supported polyethyleneimine (PEI) materials as solid sorbents and examined their CO_2 capturing behaviour for various PEI loadings (20, 35, 50 wt%), flow rates (15, 30, 45 L/h) and adsorption temperatures (30, 40, 50, 60 °C) and at 2 different CO_2 concentration (1% and 17%). The sorbents were prepared using a wetness impregnation technique and were characterized for their physical and chemical properties. Results show that 35% PEI loading has the best CO_2 capture capacity under 1% CO_2 flow with a capacity of 90.5 mg/g sorbent. However, at 17% CO_2 flow, 50% PEI loading was found to be the best choice with a capacity of 24 mg/g sorbent. The significant difference in the CO_2 adsorption capacity of sorbents between 2 different CO_2 concentrations is attributed to the strong diffusion limitation of sorbents caused by the dramatic decrease in their surface area and pore volume. We also found that the flow rate and adsorption temperature have a strong impact on the CO_2 capture capacity. Both have negative effects on the adsorption capacity. One exception was found at 40 ^oC, where the adsorption capacity is lower than that observed at 30C. This is also related to diffusion limited adsorption process. The relatively low solvent/PEI ratio and insufficient mixing time results in uneven distribution of PEI on alumina and a high degree of reduction in the surface area and pore volume of sorbent, which leads to the relatively low adsorption capacity due to high diffuison limitation. This issue needs to be solved for further studies.

Scientific Ethics Declaration

The authors declare that the scientific ethical and legal responsibility of this article published in EPSTEM journal belongs to the authors.

Acknowledgements or Notes

* This article was presented as oral presentation at the International Conference on Basic Sciences, Engineering and Technology (www.icbaset.net) held in Marmaris/Turkey on April 27-30, 2023.

*The project is fully supported by LOGOS Kimya Teknolojileri Ltd. Şti. and TÜBİTAK. All authors gratefully thanks to Research Assist. Şefik ARICI from Ege University, Biomass Energy Systems and Technologies

Application and Research Center and Atalay Yarız from Eskişehir Technical University, Department of Mechanical Engineering for their contributions on the characterization process.

References

Chen, C., Kim, J., & Ahn, W. S. (2014). CO2 capture by amine-functionalized nanoporous materials: A review. *Korean Journal of Chemical Engineering 2014 31:11*, *31*(11), 1919–1934.

Darunte, L. A., Oetomo, A. D., Walton, K. S., Sholl, D. S., & Jones, C. W. (2016). Direct air capture of CO2 using amine functionalized MIL-101(Cr). *ACS Sustainable Chemistry and Engineering*, *4*(10), 5761–5768.

Gargiulo, N., Caputo, D., & Colella, C. (2007). Preparation and characterization of polyethylenimine-modified mesoporous silicas as CO2 sorbents. In *Studies in surface science and catalysis* (Vol. 170, pp. 1938-1943). Elsevier.

Goeppert, A., Czaun, M., May, R. B., Prakash, G. K. S., Olah, G. A., & Narayanan, S. R. (2011). Carbon dioxide capture from the air using a polyamine based regenerable solid adsorbent. *Journal of the American Chemical Society*, *133*(50), 20164-20167.

Goeppert, A., Zhang, H., Czaun, M., May, R. B., Prakash, G. K. S., Olah, G. A., & Narayanan, S. R. (2014). Easily regenerable solid adsorbents based on polyamines for carbon dioxide capture from the air. *ChemSusChem*, *7*(5), 1386–1397.

Gür, T. M. (2022). Carbon Dioxide emissions, capture, storage and utilization: review of materials, processes and technologies. In *Progress in Energy and Combustion Science* (Vol. 89). Elsevier Ltd.

Li, C., Wang, X., Yang, A., Chen, P., Zhao, T., & Liu, F. (2021). Polyethyleneimine-modified amorphous silica for the selective adsorption of co2/n2 at high temperatures. *ACS Omega*, *6*(51), 35389–35397.

Lin, Y., Yan, Q., Kong, C., & Chen, L. (2013). Polyethyleneimine incorporated metal-organic frameworks adsorbent for highly selective CO2 capture. *Scientific reports*, *3*(1), 1859.

Shafeeyan, M. S., Daud, W. M. A. W., Shamiri, A., & Aghamohammadi, N. (2015). Modeling of carbon dioxide adsorption onto ammonia-modified activated carbon: kinetic analysis and breakthrough Behavior. *Energy and Fuels*, *29*(10), 6565–6577.

Wang, J., Huang, H., Wang, M., Yao, L., Qiao, W., Long, D., & Ling, L. (2015). Direct capture of low-concentration CO2 on mesoporous carbon-supported solid amine adsorbents at ambient temperature. *Industrial and Engineering Chemistry Research*, *54*(19), 5319–5327.

Xu, X., Song, C., Andresen, J. M., Miller, B. G., & Scaroni, A. W. (2002a). Novel polyethylenimine-modified mesoporous molecular sieve of MCM-41 type as high-capacity adsorbent for CO2 capture. *Energy and Fuels*, *16*(6), 1463-1469.

Xu, X., Song, C., Andresen, J. M., Miller, B. G., & Scaroni, A. W. (2002b). Novel polyethylenimine-modified mesoporous molecular sieve of MCM-41 type as high-capacity adsorbent for CO2 capture. *Energy and Fuels*, *16*(6), 1463–1469.

Yu, C. H., Huang, C. H., & Tan, C. S. (2012). A review of CO2 capture by absorption and adsorption. In *Aerosol and Air Quality Research*, 12(5), 745–769.

Author Information

Furkan Turgut
LOGOS Kimya Teknolojileri Ltd. Şti.
Ostim, 1151. Sk. No:66, 06300 Yenimahalle/Ankara, Türkiye
furkan@logoskimya.com

Simge Kostik
İzmir Yüksek Teknoloji Enstitüsü
Gülbahçe, İzmir Yüksek Teknoloji Enstitüsü, 35430 Urla/İzmir, Türkiye

Barış Erdoğan
LOGOS Kimya Teknolojileri Ltd. Şti.
Ostim, 1151. Sk. No:66, 06300 Yenimahalle/Ankara, Türkiye

Başar Çağlar
İzmir Yüksek Teknoloji Enstitüsü
Gülbahçe, İzmir Yüksek Teknoloji Enstitüsü, 35430 Urla/İzmir, Türkiye

To cite this article:

Turgut, F., Kostik, S., Erdogan, B. & Caglar, B. (2023). CO_2 capture by PEI-impregnated alumina sorbents. *The Eurasia Proceedings of Science, Technology, Engineering & Mathematics (EPSTEM), 22,* 217-226..

The Eurasia Proceedings of Science, Technology, Engineering & Mathematics (EPSTEM)
ISSN: 2602-3199

The Eurasia Proceedings of Science, Technology, Engineering & Mathematics (EPSTEM), 2023

Volume 22, Pages 227-236

ICBASET 2023: International Conference on Basic Sciences, Engineering and Technology

The Effect of Nano Graphene Reinforcement on Pin and Adhesively Bonded Sandwich Composite Structures

Mine USLU-UYSAL
Yildiz Technical University

Abstract: The subject of joining composite parts in important issue in a wide range of engineering applications. Currently mechanically-fastened and adhesively bonded joints are the two established and accepted techniques of joining used in aerospace industry for assembling composite structures. More effective adhesively bonded joints can be achieved by increasing the chemical properties of the adhesive. In this paper, nano graphene particles were added adhesive in various proportions (0.5%wt., 1%wt. and 1.5%wt.) to increase the mechanical strength of the pin and adhesively bonded (hybrid, bolted/bonded) sandwich composite structures. The mechanical properties of the newly produced nano graphene added adhesives were determined experimentally. Sandwich composite structure hybrid models with holes were created using finite elements method. The two dimensional plane strain and three dimensional analyses have been carried out. Effect of the nano graphene reinforced and hybrid structures to the all displacements were discussed on tensile property of the sandwich structures. The sensitivity of mechanical response to the compressibility of the adhesive material has been demonstrated. Numerical analysis of nano graphene reinforced hybrid joints show their strength life is longer than corresponding adhesively bonded/bolted joints Furthermore, hybrid joints can modify the tension–compression area distribution at the side of the bolt hole, thus making composite material participate more in the load bearing. This is reflected in the increased bolt hole strain and better structural performance.

Keywords: Composites, Hybrid joints, Nano graphene reinforced adhesive, Finite element analysis

Introduction

For many years, designers have been able to replace parts made from common materials such as steel and composite materials. The most obvious benefit of composite materials is that they can be designed to achieve certain material properties in the desired direction. Until now, thin composite plates are widely used in different industries. For this reason, design and analysis methods for thin composites have been widely developed (Reddy, 1997). and various techniques have been invented by manufacturers to produce more efficient and complex parts and several techniques have been invented by manufacturers to produce more complicated parts (Van Hoa, 2009).

For efficient connection designs, it is necessary to take advantage of all the properties of composite materials, which are increasingly used in aircraft structures. Some of the applications of bolt joints in aerospace industry are such as wing to fuselage joint in Boeing/MDD Harrier, Boeing/Bell V-22 Osprey, Boeing 777 and Grumman X-29 (NASA) (Heslehurts, 2013). Bolted joints, the formerly and currently preferred method for joining these structures, suffer from low joining efficiency, resulting in thicker structures in the joint region. Typically, a composite joint has been found to provide a joint efficiency of 40-50% compared to 60% for metals. (Bodjona et al., 2015).

The wing of an Airbus 380 alone consists of more than 30,000 elements, with approximately 750,000 bolted connections (Zhang & Zhao, 2012). These joints are of key importance as they constitute the weakest point that causes the element to break. The three main methods of joining composite laminates together are either

mechanical fastening, bonding, or a combination of the two, called "hybrid" bonding. Mechanical fasteners such as pins, rivets and bolts have been known to occupy a very large area in the aerospace industry for decades (Ireman et al., 1993; Khudhayer & Othman, 2011; Collings, 1997; Wei et al., 2013). The main problem with mechani.cal joints is the high stress concentrations that occur around the fastener holes and cause damage and this is more severe in composite laminates than in metal plates (Hart-Smith, 1998).

Adhesive bonded joints are structurally more useful and efficient than mechanically bonded joints, as they perform better in distributing loads and eliminate many of the problems of high stress concentrations associated with bolted connections (Hart-Smith, 1982 & Hart-Smith, 1985). Sandwich structures are also joined by film adhesive between layers. The bonded material is used to bear compressive loads and axial tension, while the adhesive is used to carry shear loads and provide support against compressive loads normal to the bonded ones. The materials used in the construction of sandwich structures can vary depending on the application. The adhesives of a sandwich structure are typically made of aluminum alloys, titanium, high tensile steel or multilayer ply composites, functionally graded materials (Kassapoglou, 2010; Paik et al., 1999; Uysal & Guven, 2015).

In this presented study, the plates made of composite material were connected to each other by both adhesive and bolted connection (hybrid connection), but with a big difference, in the new presented study, the bond strength was tried to be increased by adding nano graphene particles into the adhesive. Researchers carry out various studies in order to increase the mechanical properties and bond strength of adhesive joints. Some of these studies include the addition of powders such as copper powder, aluminum powder, calcium silicate, calcium carbonate, silicon oxide, titanium oxide, carbon nanotube to the epoxy adhesive. impact resistance, abrasion resistance, etc. carried out to improve mechanical properties (Wetzel et al., 2003; Meguid & Sun, 2004; Kilik & Davies, 1989; Zhai et al., 2006; Wetzel, 2006; Xian et al., 2006; Zhai et al., 200; Zhao et al., 2008; Gerson et al., 2010).

In these studies, it was stated that the particle reinforcement gave better results than the additive-free epoxy adhesive. In the finite element study, in which the effect of micro aluminum powder added to epoxy adhesive on mechanical properties was examined, it was stated that the addition of micro aluminum powder increased the bond strength (Kahraman, 2008). When multi-walled carbon nanotubes are added to the epoxy adhesive as reinforcement, the mechanical strength increases with 0.5% carbon nanotube addition. while it deteriorates when 1% and 2% carbon nanotubes are added (Pilawka et al., 2012). In another study, it was stated that when the carbon nanotube addition is around 1.5%, the mechanical properties increase and after this value, the mechanical properties decrease and even lower results than the additive-free epoxy adhesive (Wernik &. Meguid, 2014). The adhesive obtained with silicate nanoparticles added to the epoxy resin at the rates of 0.5%, 1%, 1.5% and 2% by weight was used in aluminum joints to provide light and high strength. The effects of silicate nanoparticles were observed in peeling and shear stresses (Charitidis, 2020). In experimental studies using two different nanoparticles, single lap and hybrid bonding joints were investigated. Appropriate nanoparticle selection was made in experimental studies, which showed an improvement of approximately 10% in tensile strength. Adhesion zones were observed by SEM (Scanning Electron Microscopy) analyzes and the distribution of nanoparticles was investigated (Borghei et al., 2019).

Connections where adhesive zone defects are due to environmental factors and galvanized steel materials are bonded with nanoparticle added adhesive were examined. Experimental studies were carried out for nanoparticles added into the adhesive zone at different temperatures and residence times, and their shear strength and tensile strength were investigated (Nascimento et al., 2021). In the study, in which nanoparticle reinforced adhesive is obtained and the distribution of these particles in the adhesive is primarily homogeneous and then functionally graded, the obtained adhesive properties are examined. The strength and local plastic deformations of the joints bonded with the obtained adhesive were observed (Jojibabu et al., 2020). In this study, in which both iron oxide particles and nanoparticles were added to improve the properties of thermoplastic adhesives, additions were made at the rates of 0.1%, 0.5% and 1% by weight. Single lap joints were adhered with these new adhesives and the loading displacement curves were obtained and interpreted as a result of the experiment (Ciardiello et al., 2021).

As can be seen from the studies on increasing the mechanical properties of adhesive joints and adhesives, it is understood that various powders are used. In addition, it is stated in the studies that the additive ratio is very important especially in the addition of carbon-based powders to the epoxy adhesive and affects the mechanical properties of the adhesive joint. For this reason, sandwich joint models were created with nano graphene reinforced adhesives at various rates within the scope of this study. In this study, the strengthening parameters in the adhesive region were well analyzed. The aim of this study is to examine the stress and strain behaviors on

hybrid composite sandwich structures bonded using nano graphene added adhesives and to evaluate the effect of nano graphene additive on bond strength.

Materials and Method

Preparation of Nano Graphene Added Epoxy Based Nanocomposite Adhesives

Nanocomposite adhesives were produced by adding 0.5%, 1% and 1.5% by weight nano graphene to the epoxy adhesive. Before preparing the nanocomposite adhesives, the nano graphene particles were dried in an oven at 120°C for 1 hour to remove moisture. While preparing the epoxy adhesive, first of all, the epoxy adhesive was weighed on a precision scale, and then the nano particles, which were weighed in a precision balance at a predetermined rate, were added to this plain epoxy adhesive. In addition, PVP (Polyvinylpyrrolidone) was added to the mixture in an equal amount with the weight of the nano particles in order to ensure homogeneous dispersion of carbon-based nano particles in the epoxy matrix. The material properties of the adhesive and nano graphene used are given in the Table 1 and Table 2.

Table1. Mechanical properties of Loctite® EA9492 adhesive

Properties	Loctite-Hysol 9464
Shear Strength (MPa)	20
Peel Strength (MPa)	10.6
Modulus of Elasticity, E (GPa)	1.65
Shear Modulus, G (GPa)	0.75
Poisson's ratio,υ	0.356

Table 2. Properties of nano graphene used in experiments

Properties	Nano Graphene
Average particle diameter (μm)	7
Modulus of Elasticity (GPa)	1000
Average particle thickness (nm)	6
Tensile Strength (GPa)	10-20
Density (g/cm^3)	~2
Surface area (m^2/g)	130

Within the scope of the presented paper, bulk samples were prepared and subjected to tensile test for the determination of mechanical properties of adhesives with 0.5%, 1% and 1.5% additives by weight. ISO 15166 standard was taken into account in the preparation of bulk samples. This standard specifies the test specimen dimensions required for the preparation of bulk specimens from two-component liquid adhesives (Figure 1).

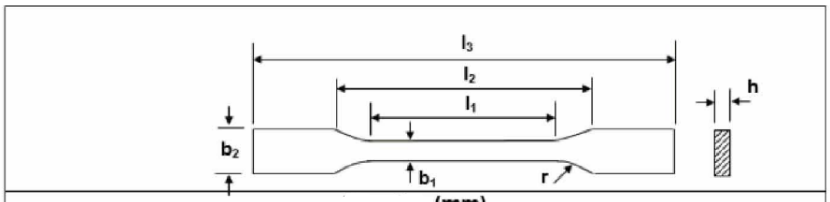

(mm)		
	A	B
l_3	≥150[1]	≥ 75
l_2	106-120	58±2
l_1	60±0.5	30±0.5
b_2	20±0.2	10±0.5
b_1	10±0.2	5±0.5
h	4±0.2	≥2±0.2
l_0	50±0.5	25±0.5
l	115±1	58±1

Figure 1. Tensile test sample dimensions according to ISO 15166 standard

In order to produce bulk samples, molds were made from PLA material using the additive manufacturing method (Figure 2(a)). Adhesives containing nano graphene, prepared, were poured into the mold as seen in Figure 2(b). In order to adjust the sample thickness (1.5 mm), a flat plate was closed over the mold and a weight was placed on it. As recommended in the adhesive data sheet, 72 hours were allowed at room temperature for

curing. In order for the adhesive to come off easily, one side of both the mold and the plate is covered with a 0.1 mm thick stretch film.

Figure 2. a) Mold prepared for bulk samples, b) bulk samples poured into the mold

After the prepared bulk samples were removed from the mold, they were sanded with fine sandpaper to remove the burrs. Tensile tests were first performed on the undoped one of these samples and the mechanical properties of the adhesive were compared with the adhesive data sheet. After this convergence, the mechanical properties of the adhesives with 0.5%, 1% and 1.5% nano graphene structure by weight were determined. It is planned to use the determined mechanical properties of nano graphene added adhesives in finite element analysis. Adhesive material properties, stress strain curve excel data obtained from tensile controls were entered into the ANSYS software.

Modeling of Sandwich Composite Structures with Pin and Adhesive

Both the adherends were composite laminated plate with layup of $[0\text{-}90]_{10s.}$ The thickness of each layer is 0.5 mm. The mechanical properties of the bonded composite material are given in the Table 3. Also, the two-hole sandwich composite plates that make up the model are shown in Figure 3(a). In Figure 3(b), the dimensions of the composite plates were given.

Table 3. Mechanical properties of composite adherends (Canyurt et al., 2010)

Properties	Composite
Modulus of Elasticity, E (GPa)	$E_{11=}22$ $E_{22=}22$ $E_{33=}9$
Shear Modulus, G (GPa)	G_{12}=5.3 G_{23}=3.1 G_{13}=3.1
Poisson's ratio,υ	υ_{xy}.0.27 υ_{yz}.0.38 υ_{xz}.0.38

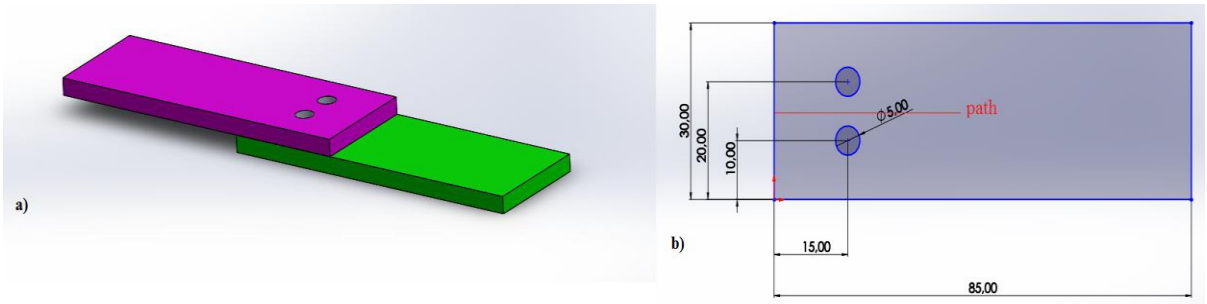

Figure 3. a) Model for composite sandwich adherend, b) Dimension of adherend

Hybrid joint models were created using the finite element method, using the bonded composite and adhesives with added 0.5%, 1% and 1.5% nano graphene, respectively. The schematic drawing of pin and adhesive bonded structure shows in Figure 4.

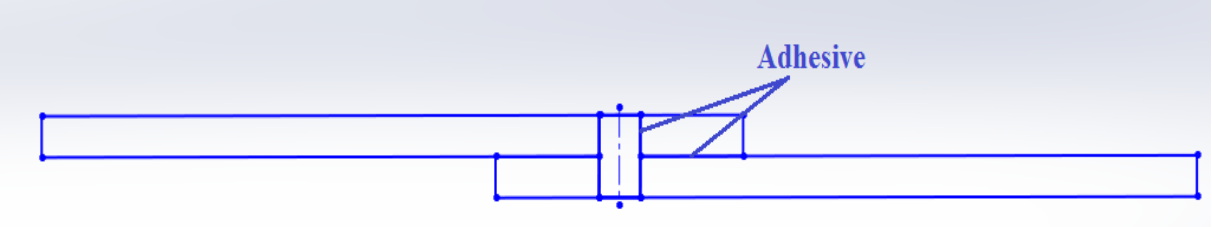

Figure 4. The schematic illustration of pin and adhesive bonded structure

Finite Element Model

The numerical model of the fixed point supported (on holes and on plates) sandwich panel is developed by using the commercial software package ANSYS. This finite element program enables the prediction of stress and strain global behavior of sandwich panel subjected to tensile load (50 MPa) cases. The thickness of one panel is 10 mm, the adhesive thickness is 1.5 mm and the total thickness of sandwich panel, t = 21.5 mm. The holes are constructed at the corners 15 cm from the edges with a diameter d of 5 cm (Figure 3). The numerical model of FGPMs sandwich panel was divided into a finite number of elements satisfying the equilibrium and compatibility at each node. The size of elements was determined for the finer mesh in the critical regions such as the holes. The mesh size was determined by the solid element constraints that the length ratio of element edges cannot be smaller than 1/20 and the angle between element edges cannot be less than 70°. Consequently, the optimal combination of mesh accuracy and elements size was found. The model has contact pairs, adhesive and adherend plates have contact position.. Surface to surface contact elements (CONTA 174 and TARGE 170) were set the overlap surface of the adherends and adhesive and pin and adhesive surfaces (Figure 5). For the details of bonding mechanics and modeling, the relevant literature (Uysal & Guven, 2015) can be consulted.

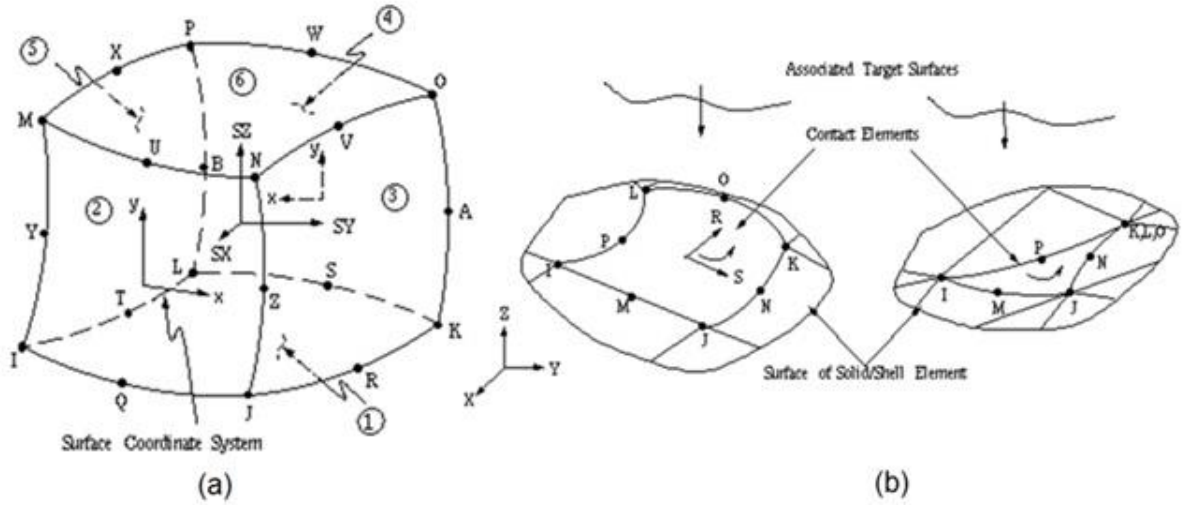

Figure 5. Element types a) Solid 95, b) Conta174 and Targe170

Results and Discussions

Normal stresses (σ_x and σ_y), shear stresses (τ_{xy}) and von mises stresses (σ_{von}) were compared for all nano graphene additions (0.5%wt., 1%wt. and 1.5%wt.) in composite sandwich structures with bolt and adhesive bonds. In Figure 6 and Figure 7, stress distributions are given for hybrid joint modeled using 0.5% nanographene added adhesive. A stress distribution image of about 35 cm from the bonding area with pins is given in these. The focus is on stress distributions in the composite plate. The image with the bolt has been removed because it looks complicated.

In Figure 6(a), the σ_x normal stress occurring under tensile load around the hole, and in Figure 6 (b), the σ_y normal stress distributions occurring in this vicinity are given.

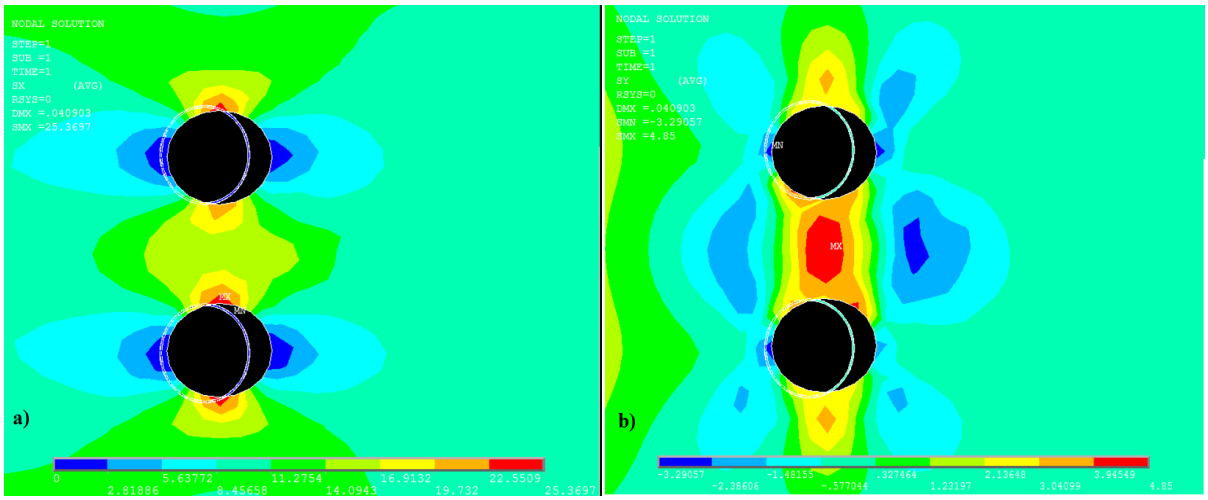

Figure 6. Stress values around the hole a) Normal stress, σ_x, b) Normal stress, σ_y

The stress and strain values of the sandwiched composite plate subjected to tensile load were determined as a result of the finite element analysis. The displacement value in the X direction is maximum at the loaded edge. Its value is 4.806 mm. The maximum stress value in the X direction is 25.369 MPa. Also, the strain value in the Y direction is 4.85 Mpa. (Figure 6). Even when the loading is longitudinal, negative shear stresses occur in the composite plate. The value of these shear stresses is 5.59 MPa. The von misses stress value calculated according to the von Misses criterion is 24.32 MPa in the sandwich plate modeled with 0.5%wt. nano graphen added adhesive (Figure 7). Comparative stress plots for hybrid joints bonded by adding other weight nano graphene are given in Figure 9 and Figure 10.

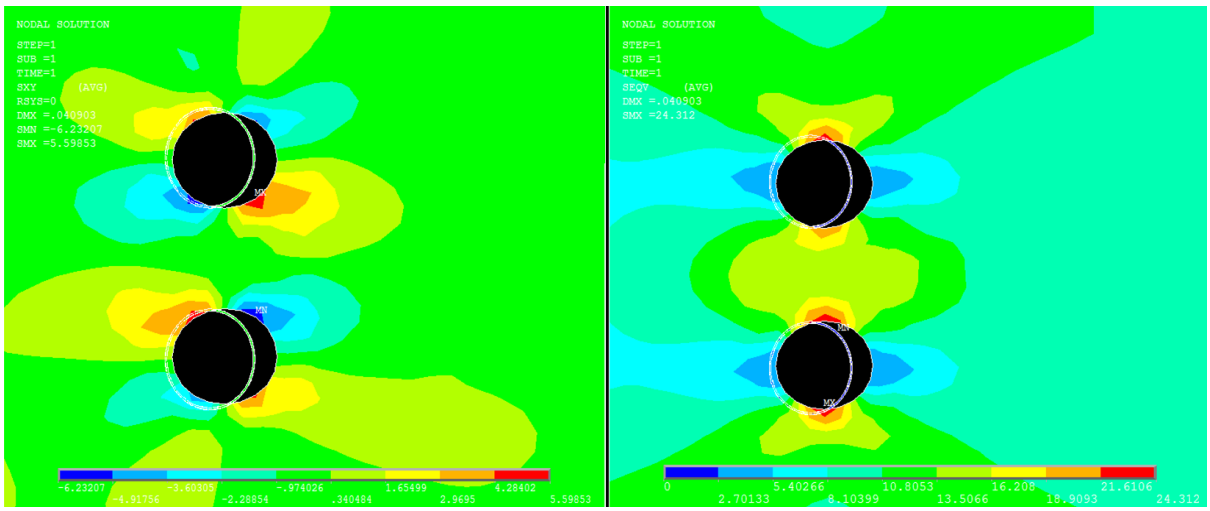

Figure 7. Stress values around the hole a) Shear Stress τ_{xy}, b) von Misses Stress, σ_{von}

After the stress analysis is done, a path is drawn in the finite element program for the more important regions and the stress values at the nodes there can be examined. The path is drawn for a distance of approximately 35 cm from the bonding place and in the middle of the composite plate (15 cm) (Figure 3(b)).

Normal stresses (σ_x and σ_y), shear stresses (τ_{xy}) and von Misses stresses (σ_{von}) behaviors are plotted on the path (Figure 8). The normal stress (σ_x) value is around 8 MPa in the fixed support, this stress increased when it came to the bolted connection position and reached a value of approximately 17.45 MPa. This is proof that, in hybrid adhesives, stress concentrations are mostly on the pin side of the composite material. These stress concentrations cause separations and delaminations in the laminated composite plates, reducing the joint strength. In this study, it was aimed to improve the strength in this region by adding nano graphene particles into the adhesive. The effects of this reinforcement are given in Figure 9 and Figure 10.

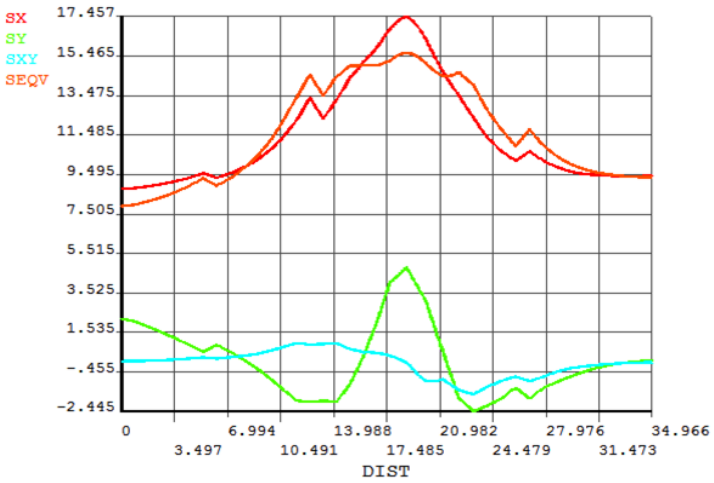

Figure 8. All stress behaviors in the adhesive bonding zone (on the composite plate)

Longitudinal tensile analysis was applied to the models to estimate the tensile strength of sandwich panels composed of composite structures.. Normal stresses (σ_x and σ_y), shear stresses (τ_{xy}) and von Misses stresses (σ_{von}) values were compared in order to understand the effects of nano graphene additions to the adhesive in single-layer lap joints. As can be seen in Figure 9a, the normal stress values in the x-direction are compared for an adhesive bonded sandwich panel with different nano graphene powder weight ratios (%). The normal stress values in the x direction is 25.36 MPa for the sandwich panel defined as 0.5%. This value is 20.80 MPa for a sandwich panel with 1.5% nano graphene powder added. The normal stress value in the x direction in 1% sandwich panel is between 0.5% and 1.5% and its value is 24.10 MPa.

For the composite sandwich panel with fixed support under tensile load, when the nano graphene powder weight fraction was increased from 0.5% to 1%, the normal stress in the y-direction (σ_y) decreased by 6%. This decrease is 23% when the ratio is increased from 0.5% to 1.5%. The highest normal stress values were calculated for 0.5% nano graphene powder and this result showed that nano graphene powder in this ratio is more compatible with the resin and responds better to tensile load.

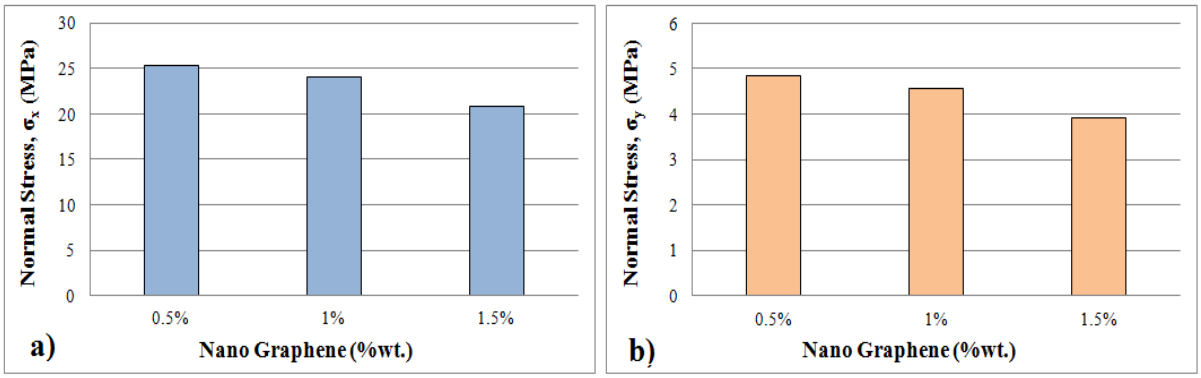

Figure 9. Effect of nano graphene weight ratio on stresses values, hybrid bond sandwich panel made of composite under tensile load, a) normal stress, σ_x b) normal stress, σ_y

When considered in terms of shear stress values, the highest shear stresses are in the junction with 0.5% nano graphene powder. The formation of 5.59 MPa in the negative direction indicates that this connection has the highest probability of separation behavior caused by shear stresses. Stress values in the negative direction determine the direction of shear stress. The shear stress value of the 1% nano graphene bond is 5.11 MPA in the negative direction, which is lower than the 0.5% nano graphene bond. (Figure 10a). The results of von misses stress analysis on the composite material are important in terms of examining the joint strength and breaking behavior of the combined geometry and determining the damage to the adherend material. The occurring and von-Mises (σvon) stress values in Figure 10 b were determined as a result of the finite element analysis. The von Mises stress value at the hybrid bonded with 1% nano graphene added was 22.61 MPa, and this value increased by 7% with 0.5% nano graphene addition. The lowest von Mises stress value was observed in the hybrid joint bonded with 1.5% nano graphene added adhesive.

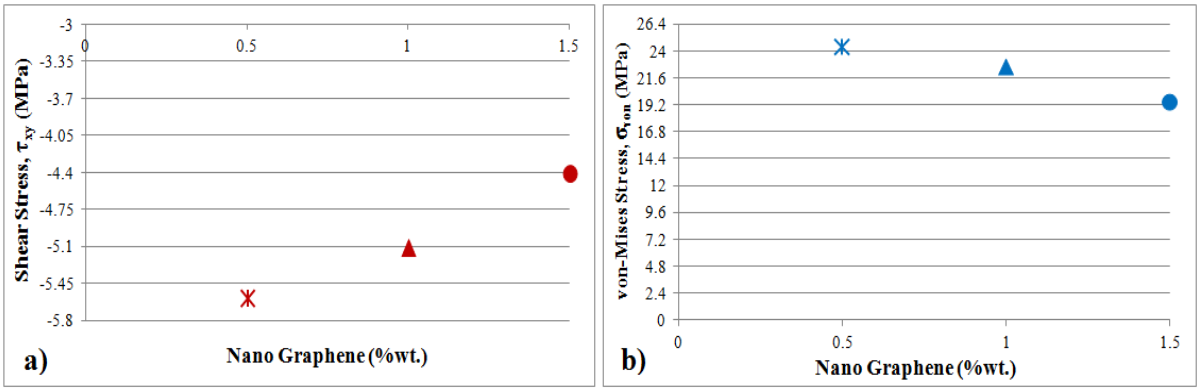

Figure 10. Effect of nano graphene weight ratio on stresses values, hybrid bond sandwich panel made of composite under tensile load, a) shear stress, τ_{xy} b) von-misses stress, σ_{von}

Conclusion

In this presented study, the behavior of heterogeneous adhesive bonds is investigated by modeling them in hybrid bonds. First, the recently experimentally developed nano graphene-added adhesive model was used in adhesive materials, and secondly, the joint was modeled as a hybrid joint with both adhesive and pin.Adhesive joints made of hybrid bonds are encountered in the aerospace industry (layered connections in aircraft and shuttle hulls), land and sea transportation (at joints in car/ship skeletons) due to their superior mechanical properties, as well as their lightness and durability. Studies on adhesive bonds made of heterogeneous adhesive and layered composite with hybrid joint geometry are rare in the literature.

In this study, it was stated that when nano graphene was added to the epoxy adhesive as reinforcement, the mechanical strength increased with 0.5% nano graphene addition, while it deteriorated when 1% and 1.5% nano graphene was added. In addition, in this study, it was stated that the value of nano graphene addition has a significant effect on the bond strength in hybrid sandwich structures formed by using layered composites, and after the appropriate value, the mechanical properties of the adhesive decrease and even lower results than the pure epoxy adhesive. It is hoped that this study will be a useful guide for future research of heterogeneous bonded hybrid connections.

Scientific Ethics Declaration

The author declares that the scientific ethical and legal responsibility of this article published in EPSTEM journal belongs to the author.

Acknowledgement

* This work was supported by Research Fund of the Yildiz Technical University. Project Number: FBA-2022-4703.

* This article was presented as oral presentation at the International Conference on Basic Sciences, Engineering and Technology (www.icbaset.net) held in Marmaris/Turkey on April 27-30, 2023.

References

Bodjona, K., Raju, K., Lim, G. H., & Lessard, L. (2015). Load sharing in single-lap bonded/bolted composite joints. Part I: model development and validation. *Composite Structures, 129*, 268-275.

Borghei, H. R., Behjat, B., & Yazdani, M. (2019). The impact of graphene nanoparticle additives on the strengt of simple and hybid adhesively bonded joints. *Journal of Composite Materials* . *53*(23), 3335-3346.

Canyurt, O. E., Meran, C., & Uslu, M. (2010). Strength estimation of adhesively bonded tongue and groove joint of thick composite sandwich structures using genetic algorithm approach. *International Journal of Adhesion & Adhesives, 30*, 281-287.

Charitidis, P. J. (2020). The effect of nanoparticles in single lap joints studied by numerical analyses. *European Journal of Engineering Research and Science. 5*(10), 1-2.

Ciardiello, R., Belingard, G., Litterio, F., & Brunella, V. (2021). Effect of iron oxide and graphene particle on joint strenght and dismounting characteristics of a thermoplastic adhesive. *International Journal of Adhesive and Adhesion, 107*, 102850.

Collings, T. A. (1977). The strength of bolted joints in multi-directional CFRP laminates. *Composites, 8*(1), 43-55.

Gerson, A. L., Bruck, H. A., Hopkins, A. R., & Segal, K. N. (2010). Curing effects of single-wall carbon naotube reinforcement on mechanical properties of filled epoxy adhesives. *Composites Part A: Applied Science and Manufacturing, 41*, 729-736.

Heslehurst, R. B. (2013). *Design and analysis of structural joints with composites materials*. Lancaster, PA: DEStech Publications, Inc.

Hoa, S. V. (2009). *Mechanics principles of the manufacturing of composite materials*. Lancaster, PA: DEStech Publications, Inc.

Ireman, T., Nyman, T., & Hellbom, K. (1993). On design methods for bolted joints in composite aircraft structures. *Composite Structures, 25*, 567-578.

Jojibabu, P., Zhang, Y. X., Rider, A. N., Wang, J., Wuhrer, R., & Prusty, B. G. (2020). High-performance epoxy-based adhesive modified with functionalized graphene nanoplatelets and triblock copolymers. *International Journal of Adhesive and Adhesion, 98*, 102521.

Kahraman, R., Sunar, M., & Yilbas, B. (2008). Influence of adhesive thickness and filler content on the mechanical performance of aluminum single-lap joints bonded with aluminum powder filled epoxy adhesive. *Journal of Materials Processing Technology, 205*, 183-189.

Kassapoglou, C. (2010). *Design and analysis of composite structures with applications to aerospace structure*. UK: John Wiley & Sons.

Khudhayer, J. J., & Othman, A. R. (2011). On fiber reinforced composite structure with bolted joint - A review. *Key Engineering Materials,471-472*, 939-944.

Kilik, R., & Davies, R. (1989). Mechanical properties of adhesive filled with metal powders. *International Journal of Adhesion and Adhesives, 9*, 224-228.

Meguid, S. A. & Sun, Y. (2004). On the tensile and shear strength on nano-reinforced composite interfaces. *Materials and Design, 25*, 289-296.

Nascimento, H., dos Reis, M. O., Monteiro, E. C., & Avila, A. F. (2021). An investigation on industrial adhesive nano-modified by graphene nanoplatelets under extreme environmental conditions. *International Journal of Adhesion and Adhesives, 111*, 102962.

Paik, J. K., Thayamballi, A. K., & Kim, G. S. (1999). The strength characteristics of aluminum honeycomb sandwich panels. *Thin Walled Structures, 35*, 205-231.

Pilawka, R., Paszkiewicz, S., & Roslaniec, Z. (2012). Epoxy composites with carbon nanotubes. *Advances in Manufacturing Science and Technology, 36*, 67-79.

Reddy, J. N. (1997). *Mechanics of laminated composite plates and shells* (2th ed.). Boca Raton, FL: CRC Press.

Smith, L. J. H. (1982). *Design methodology for bonded-bolted composite joints*. (Technical report). AFWAL-TR-81-3154, Douglas Aircraft Company.

Smith, L. J. H. (1985). Bonded-bolted composite joints. *Journal of Aircraft, 22, 993-1000.*

Smith, L. J. H. (1998). *Bolted and bonded joints*. Materials Park, OH: ASM International.

Uysal, M. U., & Guven, U. (2015). Buckling of functional graded polymeric sandwich panel under different load cases. *Composite Structures, 121*, 182-196.

Wei, J., Jiao, G, Jia, P., & Huang, T. (2013). The effect of interference fit size on the fatigue life of bolted joints in composite laminates. *Composites Part B: Engineering, 53*, 62-68.

Wernik, J. M., & Meguid, S. A. (2014). On the mechanical characterization of carbon nanotube reinforced epoxy adhesives. *Materials and Design, 59*, 19-32.

Wetzel, B., Haupert, F., & Zhang, M. Q. (2003). Epoxy nanocomposites with high mechanical and tribological performance. *Composites Science and Technology, 63*, 2055-2067.

Wetzel, B., Rosso, P., Haupert, F., & Friedrich, K. (2006). Epoxy nanocomposites - Fracture and toughening mechanisms. *Engineering Fracture Mechanics, 73*, 2375-2398.

Xian, G., Walter, R., & Haupert, F. (2006). Friction and wear of epoxy/TiO2 nanocomposites: influence of additional short carbon fibers, aramid and PTFE particles. *Composites Science and Technology, 66*, 3199-3209.

Zhai, L., Ling, G., Li, J. & Wang, Y. (2006). The effect of nanoparticles on the adhesion of epoxy adhesive. *Materials Letters, 6*, 3031-3033.

Zhai, L. L., Ling, G. P., & Wang, Y. W. (2008). Effect of nano-Al_2O_3 on adhesion strength of epoxy adhesive and steel. *International Journal of Adhesion and Adhesives, 28*, 23-28.

Zhao, H., & Li, R. K. Y. (2008). Effect of water absorption on the mechanical and dielectric properties of nano-alumina filled epoxy nanocomposites. *Composites Part A: Applied Science and Manufacturing, 39*, 602-611.

Zhang, S., & Zhao, D. (2012). *Aerospace materials handbook*. Boca Raton, FL: CRC Press.

Author Information

Mine Uslu Uysal
Yildiz Technical University
Department of Mechanical Engineering
Besiktas, 34349, Istanbul-Turkey
Contact e-mail: *mineuslu@yildiz.edu.tr*

To cite this article:

Uslu-Uysal, M. (2023). The effect of nano graphene reinforcement on pin and adhesively bonded sandwich composite structures. *The Eurasia Proceedings of Science, Technology, Engineering & Mathematics (EPSTEM), 22*, 227-236.

The Eurasia Proceedings of Science, Technology, Engineering & Mathematics (EPSTEM)
ISSN: 2602-3199

The Eurasia Proceedings of Science, Technology, Engineering & Mathematics (EPSTEM), 2023

Volume 22, Pages 237-246

ICBASET 2023: International Conference on Basic Sciences, Engineering and Technology

Variable Selection with Machine Learning in the Legalization Process for Traffic Insurance

Vedat GUNES
Anadolu Insurance

Serkan KIRCA
Anadolu Insurance

Hasar Ersan YAGCI
Muğla Sıtkı Koçman University

Nida Gokce NARIN
Muğla Sıtkı Koçman University

Abstract: In the insurance sector, the insured notifies the insurance company of which he is the customer as soon as the damage occurs. Upon this notice, a claim file is opened to the insured, and the damage file number is assigned. The claim file contains information about the product insured by the insured and the damage. This information is kept in tables in the databases of Anadolu Insurance. In the event of damage, the insured's claim can be accepted. The entire damage amount can be paid if the damage amount is partially accepted, with the examination to be carried out by the insurance company; if the damage amount is partially accepted, a part of it is paid, or the claim is rejected. The damage amount is not paid at all. When the Insured receives partial payment or the claim file is rejected, they can sue the insurance company to claim the damage amount. The litigation process is a long and bad experience for the insured. For the insurance company, in addition to customer dissatisfaction, it causes extra costs such as court, lawyer, etc. costs. The problem studied in this work is aimed to determine which variables are essential for a possible legalization process in case of partial acceptance or rejection of the claim file by using the variables in the relevant claim file by machine learning and statistical methods. While making this determination, lasso regression, information gain, chi-square test, fisher's score, Recursive Feature Elimination (RFE) with Random Forest Machine Learning algorithm, Univariate Feature Selection with bivariate statistical tests or univariate statistics like chi-square test and feature importance of Random Forest Machine Learning algorithm. Variable selection was made by using correlation coefficient and backward feature elimination methods. Variable p_value was also evaluated.

Keywords: Insurance, Legalization, Anadolu insurance, Variable selection, Machine learning, statistics

Introduction

In the insurance sector, the process of preparing a claim can be a complex and challenging experience for both the insured and the insurance company. When an insured suffers damage to their insured property, they must notify the insurance company immediately to open a claim file. The file contains information about the product insured and the damage suffered. Based on the examination of the claim file, the insurance company can either accept the claim and pay the entire damage amount or partially accept the claim and pay a portion of the amount. If the claim is rejected, the insured can sue the insurance company to claim the damage amount, leading to a lengthy and costly litigation process.

The purpose of this study is to determine which variables in the claim file are essential in predicting the likelihood of a potential legalization process in case of partial acceptance or rejection of the claim file. Machine learning and statistical methods such as lasso regression, information gain, chi-square test, fisher's score, Recursive Feature Elimination (RFE) with Random Forest Machine Learning algorithm, Univariate Feature Selection with bivariate statistical tests or univariate statistics like chi-square test and feature importance of Random Forest Machine Learning algorithm were used to select relevant variables. The variable selection process was performed using correlation coefficient and backward feature elimination methods.

The results of this study will provide valuable insights into which variables play a significant role in determining the outcome of a claim file and can aid insurance companies in making informed decisions. By identifying relevant variables, insurance companies can reduce the likelihood of a litigation process and minimize costs associated with legal fees and customer dissatisfaction.

Claim Process

The damage process starts with opening the claim file as soon as the damage and alkali notification is received and continues until the opened damage file is closed. In this process, it is aimed to ensure customer satisfaction and prevent possible costs by tracking the cost of damage. In the damage process, insurance companies have a great responsibility. The main of these responsibilities is to repair,

- Fast
- Flawless
- Complete

to ensure that it is done. In the study conducted here, the analysis and inference of the variables that will affect the legalization of the traffic damages belonging to the traffic branch in the damage process are defined as auto damage.

The legalization process can sue the Insurance company to claim the damage amount when the insured receives partial payment, or the claims file is denied. The litigation process is a long and bad experience for the insured. For the insurance company, in addition to customer dissatisfaction, it causes extra costs such as court, lawyer, etc. costs. In addition, the insured can be sued not only by the insured but also by the insurance company. For this, detecting irregularities that occur in accidents can be given as an example.

The following processes in the legalization process:

- First of all, there is a valid (valid) policy belonging to the customer.
- Occurrence of damage (i.e. hitting a tree or collision with vehicles)
- Keeping the damage reports and informing the insurance company
- Showing the vehicle to the service
- The insurance company appoints a loss adjuster, and the expert sees the intermediary at the service and starts the repair process.
- By writing the loss adjuster's report, the reflection of the loss adjuster's report to the insurance company's system
- Completing the repair process and informing the insured

sequentially, the damage process is completed.

Machine Learning Methods

The problem addressed is whether the customer of the relevant claim file will take legal action when the file is rejected or whether payment is made partially by using the variables in the report as soon as the loss adjuster's reports are reflected in the Anadolu Sigorta system. In this study, this process will be called legalization. To solve this problem, the classification method, one of the machine learning methods, was determined as the most suitable method for the problem (Uğurlu et al.,).

The subject of the study corresponds to the Supervised Learning – Classification section.

The high success score of the classification accuracy is highly correlated with the proper selection of the variables. The variable assignment is the most critical process affecting the model performance and accuracy. It should be known that when the data set is prepared, not all of the independent variables (attributes) in the data set are meaningful for the model (Kaya & Köymen, 2008). For this reason, the selection of variables should be handled before creating the model. The meaningful variables for the model should be selected, and modeling studies should be carried out specific to these variables.

Method

Preparing the Data Set Suitable for the Problem

A study-specific datamart (Li & Liu, 2017) was created using the data created in the claim process and stored in the databases belonging to Anadolu Insurance database. In the datamart developed, there are 157 variables; 156 are features, and 1 is the target variable specific to the problem. The superset of the attributes created in the data model is 810. The target variable preaches the claim file legalized (Yes / No). It was created according to the binary classification method. All the data preparation steps were developed by using IBM's Infosphere Datastage. The flow in the Datastage platform is shown in Figure 2.

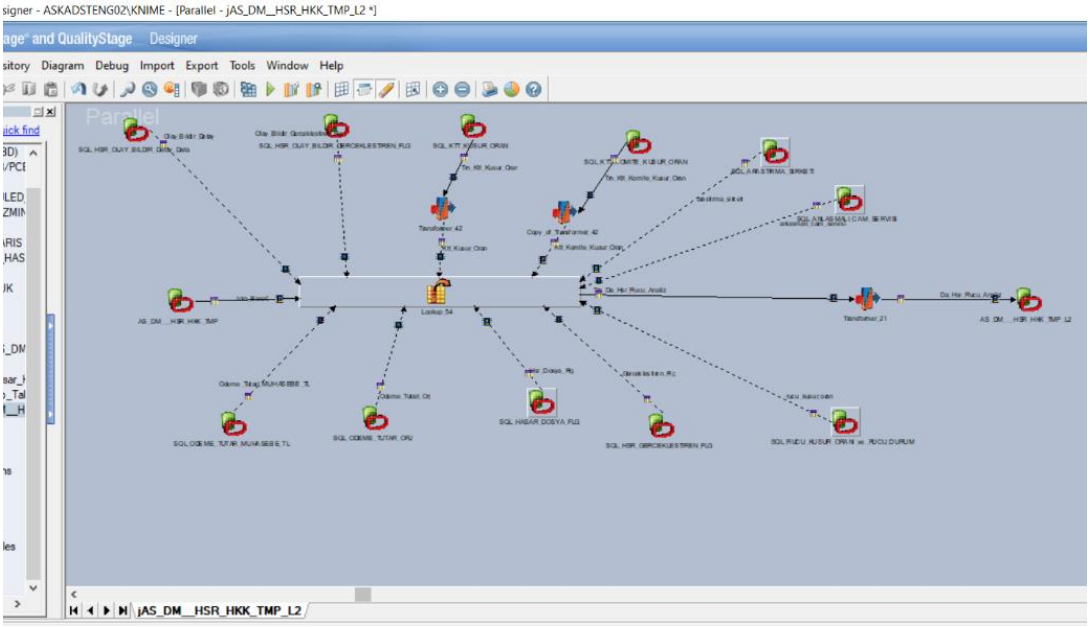

Figure 1. IBM's infosphere datastage platform

Feature Selection Methods

When the literature is examined, statistical and variable selection methods are based on machine learning algorithms (Zhang et al., 2021). Some of these algorithms are;

- Lasso Regression Feature Selection,
- Information Gain,
- Chi-Square Test,
- Fisher's Score,
- Recursive Feature Elimination (RFE),
- Univariate Feature Selection,
- Feature importance of Random Forest ML Algorithm,
- Correlation Coefficient,
- Backward Feature Elimination

methods and more are available in the literature. Let us briefly explain the above variable selection methods.

Lasso Regresyon Feature Selection

It consists of adding a penalty to different parameters of the machine learning model to reduce the freedom of the model, that is, to prevent overfitting (Kozak et al., 2020). In the linear model arrangement, the penalty is applied over the coefficients that hit each estimator. Lasso or L1 can reduce some coefficients to zero of the different regularization types. Therefore, features reduced to zero are removed from the data set before model creation.

Information Gain

Information Gain calculates the reduction in entropy from the transformation of a dataset (İlhan & Sarı, 2016).It can be used for feature selection by evaluating the information gain method outputs for each variable in the context of the target variable.

Chi-Square Test

The chi-square test is used for categorical features in a data set (Santos et al., 2012). We calculate Chi-square between each feature and target. Then select the desired number of features with the best Chi-square scores. The following conditions must be met to correctly apply chi-square to test the relationship between the various features in the dataset and the target variable. The variables should be categorical and sampled independently, and the expected frequency of the values should be higher.

Fisher's Score

The Fisher score is one of the most widely used supervised feature selection methods. The algorithm we will use returns the order of the variables in descending order according to the fisher's score. Then the variables are selected according to the problem (Sharma & Goyal, 2020).

Recursive Feature Elimination (RFE)

Recursive Feature Elimination is a wrapper-type feature selection algorithm. It means that a different machine learning algorithm is given and used at the method's core, wrapped by RFE and used to help select features. RFE, contrasts filter-based feature selections, which score each feature and choose the elements with the highest (or smallest) score. Technically, RFE is a wrapper-style feature selection algorithm that also uses filter-based feature selection internally (Garcia et al., 2017). RFE works by searching for a subset of features, starting with all features in the training dataset and successfully removing features until the desired number remains.

The final feature set is achieved by fitting the specific machine learning algorithm used at the model's core, ranking features by importance, discarding the least important features, and refitting the model. This process is repeated until a certain number of attributes remain.

Univariate Feature Selection

Univariate feature selection runs by selecting the best features based on univariate statistical tests. We compare each feature with the target variable to see if there is a statistically significant relationship between them. It is also called analysis of variance (ANOVA) (Gregorutti & Michel, 2017). We ignore other features when examining the relationship between a feature and the target variable. Because of the application steps, it is called 'univariate.'

Feature importance of Random Forest ML Algorithm

Tree-based strategies used by random forests are naturally ranked by how well they improve the purity of the node, or in other words, the reduction in impurity (Gini impurity) across all trees (Kirisci, 2022). The nodes with the most significant reduction in impurity occur at the beginning of the trees, and the notes with the most

negligible reduction in impurity appear at the end of the trees. Thus, pruning trees below a particular node can generate a subset of the most important features.

Correlation Coefficient

Correlation is a degree of the linear relationship between two or more variables (Aker, 2022). Through correlation, it can predict one variable from another. The purpose of using correlation for feature selection is that relevant variables correlate highly with the target variable. Also, the variables should be correlated with the target variable but uncorrelated among themselves. If two variables are correlated, one is estimated from the other. Therefore, if two properties are associated, the model only needs one, as the latter does not add additional information.

Backward Feature Elimination

This method works oppositely to the Advanced Feature Selection method (Akar, 2021). Here, we start with all the available features and build a model. Next, we take the variable from the model that gives the best evaluation measure value. This process is continued until the predetermined criterion is met [15].

Results and Discussion

Some specified variable selection algorithms have been selected and explained under a heading. The following variable selection algorithms were used in this study.

- Feature Importance of the Random Forest ML Algorithm
- Lasso Regression
- Information Gain
- Correlation Coefficient

Feature Importance of Random Forest ML Algorithm

When we apply the random forest feature selection algorithm to the data set, the results in figure 2 and table 1 are obtained.

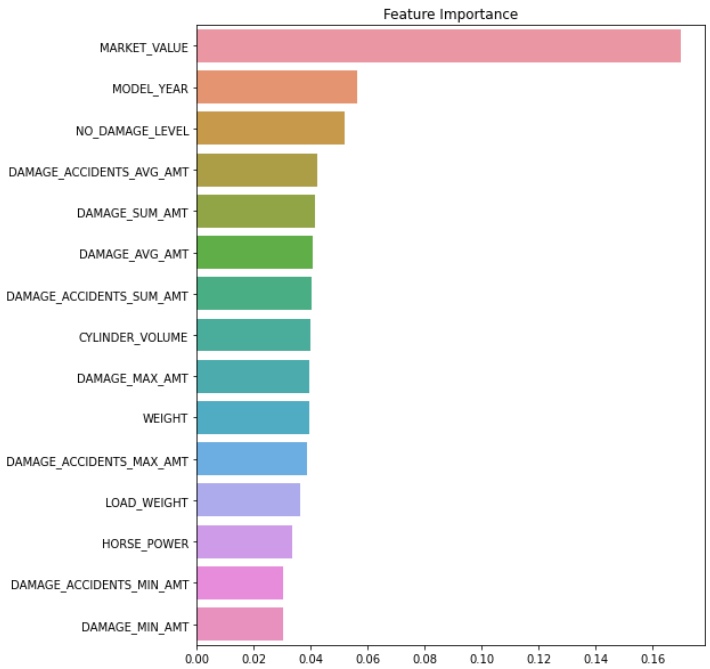

Figure 2. Random forest feature selection algorithm figural results

Table 1. Random forest feature selection algorithm values

Variables	Feature Importances
MARKET_VALUE	0.167
MODEL_YEAR	0.057
NO_DAMAGE_LEVEL	0.051
DAMAGE_ACCIDENTS_AVG_AMT	0.043
DAMAGE_SUM_AMT	0.042
DAMAGE_ACCIDENTS_SUM_AMT	0.041
CYLINDER_VOLUME	0.039
DAMAGE_MAX_AMT	0.039
DAMAGE_ACCIDENTS_MAX_AMT	0.039
WEIGHT	0.039
LOAD_WEIGHT	0.036
HORSE_POWER	0.034
DAMAGE_MIN_AMT	0.030
DAMAGE_ACCIDENTS_MIN_AMT	0.030

When Table 1 is examined, the essential variables are listed from the largest to the smallest at the variable importance level. The most important variable is the vehicle's market value, as expected. Afterward, the model year continues as the undamaged tier.

Lasso Regression

It is a regression technique in which variable selection and regularization co-occur. It is widely applied in large datasets due to its efficiency and speed. The results obtained are shown in Figure 3.

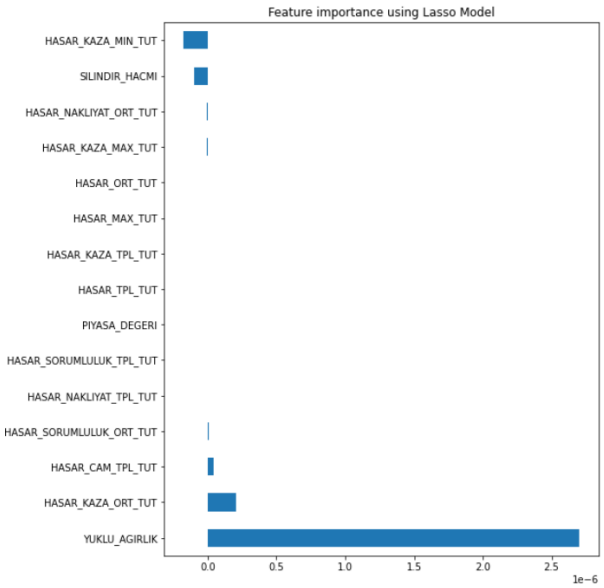

Figure 3. Lasso regression results

Figure 3 shows the variables with positive and negative effects from variable significance levels. While the minimum amount of the Caspian accident has a negative impact, the loaded weight has a positive significance, but the variable of average damage has no significant contribution.

Information Gain

It is a regression technique in which both variable selection and regularization take place at the same time. It is widely applied in large datasets due to its efficiency and speed. Information Gain calculates the reduction in

entropy from the transformation of a dataset. It can be used for feature selection by evaluating the information gain results of each variable in the context of the target variable. The results obtained are shown in Figure 4.

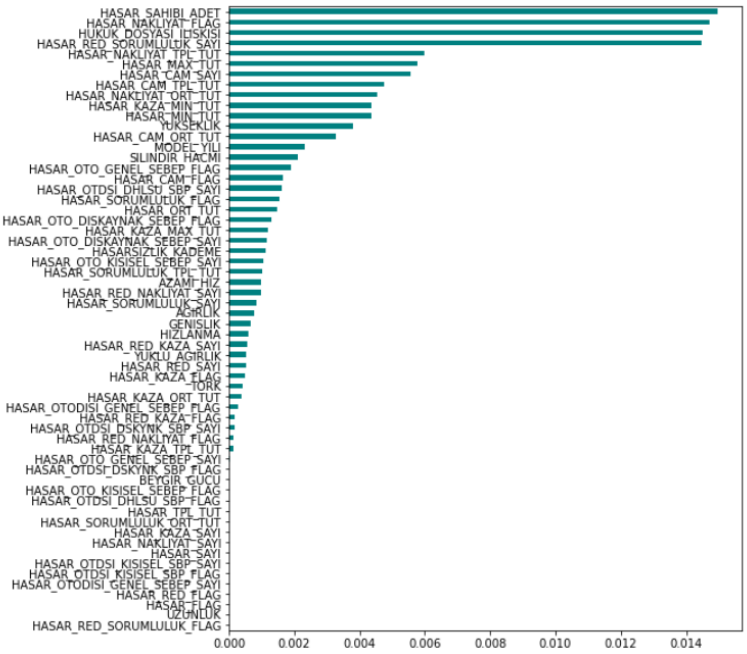

Figure 4. Information gain results

When Figure 4 is examined, the variables whose significance level is important are listed from the largest to the smallest. While the number of claimants is a vital variable, other variables are ranked according to the level of importance.

Correlation Coefficient

Correlation is a measure of the linear relationship between two or more variables. Through correlation, we can predict one variable from another. The rationale behind using correlation for feature selection is that suitable variables are highly correlated with the target. Also, the variables should be correlated to the target but uncorrelated among themselves. The results are shown in Figure 5.

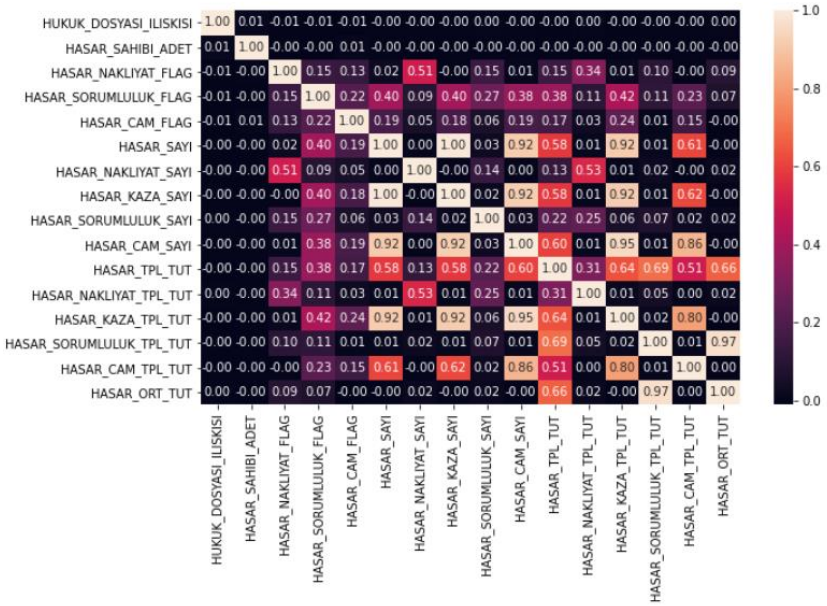

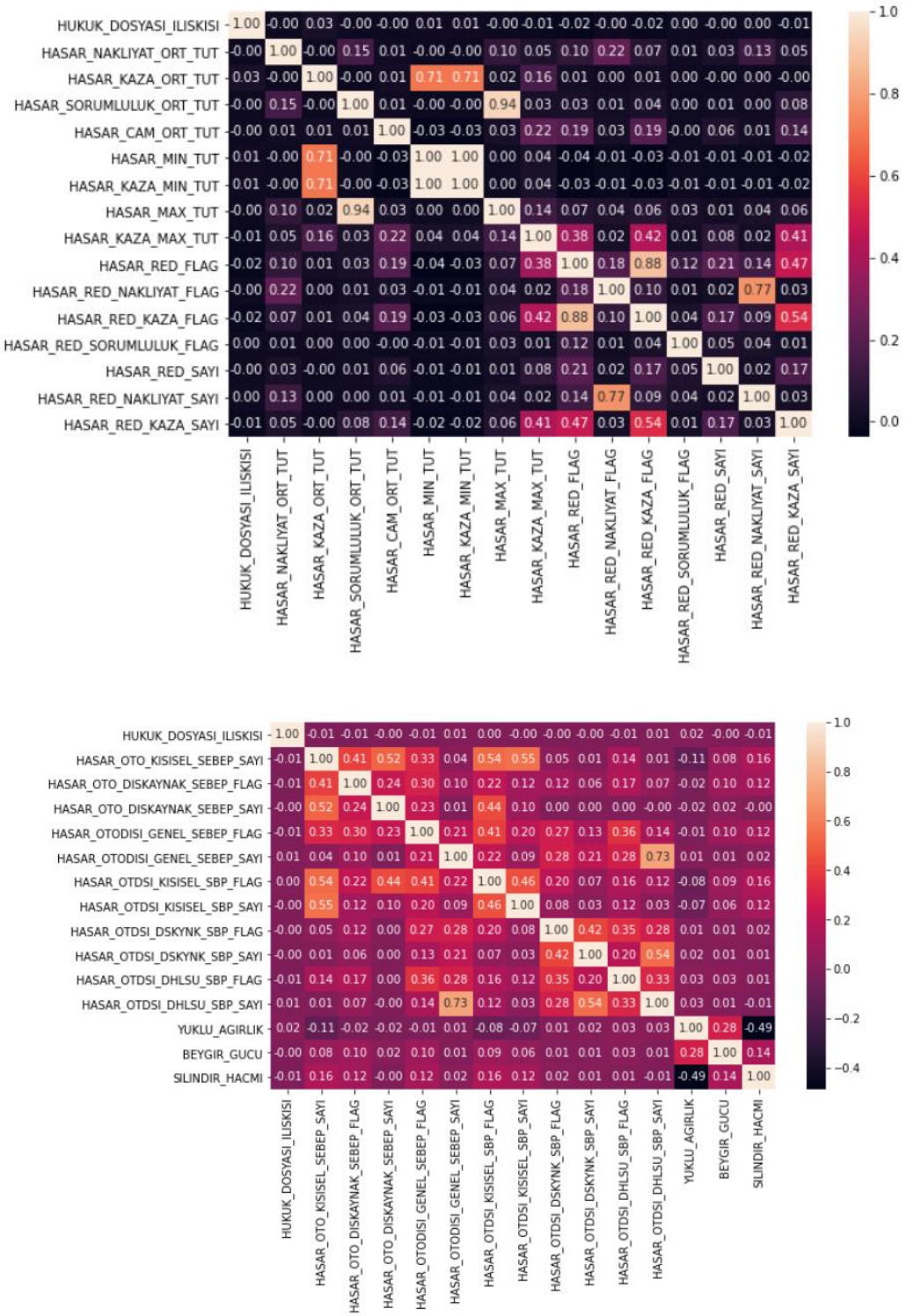

Figure 5. Correlation coefficient results

When the figures are examined, the most important factor variables with high correlation with each other should be removed from the data set because these two variables have the same effect on the target variable.

Conclusion

In this study, in summary, a classification problem was discussed. Before running machine learning algorithms, by looking at the significance levels of the variables in the data set, it was observed using more than one method

which variables would be significant for the model and which variables had a common effect on the model. There are multiple variable selection algorithms in the literature [16].

Recommendations

In the study, studies were made on some of the variable selection algorithms found in the literature according to the data set, and the results were shared. Other algorithms in the literature can be tried in study-specific or further studies. Both categorical and numerical variables can be examined separately, and a variable selection can be made according to the data type.

Scientific Ethics Declaration

The authors declare that the scientific ethical and legal responsibility of this article published in EPSTEM journal belongs to the authors.

Acknowledgements or Notes

* This work would not have been possible without the financial support of Anadolu Insurance. I am grateful to Data Management and Analytics collegues, and Data Analysis and Management Reporting team, and all of those with whom we have had the pleasure to work during this and other related projects.

* This article was presented as oral presentation at the International Conference on Basic Sciences, Engineering and Technology (www.icbaset.net) held in Marmaris/Turkey on April 27-30, 2023.

References

Akar B. (2021), Müşteriye özel fiyat tahmin çalışması, *YBS Ansiklopedi, 9, 13 – 29.*

Aker Y. (2022), Comparison of PCA and RFE-RF algorithm in bankruptcy prediction, *Gümüşhane University Journal of Social Sciences Institue. 13,* 1001 – 1008.

Garcia Y., Garcia B., Gomez M., Fernandez B., & Garcia C. J. (2017), Automatic migraine classification via feature selection committee and machine learning techniques over imaging and questionnaire data, *BMC Medical Informatics and Decision Making, 17,* 34 – 38.

Gregorutti B., & Michel B. (2017), Correlation and variable importance in random forests, *Springer link, 27, 659 – 678.*

İlhan A, & Sarı M. H. (2016), Marmara gölü'ndeki (Manisa) vimba vimba (Eğrez) Populasyonunun bazı biyolojik özellikleri. *Jurnal of Limnology and Freshwater Fisheries Research, 2,* 59 – 65

Kaya H., & Köymen K. (2008), Veri madenciliği kavramı ve uygulama alanları. *Fırat Üniversitesi Doğu Araştırmaları Dergisi, 2,* 159 – 164

Khan A, & Cotton C. (2023), Efficient attack detection in IoT devices using feature engineering-less machine learning. *https://arxiv.org/abs/2301.03532, 14,* 47- 64.

Kirisci M. (2022), Correlation coefficients of fermatean fuzzy sets with a medical application, *Journal of Mathematical Sciences and Modelling. 1,* 16 – 23.

Kozak J, Kaine K, & Juszczuk P. (2020), Permutation entropy as a measure of ınformation gain/loss in the different symbolic descriptions of financial data. *https://www.mdpi.com/1099-4300/22/3/330#, 22,* 330 – 341

Li X., & Liu J. (2017), Automatic essay scoring based on coh-metrix feature selection for Chinese English learners, *Emerging Technologies for Education, 2,* 382 – 393.

Santos D. O. V., Verspoor M., & Nerbonne J. (2012), Identifying important factors in essay grading using machine learning. *Oxford Handbook of Applied Linguistics.* 1 – 15.

Sharma S., & Goyal A. (2020), Automated essay grading: An emprical analysis of ensemble learning techniques, *Computational Methods and Data Engineering.* 343 – 362.

Uğurlu M, Doğru İ, & Arslan S.R. (2023). Karanlık ağ trafiğinin makine öğrenmesi yöntemleri kullanılarak tespiti ve sınıflandırılması. *Jurnal of the Faculty of Engineering and Architecture of Gazi Universty, 38,* 1737-1746.

Zhang S., Zhu F., Qianhao Y, & Xiaoyue Z. (2021) Identifying DNA-binding proteins based on multi-features and LASSO feature selection. *Wiley Online Library Biopolymers 112,* 17 – 28

Author Information

Vedat Güneş
Anadolu Anonim Türk Sigorta Şirketi
Rüzgarlıbahçe, Çam Pınarı Sok. No:6, 34805
Beykoz/İstanbul, Türkiye
Contact e-mail: *vgunes@anadolusigorta.com.tr*

Serkan Kırca
Anadolu Anonim Türk Sigorta Şirketi
Rüzgarlıbahçe, Çam Pınarı Sok. No:6, 34805
Beykoz/İstanbul, Türkiye

Hasan Ersan Yağcı
Muğla Sıtkı Koçman Üniversitesi
Fen Bilimleri Enstitüsü, Yapay Zeka ABD, 48000
Menteşe/Muğla, Türkiye

Nida Gökçe Narin
Muğla Sıtkı Koçman Üniversitesi
İstatistik Bölümü, Yapay Zeka Laboratuvarı, 48000
Menteşe/Muğla, Türkiye

To cite this article:

Gunes, V., Kirca, S., Yagci, H.E., & Narin, N.G. (2023). Variable selection with machine learning in the legalization process for traffic insurance. *The Eurasia Proceedings of Science, Technology, Engineering & Mathematics (EPSTEM), 22,* 237-246

The Eurasia Proceedings of Science, Technology, Engineering & Mathematics (EPSTEM)
ISSN: 2602-3199

The Eurasia Proceedings of Science, Technology, Engineering & Mathematics (EPSTEM), 2023

Volume 22, Pages 247-257

ICBASET 2023: International Conference on Basic Sciences, Engineering and Technology

Investigate the Efficiency of Project Management Software in Construction Projects

Mohamed Ahmed HAMADA
Abu Dhabi University

Abstract: Construction projects are usually regarded as massive and mostly have significant complexity and risky projects, they take longer times to be accomplished, also have a lot of phases, for that fact this research will be dedicated to finding how can project management software help in the success and deliverable of construction projects in high efficiency. Hence, project management software is used in different types of projects not only construction projects but also are used in IT projects, oil and gas projects, industrial projects …etc., this article is focused on mainly "construction projects" as mentioned earlier they are the vast and hard to delivered and overdue time can happen in most cases. The research seeks to discover the different types of project management software popularly used in construction projects and how they help or assist in such projects. The research is carried out within the commercial cities of Kazakhstan country (Almaty, Nur sultan, and Atyrau) with a qualitative mode; all data are sourced by individual interviews, recommendations, questionnaires, and observations. At the end of the research, a comprehensive result was gathered on the relative usage of project management software, with the analysis of how they are used and how they improve efficiency and support their roles in such projects.

Keywords: Project management software, Construction projects, Real estate development, Project performance

Introduction

Project management software are prepared to simplify the work of a project manager and provide more efficient results, by providing applications that can aid in planning, to manage project costs, and to track the activities and monitor schedules (Liberatore et al, 2001). The complexity of construction projects makes it to be uncertain and a times causes rising issues like mistakes, risk and changes in the future from many work plans and or stakeholders who are involve in the project. To simplify the task of the project plan and reduce the problem of uncertainty and future risks, it could be better to use some certain IT software that may assist in project schedule plan, finance and procurement of the project materials (Hamada, & Akzambekkyzy, 2022). Making project plan manually comes with a cost of paying the errors and time wasted in the old system, note that the modern software could easily find errors where it's made and show you the future outcome of each and every work plan, or excess cost that maybe wasted (Chepachenko et al, 2020).

The assorted project management software were found to address the issue of time management, project plan and control, project finance, communication and other tasks involved. The construction projects includes complicated process which require building information models somtimes, such as in UK, BIM Adoption reached 73% in 2020 (Wang & Chen, 2023) . Gantt charts were first used on large construction projects and they proved their efficiency in remarkable projects like the Hoover Dam, started in 1931. Modern IT Project management software made it easier to plan and manage large projects with up to date result.(Kuznetsov et al, 2022). As mentioned earlier the constraints of planning and managing construction projects need to be simplified using the available IT applications that are being developed nowadays, this research will try to answer the following research questions and test three research hypotheses will answer the following questions in this research:

Q1: Do construction companies in Kazakhstan use Project management software?
Q2: For which purposes do they utilize such software?
Q3: Does that software give them a positive result according the purpose that are used?
Q4: On what kind of projects do they use such software?
Q5: Does this software simplify and facilitate the work of these companies?
Q6: How effective are project management software in construction works?

Research Hypotheses

H1: Project management software have a positive impact on construction projects.
H2: Project management software simplify and reduce project workload.
H3: Project Management software are effective in Construction projects.

What are Project Management Software?

Project management software (PMS) is computer based applications designed to assist and help plan, organize, or manage resource tools as well as to develop resource estimates. Based on the specification of the software (Cobb, 2023), it can manage estimation and planning, scheduling, cost control and budget management, resource allocation, collaboration software, communication, decision-making, quality management, time management and documentation or administration systems. Numerous PC and browser-based project management software and contract management software products and services are available (Hamilton, 2001).

Project management software can:

- Help in project planning, and project setup.
- Simplify communication process within project members and stakeholders.
- Develop future changes and control the present project milestone.
- Assist in making schedule for project, or easily make changes to schedule.
- Make consistent project finance plan.
- Manage future risks.
- Manage project procurement plan.
- Manage work breakdown structure and smaller project tasks.

Projects usually have specific start and finish dates (Al-Refaie et al., 2023), with smaller tasks and work breakdown structures that lead to tangible outcomes or final project deliverables (Ahmad & Malik, 2023). For that constraints like schedule, cost, resources, budget, time and communication all depend on a project's feasibility (Moreno-Monsalve et al., 2023). So, programs are enacted of several smaller projects that, when combined, will provide a long-term business objective. Project managers oversee individual projects, and program managers supervise groups of multiple projects, focusing on a major goal. Sometimes there are functional managers who oversee smaller tasks in a project, for that project management software are built. Considereing that, there are important elements for a successful project management skills beside using software tools, such as the integration of knowledge, skill, leadership, ability and competencies which are necessary for successful construction project completion (Ghorbani, 2023).

Application of Project Management Software to Construction Projects

The construction industry is one of the most industries in which PM software is used for essential. As huge users of PM software, professionals in the construction industry have a strong interest in improving the tools and techniques available for better project planning and control (Hamada et al., 2021). Several studies demonstrated that construction managers continue to be very interested in developing better methods for project planning and management. In addition, a few studies have considered the application of these tools in PM software (Ahuja et al, 1994).

How do Software Contribute to Construction Projects?

PM software are found for the purpose of supporting most aspects of construction. They were primarily designed as solutions to specific problems that may arise during the project management process. These Solutions can be (Sun, M., & Howard , 2004):

1-Planning, Scheduling and Management
2-Computer Aided Design and Visualization
3-Building Engineering applications
4-Business information management
5-Digital Facilities Management
6-Project Integration
7-Computer cost estimation and finance

Research Problem Statement

The complexity of construction projects makes it to be uncertain and a times causes rising issues like mistakes (Gamil, & Abd Rahman, 2023), risks, and changes in the future from many work plans and or stakeholders who are involve in the project. To simplify the task of the project plan and reduce the problem of uncertainty and future risks, it could be better to use some certain IT software that may assist in project schedule plan, finance and procurement of the project materials. Making project plan manually comes with a cost of paying the errors and time wasted in the old system, consider that the modern software could easily find errors where it's made and show the future outcome of all work plans, or excess cost that maybe wasted. The assorted project management software were found to address the issue of time management, project plan and control, project finance, communication and other tasks involve. Modern IT Project management software made it easier to plan and manage large projects with up to date results. In addition, a few studies have considered the application of these tools in PM software. Over the past five years, there has been a significant increase in the usage of PM software especially by construction firms, also projects now are involving a huge amount of big data, and this type of data needs specific analytical processing (Hassanin & Hamada, 2021). For these reasons, we found a necessity to investigate the feasibility and the efficiency of software project tools in construction projects.

Research Method & Design

This study sought to explore and investigate into the implication of software towards the success of construction projects, as well as highlight their significant importance in the construction industry. The research design was explanatory and descriptive using qualitative research methods (Creswell, 2002). It was explanatory because knowledge about project Management software PMS in the construction project was discussed also, the study gives an in-depth and description on the role of PMS on construction and IT tools that facilitate the effective and efficient implementation of construction projects are described. Responses from the questionnaire was requested and assigned theoretical values to describe the data. Also information gathered was described using frequencies and percentages. In 2012 Almaty has 10% of residential construction works followed by Nur-Sultan 13% as well as Atyrau 10% (US export, 2016).

In this research, the population consists of selected contractors and construction companies, consultants and stakeholders who are undertaking construction projects in Kazakhstan (Almaty and other few regions). Contractors in the region were considered in this research. These are construction companies registered as certified companies under the law of Republic of Kazakhstan (Flagma.kz, 2020). So, to select the main sample size from the population as a reason of sample size table (Riley et al, 2021), the total population is between 200 and 300. In order to make the better representation of the sample, the higher number was selected for sample size which is 285 with 95% confidence level. In view of the given fact that some respondents may not answer the questions, we need to know the minimum respondents that we could have in our sample size. It shows the minimum number of respondents with this given formula (Tejada & Punzalan, 2012):

$n' = n / (1+ (n/N))$ n is the minimum sample size and N is the population. With our numbers, (n′) the adjusted minimum should be 130 at least.

Data Collection Method and Analysis

The main instruments used in this study were questionnaires and interviews for the quantitative and qualitative sections. The questionnaire contained an open – ended, closed – ended type of questions. Likert scales were also used in gathering some of the data. The questionnaires were made up of four sections with a total of 20 questions. The qeustionairs are distribuuted to the registered constructions companies in the big regions Kazakhstan country, there are 310 Members of Union builders of Republic of Kazakhstan, where main data of the expected population was gained, with all of the firms that operate as construction companies. Almaty region has 97 construction companies under the union from which the research data will be obtained as shown in figure (1)

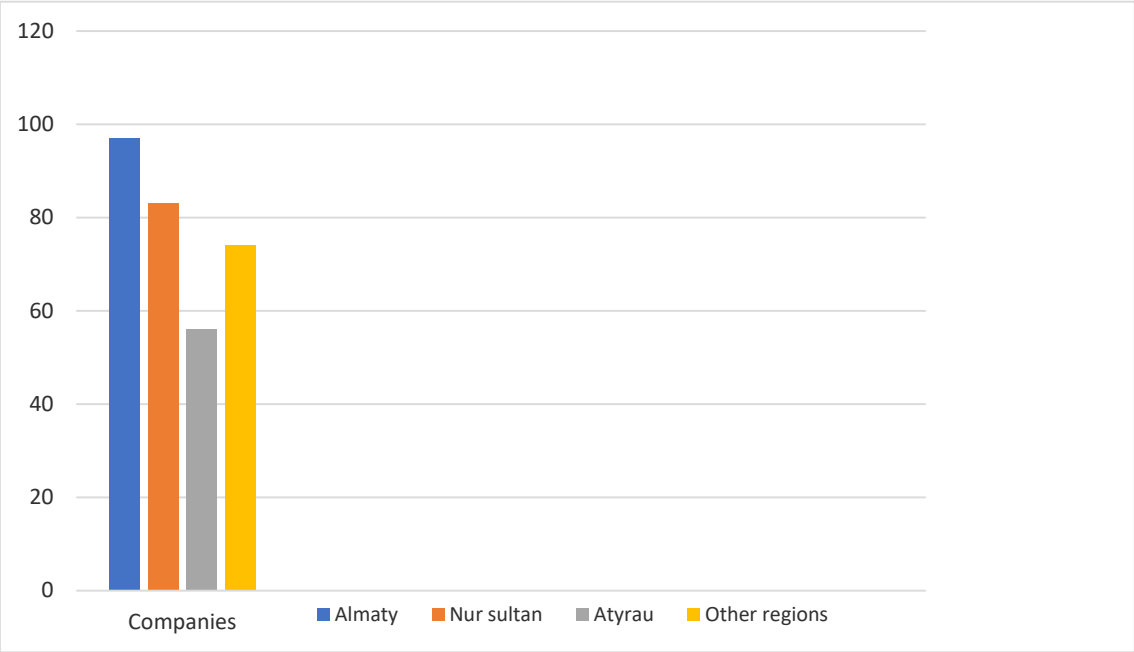

Figure 1. Distribution of construction companies in Republic of Kazakhstan.
Source: https://www.zoominfo.com/companies-search/location-kazakhstan-industry-construction

The company's background and experiences was briefly checked as shown in Figure (2), to see which will best fit for the research to find how each use IT and modern software in its projects, the target companies were identified under the members of the Union of builders in Republic of Kazakhstan. Large enterprise firms who have been operating for more than 10 years and have delivered more than 50 large projects which the researcher chose as the exact sample group. One by one meeting was held with a top official of experienced operating companies, while questionnaires were sent out to other categories.

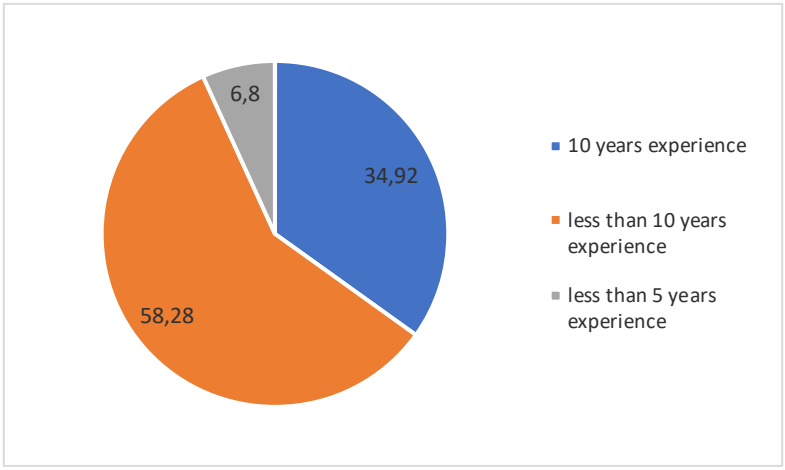

Figure 2. Categories of companies based on their years of experience.

Data gathered from the research field was analyzed qualitatively and quantitatively in a thematic system. The interviews obtained were also formatted into text. Both the literature studied, and the data gathered from the

participants and respondents were measured accurately and then SPSS was the tool used for analyzing the data which was later presented in tables, pie charts and bar graphs.

Results and Discussion

The background of respondents was first considered to ensure the respondents qualifications for the research study, and it was realized that all of them are contractors. The respondents also indicated the number of years they have been working in the construction industry. It was realized that 33% of the respondents have worked in the construction industry from six to ten years. While twenty per cent (20%) of the respondents have worked in the construction industry for less than six years (0-5years) and then the last 47% have worked in the construction industry for more than 10 years as explained in figure (3).

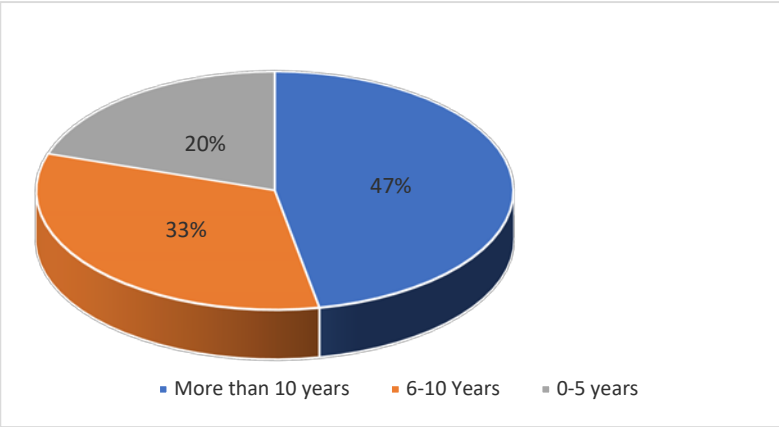

Figure. 3. Graphical representation of respondent's experience

The respondents were asked to indicate which type of construction projects their organization engages in as shown in figure (4), which indicates that most of the organizations work on housing and business centers project, they were represented by 38%. Then (12%) of the respondents said that their organizations work on Building School projects. Sixteen (16%) of the respondents indicated that their organizations work on Hotel projects. Civil Engineering Projects was indicated by 32% of the total respondents, while only 2% indicated other building projects such as building and maintenance of homes.

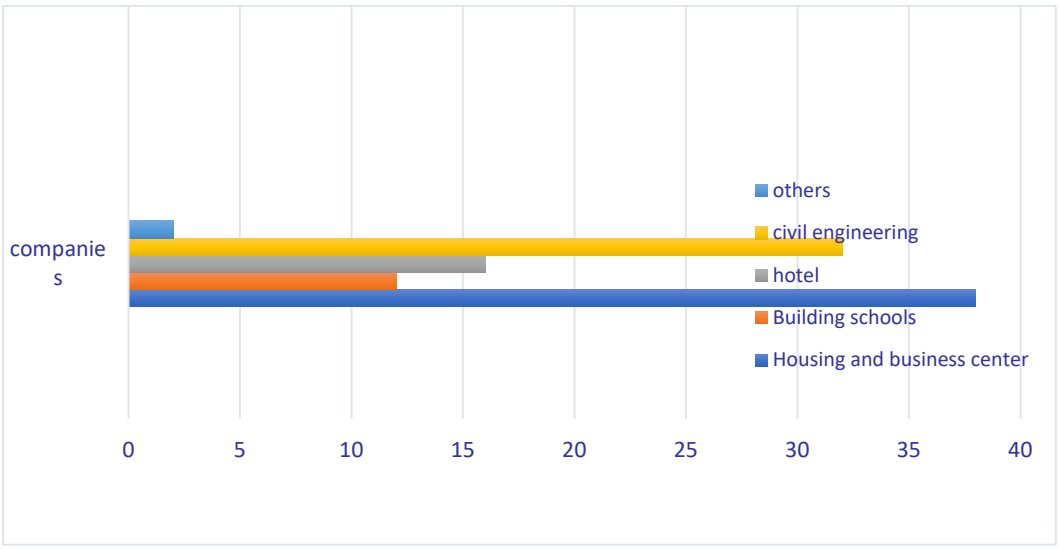

Fig. 4 Graphical representation of projects types respondents have taken part in

The questionnaire also asked respondents to indicate the main types of contracts that they are engaged in. The majority of the respondents (82%) indicated that they are engaged in Traditional Contracts while 18% of the respondents indicated that they are carried out Design-Build-Operate Contracts. The study reveals that the average duration of the projects that most of the respondents are engaged in had 12 to 18 months having the

highest frequency of 37% of responses, 33% indicated that the average duration of the projects are between 18 and 24months, 19% of the 34 respondents indicated that the average duration of the projects are between 24 and 30months while 11% of the respondents indicated that the average duration of their projects last less than 12months as explained in Figure (5)

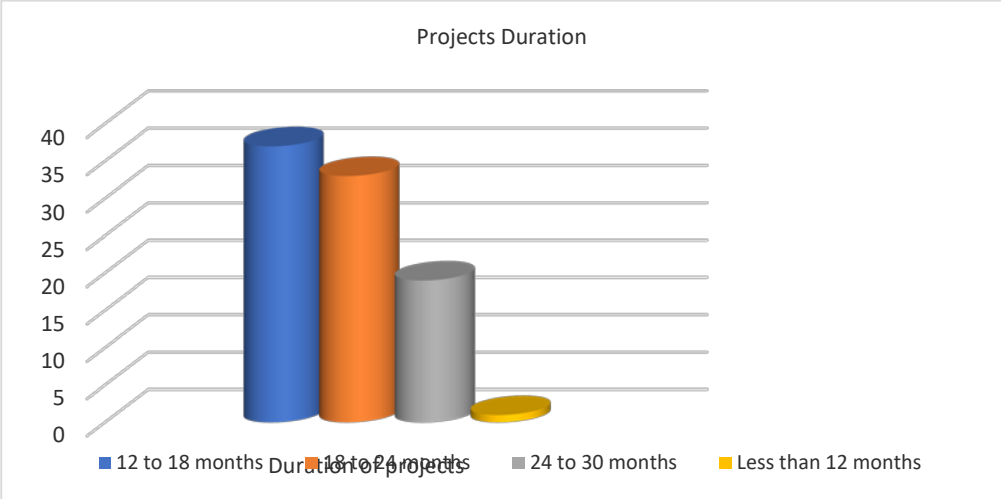

Figure 5. Graphical representation of projects duration among participants

The Role of Project Management Software in the Construction Industries

Construction respondents are heavy users of critical path analysis for projects planning and control, also resource management, scheduling, and earned value analysis for project control. The number of activities in a typical project and the use of software for all active projects were the key determinants of the usage of specific analytical techniques in the industry. The modern world of Information technology brings significant changes to our profession and the way we carry out tasks in every daily activity, likewise the project management of construction now has too much to do with software. The study shows that 92% of respondents use Project management software while only 2% are not using the IT tools and the remaining 6% use it sometimes but not always.

The participants were asked about their view on the importance of PM software, and it reveals that 78% believe that the different types of project management software are important and 13% said it's not necessarily important, and 5% agree that it's partially important. Furthermore, integrated software are in use in 34% of the total respondents' company, 61% are yet to develop such software and 5% believe that they will build PMS in the future. Table (1) and figure (6) summarize the response that collected from the participants about PM software.

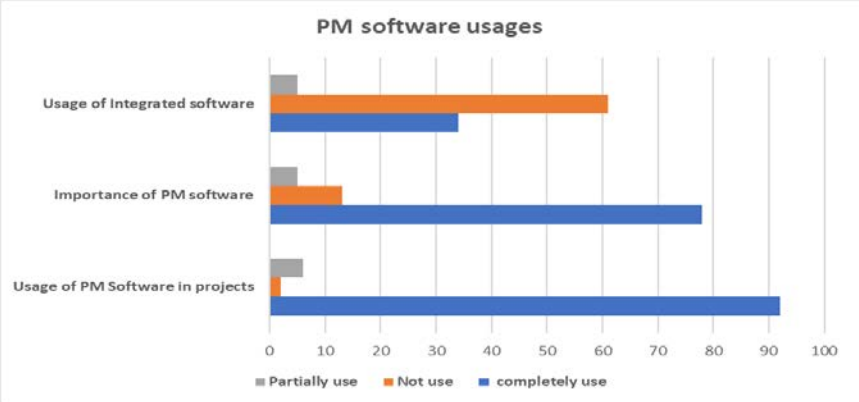

Figure 6. Importance and usages of PM software in construction projects

Table 1. Importance and usages of PM software in construction projects

Variables	Completely use	Not use	Partially use	Rank
Usage of PM Software in projects	92	2	6	1
Importance of PM software	78	13	5	3
Usage of Integrated software	34	61	5	2

Table 2. Stages at which respondents used PM software in construction projects

Project phases	Planning	Execution	Monitoring/control	Closing
At what phase do you use PM software?	37%	33%	22%	8%

Also, the respondents were asked to indicate the projects phases and aspects that they use such software in their duty. Table 2 explains the phase and Table 3 explains the project aspects. The table above show the stage or phase at which managers and stakeholders use PM software more is planning level with 37% of respondents agree to that, followed by Execution level. This might be due to the much work of planning in construction projects that consist of cost estimation, scheduling and risk plan. While in monitoring and control managers use software for communication project tracking and team development and it's the third with 22% of respondents that agree to this point. We see that only 8% participants agree the point that they use PM software at closing phase, because this is the final phase in the project and it requires a few strength and task.

Table 3. The aspects in which PM software helps respondents

Project aspects	Time Management	Cost Reduction	Managing team	Simplify Procurement
In which aspect does PM software helps you?	32%	31%	23%	14%

Table 3 prescribed the different aspects respondents use PMS at, with the highest 32% believe it saves their time in managing tasks preparing schedules or monitoring the project performance. 31% agree that it reduce cost of project, through identifying risks, simplifying works and resource allocation, while 23% manage their team using the software tools and the last 14% believe the software simplify their procurement process in managing projects.

Categories and Purpose of PM Software

This study finds the main purpose and the categories of software in construction Project management.

Table 4. Purposes of PM software in construction

Question	Planning	Cost Estimation	Team Management & Collaboration	Visual Design
For what purpose do you use PM software?	35%	17%	30%	18%

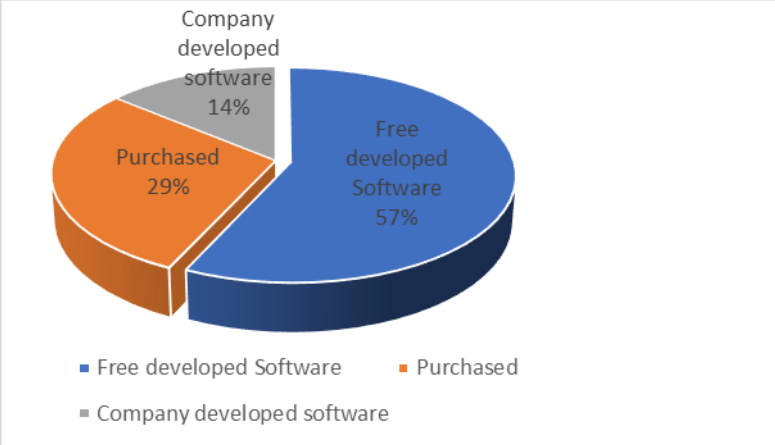

Figure 7. Graphical representation of source of PM software

As represented in Table 4 the main usage of project management software is for planning purpose as per the study, because 35% respondents showed that they use PM software for planning their project, then followed by team management and collaboration with 30%, which means that the tool is effective in solving team related issues during their projects. Visual design and cost estimation are 18% and 17% respectively, still visual design has a bit priority hence construction is something that has to do with design, but cost estimation is also important independently on it's on.

The study finds that most of the respondents rely on the free developed software on the internet with 57% agree to this fact, followed by 29% whom purchase software for their project usage and then 14% of participants use integrated company software as shown in Figure (7). The study further analyzes the main type of software being used in the construction project industry, below is a table for the result as displayed in Table 6

Table 6. PM software popularly used in construction

Software type	Microsoft Project	BIM	CAD	Other
Which among the following do you use in your projects?	47%	24%	16%	13%

The results above show the major software used in construction project is MICROSOFT PROJECT with 47% of respondents using it, then Building information modelling as the second most used software with 24% and CAD at third with 16%. Other software are also in use with 13% among respondents. These may include software that aids procurement, communication and other miscellaneous tasks in project.

Impact of Project Management Software

The following Table explains the impact factors of Software project management and tools in the construction projects and ranked according to the importance of each factor to achieve the project objectives and fulfillments. As seen from the table 7., "PM software enhance team performance or simplify project team members collaboration" in the first rank which ensure the necessity of using these types of software in construction projects.

Table 7. The impact factors of PM software that popularly used in construction projects

Impact factors of Software PM	Mean	Standard Deviation	Rank
IT tools and software are effective from the initiation to closing phase of a construction	3.84	0.96	4th
PM software have significance impact towards cost reduction throughout the project	3.82	1.14	11th
Finance and budget could be tracked and managed using PM software	3.80	1.01	6th
PM software enhance team performance or simplify project team members collaboration	3.76	0.74	1st
PM software could absolutely be used to manage communication aspect in construction	3.70	1.09	8th
Software could be used be to easily minimize onsite workload in a construction project	3.66	1.21	13th
Help in the availability of experienced & skilled labor	3.64	1.10	9th
Project delay can be managed significantly using a software to control schedule	3.62	0.97	5th
Software and IT tools could be used to manage large team as in construction project	3.56	1.07	7th
Procurement and transportation of resources could also be hastened using PM software	3.56	0.93	2nd
PM software provide a better risk management and mitigation option	3.50	0.95	3rd
Software are essential in stakeholder's relationship within a project	3.50	1.18	12th
Construction Project planning might be done properly without an IT software	3.50	1.10	10th

Regression Analysis and Testing the Research Hypotheses

In order to find the best model for data analysis, the Stepwise regression technique is used for multiple regressions, in this method, variables are input to this equation in order of their relationship with dependent variable and also this would be continuous until the entry process is significant on the model used. When variable's entry is not significant on a model, entry process will stop (Stepwise Criteria: Probability-of-F-to-enter <= .050, Probability-of-F-to-remove >= .100). As we can see, all independent variables were entered, and removal variables were found as zero. Table 8 presents coefficient determinant of *R*, *R*2 and Adjusted R. In the model, after inputting all independent variables, R is equal to 0.820 which at the end describes a strong relation between independent variables and the dependent variable. R square is equal to 0.679. This reflects that 69 percent of changes in dependent variable (positive impact) are described by these independent variables (negative impact). Here the point is R square didn't involve degree of any freedom in the analysis. Henceforth, with using Adjusted R square which it involves in the table we have R2 − Adj = 0.673, which is more reliable.

Table 8. Regression model summary

Model	R	R Square	Adjusted R	Std. Error of the Estimate
Regression	.830	.679	.673	.29230

Hypothesis Testing

Now let's use the tables above to clarify the test of research hypotheses.

Hypothesis One: In view of table 7 and the regression model in table 8, the correlation between effectiveness in project management and impact on cost reduction record 0.496 & 0.374, it shows positive relation between them. Also, according to P-value which is significant in 0.001 we can reject H0, it's mean that the first hypothesis of this study is accepted, H1: Project management Software have a positive impact on construction projects

Hypothesis Two: According to the correlation table, it shows the most positive relation with minimizing workload in comparison with managing project delay. Also tracking finance in table 7, which is 0.731, shows strong direct positive impact on managing the delay. According to P-values which are significant in 0.001 we can reject H0 and therefore second hypothesis of this study is accepted too, H2: Project management software simplify and reduce project workload.

Hypothesis Three: Based on the correlation coefficient between managing procurement and managing communication in table 7 which is 0.449, shows positive relations between them. Also, percentage of usage of PM software in table 1, which is 92%, shows how effective are software in PM. According to P-values which are significant in 0.001. We can reject H0 and then the third hypothesis of this study is accepted also, H3: Project Management software are effective in Construction projects

Conclusion

This research invistigate the importance of project management software to facilitate and support the fullfilment of the construction projects. To prescribe this importance of project management software in construction projects; We confirmed that IT and software tools have significant importance within construction project lifecycle. Most respondents clarify software can help them in planning project and simplify major planning activities like scheduling, cot estimation and managing project team members. Also, software used in construction projects, the study tested that most construction firms, they relied on Microsoft Project as their most used software. Software can save their time and reduce cost of project by making easy planning and schedule automatically. Furthermore, project management Software can assist the managers to acheive control and monitering in construction projects; the research finds that PMS are useful to construction industry managers and stakeholders for simplifying onsite and offsite workload.

Respondents who took part in the research study were all contractors and their firms were all over 10 years of experience. Due to the minimal representation of the sample size, the study picked companies that have been operating over 10 Years so as to gain valid and concrete data. This shows that the most respondents have a good idea of Kazakhstan construction industry. The main types of contracts that the respondents are involved in are

traditional contracts (82%) and design-build-operate having eighteen per cent. Out of these types of contracts the construction of housing and business centers ranked the highest with thirty-eight per cent while the least was maintenance of homes and building with only two per cent of contracts allocated. We also see that most construction works (37%) have a duration of twelve to eighteen months while the least (11%) allocated to of contracts took less than twelve months to be delivered. The study revealed that 92% of project managers use PMS in their projects, and 82% believed that PMS are important in their work and 34% used their company integrated software.

The research found that the least stage at which respondents use PMS is at the closing phase, while the main phase that the PMS is needed is planning phase. Furthermore, respondents believe that PMS are helpful in planning project with a relevant data that showed the highest percentage in this group is 35%, followed by team management and collaboration with 30% and the least is cost estimation with a statistical data of 17%. In the study we see that most of the respondents use Microsoft project as relied project management software with their highest respondents of 47%, while the other software have a statistical data of thirteen.

Recommendations and Suggestion for Further Research

This research recommends all the project managers who manage construction projects adopt modern software tools and modern technology in managing all project phases from planning the project until the closing phase. Also, there are significant impact factors discussed in the research, these factors affect the project's success, and managers should take them into their account to achieve the successful delivery of construction projects. Recommended Research areas to make further research may include:

- Apply the idea of this research in other fields or industries not only the construction industry, so this can maximize and explain the significant influence of software tools in project management.
- Maximize the role of data analysis by providing a large sample size and population to generate more findings and hidden insight from data analysis.

Scientific Ethics Declaration

The author declares that the scientific ethical and legal responsibility of this article published in EPSTEM journal belongs to the author.

Acknowledgements or Notes

* This article was presented as oral presentation at the International Conference on Basic Sciences, Engineering and Technology (www.icbaset.net) held in Marmaris/Turkey on April 27-30, 2023.

References

Ahmad, N., & Malik, A. A. (2023, February). Software project management-gap between theory and practice. In 2023 4th *International Conference on Advancements in Computational Sciences* (ICACS) (pp. 1-7). IEEE

Ahuja, H. N., Dozzi, S. P., & Abourizk, S. M. (1994). *Project management: techniques in planning and controlling construction projects*. John Wiley & Sons.

Al-Refaie, A., Al-Hawadi, A., Lepkova, N., & Abbasi, G. (2023). Blockchain of optimal multiple construction projects planning under probabilistic arrival and stochastic durations. *Journal of Civil Engineering and Management, 29*(1), 15-34

Chepachenko, N. V., Leontiev, A. A., Uraev, G. A., & Polovnikova, N. A. (2020, August). Features of the factor models for the corporate cost management purposes in construction. *In IOP Conference Series: Materials Science and Engineering, 913*(4), 042075. IOP Publishing,

Cobb, C. G. (2023). *The project manager's guide to mastering Agile: Principles and practices for an adaptive approach*. John Wiley & Sons

Creswell, J. W. (2002). *Educational research: Planning, conducting, and evaluating quantitative 7*. Prentice Hall Upper Saddle River, NJ

Export in Kazakhstan, The US export department (2016). https://2016.export.gov/kazakhstan/ doingbusinessin kazakhstan/leadingsectorsinkazakhstan/constructionandbuildingmaterials/index.asp

Flagma.kz (2020). Construction companies in Kazakhstan 2020. https://flagma.kz/en/companies/construction-companies/

Gamil, Y., & Abd Rahman, I. (2023). Studying the relationship between causes and effects of poor communication in construction projects using PLS-SEM approach. *Journal of Facilities Management, 21*(1), 102-148

Ghorbani, A. (2023). A review of successful construction project managers' competencies and leadership profile. *Journal of Rehabilitation in Civil Engineering, 11*(1), 76-95

Hamada, M. A., & Akzambekkyzy, A. (2022). Innovative governance strategy to enhance the performance and the efficiency of IT project management activities. *International Journal of Project Organisation and Management, 14*(2), 144-175.

Hamada, M. A., Abdallah, A., Kasem, M., & Abokhalil, M. (2021, April). Neural network estimation model to optimize timing and schedule of software projects. In 2021 *IEEE International Conference on Smart Information Systems and Technologies (SIST)* (pp. 1-7). IEEE

Hamilton A. J. (2001). *Managing projects for success*. London : Thomas Telford Ltd, 2001 pp 53-58.

Hassanin, M. E., & Hamada, M. A. (2022). A big data strategy to reinforce self-sustainability for pharmaceutical companies in the digital transformation era: A case study of Egyptian pharmaceutical companies. *African Journal of Science, Technology, Innovation and Development, 14*(7), 1870-1882.

Kuznetsov, N. G., Bogoslavtseva, L. V., Roshchina, L. N., Rodionova, N. D., & Kilinkarova, S. G. (2022). Priorities of software project management support of agro-industrial complex in ensuring food security. In *Business 4.0 as a subject of the digital economy* (pp. 667-669). Cham: Springer International Publishing.

Liberatore, M. J., Pollack-Johnson, B., & Smith, C. A. (2001). Project management in construction: Software use and research directions. *Journal of Construction Engineering and Management, 127*(2), 101-107.

Moreno-Monsalve, N., Delgado-Ortiz, M., Rueda-Varón, M., & Fajardo-Moreno, W. S. (2023). Sustainable development and value creation, an approach from the perspective of project management. Sustainability, *15*(1), 472.

Riley, R. D., Debray, T. P., Collins, G. S., Archer, L., Ensor, J., van Smeden, M., & Snell, K. I. (2021). Minimum sample size for external validation of a clinical prediction model with a binary outcome. *Statistics in Medicine, 40*(19), 4230-4251.

Sun, M., & Howard, R. (2004). *Understanding IT in construction*. Routledge.

Tejada, J. J., & Punzalan, J. R. B. (2012). On the misuse of Slovin's formula. The Philippine Statistician, *61*(1), 129-136

Wang, T., & Chen, H. M. (2023). Integration of building information modeling and project management in construction project life cycle. *Automation in Construction, 150*, 104832

Author Information

Mohamed Ahmed Hamada
Abu Dhabi University, Military college programs
Abu Dhabi, Al Ain , UAE
Mohamed.hamada@adu.ac.ae

To cite this article:

Hamada, M.A. (2023). Investigate the efficiency of project management software in construction projects, *The Eurasia Proceedings of Science, Technology, Engineering & Mathematics (EPSTEM), 22*, 247-257.

The Eurasia Proceedings of Science, Technology, Engineering & Mathematics (EPSTEM)
ISSN: 2602-3199

The Eurasia Proceedings of Science, Technology, Engineering & Mathematics (EPSTEM), 2023

Volume 22, Pages 258-267

ICBASET 2023: International Conference on Basic Sciences, Engineering and Technology

Application of Ultrasonic Methods for Evaluation the Anisotropy of Materials

Yonka IVANOVA
Sofia University

Abstract: The reason for anisotropy in material properties is the thermo mechanical effect in the process of plastic deformation, which creates a texture along the direction of deformation. One of the established nondestructive methods for evaluating the elastic constants in anisotropic materials is by measuring the velocities of ultrasonic waves propagating in different directions in the material. For studying the elastic anisotropy of textured media, the established measurement methods are hardly applicable because the materials are inaccessible for volumetric measurements. Moreover, the differences in the velocities of the ultrasonic waves are very small and the changes are localized in the surface and subsurface layers. The purpose of the study is to test a methodology and carry out the experimental studies to determine the anisotropy parameters of metallic materials based on the data from changes in the velocity of ultrasonic waves.

Keywords: Anisotropy, Low carbon steel sheet metal, Ultrasonic waves, Ultrasonic surface rayleigh wave, Ultrasonic subsurface wave

Introduction

The reason for the anisotropy in the properties of structural materials with crystalline structure is the thermomechanical effect in the plastic deformation process, which creates deformation texture (William, 2018). Deformation depends on the chemical composition, structure, grain structure, shape and distribution of carbides in steels, the condition of the sheet surface, the strain hardening coefficient as well as on the normal anisotropy coefficient of the sheet material (Miklyaev et al., 1986). The dependence of mechanical properties on texture direction can be useful in practice, but is usually an undesirable phenomenon. In the production of sheet materials with better mechanical and technological properties, it is necessary to perform quality control and evaluate the anisotropy of the metal sheets.

A standardized method is used to determine the anisotropy of sheet materials, which is carried out by conducting standard tensile tests according to EN ISO 6892-1:2009. The methodology requires cutting samples into at least three of the main directions 0°, 45° and 90° relative to the direction of rolling. Despite the reliability of the method, it also has its drawbacks. One of them is that a universal testing machine is needed to meet the requirements of the standard. In addition, sample preparation and testing also take time and costs.

Another method for determining the anisotropy of sheet materials is by measuring Vickers hardness. Before testing the specimens in one-dimensional tension, ten consecutive impressions with a Vickers Hardness Tester are applied to the specimens in a step of 0.50 mm, on which the diagonals are measured. After applying the 20% strain, the new diagonals of the Vickers indenter impressions on the specimens have to be measured. The determination of the anisotropy is evaluated by the anisotropy coefficient, which represents the ratio of the logarithmic ˆstrains in two mutually perpendicular directions of the examined sample bodies. The method and experimental results in the study of X5CrNi18-10 steel sheets are presented in detail in Yankov et al. (2014).

One of the well-established non-destructive methods for estimating the elastic constants of anisotropic materials is by measuring the velocities of ultrasonic waves propagating in different directions in the material (Sayers,1985; Tang et al, 2006). For investigating the elastic anisotropy of textured media, established methods are often inapplicable because the machine parts and products have limited dimensions. Furthermore, velocity differences are often very small and variations are localized in the surface and near-surface layers. The objective of the current study is to develop and test a methodology for determining an anisotropy parameter based on measurements of surface and subsurface wave velocities in several directions.

Statement of the Problem

The propagation of ultrasonic waves in an arbitrary direction in anisotropic materials is characterized by phase and group velocity differences (Viktorov, 1995). We consider dependences of ultrasonic surface wave parameters on elastic constants in the case of an orthotropic material (Barkhatov, 1999). Anisotropy of this kind arises in sheet rolling. The orthotropic material has three mutually orthogonal axes of symmetry of second order (Sedov, 1970). The orthotropy is a consequence of the technology – the randomly oriented crystals deform in a certain way (Adamescu et al.,1985). Figure 1 presented the coordinate system of an orthotropic material. In the sheets, the axis of symmetry is located along the rolling direction X_1, the axis X_2 is perpendicular to X_1, the axis X_3 is along the normal of the sheet plane (Barkhatov, 1999).

The first problem is to determine the wave propagation velocity along given medium densities, elastic physical moduli and wave propagation directions. The inverse problem is concerned with determining the components of the elasticity tensor under given density and wave propagation velocities. For these orthotropic media, the number of unknown components of the elasticity tensor is 9 (Royer et al., 1974; Landau et al., 2003; Sadd, 2009).

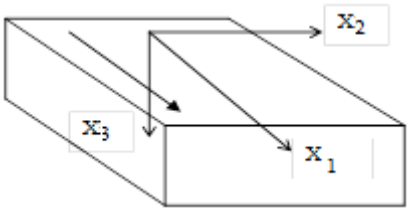

Figure 1. Coordinate system of an orthotropic material

$$C_{ij} = \begin{Vmatrix} C_{11} & C_{12} & C_{13} & 0 & 0 & 0 \\ C_{12} & C_{22} & C_{23} & 0 & 0 & 0 \\ C_{13} & C_{23} & C_{33} & 0 & 0 & 0 \\ 0 & 0 & 0 & C_{44} & 0 & 0 \\ 0 & 0 & 0 & 0 & C_{55} & 0 \\ 0 & 0 & 0 & 0 & 0 & C_{66} \end{Vmatrix}$$

Figure 2. Elasticity tensor of an orthotropic medium

An elastic wave propagating in a confined medium must satisfy the wave equation (1) (Barkhatov, 1999), (Krasilnikov, 1984) and the boundary condition for the absence of normal stresses on the material surface equation (2) at x_3=0 (Barkhatov, 1999).

$$\rho \frac{\partial^2 U_i}{\partial t^2} = C_{ijkl} \frac{\partial^2 U_k}{\partial x_j \partial x_l} \tag{1}$$

$$C_{ijkl} \frac{\partial U_k}{\partial x_l} = 0 \tag{2}$$

Among the solutions that satisfy this boundary condition, a solution in the form of a wave propagating along X_1, whose amplitude decreases in depth according to an exponential law, is searched (Royer et al., 1974) . The sought solution, inserted into the wave equation, leads to the Christoffel equation (Krasilnikov & Krylov, 1984; Barkhatov, 1999).

(3)

$$\rho V^2 U_i = C_{ijkl} N_j N_l U_k$$

According to Royer et al. (1974) and Barkhatov (1999) searching for the ultrasonic surface Rayleigh wave parameters, the problem reduces to find the eigenvalues and eigenvectors of the Christoffel equation.

$$\det\left[C_{ijkl} N_j N_l - \rho V^2 \delta_{ik}\right] = 0 \tag{4}$$

A 6th degree equation is obtained in which the ultrasonic surface Rayleigh wave velocity enters as a parameter. Each ultrasonic Rayleigh wave (URW) is a linear combination of three displacement components that propagate at the same velocity (Royer et al., 1974; Viktorov, 1995; Barkhatov, 1999).

$$U = \sum_{r=1}^{3} K^{(r)} U^{(r)} \tag{5}$$

The coefficients K and velocity are found by relation (5) in the free surface boundary conditions (2). According to (Barkhatov, 1999) after transforming the system of equations

$$\sum_{r=1}^{3} C_{i3kl} N_l^{(r)} U_k^{(u)} K^{(r)} = 0, i = 1,2,3 \tag{6}$$

we obtain a system of three equations concerning the displacement components of URW. Following Barkhatov (1999), after transformations, one can obtain a characteristic equation (7) that determines the URW velocity.

$$D.Z^2.(\delta - Z) = \left[(\delta - Z)D - Q^2\right]^2.(1 - Z) \tag{7}$$

Where

$$Z = \frac{\rho V}{C_{55}} = (\frac{V_x}{V_t})^2 ; D = \frac{C_{33}}{C_{55}} ; Q = \frac{C_{13}}{C_{55}} ; \delta = \frac{C_{11}}{C_{55}} = (\frac{V_l}{V_t})^2 = \frac{2(1-\nu)}{1-2\nu} ;$$

V_l and Vt are the velocities of longitudinal and transverse waves propagating along the X_1 axis direction and depend on four components of the elasticity tensor C_{11}, C_{33},C_{13},C_{55} ; ν is the Poisson's ratio and ρ is the density of the material.

$$\rho V_l^2 = C_{11}, \ \rho V_t^2 = C_{55}$$

By analogy with Adamescu (1985), the anisotropy coefficients A_1, A_5 have been introduced to account for the anisotropy in orthopropic materials. The coefficient A_1 represents the relative deviation of the tensile and compressive moduli along the X_1 and X_3 axes, and the coefficient A_5 characterizes the deviation of the shear moduli in the X_1 and X_2 planes from those of the isotropic material (Barkhatov, 1999).

$$A_1 = \frac{C_{11}}{C_{33}} \tag{8}$$

Where C_{11}, C_{33}, represent the in-plane tensile and compressive moduli of the X_1 and X_3 axes, respectively, and

$$A_5 = \frac{2C_{55}}{C_{11} - C_{13}} \tag{9}$$

Where C_{55} is the in-plane shear modulus of the X_1 and X_3 axes. The modulus C_{13} is a combination modulus of elasticity that characterizes the occurrence of transverse forces along the X_3 axes in tension or compression along the X_1 (Barkhatov, 1999). Then,

$$D = \frac{C_{33}}{C_{55}} = \frac{\delta}{A_1} \tag{9}$$

$$Q = \frac{C_{13}}{C_{55}} = \delta - \frac{2}{A_5} \tag{10}$$

With set anisotropy coefficients A_1, A_5 and the delta value (δ), the equation (7) is converted to (11). After transformations, equation (11) is presented in the form (12)

$$\frac{2(1-\nu)}{1-2\nu}(Z)^2\left(\frac{2(1-\nu)}{1-2\nu}-Z\right)=\left[\left(\frac{2(1-\nu)}{1-2\nu}-Z\right)\frac{2(1-\nu)}{A_1(1-2\nu)}-\left(\frac{2(1-\nu)}{1-2\nu}-\frac{2}{A_5}\right)^2\right]^2(1-Z) \tag{11}$$

$$\left(\frac{V_R}{V_t}\right)^3 AA(\nu)+B(\nu)\left(\frac{V_R}{V_t}\right)^2+CC(\nu)\left(\frac{V_R}{V_t}\right)+DD(\nu)=0 \tag{12}$$

Where V_R is the URW velocity and $Z = V_R / V_t$

$$Z^3 AA(\nu)+B(\nu)Z^2+CC(\nu)Z+DD(\nu)=0 \tag{13}$$

Where

$$AA(\nu) = D(\nu) - D(\nu)^2 \tag{14}$$

$$B(\nu)=2\delta(\nu)D(\nu)^2+D(\nu)^2-2D(\nu)Q(\nu)^2+Q(\nu)^4-D(\nu)\delta(\nu) \tag{15}$$

$$CC(\nu)=-\delta(\nu)D(\nu)^2-\delta(\nu)^2D(\nu)+2D(\nu)Q(\nu)^2\delta(\nu)-Q(\nu)^4\delta(\nu)-\delta(\nu)D(\nu)^2-Q(\nu)^4+2Q(\nu)D(\nu)^2 \tag{16}$$

$$DD(\nu)=\delta(\nu)^2D(\nu)^2-2D(\nu)Q(\nu)^2\delta(\nu)+Q(\nu)^4\delta(\nu) \tag{17}$$

The roots of the equation Z are determined in the Mathcad environment. In an isotropic material (A_1=1, A_5=1), the ultrasonic Rayleigh wave velocity depends on the Poisson's ratio ν and the transverse wave velocity. In the interval of change of Poisson's ratio ν= 0,1 to 0,265, three positive and three negative real roots are obtained.

The root Z_R, which is between 0 and 1, corresponds to a ultrasonic Rayleigh wave. When Poisson's ratio changes, the phase velocity varies in the range from 0,87.V_t to 0.97 V_t. The approximate expression for the velocity of the Rayleigh wave by (Viktorov, 1995) is presented in Figure 3 and shows a good approximation of the obtained solutions.

$$Z(\nu) = \left(\frac{0.87+1.12\nu}{1+\nu}\right)^2 \tag{18}$$

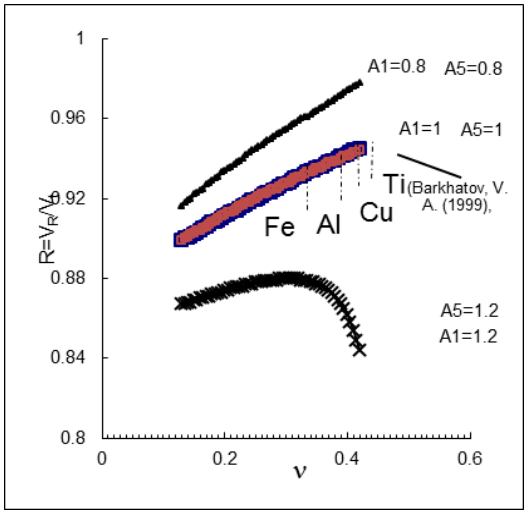

Figure 3. Dependence of the ultrasonic surface wave parameter R on the Poisson's ratio and the anisotropy parameters

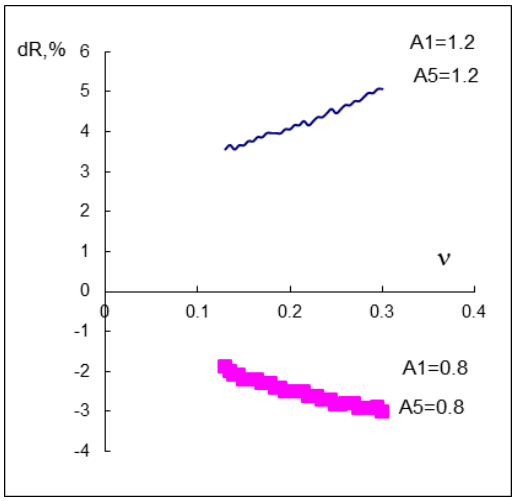

Figure 4. Relative variation of ultrasonic surface wave parameter R, %

The influence of anisotropy on the ultrasonic surface wave parameter $R = \sqrt{Z_R}$ is also given in Figure 3. When the ratios A_1 and A_5 are varied from 0.8 to 1.2, the *R* curve is shifted, but it is in the range from 0,85 to 0,98. The influence of anisotropy is weak. Figure 4 shows the relative variation $dR(v) = (R_o - R_i)/R_o$, where R_o are for an isotropic body, are R_i the values with the anisotropy accounted for. For iron with Poisson's ratio equals to 0.28 with anisotropy coefficients A_1 and A_5 equal to 1,2, the relative change in the velocities of Rayleigh waves is calculated as 4%.

In a ultrasonic Rayleigh wave, velocity dispersion is absent. The motions of the particles in this wave is along ellipses, with their major semi-axis perpendicular to the surface. The thickness of the wave localization layer is about 1.5λ, (Viktorov, 1995). Figure 5 presents the moduli of the components of the particle displacement vector in isotropic iron (Viktorov, 1995), where U3 denotes the relative amplitude of the oscillations of an ultrasonic surface wave along X_1 (along the surface) and U1 indicates the change in the relative amplitude of the oscillations along X_3 (perpendicular to the surface).

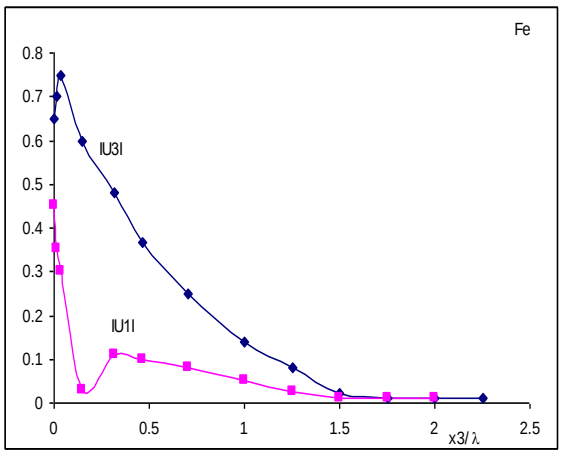

Figure 5. Moduli of the components of the Rayleigh wave displacement vector in an isotropic body

Basically the deformation in URW is a shear deformation and its velocity is close to the transverse wave velocity. The measured velocity along the X_1 direction is used to determine the shear C_{55} modulus, and along the X_2 direction the C_{44} modulus (Barkhatov, 1999).

$$C_{55} = \rho(\frac{V_R}{R})^2 \text{ along the axis } X_1 \quad (19)$$

$$C_{44} = \rho\,(\frac{V_R}{R})^2 \text{ along axis } X_2 \quad (20)$$

For Poisson's ratios greater than 0.265, equation (7) has complex-constrained roots that correspond to subsurface-longitudinal waves. According to Juozoniene, (1980) and Barkhatov (1999) the velocity of subsurface wave is close to the longitudinal wave speed. The ratio of subsurface-longitudinal wave (V_{pp}) velocity to longitudinal wave (V_l) velocity is expressed by the root of equation (7) as

$$G = \frac{\sqrt{\delta}\,\mathrm{Re}(\sqrt{Z})}{|Z|} = \frac{V_{pp}}{V_l} \tag{21}$$

where Z is the complex root, V_{pp} is the subsurface ultrasonic wave velocity. The calculations of the roots of the surface-longitudinal wave equation are shown in Figure 6.

The complex root indicates that the wave has parametric damping. The attenuation is determined by the imaginary part of the root. The attenuation ratio is the relative decrease in the amplitude of the wave over a distance of the order of the wavelength and is determined by (22)

$$K_\lambda = \frac{|U(x_1)|}{|U(x_1+\lambda)|} = \exp\ (2\pi \frac{\mathrm{Im(Z)}}{\mathrm{Re(Z)}}) \tag{22}$$

In isotropic materials, the subsurface wave parameters depend only on the Poisson's ratio. For values greater than 0.26 there exists a wave that is characterized by a complex root Z. In isotropic materials with Poisson's ratio smaller than 0 to 0.26, from the experimental point of view, no subsurface wave exists (Juozoniene,1980). Dependences of subsurface-to-longitudinal wave velocity ratio G on Poisson's ratio and anisotropy parameters are given in Figure 6. At ν ratios greater than 0.26, an unstable subsurface wave is formed, which quickly decays. The anisotropy of the elastic properties induced by deformation texture changes the solutions of the subsurface wave (Figure 6 and Figure 7). The larger the ν ratio, the smaller the layer of subsurface wave localization and the stronger the transverse waves are emitted. The attenuation ratio by (22) increases sharply (Figure 7).

The subsurface wave velocity value is close to the longitudinal wave velocity value and can be used to determine the tensile-stress modulus of the material.

$$C_{11} = \rho\ (\frac{Vpp}{G})^2 \quad \text{along } X_1 \text{ direction} \tag{23}$$

$$C_{22} = \rho\ (\frac{Vpp}{G})^2 \quad \text{along } X_2 \text{ direction.} \tag{24}$$

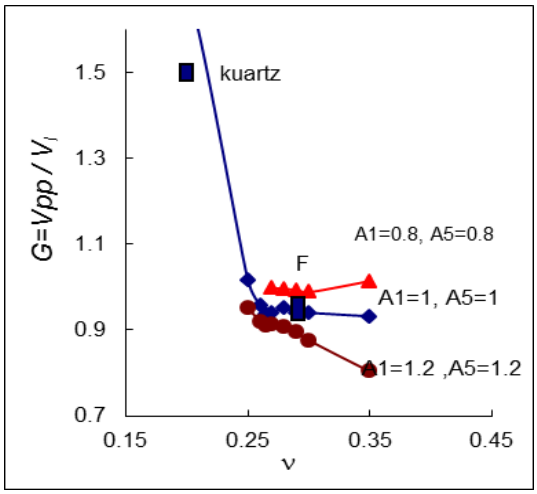

Figure 6. Subsurface-to-longitudinal wave velocity ratio and anisotropy parameters

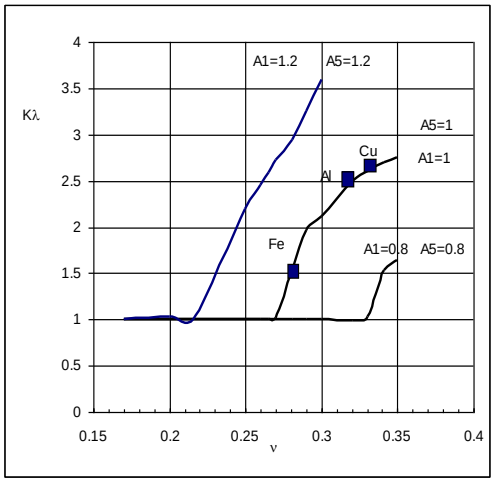

Figure 7. Subsurface wave attenuation ratio K_λ and the anisotropy parameters

As a result of the calculations performed, the dependences that relate the surface Rayleigh and subsurface wave velocities to components of the elasticity tensor were obtained. The *R* and *G* ratios are not constant and depend on the anisotropy of the material. If the data for A_1, A_5 from X-ray texture analysis are used, the values of *R* and *G* can be refined and errors in the determination of elastic moduli can be reduced.

Based on the above, it is possible to determine four of the nine independent components of orthotropic materials such as rolled sheet and plate. The measurement of the velocities of the ultrasonic surface Rayleigh and subsurface waves in the plastic deformation direction X_1 allows to determine components of the elasticity tensor C_{11} and C55. The determination of the velocities in the perpendicular direction X_2 enables the possibility to determine the components C_{22} and C_{44}.

Results and Discussion

Ultrasonic investigations with surface and subsurface waves with a working frequency of 4MHz were carried out on a low carbon metal plates (300 mm x 300 mm) with a thiknesses of 6 and 10 mm. An experimental set-up is shown in Figure 8a. A computerized ultrasonic instrument consists of a generator, a receiver of ultrasonic waves and an ultrasonic card US - expert. The ultrasonic device allows measuring the time of ultrasonic impulse with accuracy up to 1 ns and 12 bits resolution at sampling rate of 160 MHz. In order to attain a higher accuracy of investigations precautions for maintaining constant conditions for the acoustic signals generation are undertaken. The surface waves are excited by a variable angle angle transducer, at a refraction angle close to the second critical angle for the plexiglass-steel. The wavelength is on the order of 0.75 mm. The subsurface waves are excited at a refraction angle close to the first critical angle for the plexiglass-steel. Using a through transmission technique, we register and record in digital form signals emitted by transducer E and received by transducer R as shown in Figure 8a. The receiving transducer moves along the specimen covering distance ΔL.

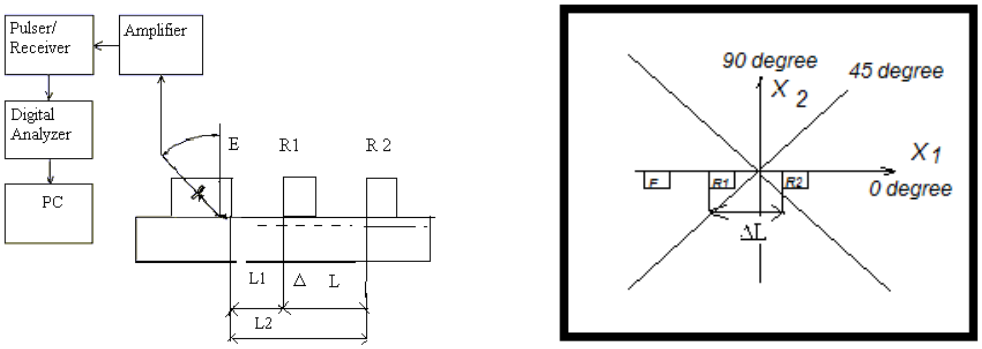

a b

Figure 8. Ultrasonic investigation of the anisotropy:
a) Experimental set-up for ultrasonic studies
b) Scheme of ultrasonic measurement of the anisotropy

The velocity of the surface waves (V_R) and subsurface waves (V_{pp}) is calculated by the formula:

$$V_{R,pp} = \frac{L_2 - L_1}{(\tau_2 - \tau_1)} = \frac{\Delta L}{\Delta \tau} \tag{25}$$

where ΔL is the distance between two positions of the receiver R, τ_1 and τ_2 are transit times of the wave obtained at distances L_1 and L_2. The transit time is registered from the beginning of the ultrasonic impulse.

The time of the recorded pulses is reported by the maximum envelope value of the signal and is measured to the nearest 1 ns. The $V_{R,pp}$ determination error is determined by $\Delta V_{R,pp}/V_{R,pp}=\Delta L/L+\Delta \tau/\tau$. For the distance ΔL=0.1 mm, L of order 50 mm and $\Delta\tau$=0,001μs, τ=10 μs the error in velocity determination is $\Delta V/V$=0,02%.The velocities of the surface and subsurface waves in the steel sheets were measured in three directions 0 °, 45° and 90° to the X_1-axis, as shown in Figure 8 b. The step of movement of the sensors is 20 mm, which is the width of the receiving transducer. For each position of the transducers, the travelling times of the ultrasonic waves at three distances 0, 50 mm and 100 mm were determined. Table 1 gives average values of surface and subsurface wave velocities in the directions 0, 45 and 90 degrees of the steel plates.

Table 1. Velocities of ultrasonic surface Rayleigh (V_R) and subsurface (V_{PP}) waves

Variables		0 degree	45 degree	90 degree
6 mm steel plate	V_R, m/s	2928	2936	2977
	V_{PP}, m/s	6001	6047	6100
10 mm steel plate	V_R, m/s	2998	2980	2989
	V_{PP}, m/s	5982	6015	6037

Anisotropy is estimated as a relative change in wave velocities. The relative variation of the Rayleigh wave velocities $dV_R = (V_{R(X1)} - V_{R(X2)})/ V_{R(X1)}$ along the X_1 and X_2 axes is about 1% for the thinner 6 mm steel plate. For the same sample, the relative change of the subsurface wave $dV_{pp} = (V_{pp(X1)} - V_{pp(X2)})/ V_{pp(X1)}$ was measured to be 1.7%, as shown in Figure 9 a. Figure 9 b shows the relative variations of the Rayleigh and subsurface waves obtained for the 10 mm thick steel plate. Less pronounced anisotropy can be observed, less than 0.5% for surface waves and about 1% for subsurface waves.

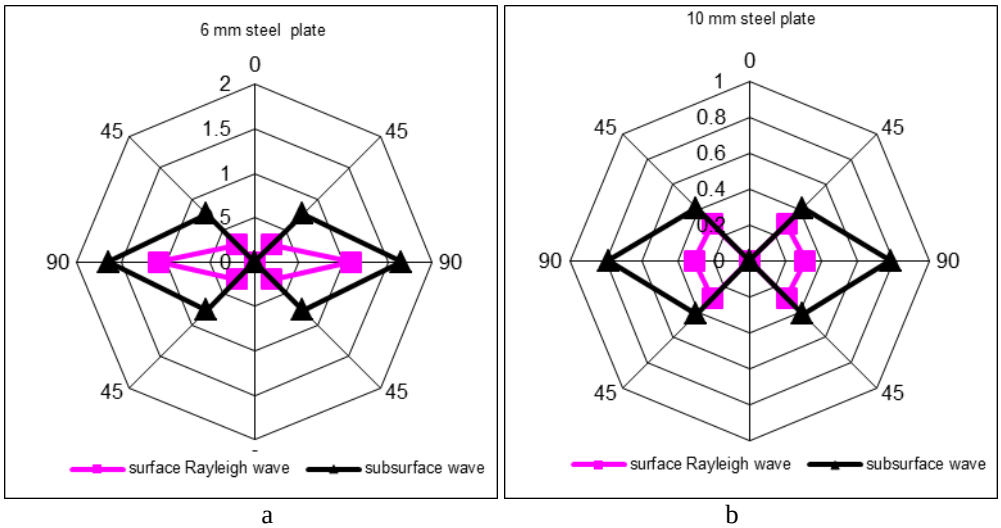

a b

Figure 9. The relative variations of the velocities of ultrasonic Rayleigh and subsurface waves on different directions: a) 6 mm steel plate; b) 10 mm steel plate

Conclusion

Based on Barkhatov (1999), this work presents a methodology for determining the anisotropy of steel sheets using ultrasonic surface waves as a result of the performed calculations, the dependences were obtained that connect the velocities of surface Rayleigh and subsurface waves with the components of the elasticity tensor of orthotropic media.

The measuring the velocities of surface and subsurface waves of rolled steel sheets in the direction of plastic deformation and in the perpendicular direction allows four of the nine independent components of orthotropic materials to be determined.

Experimental studies performed using ultrasonic methods show weak anisotropy. The anisotropy is more pronounced with the thinner steel plate. The relative variation of surface wave velocity in both directions was found to be 1%. The change in wave speed below the surface is almost approximately 2% for the 6 mm thick plate.

Recommendations

The presented research can provide new knowledge about the anisotropy of steel sheets to students and engineers to put into practice the ultrasonic methods by surface and subsurface waves for evaluation the anisotropy of metal products. Further research will be aimed at comparing the results from destructive and non-destructive methods for anisotropy assessment in orthotropic media.

Scientific Ethics Declaration

The author declares that the scientific ethical and legal responsibility of this article published in EPSTEM journal belongs to the author.

Acknowledgements or Notes

*This work has been accomplished with the financial support by the Grant No BG05M2OP001-1.002-0011-C02 financed by the Science and Education for Smart Growth Operational Program (2014-2020) and co-financed by the European Union through the European structural and Investment funds.

*This article was presented as oral presentation at the International Conference on Basic Sciences, Engineering and Technology (www.icbaset.net) held in Marmaris/Turkey on April 27-30, 2023.

References

Adamescu, R. P. Geld, E. A., & Mityushov (1985). *Anisotropy of physical properties of metals and alloys*. Moscow: Metallurgiya.

Barkhatov, V. A. (1999). Determination of the modulus of elasticity of textured metal by surface wave parameters. *Defektoscopy, 10,* 35-47.

Juozoniene, L. V. (1980). Elastic surface longitudinal waves and their use for non-destructive control. *Defektoscopy, 1,* 29-38.

Krasilnikov, V.A.,& Krylov V.V. (1984). *Introduction to physical acoustics*. Moscow: Nauka.

Landau L. D., & Lıfshıts, E. M. (2003). *Theoretical Physics, Volume VII. Theory of elasticity* (5th ed)., Moscow: Fiz.Mat.Lit.

Miklyaev, P.G., & Fridman, Y.B. (1986). *Anisotropy of mechanical properties of metals.* Moscow: Metallurgiya.

Royer, D.,& Dieulesaint E. (1974). *Elastic waves in solids.* Paris,France:Walley.

Sadd, M. (2009). *Elasticity. theory, application, and numerics.*(2nd ed). UK, Oxford:Elsevier.

Sayers, C. M. (1985). Angular dependence of the rayleigh wave velocity in polycrystalline metals with small Anisotropy. *Proc. R. Soc. Lond. A, 400,* 175-182.

Sedov, L.I. (1970). *Mechanics of continuum media*, Moscow: Nauka.

Tang, S.H., Wu, S. ,Tu, S.T.,& Kobayashi, M.(2006). Characterizing texture in polycrystalline materials by ultrasonic waves. *Theoretical and Applied Fracture Mechanics, 45*(2), 128–138.

Viktorov, I. A. (1995). *Rayleigh and lamb waves: Physical theory and applications (ultrasonic technology).* Springer.

William D., Callister, Jr., & Rethwisch D. (2018). *Fundamentals of materials, science and engineering. An integrated approach* (5 th ed). *Wiley*.

Yankov, E. H ,Gospodinov, D., & Gagov,V. (2014). Investigation on the opportunities for anisotropy determination of sheet materials by Vickers hardness test. *Proceedings Mechanics, Mechanical and Manufacturing Engineering Conference University of Ruse "Angel Kanchev", Bulgaria*. http://conf.uni-ruse.bg/bg/docs/cp14/2/2-24.pdf.

Author Information

Yonka Ivanova
Sofia University
Sofia, Bulgaria
Contact e-mail: yonivan@phys.uni-sofia

To cite this article:

Ivanova, Y.P. (2023). Application of ultrasonic methods for evaluation the anisotropy of materials. *The Eurasia Proceedings of Science, Technology, Engineering & Mathematics (EPSTEM), 22*, 258-267.

The Eurasia Proceedings of Science, Technology, Engineering & Mathematics (EPSTEM)
ISSN: 2602-3199

The Eurasia Proceedings of Science, Technology, Engineering & Mathematics (EPSTEM), 2023

Volume 22, Pages 268-273

ICBASET 2023: International Conference on Basic Sciences, Engineering and Technology

Sizing and Structural Analysis of Mechanical Bar Screen

Sezer TURGUT
TIMEX-FTS Filtration & Water Systems

Yasar YENISOY
TIMEX-FTS Filtration & Water Systems

Yaser MOHAMADI
TIMEX-FTS Filtration & Water Systems

Koray TORUN
TIMEX-FTS Filtration & Water Systems

Abstract: With the increase in the world population and improvement in industrial innovations, amount of municipal and industrial wastewater has increased dramatically. Therefore, municipal wastewater treatment systems have become a vital factor in sustaining water sources and decreasing the wastewater discharge to the environment. The first step in preliminary treatment of the wastewater is generally implemented using screening the large solid contamination. Bar screens are particularly an optimal solution for screening the wastewater in pumping stations, municipal and industrial wastewater treatment plants, and also at the inlet of the power plants. In this study, analytical method is used to determine the relationship between the screen size and the slope of streaming water channel. This correlation is now being used during the design of mechanical bar screens at our facility. In this study, Finite Element Analysis is also used to verify the structural strength of the inclined bar screen systems which have been designed, manufactured, and operated by our team. To investigate structural durability of the frames of the mechanical bar screen, static analysis is first checked by Autodesk Inventor Frame Analysis module, then Autodesk Inventor Nastran is used for detailed Finite Element Analysis.

Keywords: Wastewater, Bar screen, Analytical method, Structural analysis, Finite element analysis

Introduction

Waste treatment plants are established to reduce the possible damage of both municipal and industrial wastewater to the environment and to ensure the continuity of usable water. The treatment system consists of more than one step and different processes according to the characteristics of the wastewater. Preliminary treatment is the first of these steps. There are various treatment systems within the preliminary treatment itself. A successful mechanical preliminary treatment is important to protect the downstream processes from clogging, agglomeration, and wear in downstream equipment. One of the most commonly used methods in preliminary treatment is mechanical screening. In general, the main objectives of mechanical screening are removal of untreated solids, protection of subsequent treatment units, and improvement in the performance of treatment units. Briggs et al. (2005) examined different screen types by evaluating the effect of physical properties in the quality of outlet stream. Zabava et al. (2016) studied different equipment used in mechanical stage of the wastewater treatment plant and compared their effectiveness in removing the solid particles. It has been observed that the most effective mechanical screening approach is to use inclined bar screens for the transport of solid particles. Saju et al. (2020) investigated manual screen design for municipal waste by examining the chemical properties and behavior of various wastes in Khulna city in Bangladesh. In South Asian countries,

where the world's population is dense, it is inevitable that wastes will increase with population. As a results, waste diversity and water pollution are considerably high. By analyzing the chemical properties of the filtered water, it was clear that mechanical bar screen played a crucial rule in reducing the polluting chemical agents. Roth et al. (2018) made design optimizations for sediment removal in streams and floodplains. Similarly, Schalko & Weitbrecht (2022) used mathematical modelling for optimal design of bar screen used for removing sediments as well as large pieces of wood during floods. Ali et al. (2019) carried out a detailed study for the removal of residues in wastewater and provided a mathematical model which illustrates the relationship between water and solids. This study addressed the design of bar screens by obtaining hydrodynamic solutions for water flow, and structural analysis of the rake system used for solids drainage according to Von-mises yield criteria.

In this study, the design of an inclined mechanical bar screen is realized by 3D modeling in Autodesk Inventor and structural analysis with Autodesk Nastran software according to the Von-Mises criterion and obtaining the stress values on the bar screen. The relationship between the screen size and the slope of streaming water channel is also investigated in order to optimize the size of the mechanical bar screen. The goal is to present an improved mechanical bar screen, to effectively reduce water pollution and increase the availability of usable water.

Design of Mechanical Bar Screen

The main parts of the mechanical screen are the screen bars, the screen frame, the drive mechanism, chain group and the harrow system (Figure 1). The system starts to rotate while working with through the instrumentality the gearbox, so that the wastes are transported with a rake on the system, and discharge to the conveyor takes place from there. Conveyor is required to collect the wastes falling from the screen.

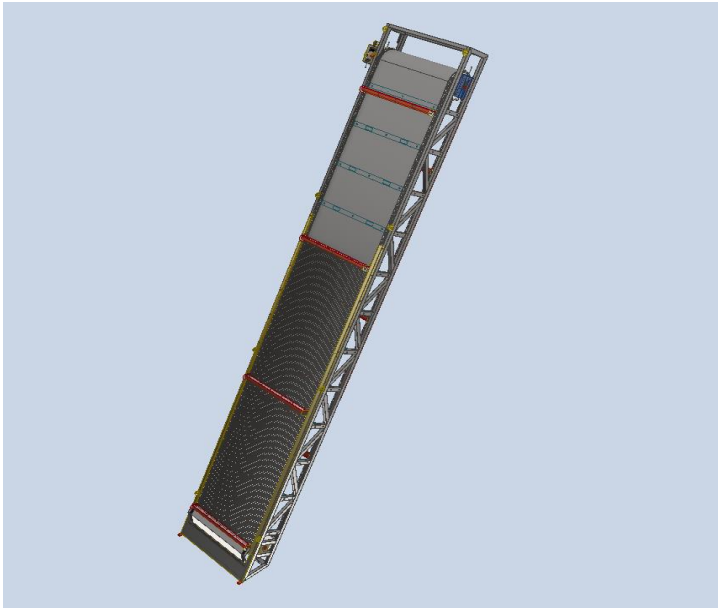

Figure 1. 3D modeling of mechanical bar screen

A safety sensor is used to cut off the energy of gearbox, and level sensor is used to operate the system, which is activated according to a certain height for water height. The level sensor acts as a float, preventing needless operation of the system. The sensor adjusted to the minimum water height continues to operate until the water drops below the adjusted height. Dimensioning is done by analytical and finite element analysis in line with the data obtained during the design of the coarse screen mesh. The work by Metcalf & Eddy (1991) includes design criteria for mechanical bar screen.

Table 1. Screen design criteria

	Manual Cleaning	Mechanical Cleaning
Velocity between screen bars (m / sn)	0.3-0.6	0.6-1
Bar section (thickness / width) (mm)	(4-8) / (25-50)	(8-10) / (50-75)
Cleaning between bars (mm)	25-75	10-50
Horizontal angle of grating with channel (degree)	45-60	70-85

Method

Analytical Method

Parameters for the analytical solution of the model are shown in the figure (Figure 2), channel width b = 1.84 m, distance between screen bars 0.02 m, slope of the channel s = 1/5000, the number of bars 52, the angle of the screen and the screen horizontal is γ = 70°, the size of the bars is 2 meters in width and 6 meters in length. Depending on the above parameters, depth of water and velocity of the flow through the screen and the approach channel is investigated at the most critical operating conditions according to the minimum and maximum flowrate.

The minimum and maximum velocity between the bars and in front of the screen are taken as, 0.9 m/s < V < 1.2 m/s. Metcalf & Eddy (1991)

$$v = \frac{Q}{A}$$

Energy losses, also known as head losses, occur as the magnitude of the velocity changes due to the screen of the channel. The height of the flow resulting from head loss is driven by the Bernoulli equation as below.

$$h = \frac{1}{0.7}\ x\ \frac{Vızgara^2 - Vızgara\ önü^2}{2\ x\ g}$$

Inside the channel, the water depth and velocity are found at points where the flowrate is minimum and maximum, according to the K coefficient. 0.3 m/s < Vmin < 0.5 m/s.

$$K = \frac{Q\ x\ n}{b^{8/3}\ x\ s^{1/2}}$$

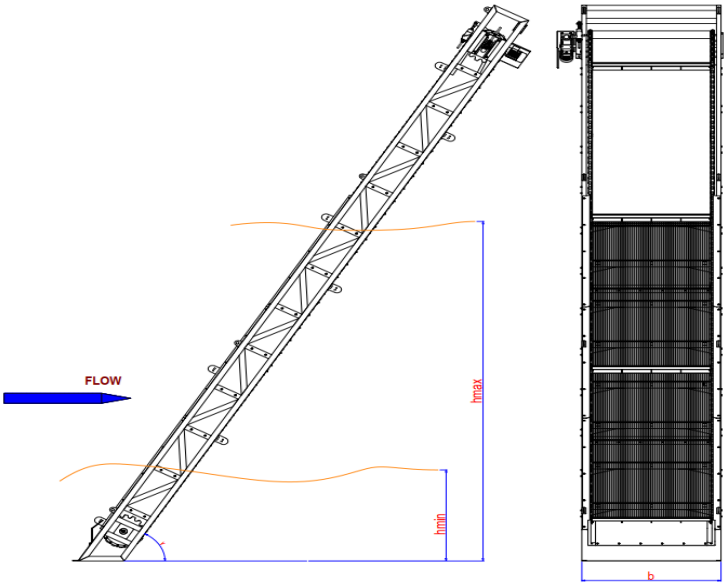

Figure 2. Schematic diagram of bar screen

Finite Element Analysis

Before fabrication stage of the designed system, it is verified by static analysis on the 3D model with the finite element method in line with the process & analytical solutions. Firstly, frame analysis for the frame of the system is examined with Autodesk Inventor Nastran software, and in the next step, static analysis is applied to the screens under a certain load.

Table 2. Properties of the materials

Material	Element Type	Mass Density	Yield Strength	Ultimate Tensile Strength	Young's Modulus	Poisson's Ratio
SS-304	Beam	8 g/ cm³	250 MPa	540 MPa	193 MPa	0.3 ul
SS-304	Bar	8 g/ cm³	250 MPa	540 MPa	193 MPa	0.3 ul

For frame analysis, the system is loaded in the z-axis direction starting at 5000 N and ending at 15000 N. Gravitational flow was estimated in this study. It will not have a high flow rate, but the result of the static analysis has been verified by loading the bars with a continuous pressure of 3 bar. The model consists of a total of 421913 nodes and 177449 elements.

Results and Discussion

The strength of the bars determined by static analysis as seen in the Figure 3, the stress values of the system analyzed according to the Von-Mises criterion are displayed. It has been understood that the bars with a result of 17.74 MPa at the place of maximum is found to be considerably lower than the material yield stress.

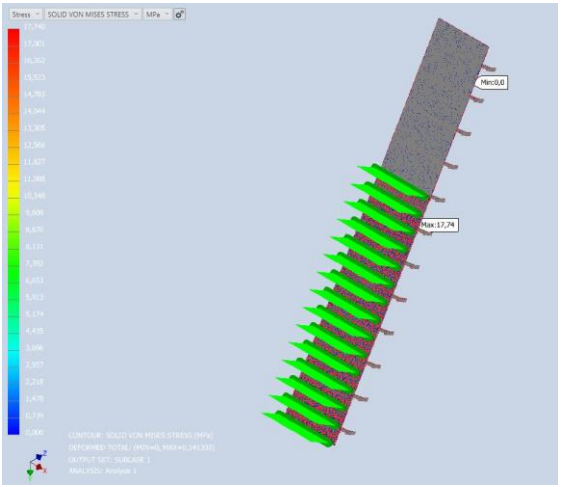

Figure 3. Stress values of mechanical bar screen

Results for the displacement are shown in Figure 4. Maximum deformation is found to be 0.14 mm which does not affect functionality of the mechanical bar screen. To minimize exerted forces due to water flow and particles to be removed from channel, reinforcement plates are placed vertically on the frame. Resulting lower deformation and decreased stress values.

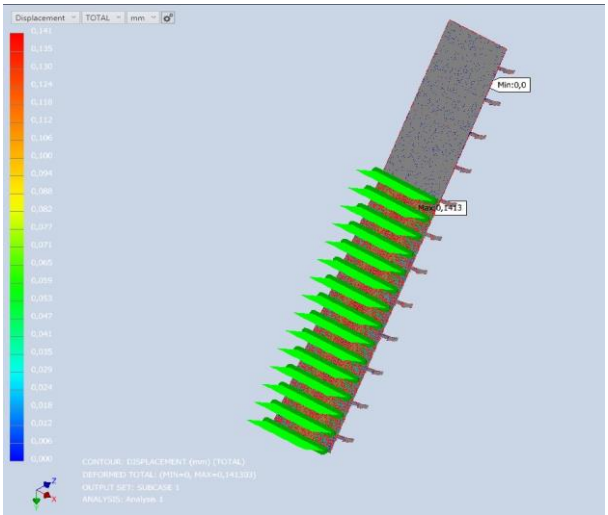

Figure 4. Displacement values of mechanical bar screen

With the analytical solution, the data shown in the Figure 5 is obtained. The results are in line with the relationship between the water height, width, and channel slope. The channel width is kept constant in the obtained data. With the result, it was seen that the water height increased as the slope decreased. The slope of the channel should be taken into account in the field studies. In the channel where the flow is constant, the relationship of the slope with the velocity can be evalueted, but with the increase of the velocity, it becomes more difficult for the screen to hold wastes.

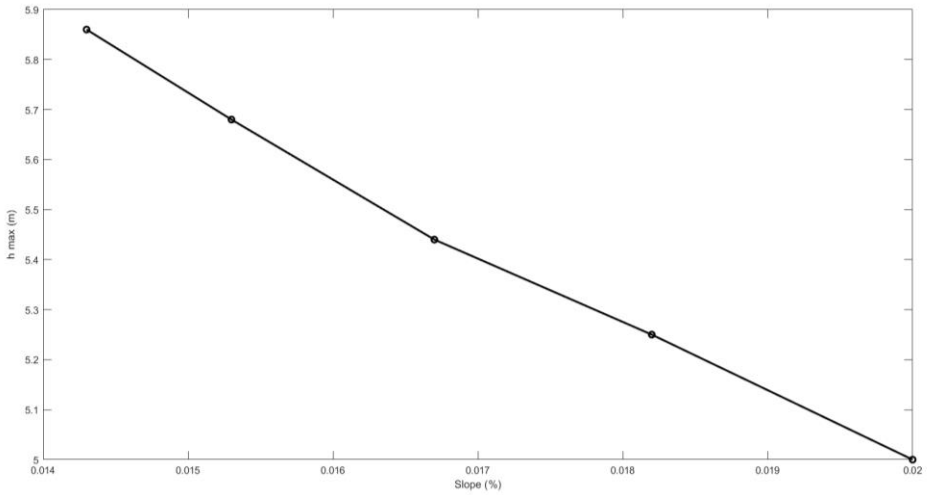

Figure 5. Slope-height relation of screens

Thanks to the mathematical modeling and structural analysis of the bar screen, the performance of the screens fabricated in our company has received positive feedbacks in the field applications. Figure 6a, Figure 6b are two examples of the units which have been designed, verified, fabricated, and commissioned in the site.

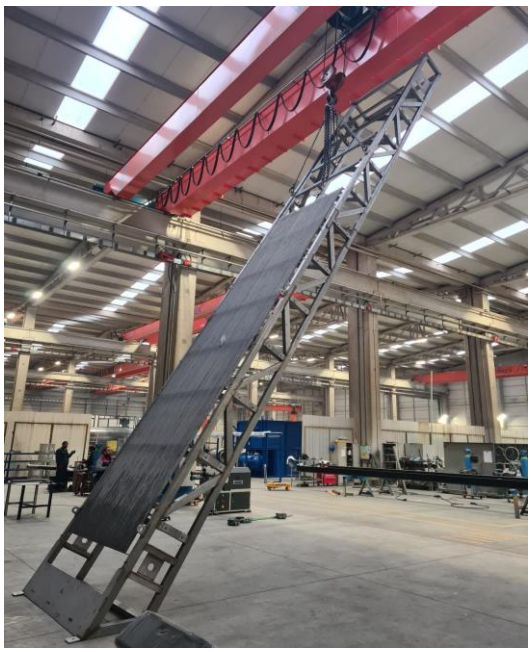

Figure 6a. Mechanical bar screen manufacturing

Figure 6b. Mechanical bar screen field application

Conclusion

The design of the system carried out by sizing the mechanical bar screen with analytical method and analyze the strength of the system with finite element analysis. It has been concluded that attention should be paid to the importance of the parameters and criteria used in the design. These issues are; maximum flow rate, width of the channel, slope of the channel, water height, head losses, distance between the screens, the process to be applied after the screen and the type of waste depending on the process.

Recommendations

Preliminary treatment, which is the first step of the purification process, consists of two processes. In this study, the coarse screen, which is the first stage, mentioned. It can be designed for fine screen by additional flow analysis with the same solution method. In addition, a brush system and irrigation method can be used for the wastes adhering to the screen for the designed coarse screen.

Scientific Ethics Declaration

The authors declare that the scientific ethical and legal responsibility of this article published in EPSTEM journal belongs to the authors.

Acknowledgements or Notes

* This article was presented as oral presentation at the International Conference on Basic Sciences, Engineering and Technology (www.icbaset.net) held in Marmaris/Turkey on April 27-30, 2023.

References

Ali, H., Kim, K. W., Bang, S. G., Chae, H. B., Shin, S. W., & Park, C. W. (2019). Numerical modeling of fluid–structure interaction between sewage water flow and bar screen to improve the screening process. *Water and Environment Journal*, *33*(4), 560-573.

Briggs, T., Ross, D., & Welp, J. (2005). Size matters: An overview of screening processes. *WEFTEC 2005*, 4339-4349.

Metcalf & Eddy. (1991). *Wastewater engineering: treatment disposal reuse* (3. Edition). McGraw.

Roth, A., Jafarnejad, M., Schwindt, S., & Schleiss, A. (2018). Design optimization of permeable sediment traps for fluvial bed load transport. In *E3S Web of Conferences*, *40*, 03009. EDP Sciences.

Saju, J. A., Rubel, S. N. R., Rahman, M. M., Nayan, S. B., & Bagchi, R. (2020). Effectiveness of manual bar screen in separating solid waste from municipal sewers of Khulna city. *Aust. J. Eng. Innov. Technol*, *2*(3), 31-41.

Schalko, I., & Weitbrecht, V. (2022). Wood blockage and sediment transport at inclined bar screens. *Journal of Hydraulic Research*, *60*(1), 164-172.

Zabava, B., Voicu, G., Ungureanu, N., Dinca, M., & Safta, V. (2016). Basic equipment for the mechanical treatment of wastewater. *Acta Technica Corviniensis-Bulletin of Engineering*, *9*(3), 57.

Author Information

Sezer Turgut
Timex-FTS Filtration & Water Systems
Ankara, Turkey
Contact e-mail: sezer@*timex.com.tr*

Yaşar Yenisoy
Timex-FTS Filtration & Water Systems
Ankara, Turkey

Yaser Mohamadi
Timex-FTS Filtration & Water Systems
Ankara, Turkey

Koray Torun
Timex-FTS Filtration & Water Systems
Ankara, Turkey

To cite this article:

Turgut, S., Yenisoy, Y., Mohamadi, Y. & Torun, K. (2023). Sizing and structural analysis of mechanical bar screen. *The Eurasia Proceedings of Science, Technology, Engineering & Mathematics (EPSTEM), 22,* 268-273.

The Eurasia Proceedings of Science, Technology, Engineering & Mathematics (EPSTEM)
ISSN: 2602-3199

The Eurasia Proceedings of Science, Technology, Engineering & Mathematics (EPSTEM), 2023

Volume 22, Pages 274-279

ICBASET 2023: International Conference on Basic Sciences, Engineering and Technology

Regional Guidance System for Cleaning Robots as a Result of Pollution of Solar Panels

Emin CANTEZ
Coskunoz Kalıp Makina A.S., R&D Center

Hasan SAHIN
Bursa Technical University

Omer Faruk EFE
Bursa Technical University

Abstract Solar energy production is provided by thermal and photovoltaic (PV) systems. Among them, PVs are considered one of the most important power generation systems that produce safe and sustainable energy. Depending on the outdoor conditions, PV systems get dirty over time due to dust, rain and environmental factors. Above the PV system When polluted, it causes a significant decrease in their efficiency. Especially in large photovoltaic power plants, it is seen that the panels are not polluted equally. But the cleaning robots system When it starts to clean, it cleans all the panels. Cleaning all clean and dirty panels causes energy consumption, material life and spare parts waste. In the system we have planned, it is planned to clean the panels by detecting the dirty panels with the camera and directing the cleaning robot only to the contaminated areas. Since only the contaminated areas will be cleaned, the energy production efficiency of the panels will increase and the cleaning time will be shortened.

Keywords Photovoltaic, Energy, Image processing, Object detection, Camera

Introduction

In recent years, global warming and the decrease in fossil fuels have increased the interest in renewable energy sources (RES) such as solar, wind, hydroelectric and geothermal energy. Among these energy sources, solar energy is one of the remarkable types of RES. Solar energy has become a more acceptable and promising energy source thanks to its enormous potential power and safe energy production (Korkmaz, 2021). Due to the disadvantages of using fossil fuels; Renewable energy sources such as wind, solar, geothermal and biomass have begun to be used. Among the renewable energy sources; Resources such as solar energy, hydraulic energy, wind energy, geothermal energy, solar energy, biomass energy, hydrogen energy, wave energy can be shown among the widely used energy sources (Önal, & Turhal, 2021). Compared with traditional energy sources, solar energy has many advantages such as abundant source, wide spread, free of environmental pollution, free use and easy accessibility (Diallo D, 2021) One of the important features of this energy is the easy installation of the systems required for production and low infrastructure costs (Pratt & Govender, 2021). Thus, solar power generation plants have become increasingly common around the world. Worldwide, the total PV power generation capacity has exceeded 625 GW at the end of 2019, while it was only 23 GW 10 years ago. The annual addition of PV capacity increased from around 8 GW in 2009 to more than 115 GW in 2019. In addition, it is estimated that PV capacity can meet the energy production of 3,518 TWh in 2030 (Khezri et al., 2022). However, various problems arise in the production and use of PV systems, such as reliability of panels, power drop, outdoor conditions and failures. PV panels are installed outdoors and are usually protected from the environment by an aluminum frame and glass lamination. However, these measures may not be sufficient due to harsh climatic

conditions and many different malfunctions may occur during installation, such as breaking or cracking the panel, falling tree branches, snow, insect marks, burn marks, shading and discoloration. In addition, manufacturing defects such as faulty soldering or connection can also cause PV panels to be damaged. Such various problems hinder the current flow of PV systems, reducing generation power and efficiency. Therefore, in solar power plants, it is necessary to monitor the operating status of the panels and replace or repair the defective units to ensure maximum efficiency (Naveen Venkatesh &Sugumaran, 2022). At this stage, by using an artificial intelligence algorithm that controls the PV lines, the system can also monitor the energy situation produced and record possible errors that occur. This artificial intelligence algorithm, which has many different versions of object recognition applications, collects recording data with the help of a camera, preventing losses during energy production. By directing the cleaning system or robots locally, it ensures that the dirty area is cleaned.

Material and Method

Deep learning helps machines understand the world and solve complex problems. It is the most popular approach for developing artificial intelligence, deep learning method, multi-layer for feature extraction and transformation nonlinear processing units. Successive layers take the output of the previous layer as input and process it (Kızrak, & Bolat, 2018).

Artificial Neural Networks (ANN)

ANN are machine systems developed for ANN to perform functions such as learning, generalizing and generating new information, inspired by the human brain, imitating the way the brain works, and are different from traditional algorithms. They use the calculation method. ANNs have fault tolerance and draw from experience, but are also hardware dependent. Neural networks contain input, weights, bias, sum function, activation function and output. A simple neural network example is given in Figure 1. Inputs can come from another neuron as well as from the outside world and form inputs to neurons. Incoming data is recorded with a weight value. It is multiplied by the bias value and added. In this way, it is known that the effect on the inputs to be produced can be adjusted. The addition function is the input by multiplying; It is the function that gives the net input of that cell by summing its values. Depends on ANN Sometimes the value of the inputs is important, sometimes the number of incoming inputs can be important (Su et al., 2021).

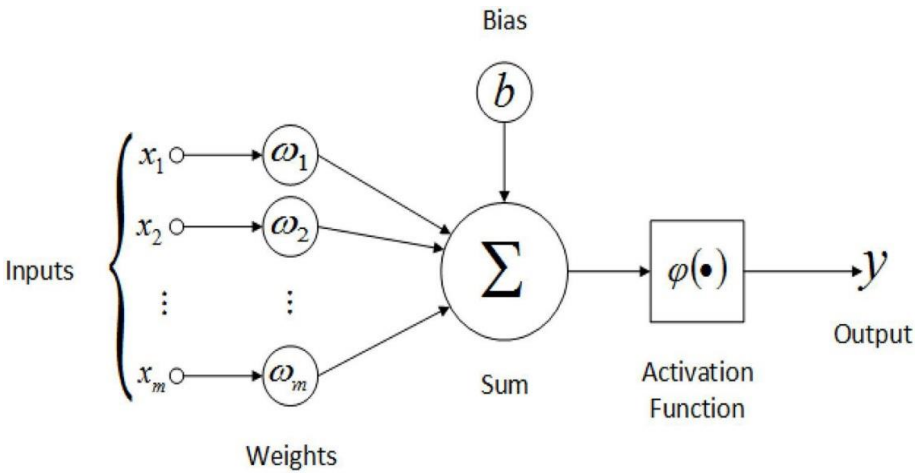

Figure 1. A simple neural network example

Convolutional Neural Networks (ESA)

People look at an image and make quick inferences about where they are in the image. ESAs created with today's computer vision field have achieved significant success in modeling the human visual system. ESA is used in many fields. Object recognition, object classification, object tracking, sentence modeling etc. ESAs consist of many layers. These are input layer, convolution layer, ReLu, pooling layer, fully connected layer, dropout layer, classification layer and output layer. The first example of Convolutional neural network is given in Figure 2.

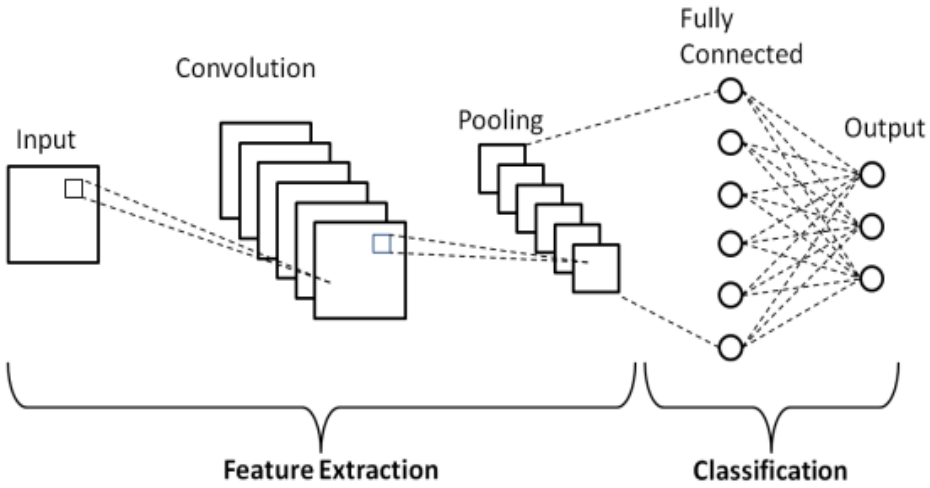

Figure 2. Convolutional neural network

Object Recognition Algorithms

Object detection is used in almost every field such as people counting, autonomous vehicles, pedestrian detection, face detection. The general purpose of object detection is to create a new image of a predefined object class in the system and determine the position of each detected object in this image using a rectangle surrounding it. There are many accurate and fast algorithms for object detection and tracking. The simplest deep learning approach for object detection and object tracking in deep learning is a convolutional neural network. An output class is obtained for each input image. Image This system can also be used to detect various objects. The biggest problem with this approach is that the object in the image can be of different sizes. As a result of this problem, it will cause the computation time to take quite a long time. Many object detection neural networks are available (Gu et al., 2018).

Examples of these are R-CNN, Fast R-CNN, Faster R-CNN, SSD, YOLO. The YoloV5 algorithm is very fast because it passes the image through the neural network in one go and predicts the class and coordinates of all objects. The most important feature that istinguishes YoloV5 from other object detection algorithms is that it is ahead of its competitors in general average sensitivity (mAP) values in real-time object detection and tracking.

WORKS DONE

Data Set Creation and Labeling

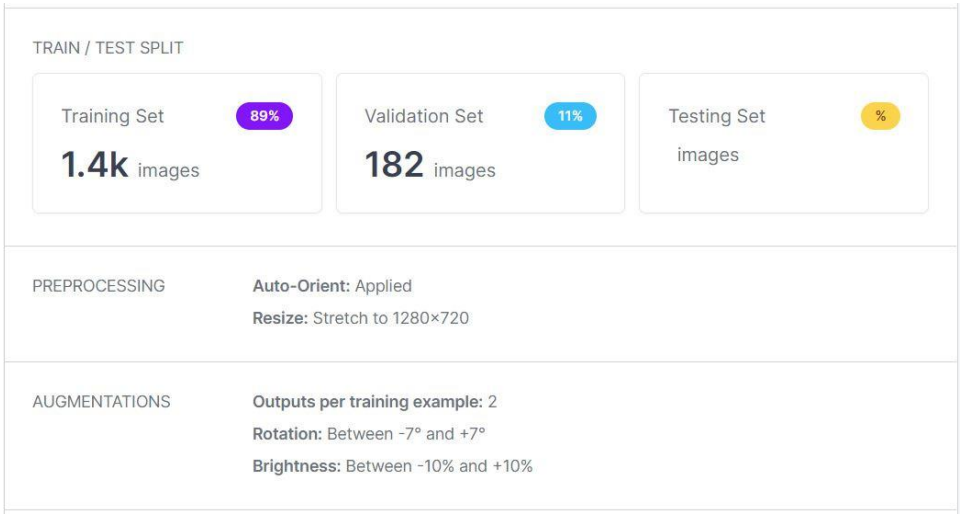

Figure 3. Data set creation

Photo recordings started with a camera placed on the solar panel. Later, a training set was created out of approximately 1600 photos. Since a data set of this size would prolong the training process, the dimensions of the photos were changed to 640x640 pixels. All photos with varying sizes in the dataset were tagged. The purpose of tagging is to save the coordinates of the object in a text file. After photo tagging, the data set is divided into training, testing, and validation. Out of 1600 photos, 1400 are reserved as training data, 180 as test data, and 20 as validation data.

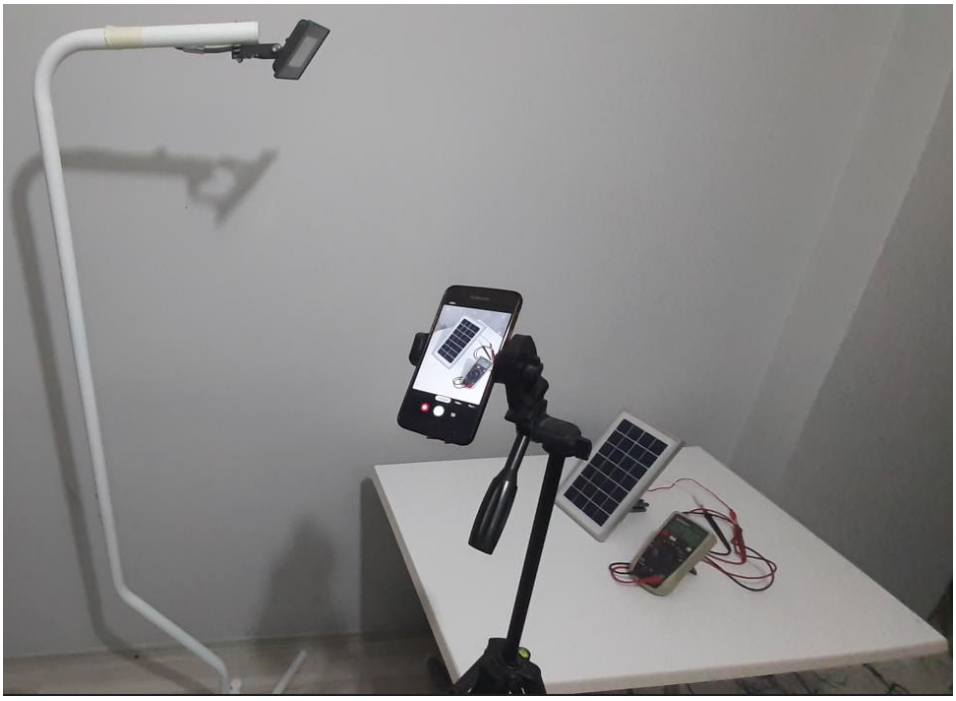

Figure 4. Experimental design

Experimental Studies

The dataset consists of 1600 photos. After the data set was created, labeling was performed for all photographs in the data set. Tagging took 20 seconds for a photo. The tagging process for all photos took approximately 10 hours. After the dataset is labeled, the neural network parameters are set. Then the training process was started and the average error graph was drawn.

epoch,	train/box_loss,	train/obj_loss,	train/cls_loss,	metrics/precision,	metrics/recall,	metrics/mAP_0.5,r	s/mAP_0.5:0.95,	val/box_loss,	val/obj_loss,	val/cls_loss,	x/lr0,	x/lr1,	x/lr2
24	0.02031,	0.010469,	0.0023938,	0.99985,	1	0.995,	0.87382,	0.015389,	0.010654,	0.0021847,	0.009241,	0.009241,	0.009241
25	0.019691,	0.010166,	0.0025404,	0.99972,	0.99999,	0.995,	0.85977,	0.015879,	0.0096076,	0.0020653,	0.009208,	0.009208,	0.009208
26	0.019951,	0.010446,	0.002476,	0.99983,	1	0.995,	0.87167,	0.014631,	0.0097833,	0.0019741,	0.009175,	0.009175,	0.009175
27	0.019876,	0.010124,	0.0025397,	0.99977,	1	0.995,	0.87352,	0.014618,	0.009336,	0.0020821,	0.009142,	0.009142,	0.009142
28	0.019108,	0.010261,	0.0024813,	0.99988,	1	0.995,	0.86519,	0.015025,	0.010086,	0.0019784,	0.009109,	0.009109,	0.009109
29	0.019029,	0.010039,	0.0024294,	0.99839,	0.99855,	0.99368,	0.86055,	0.014758,	0.0092297,	0.0020514,	0.009076,	0.009076,	0.009076
30	0.018667,	0.0097393,	0.002378,	0.99975,	1	0.995,	0.88773,	0.014694,	0.0089191,	0.0020006,	0.009043,	0.009043,	0.009043
31	0.019116,	0.0098527,	0.002407,	0.99984,	1	0.995,	0.88749,	0.01432,	0.0088664,	0.00197,	0.00901,	0.00901,	0.00901
32	0.01899,	0.0099199,	0.0023665,	0.9999,	1	0.995,	0.87814,	0.014055,	0.0087376,	0.0019037,	0.008977,	0.008977,	0.008977
33	0.018171,	0.0095334,	0.0023811,	0.99983,	1	0.995,	0.88818,	0.013712,	0.0096841,	0.0019522,	0.008944,	0.008944,	0.008944
34	0.018482,	0.0096769,	0.0022734,	0.99997,	0.99999,	0.995,	0.88841,	0.014449,	0.0093194,	0.0020367,	0.008911,	0.008911,	0.008911
35	0.018356,	0.0095748,	0.002348,	0.99983,	1	0.995,	0.90409,	0.012987,	0.0085867,	0.0018862,	0.008878,	0.008878,	0.008878
36	0.017856,	0.0095005,	0.0023077,	0.99963,	1	0.995,	0.88212,	0.015409,	0.0093945,	0.0021257,	0.008845,	0.008845,	0.008845
37	0.017897,	0.0092962,	0.0021632,	0.99994,	1	0.995,	0.87271,	0.014766,	0.0097967,	0.0019053,	0.008812,	0.008812,	0.008812
38	0.017755,	0.00929,	0.0023235,	0.99976,	1	0.995,	0.89736,	0.01372,	0.0089347,	0.00187,	0.008779,	0.008779,	0.008779
39	0.017209,	0.0091585,	0.0022492,	0.99977,	1	0.995,	0.89324,	0.013571,	0.009117,	0.0019395,	0.008746,	0.008746,	0.008746
40	0.017428,	0.0092673,	0.0023724,	0.99981,	1	0.995,	0.91298,	0.012581,	0.0086461,	0.0020069,	0.008713,	0.008713,	0.008713
41	0.017411,	0.0091622,	0.0023131,	0.99988,	1	0.995,	0.89694,	0.014029,	0.0092194,	0.0020316,	0.00868,	0.00868,	0.00868
42	0.017248,	0.0089802,	0.0022533,	0.99985,	1	0.995,	0.89401,	0.014656,	0.0096235,	0.0019942,	0.008647,	0.008647,	0.008647
43	0.017142,	0.0089809,	0.0021745,	0.99974,	1	0.995,	0.89645,	0.014057,	0.0095406,	0.0020479,	0.008614,	0.008614,	0.008614
44	0.016941,	0.0089456,	0.0022415,	0.9998,	1	0.995,	0.90858,	0.013106,	0.0091406,	0.0019873,	0.008581,	0.008581,	0.008581
45	0.016807,	0.0089965,	0.0020984,	0.9999,	1	0.995,	0.91265,	0.011744,	0.0079231,	0.0018374,	0.008548,	0.008548,	0.008548
46	0.016603,	0.0087561,	0.0021571,	0.99989,	1	0.995,	0.9012,	0.013099,	0.0083643,	0.0020121,	0.008515,	0.008515,	0.008515
47	0.016473,	0.0088255,	0.0021439,	0.99983,	1	0.995,	0.90416,	0.012285,	0.0088735,	0.0018329,	0.008482,	0.008482,	0.008482
48	0.016567,	0.0088794,	0.0021617,	0.99969,	1	0.995,	0.90378,	0.012663,	0.0088911,	0.0018187,	0.008449,	0.008449,	0.008449
49	0.016468,	0.0086328,	0.0021237,	0.9998,	1	0.995,	0.90928,	0.012281,	0.0082401,	0.0018251,	0.008416,	0.008416,	0.008416
50	0.016549,	0.0086727,	0.0021677,	0.99978,	1	0.995,	0.9104,	0.012094,	0.0082974,	0.0018455,	0.008383,	0.008383,	0.008383
51	0.01625,	0.0086281,	0.0020911,	0.99982,	1	0.995,	0.90893,	0.012131,	0.0081023,	0.0017397,	0.00835,	0.00835,	0.00835

Figure 5. Experimental results

The learning rate has an important place for the error function. The mean error function is not expected to decrease either too fast or too slowly. In this thesis study, the learning rate that most appropriately reduces the

mean error value was selected by training with different learning rates. In Figure 5, the average error graph is given when the learning rate is 0.01. As can be seen from the Figure 5, it will be seen that the average error graph decreases very rapidly. Although this learning speed has accelerated the training process, it is highly affected by the data set. For this reason, the rate of pre-education learning should be reduced.

Conclusion

After the study, an effective deep learning model has been proposed for the detection and classification of pollution in photovoltaic (PV) panel cells. Among the object detection algorithms, the YoloV5 algorithm turned out to be faster and more sensitive. The photos taken were run by this algorithm. According to the result of the algorithm, a cleaning robot will be sent to the PV panel area.

Scientific Ethics Declaration

The authors declare that the scientific ethical and legal responsibility of this article published in EPSTEM journal belongs to the authors.

Acknowledgements or Notes

* This article was presented as oral presentation at the International Conference on Basic Sciences, Engineering and Technology (www.icbaset.net) held in Marmaris/Turkey on April 27-30, 2023.

References

Acikgoz H. (2022).A novel approach based on integration of convolutional neural networks and deep feature selection for short-term solar radiation forecasting. *Appl Energy,305*. 117912..

Ali, M.U., Khan, H.F., Masud M., Kallu K.D., & Zafar, A. (2020) A machine learning framework to identify the hotspot in photovoltaic module using infrared thermography. *Solar Energy, 208,*643–651.

Amidi, A., Amidi, S., Vlachakis, D., Paragios, N., & Zacharaki, EI. (2016) A machine learning methodology for enzyme functional classification combining structural and protein sequence descriptors. *Lecture Notes in Computer Science, 9656*, 728–738.

Deitsch S, Christlein V, Berger S, Buerhop-Lutz C, Maier A, Gallwitz, F., & Riess, C. (2019). Automatic classification of defective photovoltaic module cells in electroluminescence images. *Solar Energy, 185,*455–468.

Gu, J, Wang, Z., Kuen, J, Ma, L., Shahroudy, A., & Shuai B, (2018) Recent advances in convolutional neural networks. *Pattern Recognit, 77*, 354–377.

Khezri, R., Mahmoudi, A., & Aki, H. (2022). Optimal planning of solar photovoltaic and battery storage systems for grid-connected residential sector: Review, challenges and new perspectives. *Renewable and Sustainable Energy Reviews,153*. 111763.

Kızrak, M., & Bolat, B. (2018). Derin ogrenme ile kalabalık analizi uzerine detaylı bir arastırma. *Bilişim Teknolojileri Dergisi,11*(11), 263-286.

Korkmaz, D. (2021). SolarNet: A hybrid reliable model based on convolutional neural network and variational mode decomposition for hourly photovoltaic power forecasting. *Applied Energy, 300*, 117410.

Li, B., Delpha, C., Diallo, D, Migan-Dubois A. (2021) Application of artificial neural networks to photovoltaic fault detection and diagnosis: A review. *Renewable and Sustainable Energy Review ,138.* 110512.

Naveen Venkatesh, S., & Sugumaran, V. (2022). Machine vision based fault diagnosis of photovoltaic modules using lazy learning approach. *Measurement, 191*. 110786.

Önal, Y., & Turhal, Ü. Ç. (2021). *Bilecik Şeyh Edebali üniversitesi merkez kampüsünde Güneş takipli fotovoltaik enerji sistemi uygulaması*. http://acikkaynak.bilecik.edu.tr/xmlui/bitstream/handle/11552/2558/BAP_SONU%c3%87_RAPORU_03.01.2022.pdf?sequence=1&isAllowed=y

Otamendi, U., Martinez, I., Quartulli, M., Olaizola, I.G., Viles, E., & Cambarau, W. (2021). Segmentation of cell-level anomalies in electroluminescence images of photovoltaic modules. *Solar Energy, 220*, 914–926.

Pratt, L., Govender, D., & Klein, R. (2021) Defect detection and quantification in electroluminescence images of solar PV modules using U-net semantic segmentation. *Renewable Energy,178,*1211–122

Su, B., Chen, H., Liu, K., & Liu, W. (2021) RCAG-Net: Residual channelwise attention gate network for hot spot defect detection of photovoltaic farms. *IEEE Transactions on Instrumentatation and Measurement, 70.* 1-14.

Author Information

Emin Cantez
Coşkunoz Kalıp Makina A.Ş., R&D Center
Türkiye
Contact e-mail: ecantez@coskunoz.com.tr

Hasan Şahin
Bursa Technical University
Bursa, Türkiye

Ömer Faruk Efe
Bursa Technical University
Bursa, Türkiye

To cite this article:

Cantez, E., Sahin, H., & Efe, O.M. (2023). Regional guidance system for cleaning robots as a result of pollution of solar panels. *The Eurasia Proceedings of Science, Technology, Engineering & Mathematics (EPSTEM), 22,* 274-279.

The Eurasia Proceedings of Science, Technology, Engineering & Mathematics (EPSTEM)
ISSN: 2602-3199

The Eurasia Proceedings of Science, Technology, Engineering & Mathematics (EPSTEM), 2023

Volume 22, Pages 280-284

ICBASET 2023: International Conference on Basic Sciences, Engineering and Technology

DNA Profiling of ING1 Gene in Triple Negative Breast Cancer

Alaa Anwer EZZET
Gaziantep University

Isik Didem KARAGOZ
Gaziantep University

Sibel CANGI
Gaziantep University

Tulay KUS
Gaziantep University

Abstract: Breast cancer is among the most common cancers and the second in death caused from cancers in women. Triple negative breast cancer (TNBC) is a subgroup which not expressed estrogen (ER), progesterone (PR) and HER2 receptors in breast cancer. It has 15% rate of all breast cancer and has been more aggressive and has poor prognosis. For this reason, early diagnosis has a key role because of TNBC's high relapse. Investigation of DNA methylation pattern in TNBC likewise all types of breast cancer has become an important prognostic vehicle besides assessment of gene expression profile in diagnosis cancer subtypes. DNA methylation pattern of tumor suppressor genes which is one of the epigenetic modifications has highly importance. In this study, we aimed to investigate the relationship DNA methylation pattern of ING1 (inhibitor of growth family member 1), a tumor suppressor gene and TNBC. For this purpose, we searched the methylation pattern of ING1 and breast cancer patients especially TNBC. As a result, we discussed and tried to clarified the relationship between epigenetic modifications of ING1 gene and TNBC.

Keywords: Breast cancer, Triple negative breast cancer, Epigenetic factors, DNA methylation, ING1 gene.

Introduction

Breast cancer is one of the most common cancers and ranks second in cancer-related deaths in women in around the world. While the incidence of 5-year survival in early stage localized breast cancer and ductal carcinoma *in situ* is 100%; this rate decreases to 27% in metastatic breast cancers.

TNBC is a breast cancer subtype in which estrogen (ER), progesterone (PR) and HER2 receptors are not expressed. It represents 15% of all breast cancers and has a more aggressive and worse prognosis than others. Recent studies have shown that 60% of patients have a 5-year life expectancy. The lack of receptors makes TNBCs unresponsive to hormonal and anti-HER2 therapies used in other breast cancers. And unfortunately, none of the commonly used gene expression profiling tests (Oncotype DX with 21 genes, Mamma-print with 70 genes, and PAM509) are clinically useful in patients with TNBC. Therefore, looking for DNA methylation patterns in TNBC, as in other cancers, has become important prognostic tools in determining cancer subtypes as well as gene expression tests (Fackler et al., 2020).

Epigenetic changes have a high potential to be a source of innovative biomarkers in cancer with the advantages of being stable, having specific genes at high frequency and being detectable in biological fluids in a minimally

invasive way. Among the epigenetic changes, DNA methylation plays a key role in the regulation of gene expression, and abnormal methylation is implicated in many human diseases, including cancer, by disrupting normal gene expression and regulation. The possible mechanism underlying cancer development and progression is hypermethylation of CpG (cytosine-phosphate-guanine) islands located in the promoter regions of tumor suppressor genes, which causes loss of expression or hypomethylation that causes chromosome instability and increased mutation.

Since the tumor suppressor gene ING1, whose extensive methylation patterns were not studied specifically in the TNBC subtype, In this study, we investigated the effect of the methylation pattern and gene expression of the ING1 gene in triple negative breast cancer, The Cancer Genome Atlas Program – NCI-TCGA, National Center for Biotechnology Information-NCBI and The Human Protein Atlas were selected in line with the information obtained from different sources.

ING1 (Inhibitor of Growth Family Member 1) is a tumor suppressor gene involved in many processes such as cell growth, apoptosis, aging, migration and DNA repair. It has been mapped close to the telomeric region on chromosome 13q34 in the human genome (Shimada et al., 1998; Nagashima et al., 2001; He et al., 2005). Loss of ING proteins, whose expression varies greatly in different tissues, is generally correlated with cancer progression **(**Wang et al., 2010; Li et al., 2011a) and their expression is decreased /or lost in human tumors (Walzak et al., 2008).

It has been reported that loss of ING protein expression is positively correlated with tumor progression in head and neck cancers and microvessel density in ovarian cancers (Thakur et al., 2014**)**. However, it is also known that ING knockout mice spontaneously develop tumors with a high frequency (Kichina et al., 2006; Coles et al., 2007; Saito et al., 2010).

ING genes, which are frequently suppressed in cancer cells, are rarely mutated. This suggests that the mechanism of suppression of ING expression is due to epigenetic factors (Tokunaga, et al., 2000; Gunduz et al., 2002; Campos et al., 2004; Garkavtsev et al., 2004). Indeed, it has been reported that abnormally high methylation levels on the ING1 gene promoter correlate with low transcript levels in ovarian cancers **(**Shen et al., 2005).

While the mRNA measured in the normal Hs578Bst mammary epithelial cell line is quite high, the steady-state levels of all ING1 transcript isoforms were decreased 10 to 100-fold in most breast cancer cell lines examined (Walzak et al., 2008). It is also known that ING1 expression is frequently lost in familial and sporadic breast cancers, and loss of ING1 is associated with poor prognosis in breast cancer (Toyama et al., 1999; Tokunaga, et al., 2000; Ythier et al., 2008). In addition, there is information in researches that changing ING1 levels affects the expression of genes known to be altered in breast cancer **(**Thakur et al., 2014).

The Purpose

Considering that the ING1 gene is active in normal tissues and inactive as a result of hypermethylation in the promoter regions in cancerous tissues, it is thought to be used as a marker in the prediction of TBNC. Therefore, in this study plan, it is aimed to discuss the usability of the promoter methylation pattern of the ING1 gene as a biomarker in TNBC with an aggressive course.

Results and Discussion

The ING1, ING2, ING3, ING4, and ING5 members of the growth inhibitor (ING) family of type II tumor suppressors have a variety of roles in biological processes, including growth, proliferation, DNA repair, invasion, migration, and cell death (Smolle et al., 2019**)**. Reduced ING3 expression in the nucleus has been related in research to being a stand-alone prognostic factor in breast cancer. The study provided the first in-depth description of ING3 expression in breast cancer and showed that it was a reliable predictor of breast cancer (Wu et al., 2021). While the ING2 protein is a chromatin reader and a stable member of the mSin3A/HDAC complex, other studies have connected it to lung cancer. ING2 expression was lost in various cancer subtypes, but it was still discovered to have a variety of tumor-suppressive effects in cancer cell lines (Blondel et al., 2019).

While different research discovered unmistakable proof that certain cancers exhibit diminished or even absent nuclear expression of p33ING1b in comparison to their normal counterparts, the potential utility of the ING1 gene for vaccine-based diagnostics and treatment rose when the immunogenicity of the gene was observed in breast cancer patients. ING1 is a gene therapy that can target particularly tumor cells since it plays a significant role in promoting apoptosis in tumor cells, which guards against harm to healthy cells. Because tumor suppressor genes exist in cancer cells as non-mutated wild-type alleles, they aid in the discovery of treatments. This study concluded that ING1 gene mutations are an uncommon event in cancer (Nouman et al., 2003).

Another two studies revealed ING1 as a gene whose deletion promotes and accelerates tumor development. This means that in many distinct tumor types, its expression is lost or significantly diminished (Ythier et al., 2008; Li et al., 2011b). According to a study, the epigenetic regulator ING1 may engage in new cell functions when expressed at high levels **(**Thakur et al., 2012), and a study on the ING1 gene has offered strong support for its function as a tumor suppressor in the development of cancer (Bányai et al., 2021).

Low levels of ING1 in breast cancer enhance metastasis, according to different research studies. ING1 is a suppressed gene in breast cancer cell lines that contributes to the control of gene expression, and it was demonstrated in this study that altering ING1 levels modifies the expression of genes known to be altered in breast cancer. Increased levels of ING1 are also strongly linked to both overall disease-specific survival and survival free of illness, and overexpression of ING1 helps to prevent cell migration (Thakur et al., 2014).

An initial report for the examination of ING1 mutations and expression in 452 groups of cancer samples was submitted. Breast tumors (58%) with low ING1 expression contained metastatic spread to local lymph nodes, compared to just 9% of tumors with increased ING1 expression relative to the surrounding normal tissue. Although the study found that ING1 mutagens are extremely uncommon in breast or ovarian cancer, ING1 expression was commonly decreased concurrently with breast cancer progression (Toyama et al., 1999).

According to a study, this gene's suppression is directly related to the aggressive character of TNBC, and its activation improves anti-tumor activity (Vasilatos et al., 2013). In our work, we look forward to directly linking the ING1 gene to triple-negative breast cancer, as you will see an accurate investigation of the gene and its comparison between healthy cells and precancerous cells in this type of cancer.

Conclusion

Research has found that conventional treatment methods are not completely effective in treating BC, especially TNBC, due to the poor prognosis of this cancer and its lack of response to current therapies. It has a poor prognosis and fewer treatment options, as evidenced by its higher mortality rate when compared to other subtypes of breast cancer **(**Mahmoud et al., 2022).

The research reached the possibility of using gene therapies to combat this disease, and our work was based on the possibility of using the ING1 gene to predict the event of cancer, as this gene, when over expressed, indicates that cancer does not occur, and the reverse occurs when it is underexpressed, which is a distinctive feature of the occurrence of TNBC **(**Eastlack & Alahar, 2015). In our paper, we aimed to find out that ING1 gene oligomerization is a characteristic.

Recommendations

We recommend that to investigate ING1 gene and TNBC relationship epigenetically and the other cancer types.

Scientific Ethics Declaration

The authors declare that the scientific ethical and legal responsibility of this article published in EPSTEM journal belongs to the authors.

Acknowledgements or Notes

* This article was presented as oral presentation at the International Conference on Basic Sciences, Engineering and Technology (www.icbaset.net) held in Marmaris/Turkey on April 27-30, 2023.

References.

Bányai, L., Trexler, M., Kerekes, K., Csuka, O., & Patthy, L. (2021). Use of signals of positive and negative selection to distinguish cancer genes and passenger genes. *Elife, 10*. e59629.

Blondel, A., Benberghout, A., Pedeux, R., & Ricordel, C. (2019). Exploiting ING2 epigenetic modulation as a therapeutic opportunity for non-small cell lung cancer. Cancers, *11*(10), 1601; https://doi.org/10.3390/cancers11101601

Campos, E. I., Chin, M. Y., Kuo, W. H., & Li, G. (2004). Biological functions of the ING family tumor suppressors.*Cellular and Molecular Life Sciences CMLS, 61*, 2597-2613.

Coles, A. H., Liang, H., Zhu, Z., Marfella, C. G., Kang, J., Imbalzano, A. N., & Jones, S. N. (2007). Deletion of p37Ing1 in mice reveals a p53-independent role for Ing1 in the suppression of cell proliferation, apoptosis, and tumorigenesis. *Cancer Research*, *67*(5), 2054-2061.

Eastlack, S. C., & Alahar, S.K. (2015). MicroRNA and breast cancer: Understanding pathogenesis, improving. management. *Noncoding RNA,* 17-34.

Fackler, M. J., Cho, S., Cope, L., Gabrielson, E., Visvanathan, K., Wilsbach, K., ... & Umbricht, C. B. (2020). DNA methylation markers predict recurrence-free interval in triple-negative breast cancer.NPJ Breast Cancer ,*6*(1), 3.

Garkavtsev, I., Kozin, S. V., Chernova, O., Xu, L., Winkler, F., Brown, E., ... & Jain, R. K. (2004). The candidate tumour suppressor protein ING4 regulates brain tumour growth and angiogenesis. *Nature,428*(6980), 328-332.

Gunduz, M., Ouchida, M., Fukushima, K., Ito, S., Jitsumori, Y., Nakashima. T., Nagai, N., Nishizaki, K., & Shimizu, K. (2002). Allelic loss and reduced expression of the ING3, a candidate tumor suppressor gene at 7q31, in human head and neck cancers. *Oncogene, 21,*4462–4470.

He, G. H., Helbing C. C., Wagner M. J., Sensen C. W., Riabowol, K. (2005) Phylogenetic analysis of the ING family of PHD finger proteins. *Mol Biol Evol 22*(1):104-116.

Kichina, J. V., Zeremski, M., Aris, L., Gurova, K. V., Walker, E., Franks, R., ... & Gudkov, A. V. (2006). Targeted disruption of the mouse ING1 locus results in reduced body size, hypersensitivity to radiation and elevated incidence of lymphomas. *Oncogene,25*(6), 857-866.

Li, F., Li, J., Sheng, H., Dai, L., Cheng, K., & Lin, S. (2011a). Lin Chuang er bi yan hou tou jing wai ke za zhi . *Journal of Clinical Otorhinolaryngology, Head, and Neck Surgery, 25*(21), 986–989.

Li, J., Martinka, M., & Li, G. (2008). Role of ING4 in human melanoma cell migration, invasion and patient survival. *Carcinogenesis,29*(7), 1373–1379.

Li, X., Kikuchi, K., & Takano, Y. (2011)b. ING genes work as tumor suppressor genes in the carcinogenesis of head and neck squamous cell carcinoma. *Journal of Oncology*. Article ID 963614 | https://doi.org/10.1155/2011/963614.

Mahmoud, R., Ordóñez-Morán, P.,& Allegrucci, C. (2022). Challenges for triple negative breast cancer treatment: Defeating heterogeneity and cancer stemness. *Cancers, 14(17),* 4280.

Nagashima, M., Shiseki, M., Miura, K., Hagiwara, K., Linke, S. P., Pedeux, R., Wang, X. W., Yokota, J., Riabowol, K., & Harris, C. C. (2001) DNA damage-inducible gene p33ING2 negatively regulates cell proliferation through acetylation of p53. *Proc Natl Acad Sci U S A 98*(17), 9671-9676.

Nouman, G. S., Anderson, J. J., Lunec, J., & Angus, B. (2003). The role of the tumour suppressor p33 ING1b in human neoplasia. *Journal of Clinical Pathology*, *56*(7), 491–496.

Saito, M., Kumamoto, K., Robles, A. I., Horikawa, I., Furusato, B., Okamura, S., Goto, A., Yamashita, T., Nagashima, M., Lee, T. L., Baxendale, V. J., Rennert, O. M., Takenoshita, S., Yokota, J., Sesterhenn, I. A., Trivers, G. E., Hussain, S. P., & Harris, C. C. (2010). Targeted disruption of ING2 results in defective spermatogenesis and development of soft-tissue sarcomas. *PloS One, 5*(11), e15541.

Shen, D. H., Chan, K. Y., Khoo, U. S., Ngan, H. Y., Xue, W. C., Chiu, P. M., Ip, P., & Cheung, A. N. (2005). Epigenetic and genetic alterations of p33ING1b in ovarian cancer. *Carcinogenesis,26*(4).

Shimada, Y., Saito, A., Suzuki, M., Takahashi, E., & Horie, M. (1998). Cloning of a novel gene (ING1L) homologous to ING1, a candidate tumor suppressor. *Cytogenet Cell Genetics,83*(3-4):232-235.

Smolle, E., Fink-Neuboeck, N., Lindenmann, J., Smolle-Juettner, F., & Pichler, M. (2019). The biological and clinical relevance of inhibitor of growth (ING) genes in non-small cell lung cancer. Cancers, *11*(8), 1118.

Thakur, S., Feng, X., Qiao Shi, Z., Ganapathy, A., Kumar Mishra, M., Atadja, P., Morris, D., & Riabowol, K. (2012). ING1 and 5-azacytidine act synergistically to block breast cancer cell growth. *PloS One, 7*(8), e43671.

Thakur, S., Singla, A. K., Chen, J., Tran, U., Yang, Y., Salazar, C., Magliocco, A., Klimowicz, A., Jirik, F., & Riabowol, K. (2014). Reduced ING1 levels in breast cancer promotes metastasis. *Oncotarget, 5*(12), 4244–4256.

The human protein atlas.(2022, July 30). http://www.proteinatlas.org

Tokunaga, E., Maehara, Y., Oki, E., Kitamura, K., Kakeji, Y., Ohno, S., & Sugimachi, K. (2000). Diminished expression of ING1 mRNA and the correlation with p53 expression in breast cancers. *Cancer Letters,152*(1), 15–22.

Toyama, T., Iwase, H., Watson, P., Muzik, H., Saettler, E., Magliocco, A., DiFrancesco, L., Forsyth, P., Garkavtsev, I., Kobayashi, S., & Riabowol, K. (1999). Suppression of ING1 expression in sporadic breast cancer. *Oncogene, 18*(37), 5187–5193.

Vasilatos, S., Katz, T. A., Oesterreich, S., Davidson, N. E., & Huang, Y. (2013). Targeting LSD1-HDACs crosstalk as a potential therapeutic strategy for triple negative breast cancer cells. *Cancer Research, 73*(8), 673-673.

Walzak, A. A., Veldhoen, N., Feng, X., Riabowol, K., & Helbing, C. C. (2008). Expression profiles of mRNA transcript variants encoding the human inhibitor of growth tumor suppressor gene family in normal and neoplastic tissues. *Experimental Cell Research, 314*(2), 273–285.

Wang, Q. S., Li, M., Zhang, L. Y., Jin, Y., Tong, D. D., Yu, Y., ... & Fu, S. B. (2010). Down-regulation of ING4 is associated with initiation and progression of lung cancer. *Histopathology,57*(2), 271-281.

Wu, X., Chen, C., Luo, B., Yan, D., Yan, H., Chen, F., ... & Yuan, J. (2021). Nuclear ING3 expression is correlated with a good prognosis of breast cancer. Frontiers in Oncology, 10, 589009.

Ythier, D., Larrieu, D., Brambilla, C., Brambilla, E., & Pedeux, R. (2008). The new tumor suppressor genes ING: genomic structure and status in cancer. *International Journal of Cancer, 123*(7), 1483–1490.

Author Information

Alaa Anwer Ezzat
Gaziantep University
Gaziantep, Turkey

Isık Didem Karagoz
Gaziantep University
Gaziantep, Turkey
Contact e-mail: karagoz@gantep.edu.tr

Sibel Cangı
Gaziantep University
Gaziantep,Turkey

Tulay Kus
Gaziantep University
Gaziantep, Turkey

To cite this article:

Ezzat, A.A., Karagoz, I.D., Cangi, S**.,** & Kus, T. (2023). DNA profiling of ING1 gene in triple negative breast cancer. *The Eurasia Proceedings of Science, Technology, Engineering & Mathematics (EPSTEM), 22,* 280-284.

The Eurasia Proceedings of Science, Technology, Engineering & Mathematics (EPSTEM)
ISSN: 2602-3199

The Eurasia Proceedings of Science, Technology, Engineering & Mathematics (EPSTEM), 2023

Volume 22, Pages 285-294

ICBASET 2023: International Conference on Basic Sciences, Engineering and Technology

A Preliminary Study of a Multifunctional DOC/Wet-Scrubber Capable to Reduce both Chemical and Acoustic Emissions in Marine Field

Giada KYAW OO D'AMORE
University of Trieste

Jan KAŠPAR
University of Trieste

Abstract: The reduction of ship emissions (*i.e.*, Nitrogen Oxides – NOx, Sulfur Oxides – SOx and Particulate Matter PM) are of paramount importance particularly when shipping in Emission Control Areas (ECAs) where restrictive limits on emissions are imposed by the International Maritime Organization (IMO). In such ECAs, which starting from 2025 will also include Mediterranean Sea, the use of Ultra Low Sulfur Fuel Oil (ULSFO – sulfur content ≤ 0.1 wt%) or, alternatively, an emission-equivalent Exhaust Gas Cleaning System (EGCS) is mandatory. The price of ULSFO is about twice that of the ordinary Heavy Fuel Oil, which heavily affects marine transport economics. Consequently, several EGCS concepts have been studied for the abatement of NOx, SOx and PM, yet they have big dimensions which preclude their installation on already existing ships and, therefore, making necessary the re-design of the whole propulsion system. In the presented study, the use of a Diesel Oxidation Catalyst (DOC) in series with a closed loop scrubber to reduce NOx, SOx, PM and acoustic emissions is studied with the aim to design a compact exhaust line, with multifunctional performances, that allow to be compliant with the IMO's regulations. The role of the DOC is that of oxidizing the emitted NO to improve the solubility of the NOx species in the scrubber, besides hydrocarbons and PM abatement. It is shown that the oxidation activity and stability of the Pt-based catalysts can be significantly improved by doping with acidic oxides in comparison to a conventional Pt/Al_2O_3 catalyst. This allows to design a compact EGCS which, in addition to the chemical aspects, incorporates modification aimed at minimizing acoustic emissions as well, acting as a silencer. Preliminary results assessing the validity of the integrate system on a full engine-EGSC mockup are reported in the paper.

Keywords: Diesel oxidation catalyst, Marine pollution control, Chemical emissions, Noise emissions

Introduction

Maritime transport is of great importance for the global economy, as it accounts for around 80% of worldwide trade, together with its related activities (e.g., shipbuilding, repairs, ports activities) (Adam et al., 2021). Due to the extensive use of HFO (S~ 2.5 wt%), maritime transport has accounted for approximately 10-15% of global SOx and NOx emissions. This led to an increasing concern about the global impact of maritime emissions. IMO, consistently, has restricted the limits imposed by MARPOL 73/78 Annex VI Regulation (Revised MARPOL Annex VI, 2008) on ships emissions. The more restrictive limits are imposed on SOx and NOx emissions (Figure 1) for ECAs (Emission Control Areas), i.e. SECAs (Sulfur Emission Control Areas) and NECAs (Nitrogen Emission Control Areas) (Figure 2) making TIER III NOx limits effective since January 1st, 2016 for the ships build after that date (Revised MARPOL Annex VI, 2008).

Marine engines emit various pollutants into the air: HC, CO, NOx, SOx and PM. SOx emissions depend on the sulfur content of the fuel used, while NOx emissions depend, in addition to the nitrogen content in the fuel, also on the engine speed and power rating, resulting in their strong dependency on the cruising speed. Two ways to

comply with international regulation are represented by the reduction of the ship cruising speed and/or using fuels with low sulfur and nitrogen content, e.g., VLSFO – Very Low Sulfur Fuel Oil (S ≤ 0.5 wt%) or, even ULFSO (Johnsen et al., 2019). However, such solutions heavily affect the shipping economics due to the cost of refined fuels and the slowdown of naval trade. The use of alternative fuels (e.g., LNG – Liquefied Natural Gas, Hydrogen) or alternative energy sources (e.g., electric propulsion) is compliant with the regulations but require the re-design and the refitting of the entire propulsion system, especially for the ships already in navigation, besides the higher running costs of these energy sources (Johnsen et al., 2019). Thus, the use of EGCS (Exhaust Gas Cleaning Systems) represents a viable solution to make ships eco-sustainable and economically efficient.

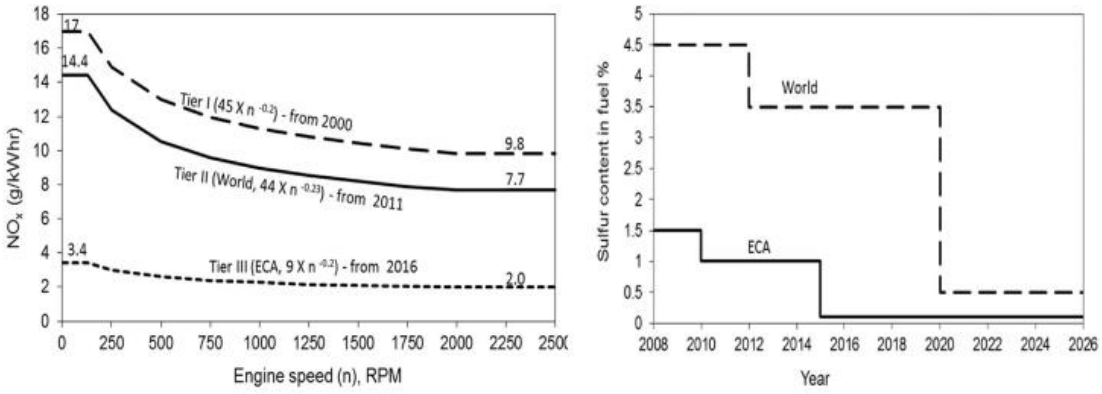

Figure 1. NOx and SOx limits.

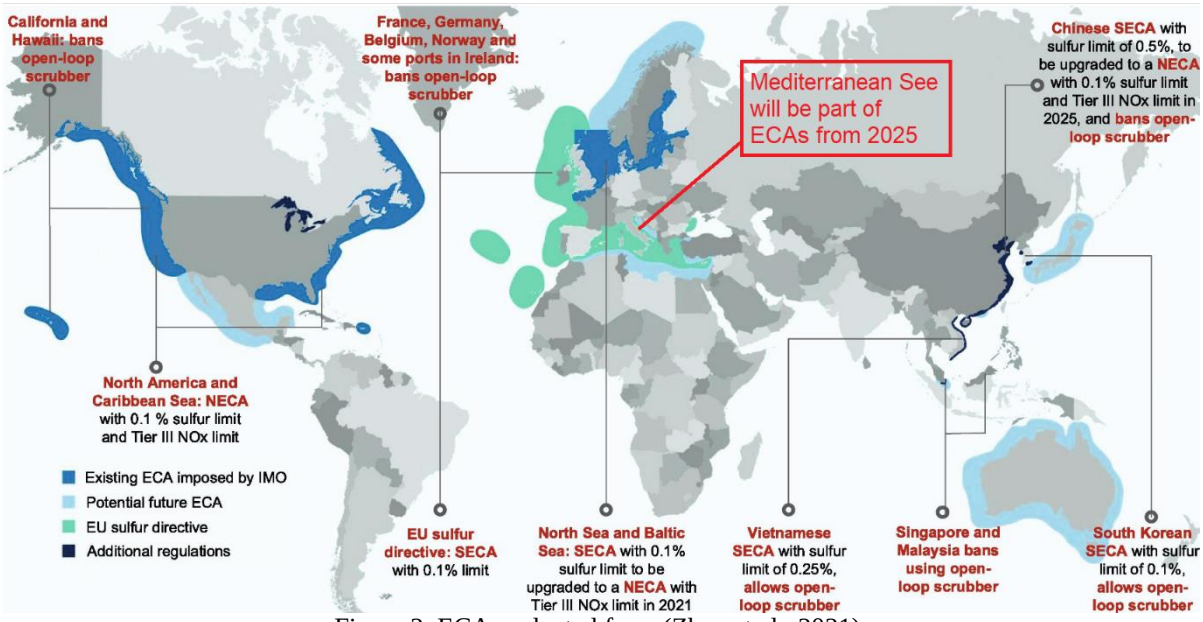

Figure 2. ECAs, adapted from (Zhao et al., 2021).

EGR (Exhaust Gas Recirculation) and SCR (Selective Catalytic Reduction) systems are effective technologies for the control of NOx emissions (Chen et al., 2015; Ushakov et al., 2020), while for SOx abatement the use of scrubber is proven to be efficient (Lindstad et al., 2017).

EGR recirculates a portion of the exhaust gas into the engine's combustion chamber, lowering its internal temperature. As a result, NOx emissions are reduced, however causing an increase in fuel consumption and engine efficiency characteristics (Huang et al., 2022; Lou et al., 2022). Therefore, it is preferred to limit the EGR ratio and use other techniques such as the SCR.

SCR systems, through the in situ production of ammonia from the decomposition of urea, allow the reduction of NOx to nitrogen (N_2) (Zhu et al., 2022). This technique can be applied efficiently to a marine engine, but due to the high sulfur content of traditional fuel, poisoning of the active sites of the catalyst can occur, reducing the SCR efficiency and leading to a possible "slip" effect of the ammonia, which is a very polluting and toxic gas. Moreover, the use of SCR requires the storage of urea on board ships (Ayre et al., 2011).

The scrubbers abate SOx by absorption in a washing liquid; sea water is used as washing liquid in open loop scrubber, while in closed loop scrubber, water with chemicals additives is used (United States Environmental Protection Agency Office of Wastewater Management Washington, DC 20460, 2011; Lindstad et al., 2016). Scrubbers are able to abet also PM.

Ships emissions are not limited to chemical pollutant, but the noise radiated by the exhaust gas is also a dangerous emission for both the passengers and the environment. Several regulations limit the noise emission during the navigation and the mooring in port (Code on Noise Level On Board Ships - Res. A.468(XII), 2012; Procedure for the Determination of Airborne Noise Emissions from Marine Vessels, 2019). For the reduction of the noise emitted by the engine and radiated in to the surrounding of the ships through the exhaust gases silencers are used along the exhaust line (Bodn et al., 2007).

The current EGCS systems previously discussed represent effective solutions, but the simultaneous application on board ships of these systems is very complex and/or not economically feasible (Kyaw Oo D'Amore, Biot, et al., 2021). Based on these observations, this work aims at developing an innovative solution that allows the simultaneous abatement of both the emmited pollutants and noise, using an EGCS which consists of an oxidation catalyst followed by a scrubber. In this paper the attention is placed in particular on the converter containing a Pt-based DOC, which serves to oxidize NO to NO_2 to improve NOx solubility in the scrubber, futher the silencing effect of the DOC converter is adressed. Figure 3 illustrates this abatement strategy which has the advantage of being very compact, allowing, in principle, the elimination of SCR, EGR and silencer.

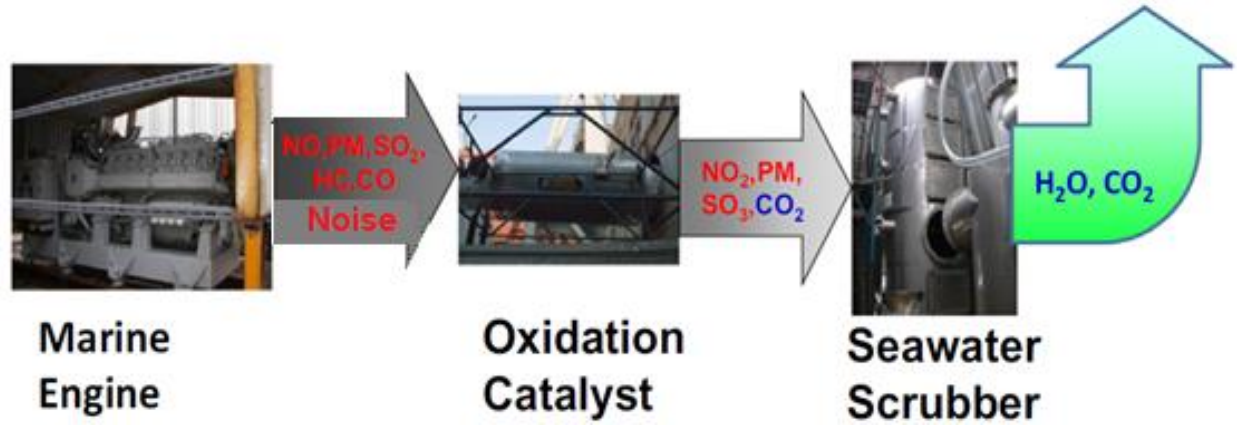

Figure 3. Abatement strategy. adapted from (Boscarato et al., 2015).

Considering that SOx and NOx emitted by the engine are mostly in the form of SO_2 and NO, due to the conditions in which combustion takes place in the engine and which do not allow for complete oxidation (EGCSA group, 2012), the ideal DOC converter should have the following characteristics:

- Able to achieve in operating conditions an average conversion of NO to NO_2 of about 50% since in the wet scrubber NO/NO_2 mixtures are further absorbed as N_2O_3 according to the following equation (Thomas et al., 2000):

$$NO + NO_2 \rightleftharpoons N_2O_3 \quad (1)$$

- To present a low oxidation activity toward SO_2 since its oxidation produces SO_3, which is responsible for acid mist in the wet scrubber, is very corrosive and can damage pipes and machinery;

- To feature a high resistance to poisoning by sulfur, i.e., it must have a low affinity to adsorb sulfites/sulfates that can cover the active sites, reducing the activity of the catalyst;

- Present high acoustic performance in terms of Transmission Loss (TL) to reduce the noise radiated by the engine.

In this paper, first a study on the effect of different doping additives to increase the resistance to sulfur poisoning of the DOC is addressed. Then, a real DOC is designed and tested on the mock-up of a marine Genset to evaluate its efficiency in NO conversion. Finally, numerical simulations are performed to evaluate the

acoustic performance of the DOC and find a geometry that increase its TL, while keeping unaffected its chemical efficiency.

Methods

Experimental Measurements to Evaluate the Efficiency of NO Oxidation

The laboratory experimental setup used to test the catalysts with different doping is reported in Figure 4).

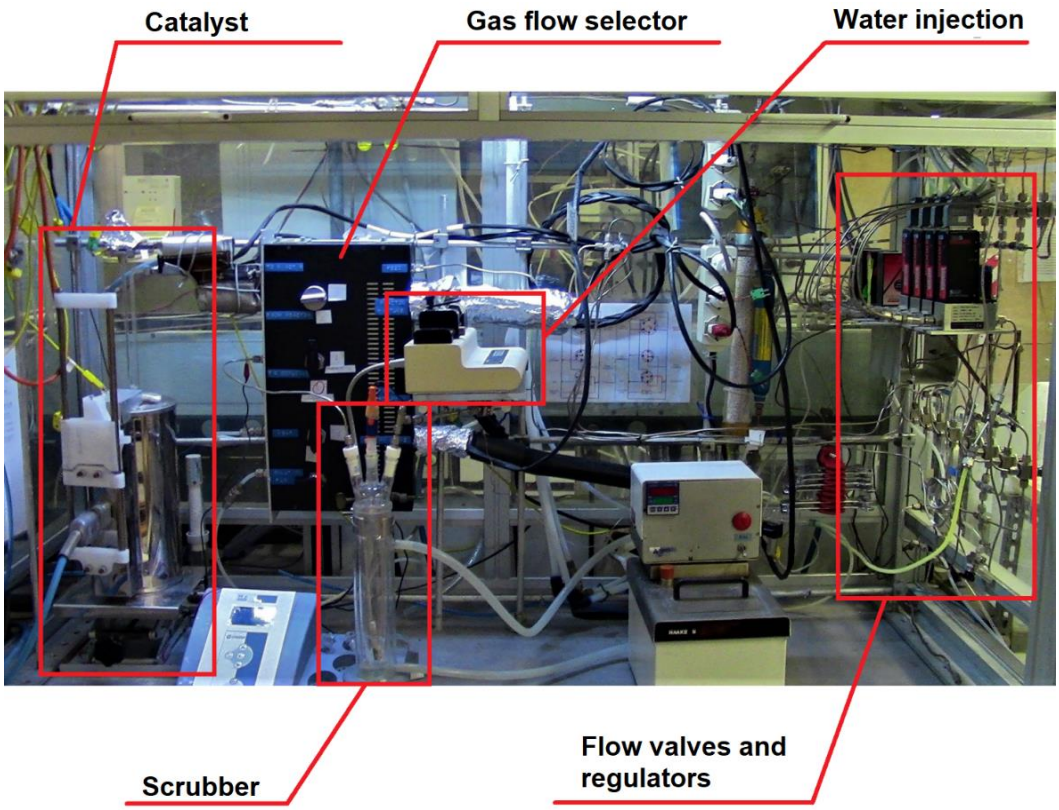

Figure 4. Laboratory experimental set-up.

The catalysts are loaded in a U-tube flow microreactor, which is connected to a gas flow selector that allows to exclude or include a saturator at the outlet of the reactor which simulates a scrubber. The inlet and outlet gas mixtures are analyzed using an on-line FTIR MKS 2000 instrument, which is provided with calibration curves for all the reactants of interest, i.e., NO, NO_2, CO_2, CO, SO_2, N_2O, H_2O, except N_2 and O_2, these species being IR inactive, whereas SO_3 is absorbed in the transfer line in order to avoid damage on the instrument. Therefore, the conversion of SO_2 is calculated as SO_2 disappearance whereas NO conversion is calculated using the formulae:

$$SO_2 \text{ conversion } (\%) = \left(1 - \frac{[SO_2]_{\text{reactor out}}}{[SO_2]_{\text{reactor int}}}\right) \cdot 100 \quad (2)$$

$$NO \text{ conversion } (\%) = \frac{[NO_2]}{[NO] + [NO_2]} \cdot 100 \quad (3)$$

A simulated exhaust is employed with the following composition is employed (mol%): SO_2 570 ppm, NO 900 ppm, O_2 9%, CO_2 6,6%, H_2O 6%, total flowrate 100 ml min^{-1}, using a Gas Hourly Space Velocity (GHSV) of 100,000 h^{-1}. $M_xZr_{1-x}O_{2\pm m}$ mixed oxide, where M is a transition metal, were synthesised by MEL Chemicals using proprietary synthesis methods aimed at incorporation of the dopant within the ZrO_2 structural framework. The dopant levels varied between 8 and 18 mol%.

Once the most promising catalyst composition has been identified, i.e., the one which has the greatest resistance to sulfur poisoning, a full-scale DOC is designed and tested on the exhaust line of a diesel generator mockup (Figure).

Figure 5. Diesel Genset mockup, DOC converter rounded in red.

Numerical Simulations to Evaluate and Optimize the Acoustic Properties of the DOC

To calculate the TL of the DOC a combined approach that uses CFD and acoustic FEM simulation is used. This methodology allows to consider the influence of the flow on the acoustic properties while keeping the computational effort reduced. The velocity, pressure and temperature fields are calculated with CFD simulations and are then imported in the FEM solver through mesh mapping to estimate the TL (Kyaw Oo D'Amore, Mauro, et al., 2022).

Settings used for CFD and FEM simulations and the characteristics of the mesh used to discretise the geometry are chosen on the basis of the results obtained in previous study (Kyaw Oo D'Amore & Mauro, 2021; Kyaw Oo D'Amore, Morgut, et al., 2022).

Having calculated the TL of the reference DOC, geometrical modifications are performed to increase the efficiency of the DOC in noise reduction. The flow resistivity and the OAR (Open Area Ratio) of the monoliths inside the DOC converter, which represent the catalytical elements, are not modified to ensure the chemical efficiency. The external steel casing geometry of the converter is changed and perforated elements are inserted to increase the TL of the DOC, also evaluating the distribution of the flow entering the monoliths (it should be as homogeneous as possible) and the generated back pressure (it must not be greater than the limit value admitted by the engine in order not to lower its efficiency) using the CFD technique.

Results and Discussion

Efficiency in NO Oxidation

Platinum catalysts represent the state of the art DOC used for PM abatement (Zhang et al., 2022), in addition their feature excellent activity for NO oxidation, with relatively good tolerance to SOx and resistance at high temperatures, present in diesel exhaust gases (Hong et al., 2017).

The activity of Pt catalysts depends on the type of support on which the active metal is dispersed. The most common support is γ-alumina (Pt/γ-Al_2O_3. The Eley-Rideal mechanism is generally accepted for NO oxidation which can occur through two paths (Figure 5): the NO can react with the oxygen adsorbed (O) on the active metal, directly giving NO_2 in the gaseous phase or the reaction produces nitrates (NO_3^-) which are adsorbed on the support and may decompose giving NO_2 or NO, depending on the operating conditions (Li et al., 2010). This

second mechanism clearly inspired research on the effects of the support in NO oxidation, either by changing the Al_2O_3 support itself for *e.g.*, CeO_2, ZrO_2, TiO_2, etc., or by a surface doping of the Al_2O_3 carrier with transition metal oxides (Hong et al., 2017). Among the supports, TiO_2 and ZrO_2 have been recognized to confer sulfur-resistance to the supported Pt particles in the oxidation of NO to NO_2. At variance with TiO_2 which has relatively low thermal stability, it is well known that structural doping can confer high thermal stability to ZrO_2-containing mixed oxides (Di Monte et al., 2005); accordingly, the latter systems are chosen for this study.

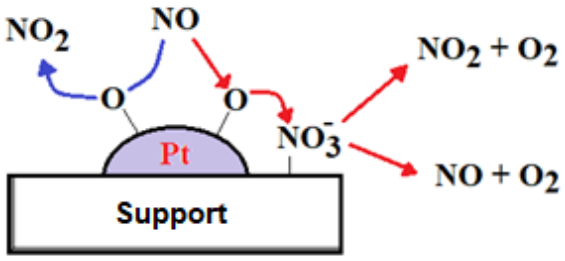

Figure 5. Eley-Rideal mechanism proposed for NO oxidation over Pt catalysts (Li et al., 2010).

Specifically, $Pt/M_xZr_{1-x}O_{2\pm m}$ catalysts with four different structural dopants were employed in the laboratory scale study with the aim to assess the following effects:

• Tungsten oxide (WO_3), to investigate the effects of acidity of the reactivity;

• Cerium oxide (CeO_2), to investigate the effects of high redox reactivity;

• Yttrium oxide (Y_2O_3), which is a neutral element that acts as a thermal stabilizer;

• Lanthanum oxide (La_2O_3), to investigate the effects of basicity of the reactivity.

As previously explained, the study on the influence of different doping on the conversion of both SO_2 and NO is first addressed to highlight the composition with higher resistance to sulfur poisoning. To evaluate the conversion as a function of time and temperature a typical analysis cycle that includes two ramps of heating and subsequent cooling from 100 °C to 500 °C was performed. Figure 6 reports the conversion vs. temperature curves for the Pt/doped-ZrO_2 samples.

Lanthanum, cerium and yttrium doped Pt/ZrO_2 samples feature similar behavior, the conversion of NO does not have a high efficiency and reaches its maximum around 425 °C (about 20%); at lower temperatures the reaction is kinetically controlled, while at higher temperatures it is thermodynamically disadvantaged. A perusal of the SO_2 conversion curves reveals that the heat-up curves present lower conversion compared to run-down part of the cycle at comparable temperatures. This hysteresis is associated to the surface adsorption of NOx and SOx-derived species, mainly on the support, which actively participates to the reaction (Figure 6): during the heating ramp adsorption mainly occurs, then, at the maximum temperature reached by the cycle (500 °C) reasonably desorption of most of the compounds present on the catalyst occurs, leaving the surface clean during the ramp-down part of the cycle (Boscarato et al., 2015). However, the catalyst is not fully regenerated as the second heating curves is lower than the first one. Noticeably, when these experiments are performed in the absence of SO_2, the hysteresis phenomenon is still present and the NO conversion is higher, in line with the poisoning effect of SO_2 (data not reported).

Tungsten is the doping that leads to the best results: the NO conversion reaches 30% at 375 °C. This is attributed to the effect of tungsten which reduces the affinity of SOx-derived species with the active sites, which remain free for NO conversion.

Based on these results, a $Pt/\gamma\text{-}Al_2O_3$ catalyst supported with 20% of WO_3 was prepared and wascoated on two metallic honeycombs there were inserted in a stainless teel casing to obtain the converter described in Figure 7. and preliminarily tested using above descbribed mock-up with the exhaust line and the diesel Genset operating at a GHSV of 100.000 h^{-1}. $\gamma\text{-}Al_2O_3$ is chosen as support instead of ZrO_2 due to its high surface area useful to achieve a high Pt dispersion that could increase the conversion of NO in a real case scenario. Preliminary results showed a NO conversion of 14% at a temperature of about 330°C, which is well-in-line with the results obtained in the model laboratory system, thus confirming the validity of the present approach. Further measurements are on-going and will be reported in a future.

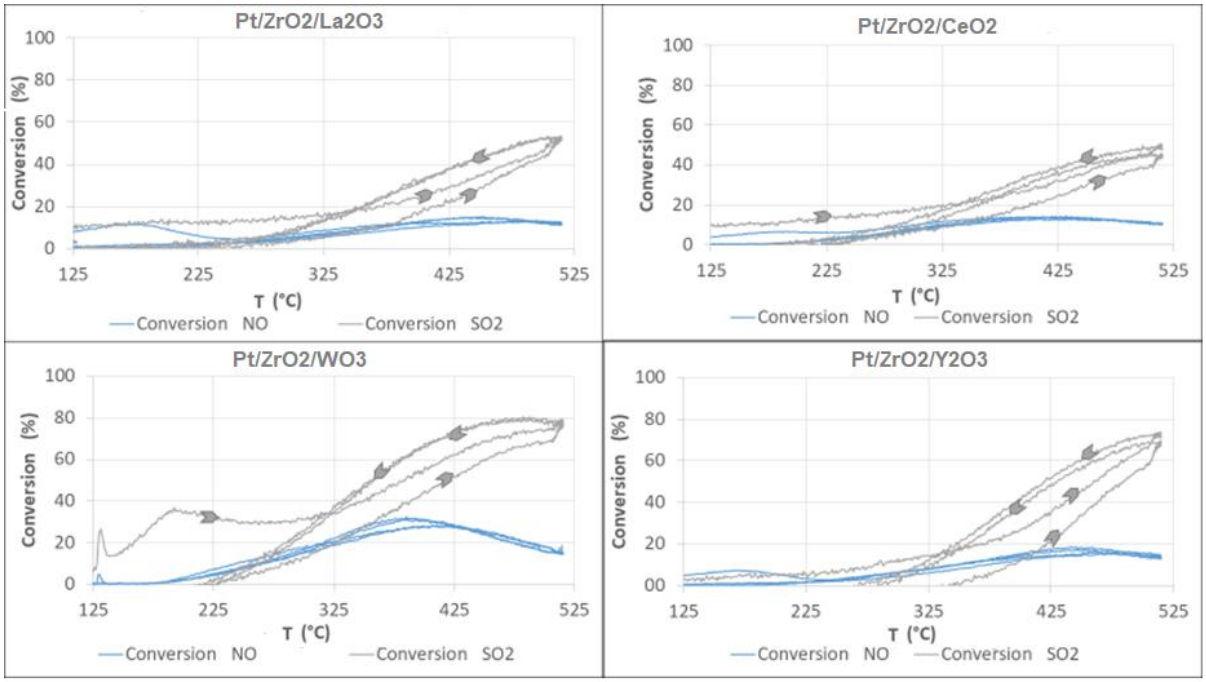

Figure 6. Comparison of conversion curves (NO to NO_2 and SO_2 to SO_3) as a function of temperature over Pt/doped-ZrO_2 catalysts.

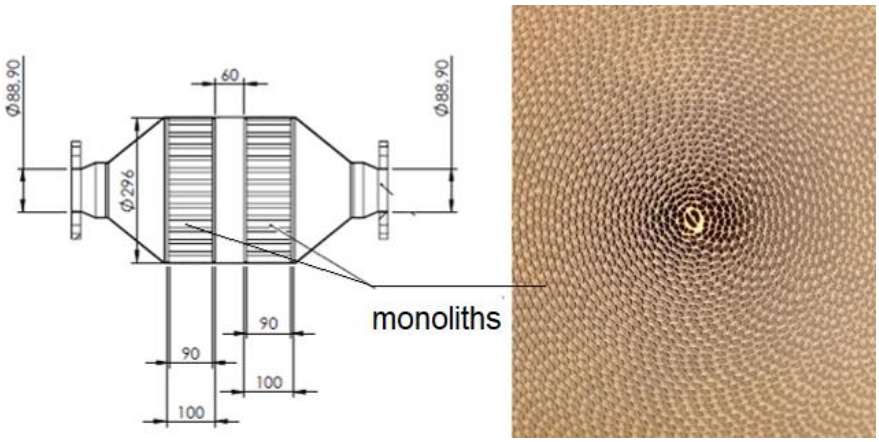

Figure 7. Scheme of the DOC converter and detail of the honeycomb structure.

Evaluation and Optimization of the Acoustic Properties of the DOC

The TL of the reference DOC (Figure 7) is evaluated with the combined CFD-FEM methodology considering a flow with characteristics as those measured on the diesel Genset mockup, .i.e., a linear flow velocity of 42.5 m/s at a temperature of 270 °C.

Figure 8 compares the TL curve calculated using the actual converted geometry (Figure 8) with the TL of a modelled DOC converter where modifications of the geometry are applied in order to improve the silencing effect of the converter, without affecting the chemicals processes occurring in the two honeycombs. Figure 9 compares the two geometrical configurations of the analyzed DOCs, whereas their main dimensions are reported in Table 1.

Remarkably, modest modifications of the converter geometry allow to increase the TL up to 10 dB in the frequency range 0-200 Hz and up to 20 Hz in the frequency range 350-650 Hz. In the frequency range 200-350 Hz a decrease of the TL curve up to 6 Hz is highlighted; for a real application this dip should not correspond with the engine frequency to maximize the overall noise reduction. Accordingly, further studied should be performed to find a configuration which allow the optimization of the TL in the whole frequency range.

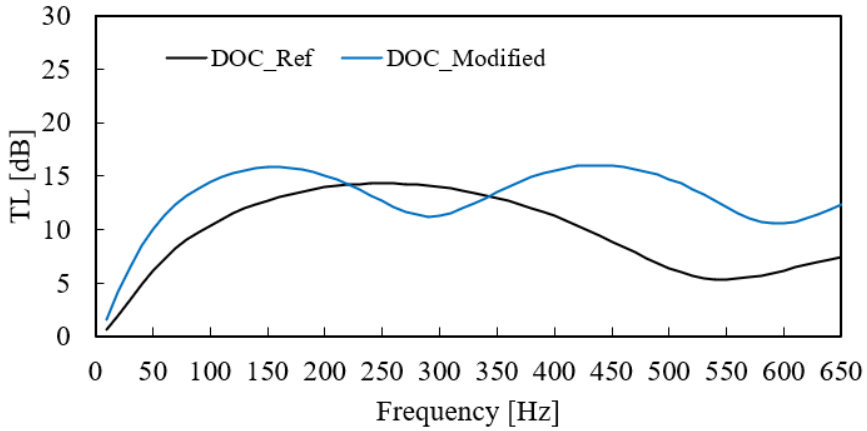

Figure 8. TL comparison, reference DOC *vs* modified one.

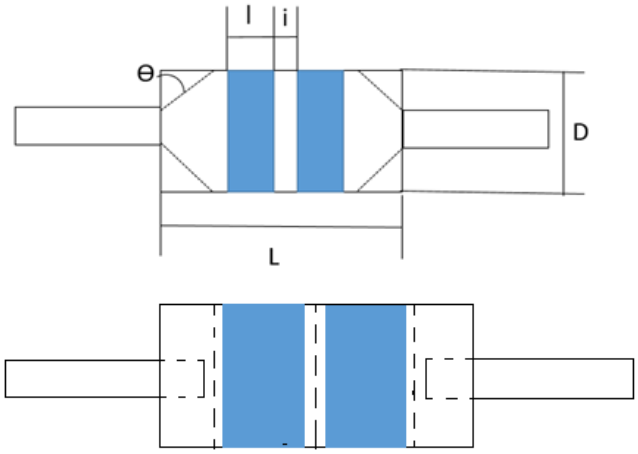

Figure 9.Comparison between geometry of reference DOC and modified one.

Table 1. Reference DOC geometry parameters *vs* modified DOC.

DOC	D	Θ	L	l	i	n_p	R	OAR	L_f
Ref	297	40	510	90	60	0	678	0.92	0
Mod	297	0	765	180	90	3	678	0.92	127.5

Conclusions

In the present work, an interdisciplinary approach to the development of an advanced multifunctional EGCS is presented. The use of a DOC for NOx abatement is proposed, replacing traditional systems on board ships such as SCR and EGR. The DOC is designed to also have noise reduction properties, aiming to also eliminate the silencer along the exhaust line of marine diesel engines, thanks to the systems integration. The wet scrubber present downstream of the DOC, can be used also for the reduction of SOx, always with a view of system integration to obtain a compact exhaust line that allow to save space on board while be compliant with the international regulations. The preliminary study presented in this paper focused on the possible doping to increase the resistance of the catalyst to sulfure poisoning and to the oxidation of SO_2. It has been seen that tungsten is the most promising doping in this sense. A good correlation between laboratory-scale measurements and DOC on a diesel Genset mockup has been highlighted and good results are obtained in increasing the acoustic properties of the DOC. Other studies are ongoing to further increase the efficiency of NOx oxidation within the DOC.

Scientific Ethics Declaration

The authors declare that the scientific ethical and legal responsibility of this article published in EPSTEM journal belongs to the authors.

Acknowledgements or Notes

* This article was presented as oral presentation at the International Conference on Basic Sciences, Engineering and Technology (www.icbaset.net) held in Marmaris/Turkey on April 27-30, 2023.

References

Adam, A. F., Moldovan, I. A. G., Nita, S. C., & Hrebenciuc, A. (2021). The importance of maritime transport for economic growth in the European union: A panel data analysis. *Sustainability*, *13*(14), 7961.

Ayre, L. S., Johnson, D. R., Clark, N. N., England, J. A., Atkinson, R. J., McKain, D. L., Ralston, B. A., Balon, T. H., & Moynihan, P. J. (2011). Novel nox emission reduction technology for diesel marine engines. *American Society of Mechanical Engineers, Internal Combustion Engine Division (Publication) ICE*, 703–710.

Bodn, H., & Glav, R. (2007). Exhaust and intake noise and acoustical design of mufflers and silencers. In M. J. Crocker (Ed.), *Handbook of noise and vibration control* (pp. 1034–1053). Hoboken, NJ, USA: John Wiley & Sons, Inc.

Boscarato, I., Hickey, N., Kašpar, J., Prati, M. V., & Mariani, A. (2015). Green shipping: Marine engine pollution abatement using a combined catalyst/seawater scrubber system. 1. effect of catalyst. *Journal of Catalysis*, *328*, 248–257.

Chen, Y., & Lv, L. (2015). Design and evaluation of an Integrated SCR and exhaust Muffler from marine diesels. *Journal of Marine Science and Technology*, *20*(3), 505–519.

Di Monte, R., & Kaspar, J. (2005). Nanostructured ceo2-zro2 mixed oxides. *Journal of Materials Chemistry*, *15*, 633–648.

EGCSA group. (2012). *A practical guide to exhaust gas cleaning systems for the maritime industry*. https://www.egcsa.com/wp-content/uploads/EGCSA-Handbook-2012-A5-size-.pdf

Hong, Z., Wang, Z. L., & Li, X. (2017). Catalytic oxidation of nitric oxide (NO) over different catalysts: an overview. *Catalysis Science & Technology*, *7*(16), 3440–3452.

Huang, H., Tian, J., Li, J., & Tan, D. (2022). Effects of different exhaust gas recirculation (egr) Rates on combustion and emission characteristics of biodiesel–biesel blended fuel based on an improved chemical mechanism. *Energies*, *15*(11), 4153.

ANNEX 13. (2008).Revised marpol. *Resolutıon MEPC,176*(58). https://wwwcdn.imo.org/localresources/en/OurWork/Environment/Documents/176(58).pdf

ANNEX 1. (2012). Adoption of the code on noise level on board ships. *Resolutıon MSC, 337*(91). https://wwwcdn.imo.org/localresources/en/KnowledgeCentre/IndexofIMOResolutions/Documents/MSC%20-%20Maritime%20Safety/337(91).pdf

Johnsen, K., Kock, F., Strøm, A., & Chryssakis, C. (2019). *Global sulphur cap 2020 update [DNV-GL technical report*. https://www.dnvgl.com/maritime/publications/global-sulphur-cap-2020.html

Kyaw Oo D'Amore, G., Biot, M., Mauro, F., & Kašpar, J. (2021). Green shipping—multifunctional marine scrubbers for emission control: silencing effect. *Applied Sciences*, *11*(19). https://doi.org/10.3390/app11199079

Kyaw Oo D'Amore, G., & Mauro, F. (2021). Numerical study on modelling perforated elements using porous baffle interface and porous region. *Journal of Engineering, Design and Technology*. https://doi.org/10.1108/JEDT-07-2021-0356

Kyaw Oo D'Amore, G., Mauro, F., Rognoni, G., Morgut, M., & Biot, M. (2022, June 15). A combined CFD-FEM approach to evaluate acoustic performances of an integrated scrubber-silencer for marine applications. Proceeding of NAV 2022: *20th International Conference on Ship & Maritime Research, Genoa-La Spezia (Italy).*

Kyaw Oo D'Amore, G., Morgut, M., Biot, M., & Mauro, F. (2022). Numerical study on the influence of porous baffle interface and mesh typology on the silencer flow analysis. *Marine Systems & Ocean Technology*, *17*(2), 71-79.

Li, L., Shen, Q., Cheng, J., & Hao, Z. (2010). Catalytic oxidation of NO over TiO_2 supported platinum clusters I. Preparation, characterization and catalytic properties. *Applied Catalysis B: Environmental*, *93*(3–4), 259–266.

Lindstad, H. E., & Eskeland, G. S. (2016). Environmental regulations in shipping: Policies leaning towards globalization of scrubbers deserve scrutiny. *Transportation Research Part D: Transport and Environment*, *47*, 67–76.

Lindstad, H. E., Rehn, C. F., & Eskeland, G. S. (2017). Sulphur abatement globally in maritime shipping. *Transportation Research Part D: Transport and Environment*, *57*, 303–313.

Lou, D., Kang, L., Zhang, Y., Fang, L., & Luo, C. (2022). Effect of exhaust gas recirculation combined with selective catalytic reduction on NO_x emission characteristics and their matching optimization of a heavy-duty diesel engine. *ACS Omega*, *7*(26), 22291–22302.

Thomas, D., & Vanderschnren, J. (2000). Nitrogen oxides scrubbing with alkaline solutions. *In Chemical Engineering and Technology 23*(5), 449–455

United states environmental protection agency office of wastewater management Washington, DC 20460. (2011). *Exhaust Gas Scrubber Washwater Effluent*. https://apps.dtic.mil/sti/pdfs/ADA553088.pdf

Ushakov, S., Stenersen, D., Einang, P. M., & Ask, T. Ø. (2020). Meeting future emission regulation at sea by combining low-pressure EGR and seawater scrubbing. *Journal of Marine Science and Technology (Japan)*, *25*(2), 482–497.

Zhang, Z., Tian, J., Li, J., Cao, C., Wang, S., Lv, J., Zheng, W., & Tan, D. (2022). The development of diesel oxidation catalysts and the effect of sulfur dioxide on catalysts of metal-based diesel oxidation catalysts: A review. *Fuel Processing Technology*, *233*, 107317.

Zhao, Y., Fan, Y., Fagerholt, K., & Zhou, J. (2021). Reducing sulfur and nitrogen emissions in shipping economically. *Transportation Research Part D: Transport and Environment*, *90*, 102641.

Zhu, Y., Zhou, W., Xia, C., & Hou, Q. (2022). Application and development of selective catalytic reduction technology for marine low-speed diesel engine: Trade-off among high sulfur fuel, high thermal efficiency, and low pollution emission. *Atmosphere*, *13*(5), 731.

Author Information

Giada Kyaw Oo D'Amore
University of Trieste
Trieste, Italy
Contact e-mail: *giada.kyawoodamore@dia.units.it*

Jan Kašpar
University of Trieste
Trieste, Italy

To cite this article:

Kyaw Oo D'Amore, G., & Kašpar, J. (2023). Preliminary study on the use of a DOC to reduce NOx emissions in marine field. *The Eurasia Proceedings of Science, Technology, Engineering & Mathematics (EPSTEM)*, *22*, 285-294.

The Eurasia Proceedings of Science, Technology, Engineering & Mathematics (EPSTEM)
ISSN: 2602-3199

The Eurasia Proceedings of Science, Technology, Engineering & Mathematics (EPSTEM), 2023

Volume 22, Pages 295-304

ICBASET 2023: International Conference on Basic Sciences, Engineering and Technology

Computational Study of Erosion Wear of Capillary Used in Laser Solder Ball Jetting Process

Suparoj PREMJARUNAN
The Sirindhorn International Thai-German Graduate School of Engineering.
King Mongkut's University of Technology

Karuna TUCHINDA
The Sirindhorn International Thai-German Graduate School of Engineering
King Mongkut's University of Technology

Kittichai SOJIPHAN
The Sirindhorn International Thai-German Graduate School of Engineering
King Mongkut's University of Technology

Abstract: Solder Ball Bumper Jetting Process is used for high precision soldering in small area with high productivity. Cemented carbide (WC-Co) is the common material used for capillary due to its high strength and good wear resistance. Small paritcle induced during soldering process could cause particle erosion wear and it is found to be one of the surface failure mostly controlling capillary in-service life. The particles were expected to be hard particle generated by surface wear in the earlier process. This research aims to study the material behavior under particle impact to increase the understanding of capillary failure based on particle impingement erosion wear using Finite Element Method (FEM). The effect of contact paramters, i.e. impact angle of particle and particle size, on failure of capillary tip was studied. The impact angle variation between 10, 30, 60, 90 degree and particle size variation of 0.5, 0.75, 1 micrometer were considered. The result showed that higher angle of impact can lead to higher stress developed while particle size effect depends strongly on the contact area which relies on impact angle. In case of 60 and 90 degree of impact, results showed a trend of decreasing developted stress with increasing particle size. While 10 and 30 degree of impact showed a trend of increasing in developed stress when particle size increased. The research results could be used as guidelines to improve the capillary design or soldering process to incrase the capillary in-service life or minimize the chance for capillary failure at unexpected short time period.

Keywords: Solder ball bumper jet, Soldering, Impact angle, Particle size, Finite element method, Erosion wear.

Introduction

Microelectromechanical systems (MEMS) are combination of mechanical and electrical structures with micron size elements (Ozevin, 2014). MEMS devices are important component to sensors and hard-disk drives (Hirano, 2007). The packaging of MEMS devices needs more advanced technology in processing in miniature area than traditional soldering method. To achieve the requirement, method of laser-based solder jetting technology, Solder Ball Bumper Jet (SB^2-Jet), have been used. The preformed solder ball of this process is singulated from solder ball reservoir to the tip of capillary. After that, the laser pulse is used to melt solder ball and molten solder ball will be jetted out from capillary tip as shown in Figure 1 (Sun, 2012). This type of Laser Solder Ball Jetting process provides high productivity and fulfills all the needs of fluxless soldering, local heating and reflow, no mechanical contact and stress during soldering (Zakel, 2002).

- Selection and peer-review under responsibility of the Organizing Committee of the Conference

The process needs high accuracy to process miniature device and the shape of capillary can affect the accuracy of the process. Research have been done to investigate the effect of capillary tip. In 2011, three types of capillary tip shapes shown in Figure 2 were studied and the effect of capillary tip on jetting accuracy is shown here in Figure 3 (Mata, 2011). Cemented carbide (WC-Co) capillary used for this process is usually be changed after capillary tip shows unacceptable defect to keep high precision of such process. Less defect can lead to higher lifetime before capillary rejected from production line which can decrease cost from capillary changing.

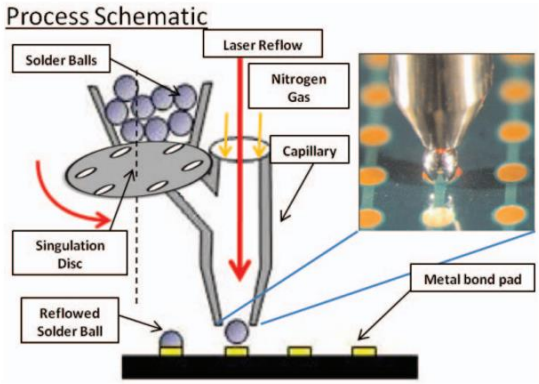

Figure 1. Principle of SB^2-Jet process (Sun, 2012)

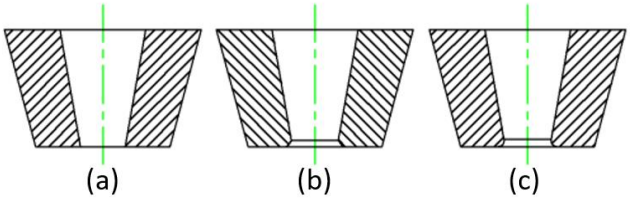

Figure 2. Shape of (a) capillary type A, (b) Capillary type B, (c) Capillary type C. (Mata, 2011)

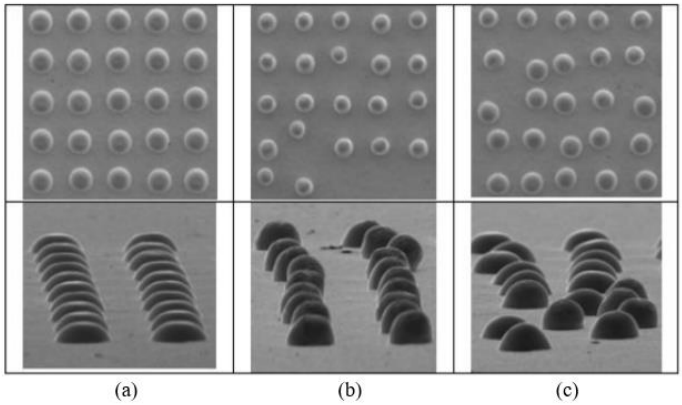

Figure 3. Jetting result of (a) Capillary type A, (b) Capillary type B, (c) Capillary type C. (Mata, 2011)

Erosive wear was found to be one of the main surface failures expected as the process involved fluid flow. The erosive wear resistance of WC-Co carbides obtained by spark plasma sintering method was studied (Wachowicz, 2021). The study showed that erosion rate depends on sintering process of WC-Co and erosion medium. This erosive wear study used quartz particle as erodent particle. The result of this study showed that larger particle impact can lead to more erosion wear. Also, larger impact angle also leads to higher surface deformation and more material removal during impact. Small particle could be induced during soldering process and could be considered as erosive particle. Erosive particle could be chromium and stainless steel from laser jetting system or WC particle from WC-Co cemented carbide capillary wall. Internal crack from manufacturing process can lead to WC grain worn out from crack surface (Mikado, 2017). The particles generated by surface wear in the earlier process, i.e. WC particle, were hard particle which is expected to has a strong effect on capillary surface defect leading to jetting inaccuracy.

This research aims to study the material behavior under particle impact to increase the understanding of capillary failure based on particle impingement erosion wear using Finite Element Method (FEM). The effect of

contact parameters, i.e. impact angle of particle and particle size, on failure of capillary tip was studied. The erosive particles were assumed to flow along with molten solder at same velocity as molten solder ball flow velocity during laser solder ball jetting process. This study focused on WC erosive particles due to higher density and Young's Modulus which developed more stress during impact and can lead to more serious failure compared to other metal particle in jetting system. FEM were used to investigate the stress distribution developed during impact and used to estimate the material removal from particle impact based on failure criteria. Higher stress developed lead to lower time for material removal, i.e. lower number of loading cycle or impact to failure. It was observed that once developed stress from particle impact exceed yield strength and exposed to the surface, surface removal take place as expected (Akchurin, 2016). The mechanical properties at room temperature were used for computational study by finite element method. At process temperature, which is around 217 degree Celsius, it is not expected for WC-Co cemented carbide to exhibit significant change in mechanical properties and failure compared to room temperature (Milman, 2013). Nanoindentation technique was employed to obtain the material properties to be used for FEM.

Method

Microstructure Analysis

Microstructure analysis carried on by Scanning Electron Microscope to specified grain size of WC grain which was used to identify size of impact particle used in this study. Grain size was measured by using ImageJ to measure multiples WC grain to find mean grain size and distribution of grain size.

Material Testing by Nanoindentation

Capillary material used in this study assumed to be made of WC-Co cemented carbide available commercially. WC-Co cemented carbide were characterized by nanoindentation technique to accurately capture the properties in small scale. The result of nanomechanical tester showed hardness and Reduced Elastic Modulus. Reduced Elastic Modulus was converted to Young's Modulus using relationship showed in Equation 1.

$$\frac{1}{E_r} = \frac{1-\nu^2}{E} + \frac{1-\nu_i{}^2}{E_i} \tag{1}$$

Where E_r, E, E_i represent Reduced Elastic modulus, Young's Modulus of testing specimen and Young's Modulus of indenter, respectively. ν and ν_i represent Poisson's ratio of testing specimen and indenter, respectively.

Maximum indentation load (F_m), Maximum indentation depth (h_m), Area of contact (A_f) and Young's Modulus (E) were used to calculate yield strain (ε_y) and strain hardening exponent (n) through numerical method according to Equation 2 and 3 (Tunvisut, 2002) to create stress-strain curve for WC material which was later used in finite element analysis.

$$\frac{F_m}{E{h_m}^2} = 73{\varepsilon_y}^{0.82} - 87.3{\varepsilon_y}^{0.98} - \left(0.24ln\varepsilon_y + 0.39\right)n^{0.26ln\varepsilon_y+0.10} \quad , \tag{2}$$

$$\frac{A_f}{{h_m}^2} = 6ln\varepsilon_y - 178{\varepsilon_y}^{0.13} + \left(4.54ln\varepsilon_y + 5.86\right)n^{0.1ln\varepsilon_y-0.1} + 155.7. \ , \tag{3}$$

Finite Element Analysis

Particle impact model was developed to simulate effect of impact angle and particle size. The stress developed near WC-Co surface from particle impact was studied. The impact angle variation between 10, 30, 60, 90 degree and particle size variation corresponding to carbide particle sizes observed were considered, i.e. 0.5, 0.75, 1 micrometer. Figure 4 showed impact model and Figure 5 showed meshing in the contact area. Impact velocity equal to 2.23 m/s was selected based on preliminary study using simplified CFD model (Premjarunan, 2023) which was applied to all cases of particle impact study. Particle material properties obtained from nanoindentation test of the hardest phase of cemented carbide specimen were used. This is to represent the worst case due to WC grain particle worn out from capillary wall.

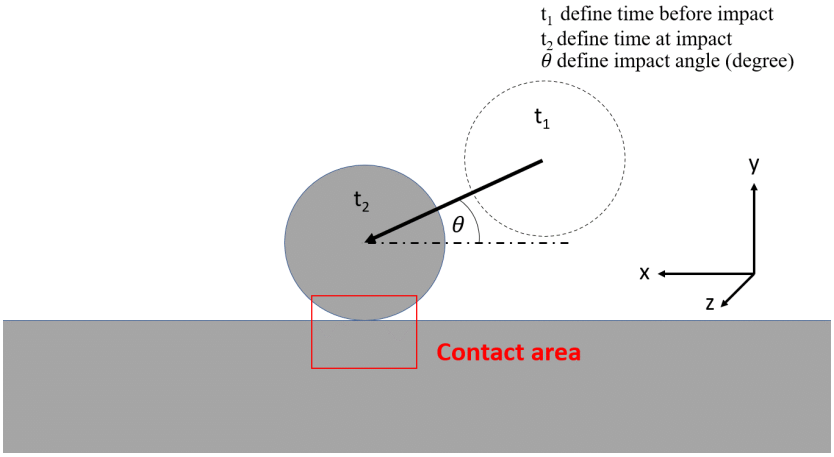

Figure 4. Impact model used in study showing impact step, impact area and impact angle.

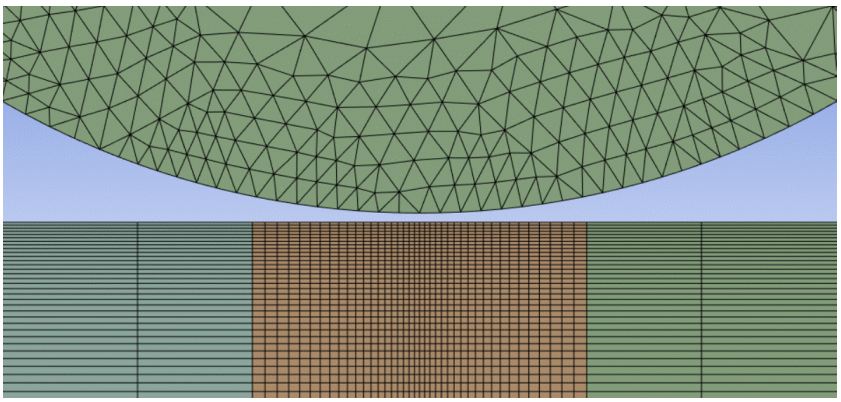

Figure 5. Finite Element model showed meshing in contact area.

The stress developed near impact surface was used to estimate wear volume. Material in the area that experienced stress more than yield strength and exposed to the surface would be the area to fail and be removed as wear debris.

Results and Discussion

Microstructure Analysis

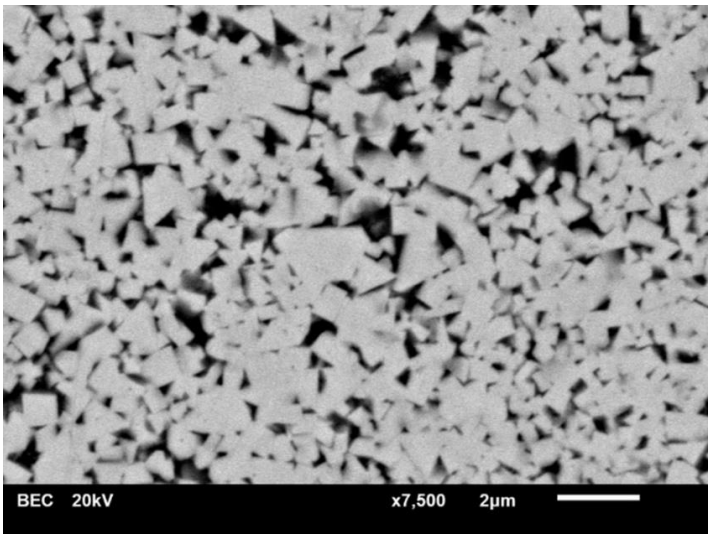

Figure 6. Example of Microstructure of commercial grade WC-Co from Scanning Electron Microscopy

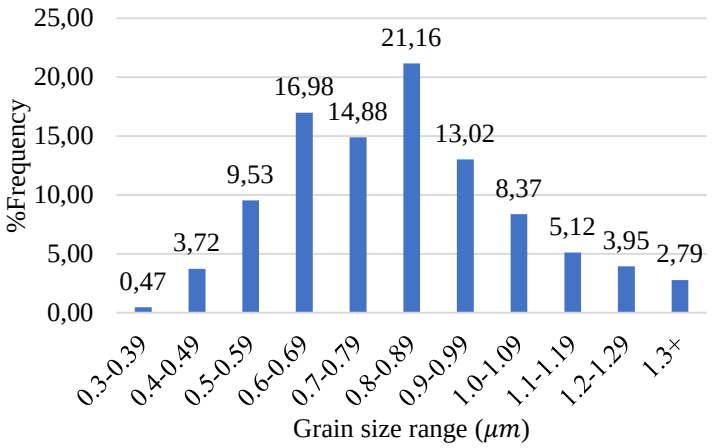

Figure 7. Carbide grain size distribution of KA10 cemented carbide measured from Figure 5.

Example of SEM micrograph shown in Figure 6 with grain size distribution result shown in Figure 7 was measured from multiple samples. Mean grain size measured from ImageJ was found to be 0.83 microns. The size distribution showed highest frequency in the range of 0.5 to 1 micrometer. The results were used to define the range of particle size studied. The variation of particle size of 0.5, 0.75, 1 micrometer were investigated assuming that grain of WC-Co at surface can be worn off early on the process.

Material Testing by Nanoindentation

The typical results obtained from nanoindentation tests including loading-unloading curve shown in Figure 8. The test results from multiple testing at different positions were used to define the properties of WC-Co Cemented carbide. The property of WC hard particle phase was obtained from the results corresponding to the area showing maximum hardness from nanoindentation test. It was used to represent hard phase carbide which was assumed to be impact particle to study the effect of impact from WC grain. Maximum indentation load, maximum indentation depth, reduced elastic modulus, and contact area were used to estimate material constant by Equation 1,2 and 3 and the results are shown in Table 2.

Table 2. Material Properties of WC-Co cemented carbide

Material	Indentation yield strength (MPa)	Strain hardening exponent	Young's Modulus (GPa)	Hardness (GPa)
Average WC-Co surface	2,130	1.62	626	28.89
Hard WC grain	3,440	1.49	781	39.24

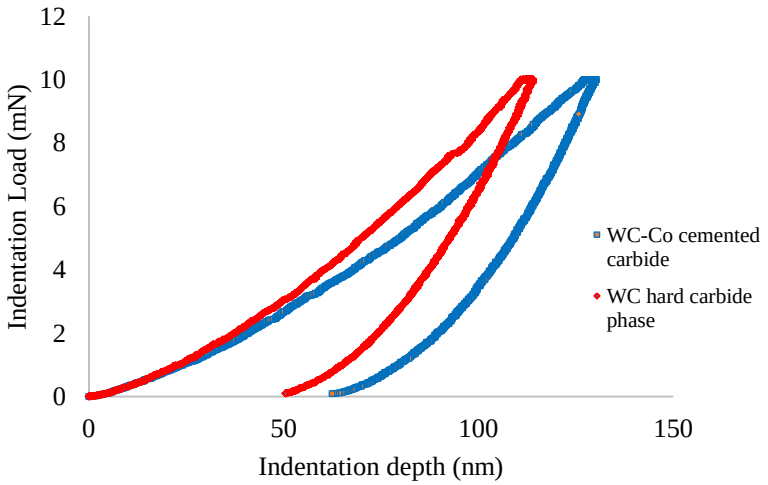

Figure 8. Loading-unloading curve of WC-Co surface

In term of temperature effect during soldering process, i.e., melting temperature of solder used in the process, other study about effect of temperature to mechanical properties showed insignificant reduction of strength until 300 degrees Celsius (Milman, 2013). Hence, the properties obtained from tests carried out at room temperature will be used to represent material properties in the FEM.

Finite Element Analysis

Von Mises stress (σ_{VM}) result of WC-Co surface from FEM showed in Figure 9-11. The particle body was hidden to inspect stress distribution contour from FEM. Distribution pattern revealed larger developed Von Mises stress during impact of particle. Larger impact particle size led to wider distribution of stress. At the same time, higher impact angle also led to larger in distribution of developed stress during impact.

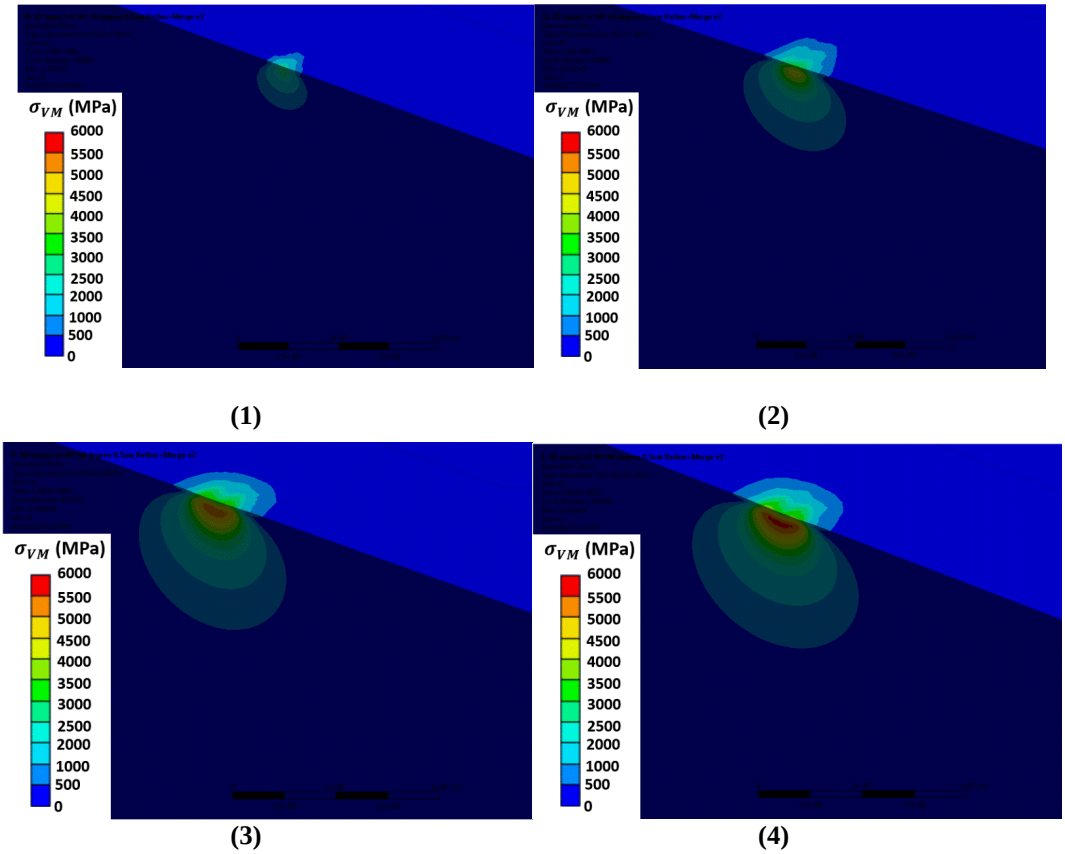

Figure 9. Von Mises Stress obtained from FEM by ANSYS Explicit Dynamics at particle size of 0.5 μm at same contour plot range of (1) Impact angle of 10-degree (2) Impact angle of 30-degree (3) Impact angle of 60-degree (4) Impact angle of 90-degree.

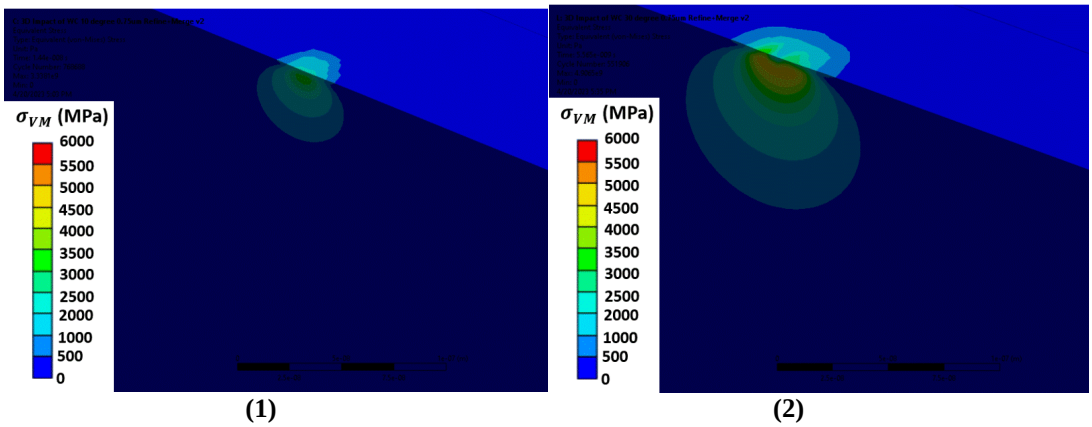

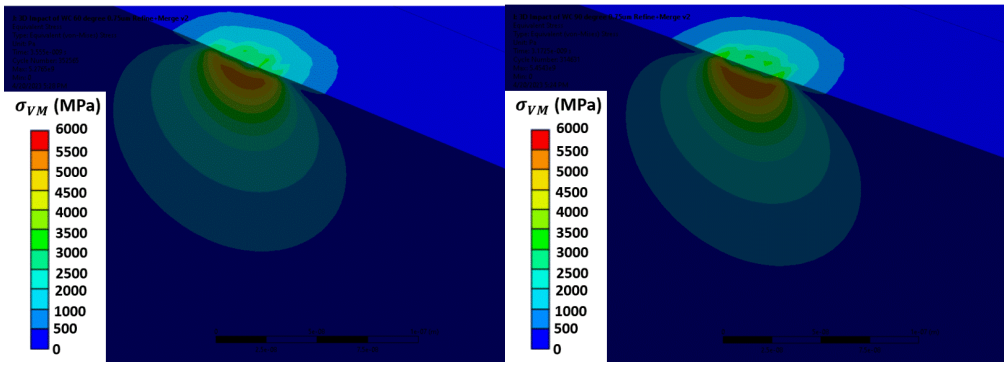

Figure 10. Von Mises Stress obtained from FEM by ANSYS Explicit Dynamics at particle size of 0.75 μm at same contour plot range of (1) Impact angle of 10-degree (2) Impact angle of 30-degree (3) Impact angle of 60-degree (4) Impact angle of 90-degree.

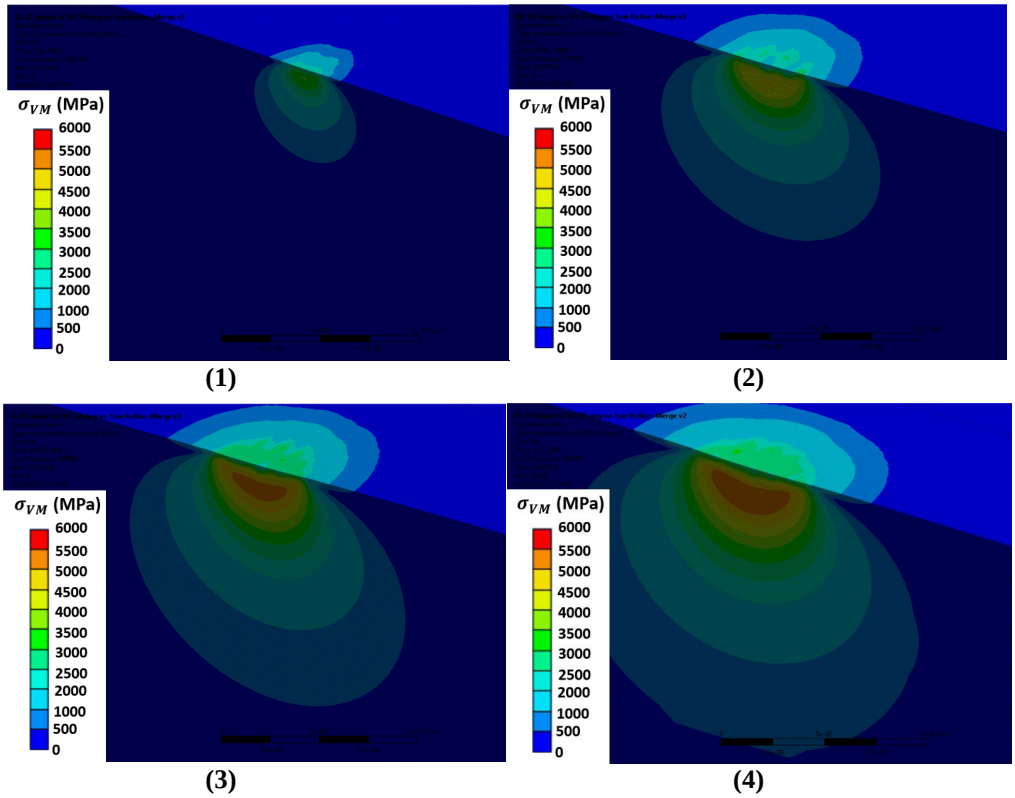

Figure 11**.** Von Mises Stress obtained from FEM by ANSYS Explicit Dynamics at particle size of 1 μm at same contour plot range of (1) Impact angle of 10-degree (2) Impact angle of 30-degree (3) Impact angle of 60-degree (4) Impact angle of 90-degree.

Relationship between maximum stress and impact angle and maximum stress and impact particle size were also considered and showed in Figure 12 and 13, respectively. The result showed effect of impact angle and impact size of particle to stress developed at WC-Co cemented carbide material.

The result plot from Figure 12 showed developed stress increased when impact angle increased. In term of particle size effect, the result from Figure 13 showed increased trend of stress when particle size increased in case of 10 and 30 degree. However, at 60 and 90 degree of impact showed stress slightly decreased when particle size increased. The result showed that Von Mises stress developed around the contact area depends on both particle size and impact angle. For the same material or material with the same density, increasing of particle size led to an increase in particle mass resulting in higher impact force expected during impact. However, particle size increasing did not found to lead to increasing developed stress in all cases because of variation of contact area from different impact angle and particle size during impact. Higher contact area would result in lower stress associated with the same impact force.

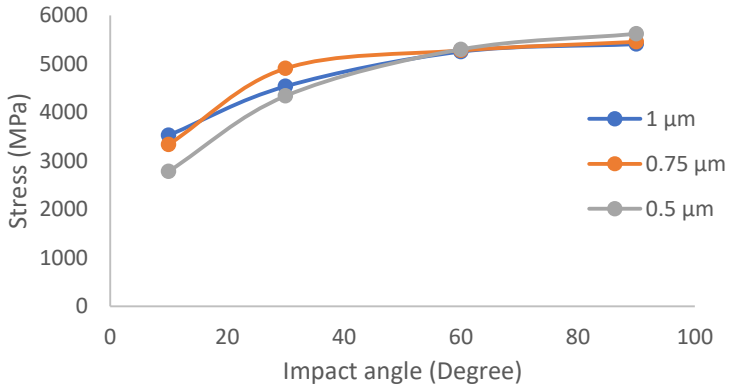

Figure 12. Developed Von Mises stress during impact of different angle of particle

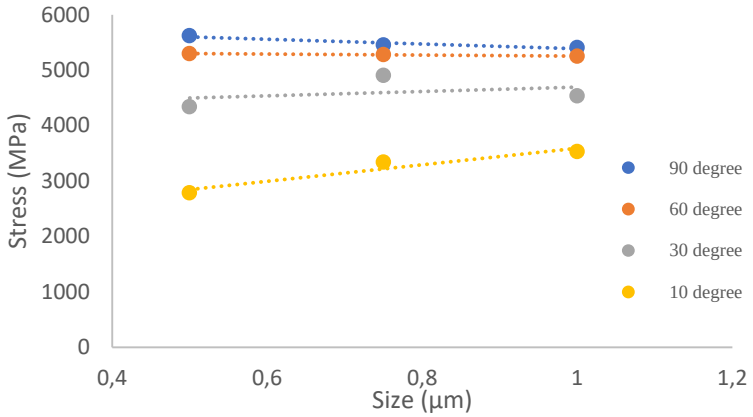

Figure 13**.** Developed Von Mises stress during impact of different size of particle

Wear depth and wear debris size was then be estimated from Von Mises stress distribution contour from finite element results. Yield criteria was used to estimate wear volume and the yield strength of WC-Co cemented carbide is 2,130 MPa as showed in result from Table 1. The stress distribution countor was replotted with different contour level range being redefined to define the wear volume more conveniently as showed in Figure 14. Wear length in 3 axes was measured and showed in Figure 14 as L_x, L_y, L_z for length in x, y, and z-axis, respectively. Wear volume ($V_{Ellipsoid}$) was calculated assuming wear shape as half ellipsoid shape using Equation 4 assuming that area under the surface which showed stress lower than yield strength was not worn out. L_x and L_z define maximum length of stress distribution at the surface while L_y defines maximum depth.

$$V_{Ellipsoid} = \frac{4}{3}\frac{(\pi L_x L_y L_z)}{2} \quad , \qquad (4)$$

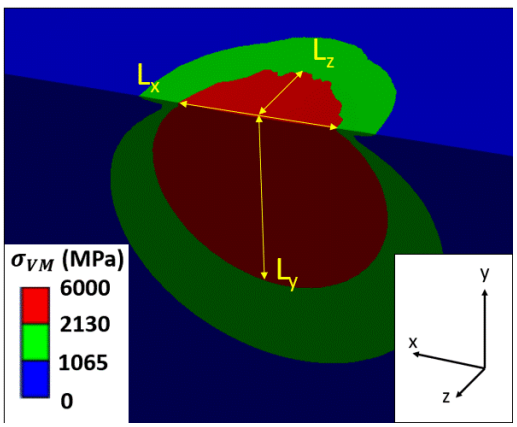

Figure 14. Redefined Von Mises stress contour for calculation of wear volume.

The calculated wear volumes from applying yield criteria to define material failure based on developed Von Mises stress during impact from FEM are shown in Figure 15. The wear volume showed that impact angle and particle size increasing can lead to increasing wear volume. Increasing in particle size led to slightly decrease in maximum Von Mises stress in some cases depending on impact angle and particle size. For cases with increasing of the area of impact which resulted in wider area with plastic deformation, i.e., area with stress higher than yield strength of material, could result in higher wear volume. Note that, in this work, material failure causing material removal based on yielding failure was assumed as it is expected that the number of cycles to failure of such material would be found shortly once plastic deformation observed.

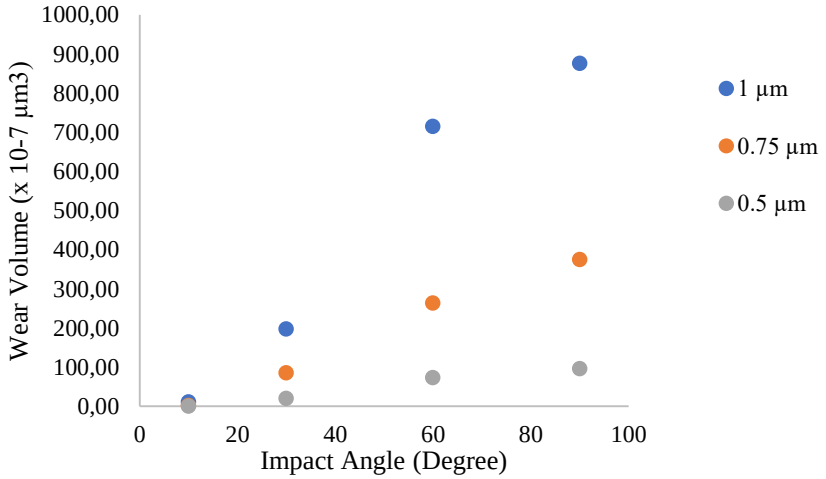

Figure 15. Calculated wear volume of different impact angle and particle size of impact particle

Conclusion

This research aims to study the effect of contact parameters, i.e., grain size of WC and impact angle, on stress distribution and failure of capillary tip made of WC-Co cemented carbide from particle impingement erosion wear using Finite Element Method (FEM). The impact angle variation between 10, 30, 60, 90 degree and particle size variation of 0.5, 0.75, 1 micrometer were considered. The result showed that increasing in impact angle led to higher stress during impact of particle. In case of impact particle size increased, results at 10 to 30 degrees showed increasing of stress when particle size increased. For higher angle of impact of 60 to 90 degrees, maximum stress showed slightly decreased trend when particle size increased due to expanded contact area during impact. However, wear volume results determined based on yield criteria showed that more wear volume were observed when impact angle increased for all particle size.

The results could be useful to improve lifetime of the specimen based on capillary surface change as it affected jetting accuracy. Reduction of grain size can lead to decreased wear volume under current assumption that WC hard particle worn out from early process was expected. Decreasing grain size can lead to lower stress distribution due to lower mass.

Recommendations

The current model could be extended to study particle erosion wear in other application with different impact conditions such as different contacting materials, impact velocity. The model can also be used to study material failure based on other failure mechanism such as micro-fracture to include the effect of initial cracks.

Scientific Ethics Declaration

The authors declare that the scientific ethical and legal responsibility of this article published in EPSTEM journal belongs to the authors.

Acknowledgements or Notes

This article was presented as oral presentation at the International Conference on Basic Sciences, Engineering and Technology (www.icbaset.net) held in Marmaris/Turkey on April 27-30, 2023.

References

Akchurin, A., Bosman, R. & Lugt, P.M. (2016). A stress-criterion-based model for the prediction of the size of wear particles in boundary lubricated contacts. Tribol Lett, *64*, 35.

Hirano, T., & Yang, H. (2007). MEMS applications in hard disk drives. *TRANSDUCERS 2007 - 2007 International Solid-State Sensors, Actuators and Microsystems Conference*, 2203-2206.

Mata, S., &Taechajedcadarungsri, S. (2011). The effects of capillary tip geometry on solder jetting accuracy in laser solder ball jetting process. *KKU Res J. 16*(6): 596-611.

Mikado, H., Ishihara, S., Oguma, N., & Kawamura, S. (2017). On the short surface fatigue crack growth behavior in a fine-grained WC-co cemented carbide. *Metals, 7*(7), 254. https://doi.org/10.3390/met7070254

Milman, Y. V. (2014). The effect of structural state and temperature on mechanical properties and deformation mechanisms of WC-Co hard alloy. *Journal of Superhard Materials, 36*, 65-81.

Ozevin, D. (2014). Micro-electro-mechanical-systems (MEMS) for assessing and monitoring civil infrastructures. In *Sensor Technologies for Civil Infrastructures (pp. 265-302e).* Woodhead Publishing.

Premjarunan, S. (2023). *Study of capillary failure in laser jet soldering process combined with CFD and FEM*. Master dissertation The Sirindhorn International Thai-German Graduate School of Engineering, King Mongkut's University of Technology North Bangkok.

Sun, W., Sun, T., Lim, K., Ding, M., Johari, B., Dinish, U. S., & Olivo, M., (2012). Effective 90° interconnections using laser solder jetting technologies. *IEEE 14th Electronics Packaging Technology Conference (EPTC).*

Tunvisut, K., Busso, E. P., O'Dowd, N. P., & Brantner, H. P. (2002). Determination of the mechanical properties of metallic thin films and substrates from indentation tests. *Philosophical Magazine A, 82*(10): 2013-2029.

Wachowicz, J., Dembiczak, T., Stradomski, G., Bałaga, Z., Jasińska, J., Rydz, D., Wilkowski, J., & Dyner, M. (2021). The analysis of erosive wear resistance of WC-Co carbides obtained by spark plasma sintering method. *Materials, 14*(23), 7326.

Zakel, E., Titerle, L., Oppert, T., & Blankenhorn, R. G. (2002). High speed laser solder jetting technology for optoelectronics and mems packaging. Proceedings: *International Conference on Electronics Packaging. (Tokyo, Japan).*

Author Information

Suparoj Premjarunan
The Sirindhorn International Thai-German Graduate School of Engineering. King Mongkut's University of Technology, North Bangkok, Thailand.
Contact e-mail: *s6209092860511@kmutnb.ac.th*

Karuna Tuchinda
The Sirindhorn International Thai-German Graduate School of Engineering. King Mongkut's University of Technology, North Bangkok , Thailand.

Kittichai Sojiphan
The Sirindhorn International Thai-German Graduate School of Engineering King Mongkut's University of Technology North Bangkok, Thailand

To cite this article:

Premjarunan, S., Tuchinda, K., & Sojiphan, K. (2023). Computational study of erosion wear of capillary used in Laser Solder Ball Jetting Process. *The Eurasia Proceedings of Science, Technology, Engineering & Mathematics (EPSTEM), 22*, 295-304.

The Eurasia Proceedings of Science, Technology, Engineering & Mathematics (EPSTEM)
ISSN: 2602-3199

The Eurasia Proceedings of Science, Technology, Engineering & Mathematics (EPSTEM), 2023

Volume 22, Pages 305-310

ICBASET 2023: International Conference on Basic Sciences, Engineering and Technology

A Study on Single Mode Laser Based Plastic-Metal Joining Process

Mehtap HIDIROGLU
Coşkunoz Holding CKM R&D Center

Emre EROGUL
Coşkunoz Holding CKM R&D Center

Ramazan OZLUTURK
Coşkunoz Holding CKM R&D Center

Tanya A. BASER
Coşkunoz Holding CKM R&D Center

Abstract: Especially in the automotive industry, the use of plastic and metal joints is preferred for weight savings. Generally, a method called “over molding” is used, where the joint strength is obtained with the plastic material that completely surrounds the metal parts, because plastic and metal cannot be bonded or welded together due to their chemical and physical differences. Today, it is used in the bonding process of joining plastics and metals, but the connection is weak. In order to overcome these problems, a promising approach has been explored by researchers in recent years. In this approach, a two-stage process is used. In the first processing step, laser radiation is applied to form microstructures on the surface of the metallic bonding partner. In the next step, the plastic is mechanically locked to the microstructures with the plastic injection method. A fast beam movement is realized by a galvometric scanning system, which allows scanning variable patterns on the metal surface. Because the process is based on a combination of sublimation and melting, the processing time is much shorter compared to conventional structuring processes. However, this study was done in slow cycles away from mass production in the laboratory setup. In this study, metal-plastic hybrid bonding experiments were carried out in 2 stages consisting of laser micro treatment of the metal surface and plastic injection process. After the injection process, the plastic is mechanically locked onto the processed surfaces.

Keywords: Laser assisted metal and plastic joining, Light weight, Plastic-metal joining.

Introduction

Usage of plastic and metal connections has a great potantial in the automotive industry in order to produce light weight vehicle body (Heckert & Zaeh,2014). A method called “overmolding” is generally used to join plastic and metals. the strength of the plastic part is improved by completely surrounding the metal. The aim of overmolding is to combine multiple plastic parts together in a seamless fashion to create a durable and uniform product (Paul et al., 2012). Plastic and metal can only be partially combined to each other due to their chemical and physical differences.

The bonding process or mechanical connection are also used in the joining of plastics and metals (Bergmann & Zaeh,2014). These connections usually require additional processes. Cost-up and increased process time issues are the main disadvantages of aformentioned processes. To overcome these problems, a promising approach has been developed by researchers in recent years. LAMP (Laser assisted Metal and Plastic Joining) method is preffered to join metal and plastics (Roesnera et al.,2011). On the other hand, it is foreseen that this method can

be used in direct joining of aluminum alloys and steel materials. Bimetallic corrosion, also called galvanic corrosion, occurs between aluminum and steel connections. Bimetallic corrosion can be prevented by combining the plastic component by sandwiching between different metal sheets with the LAMP method without additional parts or tools such as adhesives and rivets. In addition, this type of coupling provides design flexibility (Katayama & Kubata, 2007). This approach uses a two-step process. In the first processing step, the laser beam is used to create microstructures on the metal surface. In the second step, the plastic material is injected onto the metal with the plastic injection method and the plastic is mechanically locked into the microstructures. In addition to mechanical locking, a chemical bond is formed with the help of atomic diffusion (Katayama & Kubata, 2007; Roesnera et al.,2011).

In this study, method development studies were performed using LAMP in accordance with mass production speeds, starting from the laboratory level. Hybrid structures were obtained that can meet customer needs in automotive industry. Characterization and optimization of the connections were performed. A rapid beam movement was achieved with a galvometric scanning system that allows scanning of variable patterns on the metal surface. The surface treatment time was shortened. Mass production compared to traditional structuring processes.

Method

ST52 steel in 1.8 mm thickness and P6-6 GF30 plastic in 3 mm were used in this study. Hybrid joining process were performed by Ytterbium fiber laser. The laser is in Continuous Wave (CW) mode at 1070 nm wavelength. Laser beam profile is Gaussian with 1 cm diameter and it is in TEM_{00} mode. Single mode laser was used in the study. The hybrid joining process consists of 2 steps as shown in figure 1. Channels were processed on the metal surface at 400 micron intervals with the help of the experimental setup shown in Figure 2. Micro channel surface texturing studies were carried out with 7 different parameters are illustrated in Table 1.

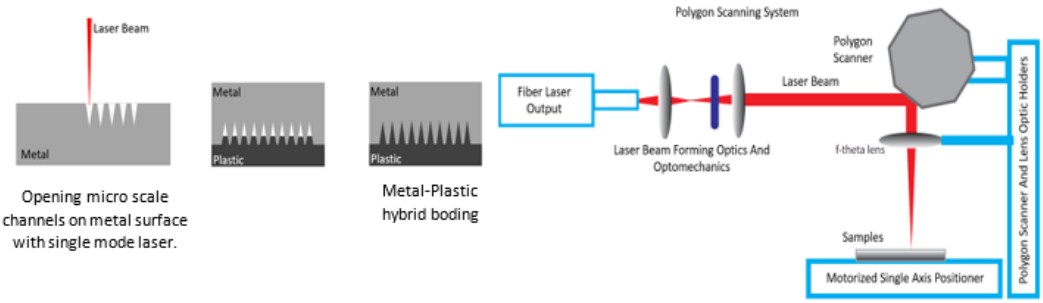

Figure 1. Hybrid joining process steps and experimental setup of polygon scaning system.

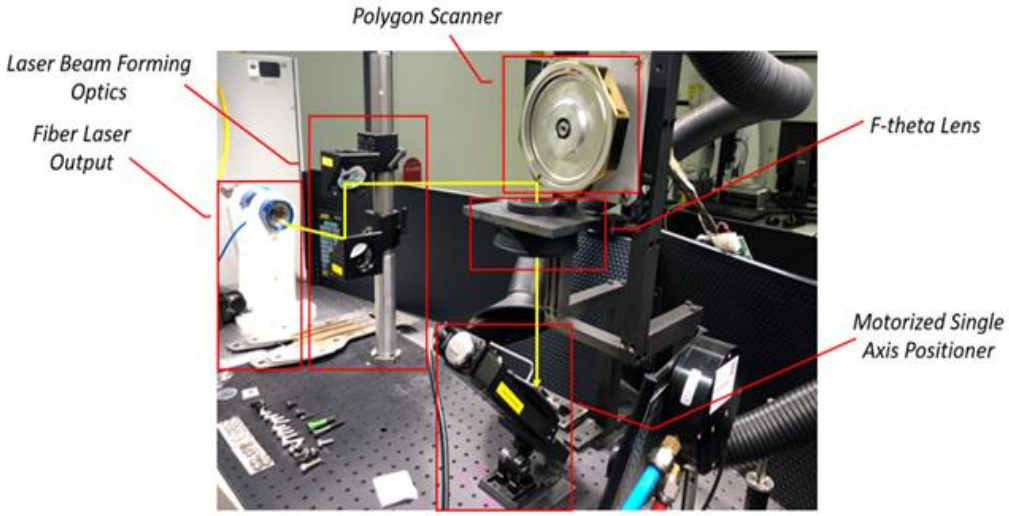

Figure 2. Laser assisted surface texturing experimental setup. In the experimental setup, the yellow arrow simulates the laser beam.

Table 1. Laser parameter matrix of laser surface structuring process.

Specimen Number	Lazer Power (W)	Polygon Speed (RPM)	Time (s)	Channel Angle (°)
S1	1500	3000	2	90
S2	2000	3000	1	90
S3	2000	3000	1,5	90
S4	2500	3000	1	90
S5	2500	3000	1,5	90
S6	2500	3000	3	90
S7	2000	3000	1,5	45

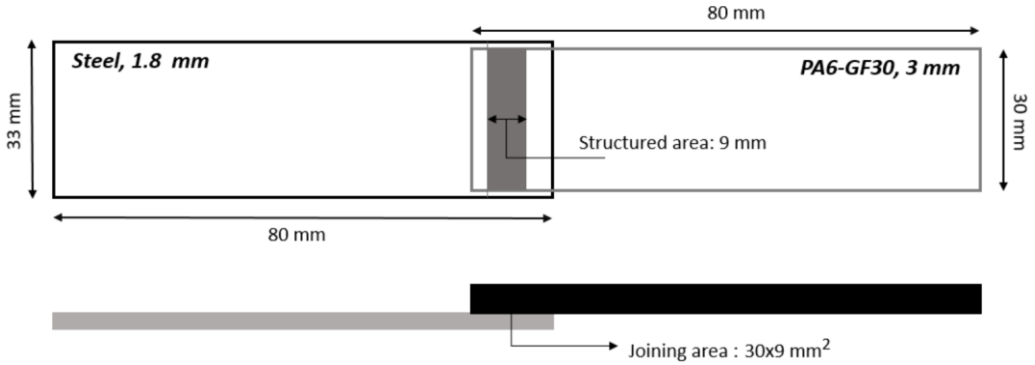

Figure 3. Tensile test specimens dimensions after plastic injection.

Tensile tests were performed at 50 kN capacity SHIMADZU equipment with 5 mm/min tensile speed rate at room temperature. The geometry of tensile test specimens after plastic injection was illustrated in Figure 3. Specimens were cut out by METKON METACUT 302 metallographic sensitive cutting equipment, and then were mold by METKON ECOPRESS 52 hot molding machine. The standard metallographic grinding and polishing were performed by METKON FORCIPOL 202 unit. Macro structural investigations were performed by Nikon SMZ745T optical microscope.

Results and Discussion

The width and depth ratios of the obtained non-angle channels were measured by optical microscope. Angled channels as well as the tensile specimens were selected considering the most appropriate depth, width ratios and channel geometries.

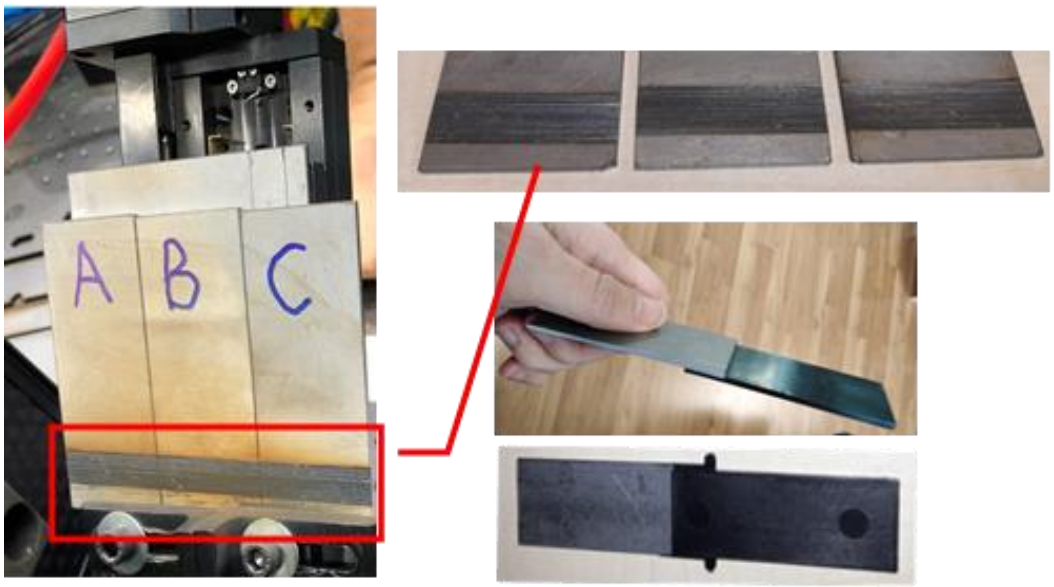

Figure 4. Surface-treated samples with channel structures and tensile test specimens (S6) and dimensions after plastic injection.

The channel geometries were determined by optical microscope using the laser parameters illustrated in Table 1. The channel depth increased with increasing laser power and/or processing time. Figure 4 shows the surface-treated specimens by laser with channel structures. Tensile test specimen geometry after plastic injection on S6 specimen was also depicted in Fig 4.

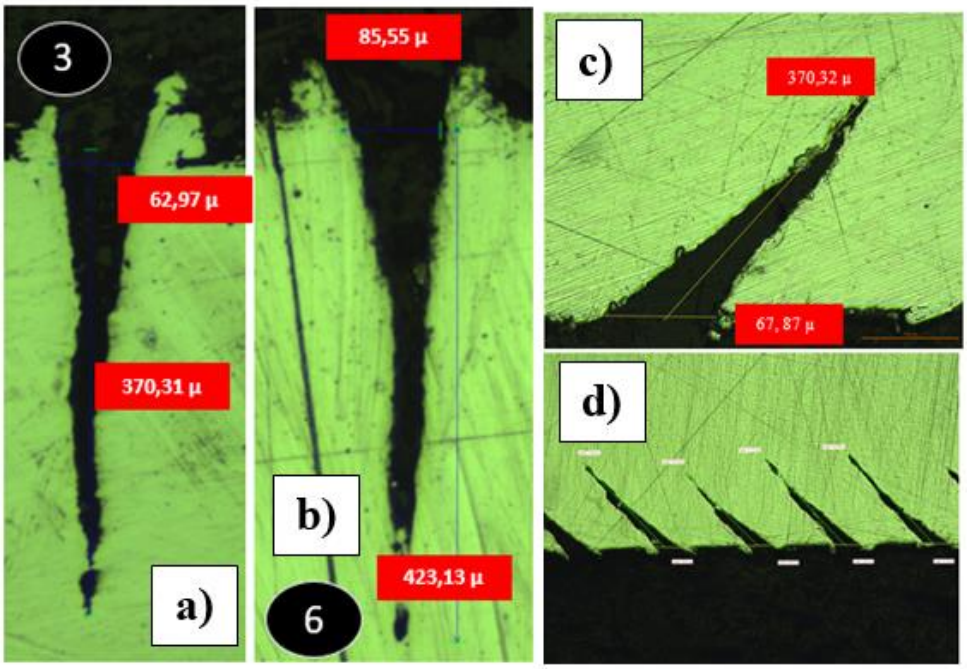

Figure 5. Macro images of metal specimens with surface textured at 0° and 45° angle; a) S3, b) S6, c) S7 and d) Cross section of S7.

Fig. 5 shows the macro section images of metal shet specimens with surface textured at 90° and 45° angle. The effect of laser power and process time on the channel geometry was also illustrated in Fig 5. It has been determined that the length and the width of the channel were increased, so the aspect ratio value was decreased.

The channel widths and depths formed on the sheet surfaces of the laser-textured samples are given in Table 2. Comparison of S1 and S2 shows that the aspect ratio increased with the increase in laser power. It has been determined that increasing the laser power in S4, S5 and S6 causes an increase in aspect ratio of S2 and S3. The aspect ratio and width-depth results of S3 and S6 showes that the channel depth increased with the increase in laser power and processing time, whereas the aspect ratio decreased as a result of the increase in channel width.

Table 2. Channel dimensions results after laser surface structuring process.

Specimen Number	Channel Edge Width (µm)	Channel Depth (µm)	Acpect Ratio (Depth/ Width)	Channel Angle (°)
S1	58,22	222,32	3,81	90
S2	55,84	276,94	4,95	90
S3	62,97	370,31	5,88	90
S4	48,71	286,45	5,88	90
S5	64,16	354,2	5,52	90
S6	85,55	423,13	4,94	90
S7	67,87	370,32	5,45	45

Tensile strength of S3, S6 and S7 specimens were obtained as ~12 MPa/mm^2, ~13 MPa/mm^2 and ~15 MPa/mm^2, respectively. It was concluded that the channel structures formed at an angle of 45 degrees to the surface in S7 with the S3 parameters increased the mechanical locking between metal and plastic. In Figure 6, the images of the broken parts of the S7 after the tensile test are shared. Fracture after tensile test in S3, S6 and S7 occurred by separating the plastic material from the channels as in Fig. 6

Figure 6. Image of broken parts from S7 specimen after tensile test.

Conclusions

The motivation point of the laser-assisted joining technique was chosen in the study. It is to develop an alternative joining technique that provides solutions to the problems of chemical compatibility, adhesion, bonding of dissimilar materials, curing problems of adhesives, extra surface applications required for adhesives, extended cycle times, and homogenization problems. The surfaces of metals formed with the laser method used in the study were functional and a part metal-plastic hybrid form was created with the back injection method to be used in plastic injection. The test results are summarized as follows:

- The relationship between the ratio of channel depth to mouth width and tensile test results play an important role to determine the optimum surface texture parameter.
- The joint strength of the S3 specimen with 90° channel geometry was obtained as 12.5 MPa/mm^2.
- The joint strength of the S6 specimen was obtained as 13.4 MPa/mm^2
- The joint strength of the S7 surface textured specimen with an angle of 45° was obtained as 15,6 MPa/mm^2
- The textured surface with a 45° angled channel structure has increased the bond strength between plastic and metal.

Scientific Ethics Declaration

The authors declare that the scientific ethical and legal responsibility of this article published in EPSTEM journal belongs to the authors.

Acknowledgements

* This article was presented as oral presentation at the International Conference on Basic Sciences, Engineering and Technology (www.icbaset.net) held in Marmaris/Turkey on April 27-30, 2023.

* The authors would like to thank, R. Taşdemir for the specimen preparation at Coşkunöz CKM R&D Center.

References

Bergmann, J.P., & Stambke, M. (2012). Potential of laser-manufactured polymer-metal hybrid joints. *Physics Procedia 39*, 84-91.

Heckert, A., & Zaeh, M. (2014). Laser surface pre-treatment of aluminium for hybrid Joints with glass fibre reinforced thermoplastics. *Physics Procedia, 56*, 1171 -1181.

Katayama, S., & Kubota, S. (2007). Laser-assisted metal and plastic joining. *Proc. of LANE 2007.*

Paul, H., Luke, M., & Henning, F. (2012). Evaluation of the joining mechanisms of polymer metal components. Proceedings of *ECC15 – 15th European Conference on Composite Materials.* Venice, Italy, 1-7

Roesnera, A., Scheik, S., Olowinskya, A., Gillnera, A., Reisgen, U., & Schleser, M. (2011). Laser assisted joining of plastic metal hybrids. *Physics Procedia 12*, 370–377.

Author Information

Mehtap Hıdıroglu
Coşkunöz CKM R&D Center
Bursa,Turkey
Contact e-mail: *mhidiroglu@coskunoz.com.tr*

Emre Erogul
Coşkunöz CKM R&D Center
Bursa,Turkey

Ramazan Ozluturk
Coşkunöz CKM R&D Center
Bursa,Turkey

Tanya A. Baser
Coşkunöz CKM R&D Center
Bursa,Turkey

To cite this article:

Hıdıroglu, M., Erogul, E., Ozluturk, R., & Baser, T.A. (2023). A study on single mode laser based plastic-metal joining process. *The Eurasia Proceedings of Science, Technology, Engineering & Mathematics (EPSTEM), 22,* 305-310.

The Eurasia Proceedings of Science, Technology, Engineering & Mathematics (EPSTEM)
ISSN: 2602-3199

The Eurasia Proceedings of Science, Technology, Engineering & Mathematics (EPSTEM), 2023

Volume 22, Pages 311-323

ICBASET 2023: International Conference on Basic Sciences, Engineering and Technology

Investigating the RSSI-based Distance Classification using Median Confidence Interval in a Multi-Device BLE Environment

Jille Anne R. VERANO
Mapúa University

Doreen Marie S. SORONGON
Mapúa University

Febus Reidj G. CRUZ
Mapúa University

Abstract: As the COVID-19 global pandemic occurred in 2020, there has been an increase in interest in using Received Signal Strength Indicator (RSSI) for strict implementations of social distancing. Bluetooth Low Energy (BLE) has been mainly used as an option for it is cost-effective and can be integrated with IoT for a wide range of applications. For a multiple-device BLE environment, the devices were calibrated, and parameters of the distance estimation were estimated using linear regression. For each device, RSSI values were acquired in various directions and distances. A confidence interval of 90% was used to create a prediction range for distance classification using the acquired RSSI. Using the range of median, BLE combinations at various distances and positions yield less than 50% of the data when classifying received RSSI values to distances of 1, 2, 3, and 4m. Irregularities from acquiring the RSSI value for various distances have been observed and can affect the classification of distance with the RSSI values. Further study is needed on other methods for the basis of interval range and minimization of irregularities.

Keywords: Social distancing, Bluetooth, Distance estimation, Confidence interval, Signal strength

Introduction

COVID-19 is an infectious disease that can spread from an infected person through small aerosols or large droplets discharged when they talk, cough or sneeze. It is mainly transmitted through respiratory discharges and can potentially spread on a large scale within communities. Due to this possibility, countries like the Philippines have declared a state of public health emergency to address concerns about its transmission. Monitoring and strict observation of regulation are physically and time demanding without the use of automation and robotics. Having tremendous access to a wireless network, sensors, and knowledge on machine learning, deep learning, and the internet of things (IoT), other studies explored various methods of reducing the transmission (Alsaeedy & Chong, 2020; Degadwala et al., 2020). Cellular networks, IoT devices for location tracking, contact, and symptom tracking, social distancing alert devices, and deep learning models for real-time monitoring are currently used risk detection methods (Alsaeedy & Chong, 2020; Degadwala et al., 2020). For establishments, several proposed automated systems ensure proper observation of social distancing. These systems primarily detect motion using image processing and background reduction to indicate human presence (Ahamad et al., 2020). Apart from this, several other detection algorithms exist, such as the pre-trained convolutional neural network (CNN) based models (Ahamad et al., 2020; Teles de Menezes et al., 2020). CNN-based models contribute to the automation filtering and feature extraction process of deep learning algorithms for object

detection and classification (Teles de Menezes et al. (2020). Several deep object detection algorithms such as You Only Look Once (YOLO), Single Shot Detector (SSD), Faster Region-based Convolutional Neural Network (Faster R-CNN), and Region-based Fully Convolutional Neural Network (R-FCN) were already studied for monitoring the adherence of the people to social distancing (Ahamad et al., 2020; Bhambani et al., 2020). Aside from the increasing interest in deep learning models as a monitoring system, IoT devices such as smart wearables have also been increasingly gaining attention in the field. IoT provides systems that are low-cost and user-friendly yet an excellent indicator of the adherence to preventive measures using ultrasound, magnetic fields, and Bluetooth Low Energy (BLE) as proximity sensors (Jeon et al., 2018; Stojanović et al., 2020). The use of AI systems and specific proximity sensors in IoT have certain limitations. With AI systems, although it provides high accuracy of proximity detection, the concern on the user's privacy arises as the exact location and appearance of the user can be observed (Bhambani et al., 2020; Jeon et al., 2018). Magnetic fields yield high accuracy and robustness; however, challenges to their portability, such as size minimization and low power design and privacy concerns, need further improvement (Bello, et al., 2020; Bian et al., 2020). The use of beacon technology in BLE allows proximity detection by using the contextual information generated by the beacons (Jeon et al., 2018; Lubis & Basari, 2020).

Emerging low power wireless technologies, such as BLE, have enabled dynamic wireless communication between devices and paved the way for IoT applications in automation, health, tracking, etc (Lubis & Basari, 2020; Polonelli et al., 2021). BLE is particularly suited to power-constrained applications, and its beacon technology offers efficient location-based services, which can be used in unmanned proximity-based applications (Jeon et al., 2018; Lubis & Basari, 2020; Polonelli et al., 2021). The neighbor discovery process (NDP) of BLE is used in proximity-based applications, where devices send information in the form of advertising packets over advertising channels to be discovered by scanners (Song et al., 2019). BLE architecture has several layers, including the Generic Access Profile (GAP), which provides different device roles such as a broadcaster, peripheral, observer, and central. BLE uses two modes of advertising PDU, one requiring an established connection and the other not requiring it (Ng et al., 2021). Moreover, proximity estimation relies on Received Signal Strength Indicator (RSSI), and filters are needed to increase its accuracy due to the factors affecting the RSSI's behavior (Cruz et al., 2018).While outdoor applications using filtered RSSI resulted in effective and efficient proximity tracking, the distance is inversely relative to the maximum distance for optimal functionality (Cruz, Garcia, et al., 2018).

Received Signal Strength Indicator (RSSI) is an indication of the power of the signal that is received from a transmitter. For distance estimation, a formula equation based on the power loss during signal propagation was used to acquire distance using transmitted power and RSSI (Amft et al., 2020; Zhang et al., 2016). Previous studies have used formulas that can estimate the distance between a transmitter and receiver using the Log-Distance Path Loss Model below: (Ivanic & Mezei, 2018; Jones et al., 2020; Onofre et al., 2016; Song et al., 2019; Tiwari et al., 2020; Zhang et al., 2016):

$$d = 10^{\left(\frac{(A-RSSI)}{10 \cdot n}\right)} \qquad (1)$$

Wherein the d is the estimated distance from the transmitter and receiver, A is the signal strength from a fixed distance of d from the transmitter and n is the path loss exponent depending on the surrounding environment. Due to the instability of RSSI, identification of the parameters in the estimation of distance varies on varying RSSI. Several studies have shown that by using known values of RSSI and its relative distance, unknown parameters such as the A and n can be acquired using the linear regression model (Ivanic & Mezei, 2018; Zhang et al., 2016). Furthermore, the model features a good distance estimation for a line-of-sight propagation (Ivanic & Mezei, 2018).

An ideal antenna radiates uniformly in all directions. However, it is not practically possible in real-life application as some antennas radiate more power in certain directions. For the antennas, the (RSSI) is the measure of the power of the radio signal received by an antenna. When the RSSI is not equal when measured at various directions, it means that the power of the received signal is not distributed equally in all directions. This non-uniform distribution of power is affected by various factors, including the performance and elevation of the antenna and the environmental conditions in which the signal is transmitted (Fang et al., 2010). Therefore, for ranging purposes, it is important to consider the non-isotropic nature of the RSSI and the factors that influence it.

In proximity detection, the data of RSSI is used to identify the user within the proximity range. However, local implementations of this, such as in a closed area, need further improvements on its proximity detection, signal

detection, and battery consumption (Lubis & Basari, 2020). Furthermore, beacon technology only employs one as transmitter and the other as the receiver with or without connection (Lubis & Basari, 2020). This technology is mostly employed for social distancing purposes. However, current BLE technology supports a dual role on a single device and therefore can be explored for device communication that does not require a connection. For most social distancing wearables, the device is only tested using the one device to one device set-up. A one device to many device set-up is more efficient to minimize the spreading of the COVID-19 disease within crowded places because this set-up limits close face-to-face contact with two or more people (Alhmiedat & Aborokbah, 2021).

Despite the increasing interest in the usage of BLE technology of ranging, there is lack of research conducted on ranging for multiple devices in an environment. This paper will include acquiring the RSSI around each transmitter and based on the acquired results, a distance classification was done using the confidence interval median. The paper investigates RSSI to distance matching using the created interval from confidence interval and the RSSI values of devices in a multi-device environment.

Method

Hardware Development

Figure 1 shows the overview schematic diagram of the wearable. The wearable would have the ESP32 module as its main component for processing and acquisition of the RSSI values. For the BLE configuration, devices would be configured as BLE broadcasters and observers. The configuration does not need to establish a connection to relay information from one another. The advertising packet of the broadcaster will be set to ADV_NONCONN_IND which does not allow connection requests and does not allow additional data to be advertised that is not included in the advertising packet. The advertising packet was configured to include the local device name, UUID, and TX power.

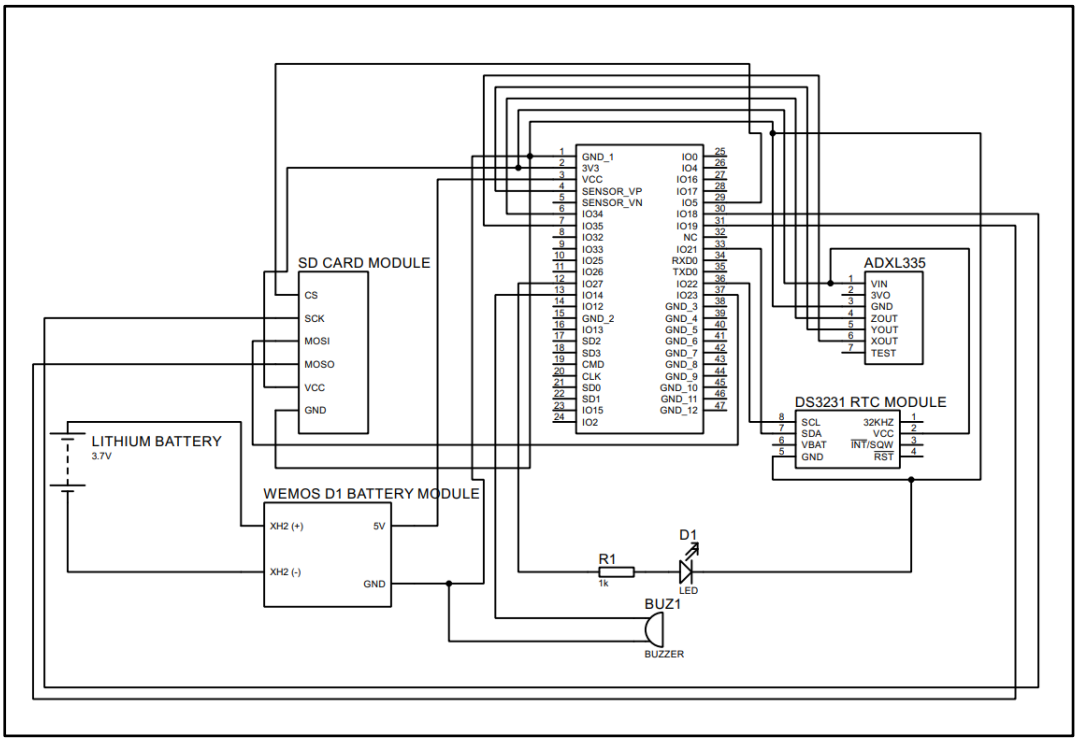

Figure 1. Schematic diagram of the hardware

RSSI Calibration and Parameter Estimation

Calibration is essential when dealing with RSSI that is susceptible to environmental interferences. According to a study (Fang et al., 2010), the RSSI value can be calibrated by means of acquiring the average deviation from the receivers. For the consistency of the power being transmitted from the transmitter for the 5 devices, 40

samples of raw RSSI values were measured at a fixed height and fixed distance of 1m direct line of sight from the transmitter using another receiving device. The five devices would take turns being the transmitter, and the acquired values would be compared to those obtained from an application that measures the RSSI in units of dBm. From the specification of the ESP32, the RSSI values acquired are in units of dBm. The average RSSI value from the application was then used to adjust the raw RSSI values. The difference between the raw RSSI with the RSSI from the application will be the offset values. For the estimation of the path loss model parameters at line of sight, different raw RSSI from different distances of 0.5, 1, 1.5, and 2m from a transmitter was acquired. Linear regression would then be applied to acquire the unknown parameters from the equation (1).

The linear regression has the equation,

$$y = mx + b \qquad (2)$$

During a signal propagation, the attenuation is expressed by the received power in the form of signal strength with the distance. From the given formula in a study (Zhang et al., 2016), this can be rearranged in the form,

$$P_d - P_{d0} = -10log(\frac{d}{d_{d0}}) \quad (3)$$

Where d is the distance between a transmitter and receiver, d0 is a fixed reference distance from the transmitter, Pd the signal strength at d and Pd0 is the signal strength at the reference distance. Letting the dependent variable y to be the signal strength, RSSI, and the independent variable x the log-distance,

$$y = P_d - P_{d0} \qquad (4)$$
$$x = log(\frac{d}{d_{d0}}) \qquad (5)$$

Then the m from the linear regression would then be,

$$m = -10n \qquad (6)$$

Acquiring the y and m from the linear regression analysis would be done to obtain an ideal value for A and n for the given environment.

RSSI Ranging and Matching

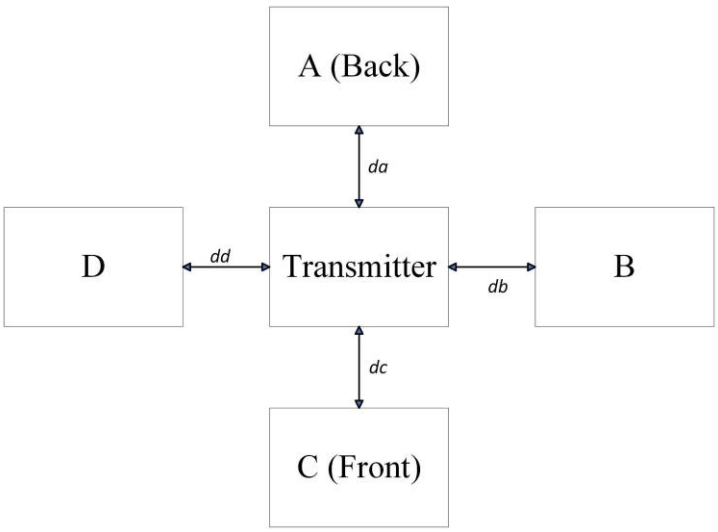

Figure 2. Location A, B, C, and D positions

The RSSI around each device being a transmitter was acquired. The considered locations for the placement of the receiver is shown in Figure 2 where location C is where the receiving device is at the front of the transmitting device, A is at the back, and B and D are at its sides. The *da*, *db*, *dc*, and *dd* correspond to the distances of the devices at positions A, B, C, and D respectively. For each device, RSSI values are stored onto

the SD card at various positions. The interval will be created from the acquired RSSI values from the five devices. For the matching of distance with the position, confidence interval is used to acquire the range in which a parameter, RSSI, of a population would most likely fall. In here, the range was acquired using the formula,

$$NQ \pm z\sqrt{NQ(1-Q)} \qquad (7)$$

Wherein N is the sample size, Q is 0.5 for median (quantile interest), and z the z-critical value. From the data, the N has the value of 205 and 90% confidence would be used where the z = 2.58. The range for the various distances from the transmitter at position A, B, C, and D is shown in Table 2.

Results and Discussion

Figure 3 represents the RSSI values at position A within distances 1m, 2m, 3m, and 4m from each device. For the 1m distance, the highest median RSSI value is at device 2. As for the distances 2m, 3m, and 4m, the highest median value of the RSSI was device 1. Although it can be observed that there are existing differences in the RSSI median values between each device, the median of each device in various distances is also observed to be like one another when looking at each box at different devices at position A. In addition the IQR or the Interquartile Range of the RSSI values is observed to be narrow. The interpretation is that the RSSI values were not spread and relatively towards a narrow range when measured at position A.

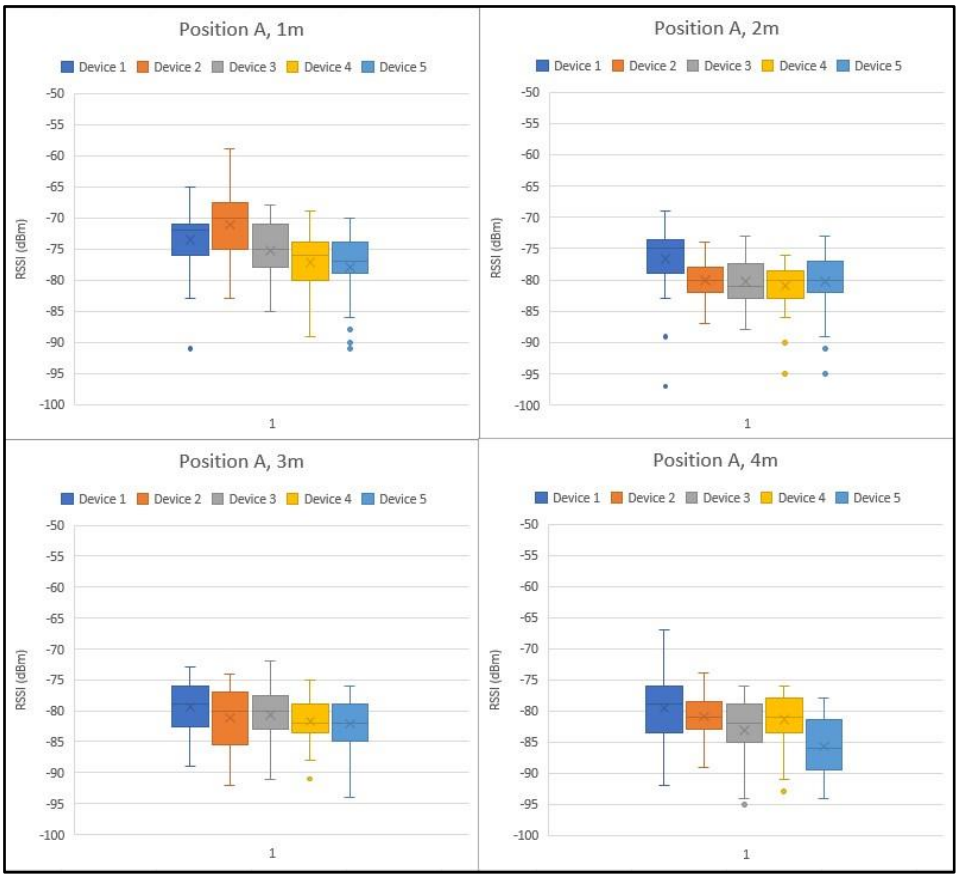

Figure 3. Box plot of RSSI values at position A

On the other hand, additional observations of the differences from the graph for the different devices for position B shown in figures 4, at 1m, devices 2-5 shared relative median RSSI values. As for 2m, the median RSSI values vary from one another for the devices except for device 3 and device 5 which remained close to one another. At 3m, the group of devices are resulted to have relative RSSI median values, such as for device 2 and device 4, and devices 1, 3, and 4. At 4m, the same behavior of the RSSI median values was observed, except for device 1 which had an entirely different RSSI median value when compared to other devices. With this, it can be observed that the devices at some distance can either have relative or non-relative values of the RSSI median. Moreover, the lengths of the box are not similar which means that the RSSI of some devices are highly variable.

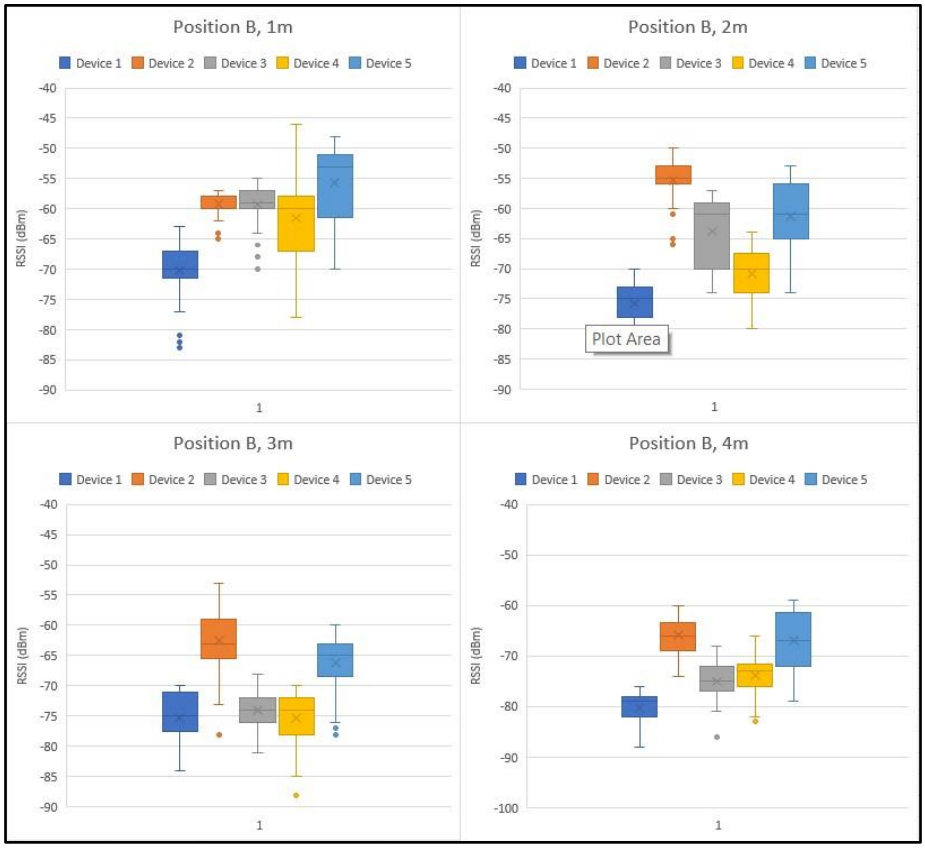

Figure 4. Box plot of RSSI values at position B

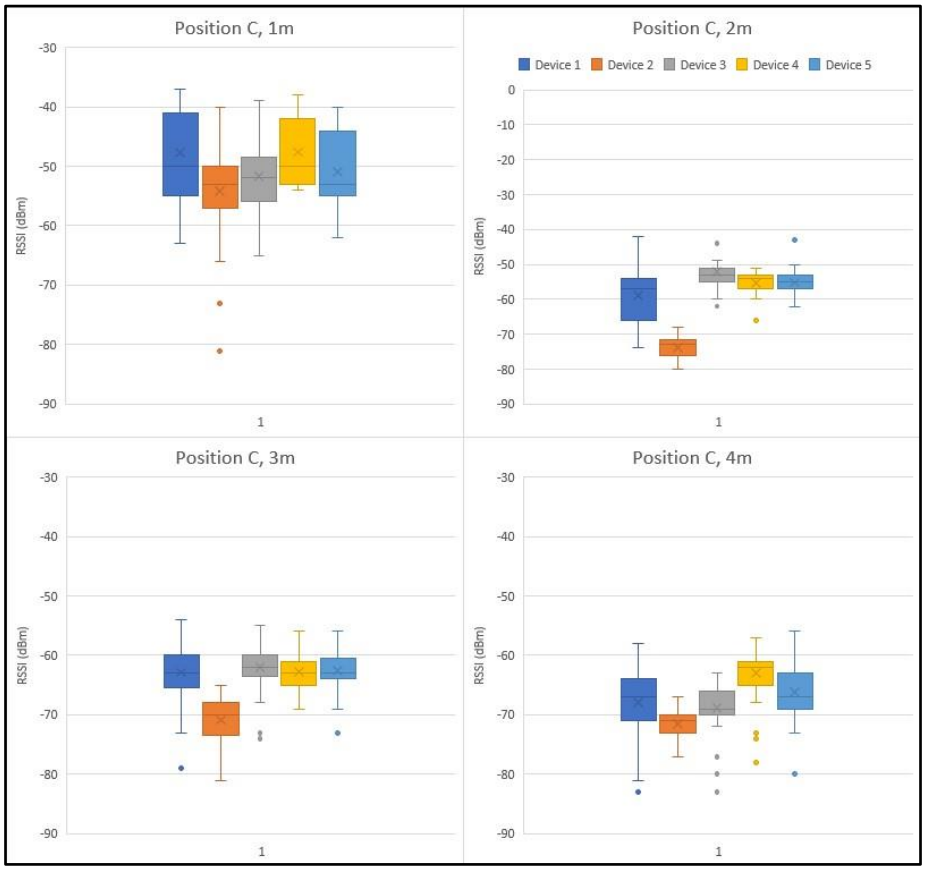

Figure 5. Box plot of RSSI values at position C

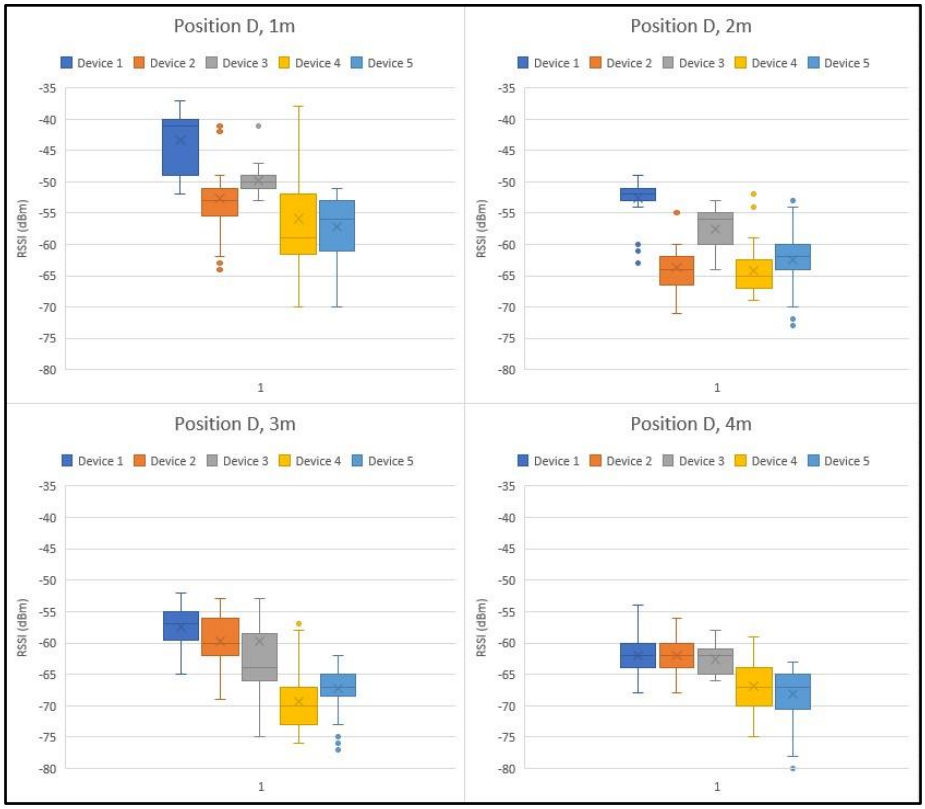

Figure 6. Box plot of RSSI values at position D

The median RSSI values at 1m are close to one another when looking at figure 5. However, comparing the box plot length in position A, a distinction between the two can be observed. Some box plots are not narrow as observed for devices 1, 4, and 5 in which the RSSI values from these devices at position C have large variability when compared to devices 2 and 3. Moreover, aside from distance 1, the RSSI median value from device 2 is not close to the median of other devices. Not only at position C but also in position D, show in figure 6, that highly variable RSSI values are observed for distance at 1m and 2m from the transmitter. Close median values of RSSI are only observed at 4m for position D.

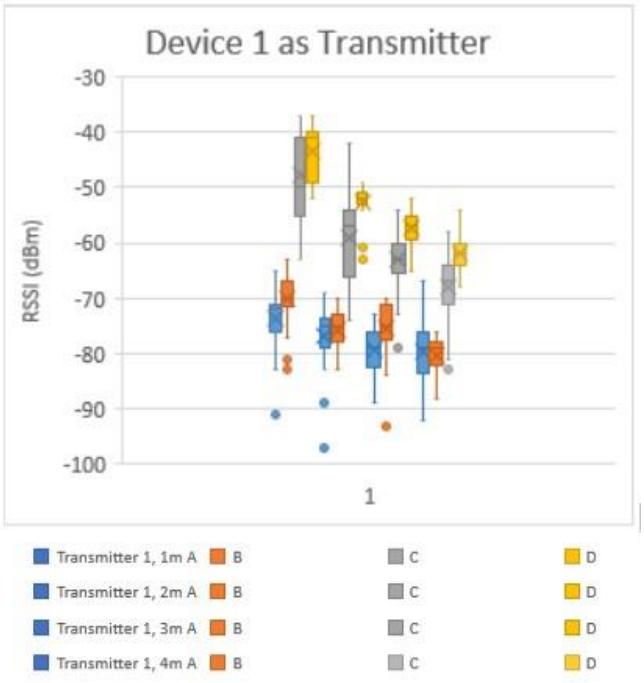

Figure 7. RSSI values from transmitter device 1.

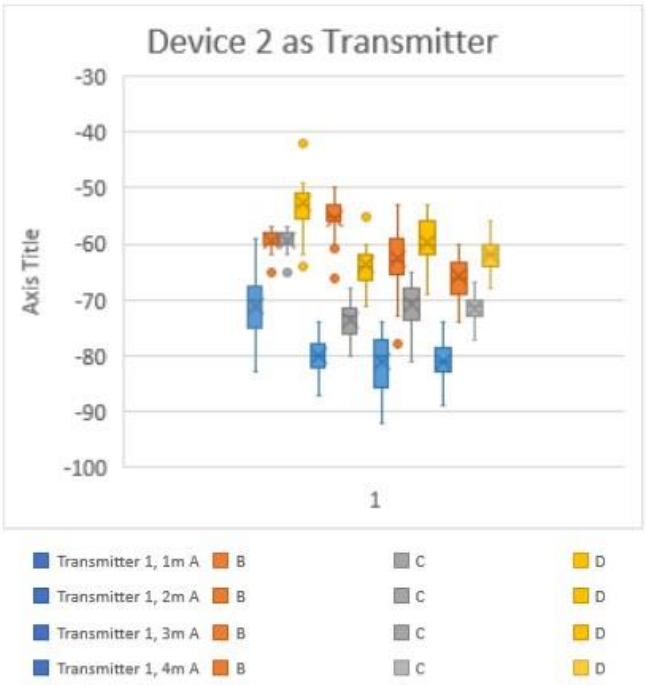

Figure 8. RSSI values from transmitter device 2.

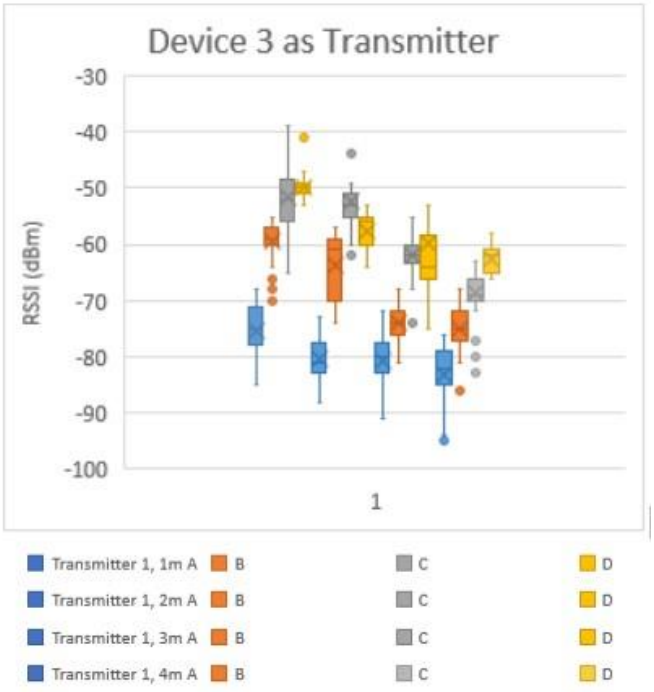

Figure 9. RSSI values from transmitter device 3.

The signal strength from the 5 devices figure 7, 8, 9, 10 and 11 shows the relationship between distance. Based on the trend of the graph, the relationship between the distance and signal strength can be observed where RSSI values at farther distances have lower RSSI values compared to near distance such as 1m. In signal propagation, attenuation is experienced due to the presence of external factors which results in loss of energy and low signal strength values received by the devices. This characteristic of signal can be observed on the acquired RSSI values where the median of the RSSI keeps decreasing as the distance from the transmitter changes from 1 to 4m for some devices. However, some devices do not exhibit the trend and can be due to the factors that influence the RSSI.

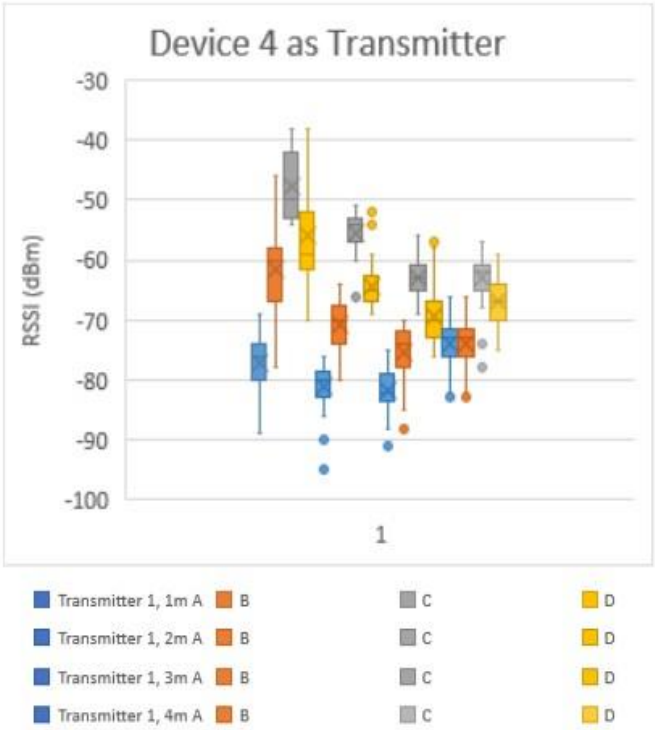

Figure 10. RSSI values from transmitter device 4.

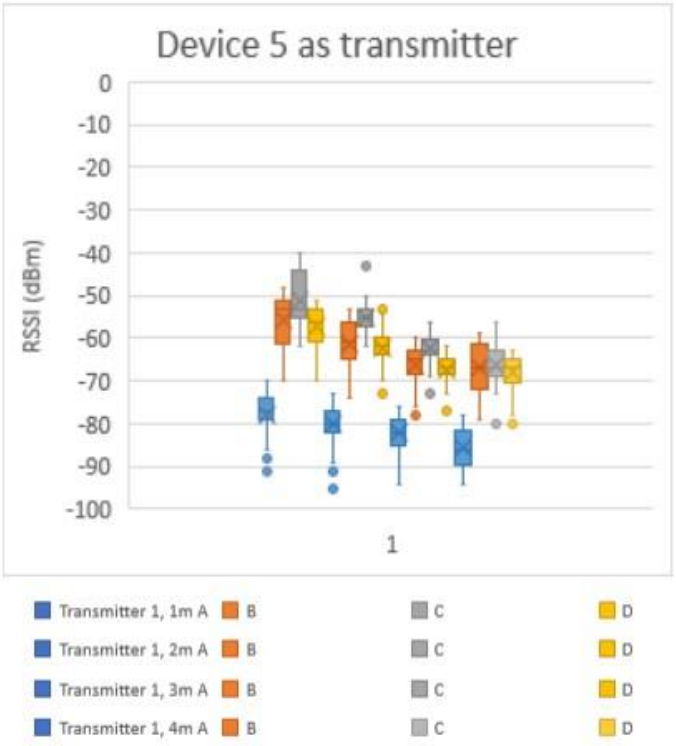

Figure 11. RSSI values from transmitter device 5.

Overall, some RSSI values acquired by the devices are highly variable at some distances. The variability observed from the set of data acquired can be due to the uncontrolled conditions such as environmental factors or factors present in the hardware such as lack of calibration of the battery level voltage of the different devices. In a study (Mitralexis & Goumopoulos, 2015), one factor that can affect the signal strength is the battery level of the device. Decreasing the battery level affects the signal strength, a weaker signal strength is received from the transmitter (Mitralexis & Goumopoulos, 2015). Therefore, a constant supply of power to the module is crucial to the usage of an RF module.

RSSI Matching based on Position

The relationship between the RSSI and distance can be observed from the combined received RSSI values at various positions as shown in Figure 12 and 13. At the various positions, observations are made by using measures of central tendency such as the median or mean to describe the RSSI values. In Figure 12 and 13, a sharp drop on the RSSI values can be observed in position B using the mean as the measure. At position C, the RSSI values are much lower compared to the D RSSI values for distance 3 and 4m. The sharp drop if RSSI values for position B can be due to the lower acquired RSSI values of Device 1 as shown in Figure 4 compared to the other devices. For low RSSI values at position C for distances 3 and 4m, this can be due to the RSSI values acquired by Device 2 where the RSSI values were close to a lower median value for all distances except at 1m shown in Figure 5.

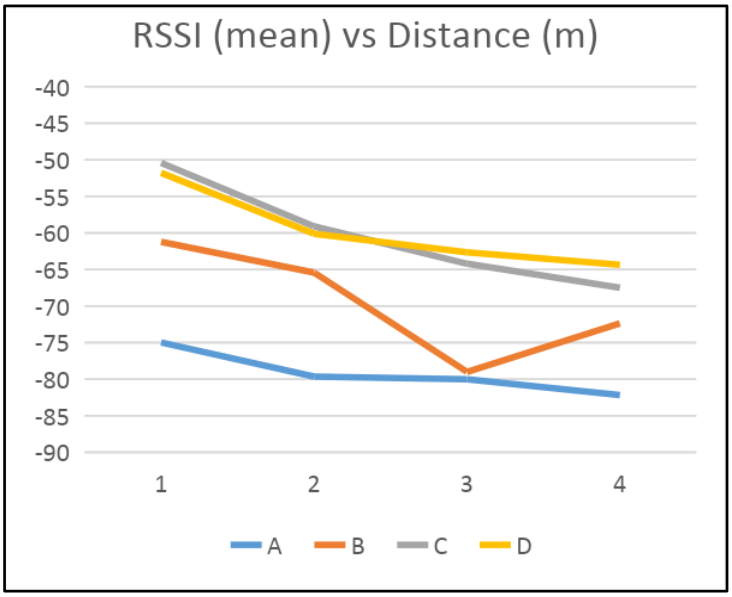

Figure 12. RSSI (mean) vs Distance at various positions

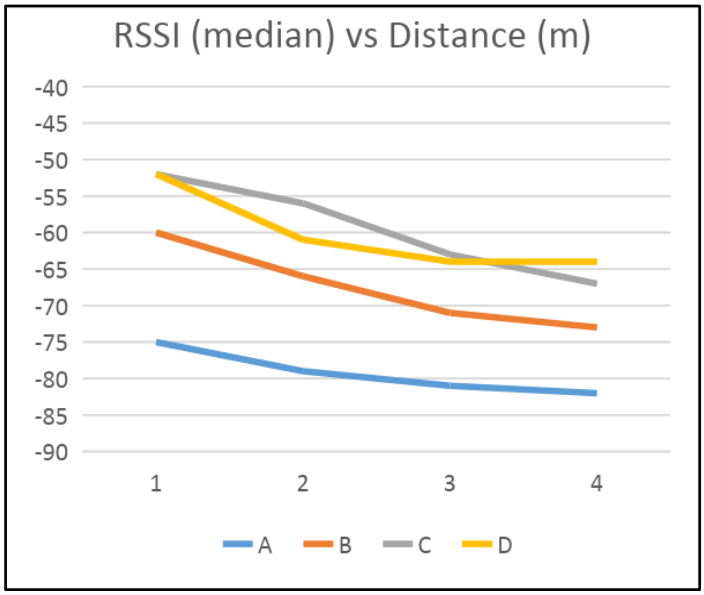

Figure 13. RSSI (median) vs Distance at various positions

RSSI (median) and RSSI (mean) have a similar trend shown, however, the graph of the RSSI (median) produces a much smoother line compared to RSSI (mean). The difference can be due to the nature of the RSSI where it is susceptible to influences and it is highly variable when there are presence of outliers in the gathered data. From the data acquired, the distinction can be due to the suspected potential outliers found from the data. Therefore, representation of the RSSI values that are not susceptible outliers can be achieved by using RSSI (median).

Table 1. Interval for various positions and distances

Position	Distance	Lower bound	Upper bound
A	1	-76	-74
	2	-80	-79
	3	-82	-79
	4	-83	-81
B	1	-60	-59
	2	-69	-63
	3	-73	-71
	4	-74	-72
C	1	-53	-51
	2	-57	-55
	3	-65	-63
	4	-69	-66
D	1	-53	-51
	2	-62	-60
	3	-65	-62
	4	-65	-63

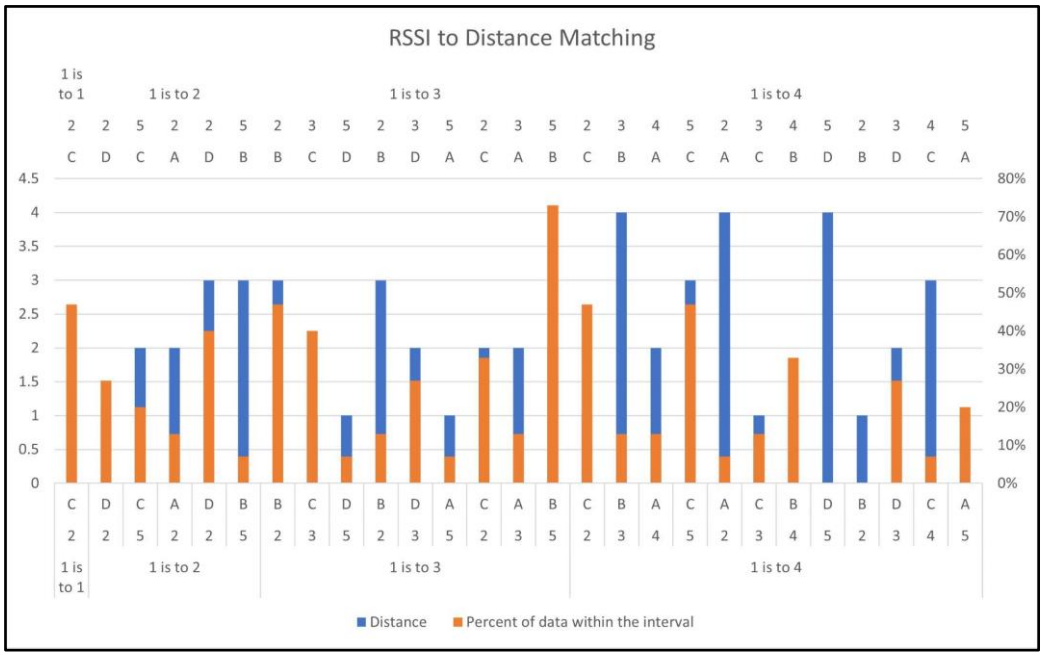

Figure 14. Percent of RSSI data within the interval

The acquired range using the confidence interval was then used to the acquired raw RSSI values from various distances and positions. Table 1 shows the various combinations of the devices where aside from the position and distance, the number of devices within the perimeter was also considered. For most of the combinations, the data falls less than 50% using the created range as shown in Figure 14. The created range was formed using the initial RSSI observations from the five devices. The low percentage from the various combinations can be due to the reliance on the individual performances of the devices, the RSSI data it gathered. As aforementioned, irregularities on the RSSI values on some of the devices were observed. The formation of irregularities can be from uncontrolled factors that affect the signal strength such as the battery level and environmental interference. It can also be due to the method used in creating the range where other methods can be considered for solving the confidence interval. Exploring improvements on the gathered data or range for it was compared might improve the matching of RSSI values to the various distances.

Conclusion

In real-life applications, antennas radiate more to certain directions than others. Observations with multiple devices in the environment show variations on the RSSI transmitted with the other devices. Using a confidence

interval-median, most of the BLE combinations have less than 50 % of the data fall within the interval. The resulting low percentage might be due to the irregularities observed from the devices. Other factors affecting RSSI should be considered and controlled as it can improve the use of the prediction range when estimating the distance.

Recommendations

The future researchers recommended to perform much stricter calibration of the devices and consider more factors that influence the RSSI. In addition, exploring other methods of creating the confidence interval range might improve the distance classification.

Scientific Ethics Declaration

The authors declare that the scientific ethical and legal responsibility of this article published in EPSTEM journal belongs to the authors.

Acknowledgements or Notes

* This article was presented as an oral presentation at the International Conference on Basic Sciences, Engineering and Technology (www.icbaset.net) held in Marmaris/Turkey on April 27-30, 2023.

*The researchers would like to express their sincerest gratitude to the Lord for providing them with faith, wisdom, strength, and guidance throughout the making of their research. To their thesis adviser, Engr. Febus Reidj Cruz, for his invaluable encouragement and expertise in every step of the completion of this paper. The researchers would also wish to thank their family and friends for their unconditional support, understanding, and patience which kept the researchers going even during the toughest challenges through the research process.

References

Ahamad, A. H., Zaini, N., & Latip, M. F. A. (2020, August). Person detection for social distancing and safety violation alert based on segmented ROI. In *2020 10th IEEE International Conference on Control System, Computing and Engineering* (ICCSCE) (pp. 113-118). IEEE.

Alhmiedat, T., & Aborokbah, M. (2021). Social distance monitoring approach using wearable smart tags. *Electronics*, *10*(19), 2435.

Alsaeedy, A. A. R., & Chong, E. K. P. (2020). Detecting regions at risk for spreading COVID-19 using existing cellular wireless network functionalities. *IEEE Open Journal of Engineering in Medicine and Biology*, *1*, 187–189.

Amft, O., Lopera, L., Lukowicz, P., Bian, S., Burggraf, P., Amft, O., & Laerhoven, K. V. (2020). Wearables to fight covid-19: From symptom tracking to contact tracing. *IEEE Pervasive Computing*, *19*(4), 53–60.

Bhambani, K., Jain, T., & Sultanpure, K. A. (2020). Real-time face mask and social distancing violation detection system using YOLO. *IEEE Xplore.*

Bian, S., Zhou, B., Bello, H., & Lukowicz, P. (2020). A wearable magnetic field based proximity sensing system for monitoring COVID-19 social distancing. *Proceedings of the 2020 International Symposium on Wearable Computers.*

Bian, S., Zhou, B., & Lukowicz, P. (2020). Social distance monitor with a wearable magnetic field proximity sensor. *Sensors*, *20*(18), 5101.

Cruz, J. C. D., Cruz, F. R. G., Sese, J., Borbon, M. D., Cacayuran, A. G., Rea, K. D., & Gammad, J. R. (2018). Faculty monitoring system with mobile application using received signal strength indication. *2018 IEEE 10th International Conference on Humanoid, Nanotechnology, Information Technology, Communication and Control, Environment and Management (HNICEM).*

Cruz, J. C. D., Garcia, R. G., Garcia, A. J. G., Manalo, K. A. A., Nworgu, V. I., & Payumo, J. B. M. (2018). Proximity tracker using received signal strength, particle filter and extended Kalman Filter. *2018 IEEE 10th International Conference on Humanoid, Nanotechnology, Information Technology, Communication and Control, Environment and Management (HNICEM).*

Degadwala, S., Vyas, D., Dave, H., & Mahajan, A. (2020). Visual social Ddstance alert system using computer vision & deep learning. *2020 4th International Conference on Electronics, Communication and Aerospace Technology (ICECA).*

ESPRESSIF. (2023). GAP API - ESP32 - — ESP-IDF programming guide v5.0.1 documentation. Docs.espressif.com.

Fang, Z., Zhao, Z., Geng, D., Xuan, Y., Du, L., & Cui, X. (2010). RSSI variability characterization and calibration method in wireless sensor network. *The 2010 IEEE International Conference on Information and Automation.*

Ivanic, M., & Mezei, I. (2018). Distance estimation based on RSSI improvements of orientation aware nodes. In *2018 Zooming innovation in consumer technologies conference (ZINC) (pp. 140-143). IEEE.*

Jeon, K. E., She, J., Soonsawad, P., & Ng, P. C. (2018). BLE beacons for internet of things applications: Survey, challenges, and opportunities. *IEEE Internet of Things Journal, 5*(2), 811–828.

Jones, N. R., Qureshi, Z. U., Temple, R. J., Larwood, J. P. J., Greenhalgh, T., & Bourouiba, L. (2020). Two metres or one: what is the evidence for physical distancing in Covid-19? *BMJ,* 370. doi: https://doi.org/10.1136/bmj.m3223

Lubis, A. F., & Basari. (2020). Proximity-based covid-19 contact tracing system devices for locally problems solution. *2020 3rd International Seminar on Research of Information Technology and Intelligent Systems (ISRITI).*

Mitralexis, G., & Goumopoulos, C. (2015). Web based monitoring and irrigation system with energy autonomous wireless sensor network for precision agriculture. *Lecture Notes in Computer Science,* 361–370.

Ng, P. C., Spachos, P., & N. Plataniotis, K. (2021). COVID-19 and your smartphone: BLE-based smart contact tracing. *IEEE Systems Journal,* 1–12.

Onofre, S., Silvestre, P. M., Pimentao, J. P., & Sousa, P. (2016). Surpassing bluetooth low energy limitations on distance determination. *2016 IEEE International Power Electronics and Motion Control Conference (PEMC).*

Polonelli, T., Schulthess, L., Mayer, P., Magno, M., & Benini, L. (2021). H-Watch: An open, connected platform for AI-Enhanced covid-19 infection symptoms monitoring and contact tracing. *2021 IEEE International Symposium on Circuits and Systems (ISCAS).*

Song, S. W., Lee, Y. S., Imdad, F., Niaz, M. T., & Kim, H. S. (2019). Efficient advertiser discovery in Bluetooth low energy devices. *Energies*, *12*(9), 1707.

Stojanović, R., Škraba, A., & Lutovac, B. (2020). A headset like wearable device to track Covid-19 symptoms. *IEEE Xplore*.

Teles de Menezes, R. S., Magalhaes, R. M., & Maia, H. (2020). Object recognition using convolutional neural networks. *Recent Trends in Artificial Neural Networks - from Training to Prediction.*

Tiwari, K. R., Singhal, I., & Mittal, A. (2020). Smart social distancing solution using bluetooth® low energy. *5th International Conference on Computing, Communication and Security (ICCCS).*

Zhang, K., Zhang, Y., & Wan, S. (2016). Research of RSSI indoor ranging algorithm based on Gaussian - Kalman linear filtering. *2016 IEEE Advanced Information Management, Communicates, Electronic and Automation Control Conference (IMCEC).*

Author Information

Jille Anne R. Verano
Mapúa University
Manila, Philippines
jarverano@mymail.mapua.edu.ph

Doreen Marie S. Sorongon
Mapúa University
Manila, Philippines

Febus Reidj G. Cruz
Mapúa University
Manila, Philippines

To cite this article:

Verano, J.A.R., Sorongon, D.M.S. & Cruz, F.R.G. (2023). Investigating the RSSI-based distance classification using median confidence interval in a multi-device BLE environment. *The Eurasia Proceedings of Science, Technology, Engineering & Mathematics (EPSTEM), 22,* 311-323.

The Eurasia Proceedings of Science, Technology, Engineering & Mathematics (EPSTEM)
ISSN: 2602-3199

The Eurasia Proceedings of Science, Technology, Engineering & Mathematics (EPSTEM), 2023

Volume 22, Pages 324-329

ICBASET 2023: International Conference on Basic Sciences, Engineering and Technology

Design of Sinus Flow Filters

Nilsu PARLAKYILDIZ
TIMEX-FTS Filtration Treatment Systems

Neset TAS
TIMEX-FTS Filtration Treatment Systems

Abstract: Based on the service reports received from agricultural irrigation companies are analysed, 2 major problems in this field stand out. First one is the damage caused by the insoluble organic and inorganic particles in the water supplied from the water source to the irrigation pipeline and the control equipment on it, and as a result, the irrigation efficiency decreases. The second problem is that the filters with different filtration degrees used to solve the first problem cause to consume a lot of energy during operation and increase the operation& maintenance costs and narrow the usage area. Separate products in different filtration degrees offered for the first problem caused the second problem, so another alternative way had to be found for a permanent solution. For this purpose, our company has designed and manufactured SinusFlow filters which is a compact product with a double stage with single motor that combines different filtration degrees in a single product with a quick manufacturing center. As a result of development of this new product, 2 different (coarse & fine) type of filters combine in a single filter. In this way, while the filtering process is carried out with a single motor with much less energy consumption, the usage area and operation & maintenance costs have been reduced.

Keywords: Filtration, Water, Agricultural irrigation

Introduction

Industrial filters are used in the field of agricultural irrigation, especially in the recent years. In order to increase the filtration efficiency in these areas and to maximize the usage area, the designs of the filters are still being developed. TIMEX is a company that has been designing and manufacturing industrial filters for agricultural irrigation since 30 years. When the technical service reports from all customers in this field are evaluated, 1 major problem stands out. This problem is that the filtration efficiency decreases as a result of the clogging of single strainer filters in a very short time due to the insoluble particles of very different particle size in the source waters used in these areas and these filters require very frequent maintenance. In order to solve this problem, our company has been designed as separate products with coarse and fine strainers for agricultural irrigation areas and integrated into the irrigation systems.

However, this situation both limited the usage area in the field and caused an excessive increase in energy consumption and expenses in the field. Upon this, our company started R&D studies and decided to realise the idea of combining 2 strainers with different microns in a single pressure vessel. Upon this, firstly, tests were conducted in laboratories with the samples taken from the fields (Landa et al., 1997). It was decided which filtration degrees were required for which sites. Then design works started. After the design calculations were completed, the production process was started and the first products were produced.

Method

The design of the related product was made according to ASME Sec VIII Div. 1 standard. The solid model has been created using Autodesk Inventor software. Solid model photos are available below (Figure 1, Figure 2, Figure 3, Figure 4).

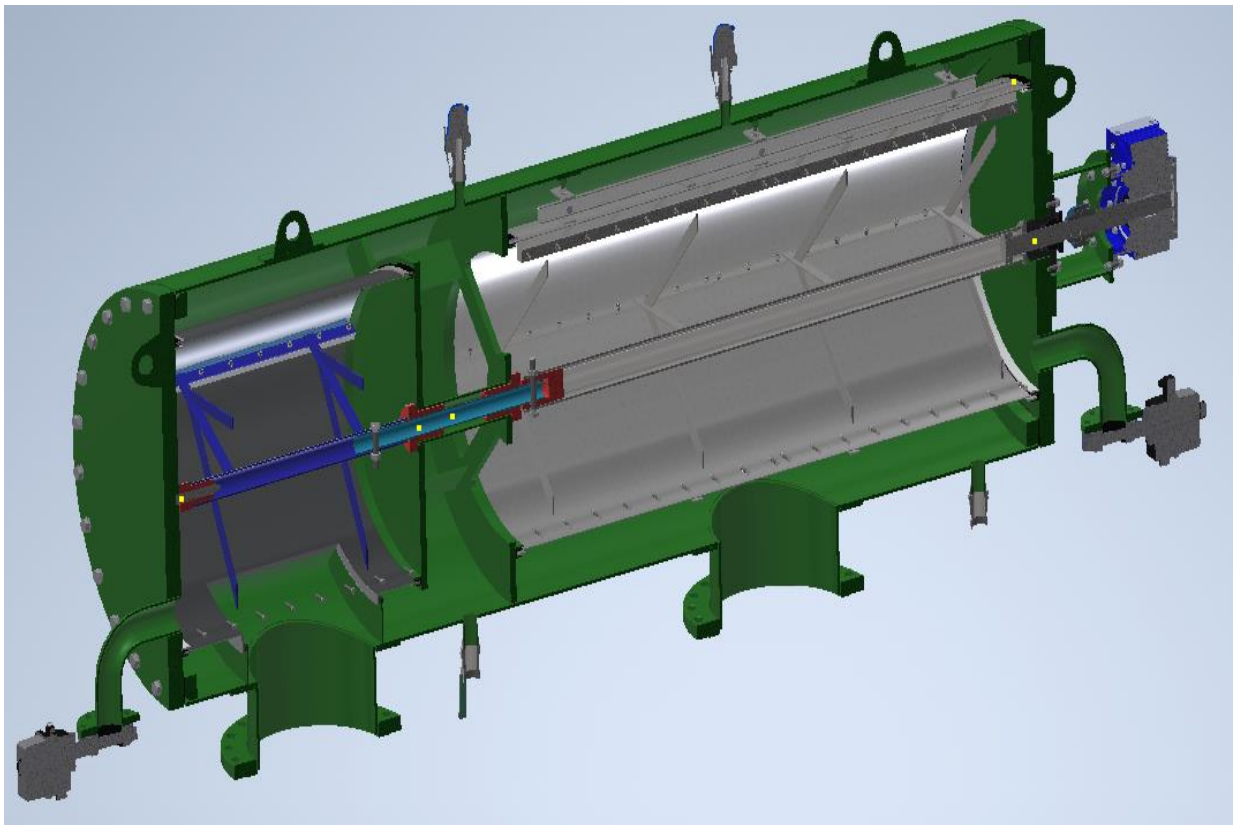

Figure 1. Section view of the sinus flow filter

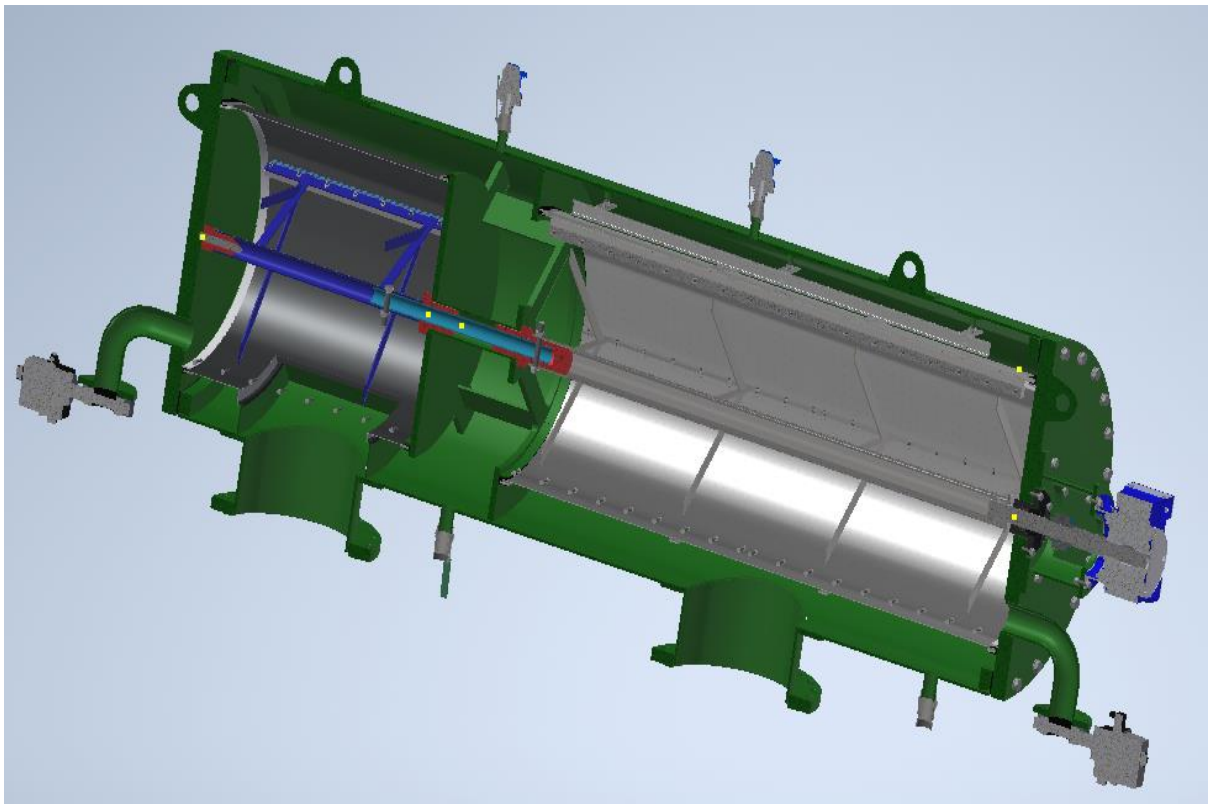

Figure 2. Section view of the sinus flow filter

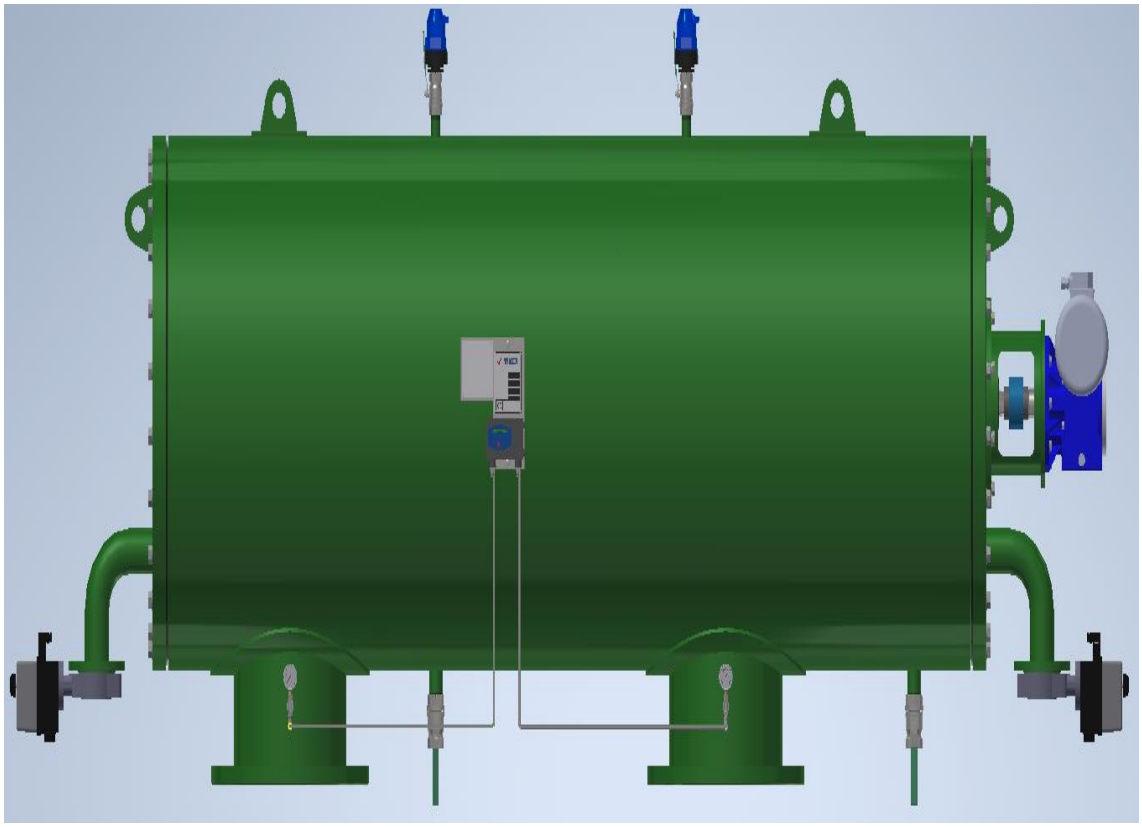

Figure 3. 3D Model of the sinus flow filter

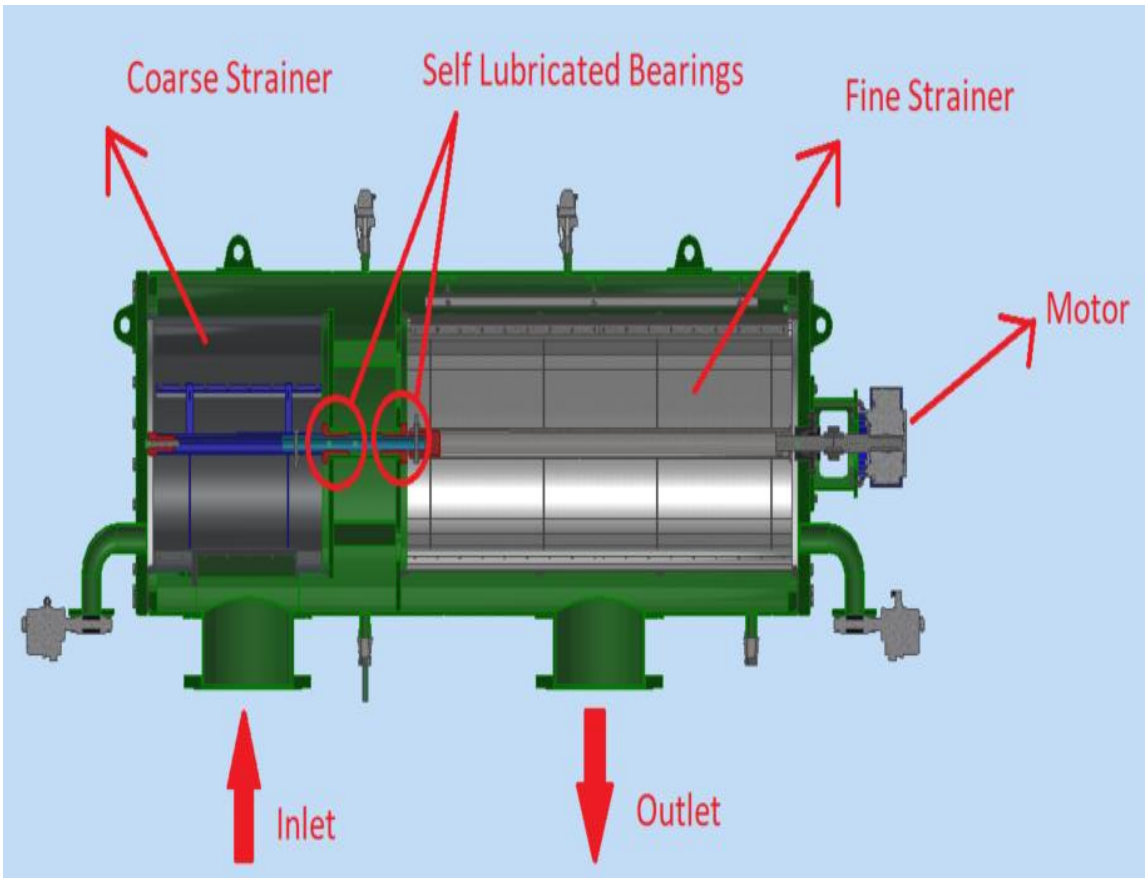

Figure 4. Section view of the sinus flow filter

As can be seen in the drawings above, a total of 2 strainers, coarse and fine, are placed in parallel in the pressure vessel. Since the sealing of fine strainer is very important, the centering of the strainer must be precise. In order to achieve this, it was decided to use rail mechanism and the centering was done in the most accurate way with this system. Another consideration while designing is to increase the velocity of the water by narrowing the area in the transition from coarse filter to fine filter, so that the particles adhere more homogeneously to the inner surface of the screen and the inner surface area is used more efficiently. Thus, it is aimed to increase filtration efficiency. In order to provide sinus flow (Kehrein, 2001), plates between two sieves were used. Other purpose of this plate is firstly to provide space for the sealing equipments to fix and to ensure the centering of the shaft.

It is aimed to maximise energy saving with this new design by a single motor instead of 2 motors. In addition to the transition from a 2-motor system to a single motor, the fact that the two-way motor movement is reduced to a single direction with the collector design made in such a way that the nozzles do not need to move horizontally is also considered for energy saving. Another expected benefit of the design of Sinus Flow filters is the compact design, which increases the usage area of the field.

Results and Discussion

The completed products were integrated into agricultural irrigation areas. (Figure 5, Figure 6, Figure 7). According to the user reports sent to us, the major results can be summarized as follows. Firstly, energy consumption in the field has decreased by 30% through this new design with a single motor. Secondly, the maintenance period of the filters is delayed with the Sinus Flow and therefore the maintenance periods are prolonged. Lastly, the usage area has increased greatly with these compact filters installed instead of many industrial filters of different micron grades used in the old systems to do the same job.

Figure 5. Sinus flow filters from agricultural field

Figure 6. Sinus flow filters from agricultural field

Figure 7. Sinus flow filters from agricultural field

Conclusion

In this article, the design of a new product for the solution of user problems based on reports from agricultural irrigation areas is discussed. To conclude, the new designed Sinus Flow filters have achieved the purpose and user problems received from the site have been solved.

Scientific Ethics Declaration

The authors declare that the scientific ethical and legal responsibility of this article published in EPSTEM journal belongs to the authors.

Acknowledgements or Notes

* This article was presented as oral presentation at the International Conference on Basic Sciences, Engineering and Technology (www.icbaset.net) held in Marmaris/Turkey on April 27-30, 2023.

References

Kehrein, S. (2001). Flow equation approach to the sine-Gordon model. *Nuclear Physics B, 592*(3), 512-562.

Landa, H., Capella, A., & Jiménez, B. (1997). Particle size distribution in an efluent from an advanced primary treatment and its removal during filtration. *Water Science and Technology, 36*(4), 159-165.

Author Information

Nilsu Parlakyildiz
TIMEX-FTS Filtration Treatment Systems
ASO 2 OSB. 2036. Street No:12 Sincan
Ankara/TURKEY
Contact e-mail: nilsu@timex.com.tr

Neşet Taş
TIMEX-FTS Filtration Treatment Systems
ASO 2 OSB. 2036. Street No:12 Sincan
Ankara/TURKEY

To cite this article:

Parlakyildiz, N. & Tas, N. (2023). Design of sinus flow filters. *The Eurasia Proceedings of Science, Technology, Engineering & Mathematics (EPSTEM), 22,* 324-329.

The Eurasia Proceedings of Science, Technology, Engineering & Mathematics (EPSTEM)
ISSN: 2602-3199

The Eurasia Proceedings of Science, Technology, Engineering & Mathematics (EPSTEM), 2023

Volume 22, Pages 330-338

ICBASET 2023: International Conference on Basic Sciences, Engineering and Technology

Analysis and Evaluation of the Maximum Runoff Formed in the River Basin of the Arda River to the Dam Wall of the Kardzhali Dam in Bulgaria

Silvia KIRILOVA
University of Architecture, Civil Engineering and Geodesy

Kameliya RADEVA
Space Research and Technology Institute, Bulgarian Academy of Sciences

Abstract: The current study tracks the change in the maximum outflow formed in the watershed of Kardjali dam, which is among the complex and nationally significant dams in Bulgaria and is subject to annual monitoring by the Ministry of environment and waters (MOEW). The maximum runoff is an extreme hydrological phenomenon with spatio-temporal variation, the exact determination of which requires in-depth knowledge of hydrographic, climatic, soil, vegetation conditions, as well as anthropogenic factors for each individual region. Investigating it in a certain territory during the operation of hydrotechnical facilities has been a current topic in recent decades. The purpose of the present study is to track the change in the maximum runoff in Arda River catchment to Kardzhali Dam for the period 1961-2021, which also includes the period recommended by the World Meteorological Organization (1961-1990). GIS database was created as a basis for analyzing the results, containing information from the soil map of Bulgaria 1968, land cover from Corine 2012, JICA project finished in 2005. As for the estimation of the maximum runoff information array of hydrometric data observed in hydrometric station 315/61700 on Arda River and data from the operation of Kardzhali Dam has been used for the purposes of the present study. The study shows that with proper management of the reservoir, there is no danger of flooding the surrounding terrain after the dam wall. The research contributes to improving the process of monitoring on the maximum outflow to the Kardzhali Dam and supports decision-making by the responsible institutions in the management of water volumes in the dam lake cup when a high wave occurs.

Keywords: Maximum runoff, Statistical analysis, Hydrometric data, GIS

Introduction

The study of the maximum runoff in a given territory and certain river basins has been an actual task in recent decades. The changes in its parameters have been subjected to additional analyzes and evaluations in consideration of climate changes, which in some cases have led to significant changes in its regime. This new challenge of engineering hydrology has led to searching for solutions on application of new computational procedures, such as mathematical modeling methods, use of analog stations, satellite observations, etc (Nedkov R. et al., 2020). Through the application of these methods and approaches, it is aimed that the maximum runoff and its parameters reach maximum correlation with the processes and phenomena that form it. With the manifestation of climate changes and with the often realized high water in the riverbeds, it is mandatory to apply the above-mentioned methods for recalculation and analysis of the maximum runoff formed within the studied watershed.

The analysis of the maximum outflow is based on the collected data in the hydrometric stations located along Arda River. The accepted period for the analysis of the maximum runoff is from 1961 until 2021, including the reference period from 1961 to 1990 adopted by the World Meteorological Organization (2017 edition, WMO-

- Selection and peer-review under responsibility of the Organizing Committee of the Conference

№1203). The calculation and formation of a hydrological series of maximum water quantities to the retaining wall of the Kardzhali dam is based on interpolation dependencies (Murdock & Gulliver, 1993), derived on the basis of maximum outflow data collected in the hydrometric stations built in the river system of the studied catchment and on data about the maximum volumes realized in the dam. The range of maximum runoff values is analyzed using non-parametric criteria for uniformity, representativeness and significance to confirm the homogeneity of the study area. Through the apparatus of mathematical statistics, the theoretical approximation of the empirical points of the hydrological order is presented and maximum water quantities with characteristic security are calculated, based on which the volume of the high wave in the water reservoir is determined. The results of the study will be of benefit for the responsible institutions to make decisions and undertake management actions for the appropriate operation of the reservoir and for maintaining the ecological balance in the area of the dam wall.

Studied Area

The present study covers the catchment of Arda River from its originating points to Kardjali Dam. The river basin is developed entirely on the territory of the country, in the south-eastern part of the Eastern Rhodopes, within the borders of the Eastern White Sea Basin Water Management Region. The catchment of Arda River borders to the north and northwest with the catchment basin of Maritsa River, to the south and southwest with our border with Greece, to the east and southeast with the catchment of Varbitsa River. The river basin is oriented from southwest to northeast and is localated in the mountain and mid-mountain hypsometric belt (Figure 1).

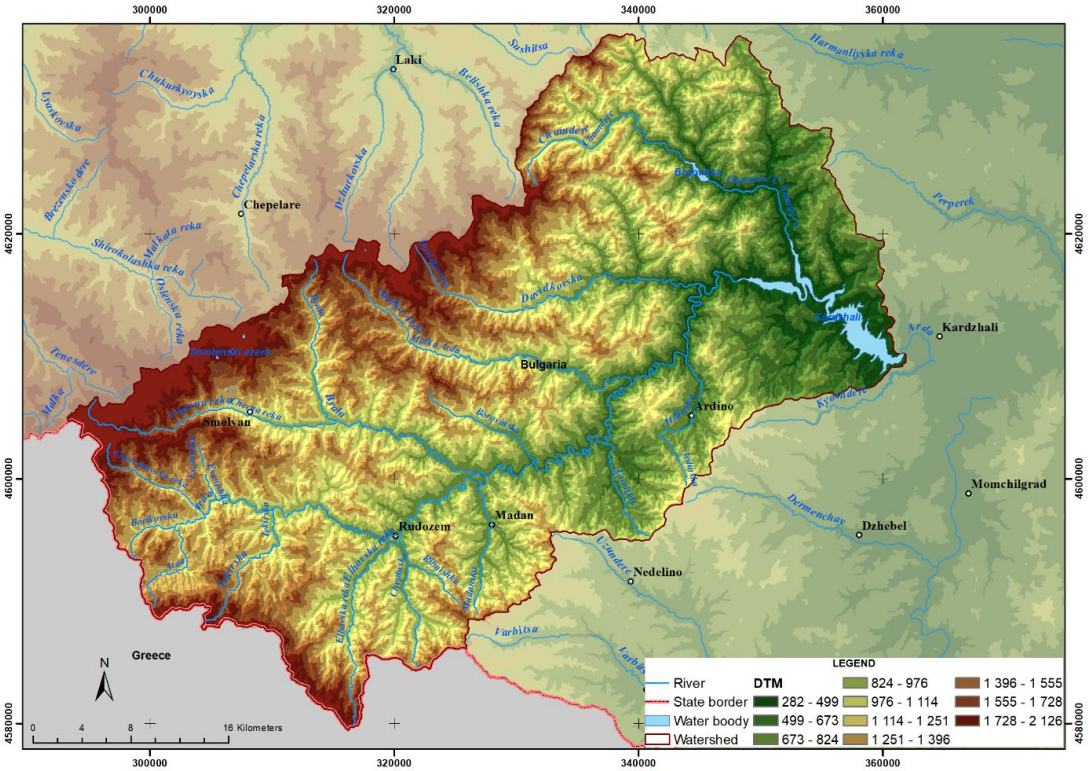

Figure1. Relief, river network and hydrometric stations in Arda river basin

The Arda River, in the section from the springs to "Kardjali" dam, forms its outflow through a well-developed river network located on the Prespa section of the Western Rhodopes and the northwestern slopes of the Yellow section of the Eastern Rhodopes. A characteristic feature of the river network's watershed is the deep valleys and steep slopes along which the river's outflow is formed with slopes reaching up to 40°. Along the length of the river section within the studied watershed, several expansions in its river bed appear, as well as mountain meanders in the area of the town of Rudozem. The section of the studied watershed falling in the foothills of the river course enters a deep, rocky and difficult-to-navigate gorge, from which it exits after the area of the Devil's Bridge (Sheitan cuprue). In this area, the gradients of the catchment slopes reach up to 45°, and the river bed reaches a width of 50 to 60 m. Its right slopes are forested with broad-leaved forests, and the left slopes are bare and collapsed by screes as shown in figure 2.

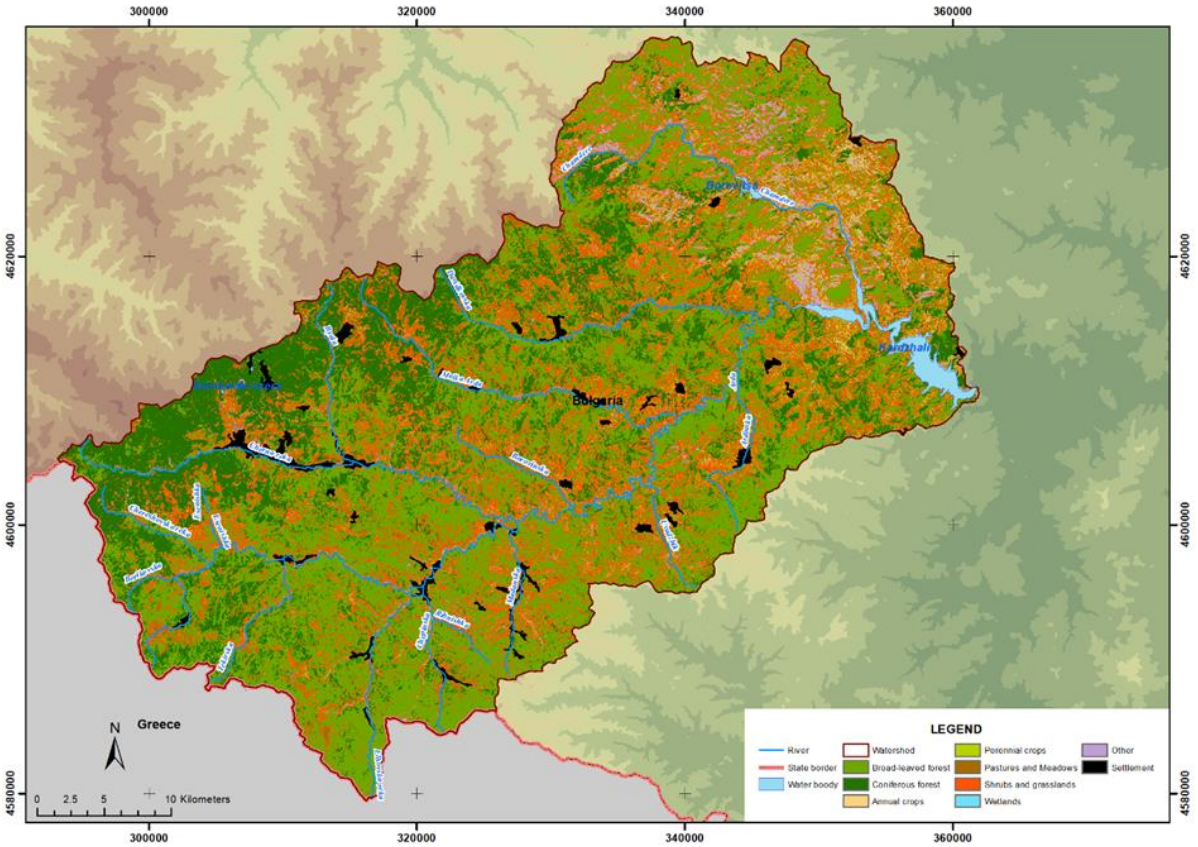

Figure 2. Land cover within the study watershed.

The main orographic characteristics of the studied watershed to Kardzhali Dam determined by GIS are presented in Table 1.

Table 1. Orographic characteristics of the studied area

River	Catchment area	Average altitude	River length	Average river slope	Average catchment slope	River network density	Forestry	Lake area incl. peatlands
-	A km^2	H m	L km	‰	Ir ‰	km^{-1}	%	%
Arda river to Kardjali Dam	1882,0	997	134,0	9.6	328	1.53	35.4	0.32

According to the classification of water bodies that have main characteristics of the river system and water bodies accepted by the Ministry of Environment and Water the surveyed watershed of this section of Arda River falls into a surface water body with code BG3AR500R020 and type code R5 (MOEW, 2016-2021).

Materials and Methods

The methodology in the present study includes determination of sustainable physicogeographical parameters, such as boundaries of the catchment basin of the dam, area, and altitude, analysis and evaluation of the data from the available monitoring system for the formation of hydrological series from maximum values of the river runoff for the surveyed area and application of a suitable mathematical apparatus for statistical processing of the data arrays for the maximum runoff (Mamdouh Sh. et al., 1993) with a view to achieving results as close as possible to the real runoff regime.

The watershed outline of the river basin and its orographic features are generated in a GIS environment using the Geospatial Hydrologic Modeling Extension (HEC-geoHMC) model. (Feldman, 2000). The model precisely and reasonably determines the orographic parameters for each specific catchment basin (Baumbach et al, 2015).

The work of the algorithm implementing the model is the verification of the input data for a digital model of the relief and the generation of raster layers, necessary for the more accurate formation and reporting of the river outflow in the specific basin (Modev & Kirilova, 2013).

The materials on which the present study was carried out are the arrays of data on the flow regime of the river within the studied watershed collected at the specific hydrometric stations from the national reference hydrometric network. These materials are determined by the number of hydrometric points and programs for monitoring and measuring runoff parameters performed with the appropriate discretization. The hydrometric stations in the watershed are presented in Table 2 and Figure 1.

Table 2. Hydrometric station from the main monitoring network of Bulgaria.

Hydrometric station N	Opening/ Closing year	River	Settlement	Catchment basin area	Average altitude	Average slope of the water basin	River length	Average River slope	River network density	Forestry
-	- / -	-	-	km^2	m	‰	km	‰	km^{-1}	%
320	1950/ 1956	Arda	Rudozem	257.7	1162	288	37.15	20.6	1.53	35.4
346/ 61330	1950/	Elhovska	Rudozem	83.9	1147	362	18.95	47.0	1.65	32.3
322/ 61050	1953/ functioning	Byala	Bostina	52.9	1293	385	12.12	51.3	1.56	52.2
322A	1950/1953	Byala	Smolyan Ustovo	66.0	1250	379	16.80	47.7	1.62	57.5
319/ 61350	1951/ functioning	Cherna	Taran	242.1	1280	348	39.35	30.8	1.93	32.2
315/ 61700	1952/ 1955/ functioning	Arda	Vehtino	857.4 858.4	1209 1172	315 332	66.65 66.90	13.5 13.5	1.69 1.69	53.5 53.5
315A	1949/1952	Arda	Stoyanov bridge	870.0	1166	329	72.6	12.9	1.76	55.0
314/ 61400	1949/ functioning	Malka Arda	Banite	114.0	1172	352	30.54	34.2	2.02	56.5
316	1949/1958	Arda	Prileptzi	1899.50	992	328	132.8	9.15	1.65	40.0
140	1932/1950	Arda	Kardjali	1987.94	969	325	138.2	8.90	1.62	40.0

The scope of the study is focused on studying the regime and in general the fluctuations of the maximum runoff by evaluating the information arrays of the maximum runoff obtained as data from the individual hydrometric stations when applying analyzes through mathematical statistics covering the verification of representativeness, uniformity and significance of the hydrometric data. Determining the forming high waters and approaches to Kardzhali dam.

After 1970, regular observations of the outflow of Arda River have been carried out at Kardzhali dam wall point. These observations are processed by means of the balance equation of the dam and allow the determination of average daily water quantities with high accuracy between 1 - 3 %. It is not possible to determine instantaneous (extreme) water quantities by means of the measuring system of Kardzhali dam. They can be calculated by means of interpolation dependencies or by transferring terms from the hydrological series of neighboring stations. The formed hydrological order of maximum water quantities to Kardzhali dam was compiled by means of interpolation and by the volumes of high waves during simultaneous observations in stations located "above" and "below" the research point and by transferring water quantities using established in practice ratios between runoff modulus and catchment area (Sabahattin Isik et al , 2008).

The methodology used in carrying out the analysis and the information array of data created by it for the maximum outflow of Arda River to Kardzhali dam are based on the main criteria used in mathematical statistics for checking and validation of the information array, through non-parametric criteria for homogeneity, representativeness and significance of the hydrological order of maximum water quantities. To analyze the homogeneity of the time series of maximum values of the river runoff, the non-parametric criteria of Pettitt's test, Buishand's test, Standard normal homogeneity test (SNHT) and von Neumann's test two-sided limited and with a confidence probability of 5% are applied (Naghettini, 2017; Kirilova, 2019).

To analyze the representativeness of the hydrological order, the non-parametric Mann-Whitney criterion is applied, which asserts that two parts of the hydrological order belong to the same general aggregation. The advantage of the criterion is that no pre-accepted probability density distribution is required to confirm the null

hypothesis. To evaluate the significance of the trend of the hydrological series of maximum water quantities, the non-parametric Mann-Kendall criterion is applied to determine whether the given time series has a monotonic upward or downward trend. The statistical capabilities of the approaches used are quite sensitive to various properties of the sample data and most often detect a monotonic trend or a sudden change under the influence of sudden climate changes (Salas, 1993).

In the analysis of the hydrological sequence of probabilistic values of the maximum runoff, the apparatus of the mathematical statistics was used, assuming a theoretical distribution of the random values. A choice was also made to approximate the empirical curve with the theoretical one, and the choice was based on minimal deviations of the empirical points from the theoretical ones (Mamdouh Sh. et al., 1993). In order to determine the volume of high waves at Kardzhali Dam under characteristic water quantities, a functional dependence was constructed between the maximum water quantity and the volume of the high wave according to the data from observed single peak annual high waves at hydrometric station 315/61700 near the village of Vehtino and at hydrometric station 140 near the town of Kardzhali.

Results and Discussion

The formed hydrological series of values from the maximum outflow, as an inflow to Kardzhali dam, is also based on the construction of the hodograph from water quantities values to the point for the period 1961 - 2021. The construction results are presented in Figure 3.

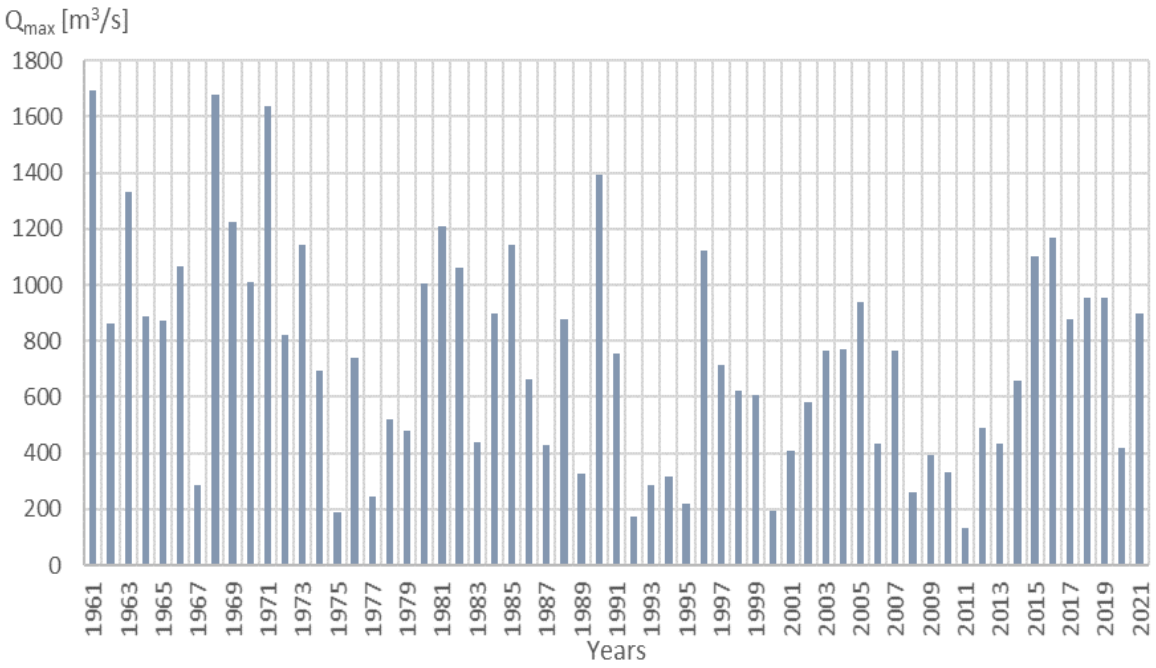

Figure 3. Hodograph of the maximum outflow for the studied period

The results of the adopted non-parametric criteria for homogeneity of the time series of maximum values of the river runoff confirm its non-homogeneity, i.e. a time change relative to the mean value of the hydrological data series is observed. Only the Pettitt's test confirms that the order is uniform.(Table3, Fig.4)

Table3. Homogeneity of the hydrological order of maximum values

Dam wall Point	River basin	p-value (bilateral criteria)				Year of change
		Pettitt's test	(SNHT)	Buishand's test	von Neumann's test	
Kardjali Dam	Arda river	0,051	0,002	0,007	0,009	1973

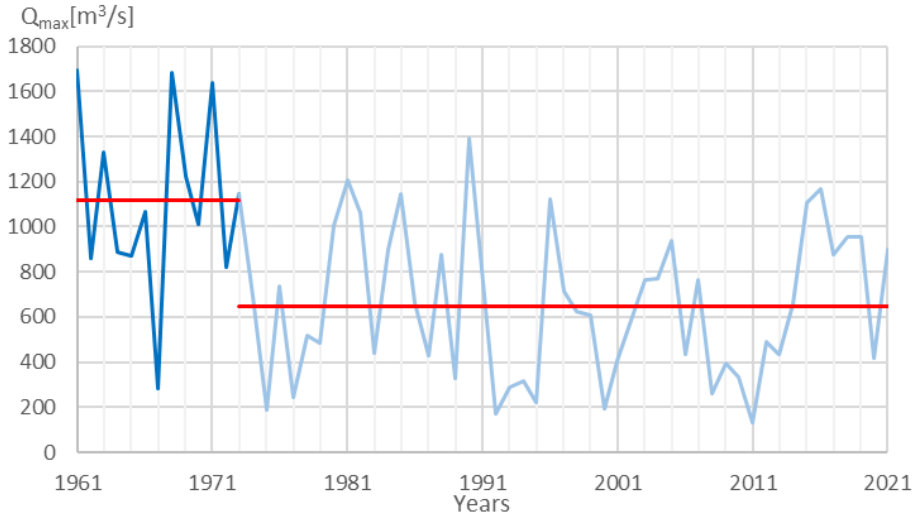

Figure 4. Chronological order of the maximum runoff with time change in 1973.

The result of the non-parametric Mann-Whitney criteria for representativeness of the hydrological series of maximum water quantities confirms that two parts of the hydrological series belong to the same general aggregation. The result of the non-parametric Mann-Whitney criteria for representativeness of the hydrological series of maximum water quantities at a confidence interval bounded from the left with a significance level α = 5% and with a quantitative estimate p = 0.998 > 0.05 confirms that the two parts of the hydrological series belong to the same general aggregation. The results of the trend significance assessment using the non-parametric Mann-Kendall test confirm that the order is statistically significant at a two-sided bounded confidence interval with a significance level α = 1% and with a quantitative assessment p = 0.029 > 0.01 where a trend is observed to reduce the maximum outflow in Kardzhali dam (WMO/TD-No. 1013, 2000).

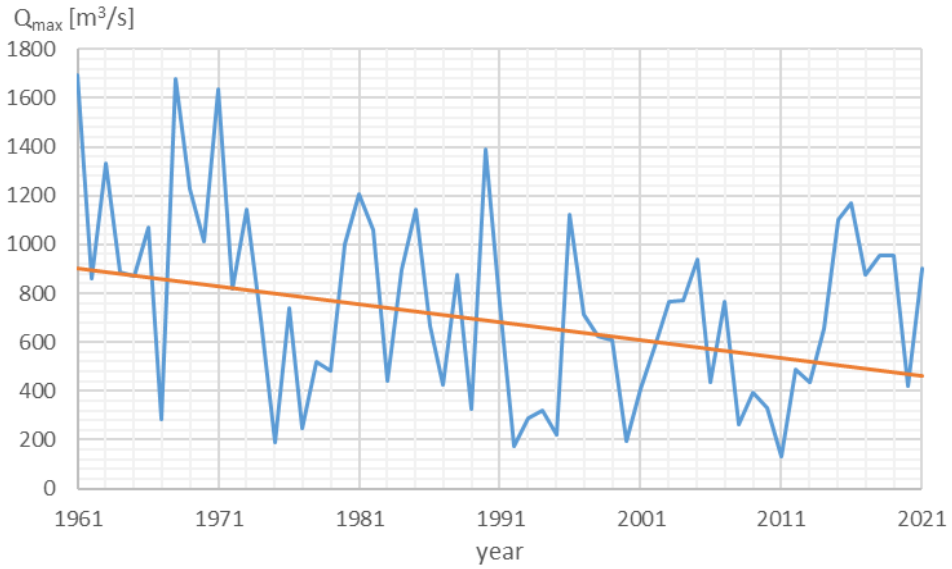

Figure 5. Chronological trend of maximum runoff for the period 1961 - 2021

The performed analyzes and evaluations show that the hydrological series is representative and can be studied with the methods of frequency analysis, which includes the statistical processing of the time series. The guarantee curve of the maximum outflow to Kardzhali dam is calculated and constructed. The statistical parameters of the hydrological order are calculated using the method of reference ordinates with an assumed lognormal distribution for the best approximation of the empirical points with the theoretical ones. The calculation results are given in Table 4 and Table 5.

Table 4. Statistical parameters of the series of maximum outflow values at Kardzhali dam

Dam wall Point	Statistic parameter			
	Qmax (m3/s)	σ (m3/s)	Cv -	Cs -
Kardjali Dam	795,0	472,9	0,60	1,35

Table 5. Values of the theoretical collateral curve of the Arda River to Kardzhali Dam

P %	0.01	0.1	1	5	10	20	50
Qp m^3/s	4252.2	3249.6	2313.2	1684.2	1409.9	1130.9	710.0

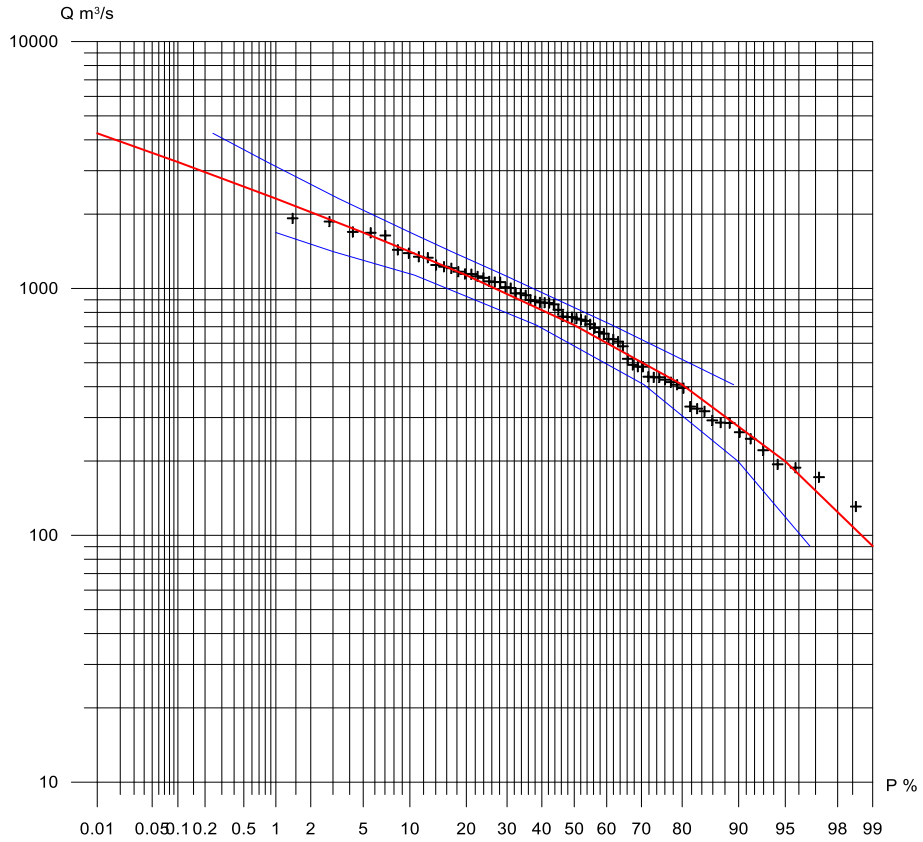

Figure 6. Theoretical supply curve of Arda River to Kardzhali Dam

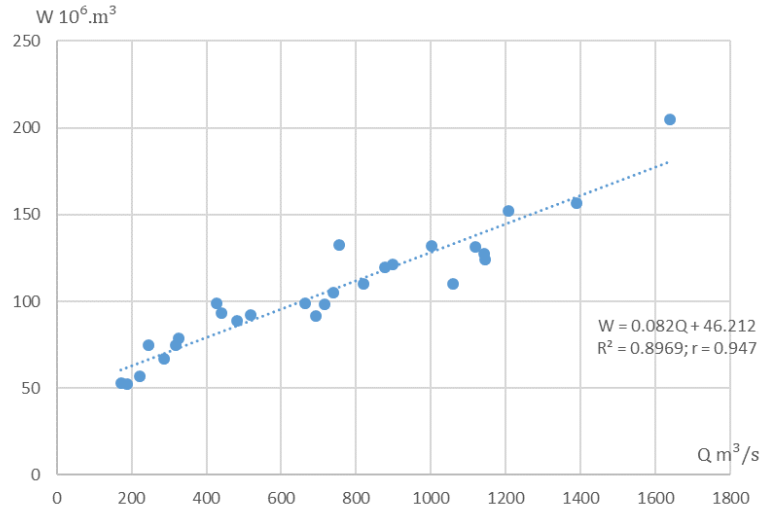

Figure 7. Dependence between the maximum amount of water and the volume of the high waves at HMS 315/61700 - Vehtino village and at HMS 140 in the town of Kardzhali

According to the data from observed single peak annual high waves at HMS 315 - village of Vehtino and at HMS 140 in the town of Kardzhali, a functional dependence between the maximum water quantity and the volume of the high wave was deduced. The results are presented graphically in Figure 7. The high correlative coefficient allows the dependence to be used to calculate the volumes of high waves with characteristic collateral to Kardzhali Dam. The results of the calculations are presented in Table 6.

Table 6. Recommended maximum water quantities and volumes of dimensional high waves determined by statistical methods

Probability %	0.01	0.1	1.0	5.0	10.0
HMS 315/61700					
Q_P [m^3/s]	3078.6	2442.4	1787.4	1309.3	1083.5
W [m^3x10^6]	298.66	246.49	192.78	153.57	135.06
Kardjali Dam					
Q_P [m^3/s]	4252.2	3249.6	2313.2	1684.2	1409.9
W [m^3x10^6]	394.89	312.68	235.89	184.32	161.82

The water quantities and volumes of dimensional high waves presented in Table 6 are obtained by a statistical method and are not tied to the rainfall that generated them.

Conclusion

The results of the present study provide prerequisites to accept that the anthropogenic pressure on the regime of the maximum runoff, expressed in dynamic changes in water consumption - for power generation, irrigation and water supply, as long as they are subject to internal balance, do not have a significant impact on structural uniformity and representativeness of the hydrological order. Additionally, with the climate change within the boundaries of the studied catchment, a trend for maximum outflow decrease of Arda River to Kardzhali Dam is observed. The results of the present study can be used with sufficient accuracy in the design, planning and exploitation of water resources, in conditions close to natural ones. The obtained values for the maximum water quantities at Kardzhali dam can be used as a basis for verification of results in subsequent developments and application of appropriate solutions related to the effective management of the hydroelectric node/Kardzhali dam.

Scientific Ethics Declaration

The authors declare that the scientific ethical and legal responsibility of this article published in EPSTEM journal belongs to the authors.

Acknowledgements or Notes

* This article was presented as oral presentation at the International Conference on Basic Sciences, Engineering and Technology (www.icbaset.net) held in Marmaris/Turkey on April 27-30, 2023.

References

Baumbach, T., Burckhard Suzette R., & Kant, J. M. (2015). *Watershed modeling using arc hydro tools. GeoHMS, and HEC-HMS*. Published by South Dakota State University (SDSU), College of Engineering, Civil and Environmental Engineering Department, and Water and Environmental Engineering Research Center, Brookings, SD 57007, 2-2015.

Feldman A. D. (2000). *Hydrologic modeling system HEC-HMS: Technical Reference Manual*. US Army Corps of Engineers, Hydrologic Engineering Center. NSN 7540-01-280-5500

Isik, S., & Singh, V. P. (2008). Hydrologic regionalization of watersheds in Turkey. *Journal of Hydrologic Engineering*, *13*(9), 824-834.

Kirilova S., (2019). *Homogeneity of hydrological series in the context of hydrotechnical planning and design*, Conference Proceedings "Climate, atmosphere and water resources during climate change. First

scientific conference, Bulgarian Academy of Sciences, Climate, Atmosphere and Water Research Institute., ISBN: 2683-0558, (p. 39-47).

Mamdouh Sh. et al. (1993). *Statistical analysis in water resources engineering*, A.A. Balkema, Rottterdam, Broookfild.

Ministry of Environment and Waters. (2016). River basin management plans in east aegean river basin directorate. https://earbd.bg/indexdetails.php?menu_id=609

Modev, St., & Kirilova. (2013). Characteristics of the geographical information system for the Nestos River Catchment, *Vodno Delo*, *3-4,* 23-28.

Murdock, R. U., & Gulliver, J. S. (1993). Prediction of river discharges at ungauged sites with analysis of uncertainty. *Journal of Water Resources Planning and Management*, *119* (4), 473–487.

Naghettini, M. (2017). *Fundamentals of statistical hydrology*. Springer, ISBN: 978-3-319-43561-9.

Radeva, K., Nedkov, R., Kirilova, S., & Georgiev, N. (2020, August). Optical and SAR data for application of Interim Ecological Monitoring (IEM) on Studena Dam, Bulgaria. In *Eighth International Conference on Remote Sensing and Geoinformation of the Environment (RSCy2020) (Vol. 11524, pp. 149-157*). SPIE.

Salas J. D. (1993). *Analysis and modeling of hydrological time series.* Handbook of Hydrology. New York, ISBN: 9780070397323.

World Meteorological Organization (2017). *Guidelines on the calculation of climate normal*. WMO-№1203

World Meteorological Organization (2000). *Detecting trend and other changes in hydrological data*. WMO/TD-No. 1013. https://water.usgs.gov/osw/wcp-water/detecting-trend.pdf, checked on 30.03.2023.

Author Information

Silvia Kirilova
University of Architecture, Civil Engineering and Geodesy, Hydraulics and Hydrology Department. 1164, 1 Hristo Smirnenski Blvd., Sofia, Bulgaria
Contact e-mail: *spacedgclima@gmail.com*

Kameliya Radeva
Space Research and Technology Institute, Bulgarian Academy of Sciences, 1113, str. "Acad. Georgy Bonchev" bl. 1 Sofia, Bulgaria

To cite this article:

Kirilova, S. & Radeva, K. (2023). Analysis and evaluation of the maximum runoff formed in the river basin of the Arda river to the dam wall of the Kardzhali dam in Bulgaria. *The Eurasia Proceedings of Science, Technology, Engineering & Mathematics (EPSTEM), 22,* 330-338.

The Eurasia Proceedings of Science, Technology, Engineering & Mathematics (EPSTEM)
ISSN: 2602-3199

The Eurasia Proceedings of Science, Technology, Engineering & Mathematics (EPSTEM), 2023

Volume 22, Pages 339-347

ICBASET 2023: International Conference on Basic Sciences, Engineering and Technology

Investigation of Design Parameters in Tensile Loads of the Diamond Joints in Composite Structures with a Finite Element Approach

Mine USLU-UYSAL
Yildiz Technical University

Abstract: Adhesively bonded joining in composite structures is carried out using mechanical or adhesive techniques with commonly single or double lap. In laminated structure elements joined in this way, damage generally occurs at the upper layer. That is loading capacity goes down due to the fact that the axial width goes up. In this paper, mechanical joints with joint lock in the shape of diamond are offered to replace adhesively bonded butt joints. E-glass/vinyl ester composite laminates was used as the plate material in the system, the diamond material in the middle was composite, aluminum and steel and Loctite Hysol 9464 was used as the adhesive material. Finite element models were performed in different values of the ratio of the end height of diamond to the height of the specimen (c/height), the ratio of the upper height of diamond to the end height of diamond (a/c) and the ratio of the half-length of diamond to the height of specimen (b/height). Using these dimension values, the effects of the joint geometry parameters are evaluated. Diamond joints model was analyzed by using finite elements method and obtained stresses values. These stresses values were examined and the appropriate design parameters for the diamond lock were decided. Before damage occurs in a composite structure, damage to the diamond lock is seen, and with this important observation, the life of composite structures can be extended by repairing the diamond lock.

Keywords: Diamond joint, Composite, Tensile load, Joint types, Finite element analysis

Introduction

For composite materials are widely used in mechanical and structural components due to their high specific strength and stiffness-to-weight ratios. Composites can also be designed and optimized in many ways, for example; The requirement for different strength and stiffness in various aspects dictated by the design and performance of a structural component. Compared to metal structures, modeling and analysis of composite structures is a challenging task. The load-bearing capacity of composite materials continues to be severely limited due to weaknesses in the joints or joints to the main structure. Because composite materials do not have anisotropy and homogeneous properties, their response to loading is more complex than metallic structures. For a reliable design of composite structures, it is necessary to thoroughly understand their behavior under static and dynamic loading under various environmental conditions, and to determine the lifetime of the joint. The development of such design methods depends on test data, analytical and computer modeling and numerical models created using finite element techniques.

Composite materials are found in industrial sectors such as aerospace, marine and automotive. Most of the giant structures in these sectors consist of two or more joints. The purpose of these connections is to transfer force through the main structure by combining two or more materials. The biggest problem in composite joints is the weakness in the joints. In the joints of composite structures, the damage strength of the composite material, the direction of the first damage and the production method are important. For this reason, many studies on the joining of composite materials have taken place in the literature. (Morgado et al., 2022; Silva & Adams, 2007; Santos et al., 2019; Kötter et al., 2020; Purimpat et al., 2013; Gunnion & Herzberg, 2006; Moya-Sanz et al.,

2017; Sebastiani et al., 2019; Kumar et al., 2006). In present paper, E-glass/vinylester laminates was used as composite material.

E-glass fiber has better tensile and good compressive strength and good stiffness, besides it has poor impact resistance. E-glass is the most widely used fiber reinforcement in composite materials. Polyesters are high performance and good engineering polymers that find use in different applications (Davallo et al., 2010). Woven fabric composites are more resistant to damage than non-woven fabrics if a delamination is present. Due to the non-planar interlayer structure of woven fabric composites, a delamination crack will interact with the woven structure during propagation, resulting in significant crack growth resistance. Vinylester resins have higher toughness values compared to polyester resins (Young, 1997). Glass-polyester composites are already well established. But if the glass/vinyl ester composite can provide sufficient toughness, then the use of vinyl esters in composites may be more attractive. In present paper, E-glass/vinyl ester composite materials were bonded in the form of butts with the help of a diamond aluminum.

A general discussion of adhesion, adhesives, and especially adhesive bonds and repairs in metallic alloys, polymers and composite materials can be found in (Kinloch, 2004; Baldan, 2004(a); Baldan, 2004(b)). Some representative studies on lap joints and mechanical behavior of lap joints can be found in (Keller & Vallée, 2005; Zhang & Keller, 2008; Ascione, 2009; Goyal & Johnson, 2008; Castro & Keller, 2008). Fewer studies in literature deal with butt joints (Ascione, 2009; Adams et al., 1978; Adams & Coppendale, 1979; Öchsner & Grácio, 2007; Öchsner et al., 2007; Ikegami et al., 1996; Sampaio et al., 2004; Taib et al., 2006).

While Adams et al. (1978) and Adams & Coppendale (1979) were more concerned with the stress analysis of axisymmetric butt-joints, some other articles were concerned with the determination of elastic constants as well as evaluation procedures for butt-joint testing of adhesive technology (Öchsner & Grácio, 2007), To date, only a few studies have examined the effect of adhesive thickness and geometry on the stiffness of bonded butt joints (Öchsner & Grácio, 2007; Öchsner et al., 2007; Ikegami et al., 1996; Sampaio et al., 2004; Taib et al., 2006). In general, as an alternative to welded joints, joints with different geometries (mainly aluminum/epoxy systems as in this study) are used. At butt joints, the bonded area is not excessively large and the nominal shear stress (tensile force/bond area) is nearly constant for a constant adhesive thickness. The thickness of the adhesive layer is the most important main geometric effect. A tensile test may show cohesive failure, adhesive failure, or mixed failure, depending on the adhesive/adhesive materials, surface coating, and adhesive thickness.

Tensile tests are used for determining the strength of a given butt joint, but these tests do not provide all the key parameters to be used directly in engineering design and estimating the strength of a bonded/connected system with arbitrary geometry is still a challenge. In general, complex finite element simulations are required (Castagnetti & Dragoni, 2009). In the butt joint method, the adhesive bonding technique is generally used throughout the thickness. In this type of joints, inclined or stepped joints are preferred more than simple butt joints in order to prevent peeling stress and reduce its value. Although different joint types are used in butt jointing, shear stress negatively most biggest affects joint life.

In this presented paper, mechanical butt joints with diamond shaped joint locks are proposed instead of glued butt joints. In mechanical butt jointing, diamond-shaped joint lock elements are used to fix the composite laminate plates face to face with a tight fit procedure. The main purpose of this study is to examine the effects of changes in the material and geometric parameters of the diamond joint lock components on the maximum load carrying capacity of the joint using the finite element method.

Materials and Method

Preparation of Design Parameters of the Diamond Lock Joints in E-glass/Vinylester Laminates

In this study, material models with diamond geometry shown in Figure 1 were prepared by using three types of materials: composite, aluminum and steel. Finite element models are performed in different values of the ratio of the end height of diamond to the height of the specimen (c/height), the ratio of the upper height of diamond to the end height of diamond (a/c) and the ratio of the half-length of diamond to the height of specimen (b/height) (Table 1). Using these dimension values, the effects of the joint geometry parameters are evaluated.

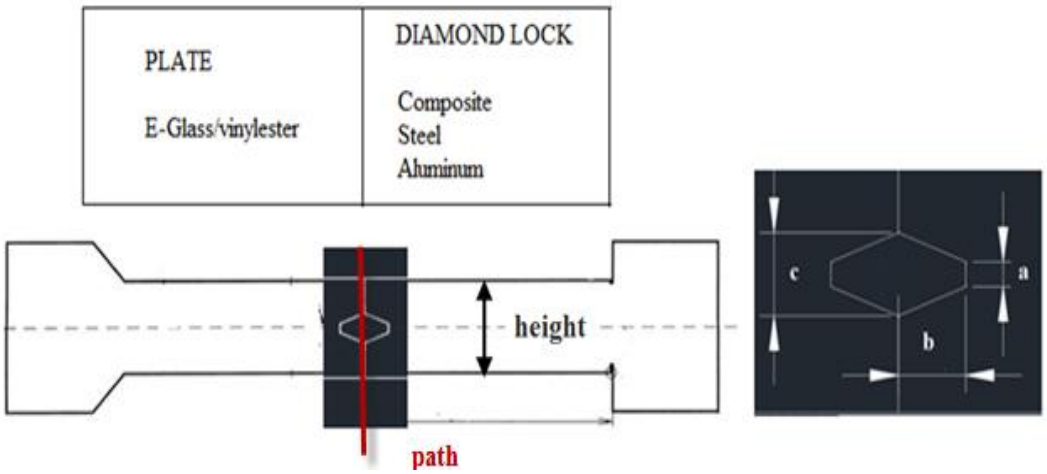

Figure 1. Composite laminates combined with diamond lock and diamond geometric parameters

As seen in Figure 1, specimen dimensions were chosen as follows: specimen height (h) is 20 mm, total specimen jaw length L=160 mm and specimen thickness t= 5 mm. Keeping constant the specimen's main dimensions (h, L, t) that are joined in mechanic butt joint, the end width (c), middle width (a) and half the length (b) of the joint lock in the shape of diamond were changed. To see the effects of geometric parameters on tensile loads, several models were performed by changing the ratio of the end width of diamond to the width of the specimen (c/height) and the ratio of the middle width of diamond to the end width of diamond (a/c) from 0.3 to 1.2. In these finite element models, the ratio of the half-length of diamond to the width of the specimen (b/height) was chosen as 0.3, 0.6 and 0.9. The dimensions of diamond lock joint components are given in Table 1. Half specimens are jointed with diamond joint components by using tight fitting. Diamond parts used as joining components were made up of both metal (steel and aluminum) and composite materials. Therefore, the effect of the diamond material on tensile load was considered as well.

Table1. Diamond lock component dimension parameters

Dimension Ratio		c/height				Dimension (mm)
		0.3	0.6	0.9	1.2	
		6	12	18	-	c
a/c	0.3	1.8	3.6	5.4	-	a
	0.6	3.6	7.2	10.8	-	
	0.9	5.4	10.8	17.2	-	
	1.2	7.2	14.4	-	-	
b/height	0.3	6				b
	0.6	12				
	0.9	18				

In this study, the composite material, whose material properties are given in Table 2, was used in both plate and diamond geometry. Tensile properties such as longitudinal modulus (E_{11}), transverse modulus (E_{22}), transverse modulus (E_{33}), Poisson's ratio (υ_{xy}) etc. are given in Table 2. The laminated composite material is 10 layers and directions 0° and 90°, one layer thickness is 0.5 mm.

Table 2. Mechanical properties of composite adherends

Properties	Composite
Modulus of Elasticity, E (GPa)	$E_{11=}22$ $E_{22=}22$ $E_{33=}9$
Shear Modulus, G (GPa)	G_{12}=5.3 G_{23}=3.1 G_{13}=3.1
Poisson's ratio,υ	υ_{xy}.0.27 υ_{yz}.0.38 υ_{xz}.0.38

Steel S235JR and Aluminum 5083 are used as a diamond lock and their mechanical properties are given in Table 3.

Table 3. Mechanical properties of steel and aluminium diamond lock

Materials	Modulus of Elasticity (GPa)	Poisson Ratios
Aluminum 5083	70	0.3
Steel S235JR	235	0.3

Modeling of Diamond Lock Joints in Composite Structures

The thickness of the adhesive layer is 0.1 mm. In the Figure 2 , the schematic illustration of adhesives areas in the model can be seen. The mechanical properties of the adhesive material are given in the Table 4. It is an adhesive applied by mixing epoxy and hardener in a ratio of 1:1, by weight and volume. The same type of materials (metal, ceramic, plastic, etc.) and different materials (composite, etc.), It is an ideal adhesive for bonding. The main mechanical properties specified by the manufacturer for the adhesive with a setting time of 180 minutes after application are given in Table 4.

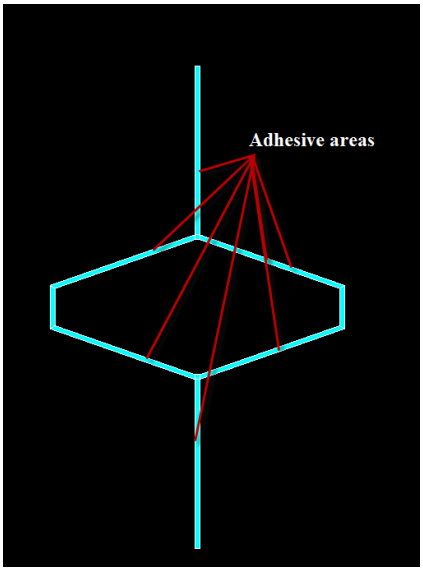

Figure 2. The schematic illustration of adhesives areas in the model

Table 4. Mechanical properties of adhesive

Properties	Loctite-Hysol 9464
Shear Strength (MPa)	20
Peel Strength (MPa)	10.6
Modulus of Elasticity, E (GPa)	1.65
Shear Modulus, G (GPa)	0.75
Poisson's ratio,υ	0.356
Mixture by volume rate	1:1

Finite Element Model

The finite element model of fixed pointed diamond lock joint was developed using the commercial software package ANSYS. This finite element program provides an estimate of the overall strain behavior of the composite panel when subjected to a tensile load (30 MPa). The thickness of one panel is 10 mm, the adhesive thickness is 1 mm.

When drawing the first aluminum lock model, 0.3-0.3-0.3A is selected the name of the model, the explanation for this is as follows; The values c/height =0.3, a/c=0.3 and b/height =0.3 are selected from the Table 1 and a model is created by drawing the corresponding diamond in the shape of c=6 mm, a=1.8 mm and b=6 mm by using aluminum material (A). All models are named according to this rule. The numerical model of the panel is divided into a finite number of elements that ensure stability and cohesion at each node. As a result, the optimal

combination of mesh accuracy and element size was found (Figure 3).Element edge is selected as 0.025mm. The model has contact pairs, the contact position of the adhesive and adherend plates. The relevant literature (Uysal and Güven, 2015) can be consulted for bonding mechanics and modeling details.

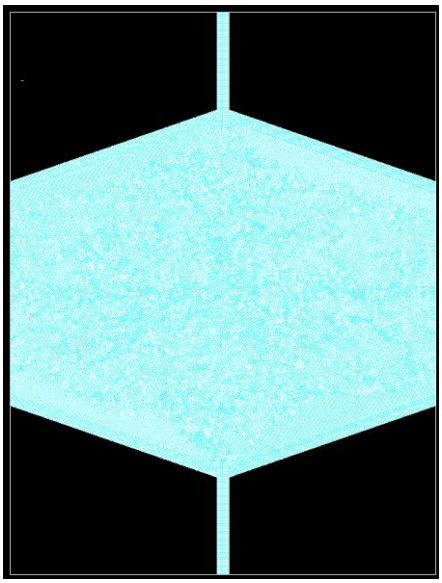

Figure 3. The mesh detail in diamond and adhesives areas

Results and Discussions

The diamond-shaped connection lock components used in the finite element analysis are modeled using both steel (S235 JR) and aluminum (Aluminum 5083) and composite (E-glass/vinylester composite) materials. In this paper, the load carrying capacities of the models were investigated by changing both the geometrical parameters and the materials of the diamond lock elements. Figure 4 shows the variation of metal and composite diamond on maximum von-Misses stresses (σ von-misses) for different b values (diamond half length value). The most suitable b compatibility for all materials seems to be 12 mm. For this reason, length b was chosen as 12 mm.

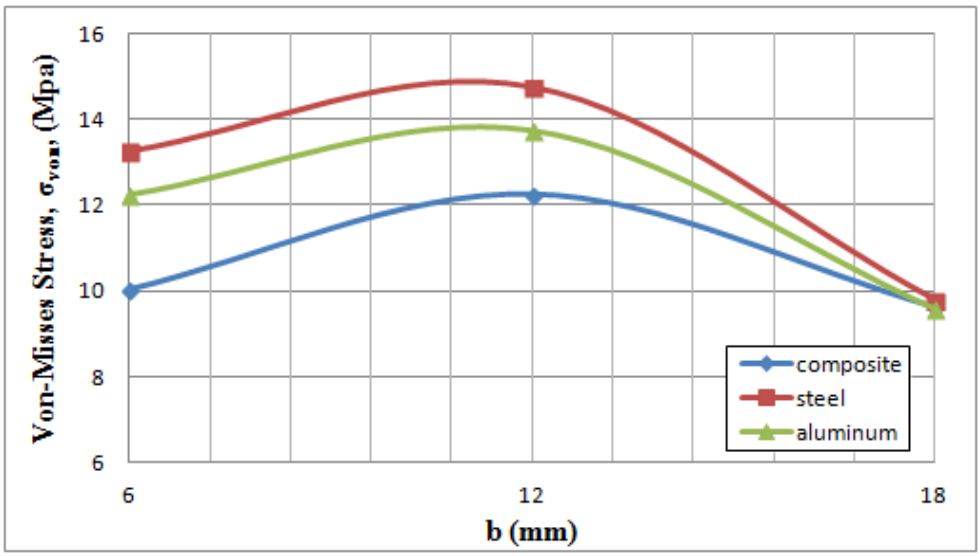

Figure 4. Von-Misses stress respect to diamond half length (b) parameters.

The changes in the load carrying capacity of the samples made with various (a/c) ratios according to the (c/h) ratio of the diamond key element are shown in the Figure 5. As seen in Figure 5, it depends on the load carrying capacity (c/h) ratio. When the a/c ratio is equal to 0.3 and the c/h ratio is equal to 0.6, the load carrying capacity for both metal(steel and aluminum) and composite diamond locks is maximum. As a result, it can be concluded that the choice of diamond width is very important in terms of load carrying capacity.

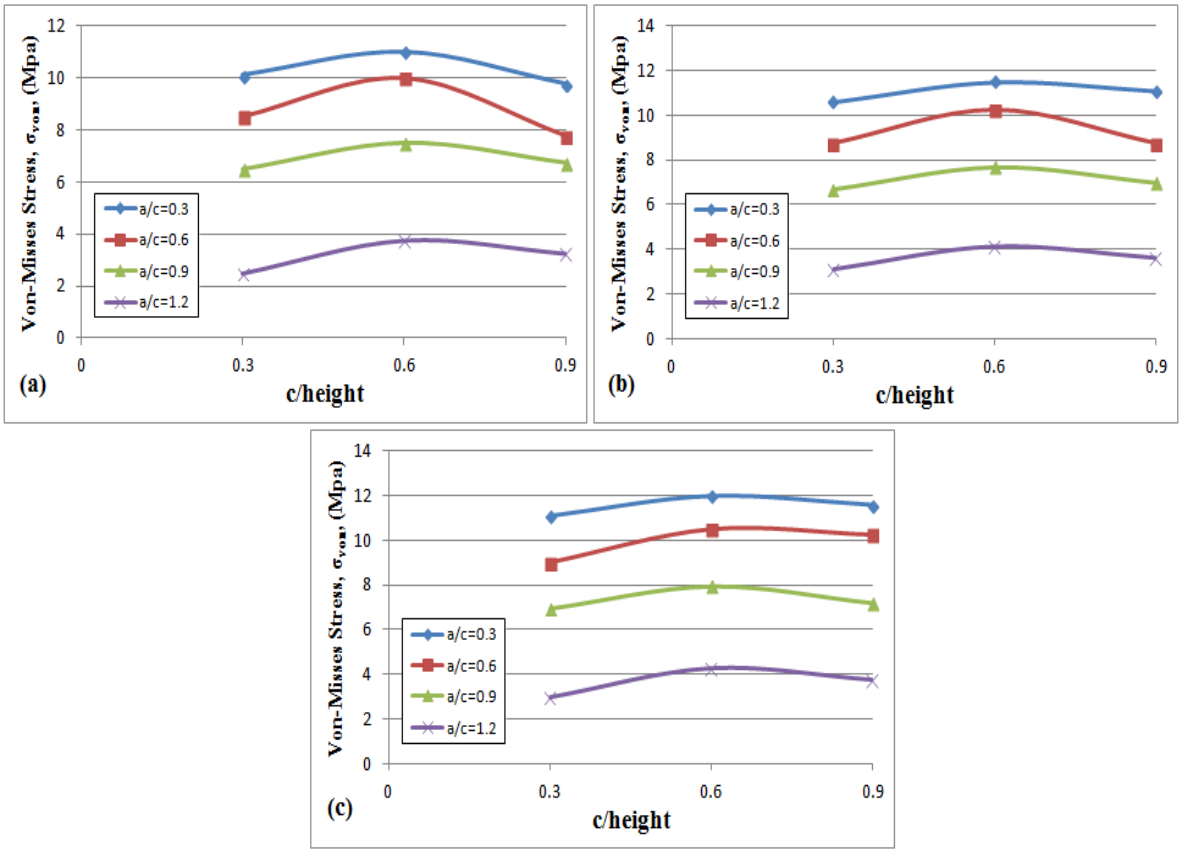

Figure 5. Von-Misses stress respect to c/height parameters for
a) Composite diamond b) Aluminum diamond , c) Steel diamond

The variation in the maximum von misses stresses with respect to the a/c ratio is shown in Figure 6. When the c/height ratio is 0.6 and the a/c ratio is equal to 0.3, the load carrying capacity of both metal and composite diamonds is maximum. The decrease in the maximum load with the increase of the a/c ratio shows the importance of the diamond middle width. As the middle width of the diamond decreases, the shape of the diamond lock element begins to resemble a square or rectangular shape. The diamond lock element starts to lose its locking feature and this causes the load carrying capacity to decrease. When the a/c ratio is equal to 1, the square or rectangular lock element is no longer load-bearing.

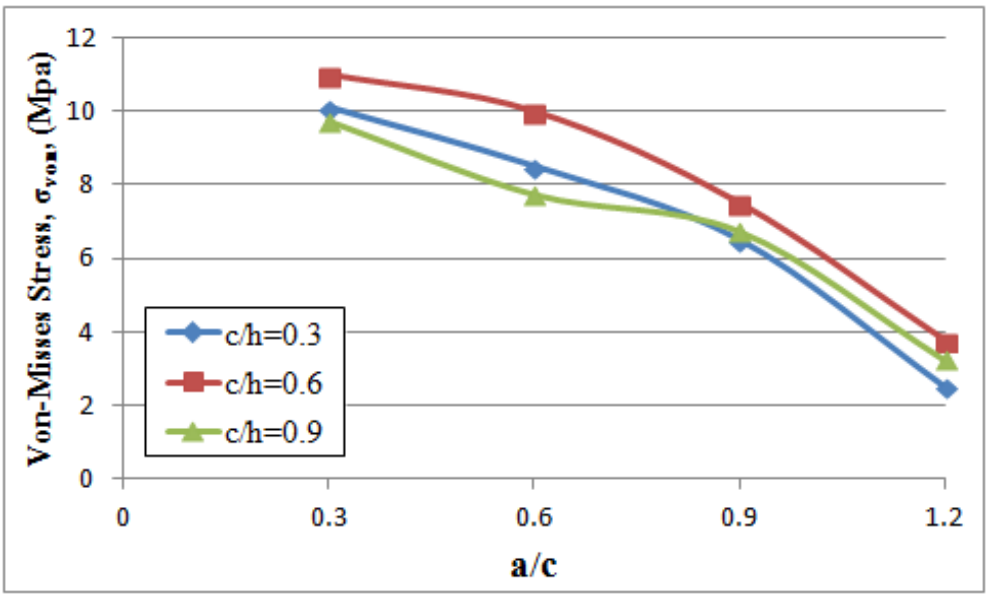

Figure 6. Von-Misses stress respect to a/c parameters

Path that appears as a red line in the diamond lock model is drawn in Figure 1. The path is exactly 20 mm and runs right through the middle of the adhesive layer and also the model. Normal stresses (σ_y), shear stresses (τ_{xy}) values were taken from the path in the solution for the model named 03-03-03A. (on the aluminum model, the values c/height =0.3, a/c=0.3 and b/height =0.3 are selected from the Table1). Since the shape is symmetrical, symmetry is observed in all stresses. The distributions of stresses are similar in other models.

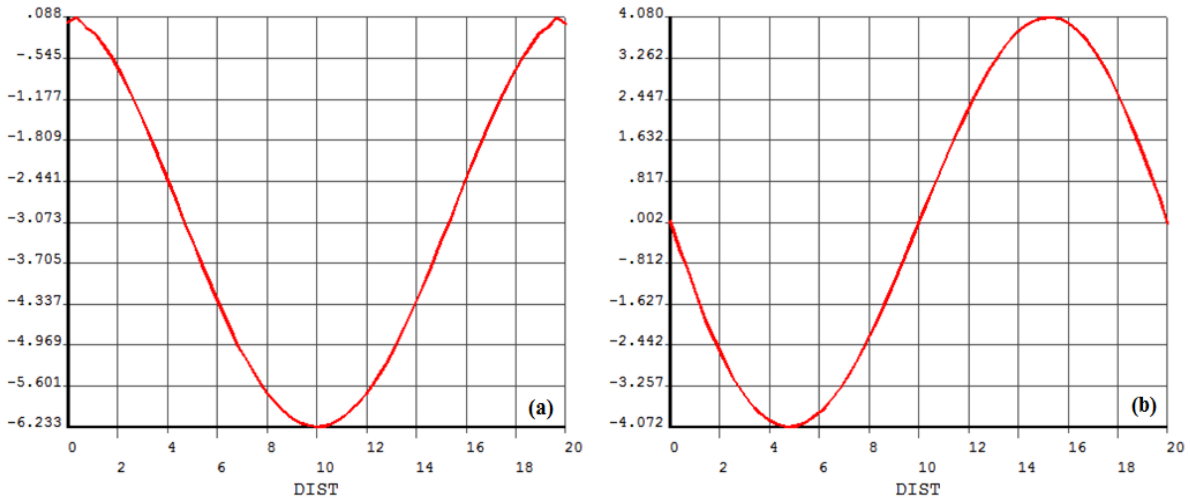

Figure 7. a) Normal stresses (σ_y) and b) Shear stresses (τ_{xy}) distributions on the path

Conclusion

In this presented study, effects of joints in the shape of diamond, its materials and geometric parameters on the load capacity were all considered by using finite element method. E-glass/vinyl ester composite materials, aluminum 5083 and S235JR steel was chosen for diamond lock material parameters. Models were made in different values of the ratio of the end height of diamond to the height of the specimen (c/height), the ratio of the upper height of diamond to the end height of diamond (a/c) and the ratio of the half-length of diamond to the height of specimen (b/height). Diamond joints model was analyzed and obtained stress values. The stress values were examined and the appropriate design parameters were decided for diamond joints. At high values of the ratio of the middle width of diamond to the width of diamond (a/c), von-misses stress decreases gradually. When (a/c) reaches 1, since angled surface disappears, diamond carries no load. For this reason, in such cases, adhesively bonding technique is preferred and the adhesive material holds the joint together. Compared to the composite diamond samples, the steel and aluminum diamond samples have higher load carrying capacities. While the ratio of c/height increases, it is concluded that load carrying capacity decreases gradually. In a specimen that has a constant height, when diamond end width rises, it suffers from the weakened area at both sides of diamond joint component and its load carrying capacity decreases. The ratio of c/height can become 0.6 for composite diamonds model. The mechanical butt joint technique can be used together with the bonding technique. In this case, the negative effects on adhesive joints can be minimized by changing the material and size parameters in diamond lock. It is also possible to have different joint load carrying capacities by changing the shape of the diamond locks.

Scientific Ethics Declaration

The author declares that the scientific ethical and legal responsibility of this article published in EPSTEM journal belongs to the author.

Acknowledgement

This article was presented as oral presentation at the International Conference on Basic Sciences, Engineering and Technology (www.icbaset.net) held in Marmaris/Turkey on April 27-30, 2023.

References

Adams, R. D., & Coppendale, J. (1979). The stress–strain behaviour of axially loaded butt joints. *The Journal of Adhesion*, *10*, 49-62.

Adams, R. D., Coppendale, J., & Peppiatt, N. (1978). Stress analysis of axisymmetric butt joints loaded in torsion and tension. *The Journal of Strain Analysis for Engineering Design*, *13*, 1-10.

Ascione, F. (2009). Mechanical behaviour of FRP adhesive joints: a theoretical model. *Composites: Part B*, 40, 116-124.

Baldan, A. (2004a). Adhesively-bonded joints and repairs in metallic alloys, polymers and composites materials: adhesives, adhesion theories and surface pretreatment. *Journal of Material Science*, *39*, 1-49.

Baldan, A. (2004b). Adhesively-bonded joints in metallic alloys, polymers and composite materials: mechanical and environmental durability performance. *Journal of Material Science*, *39*, 4729-4797.

Castagnetti, D., & Dragoni, E. (2009). Standard finite element techniques for efficient stress analysis of adhesive joints, *International Journal of Adhesion and Adhesives*, *29*, 125-135.

Castro, J., & Keller, T. (2008). Ductile double-lap joints from brittle GFRP laminates and ductile adhesives, Part II: numerical investigation and joint strength prediction. *Composites: Part B*, *39*, 282-291.

Davallo, M., Pasdar, H. & Mohseni, M. (2010). Mechanical properties of unsaturated polyester resin, *International Journal of ChemTech Research*, *2*(4), 2113-2117.

Dos Santos, D. G., Carbas, R. J. C., Marques, E. A. S., & Da Silva, L. F. M. (2019). Reinforcement of CFRP joints with fibre metal laminates and additional adhesive layers. *Composites Part B: Engineering*, *165*, 386-396.

Goyal, V. K., Johnson, E. R., & Goyal, V. K. (2008). Predictive strength-fracture model for composite bonded joints. *Composite Structures*, *82*, 434-446.

Gunnion A. J., & Herzberg I. (2006). Parametric study of scraf joints in composite structures, *Composite Structures*, *75*, 364-376.

Ikegami, K., Fujii, T., Kawagoe, H., Kyogoku, H., Motoie, K., Nohno, K., Sugibayashi, T. & Yoshida, F. (1996). Benchmark tests on adhesive strengths in butt, single and double lap joints and double-cantilever beams. *International Journal of Adhesion and Adhesives*, *16*, 219-226.

Keller, T., & Vallée, T. (2005). Adhesively bonded lap joints from pultruded GFRP profiles. Part II: joint strength prediction. *Composites: Part B*, *36*, 311-350.

Kinloch, A. J. (1987). *Adhesion and adhesives: science and technology*. New York, NY: Chapman & Hall.

Kötter, B., Karsten, J., Körbelin, J., & Fiedler, B. (2020). CFRP thin-ply fibre metal laminates: Influences of ply thickness and metal layers on open hole tension and compression properties. *Materials*, *13*(4), 910

Kumar S. B., Sridhar I., Sivashanker S., Osiyemi S. O., & Bag A. (2006). Tensile failure of adhesively bonded CFRP composite scarf joints, *Materials Science and Engineering B*, *132*, 113-120.

Moya-Sanz, E. M., Ivañez, I., & Garcia-Castillo, S. K. (2017). Effect of the geometry in the strength of single-lap adhesive joints of composite laminates under uniaxial tensile load. *International Journal of Adhesion and Adhesives*, *72*, 23-29.

Morgado, M. A., Carbas, R. J. C., Dos Santos, D. G., & Da Silva, L. F. M. (2020). Strength of CFRP joints reinforced with adhesive layers. *International Journal of Adhesion and Adhesives*, *97*, 102475.

Öchsner, A., & Grácio, J. (2007). An evaluation of the elastic properties of an adhesive layer using the tensile-butt joint test: procedures and error estimates. *International Journal of Adhesion and Adhesives*, *27*, 129-135.

Öchsner, A., Stasiek, M., Mishuris, G., & Grácio, J. (2007). A new evaluation procedure for the butt-joint test of adhesive technology: determination of the complete set of linear elastic constants. *International Journal of Adhesion and Adhesives*, *27*, 703-711.

Purimpat, S., Jérôme, R., & Shahram, A. (2013). Effect of fiber angle orientation on a laminated composite single-lap adhesive joint. *Advanced Composite Materials*, *22*, 139-149.

Sampaio, E. M., Bastian, F. L., & da Costa, H. S. M. (2004). A simple continuum damage model for adhesively bonded butt joints. *Mechanics Research Communications*, *31*(4), 443-449.

Sebastiani, G., Pfeifer, S., Röber, L., Katoh, J., Yamaguchi, Z., & Takada, S. (2019). Bonding strength of FRP-metal hybrids. *Technologies for Lightweight Structures*, *3*(1), 1-8.

Silva L. F. M., & Adams, R. D. (2007). Techniques to reduce the peel stresses in adhesive joints with composites. *International Journal of Adhesion and Adhesives*, *27*, 227-235.

Taib, A. A., Boukhili, R., Achiou, S., Gordon, S., & Boukehili, H. (2006). Bonded joints with composite adherends. Part I. Effect of specimen configuration, adhesive thickness, spew fillet and adherend stiffness on fracture. *International Journal of Adhesion and Adhesives*, *26*, 226-236.

Uysal, M. U., & Guven, U. (2015). Buckling of functional graded polymeric sandwich panel under different load cases. *Composite Structures*, *121*, 182-196.

Young, R. E. (1997). Vinyl ester resins. In: P. K. Mallich (Ed.), *Unsaturated polyester technology* (pp. 315-420). New York, NY: Marcel Dekker, Inc.

Zhang, Y., & Keller, T. (2008). Progressive failure process of adhesively bonded joints composed of pultruded GFRP. *Composites Science and Technology*, *68* (2), 461-470.

Author Information

Mine Uslu Uysal
Yildiz Technical University
Department of Mechanical Engineering
Besiktas, 34349, Istanbul-Turkey
Contact e-mail: *mineuslu@yildiz.edu.tr*

To cite this article:

Uslu-Uysal, M. (2023). Investigation of design parameters in tensile loads of the diamond joints in composite structures with a finite element approach. *The Eurasia Proceedings of Science, Technology, Engineering & Mathematics (EPSTEM), 22*, 339-347

The Eurasia Proceedings of Science, Technology, Engineering & Mathematics (EPSTEM)
ISSN: 2602-3199

The Eurasia Proceedings of Science, Technology, Engineering & Mathematics (EPSTEM), 2023

Volume 22, Pages 348-358

ICBASET 2023: International Conference on Basic Sciences, Engineering and Technology

NMR Spin Echo Study of Domain Wall Pinning in Magnets in Combination with an Additional Magnetic Video-Pulse

Tsisana GAVASHELI
Ivane Javakhishvili Tbilisi State University

Grigor MAMNIASHVILI
Ivane Javakhishvili Tbilisi State University

Tatiana GEGECHKORI
Ivane Javakhishvili Tbilisi State University

Abstract: NMR spin echo at application of an additional magnetic video-pulse is a convenient method to study the domain wall pinning in magnetic materials. Domain wall (DW) pinning is the critical amplitude of the magnetic video-pulse (MVP) below which the DW is fixed. For its assessment, two alternative NMR methods were chosen. In the first case, the pinning of DW was measured by the action of MVP on a two-pulse echo signal, and in the second one, the pinning was measured at the combined action of MVP and radiofrequency (RF) pulses on the nuclear spin system in DW during the process of formation a single-pulse echo, by means of generation of the so-called magnetic echo signal. DW pinning was studied by these two methods in magnets (lithium-zinc ferrite and cobalt micropowder samples).

Keywords: Nuclear spin echo, Magnetic video-pulse, Two-pulse echo, Domain wall mobility, Pinning.

Introduction

Nuclear magnetic resonance (NMR) in magnets is currently a powerful microscopic method for characterizing various magnetic materials (Turov & Petrov, 1972; Wurmehl & Kohlhepp, 2008; Shmyreva, et al., 2016; Mamniashvili et al., 2016). One of its advantages is the ability to give valuable information about the properties of domain walls (DWs). The inclusion of additional magnetic video- pulses (MVP), capable of causing the DW displacement, makes it possible to study the DW pinning, expanding the potential of the NMR method.

In particular, it was shown in (Pleshakov et al., 2016; Gavasheli et al., 2020), that the use of nuclear spin echoes from nuclei in DWs of lithium ferrite and cobalt nanowires in combination with magnetic video-pulse (MVP) is a convenient method for studying the pinning of DWs in these systems. This method is also of a great interest for the study of magnets for applications in information recording devices and sensors. For the first time, the dynamics of DW under the action of an MVP in a single-crystal of a ferrite sample was investigated by Galt (Galt, 1954). It was shown that the dynamics of DW is described by the linear dependence of the DW velocity υ on the applied MVP:

$$\upsilon=S(H-H_0)$$

where S is the mobility of the DW and H_0 is the DW pinning - the critical field below which the DW is fixed.

The original technique of MVP exposure was used in (Pleshakov et al., 2016), which consisted in exposing of the nuclear spin system in the lithium-zinc ferrite sample with a sequence of two pairs of RF pulses in

combination with an additional long-term MVP. The effect of MVP was investigated by the effect on the signals of stimulated and two-pulse echoes (TPE) formed when three or two pulses, correspondingly, are combined in the sequence. In this case, the MVP overlapped, respectively, the second and the third radiofrequency (RF) pulses, as well as the intervals between them and the signals, respectively, of the stimulated and two-pulse echoes. Under the applied MVP the echo signals are suppressed due to the inhomogeneous phase changes of rephasing nuclear isochromates which are proportional to the DW displacements and hyperfine field (HFF) anisotropy. Figure. 1a shows the result of the combined action of the MVP on the TPE signals at zero magnetic field (*1*) and the external magnetic field H_e = 1000 Oe (*2*), Figure 3 (Pleshakov et al., 2016), and Figure 1b shows a modified by us Figure 1a, taking into account the existence of pinning field H_0 (*1*) and using the same experimental points as in Figure 1a.

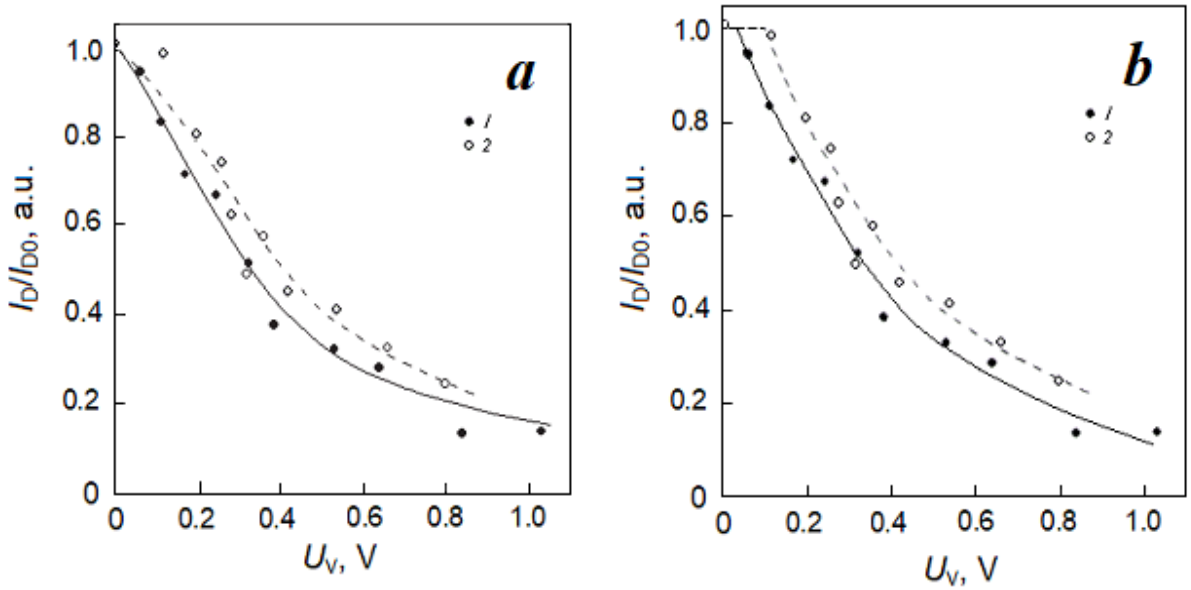

Figure 1. (a) - The dependence of the normalized amplitude of the two-pulse echo (TPE) signal on the amplitude of the magnetic video-pulse (MVP) (Pleshakov et al., 2016).
(b) – The modified dependence of the normalized TPE amplitude (a) on the amplitude of the MVP. *1* - H_e = 0 Oe; *2* – H_e = 1000 Oe.

A similar effect of the MVP action on the stimulated echo was also shown in (Pleshakov et al., 2016). The dependence modified in this way shows that the results obtained in (Pleshakov et al., 2016) also indicate the possibility of mesuring the pinning field H_0 of the DW, which is determined by the MVP amplitude, below which DWs are pinned and motionless. The aim of our further research is an alternative proof by two NMR methods: by the MVP action on TPE and by the combined action of RF and MVP, of the presence of DW pinning field H_0, corresponding to the MVP amplitude below which DW is fixed.

The methodology of (Mamniashvili et al., 2015; Pleshakov et al., 2016; Gavasheli et al., 2020) is used for the study of the dependence of the pinning force H_0 in cobalt micropowders on the duration of MVP τ_m and the magnitude of the external magnetic field H_e. As it known (Mamniashvili et al., 2015), cobalt and lithium-zinc ferrite are very different in their NMR properties: in cobalt, the anisotropy of the hyperfine field (HFF) is an order of magnitude higher than its value for lithium ferrite. In addition, the value of the NMR amplification factor η in lithium ferrite is about 10^3 times higher than the value of amplification factor η in cobalt, which indicates a much greater mobility of DWs in lithium-zinc ferrite as compared to cobalt. We can obtain a preliminary estimate of the dependence of H_0 on the length of MVP from Figure 2, obtained on the basis of Figure 2 from Rassvetalov and Levitski (1981), if it is modified similarly to Figure 1 from (Gavasheli et al. (2021) or Figure 1 from Gavasheli et al. (2022), taking into account the presence of pinning force H_0.

Figure 2 shows the dependence of TPE (for A-sites of nickel ferrite) on the duration of MVP at H = 2(*1*), 4(*2*), 10 Oe (*3*). Analysis of the dependence of H_0 on τ_m in this figure shows that for τ_m and H_0 (representing the intersection points of dependences *1*, *2* and *3* with the axis τ_m in Fig. 1), the relation $A_m = H_0 \cdot \tau_m$=const, holds for all H, i.e. the pinning force H_0 is inversely proportional to τ_m. The value A_m, which is the area of the MVP, is constant for all threshold values of τ_m, when the TPE intensity begins to decrease due to the tear-off from the pinning centers.

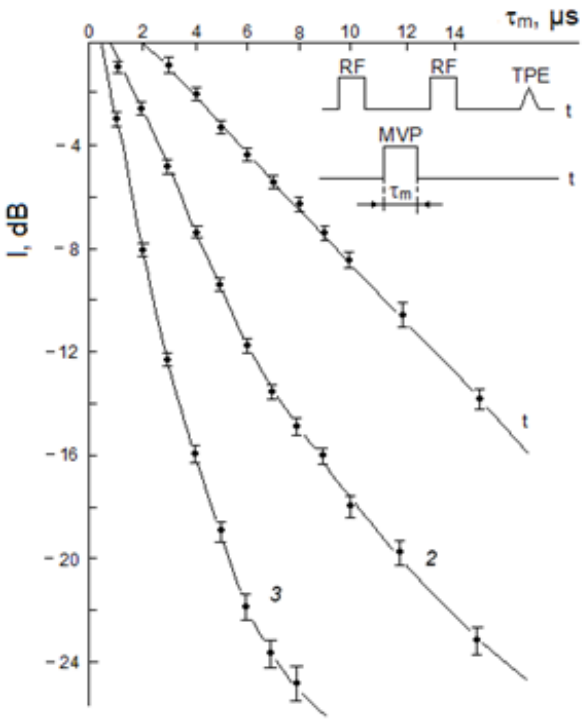

Figure 2. Dependence of TPE (A –sites of nickel ferrite) on the duration of MVP τ_m at H = 2 Oe (*1*), 4 Oe (*2*), 10 Oe (*3*).

We also note that earlier in (Mamniashvili et al., 2015; Pleshakov et al., 2016; Gavasheli et al., 2020) the dependence of H_0 on the external magnetic field H_e was not studied. As is known (Pleshakov et al., 2016), the application of a large constant magnetic field reduces the number of DWs, and the remaining ones are distributed over pinning centers, which contribute to a greater pinning. The purpose of this work is to study the experimental dependence of H_0 on τ_m and H on the example of the effect of MVP on the TPE and ME signals observed from ^{59}Co nuclei in the DWs of a cobalt micropowder.

Experimental Results and Their Discussion

The block diagram of the experimental setup is shown in Figure 3: RF excitation pulses are generated by generator *1*. Next, a sequence of NMR excitation echo pulses is fed into resonator *2* with the ring-shaped lithium ferrite sample used. The RF field of the pulses excites the echo signal in the upper coil of the resonator *2*. Then these pulses, together with the echo signal S, enter the receiver *3* and are recorded by the oscilloscope *4*. The channel *5* generates MVP pulses applied to the lower winding of the resonator. A description of the NMR spectrometer and MVP unit is given in (Gavasheli et al., 2020). The experimental results were obtained at T = 77 K. The echo signal amplitude was measured in the presence and absence of a MVP with amplitude H.

We used samples of lithium-zinc ferrite $Li_{0.5}Fe_{1.0}Zn_{0.15}O_4$, which were rings with a diameter of 12-15 mm and a weight of 5-8 g, enriched in the ^{57}Fe isotope to 96.8% in order to increase the intensity of the echo signal (Mamniashvili et al., 2015). The NMR spectrum of lithium ferrite at T = 77 K consists of two well-resolved lines, where the low-frequency line belongs to the tetrahedral sites A, and the high-frequency line to the octahedral sites B. The ^{57}Fe NMR spectrum of the spin echo of the polycrystalline sample of lithium-zinc ferrite under study is shown in Figure 4.

Because of the large angles of electronic magnetization M rotation associated with DW displacement, the displacement of the DW under the action of MVP in between RF pulses, even being insignificant, can be accompanied by a large rotation of M. In this case, the rotation of M inside the DW is proportional to the displacement of the DW. This process is accompanied by abrupt inhomogeneous changes of dephasing isochromate frequencies proportional to the displacement of the DW due to anisotropy of the HFF in magnetic material (Gavasheli et al., 2020), resulting in the echo signal suppression.

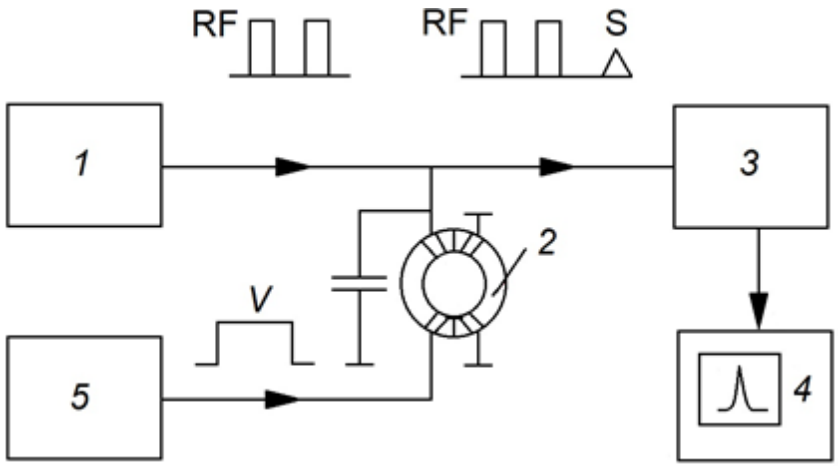

Figure 3. Block diagram of the experimental setup: *1* - RF pulse excitation generator; *2* - resonator with a ring-shaped sample of lithium-zinc ferrite; *3* - RF receiver; *4* - oscilloscope; *5* - channel of formation of MVP.

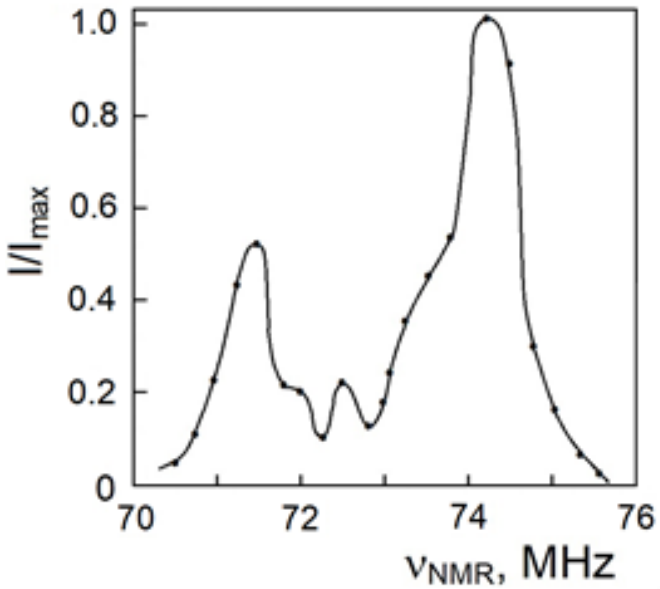

Figure 4. NMR spectrum of ^{57}Fe nuclei in polycrystalline lithium-zinc ferrite, T = 77 K.

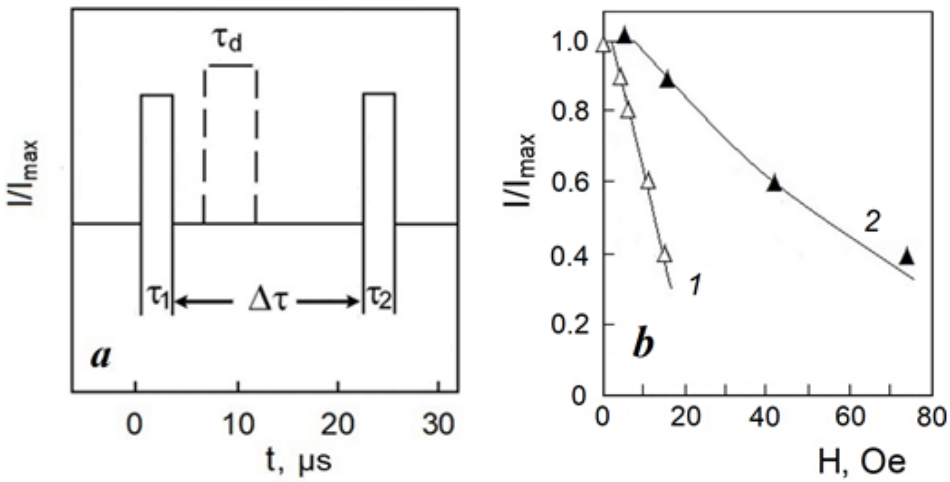

Figure 5. (a) - Position of the MVP acting in the interval between RF pulses. (b) Amplitude diagrams of the effect of MVP on a two-pulse echo (TPE) in lithium-zinc ferrite at frequencies of 71 and 74 MHz, curves – 2 and 1, corresponding to A and B positions respectively, the duration of the MVP τ_d =1.0 μs, T = 77 K.

The MVP amplitude at which the TPE intensity begins to decline, associated with the onset of the DW motion, is naturally related to the DW pinning field H_0. The diagram showing the effect of MVP acting in the time interval between two RF pulses on TPE is presented in Figure 5. In Figure 5b one can see also a significant increase in the pinning field H_0 upon passing from octahedral B to tetrahedral A positions.

Analysis of the dependence of the MVP effect on echo signals in the studied samples shows a significant, up to one order of magnitude, increase in DW mobility and a decrease in the pinning force in lithium ferrite as compared to cobalt (Gavasheli et al., 2020). A particularly large MVP effect on the TPE is observed for the echo signal from nuclei located in octahedral B-sites of lithium ferrite at a frequency of 74 MHz with a higher anisotropy HFF (Doroshev et al., 1972), compared to the echo from the nuclei in tetrahedral positions A at a frequency of 71 MHz, Figure 5b.

The pinning field H_0 could be measured also at the combined action of MVP and radiofrequency (RF) pulse on the nuclear spin system in DW at the process of formation a single-pulse echo (SPE), by means of generation of the so-called stimulated magnetic echo (ME) signal (Gavasheli et al., 2020). The ME is formed at combined application of RF and MVP pulses due to an abrupt non-adiabatic change of effective magnetic field $\vec{H}_{eff} = \frac{1}{\gamma_n}(\Delta\omega_j\vec{z} + \omega_1\vec{y})$ in the rotating coordinate system (RCS), where γ_n is the nuclear gyromagnetic ratio, $\vec{z}$ and $\vec{y}$ are unit vectors in RCS, $\Delta\omega_j=\omega_{NMR} - \omega_{RF}$ is the detuning for the j-th isochromate, $\omega_1=\gamma_n\eta H_1$ is the pulse amplitude in frequency units and η is the RF field amplification factor. In this case the application of MVP is equivalent to the application of additional RF pulse which in combination with two other RF pulse analogs, corresponding to the RF pulse edges, forms a ME signal (Gavasheli et al., 2020). In lithium ferrite, the oscillogram of the observed signal of a stimulated ME followed by the single-pulse echo (SPE) signal is shown at 71 MHz in Figure 6a, and dependences of ME and SPE intensities on the MVP amplitude were obtained, Figure 6b, similar to the corresponding dependences in cobalt (Gavasheli et al., 2020).

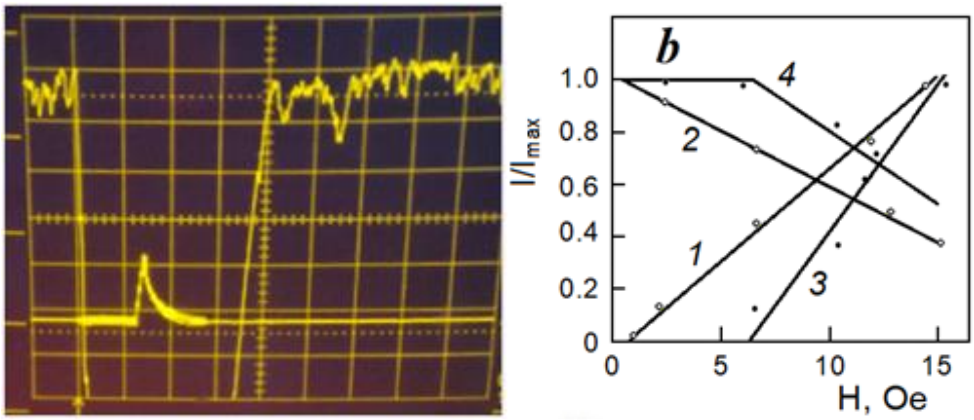

Figure 6. (a) Oscillogram of the magnetic and subsequent SPE echo signals in lithium-zinc ferrite (upper beam), NMR = 71 MHz, T = 77 K, the lower beam shows the duration of the radio frequency magnetic pulses as well as the amplitude of the magnetic video-pulse; (b) dependences of the signals of the magnetic (*1*,*3*) and single-pulse (*2*,*4*) echoes on the amplitude of the magnetic video pulse at frequencies of 74 and 71 MHz, respectively:

τ_{RF} = 15 μs, τ_d = 0.5 μs, T=77 K.

The amplitude of MVP at which the ME appears, Figure 6b, correlates with the MVP amplitude acting on the TPE, at which its decrease begins, which is associated with the DW pinning field H_0, Fig. 4b, giving an alternative way to measure DW pinning force H_0 and mobility in magnets.

The observed experimental dependences of the SPE and TPE signals can be understood taking into account that, according to (1), under the action of the MVP, the DW reversibly shifts at a distance Δx proportional to the MVP amplitude $\Delta x \sim \upsilon\,\tau_d = S\,(H-H_0)\,\tau_d$, when the MVP amplitude exceeds the values of the pinning field H_0. In the Δx layer, the nuclei under the combined action of RF and MVP experience the effect of a jump-like change in the magnitude and direction of the effective magnetic field H_{eff} in the RCS, due to the corresponding change in the local HFF and factor η. Therefore, according to the nonresonant model of the SPE formation (Gavasheli et al., 2020), the effect of the MVP is equivalent to the effect of the second RF pulse in combination

with two RF pulse analogs corresponding to the RF pulse edges, resulting in formation of the three-pulse ME signal. The ME amplitude is proportional to the number of nuclei in a Δx layer formed when the DW is displaced: $I_{ME} \sim \Delta x/L$, where L is the width of the excited section of the DW under the action of an RF pulse. These nuclei do not contribute in SPE formation due to the loss of phase coherence and, correspondingly, I_{SPE} is proportional the number of nuclei in the remaining part of excited by RF pulse DW section $I_{SPE} \sim (L - \Delta x)/L$. In this case, the jump-like change in the NMR frequency in the RCS at combined action of RF and MVP, must satisfy the condition $\Delta\omega'_j\tau_d << 1$, or, in other words, the precession period of the nuclei in the RCS $\Delta\omega'_j=(\Delta\omega^2+\omega_1^2)^{1/2}$ should be larger as compared with τ_d. When the MVP is applied to the TPE in the interval between RF pulses, nuclei precess in the local HFF with a frequency $\omega_j=\gamma_n H_{HFF}$ and, therefore, the new condition $\omega_j\tau_d << 1$ should be fulfilled to observe an additional ME signal, which requires that a nanosecond duration of the MVP τ_d must be used, as in case of observing an inverse echo signal (Ignatchenko et al., 1963), which in our case is not satisfied. Therefore, the effect of MVP on TPE leads only to a decrease in the intensity of TPE, proportional to a DW displacement Δx: $I_{TPE} \sim (L - \Delta x)/L$, due to the loss of phase coherence of nuclei in this layer. These qualitative considerations make it possible to understand the obtained experimental dependences of the ME, SPE and TPE signals under the action of MVP.

The measurements were carried out on a phase-incoherent spin echo spectrometer (Gavasheli et al., 2022; Mamniashvili & Gegechkori, 2023) in the frequency range of 200–400 MHz at a temperature of 293 K. In the range of 200–400 MHz, a commercial Lecher-type generator with a two-wire line, including two inductors with different numbers of turns, was used. For pulse lengths in the range from 0.1 to 50 μs, the maximum amplitude of the RF field produced on the sample was about 3.0 Oe, and the front steepness was no worse than 0.15 μs. Receiver dead time ~ 1 μs.

The scheme of the experiment on pulsed magnetic action is given in (Gavasheli et al., 2022; Mamniashvili & Gegechkori, 2023).

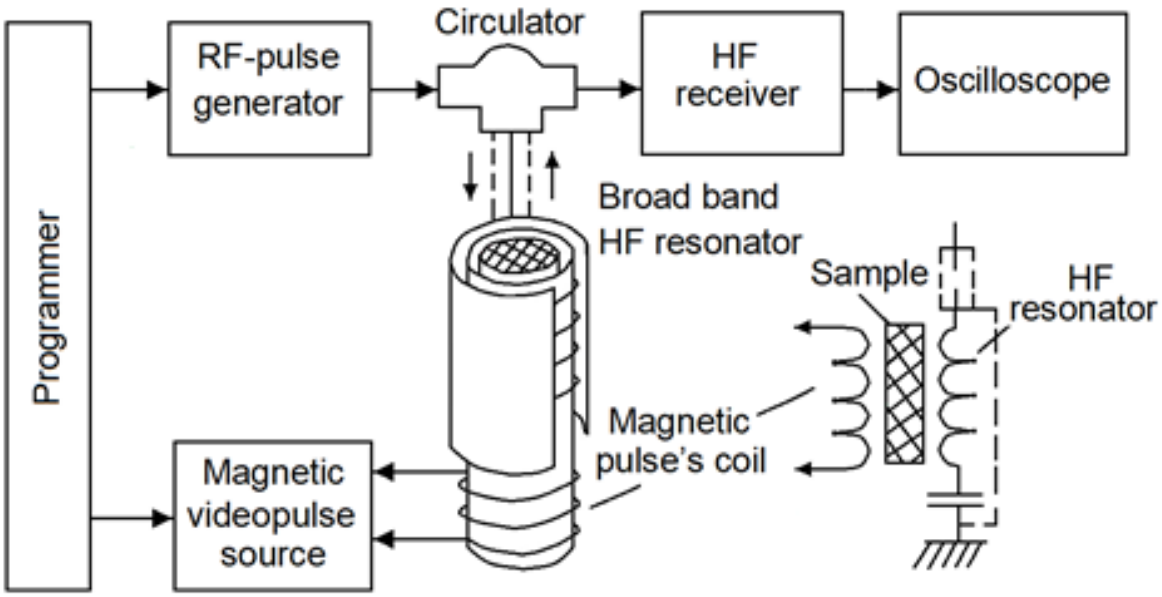

Figure7. NMR spectrometer setup

The MVP was created by a gated current stabilizer of adjustable amplitude and an additional copper coil, which made it possible to obtain magnetic field pulses of the order of 500 Oe for a sample size of ~10 mm.

Cobalt micropowders were obtained by the alloying method (Gavasheli et al., 2022; Mamniashvili & Gegechkori, 2023) with an average grain size of ~10 μs. Characteristic parameters of RF pulses: duration - a few microseconds, a delay between them - tens of microseconds, a carrier frequency of 213 MHz at T = 293 K coincides with the frequency of the nuclei in the centres of the DW of the face-centred cubic (fcc) phase of cobalt.

The oscillograms of the experiments are shown in Figure 8.

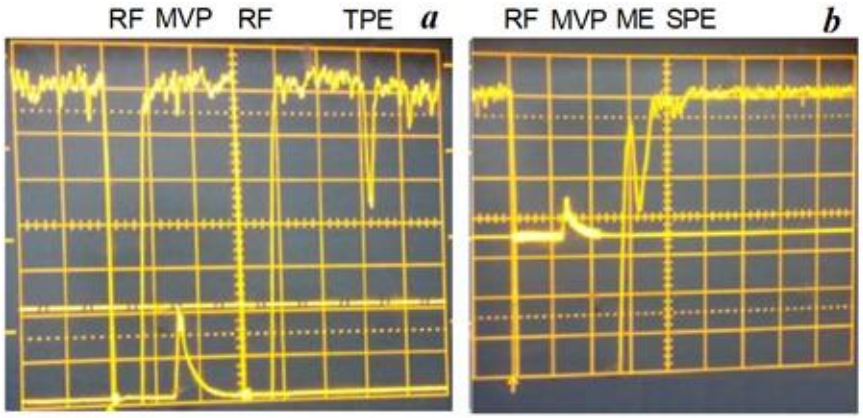

Figure 8. Oscillogram of the TPE signal in cobalt (upper beam) and the wavemeter signal showing the position of RF and MVP pulses (lower beam) (a); oscillogram of the ME and RPE signals in cobalt, the lower beam shows the duration and position of the RF pulse, as well as the position of the MVP (b).

The NMR spectrum of the studied cobalt sample is shown in Figure 9 a. Comparison of curves *1* and *4* in Figs. 9b indicates a much higher magnetic hardness of cobalt compared to lithium-zinc ferrite. Curves *2* and *3* in Figs. 9b demonstrate similar dependences of the relative intensity I/I_{max} of the TPE and ME signals on the magnetic field H_e, which reflects the same mechanisms of their formation (Mamniashvili et. al., 2022). Figure 8 shows oscillograms explaining the scheme of the experiment and Figure 9b shows the dependences of the TPE on the MVP amplitude under the action of an external H_e field and the corresponding results for the ME.

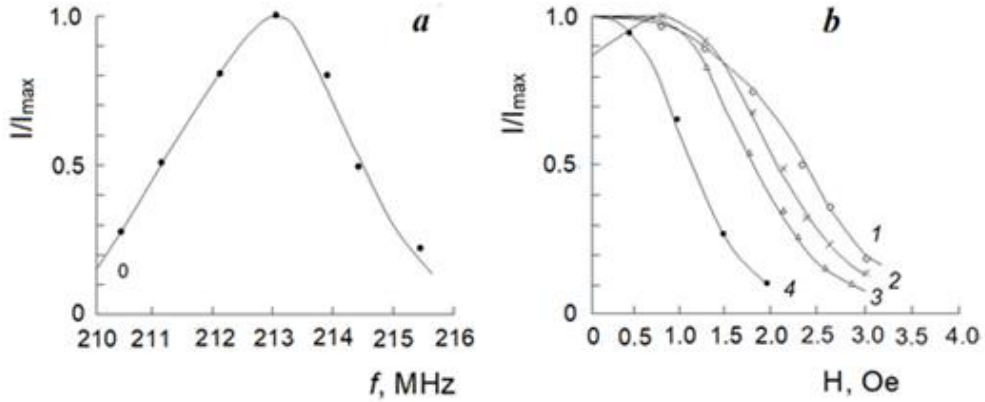

Figure 9. ^{59}Co NMR spectrum of the investigated Co micropowder (a) a change in the relative intensities I/Imax of echo signals in cobalt with increasing constant magnetic field H_e: curves *1*, *2*, *3* – TPE, SPE, and ME, respectively, *4* - TPE in lithium-zinc ferrite (b); T=293K.

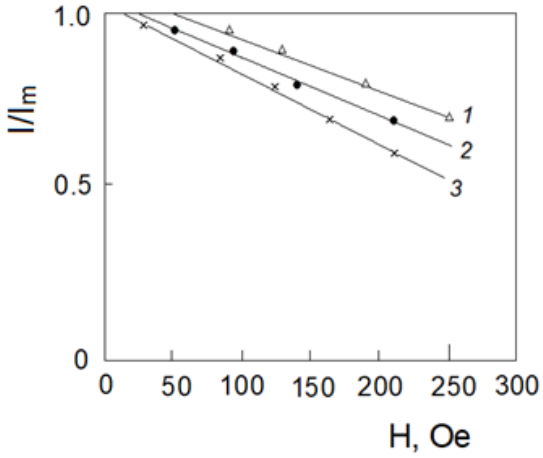

Figure 10. Dependence of the normalized TPE intensity I/I_m on the MVP amplitude H: *1-3* at τ_m =1, 2, and 3 μs, respectively.

Let us present the results of the study of the pinning force H_0 under the action of an additional MVP, depending on the duration of the MVP τ_m, on the TPE signals in a cobalt micropowder, Figure 10. Analysis of the obtained results in Figure 10 shows that in the case of cobalt the relation $A_m = H_0 \cdot \tau_m$=const, also holds according to which the MVP threshold area is constant for all MVP durations. This coincides with a similar conclusion for the MVP threshold area in the case of nickel ferrite, Figure 6.

It should be noted that for the first time such a relation was established in the NMR study of the pinning force H_0 of the ME signal dependence on τ_m (Gavasheli et al., 2022; Mamniashvili & Gegechkori, 2023) in cobalt. And A_m is the threshold area of the MVP, corresponding to the beginning of the displacement of the DW under the action of the MVP. The physical meaning of this result can be understood if we take into account that, according to the one-dimensional DW model (Konishi et. al., 1976), the DW displacement x under the action of a short MVP with amplitude H and duration τ_m is determined by the relation

$$x=C\cdot H\cdot\tau_m,$$

Where C is a constant characteristic of the material under study. Thus, the same displacement of the DW corresponds to any of the threshold values of the MVP, and it is natural to associate it with the width of the potential well in which the DW is located in the initial state. We also note that a similar relationship between H and τ_m was established in the study of Permalloy films by the Kerr magneto-optical method (Bartran & Bourne, 1973).

Let us further investigate the dependence of H_0 on the magnitude of the external magnetic field H_e at a fixed MVP duration τ_m =1 μs.

The results obtained by two alternative methods show an increase in the pinning force in cobalt with increasing H_e in accordance with (Pleshakov et al., 2016), but in a larger range (up to 3 kOe) compared to 1 kOe in lithium-zinc ferrite [5] and confirm the possibility of studying the force pinning of H_0 in cobalt micropowders by two alternative NMR methods using additional MMI. In contrast to [5], an increase in the pinning force in cobalt is observed in a wider range of external constant magnetic field H_e due to the higher magnetic hardness of cobalt compared to lithium-zinc ferrite (~3 kOe in cobalt compared to ~1 kOe in lithium-zinc ferrite).

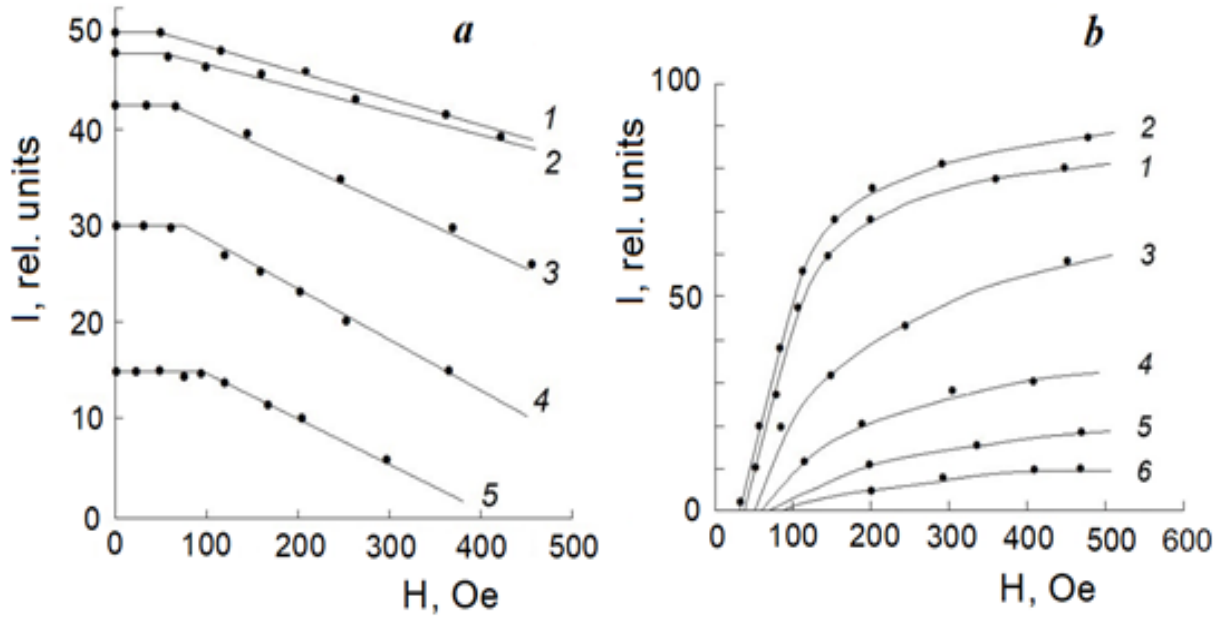

Figure 11. Dependences of the TPE intensity on the MVP amplitude in cobalt in the interval between RF pulses at H_e=0 (*1*), 0.8 (*2*), 1.9 (*3*), 2.3 (*4*), and 3 kOe (*5*) (a) and the intensity ME on the MVP amplitude in cobalt at H_e = 0 (*1*), 0.8 (*2*), 1.3 (*3*), 2.3 (*4*), 2.6 (*5*), and 2.8 kOe (*6*).

Based on the data in Fig. 11, it is possible to construct the dependence of the pinning force H_0 on the magnitude of the external field H_e, Figure 12.

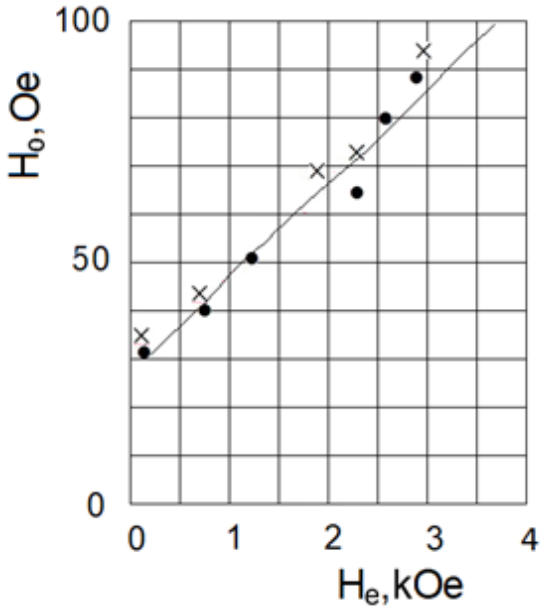

Figure 12. Dependence of the pinning force H_0 on the magnitude of the external constant magnetic field H_e on the threshold of the ME signal generation (x) and the influence of the MVP on the TPE amplitude (•).

Thus, it has been established that up to external fields ~ 3 kOe, a linear dependence of H_0 on H_e is observed. This indicates that, at higher H_e, the DWs are distributed over positions corresponding to the parameters of the potential walls providing stronger pinning. We also note a feature of the data in Figure 11, which consists in the fact that the rate of suppression of the TPE signal increases with increasing H_e, in contrast to that observed in lithium ferrite (Pleshakov et al., 2016), which is due to the differences in the NMR properties of cobalt and lithium ferrite noted above (Mamniashvili et. al., 2021).

Conclusions

It is shown that the excitation of nuclear spin echo signals in combination with a magnetic video-pulse is a convenient method for evaluation the domain wall pinning field in magnetic materials on example of a lithium-zinc sample. Two different methods were applied to evaluate the domain wall pinning in a lithium-zinc ferrite. In the first case, the pinning of domain walls was measured by the action of magnetic video-pulse on a two-pulse echo signal, and in the second one, the pinning was measured at the combined action of magnetic video-pulse and RF pulses on the nuclear spin system in domain walls in the process of formation of a single-pulse echo, by means of generation of the so-called magnetic echo signal.

Qualitative considerations are presented making it possible to understand the obtained experimental dependences of the single-pulse, magnetic and two-pulse echo signals under the action of a magnetic video-pulse.

In the present work, for the first time, the pinning force of domain walls was studied by the NMR two-pulse spin-echo method under the action of an additional magnetic video-pulse in cobalt. It was shown that the pinning value H_0 is inversely proportional to the length of the magnetic video-pulse τ_m. In addition, the area of the magnetic video pulse turned out to be constant for all threshold durations of the magnetic video pulse.

The dependence of the pinning force H_0 on the external constant magnetic field H_e is studied. It is shown that up to ~ 3 kOe there is a linear dependence of H_0 on H_e. This indicates that as the H_e increases the domain walls are distributed over sites corresponding to the stronger pinning centers.

The degree of pinning (pinning force) of domain walls in cobalt micropowder has been studied by two alternative NMR methods: by the action of a magnetic video pulse on a two-pulse echo and by the threshold for generating of the magnetic echo signal under the action of an additional magnetic video-pulse. A linear dependence of the pinning force on the amplitude of the magnetic video pulse is established in a wider range of the external magnetic field (up to ~ 3 kOe) compared to the softer lithium-zinc ferrite (observed up to 1 kOe).

Scientific Ethics Declaration

The authors declare that the scientific ethical and legal responsibility of this article published in EPSTEM journal belongs to the authors.

Acknowledgements or Notes

* This article was presented as oral presentation at the International Conference on Basic Sciences, Engineering and Technology (www.icbaset.net) held in Marmaris/Turkey on April 27-30, 2023.

* This work was supported by Shota Rustaveli National Science Foundation of Georgia (Grant # STEM-22-1339).

References

Bartran, D., & Bourne, H. (1973). Domain wall velocity and interrupted pulse experiments. *IEEE Transactions on Magnetics*, *9*(4), 609-613.

Doroshev, V. D., Klochan, V. A., Kovtun, N. M., & Seleznev, V. N. (1972). The effect of dipole and anisotropic hyperfine fields on NMR of Fe^{57} in lithium ferrite $Li_{0.5}Fe_{2.5}O_4$. *Physica Status Solidi A*, *9*(2), 679-689.

Galt, J. K. (1954). Motion of individual domain walls in a nickel-iron ferrite. *Bell Labs Technical Journal*, *33*(5), 1023-1054.

Gavasheli, T. A., Mamniashvili, G. I., Shermadini, Z. G., Zedginidze, T. I., Petriashvili, T. G., Gegechkori, T. O, & Janjalia, M. V. (2020). Investigation of the pinning and mobility of domain walls in cobalt micro- and nanowires by the nuclear spin echo method under the additional influence of a magnetic video pulse. *Journal of Magnetism and Magnetic Materials*, *500*. 166310.

Gavasheli, T., Gegechkori, T., Mamniashvili, G., & Gvedashvili, G. (2021). NMR spin echo study of domain wall pinning in lithium ferrite in combination with an additional magnetic video-pulse. *Proceedings of the XXVI International Seminar/Workshop on Direct and Inverse Problems of Electromagnetic and Acoustic Wave Theory (DIPED-2021)*, (pp. 199-202). IEEE.

Gavasheli, T., Mamniashvili, G., Ghvedashvili, G., & Gegechkori, T. (2022). NMR spin-echo study of the domain wall pinning in cobalt micropowders. *Proceedings of the 2nd Ukrainian Microwave Week (UkrMW)*, (pp. 405-409). IEEE.

Ignatchenko, V. A., Mal'tsev, V. K., Reihgardt, A. E., & Tsifrinovich, V. I. (1983). New mechanism for formation of nuclear-spin echo. *JETP Letters*, *37*(9), 520-522.

Konishi, S., Mizuno, K., Watanabe, F., & Narita, K. (1976). Domain wall displacement under pulsed magnetic field. *AIP Conference Proceedings*, *34*(1), 145-147.

Mamniashvili, G. I., Gegechkori, T. O., Akhalkatsi, A. M., & Gavasheli, T. A. (2015). On the role of the hyperfine field anisotropy in the formation of a single-pulse NMR spin echo in cobalt. *Journal of Superconductivity and Novel Magnetism*, *28*(3), 911-916.

Mamniashvili, G., Zviadadze, M., Gegechkori, T., & Shermadini, Z. (2016). NMR spectroscopy of magnets using arbitrary number and duration radio-frequency pulses. *International Journal of Trend in Research and Development*, *3*(2), 434-473.

Mamniashvili, G. I., Gegechkori, T. O., & Gavasheli, Ts. A. (2021). Study of the nature of the NMR signal in lithium ferrite upon exposure to a low-frequency magnetic field. *Physics of Metals and Metallography*, *122*(9), 841-846.

Mamniashvili, G., Gegechkori, T., Janjalia, M., & Gogishvili, P. (2022). Investigation of the single-pulse NMR echo origin in cobalt using additional magnetic video-pulses. *Magnetic Resonance in Solids*, *24*, 22102.

Mamniashvili, G. I., & Gegechkori, T. O. (2023). Investigation of the characteristics of domain wall fixation centers in cobalt by nuclear magnetic resonance. *Journal of Applied Spectroscopy*, *89*(6), 1076–1079.

Pleshakov, I. V., Popov, P. S., Kuz'min, Yu. I., & Dudkin, V. I. (2016). NMR study of domain wall pinning in a magnetically ordered material. *Technical Physics Letters*, *42*(1), 59-62.

Rassvetalov, L. A., & Levitski, A. B. (1981). Influence of a pulsed magnetic field on the nuclear spin echo in some ferromagnets and ferrimagnets. *Soviet Physics, Solid State*, *23*(11), 3354- 3359.

Shmyreva, A. A., Matveev, V. V., & Yurkov, G. Y. (2016). Nuclear magnetic resonance in magnetic nano-materials as an effective technique to test and/or to certificate local magnetic properties. *International Journal of Nanotechnology*, *13*(1-3), 126-135.

Turov, E. A., & Petrov, M. P. (1972). *Nuclear magnetic resonance in ferro- and antiferromagnets*. New York, NY: Halsted (Wiley).

Wurmehl, S., & Kohlhepp J. T. (2008). Nuclear magnetic resonance studies of materials for spintronic applications. *Journal of Physics D: Applied Physic*s, *41*(17).

Author Information

Tsisana Gavasheli
Ivane Javakhishvili Tbilisi State University
Tbilisi, Georgia
Contact e-mail: *tsismari.gavasheli@tsu.ge*

Grigor Mamniashvili
Ivane Javakhishvili Tbilisi State University
Tbilisi, Georgia

Tatiana Gegechkori
Ivane Javakhishvili Tbilisi State University
Tbilisi, Georgia

To cite this article:

Gavasheli.T., Mamniashvili G., & Gegechkori T., (2023). NMR spin echo study of domain wall pinning in magnets in combination with an additional magnetic video-pulse, *The Eurasia Proceedings of Science, Technology, Engineering & Mathematics (EPSTEM), 22*, 348-358.

The Eurasia Proceedings of Science, Technology, Engineering & Mathematics (EPSTEM)
ISSN: 2602-3199

The Eurasia Proceedings of Science, Technology, Engineering & Mathematics (EPSTEM), 2023

Volume 22, Pages 359-363

ICBASET 2023: International Conference on Basic Sciences, Engineering and Technology

On gr-Quasi-Semiprime Submodules

Khaldoun AL-ZOUBI
Jordan University of Science and Technology

Shatha ALGHUEIRI
Jordan University of Science and Technology

Abstract: Let G be a group. A ring R is called a graded ring (or G-graded ring) if there exist additive subgroups R_α of R indexed by the elements $\alpha \in G$ such that $R = \oplus_{\alpha\in G} R_\alpha$ and $R_\alpha R_\beta \subseteq R_{\alpha\beta}$ for all $\alpha, \beta \in G$. If an element of R belongs to $h(R) = \cup_{\alpha\in G} R_\alpha$, then it is called a homogeneous. A Left R-module M is said to be *a graded R-module* if there exists a family of additive subgroups $\{M_\alpha\}_{\alpha\in G}$ of M such that $M = \oplus_{\alpha\in G} M_\alpha$ and $R_\alpha M_\beta \subseteq M_{\alpha\beta}$ for all $\alpha, \beta \in G$. Also if an element of M belongs to $\cup_{\alpha\in G} M_\alpha = h(M)$, then it is called a homogeneous. A submodule N of M is said to be *a graded submodule of M* if $N = \oplus_{\alpha\in G}(N \cap M_\alpha) := \oplus_{\alpha\in G} N_\alpha$. Let G be a group with identity e. Let R be a G -graded commutative ring and M a graded R-module. A proper graded submodule S of M is said to be *a graded semiprime (*shortly gr *-semiprime) submodule* if whenever $r^n m \in S$ where $r \in h(R)$, $m \in h(M)$ and $n \in Z^+$, then $rm \in S$. In this work, we introduce the concept of graded quasi-semiprime (shortly gr-quasi-semiprime) submodule as a generalization of gr-semiprime submodule and give some basic properties of these classes of graded submodules. We say that a proper graded submodule S of M is a gr-quasi-semiprime submodule if $(S:_R M) = \{r \in R: rM \subseteq S\}$ is a gr-semiprime ideal of R.

Keywords: Graded quasi-semiprime submodule, Graded semiprime submodule, Graded prime.

Introduction

Throughout this paper all rings are commutative with identity and all modules are unitary. Graded semiprime submodules of graded modules over graded commutative rings, have been introduced and studied in Farzalipour et al., 2012; Lee et al., 2012; Al-Zoubi et al., 2017). Also, the concept of graded semiprime ideal was introduced by Lee and Varmazyar in Lee (2012) and studied in Farzalipour et al. (2013). Recently, Al-Zoubi et al. (2017) introduced and studied the concept of graded semi-radical of graded submodules in graded modules.

Here, we introduce the concept of graded quasi-semiprime submodules of graded modules over a commutative graded rings as a generalization of graded semiprime submodules and investigate some properties of these classes of graded submodules. Let R be a G-graded ring, M a graded R-module and N a graded submodule of M. Then $(N:_R M)$ is defined as $(N:_R M) = \{r \in R: rM \subseteq N\}$. It is shown in Atani (2006) that if N is a graded submodule of M, then $(N:_R M)$ is a graded ideal of R. The annihilator of M is defined as $(0:_R M)$ and is denoted by $Ann_R(M)$. A proper graded submodule N of M is said to be *a graded semiprime submodule* if whenever $r \in h(R)$, $m \in h(M)$ and $n \in Z^+$ with $r^n m \in N$, then $rm \in N$, (Farzalipour et al., 2012). A proper graded ideal I of R is said to be graded semiprime ideal if whenever $r, s \in h(R)$ and

$n \in Z^+$ with $r^n s \in I$, then $rs \in I$, (Farzalipour et al., 2013). For more information about the properties of graded rings and graded modules see Nastasescu et al. (1982), Nastasescu et al. (2004) and Hazrat (2016).

Results and Discussion

Definition 1. Let R be a G-graded ring and M a graded R-module. A proper graded submodule N of M is said to be *a graded quasi-semiprime submodule of* M if $(N:_R M)$ is a graded semiprime ideal of R.

Theorem 2. *Let R be a G-graded ring, M a graded R-module and N a proper graded submodule of M. If N is a graded semiprime submodule of M, then N is a graded quasi-semiprime submodule of M.*

Proof. By Al-Zoubi et al. (2017).□

The next example shows that a graded quasi-semiprime submodule is not necessarily graded semiprime submodule.

Example 3. Let $G = \mathbb{Z}_2$, $R = \mathbb{Z}$ be a G-graded ring with $R_0 = \mathbb{Z}$ and $R_1 = \{0\}$. Let $M = \mathbb{Z} \times \mathbb{Z}$ be a graded R-module with $M_0 = \mathbb{Z} \times \{0\}$ and $M_1 = \{0\} \times \mathbb{Z}$. Now, consider a submodule $N = 4\mathbb{Z} \times \{0\}$ of M. Then it is a graded submodule and $(N:_R M) = \{0\}$ is a graded semiprime ideal of R, and so N is a graded quasi-semiprime submodule of R. But the graded submodule N is not graded semiprime submodule of M, since $2^2(3,0) \in N$ but $2(3,0) \notin N$.

Example 4. Let $G = \mathbb{Z}_2$, $R = \mathbb{Z}$ be a G-graded ring with $R_0 = \mathbb{Z}$ and $R_1 = \{0\}$. Let $M = \mathbb{Z}_8$ be a G-graded R-module with $M_0 = \mathbb{Z}_8$ and $M_1 = \{0\}$. Now, consider a submodule $N =< 4 >$ of M. Then it is a graded submodule and $(N:_R M) = 4\mathbb{Z}$ is not a graded semiprime ideal of R since $2^2 1 = 4 \in 4\mathbb{Z}$ but $2 \cdot 1 = 2 \notin 4\mathbb{Z}$. Then N is not graded quasi-semiprime submodule of M.

Recall that a graded R-module M is called *a graded multiplication* if for each graded submodule N of M, we have $N = IM$ for some graded ideal I of R. If N is graded submodule of a graded multiplication module M, then $N = (N:_R M)M$.

Theorem 5. *Let R be a G-graded ring, M a graded multiplication R -module and N a proper graded submodule of M. Then N is a graded quasi-semiprime submodule of M if and only if N is a graded semiprime submodule of M.*

Proof. By Al-Zoubi et al.(2017)

Theorem 6. *Let R be a G-graded ring, M a graded multiplication R-module and N a proper graded submodule of M. Then the following statements are equivalent:*

1. *N is a graded quasi-semiprime submodule of M.*
2. *If whenever $I^k M \subseteq N$, where I is a graded ideal of R and $k \in \mathbb{Z}^+$, then $IM \subseteq N$.*

Proof. $(i) \Rightarrow (ii)$ By Theorem 5 and Farzalipour et al. (2012).

$(ii) \Rightarrow (i)$ Let $r^k s \in (N:_R M)$ where $r, s \in h(R)$ and $k \in \mathbb{Z}^+$. So $r^k sM \subseteq N$. Let $I = (rs)$ be a graded ideal of R generated by rs. Then $I^k M \subseteq N$. By our assumption we have $IM = (rs)M \subseteq N$. This

yields that $rs \in (N:_R M)$. So $(N:_R M)$ is a graded semiprime ideal of R. Therefore N is a graded quasi-semiprime submodule of M. □

Recall that a proper graded ideal I of a G-graded ring R is said to be *a graded prime ideal* if whenever $r, s \in h(R)$ with $rs \in I$, then either $r \in I$ or $s \in I$ Refai et al. (2004). A proper graded ideal J of R is said to be *a graded primary ideal* if whenever $r, s \in h(R)$ with $rs \in J$, then either $r \in J$ or $s^n \in J$ for some $n \in \mathbb{Z}^+$ Refai et al.(2004).

Theorem 7. *Let R be a G-graded ring, M a graded R-module and N a graded quasi-semiprime submodule of M. If $(N:_R M)$ is a graded primary ideal of R, then $(N:_R M)$ is a graded prime ideal of R.*

Proof. Suppose that $(N:_R M)$ is a graded primary ideal of R. Let $rs \in (N:_R M)$ and $r \notin (N:_R M)$. Then $s \in Gr\big((N:_R M)\big)$ as $(N:_R M)$ is a graded primary ideal of R. Hence $s^k \in (N:_R M)$ for some $k \in \mathbb{Z}^+$. Since $(N:_R M)$ is a graded semiprime ideal of R, we have $s \in (N:_R M)$. Therefore $(N:_R M)$ is a graded prime ideal of R. □

Let R be a G-graded ring, M a graded R-module and N a graded submodule of M. The graded envelope submodule $RGE_M(N)$ of N in M is a graded submodule of M generated by the set $GE_M(N) = \{rm : r \in h(R), m \in h(M)$ such that $r^n m \in N$ for some $n \in \mathbb{Z}^+\}$ (Atani et al., 2010).

Theorem 8. *Let R be a G-graded ring, M a graded multiplication R-module and N a proper graded submodule of M. Then N is a graded quasi-semiprime submodule of M if and only if $N = RGE_M(N)$.*

Proof. Suppose that N is a graded quasi-semiprime submodule of M. Then N is a graded semiprime submodule of M by Theorem 5. Clearly, $N \subseteq RGE_M(N)$. Now, let $x \in GE_M(N)$. Then $x = rm$ for some $r \in h(R)$, $m \in h(M)$ and there exists $k \in \mathbb{Z}^+$ such that $r^k m \in N$. Then $rm \in N$ as N is a graded semiprime submodule of M. Hence $GE_M(N) \subseteq N$. This yields that $RGE_M(N) \subseteq N$. Thus $N = RGE_M(N)$. Conversely, suppose that $N = RGE_M(N)$. Let $r \in h(R)$, $m \in h(M)$ and $k \in \mathbb{Z}^+$ such that $r^k m \in N$, so by the definition of the set $GE_M(N)$ we have $rm \in GE_M(N)$. Then $rm \in N$ as $GE_M(N) \subseteq RGE_M(N) = N$, so N is a graded semiprime submodule of M. Therefore N is a graded quasi-semiprime submodule of M by Theorem 2. □

Let R be a G-graded ring and M, M' be two graded R-modules. Let $f: M \to M'$ be an R-module homomorphism. Then f is said to be *a graded homomorphism* if $f(M_\alpha) \subseteq M'_\alpha$ for all $\alpha \in G$ (Nastasescu et al., 2004).

Theorem 9. *Let R be a G-graded ring, M, M' be two graded R-modules and $f: M \to M'$ a graded epimorphism.*

1. *If N is a graded quasi-semiprime submodule of M such that $ker(f) \subseteq N$, then $f(N)$ is a graded quasi-semiprime submodule of M'.*
2. *If N' is a graded quasi-semiprime submodule of M', then $f^{-1}(N')$ is a graded quasi-semiprime submodule of M.*

Proof. (i) Suppose that N is a graded quasi-semiprime submodule of M and $ker(f) \subseteq N$. It is easy to see that $f(N) \neq M'$. Now let $r^k s \in (f(N):_R M')$ where $r, s \in h(R)$ and $k \in \mathbb{Z}^+$, it follows that,

$r^k sM' \subseteq f(N)$. Then $r^k sM' = r^k sf(M) = f(r^k sM) \subseteq f(N)$ since f is an epimorphism. This yields that $r^k sM \subseteq N$ since $ker(f) \subseteq N$, i.e., $r^k s \in (N:_R M)$. Since N is a graded quasi-semiprime submodule of M, we get $rs \in (N:_R M)$, i.e., $rsM \subseteq N$. Hence $f(rsM) = rsf(M) = rsM' \subseteq f(N)$, i.e., $rs \in (f(N):_R M')$. Therefore, $f(N)$ is a graded quasi-semiprime submodule of M'.

(ii) Suppose that N' is a graded quasi-semiprime submodule of M'. It is easy to see that $f^{-1}(N') \neq M$. Let $r^k s \in (f^{-1}(N'):_R M)$ where $r, s \in h(R)$ and $k \in \mathbb{Z}^+$, it follows that, $r^k sM \subseteq f^{-1}(N')$. Then $r^k sf(M) = r^k sM' \subseteq N'$, i.e., $r^k s \in (N':_R M')$. Then $rs \in (N':_R M')$ as N' is a graded quasi-semiprime submodule of M'. So $rsM' = rsf(M) = f(rsM) \subseteq N'$. It follows that $rsM \subseteq f^{-1}(N')$. So $rs \in (f^{-1}(N'):_R M)$. Therefore $f^{-1}(N')$ is a graded quasi-semiprime submodule of M.

Theorem 10. *Let R be a G-graded ring, M a graded R-module and K a proper graded submodule of M. If N is a graded quasi-semiprime submodule of M with $N \subseteq K$ and $(N:_R M)$ is a graded maximal ideal of R, then K is a graded quasi-semiprime submodule of M.*

Proof. Suppose that $N \subseteq K$, it follows that $(N:_R M) \subseteq (K:_R M)$. By (Atani, 2006, Lemma 2.1), $(K:_R M)$ is a proper graded ideal of R. Then $(N:_R M) = (K:_R M)$ as $(N:_R M)$ is a graded maximal ideal of R. This yields that $(K:_R M)$ is a graded semiprime ideal of R. Therefore K is a graded quasi-semiprime submodule of M.

Theorem 11. *Let R be a G-graded ring, M a graded R-module and N and K be two graded quasi-semiprime submodules of M. Then $N \cap K$ is a graded quasi-semiprime submodule of M.*

Proof. Let $r^k s \in (N \cap K:_R M)$ where $r, s \in h(R)$ and $k \in \mathbb{Z}^+$. This yields that $r^k s \in (N:_R M) \cap (K:_R M)$. Since $(N:_R M)$ and $(K:_R M)$ are graded semiprime ideals of R, we have $rs \in (N:_R M) \cap (K:_R M)$ and so $rs \in (N \cap K:_R M)$. Therefore $N \cap K$ is a graded quasi-semiprime submodule of M.

Let R be a G-graded ring and M be a graded R-module, M is called a graded semiprime module if (0) is a graded semiprime submodule of M.

Definition 12. Let R be a G-graded ring and M be a graded R-module. Then M is said to be *a graded quasi-semiprime module* if $Ann_R N$ is a graded semiprime ideal of R, for every non-zero graded submodule N of M.

Theorem 13. *Let R be a G-graded ring and M be a graded R -module. If M is a graded semiprime module, then M is a graded quasi-semiprime module.*

Proof. Suppose that M is a graded semiprime module. Then 0 is a graded semiprime submodule of M. Now, Let N be a non-zero graded submodule of M and $r^k s \in Ann_R N$ where $r, s \in h(R)$ and $k \in \mathbb{Z}^+$. It follows that $r^k sN = 0$. Then $rsN = 0$ as 0 is a graded semiprime submodule of M. Hence $rs \in Ann_R N$, it follows that $Ann_R N$ is a graded semiprime ideal of R. Therefore M is a graded quasi-semiprime module.

Scientific Ethics Declaration

The authors declare that the scientific ethical and legal responsibility of this article published in EPSTEM journal belongs to the authors.

Acknowledgements or Notes

This article was presented as poster presentation at the International Conference on Basic Sciences, Engineering and Technology (www.icbaset.net) held in Marmaris/Turkey on April 27-30, 2023.

References

Al-Zoubi, K., Abu-Dawwas, R., & Al-Ayyoub, I. (2017). Graded semiprime submodules and graded semi-radical of graded submodules in graded modules. *Ricerche di Matematica, 66*(2), 449–455.

Atani, S.E., & Saraei, F.E.K. (2010). Graded modules which satisfy the gr-radical formula. *Thai Journal of Mathematics, 8*(1), 161–170.

Atani, S.E. (2006). On graded prime submodules. *Chiang Mai Journal of Science, 33*(1), 3–7.

Farzalipour, F., & Ghiasvand, F. P. (2013). On graded semiprime and graded weakly semiprime ideals. *International Electronic Journal of Algebra, 13*, 15–22.

Farzalipour, F., & Ghiasvand, F. P. (2012). On graded semiprime submodules. *Word Academy Science Eng. Technology, 68*, 694–697.

Hazrat, R. (2016). *Graded rings and graded grothendieck groups*. Cambridge: Cambridge University Press.

Lee, S.C. & Varmazyar, R. (2012). Semiprime submodules of graded multiplication modules. *Journal of the Korean Mathematical Society, 49*(2), 435–447.

Nastasescu, C., & Van Oystaeyen, F. (1982). *Graded and filtered rings and modules, lecture notes in mathematics* (p.758), New York, NY: Springer.

Nastasescu, C., & Van Oystaeyen, F. (1982). *Graded ring theory* (p.28), Amsterdam: North-Holland.

Nastasescu, C., & Van Oystaeyen, F. (2004). *Methods of graded rings*. Berlin-Heidelberg: Springer-Verlag.

Refai, M., & Al-Zoubi, K. (2004). On graded primary ideals. *Turkish Journal of Mathematics, 28*, 217–229.

Author Information

Khaldoun Al-Zoubi
Jordan University of Science and Technology
Irbid, Jordan
Contact e-mail: kfzoubi@just.edu.jo

Shatha Alghueiri
Jordan University of Science and Technology
Irbid, Jordan

To cite this article:

Al-Zoubi, K. & Alghueiri, S. (2023). On gr-quasi-semiprime submodules. *The Eurasia Proceedings of Science, Technology*, Engineering *& Mathematics (EPSTEM), 22*, 359-363.

The Eurasia Proceedings of Science, Technology, Engineering & Mathematics (EPSTEM)
ISSN: 2602-3199

The Eurasia Proceedings of Science, Technology, Engineering & Mathematics (EPSTEM),

2023 Volume 22, Pages 364-376

ICBASET 2023: International Conference on Basic Sciences, Engineering and Technology

Economic Impacts of Expected Istanbul Earthquake: Scenario Generation

Mujgan Bilge ERIS
Yeditepe University

Cagla ALPARSLAN
Yeditepe University

Melis Almula KARADAYI
Istanbul Medipol University

Ayla ALKAN
Istanbul Beykent University

Duygun Fatih DEMIREL
Istanbul Kultur University

Eylul Damla GONUL-SEZER
Yeditepe University

Abstract: It is difficult to make precise estimations about the time, location, and magnitude of earthquakes which can cause significant consequences such as massive casualties and economic losses. Although the earthquakes cannot be prevented, minimization of losses can be achieved with effective disaster management. In this study, four most likely scenarios that are put forward by the geological engineers and scientists are evaluated to illustrate the potential impacts of a possible earthquake. Therefore, effects of an earthquake on physical damage, sectoral growth and post-earthquake government expenditures, tax revenues, investments, imports, and exports are numerically estimated. Additionally, since Istanbul has an intense economic relations and workforce flow beyond its borders, it is evaluated as a whole with Kocaeli and Tekirdağ provinces. The impact of the earthquake is privatized on the basis of Istanbul, Kocaeli and Tekirdağ districts. Considering the location of the fault lines and length of breaks, it is thought that different districts would be affected by the earthquake in different degrees, and impacts of scenarios are created in this direction. Damage rates in different districts due to different magnitudes are predicted by taking 17 August 1999 Izmit Bay Earthquake as a basis. As a result of this study, the damage rates of the building stock and industrial facilities, number of casualties, sectoral and expenditure change rates in the districts of Istanbul, Tekirdağ and Kocaeli are determined. In addition, the change rates in physical, sectoral, and expenditure areas are also reflected on the rest of Türkiye. Thus, the results obtained from the scenarios will help to generate certain policy strategies after the earthquake and contribute to reducing economic, social, and physical damage.

Key Words: Natural disaster, Earthquake, Scenario analysis, Disaster economics, Loss estimation

Introduction

Throughout history, earthquakes caused both losses of life and severe economic damage. Due to its nature, it is not possible to predict the time and the location of earthquakes. However, it is possible to minimize the losses

by estimating the impacts of an earthquake. To minimize the losses and make effective plans, generating several earthquake scenarios is important since they picture what kind of situation can be faced in a possible disaster event (Lednická, 2006; Hempen, 2007). In other words, developing earthquake scenarios and analyzing the results have a major role to mitigate the damages and taking precautions. Additionally, scenario generations are critical for determining the policies specifically for post-earthquake recovery processes (Rodgers et. al.,2020).

After the 17 August 1999 earthquake in Istanbul, it is known that a major seismic tension has accumulated under the Marmara Sea and a massive earthquake is being awaited for Istanbul (Bohnhoff et al., 2013; Lange et al., 2019; Şimşek et.al.,2021). Therefore, it becomes vital to understand and analyze the outcomes of an expected Istanbul earthquake with the help of possible scenarios. This paper investigates the degree of damage and impacts of a possible earthquake based on the four most likely scenarios developed by geological engineers and scientists. According to these four scenarios, the fault segments with a high risk of break in Istanbul are evaluated. Additionally, although this earthquake is mainly expected to occur in Istanbul, it is not surprising to expect its effects beyond its borders. Therefore, Istanbul is evaluated as a whole with its surrounding provinces Kocaeli and Tekirdağ since it has direct economic relations with these two provinces.

Last but not least, the analysis is performed at the district level for Istanbul, Kocaeli, and Tekirdağ to illustrate the impacts of the scenarios, namely, where the earthquake occurred and at what magnitude. It can be noted that the location and the magnitude of an earthquake are one of the first selected factors while predicting the damages (Mader,1994). Therefore, considering different earthquake magnitudes, in other words, earthquake shocks at the district level gives more realistic results while evaluating the impact of the scenarios. According to the results of scenario evaluations, physical damages, and economic factors are decided to examine. In detail, the number of dead and injured people, damaged buildings and industrial facilities, post-earthquake changes for eleven sectors, and government expenditures, tax incomes, investments, import, and export amounts are estimated numerically. After that, these results are reflected in the Rest of Türkiye to examine the effects in a wider context.

Literature Review

Scenario generations for disaster management, particularly for earthquakes have been studied for years (Mader et.al.,1994; Villacis et al.,2000; Isık et al.,2019). These scenarios are mainly used to assess the risks after an earthquake and determine the government policies or emergency actions (Durukal et.al.,2002, Özmen 2002; Erdik, 2003; Young et. al.,2019). Some of these studies focused on earthquake scenarios in developing countries rather than industrialized ones since the scenarios are highly dependent on whether the earthquake happened in economically developed or developing countries (Erdik, 1994; Villacís et al.,1997). On the other hand, in literature, most of the articles about scenario generation and loss estimation in Türkiye are focused on the Marmara region (Durukal et.al., 2002; Erdik et.al.,2008, Strasser et.al.,2008, Demircioglu et al.,2009). It is reasonable since the economic activities are mostly concentrated in the Marmara region and population density is high. Additionally, an earthquake with a magnitude of 7 or more is expected with a %2 annual probability on the main Marmara fault line (Durukal et.al, 2008).

It is known that the first earthquake damage scenario is developed by the Research Division of the General Directorate of the Ministry of Public Works and Settlement based on 1894 earthquake results (Erdic et al.,1994). However, in this study, Istanbul is not considered specifically, in other words, the global damage in the region is predicted rather than the whole of Istanbul. Thus, Erdic et al. (1994) investigated a scenario earthquake with 7-7.5 Mw magnitude and predicted the direct losses in Istanbul. Additionally, he mentioned the earthquake disaster master plan which is prepared for Istanbul with two scenarios; medium and high-intensity earthquakes with 100 and 500 years return periods. Similarly, Özmen (2002) generated an earthquake scenario in Istanbul with a magnitude of 7.8 Mw which occurs at the nearest part of the Northern Boundary Fault where the surface rupture length is accepted as 140 km. Then, the number of buildings with severe, moderate, and minor damage is computed by using the damage estimates in the regions which are affected by different severities. In addition, the expected number of dead and injured people is also determined. Durukal et.al., (2002) examined the average damage rates for industrial facilities to analyze the possible industrial losses during the Kocaeli earthquake. The mean damage ratio for industrial enterprises is determined as %3 for 7 Mw, %8 for 8 Mw, and %20 for 9 Mw magnitude earthquake. Moreover, the loss ratios for different sectors are predicted by considering the equipment and machinery losses in case of a 9 Mw magnitude earthquake. After, Durukal et.al., (2008) used this information to predict the expected industrial losses in Istanbul. In their article, while the overall loss for industrial buildings is found as between 6 and 8%, the business interruption for chemical, textile, and automotive sectors is computed as 50, 30, and 20%, respectively. Furthermore, according to Erdik et.al. (2011),

2%-4% of the buildings are expected to have severe damage while %9-%15 have moderate and 20%-34% have light damage in Istanbul in the case of a 7.25 Mw earthquake.

The most recent report that predicts the overall loss for an expected Istanbul earthquake is prepared by the prepared by the Kandilli Observatory and Earthquake Research Institute. According to their findings, if an earthquake occurs at night with a magnitude of 7.5 Mw, there will be 17% of moderate or higher-level damaged buildings and approximately 14,150 people will lose their life. Additionally, they showed that while the financial losses due to structural damage can be expected to be around 68 billion TL, non-structural damages will be around 120 billion TL. In addition, according to TÜSİAD and TURKONFED ‘s report 25 to 300 billion dollars of economic damage is expected in case of a 7.5 Mw scenario earthquake.

Methodology

The study first provides the estimations about the physical, sectoral, and economic variables for Istanbul, Kocaeli, and Tekirdağ districts through numerical analysis. Secondly, the most likely expected scenarios for the Istanbul earthquake are explained and earthquake shocks are created for each district to illustrate the impact of four determined scenarios. Finally, post-earthquake results regarding the physical damage, and sectoral and economic changes are shown for Istanbul, Tekirdağ, and Kocaeli provinces. Additionally, analysis is performed for the remaining provinces of Türkiye to show how they will be affected in case of an expected Istanbul earthquake which will occur in the heart of the country.

Pre-Earthquake Estimations

The physical variables which can be considered as population, the number of residential buildings, and industrial facilities are determined separately for Istanbul, Kocaeli, and Tekirdağ provinces at the district level. The required data are obtained from TURKSTAT and the Ministry of Industry for the year 2020. However, the data for number of buildings is not available for the districts of Tekirdağ and Kocaeli provinces. Therefore, due to its closeness and similar regional characteristics, the number of buildings in Kocaeli province is assumed by considering the Tuzla district. Likewise, the Büyükçekmece district is used for examinations to represent Tekirdağ province.

Secondly, the size of the eleven sectors for the districts is predicted by using Gross Domestic Product (GDP) data in terms of economic activity. In that sense, the GDP by province is allocated on the basis of population, the number of buildings, or industrial facilities to these sectors for each district. For instance, to determine the size of the construction sector in a particular district, the number of buildings in that district is divided by the total number of buildings in the province to which it belongs. Then, this calculated ratio is used to distribute the relevant province's GDP to the relevant district. Similarly, economic variables such as government expenditures, tax incomes, and investments are obtained by applying the same approach. On the other hand, export and import amounts are derived from the Province Industry Status Reports for Istanbul, Tekirdağ, and Kocaeli. These shares are used to predict the import and export values for the districts.

Scenario Generation

The four most likely scenarios which are developed by the experts are studied and listed as follows:

Scenario 1: The magnitude of 6.9 earthquake caused by a 37 km fault break in Gulf.

Scenario 2: The magnitude of 7.4 earthquake caused by a 108 km fault break in the Central Marmara Basin.

Scenario 3: The magnitude of 7.5 earthquake caused by a 119 km fault break which starts in the Gulf and goes through the middle of the Marmara Sea.

Scenario 4: The magnitude of 7.7 earthquake occurred by a 174 km fault break that started from the Gulf and reached the end of the Marmara Sea, rupturing the entire Central Marmara Basin.

According to the impact of scenarios, the earthquake shocks are created for each district of Istanbul, Kocaeli, and Tekirdağ. These shocks vary between 6 to 10 in terms of Mercalli magnitude. While determining the

different magnitudes for the districts in line with scenarios, the closeness of the districts to fault lines and the Marmara Sea as well as their resistance to the earthquake are considered. For instance, if Scenario 2 occurs, the coastline of Istanbul is expected to be severely affected. Since the distance of the fault breaks to city center is approximately 20 kilometers, the coastal districts with this proximity will experience the earthquake more severely.

To analyze the impacts of an earthquake with varying magnitudes, an Excel file is prepared. By using this file, it is possible to observe how the damage caused by an earthquake will change as the magnitude of an earthquake changes on a district basis. Since the different magnitudes directly affect the number of damaged buildings, industrial facilities, and the number of casualties, outputs of an earthquake such as physical damages, changes in sector sizes, and in other economic variables can be observed easily with the help of this excel.

In the study, firstly, the ratios for the physical damages are estimated. The number of severely, moderately, and slightly damaged, and undamaged buildings as well as the number of casualties based on different Mercalli magnitudes are extrapolated by using the data from Özmen (2000)'s study. The building damage ratios for the regions affected by the 17 August 1999 Izmit Bay earthquake at different Mercalli magnitudes are shown in Table 1 below. Besides that, severely, moderately, and slightly damaged, and undamaged ratios for industrial facilities are obtained by multiplying the building damage ratios given in Table 1 by 0.75. The coefficient of 0,75 is used for this prediction since the earthquake resistance is higher for the industrial facilities than the residential buildings (T.B.D.,2018).

Subsequently, ratios for the casualties are predicted regarding different Mercalli magnitudes. For instance, ratios for the number of dead people are calculated by multiplying the ratio of severely damaged buildings for each magnitude with 26%. It can be noted that, 26% is obtained by dividing the number of dead people in 17 August 1999 Izmit Bay to the number of severely damaged buildings. Similar calculations are also performed to assume the ratios for the number of injured people. Firstly, the coefficient of 2.51 is found by dividing the number of injured people to the number of dead people in 17 August 1999 Izmit Bay Earthquake, then, it is multiplied with the severely damaged buildings' ratio.

Table 1. Damage ratios for the buildings affected by the 17 August 1999 Izmit Bay Earthquake at different magnitudes (Özmen,2000)

Mercalli Magnitude	Severely Damaged Buildings (%)	Moderately Damaged Buildings (%)	Slightly Damaged Buildings (%)	Undamaged Buildings (%)
6	0,04	0,22	0,24	99,50
7	0,91	2,67	2,59	93,83
8	2,82	4,41	5,31	87,46
9	15,7	18,16	22,75	43,39
10	33,06	15,29	19,14	32,51

Table 2. Damage ratios for the industrial facilities and casualties affected by the 17 August 1999 Izmit Bay Earthquake at different magnitudes

Mercalli Magnitude	Severely Damaged Industrial Facilities (%)	Moderately Damaged Industrial Facilities (%)	Slightly Damaged Industrial Facilities (%)	Undamaged Industrial Facilities (%)	Number of Deaths (%)	Number of Injuries (%)
6	0,03	0,17	0,18	99,63	0,01	0,10
7	0,68	2,00	1,94	95,37	0,24	2,29
8	2,12	3,31	3,98	90,60	0,73	7,09
9	11,78	13,62	17,06	57,54	4,08	39,49
10	24,80	11,47	14,36	49,38	8,60	83,15

Post-Earthquake Estimations

According to the calculated ratios given in the previous section, the post-earthquake values of physical, sectoral, and economic variables are estimated at the district level for different earthquake magnitudes. In other words, the current number of buildings and industrial facilities in the districts are multiplied by the ratios provided in

Tables 1 and 2 to illustrate the impact of a possible earthquake. Similarly, the number of deaths and injuries is obtained by multiplying the current population in the districts with the relevant ratios.

On the other hand, the district-based sectoral sizes are found by considering the post-earthquake values of the number of buildings, industrial facilities, and/or population. In addition, the current status of the sectors in relevant districts is taken into account for the calculations. For instance, while predicting the agriculture, forestry, and fisheries sector size of each district, the agricultural land size of the districts is accounted in for calculations ("Agricultural land size by sufficient income in Türkiye provinces and districts," n.d.). The areas with larger agricultural land sizes are thought to be more affected by an earthquake, and the importance weight coefficients in the formulas are determined accordingly.

Then, post-earthquake expenses, taxes, and changes in trade are examined. The government expenditures are estimated by weighting the number of severely and moderately damaged buildings and industrial facilities. Then, these ratios are multiplied by the pre-earthquake value of government expenditures. In the same manner, tax revenues, investments exports, and imports are calculated. In these calculations, an increase in government expenditures due to the government's earthquake relief efforts, and a decrease in tax revenues are assumed. Besides these, import and export amounts are figured out. Likewise, the calculations are performed by using pre and post-earthquake sector values and their importance weights in related districts.

Finally, the sectoral and economic impact of an Istanbul earthquake is demonstrated on a provincial basis for the Rest of Türkiye. Incidentally, the pre-earthquake values for the remaining provinces are obtained from TURKSTAT for the year 2020. To illustrate the impact, percentage changes in sectors and economic variables covering Istanbul, Kocaeli, and Tekirdağ provinces are calculated using their pre- and post-earthquake values. Therefore, İstanbul, Kocaeli, and Tekirdağ are evaluated as a whole while analyzing the effects of an earthquake on the Rest of Türkiye. Subsequently, the earthquake impact levels for the remaining provinces are determined by considering the percentage intervals which the calculated percentage changes fall into. Percentage intervals are defined as % 0-10, %10-20, %20-30, %30-40, and %40-50. Therefore, depending on which interval the calculated percentage change falls into, a corresponding impact level is assigned in an Excel file with the help of if functions. Then, the post-earthquake values are found by multiplying these impact levels with pre-earthquake values. For instance, if the percentage change in the agriculture sector is determined between 40% and 50%, then the sectoral impact level of the province is determined, accordingly. As a result, the post-earthquake agriculture sector size for the province is computed regarding these impact levels. Additionally, in that case, it is not surprising to expect a higher decrease the in agriculture sector for the remaining provinces.

Results and Discussion

This study evaluates four potential scenarios proposed by geological engineers and scientists to illustrate the expected social and economic impacts of an earthquake expected to occur in the Istanbul region. Due to Istanbul's economic and geological importance to its neighbours, the region is evaluated as a whole with Tekirdağ and Kocaeli.

Scenario I

In the first scenario, it is assumed that an earthquake with a magnitude of 6.9 occurred as a result of a fracture with a length of 37 km in the Gulf. Table 3 shows the expected damages for the buildings, industrial facilities, and the total of all constructions in the Istanbul region. While 92.58% of the buildings are expected to stay undamaged, this ratio is 95.99% for industrial facilities.

Table 3. Expected damages for constructions in Istanbul region for scenario 1

Construction Type	Severely Damaged	Moderately Damaged	Slightly Damaged	Undamaged
Buildings	29209	38339	46168	1420465
Industrial Facilities	307	454	528	30840
Total	29516	38793	46696	1451305

Figure 1 shows the casualties and migration. Based on this figure, it can be inferred that an increase in migration from the affected region to other cities is expected due to the extensive damage to buildings.

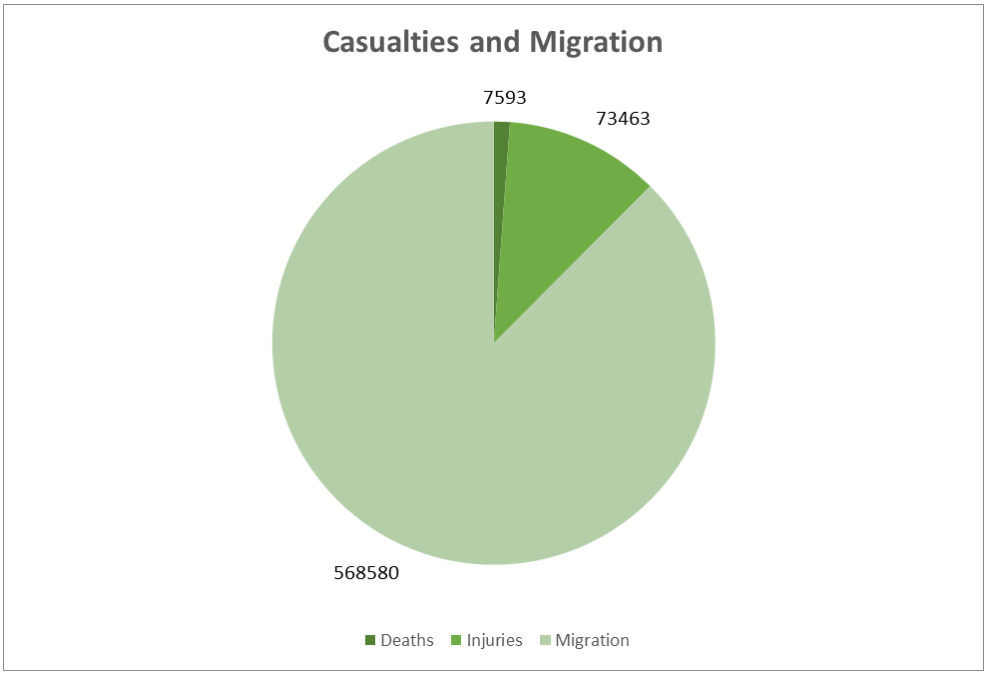

Figure 1. Expected casualties and migration in Istanbul region for scenario 1

As mentioned before, for this study, Türkiye is divided into two regions, Istanbul region and the Rest of Türkiye. Considering Istanbul's significant role in both the social and economic aspects of Türkiye, it is anticipated that the impacts of such an earthquake extend beyond the borders of the region and have an effect on the entire country. In Table 4, the changes in some economic variables in both regions after the earthquake are demonstrated. Since the government expenditures are transferred to the region, it is expected that the expenditures in the disaster region will increase. However, for a certain period, people affected by the earthquake will not be charged any taxes, which results in a decrease in tax revenues in that region. Furthermore, it is expected that investments in the region increases compared to the rest of the country.

Table 4. Expected change rates in economic variables for Istanbul region the and rest of Türkiye for scenario 1

	Change in Istanbul Region (%)	Change in Rest of Türkiye (%)
Government Expenditures	3.139	-0.431
Tax Revenues	-5.029	0
Investments	1.524	-0.444

Table 5 shows the changes in the total of sectors, imports, and export for the Istanbul region, the Rest of Türkiye, and the country as a whole. Even though there are declines in those variables in the Istanbul region, the earthquake does not have a notable impact on the rest of the country. Table 5 provides evidence that the earthquake has a greater impact on exports than imports.

Table 5. Expected change rates in sectors, imports and exports in Türkiye for scenario 1

	Change in Total of Sectors (%)	Change in Import (%)	Change In Export (%)
Istanbul Region	-3.103	-1.568	-2.058
Rest of Türkiye	0	0	0
Türkiye	-1.112	-1.011	-1.154

In this study, eleven different sectors are evaluated. Table 6 provides a general overview of the effects of the disaster on sectors, whereas Table 6 shows it in a more detailed manner by dividing it into eleven subcategories. From the table, it can be seen that the changes in the Istanbul region vary depending on the sector. Some sectors experience a substantial decrease, while others experience a more moderate one. Since this scenario is based on a relatively small-scale earthquake, the rest of Türkiye is not affected by it on the sector level.

Table 6. Expected change rates in subcategories of sectors in Istanbul region and the rest of Türkiye for scenario 1

	Change in Istanbul Region (%)	Change in Rest of Türkiye (%)
Agriculture, Forestry and Fishing	-1.577	0
Manufacturing, Mining, Quarrying and Other Industries	-2.060	0
Manufacturing Industry	-3.431	0
Building	-2.081	0
Wholesale And Retail Trade, Transportation And Storage, Accommodation And Food Service Activities	-5.682	0
Information and Communication	-0.615	0
Finance and Insurance Activities	-1.630	0
Real Estate Activities	-2.439	0
Professional, Scientific, Technical, Administrative and Support Service Activities	-1.569	0
Public Administration and Defense, Education, Human Health and Social Service Activities	-1.304	0
Other services	-0.734	0

Scenario II

In the second scenario, an earthquake with a magnitude of 7.4 caused by a 108 km fault break in the Central Marmara Basin is evaluated. The physical impacts of the earthquake are displayed in Table 7 based on the damage to constructions in the region. It is expected that 83.69% and 84.69% of the constructions will be undamaged for buildings and industrial facilities, respectively. In this scenario, there is not a vital difference depending on the construction type.

Table 7. Expected damages for constructions in Istanbul region for scenario 2

Construction Type	Severely Damaged	Moderately Damaged	Slightly Damaged	Undamaged
Buildings	93641	70588	85929	1284023
Industrial Facilities	1769	1411	1737	27212
Total	95410	71999	87666	1311235

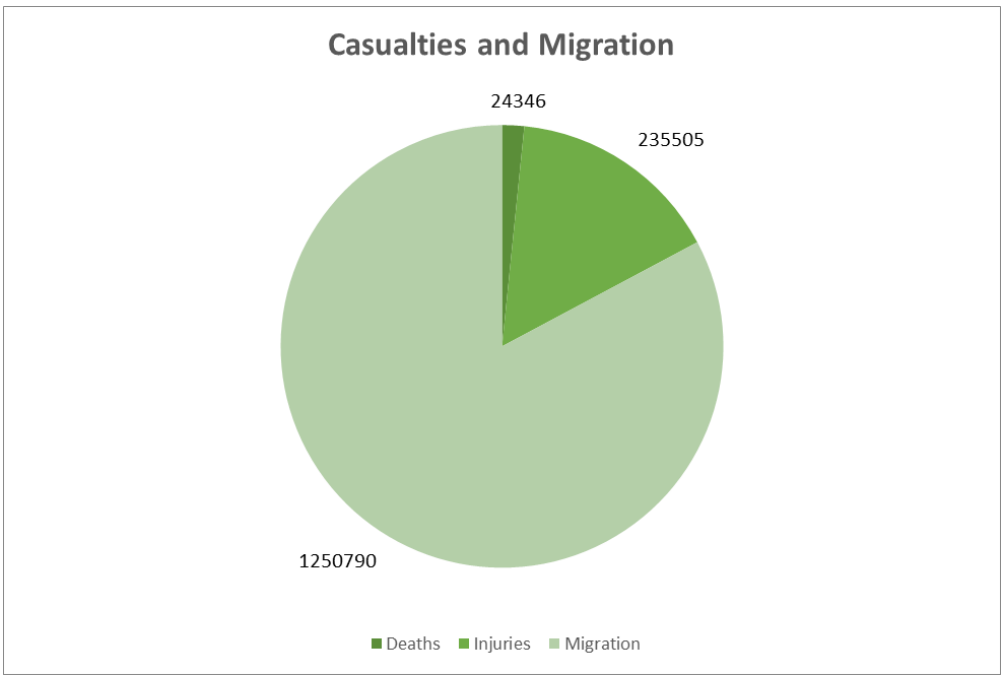

Figure 2. Expected casualties and migration in Istanbul region for scenario 2

In Figure 2, the social impacts are presented. Due to damage to the buildings and industrial facilities, local people are likely to migrate to other regions. Moreover, because of its scale compared to the first scenario, the expected casualties are relatively high in this scenario The economic impacts of the earthquake can be seen in Table 8. Though the Rest of Türkiye is not affected significantly, there is a substantial increase in investments and government expenditures for the Istanbul region.

Table 8. Expected change rates in economic variables for Istanbul region and the Rest of Türkiye for scenario 2

	Change in Istanbul Region (%)	Change in Rest of Türkiye (%)
Government Expenditures	7.390	-0.431
Tax Revenues	-9.452	0
Investments	7.923	-0.444

Table 9 and Table 10 display the effects on total sectors and the subcategories respectively. In this case, the decline is more significant compared to the first scenario. Additionally, for some sectors, the impacts surpassed the borders of Istanbul, which causes a decline in some sectors in the Rest of Türkiye.

Table 9. Expected change rates in sectors, import and exports in Türkiye for scenario 2

	Change in Total of Sectors (%)	Change in Import (%)	Change In Export (%)
Istanbul region	-9.720	-8.008	-7.243
Rest of Türkiye	-0.611	0	0
Türkiye	-3.876	-5.163	-4.061

Table 10. Expected change rates in subcategories of sectors in Istanbul region and the Rest of Türkiye for scenario 2

	Change in Istanbul Region (%)	Change in Rest of Türkiye (%)
Agriculture, Forestry And Fishing	-2.692	0
Manufacturing, Mining, Quarrying and Other Industries	-4.619	0
Manufacturing Industry	-6.193	0
Building	-8.918	0
Wholesale And Retail Trade, Transportation And Storage, Accommodation And Food Service Activities	-18.229	-2.451
Information and Communication	-7.127	0
Finance and Insurance Activities	-12.658	-2.530
Real Estate Activities	-10.494	-2.208
Professional, Scientific, Technical, Administrative and Support Service Activities	-7.319	0
Public Administration and Defense, Education, Human Health and Social Service Activities	-3.557	0
Other services	-2.783	0

Scenario III

In the third scenario, the evaluation is made based on an earthquake with a magnitude of 7.5 earthquake caused by a 119 km fault break which starts in the Gulf and goes through the middle of the Marmara Sea. This scenario examines a relatively larger-scale earthquake. The damages on the different types of constructions are presented in Table 11. The study indicates that 74.37% of the buildings will be undamaged, while this ratio is 79.45% for the industrial facilities. It can be inferred from the table that the disaster has a more catastrophic impact on buildings compared to industrial facilities.

Figure 3 demonstrates the casualties which are expected to be relatively higher than the other two scenarios examined. In addition, when taken into account together with Table 11, it is evident that due to the damage in

constructions, people resident in the area are likely to relocate to other cities for both residential and economic purposes.

Table 11. Expected damages for constructions in Istanbul region for scenario 3

Construction Type	Severely Damaged	Moderately Damaged	Slightly Damaged	Undamaged
Buildings	145765	110493	136915	1141008
Industrial Facilities	2395	1878	2328	25527
Total	148160	112371	139243	1166535

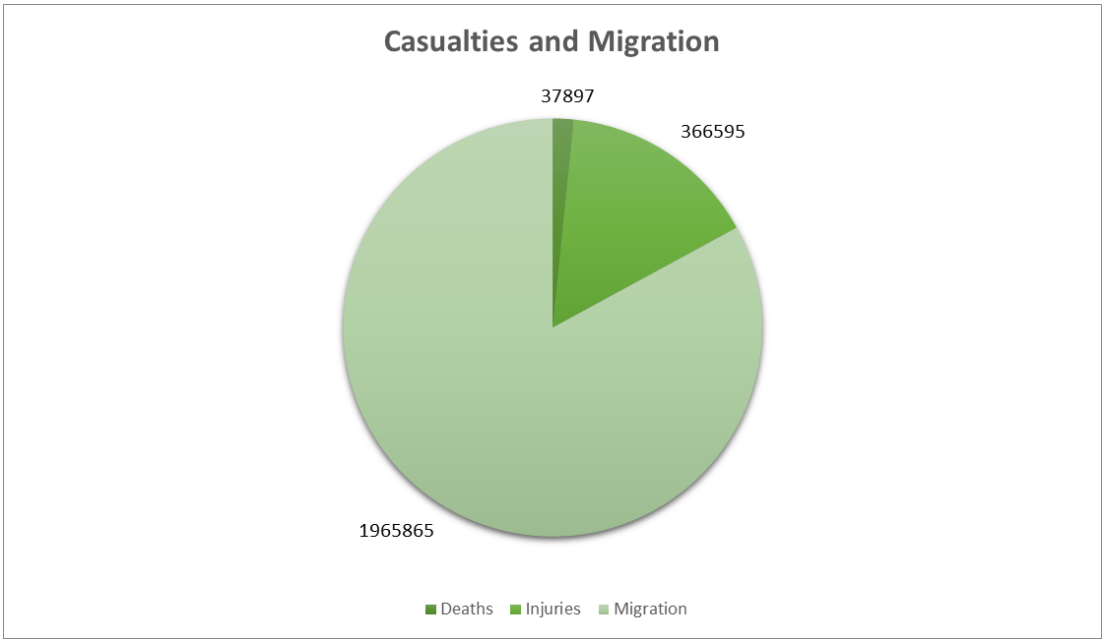

Figure 3. Expected casualties and migration in Istanbul region for scenario 3

According to Table 12, the Istanbul region is significantly affected by the earthquake with huge increases in government expenditures and investments in the disaster region. Moreover, in this scenario, the Rest of Türkiye is significantly affected by the earthquake on the economic level.

Table 12. Expected change rates in economic variables for Istanbul region and the rest of Türkiye for scenario 3

	Change in Istanbul Region (%)	Change in Rest of Türkiye (%)
Government Expenditures	11.585	-1.875
Tax Revenues	-15.895	-3.084
Investments	10.414	-1.951

Based on the results presented in Table 13 and Table 14, there is a significant decrease in the sectoral variables for the Istanbul region. Depending on the intensity of the earthquake, in this case, the changes in the Rest of Türkiye is also notable, specifically in some sectors.

Table 13. Expected change rates in sectors, imports and exports in Türkiye for scenario 3

	Change in Total of Sectors (%)	Change in Import (%)	Change in Export (%)
Istanbul region	-13.814	-10.311	-9.908
Rest of Türkiye	-1.264	-2.717	0
Türkiye	-5.763	-7.613	-5.555

Table 14. Expected change rates in subcategories of sectors in Istanbul region and the rest of Türkiye for scenario 3

	Change in Istanbul Region (%)	Change in Rest of Türkiye (%)
Agriculture, Forestry And Fishing	-4.804	0
Manufacturing, Mining, Quarrying and Other Industries	-7.114	0
Manufacturing Industry	-9.949	0
Building	-12.112	-2.299
Wholesale And Retail Trade, Transportation And Storage, Accommodation And Food Service Activities	-25.698	-5.569
Information and Communication	-9.068	0
Finance and Insurance Activities	-15.785	-2.530
Real Estate Activities	-14.388	-2.208
Professional, Scientific, Technical, Administrative and Support Service Activities	-9.798	0
Public Administration and Defense, Education, Human Health and Social Service Activities	-5.203	0
Other services	-3.790	0

Scenario IV

The last scenario is generated based on an earthquake with a magnitude of 7.7 earthquake caused by a 174 km fault break that started from the Gulf and reached the end of the Marmara Sea, rupturing the entire central Marmara Basin. This scenario demonstrates the most destructive outcomes among the four scenarios. In Table 15, the impacts of the earthquake on different types of constructions are presented. According to that, only 63.60% of the buildings are expected to be stayed undamaged, while for the industrial facilities, 69.59% of them stay undamaged.

Table 15. Expected damages for constructions in Istanbul region for scenario 4

Construction Types	Severely Damaged	Moderately Damaged	Slightly Damaged	Undamaged
Buildings	236888	144107	177462	975724
Industrial Facilities	4350	2434	2983	22361
Total	241238	146541	180445	998085

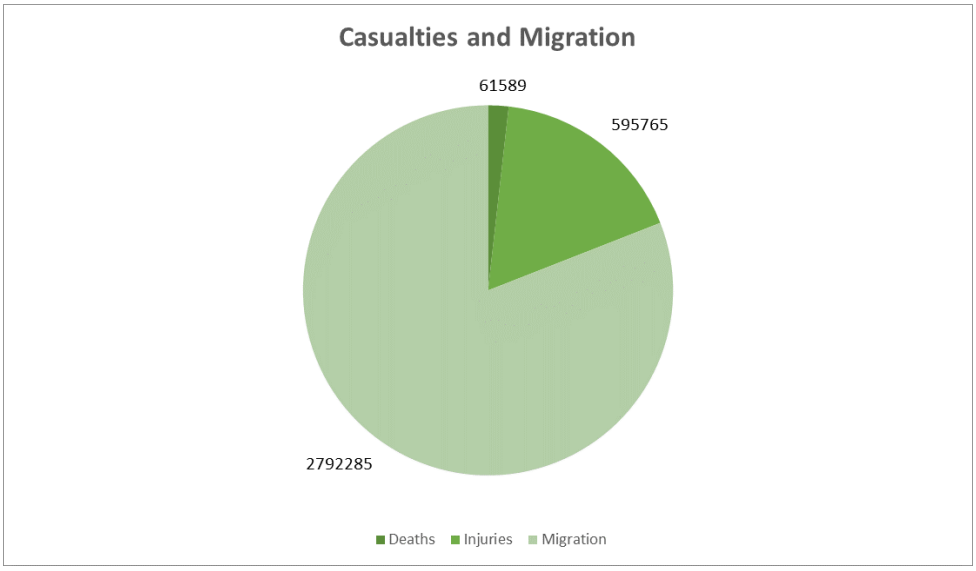

Figure 4. Expected casualties and migration in Istanbul region for scenario 4

In Figure 4, the expected casualties and the people likely to migrate are demonstrated. Since this is the scenario that is expected to cause more devastating outcomes, the casualties are substantially higher compared to others. Due to the damage to both residential and industrial constructions, most of the residents in the area are expected to relocate to a new region which results in a higher migration rate. Since this scenario studies a larger-scale earthquake, its impacts are expected to be more profound. Such an earthquake with this intensity is predicted to have a significant impact throughout the country. The impacts on some economic variables are presented in Table 16.

Table 16. Expected change rates in economic variables for Istanbul region and the rest of Türkiye for scenario 4

	Change in Istanbul Region (%)	Change in Rest of Türkiye (%)
Government Expenditures	18.847	-1.875
Tax Revenues	-25.313	-6.538
Investments	17.787	-1.951

Due to the magnitude of impact in this scenario, the most significant changes occur in this one which can be inferred by the huge decreases in economic variables. The values of sectors are critically decreased for both the Istanbul region and the Rest of Türkiye. Also, there are notable decreases in both imports and exports for the whole country. The findings can be observed in Table 17 and Table 18.

Table 17. Expected change rates in sectors, imports and exports in Türkiye for scenario 4

	Change in Total of Sectors (%)	Change in Import (%)	Change In Export (%)
Istanbul region	-21.869	-15.555	-14.642
Rest of Türkiye	-4.591	-2.717	-2.746
Türkiye	-10.784	-10.995	-9.416

Table 18. Expected change rates in subcategories of sectors in Istanbul region and the Rest of Türkiye for scenario 4

	Change in Istanbul Region (%)	Change in Rest of Türkiye (%)
Agriculture, Forestry And Fishing	-8.916	0.000
Manufacturing, Mining, Quarrying and Other Industries	-11.005	-2.781
Manufacturing Industry	-14.085	-2.951
Building	-17.990	-2.299
Wholesale And Retail Trade, Transportation And Storage, Accommodation And Food Service Activities	-41.066	-16.093
Information and Communication	-17.095	-3.330
Finance and Insurance Activities	-27.498	-5.681
Real Estate Activities	-22.034	-5.227
Professional, Scientific, Technical, Administrative and Support Service Activities	-16.672	-2.628
Public Administration and Defense, Education, Human Health and Social Service Activities	-8.185	0.000
Other services	-6.131	0.000

Conclusion

In this study, four different scenarios suggested by the experts of the subject were examined to illustrate the impacts of an earthquake on physical and economic variables for the expected Istanbul earthquake. These scenarios include four different earthquakes, ranging from relatively smaller to larger scales, resulting from the rupture of different fault lines. Due to Istanbul's economic relations with its neighbours Tekirdağ and Kocaeli, it is considered as a whole with these two cities, and the study is carried out in this direction.

It is known that depending on the location and the length of the rupture, the effects of the earthquake vary from district to district. Thus, for each district different intensity levels are assigned and the Mercalli scale is used for

this purpose. When the findings are evaluated, in Scenario 1 the impact on both physical and economic variables is relatively small in the Istanbul region whereas the rest of the country is not affected substantially. However, in Scenario 4 which represents a relatively larger-scale earthquake, it causes severe economic and social impacts in the Istanbul region, while having significant effects in the Rest of Türkiye, especially on the economic level.

Scientific Ethics Declaration

The authors declare that the scientific ethical and legal responsibility of this article published in EPSTEM journal belongs to the authors.

Acknowledgements or Notes

* This article was presented as oral presentation at the International Conference on Basic Sciences, Engineering and Technology (www.icbaset.net) held in Marmaris/Turkey on April 27-30, 2023.

* This study has been funded by TÜBİTAK-1001 "Special Call for Earthquake Research", Project Number: 121k925, Project Title: Analysing the Dynamic Impacts of the Expected Istanbul Earthquake on the Economy of Istanbul: An Input-Output Economic Model Integrated to a System Dynamics Model.

References

Bohnhoff, M., Bulut, F., Dresen, G., Malin, P. E., Eken, T., & Aktar, M. (2013). An earthquake gap south of Istanbul. *Nature Communications*, *4*(1), 1999.

Demircioglu, M. B., Erdik, M., Hancilar, U., Sesetyan, K., Tuzun, C., Yenidogan, C., & Zulfikar, A. C. (2009). Technical manual-earthquake loss estimation Routine ELERv1. 0. *Bogazici University, Department of Earthquake Engineering, Istanbul, 133*.

Durukal, E., Uskan, E., Sesetyan, K., & Demircioglu, M. B. (2002). Earthquake risk assessment for industrial facilities in Istanbul. *Bogazici University, Department of Earthquake Engineering, Istanbul*.

Durukal, E., Erdik, M., & Uçkan, E. (2008). Earthquake risk to industry in Istanbul and its management. *Natural Hazards, 44*, 199-212.

Erdik, M. (1994). *Developing a comprehensive earthquake disaster masterplan for Istanbul* (pp. 125-166). Springer Netherlands: Springer.

Erdik, M. (2013). Earthquake risk in Turkey. *Science, 341*(6147), 724-725.

Erdik, M., & Durukal, E. (2008). Earthquake risk and its mitigation in Istanbul. *Natural Hazards, 44,* 181-197.

Hempen, G. (2007). New Madrid earthquake scenario- An overview. *The Cusec Journal 12*(1), 1-12.

Işık, E., Sağır, Ç., Tozlu, Z., & Ustaoğlu, Ü. S. (2019). Determination of urban earthquake risk for Kırşehir, Turkey. *Earth Sciences Research Journal*, *23*(3), 237-247.

Istanbul Metropolitan Municipality (2019). Istanbul earthquake loss estimation and risk assessment project report. https://depremzemin.ibb.istanbul/calismalarimiz/tamamlanmis-calismalar/ istanbul-ili-olasi-deprem-kayip-tahminlerinin-guncellenmesi-projesi/.

Lange, D., Kopp, H., Royer, J. Y., Henry, P., Çakir, Z., Petersen, F., ... & Géli, L. (2019). Interseismic strain build-up on the submarine North Anatolian Fault offshore Istanbul. *Nature Communications*, *10*(1), 3006.

Lednická, M., Kaláb, Z., Hrubesová, E., & Korínek, R. (2006). Contribution to evaluation of technical seismicity effect on buildings-case study. *Earth Sciences Research Journal, 10*(1), 7-14.

Mader, G. G. (1994). Creating the scenario and drafting earthquake hazard reduction initiatives. *Issues in Urban Earthquake Risk*, 103-113.

Ministry of Agriculture and Forestry. (n.d.). Agricultural land size by sufficient income in Turkey provinces and districts [Excel file]. https ://www.tarimorman.gov.tr/Belgeler / Duyurular /T % C 3%BCr kiye%20 %C4%B0l%2 0%C4%B0l%C3%A7e%20Baz%C 4%B1nda%20Yeter%20Geli rli%20Tar%C 4%B1msal%20Arazi%20B%C3%BCy %C3%BCkl%C3%BCkleri.xlsx.

Ministry of Industry and Technology. (2020). Istanbul provincial industry status report. https://www.sanayi.gov.tr/UserFiles/ist_ilmuhaberi_2020.pdf.

Ministry of Industry and Technology (2020). Kocaeli provincial industry status report. April 7, 2023, https://www.sanayi.gov.tr/UserFiles/ist_ilmuhaberi_2020.pdf.

Ministry of Industry and Technology (2020). Tekirdag provincial industry status report. https://www.sanayi.gov.tr/UserFiles/ist_ilmuhaberi_2020.pdf.

Özmen, B. (2000). *17 Ağustos 1999 İzmit körfezi depreminin hasar durumu rakamsal verilerle*. İstanbul: Türkiye Deprem Vakfı.

Özmen, B. (2002). İstanbul ili İçin deprem senaryosu. *Türkiye Mühendislik Haberleri, 1*(417), 23-28.

Rodgers, J., Su, G., Qi, W., Milledge, D., Densmore, A., Davis, C., ... & Guo, C. (2020). Creating an earthquake scenario in China: A case study in Weinan City, Shaanxi province. *International Journal of Disaster Risk Reduction*,*42*, 101305.

Şimşek, P., & Gündüz, A. (2021). A big earthquake awaits İstanbul: Mini review. *Afet ve Risk Dergisi, 4*(1), 53-60.

Strasser, F. O., Bommer, J. J., Şeşetyan, K., Erdik, M., Çağnan, Z., Irizarry, J., ... & Lindholm, C. (2008). 6A comparative study of European earthquake loss estimation tools for a scenario in Istanbul. *Journal of Earthquake Engineering, 12*(S2), 246-256.

TURKSTAT. (2021).Export by provinces,2013-2022 (general trading system). https :// data. tuik .gov.tr/Bulten/Index?p=Ucretli-Calisan-Istatistikleri-Ocak-2021-37498&dil=1.

TURKSTAT (2021). Import by provinces,2013-2022 (general trading system). https: //data. tuik. gov.tr /Bulten/Index?p=Ucretli-Calisan-Istatistikleri-Ocak-2021-37498&dil=1.

TÜRKONFED & TÜSİAD. (2021). Istanbul earthquake scenario business preparedness report. https://turkonfed.org/Files/ContentFile/turkonfedIstanbulearthquakescenariobusinesspreparedness report-7446.pdf

Villacís, C., Tucker, B., Yepes, H., Kaneko, F., & Chatelain, J. L. (1997). Use of seismic microzoning for risk management in Quito, Ecuador. *Engineering Geology, 46*(1), 63-70.

Yönetmeliği, T. B. D. (2018). *Deprem etkisi altındaki binaların tasarımı için esaslar*. Ankara: Türkiye.

Young, J.,,Njambi-Szlapka, S., & Rodgers, J. (2019). *Practical science for uncertain futures. Working paper 563*. https://cdn.odi.org/media/documents/odi-lb-scenarios-wp563-nov19-final.pdf

Author Information

Müjgan Bilge Eris
Yeditepe University
Istanbul, Türkiye
Contact e-mail: *mujganbilge.eris@std.yeditepe.edu.tr*

Çagla Alparslan
Yeditepe University
Istanbul, Türkiye

Melis Almula Karadayı
İstanbul Medipol University
Istanbul, Türkiye

Ayla Alkan
Istanbul Beykent University
Istanbul, Türkiye

Duygun Fatih Demirel
İstanbul Culture University
Istanbul, Türkiye

Eylül Damla Gönül-Sezer
Yeditepe University
Istanbul, Türkiye

To cite this article:

Eris, M.B., Alparslan, C., Karadayi, M. A., Alkan, A., Demirel, D. F., & Gonul-Sezer E. D. (2023). Economic impacts of expected Istanbul earthquake: Scenario generation. *The Eurasia Proceedings of Science, Technology, Engineering & Mathematics (EPSTEM), 22*, 364-376.

The Eurasia Proceedings of Science, Technology, Engineering & Mathematics (EPSTEM)
ISSN: 2602-3199

The Eurasia Proceedings of Science, Technology, Engineering & Mathematics (EPSTEM), 2023

Volume 22, Pages 377-388

ICBASET 2022: International Conference on Basic Sciences, Engineering and Technology

Are the Young Investors Ready for Cryptocurrency Investments in Malaysia?

Hayati YUSOF
Universiti Tunku Abdul Rahman

Zulnurhaini ZOLKAPLY
Universiti Tunku Abdul Rahman

Muhammad Ashraf ANUAR
Universiti Tunku Abdul Rahman

Abstract: Cryptocurrency or the virtual currency is the latest development in investment. It is a medium to exchange goods and services for virtual payments, an alternative diversification tool for investors and it features an attractive store of value for wealth creation. There was an attempt to urge the Malaysian authority to legalise cryptocurrency recently in order to attract the youth's involvement in it. Even though there was an overwhelming interest detected among the country's young investors, these groups have held back their interest due to the fear of the cryptocurrency's unknown and vague territories. To date, cryptocurrency studies involving developing countries like Malaysia are still lacking as most past studies were conducted in developed countries. This research is undertaken to examine the interest and awareness of private undergraduate students on cryptocurrency's potentials as virtual money and wealth creation. Based on the analysis conducted, about more than half of the potential investors admitted that they had little knowledge of the virtual currency despite the high probability of them showing interests to make cryptocurrency investments once they graduated or started working. These potential investors also believe that cryptocurrency investments help to improve the effectiveness, profitability and the value of their monetary investments. The contribution of this quantitative research lies in the youngsters' perceptions of their perceived value and perceived risk (Consumer Behaviour Theory) towards their intention to adopt cryptocurrency. Apart from educating the youth about the virtual currency, this research seeks more regulators' attentions in managing cryptocurrency developments and its transparency in Malaysia

Keywords: Cryptocurrency, Bitcoin, Investment, Behavioural intention, Readiness

Introduction

Cryptocurrency is a virtual or digital currency that operates on peer-to-peer network without intermediaries and uses cryptography to secure and verify transactions. It is decentralised which means there is no central authority such as a government or financial institution (like the central bank) that controls cryptocurrencies and they require no financial intermediaries. In 2009, the first well-known cryptocurrency known as Bitcoin was introduced. Bitcoin was created by Satoshi Nakamoto (probably a nickname) and there are thousands of other cryptocurrencies or altcoins have been created since then (Ter Ji-Xi, Salamzadeh & Teoh, 2021). One of the key features of cryptocurrencies is its fixed or limited supply compared to fiat currencies that can be printed by the governments. The transactions on the cryptocurrency network are faster and cheaper than traditional banking transactions and the cryptocurrency transactions are recorded on a blockchain which is maintained by nodes around the world. Blockchain and the virtual currencies might be changing the face of financial services worldwide soon but there are challenges towards cryptocurrency adoption such as security risks, price volatility

and regulatory uncertainty. The use and adoption of cryptocurrencies continue to grow and has become a vital part in global financial landscape. In developing countries, cryptocurrencies have gained popularity in some ways, for example cryptocurrencies can reduce remittance fees for cross-border transactions, peer-to-peer transaction to replace traditional payment method and as an investment opportunity that is not tied to local currency or stock market.

Although the acceptance of cryptocurrency is growing, it remains to be seen how fast it will become a mainstream form of payment and investment. In developing countries, for example, there are still lacking of regulatory frameworks involving cryptocurrencies, the security risks are ambiguous and their high volatility nature is unpredictable. Furthermore, not all potential investors understand the underlying technology and the risks involved in cryptocurrency investment. As with any investment, in-depth research and due diligence on the risks and value is important before investing. Research on cryptocurrency especially in developing countries is still lacking, albeit its acceptance is steadily growing in recent years. In Malaysia, for example, research on the acceptance of cryptocurrency and the significant factors contributed to its adoption is very limited compared to other financial technology such as e-wallet and internet banking (Ter Ji-Xi, Salamzadeh & Teoh, 2021). Other researchers have also reported the lack of quantitative academic literature on the intention to adopt cryptocurrency in Malaysia (Al-Amri, Zakaria, Habbal, & Hassan, 2019). There are still many developing countries that are uninformed of cryptocurrency and according to the founder of Tokenize Exchange, Hong Qi Yu, less than 2% of Malaysians know about it (Aziz, 2019). Malaysian Ministry of Communication and Multimedia claims that the younger generations, who are the active cryptocurrency users so far, may benefit from the cryptocurrency if the government can legalise these digital assets (Sundarajan, 2022). However, the uncertainty and the consequences of cryptocurrency investment can adversely affect the potential investor's decision.

Hence, this research aims to bridge the gap in academic research regarding younger generation in Malaysia and their perception on risk and value of cryptocurrency and to generate better knowledge on the significant factors that may influence their intention to adopt cryptocurrency investment. In this study, Consumer Behaviour Theory has been adopted to articulate perceived risk (PR) and perceived value (PV) as constructs towards the intention to adopt cryptocurrency among young Malaysians. In addition, this research attempts to explore whether or not the undergraduate students in Malaysia are ready to adopt cryptocurrency investment in the future. The findings from this study will be able to answer questions on the level of cryptocurrency readiness among the potential future investors in the country and also, their perception on the cryptocurrency risks and values. This could provide more insights to the Malaysian policymakers and regulators in dealing with cryptocurrency investments in the country. The next section of this paper is the review of literature, followed by research methodology and data analysis. Conclusion and discussion are presented at the end of the article.

Literature Review

Cryptocurrency has been an academic interest more than a decade ago since the first release of most popular cryptocurrency, Bitcoin in 2009 (Farell, 2015). Academic research in cryptocurrency is still lacking and in its infancy stage. The conceptual framework in this study is primarily the Consumer Behaviour Theory and it is the most suitable framework to understand youngsters' perceptions on cryptocurrency. One dependent variable which is the consumers' intention to adopt cryptocurrency as a potential investment and two independent constructs which are the perceived risk (PR) and perceived value (PV) were adopted in this research.

Intention to Adopt Cryptocurrency

Mamman, Ogunbado, and Abu-Bakr (2016) define intention as "how hard persons are willing to try and how much determinations they are planning to use towards performing a behaviour". In the context of technology acceptance, the influence of beliefs on behavioural intention must be investigated to improve use (Brusso, 2015). One of the focal points in cryptocurrency existing research is on the intention towards cryptocurrency adoption especially in developing countries. A few major technology companies like Microsoft, Amazon and Tesla have already accepted cryptocurrency payments, but many consumers around the world are still unfamiliar with this trend. Current literature in cryptocurrency among developing countries is growing and increasing, albeit its infancy stage. A study conducted by Ter Ji-Xi, Salamzadeh and Teoh (2021) reported three factors: performance expectancy, effort expectancy and facilitating condition, are significant to consumers' behaviour towards cryptocurrency adoption in Malaysia. Another research in other developing country like India has also reported the factors that influence consumers' intention to adopt mobile banking were quite like Ter Ji-Xi,

Salamzadeh and Teoh's (2021) findings, except for facilitating condition is placed by social influence (Kishore & Sequeira, 2016). Other researchers have also studied the significant factors on the intention to use cryptocurrency among potential users in Saudi Arabia. They have also added in new possible factors which turned out to be significant in terms of adoption and have claimed that human, financial and technology-related factors influence the behavioural intention (Alaklabi & Kang, 2022). The factors influencing intention to adopt cryptocurrency as well as the results in previous studies, cannot be generalised similar for all cultural contexts. Therefore, further research is essential to understand what factors motivate or deter consumers all around the world in accepting cryptocurrency.

Perceived Risk

Perceived risk was originally theorised by Bauer back in 1960 to consumer behaviour research. It is defined as the risk that consumers anticipate on uncertainty and consequences which can adversely affect their purchase decisions (Bauer, 1960). Since then, the theory has been expanded and conceptualised into multi-dimensional constructs such as financial risk, functional risk, physical risk, psychological risk, social risk and time risk (Pathak & Pathak, 2017). In academic research, perceived risk is a vital content and many research results exhibit consumers' risk perception as an obstacle toward consumers' adoption intention such as the intention to purchase or the intention to use a new technology. However, there are quite several research that report contradictory results which shows perceived risk is not a significant factor of consumers' behaviour intention.

Consumers' risk perception in the context of cryptocurrency is defined as consumers' subjective evaluation on the losses or possible danger associated with the cryptocurrency use (Mendoza-Tello, Mora, Pujol-López & Lytras, 2018). This self-evaluation is formed by individual's past experiences, word of mouth and advertisements (Shiau, Dwivedi & Lai, 2018) which can affect consumers' motivation and can cause an individual to exhibit a contrasting reaction (Kauffman & Wang, 2001). Research results in financial technology research regarding consumers' usage intention have not been consistent. Perceived risk was found significant towards consumers' intention in adopting mobile banking in rural areas (Kishore & Sequeira, 2016), mobile wallets (Shin, 2009) and internet shopping (Faqih, 2016). Conversely in other research, perceived risk was not a significant predictor to the use intention of mobile banking among consumers in Pakistan (Farah, Hasni & Abbas, 2018). Risk perception on cryptocurrency adoption among consumer is also inconsistent. Some researchers found that perceived risk has significant influence on consumers' behavioural intention to use cryptocurrency (Abramova & Böhme, 2016; Chan, Chiew, Chong, Foong & Lee (2018). On the other hand, Mendoza-Tello et al. (2018) claimed that perceived risk has no significance to explain the intention to adopt cryptocurrencies for electronic payment. Considering cryptocurrency is still a novel technology in Malaysia and the uncertainties are not well-known yet among Malaysians, thus the hypothesis is proposed as follow:

H1: Perceived risk has a negative relationship with consumers' intention to adopt cryptocurrency in Malaysia.

Perceived Value

According to Zeithaml (1988), perceived value is defined as "consumers' overall assessment of product utility based on the perception they are given and received". In this perspective, 'given' and 'received' components reveal the benefit and sacrifice which can be in monetary or non-monetary terms. Based on this trade-off between the benefit and sacrifice components, consumers tend to make their own overall assessment of a product or service utility. Many researchers have applied this perceived value as a factor to investigate consumers' intention in field of tourism and hospitality (El-Adly & Eid, 2015). Financial technology researchers have also adopted perceived value as one of their indicators, for example a study conducted by Xie, Huang and Ye's in 2021 reported that perceived value is significant to consumers' adoption intention of Fintech services. Perceived value is also a significant factor that influence the intention to use mobile applications on mobile devices (Shaw & Sergueeva, 2019).

In the context of cryptocurrency research, perceived value is reported to be significant in a number of research; however, the value concept may be different from the common view that value as a utility concept. The value concept is broader, more complex and consists of a multi-dimensional view (García-Monleón, Erdmann & Arilla, 2023). Perceived value in a research conducted by Pakrou and Amir (2016) has resulted in a positive and meaningful relationship with consumers' intention to use Bitcoin in Iran. Other research conducted by Moysidou and Spaeth (2016) in crowdfunding reported that perceived value is relevant for crowd funders' decision making.

Hence, the perceived value has been hypothesised as follow:

H2: Perceived value has a positive relationship with consumers' intention to adopt cryptocurrency in Malaysia.
Figure 1 presents the conceptual framework adopted in this research to explore the relationship of perceived risk (PR) and perceived value (PV) and the intention to adopt cryptocurrency among young investors in Malaysia (AD).

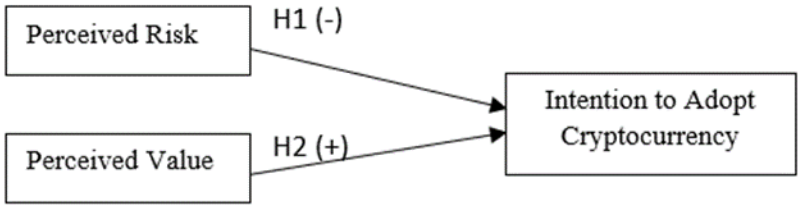

Figure 1. Conceptual framework

Research Methodology

This section explained the methods or process used in the instrument adoption, sampling, data collection and analysis. A five-point Likert scale (1- Strongly Disagree to 5 – Strongly Agree) of research instruments were adopted from a past study. The three constructs involved two independent variables, they are Perceived Risk (PR) and Perceived Value (PV) and one dependent variable which is the intention to adopt cryptocurrency (AD). This study adopted the deductive quantitative approach by the use of an online survey questionnaire. The language used for the survey questionnaire is English. Convenient sampling (a non-probability sampling approach) is used in which the researchers personally approach the potential respondents who were completing their undergraduate programmes at the time. This group was chosen as they represented the tech-savvy group who have the potentials to invest when they work or after graduation. Furthermore, this study focused on these young and potential cryptocurrency investors in a developing country as past studies involved existing, older and matured users or conducted in mostly developed countries. To continue further, in non-probability sampling, the elements in the population do not have any probabilities of being chosen in the sample. Thus, the findings from the sample may not be able to easily represent the whole population. However, at times, researchers turn to non-probability sampling in order to obtain some preliminary information in a quick and cheap manner (Sekaran, 2016).

Data have been collected between July to December 2022 involving 330 undergraduate students who have had an exposure to the digital platforms and virtual currencies. Based on G*Power estimation, the secured data collection is sufficient for its intended purpose. IBM SPSS and SmartPLS were used to analyse the data collected. Data were then analysed for validity and reliability purposes, multicollinearity problems, multiple linear regression and structured model testing.

Data Analysis

This section elaborated in detail the background of the respondents, validity and reliability of the study, multicollinearity test conducted, multiple linear regression results and the SmartPLS path co-efficient modelling.

Profile of Respondents

This study adopted the responses from 330 respondents. Overall, there are 152 (46.1%) male respondents as compared to 178 (53.9%) female respondents. Majority of the respondents are aged between 20-24 years (259;78.5%), followed by 68 respondents aged below 20 years old and three (0.9%) aged more than 24 years. Most of the respondents have some working experience before (264; 80%) while the other 66 respondents (20%) whether had no working experience or rather unsure of their past working experience. In addition, 227 (68.8%) said they did not have any investing experience with a small portion of 23.9% (79 respondents) admitted of their involvements in some investment activities. A big number of 157 (47.6%) admitted of having a little knowledge on cryptocurrency while another 95 (28.8%) said they had no knowledge at all. 68 respondents

(20.6%) claimed they have a slightly more knowledge while about 10 respondents (3%) have good knowledge of the virtual money.

Table 1. Profile of respondent

Item	Total	Percentage (%)
Gender		
Male	152	46.1
Female	178	53.9
Age		
Below 20 years old	68	20.6
Between 20-24 years	259	78.5
Between 25-29 years	2	0.6
30 years and above	1	0.3
Working Experience		
Yes	264	80
No	58	17.6
Not sure	8	2.4
Investment experience		
Yes	79	23.9
No	227	68.8
Not sure	24	7.3
Cryptocurrency knowledge		
None at all	95	28.8
A little	157	47.6
A moderate amount	68	20.6
A lot	8	2.4
A great deal	2	0.6

Reliability of the Instrument

This study used the Cronbach coefficient alpha to measure for inter-item reliability. Table 2 presents the Cronbach alpha for 330 respondents. Referring to Sekaran's (2003) rule of thumb for inter-item reliability, all the constructs meet the reliability test of being excellent with Cronbach alpha value between 0.8-0.95.

Table 2. Inter-item reliability

Item	Cronbach alpha value	Reliability
Intention to adopt cryptocurrency	0.894	Excellent
Perceived Risk (PR)	0.842	Excellent
Perceived Value (PV)	0.888	Excellent

Validity of the Instrument

Since this study adopted a similar questionnaire from Sukumaran, Bee and Wasiuzzaman (2022), a face validity is assumed to have been passed as they tested the questionnaire to existing and potential investors. On the face of it, the questionnaire seemed to measure what it is intended to measure. Construct validity is met if the results obtained from the use of the questionnaire fits the theories around which it is designed. Construct validity can be achieved through convergent and discriminant validity. Furthermore, convergent validity can be achieved if two instruments testing the same concept have high correlations while discriminant validity shows two uncorrelated variables in theory and practice (Sekaran, 2003). In this study, construct validity is achieved via a correlational analysis. The inter-item reliability can also be used to fulfil convergent validity. Correlational analysis using item-to-total-correlation has been conducted to measure the validity of the instrument. Referring to Pearson correlation test in Table 3, all perceived value (PV) constructs are moderate and positively correlated (r between 0.4 and 0.5) with the intention to adopt cryptocurrencies. On the contrary, all perceived risk (PR) constructs have a low and mostly negative correlation with the intention to adopt cryptocurrencies. This signals that the researchers dealt with high risk-averse groups of respondents, it is acceptable that humans (in this case young potential investors) are naturally trying to avoid risks when they deal with the unknowns. As an alternative, using SmartPLS, the HTMT, Fornell Larcker and cross-loading results ensured that the study met the discriminant validity requirement.

Table 3. Pearson correlation test

Main construct	Detailed construct	Intention to adopt cryptocurrency (AD1: How likely are you to invest in cryptocurrency in the near future?)	Intention to adopt cryptocurrency (AD2: I have plans to invest in cryptocurrencies in the near future)	Intention to adopt cryptocurrency (AD3: There is a high probability that I will invest in cryptocurrency after graduation or when I work)
Perceived Risk (PR)	PR1	0.031	-0.019	-0.049
	PR2	0.04	-0.020	-0.014
	PR3	-0.023	-0.003	-0.079
Perceived Value (PV)	PV1	0.505 significant at 0.01 level	0.460 significant at 0.01 level	0.521 significant at 0.01 level
	PV2	0.484 significant at 0.01 level	0.454 significant at 0.01 level	0.490 significant at 0.01 level
	PV3	0.531 significant at 0.01 level	0.449 significant at 0.01 level	0.531 significant at 0.01 level
	PV4	0.503 significant at 0.01 level	0.482 significant at 0.01 level	0.510 significant at 0.01 level
	PV5	0.515 significant at 0.01 level	0.478 significant at 0.01 level	0.489 significant at 0.01 level

Multicollinearity Test

Multicollinearity test is conducted to ensure that no high relationships (> 0.90) existed among the constructs. Table 4 indicated that all constructs (perceived risk, PR and perceived value, PV) have variance inflation factor (VIF) values below 10, thus, there is no multicollinearity problem existed in this study.

Table 4. Multicollinearity test

Construct	Unstandardised B	Coefficient std. error	Standardised coefficient beta	t	Sig.	Collinearity tolerance	Statistics VIF
Constant	3.126	0.245		12.743	<0.001		
PR1	0.030	0.095	0.029	0.318	0.751	0.359	2.783
PR2	0.057	0.089	0.057	0.640	0.523	0.384	2.603
PR3	-0.070	0.068	-0.072	-1.027	0.305	0.622	1.608
Constant	0.703	0.185		3.800	<0.001		
PV1	0.179	0.068	0.166	2.654	0.008	0.492	2.034
PV2	0.055	0.071	0.051	0.766	0.444	0.429	2.330
PV3	0.215	0.069	0.210	3.142	0.002	0.431	2.321
PV4	0.107	0.068	0.104	1.579	0.115	0.438	2.281
PV5	0.199	0.060	0.205	3.322	<0.001	0.503	1.990

Dependent Variable: AD1 – How likely are you going to invest in cryptocurrency in the near future (after graduation or when working?)

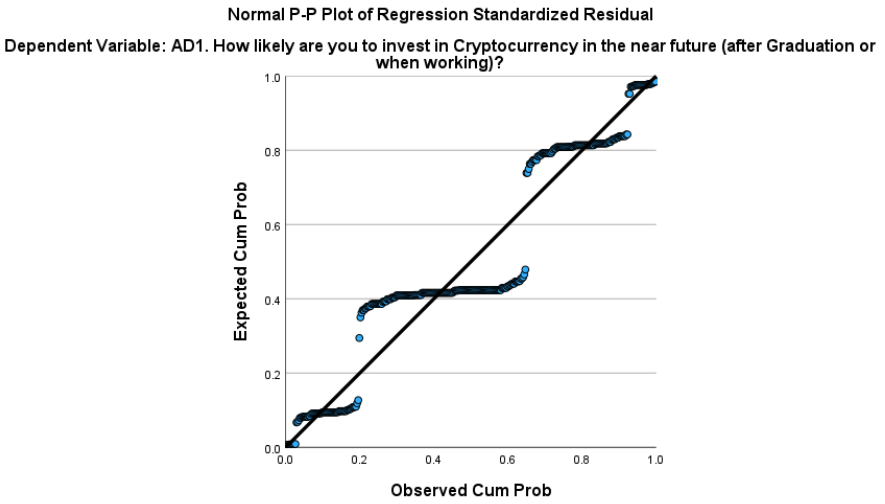

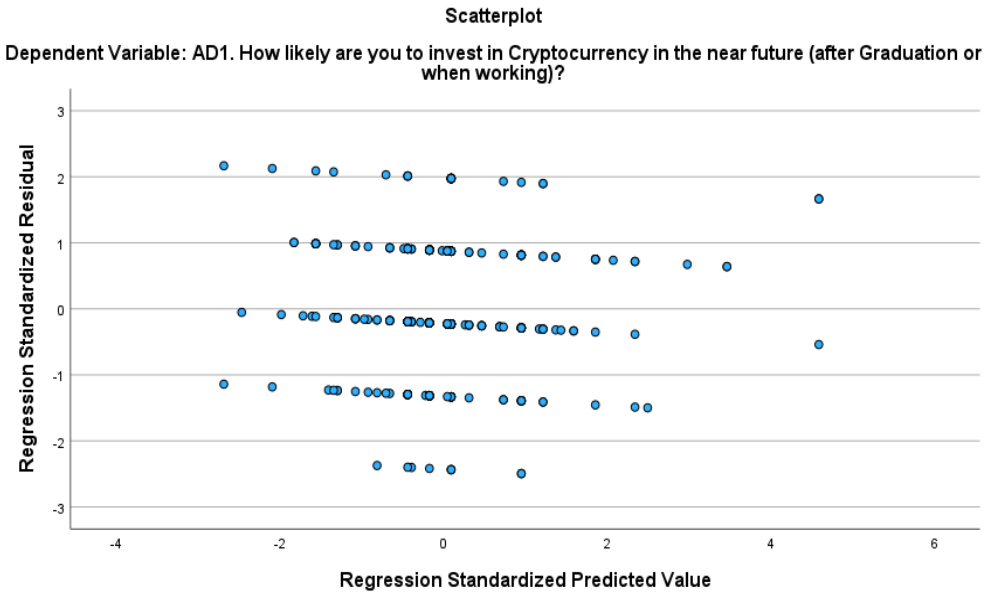

Figure 2. Homoscedasticity test for perceived risk (PR)

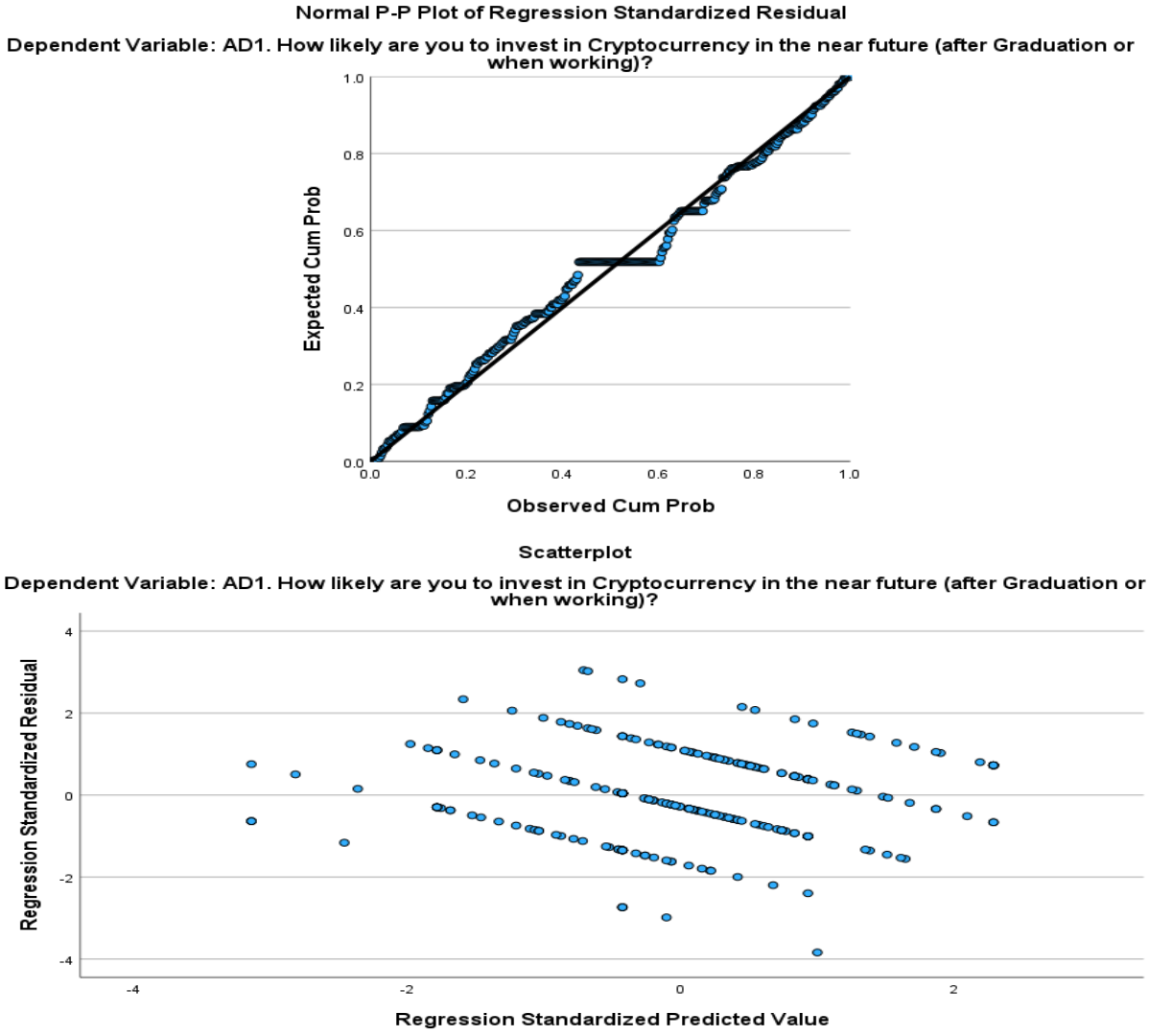

Figure 3. Homoscedasticity test for perceived value (PV)

The normal P-Plot in Figure 2 represented perceived risk (PR). It is different from the normal P-Plot for perceived value (PV) in Figure 3. The scatterplot of the residual for PV (Figure 3) is more common or acceptable (normal) as compared to PR in Figure 2. The scatterplot of residual for perceived risk (Figure 2) did not follow a straight line. In future, probably the questions to represent PR should be revised and/or replaced; however, after revision and/or replacement, if they still produce similar or consistent results, then, perhaps present or future researchers deal with significantly high risk-averse future investors. Alternatively, Table 5 showed variance inflation factor (VIF) values below 0.5 which mean there is no multicollinearity problem in this study.

Table 5. Variance Inflation Factor (VIF)

Construct	VIF
AD1.How likely are you to invest in Cryptocurrency in the near future after Graduation or when working?	2.848
AD2.I have plans to invest in cryptocurrencies in the near future.	2.955
AD3.There is a high probability I will invest in Cryptocurrency after Graduation or when I work.	3.328
AD4.I will encourage others to invest in Cryptocurrencies.	1.781
PR1.Investing in Cryptocurrencies is risky.	2.783
PR2.There is too much uncertainty associated with investing in Cryptocurrencies.	2.603
PR3.Compared with other currencies/investments Cryptocurrencies are riskier.	1.608
PV1.Using Cryptocurrencies in trading helps me improve the effectiveness, profitability and investments of my money.	2.034
PV2.I find that trading in cryptocurrencies can save money as it allows me to invest quickly and inexpensively with lower transaction costs.	2.33
PV3.Using Cryptocurrency helps me to improve my financial performance because I have total control over my money.	2.321
PV4.I will be satisfied with my Cryptocurrency investment decisions.	2.281
PV5.Investing in Cryptocurrencies will increase opportunities to achieve important goals for me.	1.99

Multiple Linear Regression (MLR)

In this study, the R square value in Table 6 is 0.380 (adjusted R square 0.365). It means that about 38% of the intention to adopt cryptocurrency can be influenced by the two chosen independent variables (perceived risk and perceived value) while the other 62% of the determinants are not captured in this study. This will be elaborated further in the findings and discussion section.

Table 6. Model summary

Model	R	R Square	Adjusted R Square	Std. Error of the estimate
1	0.617	0.380	0.365	0.72111477826

Predictors: All PR and PV constructs
Dependent Variable: AD1 - How likely are you going to invest in cryptocurrency in the near future (after graduation or when working?)

Table 7 describes the Multiple Linear Regression result. The F-value 24.633, p-value less than 0.05 indicated that the independent variables (PR and PV) statistically significantly predict the dependant variable (AD - Intention to adopt cryptocurrency) and the overall regression model is a good fit for the data.

Table 7. ANNOVA[a] (Multiple linear regression)

Model		Sum of squares	df	Mean square	F	Sig.
1	Regression	102.475	8	12.809	24.633	<0.001[b]
	Residual	166.922	321	0.520		
	Total	269.397	329			

a. Dependant variable: AD1 - How likely are you going to invest in cryptocurrency in the near future (after graduation or when working?)
b. Predictors (constant): PR1, PR2, PR3, PV1, PV2, PV3, PV4, PV5

By using SmartPLS 4 (Ringle, Wende & Becker, 2022), the researchers ran a path co-efficient loading. The result is shown in Figure 4 below. Perceived risk (PR) has a significant and negative relationship with the intention to adopt cryptocurrency with a beta value of -0.022 (p-value = 0.000, less than 0.05) while perceived value (PV) has a significant and positive relationship with the intention to adopt cryptocurrency (beta value 0.735, p-value = 0.000, less than 0.05). Hence, both hypotheses H1 and H2 are supported.

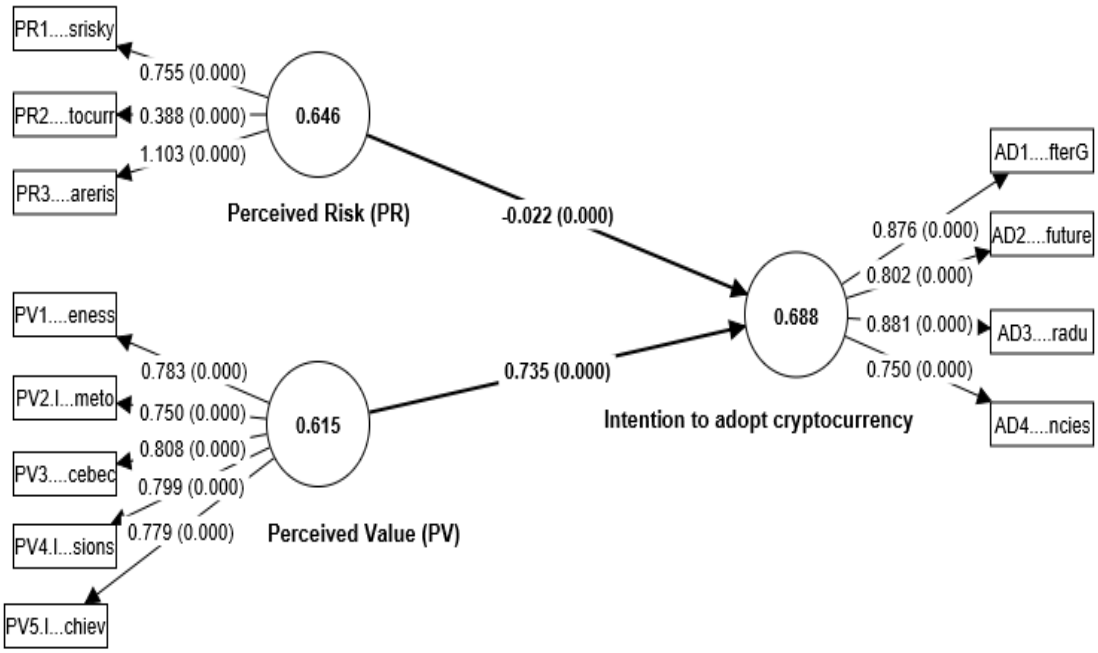

Figure 4. Path co-efficient loading

Discussion

In the past, results in financial technology research regarding consumers' usage intention have not been consistent. This study found perceived risk (PR) has a significant, negative relationship with the adoption of cryptocurrency. This is consistent with Kishore and Sequeira's (2016) mobile banking adoption, Shin's (2009) mobile wallet adoption and Faqih's (2016) internet shopping adoption. In contrast, this finding is not consistent with the findings of Farah, Hasni and Abbas (2018) in Pakistan's mobile banking adoption, Mendoza-Tello *et al.* 's (2018) cryptocurrency study as well as the finding in Sukumaran, Bee and Wasiuzzaman (2022) in which perceived risk has an insignificant influence on cryptocurrency adoption. Besides, this study dealt with high risk-averse individuals with limited investment experience and with only small knowledge about cryptocurrency investments. Perhaps, the authority, relevant agencies and academic institutions should encourage more exposure/involvements, education and training to these young generations as part of their financial literacy journeys. Mock or trial investment programmes should be conducted in workshops at the school, university or workplace entry levels. In addition, revised/more relevant or in-depth questions should be asked to gather more understanding towards the youth's perceptions on virtual investments and risk taking. Probably technology risks also are a contributor in shaping their perceptions.

Overall, perceived value (PV) is found to be significant and consistent with past studies such as in Xie, Huang and Ye's (2021) study of customers' intention to adopt Fintech services, the use of mobile applications in Shaw and Sergueeva (2019) and the intention to use Bitcoin in Iran by Pakrou and Amir (2016). It is quite true that the value concept in technology adoption (in this case involving blockchain and cryptocurrency) is more complex and multidimensional, but it is also obvious that these potential investors knew what they want in return for their financial investments and wealth creation. Having brought up in an Asian multicultural society, the value of currency, material wealth and business sense/entrepreneurial spirits seem familiar among the digital native. On average, most respondents are found to be slightly agree (mean 3.34) that cryptocurrency investments may help them to be more effective investors, make higher returns and improve their financial decisions; cryptocurrency/technology allows them to perform quick investments at lower transaction costs; produces improved financial results; and helps them to achieve important life goals.

It is noted that the two constructs (PR and PV) only captured 38% of the young investors' intentions to adopt cryptocurrency, thus this study may have missed the other significant factors that influence adoption intention (62%). These other factors might be more significant in shaping human perceptions toward risk taking behaviour and value of investments.

Conclusion and Recommendation

In conclusion, this study shared some insights for the authority, academia and service providers to understand the perceptions of potential cryptocurrency investors in Malaysia. Two independent constructs (perceived risk and perceived value) have been tested against the dependant variable of the intention to adopt cryptocurrency. It is found that both constructs significantly affecting the behavioural intention towards cryptocurrency adoption, perceived risk with a negative relationship while perceived value has a positive relationship. The youth, while being young and with insufficient investment experience, have shown some remarkable signs of being risk averse toward cryptocurrency. This is contributed to the fact that cryptocurrency and technology adoption involved security risk and cybercrimes, it is its unsecured nature and the risk of a collapsed system that are feared most by investors and wealth builders. The authority is responsible to develop and implement an ideal regulatory framework to protect investors' confidence while addressing their fear when dealing with perceived risk (Wong, Teoh, Yap & Saleh, 2022). Theoretically, this study contributes to the body of knowledge by focusing on the behavioural intentions of potential investors, in understanding their strengths and limitations toward virtual investments. The academia and government agencies may join hands in educating and providing sufficient exposure to the potential investors as parts of their financial literacy education. An introduction to the implementation of government-backed digital currencies is most welcomed (Wong et al., 2022).

This study is not without limitation, in terms of time, number of respondents, and types of constructs used to be generalised for all young, potential investors. Future researchers are recommended to adopt more constructs or questions to probe into the young investors' perceptions of intention to adopt cryptocurrency such as technology risk, privacy issues, social circle, incentives and motivations such as government support, stability, life goals/psychology, etc. The researchers felt that more contributions are needed to give insights on different investors' behavioural intention as these serve as a guide to the authority to make transparent of the dark territories of the virtual investments as well as to provide safe and controlled environments and opportunities to all.

Scientific Ethics Declaration

The authors declare that the scientific ethical and legal responsibility of this article published in EPSTEM journal belongs to the authors.

Acknowledgements or Notes

* This article was presented as oral presentation at the International Conference on Basic Sciences, Engineering and Technology (www.icbaset.net) held in Marmaris/Turkey on April 27-30, 2023.

References

Abramova, S., & Böhme, R. (2016). Perceived benefit and risk as multidimensional determinants of bitcoin use: A quantitative exploratory study. *Thirty Seventh International Conference on Information Systems*, Dublin

Alaklabi, S., & Kang, K. (2022). The extended TRA model for the assessment of factors driving individuals' behavioral intention to use cryptocurrency. *Interdisciplinary Journal of Information, Knowledge, and Management, 17*, 125-149. https://doi.org/10.28945/4948

Al-Amri, R., Zakaria, N. H., Habbal, A., & Hassan, S. (2019). Cryptocurrency adoption: current stage, opportunities, and open challenges. *International Journal of Advanced Computer Research*, *9*(44), 293-307.

Aziz, A. (2019). *Luno Malaysia back in business*. Retrieved December 1, 2019, from The Malaysian Reserve website, available at: https://themalaysianreserve.com/2019/10/23/luno-malaysia-back-in-business/

Bauer, R. A. (1960). Consumer behavior as risk raking. In Proceedings of the *43rd Conference of the Dynamic Marketiing for a Changing World*, ed. R. S. Hancock (Chicago, IL: American Marketing Association), 389–398.

Brusso, R. C. (2015). *Employee behavioral intention and technology use: mediating processes and individual difference moderators*. Old Dominion University.

Chan, K. H., Chiew, S. M., Chong, J. Y., Foong, P. Y., & Lee, X. Z. (2018). *Acceptance of Cryptocurrency among Ipoh residents*. Doctoral dissertation, UTAR.

El-Adly, M. I., & Eid, R. (2015). Measuring the perceived value of malls in a non-Western context: the case of the UAE. *International Journal of Retail & Distribution Management*, *43*(9), 849-869.

Faqih, K.M.S. (2016), An empirical analysis of factors predicting the behavioral intention to adopt internet shopping technology among non-shoppers in a developing country context: does gender matter?, *Journal of Retailing and Consumer Services*, *30*, 140-164,

Farah, M. F., Hasni, M. J. S., & Abbas, A. K. (2018). Mobile-banking adoption: empirical evidence from the banking sector in Pakistan. *International Journal of Bank Marketing*, *36*(7), 1386-1413.

Farell, R. (2015). *An analysis of the cryptocurrency ındustry*.. https://repository.upenn.edu/wharton_research_scholars/130

García-Monleón, F., Erdmann, A., & Arilla, R. (2023). A value-based approach to the adoption of cryptocurrencies. *Journal of Innovation & Knowledge*, *8*(2), 100342.

Kauffman, R. J. & Wang, B. (2001). New buyers' arrival under dynamic pricing market microstructure: the case of group-buying discounts on the internet. *J. Manag. Inform. Syst. 18*, 157–188.

Kishore, K.S.V. & Sequeira, A.H. (2016), An empirical investigation on mobile banking service adoption in rural Karnataka, *SAGE Open*, *6*(1), pp. 1-21.

Mamman, M., Ogunbado, A. F., & Abu-Bakr, A. S. (2016). Factors influencing customer's behavioral intention to adopt Islamic banking in Northern Nigeria: a proposed framework. *IOSR Journal of Economics and Finance (IOSR-JEF)*, *7*(1), 51-55.

Mendoza-Tello, J.C., Mora, H., Pujol-López, F.A. & Lytras, M.D. (2018), Social commerce as a driver to enhance trust and intention to use cryptocurrencies for electronic payments. *IEEE Access*, *6*, 50737-50751.

Moysidou, K., & Spaeth, S. (2016, August). Cognition, emotion and perceived values in crowdfunding decision making. In *Open and User Innovation Conference, Boston, USA*.

Pakrou, M., & Amir, K. (2016). The relationship between perceived value and the intention of using bitcoin. *The Journal of Internet Banking and Commerce*, *21*(2),1-18.

Pathak, V. K., & Pathak, A. (2017). Understanding perceived risk: A case study of green electronic consumer products. *Management Insight*, *13*(1), 33-37.

Ringle, C. M., Wende, S., & Becker, J.-M. (2022). *SmartPLS 4. Oststeinbek: SmartPLS GmbH*, http://www.smartpls.com.

Sekaran, U. (2003). *Research Method for Business*, Carbondale.

Sekaran, U. & Bougie, R. (2016). *Research methods for business: A skill building approach*. John Wiley & Sons.

Shiau, W.-L., Dwivedi, Y. K., and Lai, H.-H. (2018). Examining the core knowledge on facebook. *Intern. J. Inform. Manag. 43*, 52–63.

Shaw, N., & Sergueeva, K. (2019). The non-monetary benefits of mobile commerce: Extending UTAUT2 with perceived value. *International Journal of Information Management*, *45*, 44-55.

Shin, D.H. (2009), Towards an understanding of the consumer acceptance of mobile wallet, *Computers in Human Behavior*, *25*(6),1343-1354.

Sukumaran, S., Bee, T. S., & Wasiuzzaman, S. (2022). Cryptocurrency as an investment: The Malaysian Context. *Risks*, *10*(4), 86.

Sundararajan, S. (2022, March 21). *Malaysian Ministry wants crypto legal to promote adoption among youth. FXEMPIRE*. Retrieved on August 3, 2022 from Malaysian Ministry Wants Crypto Legal to Promote Adoption Among Youth (fxempire.com)

Ter Ji-Xi, J., Salamzadeh, Y. & Teoh, A.P. (2021), Behavioral intention to use cryptocurrency in Malaysia: an empirical study, *The Bottom Line*, *34*(2), 170-197. https://doi.org/10.1108/BL-08-2020-0053

Wong, S. C., Teoh T.T.M., Yap, K.H.A. & Saleh, Z. (2022). Determinants of cryptocurrency adoption behavior in Malaysia. *Jurnal Pengurusan*, *65*, 1-15.

Xie, J., Ye, L., Huang, W., & Ye, M. (2021). Understanding FinTech platform adoption: im-pacts of perceived value and perceived risk. *Journal of Theoretical and Applied Electronic Commerce Research*, *16*(5), 1893-1911.

Zeithaml, V. A. (1988). Consumer perceptions of price, quality, and value: a means-end model and synthesis of evidence. *Journal of Marketing*, *52*(3), 2-22.

Author Information

Hayati Yusof
Universiti Tunku Abdul Rahman
Kampar Campus, Jalan Universiti
Bandar Barat, 31900 Kampar
Perak, Malaysia.
Contact e-mail: *hayati@utar.edu.my*

Zulnurhaini Zolkaply
Universiti Tunku Abdul Rahman
Kampar Campus, Jalan Universiti
Bandar Barat, 31900 Kampar
Perak, Malaysia.

Muhammad Ashraf Anuar
Universiti Tunku Abdul Rahman
Kampar Campus, Jalan Universiti
Bandar Barat, 31900 Kampar
Perak, Malaysia.

To cite this article:

Yusof, H., Zolkaply, Z. & Anuar, M.A. (2023).Are the young investors ready for cryptocurrency investments in Malaysia? *The Eurasia Proceedings of Science, Technology, Engineering & Mathematics (EPSTEM), 22*, 377-388.